ABSTRACT

Title of Dissertation:	DESIGN AND SYNTHESIS OF NEW SULFONATED CNN LIGAND SCAFFOLDS FOR PLATINUM CATALYZED H/D EXCHANGE APPLICATIONS
	Morgan Jacob Kramer, Doctor of Philosophy, 2023
Dissertation directed by:	Professor Andrei N. Vedernikov, Department of Chemistry and Biochemistry

The use of platinum group metals for the activation and functionalization of C-H bonds has been a topic of substantial interest over the past 60 years. Specifically, platinum-based complexes represent a particularly promising avenue due to their ability to form air- and water-stable species that are capable of reacting with some of the most inert C-H bonds within organic substrates. Over the decades of research contributing to this field, platinum complexes have frequently been angled towards fundamental mechanistic analysis of homogeneous C-H bond activation. In turn, the development of homogenous Pt^{II}-based catalytic systems has remained underdeveloped for the practical applications in C-H bond functionalization and, in particular, deuteration of complex organic molecules, including pharmaceuticals. The latter direction is now attracting a significant interest by the pharmaceutical industry. In this work the kinetic and thermodynamic selectivity of our new catalyst, a Pt^{II} sulfonated CNN-pincer complex **1.5**, in the H/D exchange reaction between

aromatic substrates and wet TFE-d_1 was screened across thirty-four aromatic substrates with the catalysts TON up to 300 (Chapter 2). A kinetic preference of **1.5** for electron-rich C-H bonds and substrates were firmly established and a novel scale of Hammett-like σ_X^M constants was introduced to characterize the reactivity of the substrates' C(sp^2)–H bonds in transition-metal-mediated C-H activation. To greatly enhance our Pt^{II} catalysts' useful life, we used their rigid covalent immobilization to mesoporous silica nanoparticles (immobilized complex **3.5**). The resulting robust material served as an efficient H/D exchange catalyst utilizing cheaper sources of exchangeable deuterium, AcOD-d_4, and D_2O, with the catalyst's TON up to 1600 (Chapter 3). To understand our novel catalyst's structure – activity relationship, a series of benzene fragment – R-substituted analogs of **1.5** (R = MeO, tBu, iPr, F, Cl, CF_3) were synthesized and explored in the H/D exchange of a series of aromatic compounds (Chapter 4). Surprisingly, the complex **4.1-tBu** (R = ^{t}Bu) stood out as a most robust homogeneous catalyst compatible with AcOD-d_4 and D_2O at 120 ^{o}C as deuterium sources that can work *under air*. Thanks to this finding, the substrates scope for the H/D exchange with AcOD-d_4 catalyzed by **4.1-tBu** was expanded to include eight pharmaceuticals, some alkenes, with signs of engagement of some C(sp^3)-H bond donors. A novel photo-induced (violet light) room temperature H/D exchange catalyzed by **4.1-OMe** was discovered with a substantially different substrate selectivity, as compared to the thermal reaction at 80 ^{o}C. These observations may provide some important insight into the mechanism of Pt^{II}-mediated C-H activation. Finally, Chapter 5 summarizes the results of this work and suggests some future directions for this area of research.

DESIGN AND SYNTHESIS OF NEW SULFONATED CNN LIGAND SCAFFOLDS FOR PLATINUM CATALYZED H/D EXCHANGE APPLICATIONS

by

Morgan Jacob Kramer

Dissertation submitted to the Faculty of the Graduate School of the
University of Maryland, College Park, in partial fulfillment
of the requirements for the degree of
Doctor of Philosophy
2023

Advisory Committee:
Professor Andrei N. Vedernikov, Chair
Professor Daniel Falvey
Professor Jeffery Davis
Professor Efrain Rodriguez
Professor Ganesh Sriram, Dean's Representative

Dedication

To my late Father, you likely never knew it, but my love for science began with you.

Acknowledgements

I want to start by thanking my research advisor, Professor Andrei Vedernikov, whom I affectionately refer to as “AV”. I have learned so much from him from all of our conversations over the years. He has provided me with a solid foundation for scientific critical thinking and questioning that I greatly appreciate. I know that none of this would have been possible without his dedication to his group.

I would also like to thank my lab mates; Michael Hitt, Jiaheng Ruan, Diandra Soemardi, Zhehao Yuan, and Brian Horlor. Each of these people has had a significant impact on my development as scientist and I appreciate all of you. Michael and I both came into this Ph.D. program together and have been in this from the start. I have always valued having him around to share ideas and commiserate over failed experiments. He is a good friend and lab mate, and I can’t imagine what this would have been like without him.

To my extremely talented undergraduate researchers Derek Lai and Andrew Norris. Derek became a master of Suzuki couplings and columns during his time working with me and has helped me out immensely. Andrew’s willingness to learn and challenge himself has always been inspiring. I appreciate both of your efforts and contributions and I hope that I have left a positive impact on you both.

There are many people who I have met along the way who inspired me and helped me get to this point. My high school physics teacher Mr. Charlie Wilson, he saw potential in me and provided me with the inspiration I needed to believe that I could pursue a career in science and that it really was possible after all. My undergraduate research advisor from Elmira College, Dr. Jared Baker showed me how scientifically deep you must go in order

to really start answering research questions. He was an excellent mentor and educator, and I am grateful to have had the opportunity to learn from him.

I must thank my brother Seth Kramer and Bryan Boynton; you guys helped me maintain my sanity throughout this journey, friends who game together, stay together.

Finally, a very special thanks goes out to my best friend and partner, Dr. Charlotte Wentz. I can't even begin to express just how much you have done for me. You have shown me so much kindness and patience over the years and you have helped shape me into a better version of myself, we have grown and overcome so much together I am so thankful that you came into my life. I am so proud of who you have become, and I can't wait to keep spending my life with you.

Table of Contents

Dedication ii
Acknowledgments iii
Table of Contents v
List of Tables. vii
List of Figures viii
List of Charts xiii
List of Schemes xiv
List of Abbreviations xvii

Chapter 1: Current Trends and Applications of Catalytic H/D Exchange of Aromatic Substrates 1
1.1 Introduction 2
1.2 C-H bond activation and H/D Exchange 6
1.3 The Role of Ligands: Design and Application 11
1.4 Background and Past Work 17
1.5. Research Goals and Strategy 24

Chapter 2: Catalytic Deuteration of C(sp^2)-H Bonds of Substituted (Hetero)Arenes by a Pt^{II} CNN-Pincer Complex in a D_2O - 2,2,2-Trifluoroethanol-d_1 System: the Effect of Substituents on the Reaction Rate and Selectivity 26
2.1 Introduction 27
2.2 Results and Discussion 29
2.2.1 Experimental setup and expected degree of substrates' deuteration 29
2.2.2 Stability of catalyst **1.5** Background H/D exchange reactivity with TFE-d_1 33
2.2.3 Reaction kinetics model and initial rates of C-H activation 35
2.2.4 Reactivity of benzene derivatives 2.2-2.12 39
2.2.5 DFT modeling of the effect of substituents on kinetics 42
2.2.6 Novel Hammett constants σ_X^M for metal-assisted C-H bond activation 46
2.2.7 Regioselectivity of H/D exchange 47
2.2.8 Ibuprofen and Naproxen substrates 53
2.3 Conclusions 54
Supporting Information 55-90

Chapter 3: H/D Exchange Catalysis of Aromatic C-H bonds and TFE-d_1, AcOD-d_4, *and* D_2O Enabled by Covalent Immobilization of a Sterically Rigid Molecular Sulfonated CNN-Pt^{II}-OH_2 Complex 91
3.1 Introduction 92
3.2 MSN-immobilization of a Novel Sulfonated Pre-ligand 97
3.2.1 Synthesis of a $Si(OEt)_3$-substituted Sulfonated Pre-ligand 97
3.2.2 Immobilization of the novel $Si(OEt)_3$-substituted Pre-ligand on MSN 103
3.2.3 Synthesis of Molecular and MSN-immobilized Pt^{II} Aqua Complexes 105
3.2.4 Synthesis of a Novel Molecular Pt^{II} Complex 105
3.2.5 Synthesis of an MSN-immobilized Pt^{II} Aqua Complex 108
3.3 MSN Materials Characterization 111
3.4 Aromatic H/D Exchange Catalyzed by 3.5 and 3.5-FC 116

3.4.1 Extent of Deuteration for H/D exchange by 3.5 and comparison to 1.5..... 116
3.4.2 Expansion of reaction conditions and substrate scope when using 3.5 121
3.4.3 Discussion for Chart 3.3 123
3.4.4 Discussion for Chart 3.4 and some mechanistic insight 126
3.4.6 Discussion for Chart 3.5 132
3.4.7 Catalytic performance of a molecular analog of 3.5..... 141
3.4.8 Recyclability of MSN-immobilized catalyst 3.5 145
3.4.9 Evidence of Pt^{II} acting as the active catalyst of the H/D exchange by 3.5 . 149
3.5 Conclusions..... 151
Supporting Information..... 153-217

Chapter 4: Ligand Structural Effects on H/D Exchange Catalysis: A Thermal and Photochemical Approach 218
4.1 Introduction..... 219
4.2 Results and Discussion 223
4.2.1 Preparation of Ligands 4.7-X..... 223
4.2.1.1 Preparation of Pre-Ligand 4.5-X (Suzuki coupling)..... 224
4.2.1.2 Preparation of Pre-Ligand 4.6-X (S_NAr)..... 225
4.2.1.3 Preparation of Pre-Ligand 4.7-X (Sulfonation) 227
4.2.2 Preparation of Pt Complexes 4.8-X and 4.1-X 228
4.2.2.1 Preparation of Pt-Cl Complexes 4.8-X 229
4.2.2.2 Preparation of Pt-OH_2 Complexes 4.1-X..... 229
4.2.3 Kinetic Screening and Catalysis by 4.1-X 231
4.2.4 Comparison of the Performance of Catalysts 1.5 and 4.1-X 238
4.2.5 Substrate Scope and Extent of Deuteration Experiments using 4.1-tBu 243
4.2.5.1 Monosubstituted Benzene Derivatives (4.9 – 4.20)..... 244
4.2.5.2 Polysubstituted arenes and heteroaromatics (4.21 – 4.29)..... 246
4.2.5.3 Deuteration of Selected Pharmaceutical Substrates 4.30 – 4.37..... 249
4.2.5.4 Olefin Substrates (4.38-4.42)..... 250
4.2.5.5 Deuteration of Substrates' C(sp^3)-H Bonds..... 255
4.3 Development of more reactive thermal catalysts Exchange 258
4.3.1 Preparation of 4.50-tBu..... 259
4.3.1.1 Preparation of Pre-Ligand 4.47-tBu (S_NAr)..... 260
4.3.1.2 Preparation of Pre-Ligand 4.48-tBu (Sulfonation) 261
4.3.1.3 Preparation of Pt-Cl Complexes 4.49-tBu 262
4.3.1.4 Preparation of Pt-OH_2 Complexes 4.50-tBu..... 263
4.3.2 Reactivity of 4.50-tBu in H/D exchange reactions 264
4.4 Mechanistic Insight and Photo-induced Catalytic C-H Activation..... 271
4.5 Conclusions..... 285
Supporting Information..... 287-452

Chapter 5: Conclusions and Future Directions 453
5.1 A brief summary 454
5.2 Future Directions: Expansion into Alkyl H/D exchange 465
5.3 Conclusions..... 467
References..... 469

List of Tables

Table 2.1. The H/D exchange rate constants k_c (eq 2.3) and the corresponding Gibbs energies of activation for the H/D exchange between specific C(sp^2)-H bonds of substrates **2.1-2.13** and wet TFE-d_1 catalyzed by **1.5** at 80 °C 37
Table 2.2. The Hammett-type σ_X^M constants for metal-assisted C-H bond activation reactions 47
Table 3.4. Comparison of the catalytic activity of immobilized catalyst, **3.5**, its molecular variant, **3.5-FC**, and a benchmark complex **1.5**, in H/D exchange of benzene and different sources of exchangeable deuterium 142
Table 3.5. Comparison of the catalytic activity of immobilized catalyst, **3.5**, and its molecular variant, **3.5-FC**, in H/D exchange of thiophene and different sources of exchangeable deuterium..... 144
Table 3.6. Recyclability study of complex **3.5** under various conditions for the H/D exchange of thiophene. 147
Table S3.1. Immobilized catalyst recyclability for thiophene under various reaction conditions..... 191
Table 4.1. Substrate C(sp^2)-H bond-averaged values $k_{X,all}$ resulting from kinetics screening of Catalysts **4.1-X** using substrates **6** - **10** in TFE-d_1 at 80 °C. 234
Table 4.2. Substrate *meta*-C(sp^2)-H bond values $k_{X,meta}$ resulting from kinetics screening of catalysts **4.1-X** using substrates **4.6 – 4.10** in TFE-d_1 at 80 °C..... 234
Table 4.3. Hammett Plot slopes (ρ) of the meta C-H positions for catalysts **4.1-X** in TFE-d_1 at 80°C. 237
Table 4.4. A summary of catalysts **4.1-X** performance, k_X-(M^{-1} h^{-1}), using benzene as a substrate (1.12 M), catalysts loading 0.05-0.2 mol%, and various deuterium sources at 80°C or 120 °C. 238
Table 4.5. Hammett Plot slopes (ρ) of the *meta*-C-H bonds of X-substituted benzene derivatives for catalysts **4.1-tBu** and **4.50-tBu** under various conditions. 268
Table 4.6. Light source comparison and effects on the observed rate constant $k_{x,all}$ for the H/D exchange of benzene catalyzed by **1.5**. 273
Table 4.7. Catalyst performance comparison and the observed rate constant $k_{x,all}$ for the H/D exchange of benzene under photochemical conditions..... 274
Table 4.8. Relative reactivity of PhF, PhOMe and C_6H_6 in their H/D exchange reactions with TFE-d_1 catalyzed by **4.1-OMe** under thermal and photochemical conditions 276
Tables S4.1-S4.6. Experimental Parameters for **4.1-X** kinetic screening. 315-314
Table S4.6. Substrate C(sp^2)-H bond-averaged values $k_{X,all}$ resulting from kinetics screening of catalysts **4.1-X** using substrates **6** - **10** in TFE-d_1 at 80 °C. 318
Table S4.7. Substrate *meta*-C(sp^2)-H bond values $k_{X,meta}$ resulting from kinetics screening of catalysts **4.1-X** using substrates **4.6 – 4.10** in TFE-d_1 at 80 °C..... 318
Table S4.8. Substrate *para*-C(sp^2)-H bond values $k_{X,meta}$ resulting from kinetics screening of catalysts **4.1-X** using substrates **4.6 – 4.10** in TFE-d_1 at 80 °C 319
Table S4.9 Substrate *ortho*-C(sp^2)-H bond values $k_{X,meta}$ resulting from kinetics screening of catalysts **4.1-X** using substrates **4.6 – 4.10** in TFE-d_1 at 80 °C..... 319
Table S4.10. TON-24 for **4.1-X** complex screening profile in 0.45 mL TFE-d_1 solution at 80°C..... 324

List of Figures

Figure 1.1. Origins of the KIE for carbon bonds to hydrogen isotope 3
Figure 1.2. Some common pharmaceutical compounds bearing aromatic C-H bonds..... 4
Figure 1.3. Sanford's structure activity relationship for Pt^{II} and substituted diimine complexes for H/D exchange and oxidation of arenes 14
Figure 1.4. Multidentate ligand scaffolds for the for the $2e^-$ oxidation of Pt^{II} or Pd^{II}..... 17
Figure 2.1. Concentration of $C(sp^2)$-D bonds of anisole-d_x resulting from reaction (**2.1**) catalyzed by complex **1.5**..... 37
Figure 2.2. A DFT-optimized structure of the transition state $\mathbf{TS_{Ar\text{-}X}}$ for the oxidative addition of a *p*-xylene $C(sp^2)$-H bond..... 40
Figure 2.3. A plot of Gibbs energies of activation of reaction (2.1) involving *m*- and *p*-CH bonds of monosubstituted benzene derivatives 42
Figure 2.4. Plots of the DFT-calculated values of the Gibbs energies of activation of reaction (2.5) vs. the experimental values $\Delta G_{353}^{\#}$(exp) 45
Figure 2.5. ^{1}H-NMR spectra (aromatic region) demonstrating the progress of the H/D exchange between N,N-dimethylaniline and wet TFE-d_1 catalyzed by complex **1.5** at 80^{o}C..... 48
Figure 2.6. A qualitative frontier molecular orbital diagram illustrating FMO interactions between frontier orbitals of the LPt fragment and the corresponding C-H bonds of thiophene..... 50
Figure S2.1. Synthesis of $(C_6H_4$-DPMS)$PtOH_2$, **1.5**..... 56
Figure S2.2. H/D exchange reaction scheme for protio-arenes by **1.5**. 57
Figure S2.3. List of aromatic substrates inactive in reaction (2.1) 57
Figure S2.4. Sequential ^{1}H-NMR spectra demonstrating the progress of the H/D exchange between anisole and wet TFE-d_1 catalyzed by complex 1.5 at 80 ^{o}C..... 73
Figure S2.5. Initial rate of reaction catalyzed by **1.5** with benzene at 80^{o}C..... 75
Figure S2.6. Initial rate of reaction catalyzed by **1.5** with anisole at 80^{o}C..... 76
Figure S2.7. Initial rate of reaction catalyzed by **1.5** with N,N dimethylaniline at 80^{o}C 77
Figure S2.8. Initial rate of reaction catalyzed by **1.5** with fluorobenzene at 80^{o}C 79
Figure S2.9. Initial rate of reaction catalyzed by **1.5** with phenol at 80^{o}C 80
Figure S2.10. Initial rate of reaction catalyzed by **1.5** with chlorobenzene at..... 81
Figure S2.11. Initial rate of reaction catalyzed by **1.5** with bromobenzene at 80^{o}C..... 82
Figure S2.12. Initial rate of reaction catalyzed by **1.5** with nitrobenzene at 80^{o}C 83
Figure S2.13. Initial rate of reaction catalyzed by **1.5** with benzoic acid at 80^{o}C..... 84
Figure S2.14. Initial rate of reaction catalyzed by **1.5** with thiophene at 80^{o}C 85
Figure S2.15. Initial rate of reaction catalyzed by **1.5** with indole at 80^{o}C..... 86
Figure S2.16. Initial rate of reaction catalyzed by **1.5** with benzodioxole at 80^{o}C..... 87
Figure S2.17. Initial rate of reaction catalyzed by **1.5** with mesitylene at 80^{o}C..... 88
Figure S2.18. Initial rate of reaction catalyzed by **1.5** with p-xylene at 80^{o}C 89
Figure 3.1. Comparison of CNN-Pincer ligand Pt-OH2 Complexes and the past work motivations for this study..... 93
Figure 3.2. Comparison of Pt^{II}-OH_2 complexes computationally predicted ΔG# for the C-H activation of CH_4 in the gas phase at 80^{o}C and the corresponding rates of dimerization. 95

Figure 3.3. Illustration of the surface dilution effect and tripodal immobilization strategy for MSN supported **3.5**. 96
Figure 3.4. ORTEP drawing (50% probability ellipsoids) of **3.5-FC**..... 107
Figure 3.5. ^{1}H-NMR for KOH digest of an isolated MSN-derived product of a reaction of **3.16** and $Hg(ClO_4)_2$ in D_2O..... 111
Figure 3.6. (A) SEM Image of **3.5**; (B) TEM image of **3.5** C) EDS image overlay showing O in blue, Si in purple, and Pt in green; and (D) Molecular drawing of **3.5**.... 111
Figure 3.7. N_2 sorption isotherm displaying historetic behavior of **3.5**. 115
Figure 3.8. N_2 sorption isotherm overlay of SBA-16, **3.15**, **3.16** and **3.5**. 115
Figure 3.9. Superimposed ^{1}H-NMR spectra for the H/D exchange reaction between thiophene and AcOD-*d*$_4$ after 24 hours at 120^{o}C catalyzed by **3.5**..... 122
Figure 3.10. Aromatic region of ^{2}H NMR spectra for the H/D exchange reaction between thiophene and AcOD-*d*$_4$ after 24 hours at 120^{o}C catalyzed by **3.5**..... 122
Figure S3.1. Aromatic region overlay of initial and final ^{1}H-NMR spectra for Thiophene in AcOD-d_4 190
Figure S3.2. Aromatic region ^{2}H-NMR spectra for Thiophene in AcOD-d_4 after 24 hours 190
Figure S3.3. SEM and TEM images of SiO_2 nanoparticles synthesized in the absence of added ligand..... 194
Figure S3.4. N_2 Sorption of SiO_2 nanoparticles synthesized in the absence of added ligand..... 194
Figure S3.5. SEM and TEM images of immobilized ligand **3.15**..... 195
Figure S3.6. N_2 Sorption of immobilized ligand **3.15** 195
Figure S3.7. SEM and TEM images of **3.16**..... 196
Figure S3.8. EDS images of **3.16**..... 196
Figure S3.9. N_2 Sorption of immobilized Pt-Cl, **3.16**..... 197
Figure S3.10. SEM and TEM images of **3.5**..... 197
Figure S3.11. EDS images of **3.5**..... 198
Figure S3.12. N_2 Sorption of immobilized complex **3.5**..... 198
Figure S3.13. ^{1}H-NMR for 2-fluoro-6-(4-bromophenyl) pyridine **3.7** in $CDCl_3$ 200
Figure S3.14. ^{19}F-NMR for 2-fluoro-6-(4-bromophenyl) pyridine **3.7** in $CDCl_3$..... 201
Figure S3.15. ^{13}C-NMR for 2-fluoro-6-(4-bromophenyl) pyridine **3.7** in $CDCl_3$ 202
Figure S3.16. ^{1}H-NMR for 2-(4-bromobutylphenyl)-6-(pyridin-2-ylmethyl) pyridine **3.8** in $CDCl_3$..... 203
Figure S3.17. ^{13}C-NMR for 2-(4-bromobutylphenyl)-6-(pyridin-2-ylmethyl) pyridine **3.8** in $CDCl_3$..... 204
Figure S3.18. ^{1}H-NMR for 2-(4-bromobutylphenyl)-6-(pyridin-2-ylmethyl) pyridinium sulfonate **3.11** in DMSO-*d*$_6$..... 205
Figure S3.19. ^{13}C-NMR for 2-(4-bromobutylphenyl)-6-(pyridin-2-ylmethyl) pyridinium sulfonate **3.11** in DMSO-*d*..... 206
Figure S3.20. ^{1}H-NMR for Crude lithium 2-(4-trimethoxysilylphenyl)-6-(pyridin-2-ylmethyl) pyridine sulfonate **3.3** in DMSO-*d*$_6$..... 207
Figure S3.21. ^{1}H-NMR of **3.15-Digest** resulting from KOH digestion of **3.15** in D_2O 208
Figure S3.22. ^{1}H-NMR of **3.5-Digest** resulting from KOH Digestion of Immobilized Pt-OH_2 Complex **3.5** in D_2O..... 209
Figure S3.23. ^{1}H-NMR for 2-fluoro-6-phenyl pyridine in $CDCl_3$..... 210

Figure S3.24. ^{13}C-NMR for 2-fluoro-6-phenyl pyridine in $CDCl_3$. 211
Figure S3.25. ^{1}H-NMR for 2-phenyl-6-(pyridin-2-ylmethyl) pyridine **3.8-FC** in $CDCl_3$ 212
Figure S3.26. ^{13}C-NMR for 2-phenyl-6-(pyridin-2-ylmethyl) pyridine **3.8-FC** in $CDCl_3$ 213
Figure S3.27. ^{1}H-NMR for 2-phenyl-6-(pyridin-2-ylmethyl) pyridinium **3.11** in DMSO-*d*$_6$. 214
Figure S3.28. ^{13}C-NMR for 2-phenyl-6-(pyridin-2-ylmethyl) pyridinium sulfonate **3.11** in DMSO-*d*$_6$ 215
Figure S3.29. ^{1}H-NMR for 2-phenyl-6-(pyridin-2-ylmethyl) pyridine Pt-Cl Complex **3.16-FC** in DMSO-*d*$_6$..... 216
Figure S3.30. ^{13}C-NMR for 2-phenyl-6-(pyridin-2-ylmethyl) pyridine Pt-Cl Complex **3.16-FC** in DMSO-*d*$_6$..... 217
Figure S3.31. ^{1}H-NMR for 2-phenyl-6-(pyridin-2-ylmethyl) pyridine Pt-OH_2 Complex **3.5-FC** dissolved in DMSO-*d*$_6$ 218
Figure S3.32. ^{13}C-NMR for 2-phenyl-6-(pyridin-2-ylmethyl) pyridine Pt-OH_2 Complex **3.5-FC** dissolved in DMSO-*d*$_6$ 219
Figure 4.1. Other catalytic systems for aromatic H/D exchange as described in the literature. 220
Figure 4.2. Comparison of CNN-Pincer ligand Pt-OH_2 Complexes and the past work motivations for this study..... 222
Figure 4.3. Kinetic screening assay for aromatic H/D exchange catalyzed by complexes **4.1-X** 231
Figure 4.4. Hammett Plot of Log (k_{meta}) vs σ_x^M meta, H_nSub substituent effects on rate for catalysts **4.1-X**. 236
Figure 4.5. A DFT-optimized geometry of an AcOH adduct derived from **4.1-tBu** via aqua ligand substitution. 267
Figure 4.6. Hammett Overlay of Log($k_{X,meta}$) vs σ_x^M meta for **4.1-tBu** and **4.50-tBu** under various conditions. 268
Figure 4.7. Visualizations of the HOMO (predominantly a Pt d_{xz} orbital) and LUMO+3 (predominantly Pt-O σ^* orbital) for **4.1-OMe** that are involved in an electronic transition resulting in a weakened Pt-OH_2 σ-bond. 272
Figure 4.8. Benzene C-D bond formation vs time for the photo-induced H/D exchange reaction in TFE-*d*$_1$ catalyzed by **4.1-OMe**..... 276
Figure 4.9. Hammett-Type plot for the relative rates of H/D exchange with TFE-*d*$_1$ for *meta*-C-H bonds of anisole and fluorobenzene vs benzene C-H bonds catalyzed by **4.1-OMe** at 80 ^{o}C and under violet LEDs..... 280
Figure 4.10. Hammett-Type plot for the relative rates of H/D exchange with TFE-*d*$_1$ for for *meta*-C-H bonds of anisole and fluorobenzene vs benzene C-H bonds catalyzed by **4.1-OMe** at 80 ^{o}C and under violet LEDs. 280
Figure 4.11. Simplified diagram depicting the relative energy levels of the transition state TS_1 corresponding to arene coordination to a Pt^{II} center and the transition state TS_2 that corresponds to the arene C-H bond cleavage under thermal conditions (left) and under photochemical conditions (right) 282
Figure S4.1. ^{2}H NMR Overlay for the H/D exchange reaction of Benzene in TFE-*d*$_1$ by p-tBu DPMS Pt-OH_2 at 80 ^{o}C..... 317

Figure S4.2. 24 Hour Yields for Arene Screening of **4.1-CF$_3$** in 0.45 mL TFE-d_1 solution at 80^{o}C. 320
Figure S4.3. 24 Hour Yields for Arene Screening of **4.1-F** in 0.45 mL TFE-d_1 solution at 80^{o}C. 320
Figure S4.4. 24 Hour Yields for Arene Screening of **4.1-Cl** in 0.45 mL TFE-d_1 solution at 80^{o}C. 321
Figure S4.5. 24 Hour Yields for Arene Screening of **4.1-iPr** in 0.45 mL TFE-d_1 solution at 80^{o}C. 321
Figure S4.6. 24 Hour Yields for Arene Screening of **4.1-tBu** in 0.45 mL TFE-d_1 solution at 80^{o}C. 322
Figure S4.7. 24 Hour Yields for Arene Screening of **4.1-OMe** in 0.45 mL TFE-d_1 solution at 80^{o}C. 322
Figure S4.8. 24 Hour Yields for Arene Screening of **4.1-tBu** in 0.5 mL AcOD-d_4 solution at 80^{o}C. 323
Figure S4.9. 24 Hour Yields for Arene Screening of **4.1-tBu** in 0.5 mL AcOD-d_4 solution at 120^{o}C. 323
Figure S4.10.- Figure S4.91. NMR Characterization of synthetic intermediates leading to the production of **4.1-X** and **4.50-X** 362-442
Figure S4.93. ^{2}H-NMR for the H/D Exchange reaction of Acetaminophen in AcOD-*d*$_4$ catalyzed by **4.1-tBu** 443
Figure S4.94. ^{2}H-NMR for the H/D Exchange reaction of Duloxetine in AcOD-*d*$_4$ catalyzed by **4.1-tBu** 444
Figure S4.95. ^{2}H-NMR for the H/D Exchange reaction of Ibuprofen in AcOD-*d*$_4$ catalyzed by **4.1-tBu** 445
Figure S4.96. ^{2}H-NMR for the H/D Exchange reaction of Ibuprofen in AcOD-*d*$_4$ catalyzed by **4.1-tBu** 446
Figure S4.97. ^{2}H-NMR for the H/D Exchange reaction of Guaifenesin derivative in AcOD-*d*$_4$ catalyzed by **4.1-tBu** 447
Figure S4.98. ^{2}H-NMR for the H/D Exchange reaction of Melatonin in AcOD-*d*$_4$ catalyzed by **4.1-tBu** 448
Figure S4.99. ^{2}H-NMR for the H/D Exchange reaction of Amitriptyline in AcOD-*d*$_4$ catalyzed by **4.1-tBu** 449
Figure S4.100. ^{2}H-NMR for the H/D Exchange reaction of indole in AcOD-*d*$_4$ catalyzed by **4.1-tBu** 450
Figure S4.101. ^{2}H-NMR for the H/D Exchange reaction of thiophene in AcOD-*d*$_4$ catalyzed by **4.1-tBu** 451
Figure S4.102. ^{2}H-NMR for the H/D Exchange reaction of 1,2 dichlorobenzene in AcOD-*d*$_4$ catalyzed by **4.1-tBu** 452
Figure S4.103. ^{2}H-NMR for the H/D Exchange reaction of 1,2 dimethoxybenzene in AcOD-*d*$_4$ catalyzed by **4.1-tBu** 453
Figure 5.1. Key conclusions from the reactivity of **1.5** towards arene C-H bonds in wet TFE-*d*$_1$ at 80 ^{o}C 454
Figure 5.2. Immobilization strategy for **3.5** and some key results from utilizing **3.5** as an H/D exchange catalyst 456
Figure 5.3. Kinetic screening results for **4.1-X** complexes in TFE-*d*$_1$ at 80^{o}C. 457

Figure 5.4. Selected results from deuteration studies involving substituted arenes, pharmaceuticals, alkenes, and C(sp^3)-H bearing substrates..... 459
Figure 5.5. Photochemically induced H/D exchange between TFE-d_1 and benzene catalyzed by **4.1-X** at room temperature..... 460
Figure 5.6. Relative rates of H/D exchange of anisole or fluorobenzene vs benzene in TFE-d_1 under thermal (80 ^{o}C) and photochemical conditions (25 ^{o}C). 461
Figure 5.7. Simplified reaction energy diagrams comparing the relative energies of two transition states, TS_1, representing the barrier associated with ligand exchange in **4.1-X** and TS_2 representing the barrier for C-H activation of the resulting Pt^{II}-substrate complex. 462
Figure 5.8. A comparison of the efficiency of various Pt^{II} complexes synthesized in this work and those reported in the literature acting as catalysts of H/D exchange reactions of benzene and selected sources of exchangeable deuterium under thermal conditions. ... 463
Figure 5.9. Proposed H/D exchange and possible C-H functionalization schemes utilizing complex **5.9**..... 467

List of Charts

Chart 1.1. Pt^{II}-OH_2 Complexes **1.5**, **1.6**, **1.7** CNN-pincer ligand complexes 22
Chart 2.1. Pt^{II} aqua complexes **1.5, 1.6** and **1.7** 28
Chart 2.2. Aromatic substrates H_nSub studied in this work and the extent of their deuterium incorporation 31
Chart 2.3. Aromatic substrates H_nSub that either engage in side reactions or are inactive in H/D exchange by **1.5** 32
Chart 2.4. Pharmaceuticals **2.30** and **2.31** probed in H/D exchange experiments 32
Chart 2.5. Rh(III) complex **2.33** used in combination with 3 equiv. AgOTf for catalytic H/D exchange between substituted benzene substrates and CF_3CO_2D at 100 ^oC 51
Chart 3.1. The extent of deuteration of substrates used for catalyst performance screening in the H/D exchange with 0.150 M D_2O in TFE-*d*$_1$ catalyzed by 0.03-0.3 mol% **3.5** achieved after 24 hours of reaction at 80 ^oC 119
Chart 3.2. The extent of deuteration of substrates used for catalyst performance screening in the H/D exchange with 0.150 M D_2O in TFE-*d*$_1$ catalyzed by 0.03-0.3 mol% **1.5** achieved after 24 hours of reaction at 80 ^oC 119
Chart 3.3. 24-hour extent of deuteration results for H_nSub under various conditions catalyzed by **3.5** 123
Chart 3.4. 24-hour extent of deuteration results for H_nSub in AcOD-*d*$_4$ by **3.5** 125
Chart 3.5. 24-hour extent of deuteration results for H_nSub in AcOD-*d*$_4$ and 1:1 AcOD-*d*$_4$:D_2O solutions catalyzed by **3.5** 131
Chart S3.1. Summary of aromatic substrates screened for TFE-d_1, AcOD-d_4 and neat D_2O as solvents and deuterium sources 174
Chart S3.2. Summary of aromatic substrates screened with 1:1 D_2O /AcOD-d_4 mixture as the solvent and deuterium source 175
Chart 4.1. The average observed rate constants, $k_{X\text{-all}}$, for X-substituted benzene substrates (X = NO_2, F, H, OH, OMe) with **4.1-tBu** and **4.50-tBu** as catalysts 266
Chart S4.1. List of unsuccessful Substrates for H.D Exchange catalyzed by **4.5-tBu** .. 334
Chart S4.2-S4.24. Initial rate data for kinetic screening of 4.1-X derivatives for the H/D exchange of various arenes 339-361

List of Schemes

Scheme 1.1. Two main H/D exchange strategies for aromatic substrates..... 5
Scheme 1.2 Generalized diagram for C-H activation followed by C-X or C-D bond formation..... 7
Scheme 1.3 Traditional mechanisms for C-H activation mediated by homogenous metal complexes..... 7
Scheme 1.4 Garnett and Hodges' system for aromatic H/D exchange catalyzed by Na_2PtCl_4..... 8
Scheme 1.5. The currently accepted mechanism for the Shilov system for methane C-H oxidation..... 9
Scheme 1.6. The Catalytica System for the direct functionalization of methane..... 12
Scheme 1.7 Mechanistic study of the C-H activation reverse reaction enabled by diimine ligands..... 13
Scheme 1.9. **a)** Complex **1.2** hydrogen bonding stabilization by the pendant sulfonate group and its inability to carry out C-H activation. **b)** Proof of concept that the N,N ligated Pt^{II} center is capable of C-H activation..... 20
Scheme 1.10. dpms and C_6H_4-dpms structural comparison and a side-on perspective of their corresponding Pt^{II}-OH_2 complexes..... 21
Scheme 1.11 CNN Ligated Pt^{II} bimolecular deactivation pathway..... 23
Scheme 2.1. Background and Pt-catalyzed H/D exchange between a substrate H_nSub and TFE-d_1..... 34
Scheme 2.2. A proposed reaction sequence involved in the H/D exchange between arene C(sp^2)-H bonds and TFE-d_1 catalyzed by complex **1.5.**..... 36
Scheme 3.1. Synthetic strategy for the production of **3.4** and past strategies for covalent ligand immobilization..... 97
Scheme 3.2. Past synthetic strategy for the generation of cyclopenteno-fused sulfonated CNN pincer ligands..... 98
Scheme 3.3. Synthetic scheme for the production of the pre-ligand **3.10. Step A)** Suzuki coupling..... 99
Scheme 3.4. Silylation reaction for the conversion of **3.10** to **3.12-3.14**..... 101
Scheme 3.5. The covalent immobilization of **3.3** on MSNs..... 103
Scheme 3.6. KOH digest of **3.15** for the purpose of quantitation of ligand loading and validation of immobilization..... 105
Scheme 3.7 (Top) Synthesis of a molecular pre-ligand **3.11**. (Bottom) Metalation and subsequent ligand exchange of free and immobilized complexes..... 106
Scheme 3.8. KOH digests of **3.15, 3.16,** and **3.5** and the corresponding *o*-pyridyl signal used for ^1H NMR analysis of the extent of metallation of **3.15**..... 109
Scheme 3.9. Initial conditions for catalyst screening for aromatic H/D exchange in aqueous TFE-d_1 at 80 °C..... 117
Scheme 3.10. Expanded conditions of H/D exchange reaction involving H_nSub and AcOD or D_2O as deuterium sources and **3.5** as a catalyst..... 121
Scheme 3.11. One possible directing group-mediated C-H activation pathway leading to the *ortho* selectivity of **3.26**..... 130
Scheme 3.12. Evaluation of the catalytic activity of a molecular complex **3.5-FC** in H/D exchange reaction between two deuterium sources and selected substrates H_nSub..... 142

Scheme 3.13. A potentially competitive formation of **3.16** and Pt(0) and Pt(IV) disproportionation products 150
Scheme 3.14. Assessment of a relative activity of **3.16** and **3.5** in catalytic aromatic H/D exchange with TFE-d_1 151
Scheme S3.1. Synthesis of 2-fluoro-6-phenylpyridine **S3.1**. 156
Scheme S3.2. Synthesis of 7-(6-phenylpyridin-1-ium-2-yl)-6,7-dihydro-5*H*-cyclopenta[*b*]pyridine-7-sulfonate **3.11** 158
Scheme S3.3. Synthesis of **3.5-FC** 160
Scheme S3.4. Synthesis of 2-fluoro-6-(4-bromophenyl) pyridine **3.7** 162
Scheme S3.5. Synthesis of 7-(6-(4-bromophenyl)pyridin-1-ium-2-yl)-6,7-dihydro-5H-cyclopenta[b]pyridine-7-sulfonate **3.10** 164
Scheme S3.6. Synthesis of lithium 7-(6-(4-triethoxyphenyl)pyridin-2-yl)-6,7-dihydro-5H-cyclopenta[b]pyridine-7-sulfonate **3.12** 166
Scheme S3.7. Immobilization of lithium 7-(6-(4-triethoxyphenyl)pyridin-2-yl)-6,7-dihydro-5H-cyclopenta[b]pyridine-7-sulfonate **3.3** 168
Scheme S3.8. KOH Digestion of Immobilized Ligand, **3.15**, to produce 7-(6-(4-trihydroxyphenyl)pyridin-2-yl)-6,7-dihydro-5H-cyclopenta[b]pyridine-7-sulfonate **3.15-Digest** 169
Scheme S3.9. Cyclometallation of immobilized ligand, **3.15** to yield Pt-Cl complex, **3.16** 170
Scheme S3.10. Digestion of Immobilized Complex **3.16** to produce **3.16-Digest** 171
Scheme S3.11. Conversion of immobilized Pt^{II}-Cl complex **3.16** to immobilized Pt^{II} aqua complex **3.53** 164
Scheme S3.12. Assessment of a relative activity of **3.16** and **3.5** in catalytic aromatic H/D exchange with TFE-d_1, **3.16** 192
Scheme 4.1. Synthetic scheme to produce the series of ligands **4.7-X**. All reported yields are determined after isolation 223
Scheme 4.2. Synthetic scheme for the synthesis of Pt complexes **4.8-X** and **4.1-X** 229
Scheme 4.3. Aromatic substrate scope for catalytic C(sp^2)-H H/D exchange reaction catalyzed by **4.1-tBu**. Values are reported as % D incorporation after 72 hr @ 120 °C in AcOD-d_4. 244
Scheme 4.4. Summary of catalytic H/D exchange on some pharmaceutical compounds catalyzed by **4.1-tBu** in AcOD-d_4 @ 120 ^oC 248
Scheme 4.5. A proposed mechanism for the hydroarylation of olefins 251
Scheme 4.6. Intramolecular deuteration of 4.1-tBu in AcOD-d_4 252
Scheme 4.7. Attempted hydroarylation of styrene catalyzed by **4.1-tBu** 252
Scheme 4.8. Catalytic H/D exchange of some olefins catalyzed by **4.1-tBu** / AcOH-d_4 at 100 ^oC after 24h. Values is the drawings show %D incorporation 253
Scheme 4.9. Catalytic H/D exchange of C(sp^3)-H bonds of some simple alkanes and their derivatives by **4.1-tBu** / AcOH-d_4 at 140 ^oC after 24. 257
Scheme 4.10. Comparison of stability of **3.5-FC** and **4.50-tBu** under thermal H/D exchange conditions 259
Scheme 4.11. Preparation of complex **4.50-tBu** 260
Scheme 4.12. Photo-induced H/D exchange of benzene in TFE-d_1 catalyzed by **2.1** 272

Scheme 4.13. Photo-induced H/D exchange of benzene in TFE-d_1 catalyzed by **4.1-X** 275
Scheme 4.14. Previously reported reaction sequence for the H/D exchange between arene C(sp^2)–H bonds and TFE-d_1 catalyzed by **1.5**. 282
Scheme S4.1. Generalized ligand synthesis 289
Scheme S4.2. Generalized Pt-OH_2 complex synthesis..... 304
Scheme S4.3. Synthetic scheme for the production of **4.50-tBu** 312
Scheme S4.4. Reaction scheme for kinetic studies for H/D exchange catalyzed by **4.1-X** 395
Scheme 5.1. Biphasic reaction conditions for the stoichiometric C-H activation of benzene and dehydrogenation of cyclohexane by **5.6** 465

List of Abbreviations

Alk	alkyl
Ar	aryl
aq.	aqueous
bqpms	benzoquinolyl-2-pyridylmethanesulfonate
bqcpps	benzoquinolyl-cyclopentenopyridylmethanesulfonate
bpy	2,2'-bipyridyl
bpym	bipyrimidine
bn	benzyl
bz	benzoyl
calcd	calculated
C-H or CH	carbon-hydrogen bond
C-D or CD	carbon-deuterium bond
CF_3	trifluoromethyl
d_x	number of deuterium atoms
DCM	dichloromethane
DFT	Density Functional Theory
DMSO	dimethylsulfoxide
dpm	di-2-pyridylmethane
dpms	di-2-pyridylmethanesulfonate
EDX	Energy-Dispersive X-rap spectroscopy
EIE	Equilibrium Isotope Effect
ESI-MS	electrospray ionization mass spectrometry
g	grams
eq.	equivalence
H/D exchange	hydrogen-deuterium exchange
Hr	hours
HOMO	Highest Occupied Molecular Orbitals
Hz	Hertz
iPr	isopropyl
JY	J. Young Valve
k_x	Rate Constant
kcal	kilocalorie(s)
KIE	Kinetic Isotope Effect
LUMO	Lowest Occupied Molecular Orbitals
C-M	Carbon-Metal Bond
m	*meta*
M	Molarity (moles per liter)
Me	methyl
MeOH	methanol
mg	milligram(s)
MHz	megahertz
min	minute(s)
mL	milliliter(s)
mM	millimole(s) per liter

mmol	millimole(s)
mol	mole(s)
MSN	Mesoporous Silica Nanoparticles
m/z	mass to charge ratio
NHC	N-heterocyclic carbene
NMR	nuclear magnetic resonance
o	*ortho*
OA	Oxidative Addition
OMe	methoxy
ORTEP	Oak Ridge Thermal Ellipsoid Plot
OSDR	Observed vs Statistical Deuterium Incorporation Ratio
p	*para*
Ph	phenyl
psi	pounds per square inch
RDS	Rate-Determining Step
RE	Reductive Elimination
rt or RT	room temperature
σ_x	Hammett-Parameter for position, x
s	second(s)
SEM	Scanning Electron Microscopy
TEM	Transmission Electron Microscopy
tBu	tertiary butyl
TFE	2,2,2-trifluoroethanol
THF	tetrahydrofuran
v/v	volume to volume ratio
wt.%	weight percent
XRD	X-ray diffraction
µL	microliter(s)
µM	micromole(s) per liter
µmol	micromole(s)

Chapter 1: **Current Trends and Applications of Catalytic H/D Exchange of Aromatic Substrates**

1.1 *Introduction*

Deuterium is a stable nonradioactive isotope of hydrogen differing from the lightest and more abundant protium by the mass of only a neutron. Since its initial discovery by Harold Clayton Urey in 1931,[1-2] deuterium has been shown to be a rather rare isotope, comprising approximately only one hundredth of a percent of all hydrogen naturally occurring on Earth.[3-4] When a protium atom in a polyatomic species is exchanged with a deuterium atom, both physical and chemical properties of that species are appreciably affected. In fact, deuterium atoms act as weakly electron-donating substituents affecting reactivity of nearby groups. For instance, deuterated amines had a slight increase in their basicity[5] and, similarly, phenols and carboxylic acids with deuterium atoms either in their hydrocarbon backbone or in the hydroxyl itself, showed a decrease in their acidity and lipophilicity when compared to their protium counterparts.[6] These phenomena are a manifestation of the deuterium equilibrium isotope effect (EIE). Similarly, the deuterium kinetic isotope effect (KIE) is defined as the ratio of a reaction rate constants, k_H/k_D, associated with substitution of protium atoms with deuterium atoms. If an X-H bond is being broken or formed in a reaction, the deuterium kinetic isotope effect is termed as primary. The kinetic deuterium isotope effect is, most typically, associated with the difference in the zero-point vibrational energies (ZPE) of protio- vs deuterio-substituted reactants, that include all vibrational modes of the reactants and transitions state. For primary deuterium KIE, the ratio of ZPEs of species under consideration is often approximated as the ratio of ZPEs of the reacting X-H and X-D bonds (X = C or O). The ZPEs, in turn, are inversely proportional to the square root of the reduced mass of the bound atoms, X and H, or X and D, respectively. Theoretically, the nearly 2-fold increase in

atomic mass of a deuterium versus protium atom results in a small, ≤1 kcal/mol, increase of the bond dissociation energy and a slight shortening of C-D bonds vs C-H bonds (**Figure 1.1**). Assuming that the ZPE difference for a reacting C-H vs C-D bond disappears in a reaction transition state, the deuterium kinetic isotope effect of ~7 can be expected at 298K.

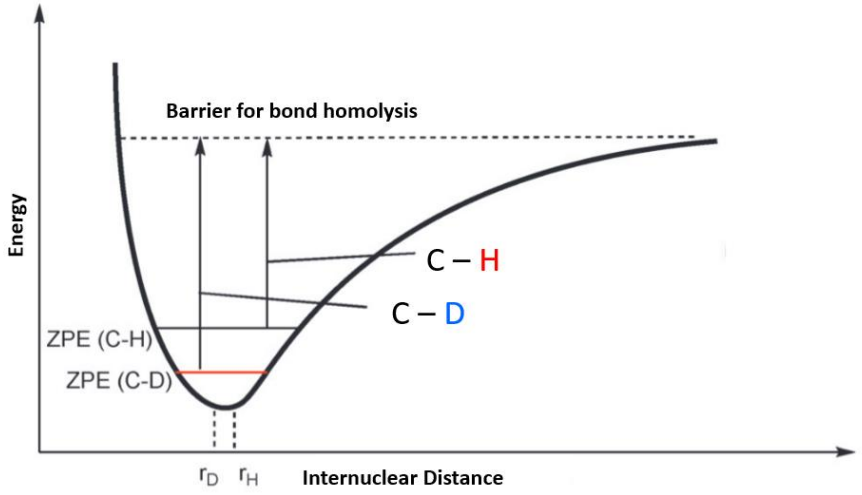

Figure 1.1. Origins of the KIE for carbon bonds to hydrogen isotopes. Lower zero-point energy of C-D corresponds to a larger activation energy barrier for bond homolysis.

While these effects have been previously elucidated in some fundamental studies,[5-6] recent attention in this area has been focused on pharmaceutical compounds for modulating drug efficiency and reducing the rate of drug metabolism *in vivo*.[1] To date, there are over 20 deuterated pharmaceutical compounds in clinical trials for in patient use, and one drug, deutetrabenazine (**Figure 1.2**), that is already approved and distributed for patient use.

This recent success and new-found utility for deuterated pharmaceuticals has increased the demand for improved methods for the catalytic installation of deuterium atoms into complex organic substrates. Generally, it is advantageous to utilize intact molecules and exchange their already established C-H bonds with newly formed C-D Bonds via a process known as H/D exchange. Aromatic backbones are ubiquitous structures in pharmaceutical

compounds (**Figure 1.2**) and may be utilized as model or targets compounds for H/D exchange.

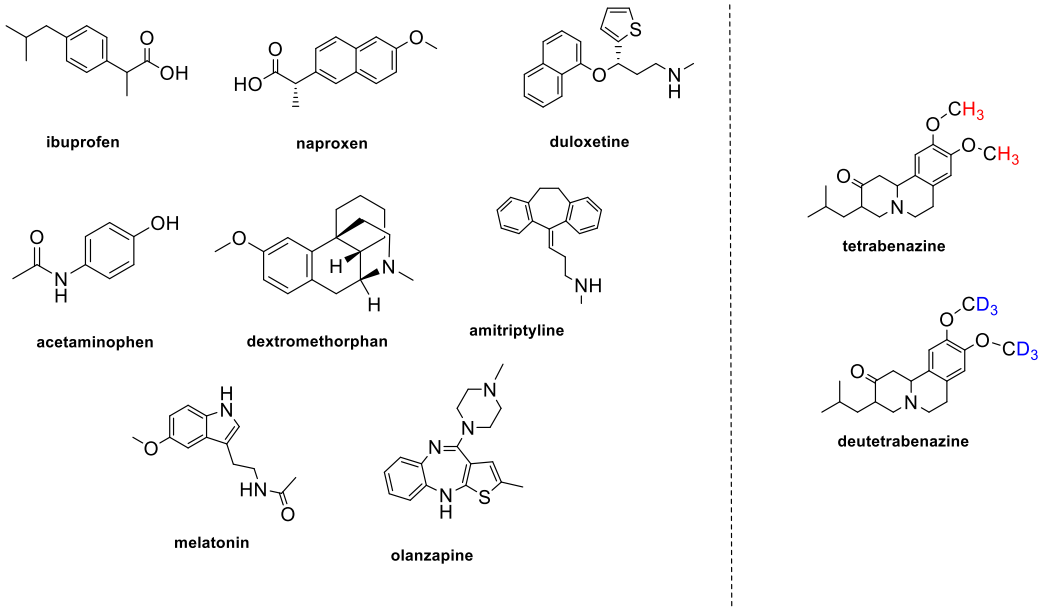

Figure 1.2 Left: Some common pharmaceutical compounds bearing aromatic C-H bonds Right: tetrabenazine and the deuterated counterpart deutetrabenazine.

This method provides minimal disturbance to the synthesis of complex materials and enables the direct conversion of the protio compounds to deuterium-enriched materials. Exchanging a hydrogen atom for deuterium presents the smallest possible change that can be made to a molecular substrate. Currently, the methods of direct H/D exchange are broken up into two major categories: Acid or base – catalyzed deuteration or transition metal – catalyzed deuteration (hetero or homogenous) (**Scheme 1.1**)

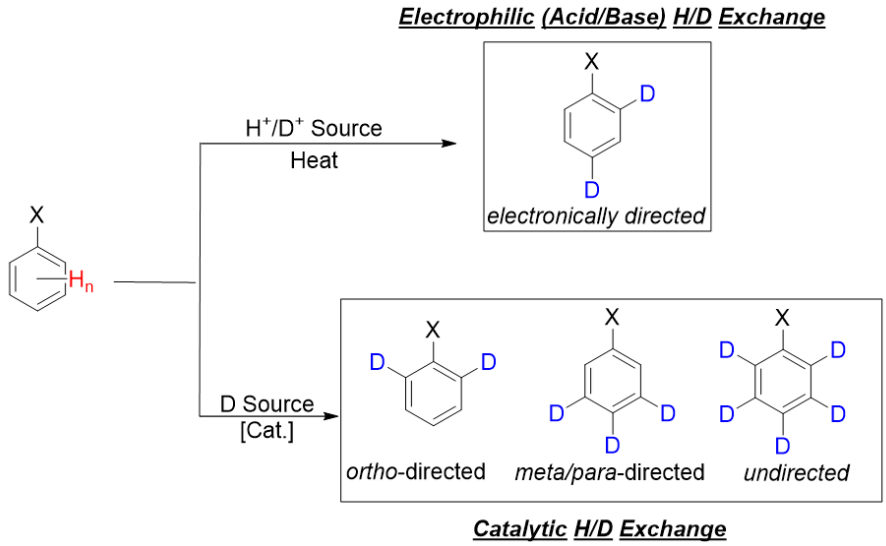

Scheme 1.1. Two main H/D exchange strategies for aromatic substrates

There are numerous advantages to both avenues of H/D exchange, for the case of acid or base – catalyzed H/D exchange, the reactions are typically very simple. Often, they utilize strong acids and elevated temperatures to exchange electronically activated C-H bonds. This category of H/D exchange methodology is among the oldest documented processes for aromatic H/D exchange and is still utilized today. However, the generality of such an approach is poor, and the selectivity arising from this process is controlled electronically and the harsh reaction conditions used are sometimes prohibitive for the H/D exchange of complex molecules bearing a wide range of various functional groups. Transition metal (TM) - catalyzed H/D exchange demonstrates a wider range of possible selectivites, ranging from complete deuteration, such as the case of undirected H/D exchange, which can be particularly advantageous for maximum deuterium enrichment, to site selective *ortho*- or *meta/para*-directed H/D exchange. Furthermore, TM-catalyzed approaches to aromatic H/D exchange often utilize much milder reactions conditions than

their acid/base - catalyzed H/D exchange counterparts, such as the use of mild deuterium sources and low temperatures. This control of H/D exchange selectivity and the use of more mild reaction conditions are critically important factors that makes TM-catalyzed H/D exchange such an attractive solution for the deuterium enrichment of complex organic molecules.[7-8]

1.2 C-H bond activation and H/D Exchange

TM-catalyzed H/D exchange and the field of C-H bond activation by transition metal compounds have been an active avenue of research for several decades since their discovery in 1960's.[10] It is important to note, that TM-catalyzed H/D exchange and the field of C-H bond functionalization by transition metal complexes are closely related via a common reaction pathway that involves the cleavage of a C-H bond and formation of a C-D or C-X bond. In fact, a catalysts' propensity for general C-H bond functionalization chemistry is often first probed by assessing its viability to perform H/D exchange. From this perspective, H/D exchange reactions can be thought of as the most fundamental or trivial examples of C-H functionalization, where X = D for the the produced C-X bonds (**Scheme 1.2**). Note that C-H bond cleavage may not be always reversible under specific conditions of a C-H bond functionalization by transition metal complexes (e.g., the subsequent steps are much faster than C-H bond cleavage), so that while C-H bond functionalization can happen in such systems the H/D exchange may not be observable.

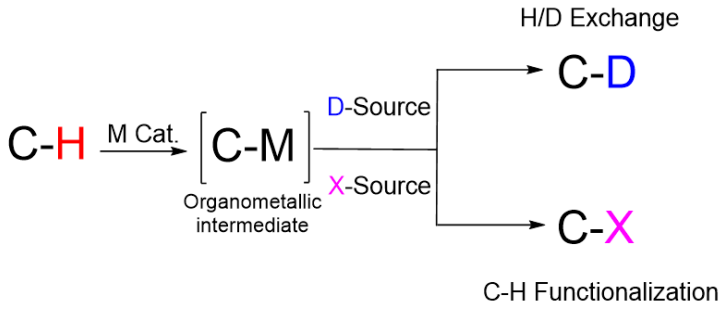

Scheme 1.2 Generalized diagram for C-H activation followed by C-X or C-D bond formation.

The common intermediate responsible for the formation of C-X or C-D bonds is a reactive organometallic C-M intermediate that results from a transition metal assisted C-H bond cleavage (Scheme 1.2). The formation of this intermediate is of critical importance to the field of C-H activation and H/D exchange since it is the species responsible for subsequent organic functionalization. Thus, the definition of C-H activation that will be adhered to in this thesis will be in reference to the reactions between a C-H bond and a transition metal complex to yield discrete complexes bearing transition metal-carbon bonds via a two-electron (radical-free) pathway.[9]

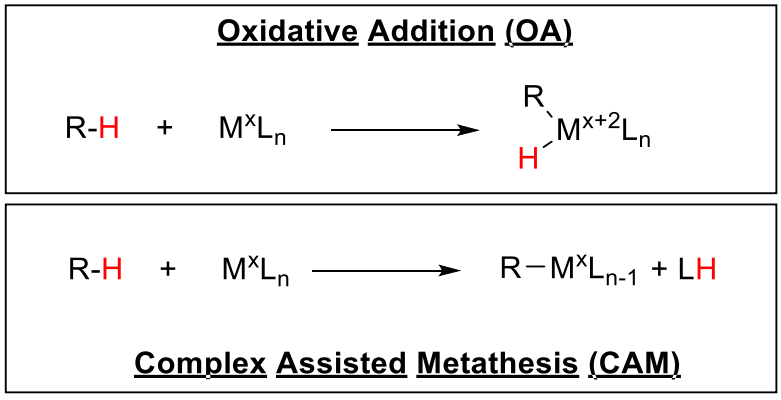

Scheme 1.3 Traditional mechanisms for C-H activation mediated by homogenous metal complexes

The two most commonly proposed mechanisms for C-H activation are oxidative addition (OA) and complex-assisted metathesis (CAM) (**Scheme 1.3**). The major difference between these two pathways lies in the identity of the generated C-M intermediate, for the case of the OA pathway, the oxidation state of the transition metal increases (usually by 2) and for CAM, the oxidation state of the metal does not change. In general, it is required to regenerate the reactive intermediate during the reaction cycle in order to allow for the overall process to be catalytic. For processes that are catalyzed by transition metal complexes, the overall reaction must proceed catalytically in order for its use to be practical.

The first discovery of homogenous C-H activation catalysis began in 1967 with Garnett and Hodges in their seminal work where they utilized $Na_2[Pt^{II}Cl_4]$ in an aqueous acetic acid/HCl mixtures that promoted the H/D exchange of arenes (Scheme 1.4).[10]

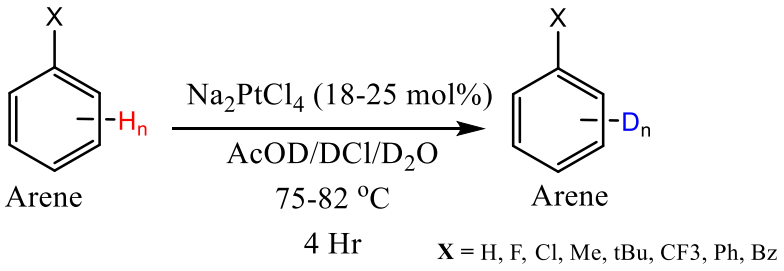

Scheme 1.4 Garnett and Hodges' system for aromatic H/D exchange catalyzed by Na_2PtCl_4.

This system was applied across an array of substituted aromatic compounds, mono- and polycyclic, and they found that H/D exchange occurred independent of the electronic effects of the arene substituent. The extent of deuteration for these arenes was universally low, ranging from 1.57-3.0% for the polycyclic substrates and only going as high as 10.7%

deuteration for benzene (which corresponds to the catalyst turnover number of about 3), alongside a rather slow reaction kinetics. Despite these facts, this work gave the first indication that homogenous Pt^{II} catalysts can activate arene C-H bonds and served as inspiration for research in the coming decades.

Shortly after this initial discovery, Shilov and co-workers expanded the substrates scope for this Pt^{II} catalyzed H/D exchange process to include alkanes and even methane (Scheme 1.5). Importantly, Shilov expanded the catalytic potential of simple $[Pt^{II}Cl_4]^{2-}$ salts beyond just H/D exchange reaction through the inclusion of $[Pt^{IV}Cl_6]^{2-}$ as a stoichiometric oxidant which enabled the partial oxidation of alkanes.[11-12]

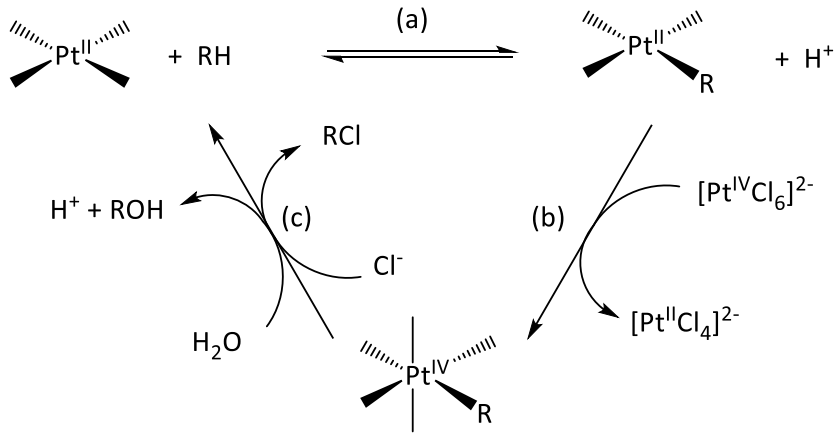

Scheme 1.5. The currently accepted mechanism for the Shilov system for methane C-H oxidation. (A) the initial C-H activation of methane to form Pt^{II}-R (R= Me), (B) the subsequent oxidation of Pt^{II}-R to Pt^{IV}-R by $[Pt^{IV}Cl_6]^{2-}$, (C) the reductive elimination of RCl or ROH via nucleophilic attack on Pt^{IV}-R.

Over the course of about 20 years of continued research the currently accepted mechanism for the Shilov system was proposed which is shown above in Scheme 1.5. The first step in this cycle involves an alkane (initially, methane) C-H activation (either by OA or CAM) to yield the Pt^{II}-R intermediate. This intermediate is of critical importance for the

subsequent formation of R-X, or in the case of H/D exchange reaction, R-D bonds. The second step in this reactions (Scheme 1.5, (b)) is the critical oxidation step which yields the highly reactive Pt^{IV}-R intermediate. The electrophilicity of the Pt^{IV} center enables the subsequent nucleophilic attack (for R = alkyl) at carbon to regenerate the catalyst and yield the functionalized alkane, R-X (where X = Cl or OH).

Interestingly, this line of research that led to the catalytic functionalization of alkanes began with an initial discovery of a catalytic H/D exchange reaction between acidic deuterium sources and aromatic substrates, thereby highlighting the important role that H/D exchange has on the field of C-H activation/functionalization. There have been examples of virtually every transition metal serving as a catalyst for either C-H activation or C-H functionalization reactions. Major contributions to this field were made by Shilov himself, as well as by more contemporary researchers such as Bergman, Jones, Labinger and Bercaw, Tilset, Hartwig, Periana, Chirik, Yu, and many others.[13-20] For the purposes of this thesis, I will focus specifically on homogenous Pt-based systems for C-H activation and H/D exchange.

Since the initial developments by Garnett, Hodges, the subsequent advancements in the late 1970-80s were focused on the development of non-oxidative avenues for direct C-H functionalization catalyzed by simple Pt^{II} salts. Ultimately, this direction of research elucidated the important and fundamental mechanisms of C-H activation that were described above in Schemes 1.2 and 1.3. There were significant limitations to utilizing simple $[Pt^{II}Cl_4]^{2-}$ salts for catalytic C-H activation and H/D exchange chemistry. At the high temperatures and catalyst concentrations required for catalytic turnovers, the catalyst lacked stability, and frequently underwent disproportionation to yield Pt^0 and Pt^{IV} and

exhausting the catalyst in the process.[21] Therefore, in order to fully explore the potential of these systems, and to properly exploit the reactive Pt-R intermediate, the stability of the catalyst must be improved.

1.3. The Role of Ligands: Design and Application

The ligand environment surrounding a reactive metal center is of critical importance in modulating the different pathways for reactivity. For example, in the Shilov-type reactions previously discussed, four chloride ligands surround the Pt^{II} center and five chlorides surround the Pt^{IV}-R fragment. Their strong electron withdrawing effects impart a significant electronic influence on the observed reactivity of the system. This results in a highly electron deficient Pt^{IV}-R, which can readily reductively eliminate and yield functionalized material. For the pre-catalyst $[Pt^{II}Cl_4]^{2-}$, the chloride ligands do little to prevent (and possibly encourage) the bimolecular disproportionation of $[Pt^{II}Cl_4]^{2-}$. From a kinetic perspective, the ligand environment can also influence the overall rate of a reaction. Gol'dshleger and Shteinman studied various complexes of the type $Pt^{II}X_n$ (where X = Cl, H_2O, NH_3, Br, NO_2, pyridine, DMSO, and PPh_3) on the rate of H/D exchange of cyclohexane. In general, they observed that the rate of H/D exchange did not merely reflect the ease of ligand substitution. Instead, rapid rates of H/D exchange were only observed when the ligands bound to Pt are of weak/low *trans* effect.[21-22]

Perhaps the most interesting but dramatic example of utilizing ligand scaffolds to stabilize and enable chemistry at Pt^{II} might have been realized by Periana and co-workers in their famous Catalytica system for direct methane oxidation.[9a, 23] The Catalytica system

uses a (bpym)$Pt^{II}Cl_2$ (bpym = bipyrimidine) catalyst that is stable in concentrated sulfuric acid at temperatures in excess of 220 ºC.

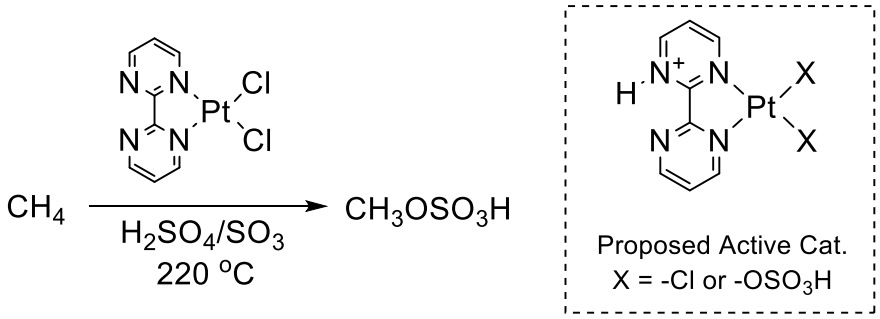

Scheme 1.6. The Catalytica System for the direct functionalization of methane[9a]

The bpym ligand was thought as a platform for stabilizing the Pt^{II} center under harsh reaction conditions and also enabling an electronic tuning of the metal center itself. The bpym ligand becomes protonated during the reaction, and in turn, increases the electrophilicity of the Pt^{II} center. The protonation of a chloride ligand converts it to a better leaving group and allows to facilitate its displacement with hydrogen sulfate ligand which is then displaced with methane, the step being turnover-limiting. The subsequent C-H activation of methane yields the critical Pt^{II}-CH_3 intermediate. Similar to the Shilov system, the Pt^{II}-CH_3 intermediate is then oxidized, this time, by SO_3, and eventually leads to the production of $MeOSO_3H$ and the regeneration of the (bpym)$Pt^{II}X_n$ complex. Numerous other transition metals have been used in the Catalytica system, including, Pd, Rh, Ir, Au, Co, V, Fe, Cu, Hg and even Eu, and even still Pt was consistently higher performing in terms of TOF and TON.[24] Dramatically, the importance of the bpym ligand in the Periana's system and the validity of proposed reaction mechanism was questioned after a groundbreaking discovery of a very high catalytic activity of K_2PtCl_4 in oleum at converting methane to $MeSO_4H$ that would not require the presence of bpym ligand.

Interestingly, the work by Schüth *et. al.* demonstrates that simple K_2PtCl_4 were capable of catalytically functionalizing methane[9b] in the absence of Periana's bpym ligand. In fact, they concluded that through the addition of bpym, there was a significant decrease in the catalyst turnover frequency (TOF), catalyst turnover number (TON), and the initial rate of the reaction. [9b] Thereby demonstrating how even well-accepted and established catalytic systems can be misunderstood about the important role the ligand environment has on catalysis.

Other research groups have also explored the use of ligands for both the enhancing of reactivity and for the stabilization of Pt^{II}. Notably, Tilset and co-workers developed a bidentate diimine ligand for probing the mechanism of protonation of a (diimine)$Pt^{II}Me_2$ species, which is a microscopic reverse of methane activation by (diimine)$Pt^{II}Me^+$. This work demonstrated the kinetic preference of protonation of the Pt center as opposed to direct protonation of a methyl ligand to form methane. Protonation of the (diimine)$Pt^{II}Me_2$ occurred to yield $[(diimine)Pt^{IV}Me_2H]^+$ first, followed by the reductive elimination of methane to yield the $[(diimine)Pt^{II}Me(CH_4)]^+$ sigma complex of methane. These two species can exist in equilibrium as they represent each half of the microscopic-reversibility of the activation of methane C-H bonds. Finally, methane can then be displaced by acetonitrile to yield $[(diimine)Pt^{II}Me(MeCN)]^+$, thereby driving the reaction forward (Scheme 1.7).

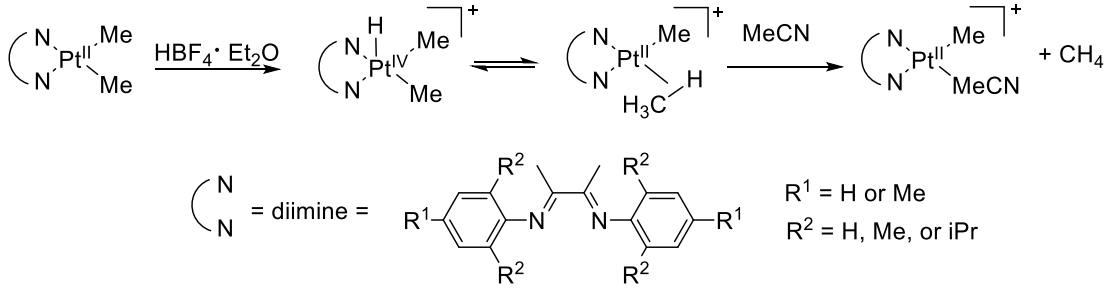

Scheme 1.7 Mechanistic study of the C-H activation reverse reaction enabled by diimine ligands

The steric protection offered by the bulky diimine ligand (when R^2 = iPr) effectively blocks the direct protonation of the methyl ligand and thereby suggests Pt as the protonation site. This work was of great mechanistic importance and was among the first examples to provide definitive evidence of an OA pathway versus a CAM for C-H activation by Pt^{II}.[25-26] The implications of this mechanistic insight enabled by this unique ligand scaffold was further expanded upon by Chen in 2004, where it was applied for the catalytic deuteration of arenes.[27] Chen and co-workers discovered that H/D exchange of benzene occurred in the presence of some (diimine)$Pt^{II}Me_2$ and acidic deuterium sources such as AcOD at 85 ºC. This system was long-lived, and robust enough to deliver TONs up to ~1500, with the maximum deuterium incorporation of about 2.6±0.3 D atoms / benzene molecule, which represented a staggering improvement of catalytic activity over the historical system developed by Garnett and Hodges.[27-28] No subsequent studies by Chen were performed to explore possible application of his catalytic system for catalytic deuteration of organic substrates. Chen's chemistry was later re-investigated and expanded by Sanford to include a structure/activity relationship of a series of (diimine)$PtCl_2$ complexes and the effects the modifications in the diimine ligands had on H/D exchange catalysis with benzene used to probe the catalysts' activity.[55, 56]

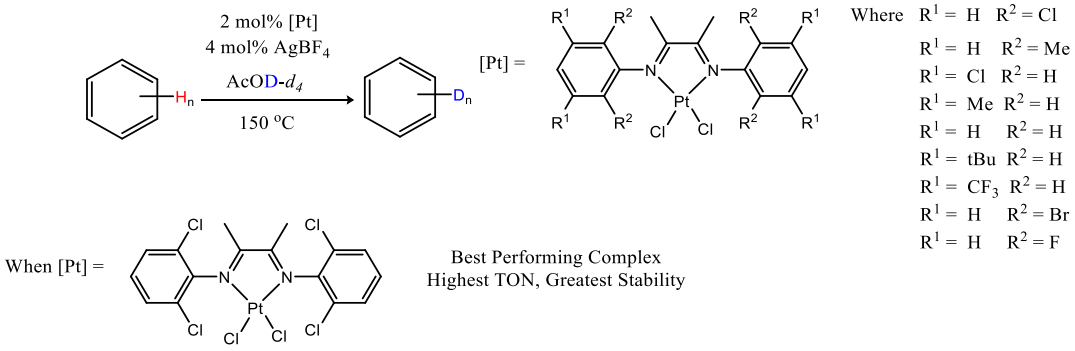

Figure 1.4. Sanford's structure activity relationship for Pt^{II} and substituted diimine complexes for H/D exchange and oxidation of arenes.[55]

Sandford *et. al.* discovered that steric crowding of the *ortho* positions on the aryl substituents in the diimine ligands with large halogens (such as Cl or Br) lead to greater catalyst lifetimes and higher TON when compared to any of the other derivatives screened. This variation in ligand design allows for a steric crowding of the TM center alongside an electron withdrawing effect due to the polarity of the C-Cl bond. Similar steric crowding was attempted with R^2 = Me, however the overall performance of the catalyst was not dramatically improved. The most active catalyst had R^1 = H and R^2 = Cl (Fig. 1.4) and the catalyst TON was 180 after 24 hours, whereas for R^1 = H and R^2 = Me the TON was only 50. Thereby suggesting that the presence of a halogen in the R^2 position provides a unique advantage, either through increasing the electrophilicity of the TM center, or by providing a potential lone pair donor to the metal center after Cl abstraction by $AgBF_4$ to yield a $14e^-$ intermediate. Steric, electronic, and halogen-specific effects have all been proposed as possible explanation for this enhanced catalyst performance. Regardless of the explanation, it is made clear by Sandford *et. al.* that even subtle variations in the ligand scaffold can lead to a profound impact on catalyst performance.[55,56]

Since Periana's works, numerous groups have aimed to incorporate ligands into their systems to enhance catalyst stability and reactivity. Multidentate ligands were designed to facilitate the change in oxidation state of the Pt center throughout the reaction cycle (Figure 1.3).[29-39] The key design feature of the ligands arises from their multidenticity and allow for multiple different binding modes from various donor atoms throughout the course of the reaction. The presence of labile or semi-labile donor atoms enables conformational changes to the complex throughout the course of the reaction. When considering a $2e^-$ oxidation pathway for Pt^{II} to Pt^{IV}, the product is stabilized by additional donor atoms. Therefore, the presence of an additional donor already covalently attached to the ligand scaffold provides a readily accessible ligand primed for association to the oxidized metal center. Typically, these reactions were performed starting from LPt^{II}-R type complexes, in order to emulate the reactive Pt^{II}-R intermediate that would typically be generated in the Shilov system. This strategy was chosen in attempt to enable the facile oxidation of the LPt^{II}-R to LPt^{IV}-R type complexes by O_2, which would then be primed for subsequent Shilov-type functionalization with O_2 as an inexpensive and environmentally benign oxidant. [29-39]

Interestingly, this concept is not unique only to oxidation by O_2 and relates back to C-H activation and H/D exchange through the same concept realized through the OA of R-H bonds by Pt^{II}. Considering that these ligand scaffolds can reduce the energy required to access the Pt^{IV}-R intermediate needed for functionalization chemistry, then the same rationalization can be applied to facilitating the OA of C-H bonds from Pt^{II}-L species to generate the transient intermediate Pt^{IV} OA complex (Scheme 1.3).

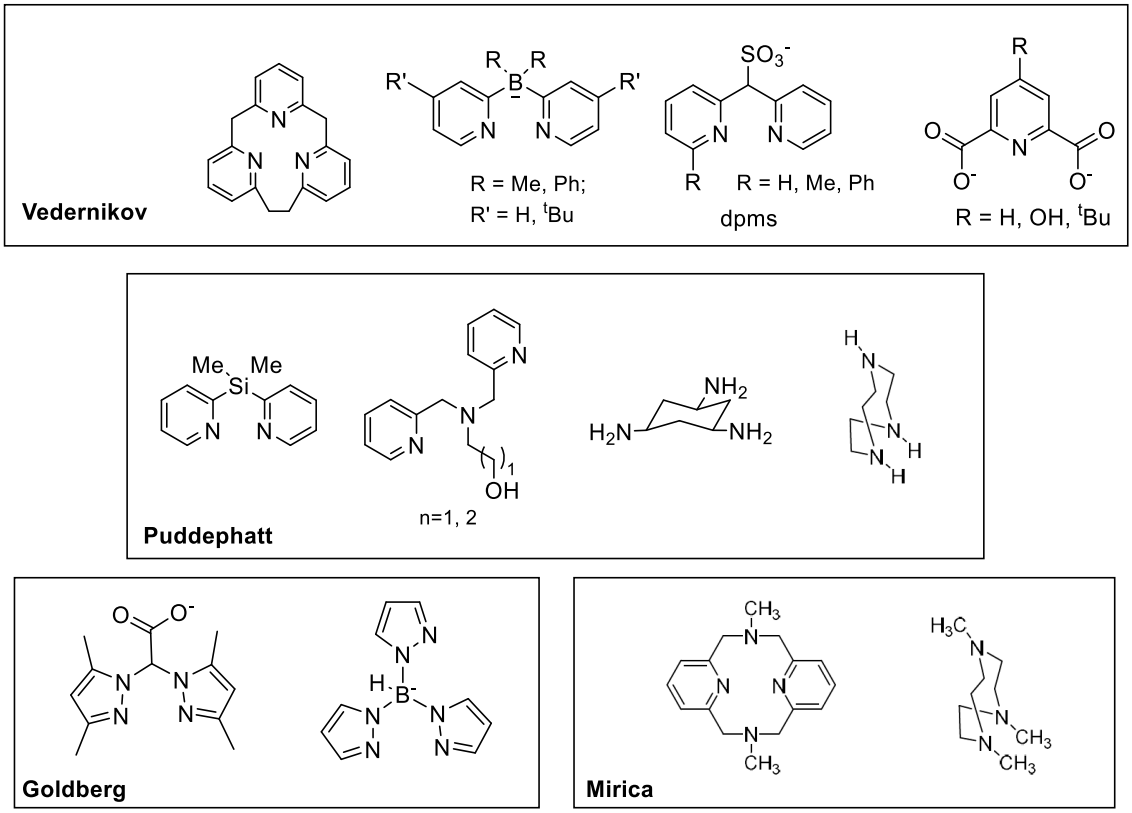

Figure 1.3 Multidentate ligand scaffolds developed by Vedernikov[29-35], Puddephatt[37-39], Goldberg[31] and Mirica[32,36] for the for the 2e$^-$ oxidation of Pt^{II} or Pd^{II}

1.4. Background and Past Work

The work presented in this thesis builds upon the prior work utilizing di-(2-pyridyl) methanesulfonate (dpms) ligand and its derivatives (Figure 1.3). Some of the first results utilizing this ligand backbone began in the early 2000's where monohydrocarbyl (dpms)Pt^{II} complexes were able to undergo aerobic oxidation, thereby eliminating the need for expensive stoichiometric $H_2Pt^{IV}Cl_6$ as an oxidant. This completed a critical step in the overall Shilov cycle (Scheme 1.5 (b)) where the Pt^{IV}-R type species is generated from the preformed Pt^{II} hydrocarbyl complex (Scheme 1.8). The Pt^{IV}-R generated can then undergo reductive elimination in acidified water to yield MeOH and Me_2O. This reductive elimination is facilitated by the presence of the labile sulfonate group which allows for

access to 5-coordinate intermediates and facile isomerization. When the R group is placed *trans* to the sulfonate (when R = Alkyl), reductive elimination of C-O or even C-N coupled products were observed. [30] The corresponding Pt^{II} dinuclear complex **1.1**, is poorly soluble in aqueous or alcohol solvents and is chemically inert towards C-H activation on methane or benzene under these reaction conditions.

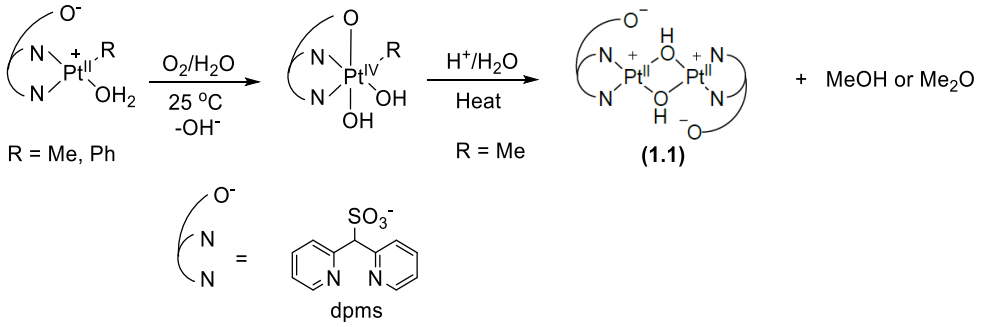

Scheme 1.8. Example of oxidation of (dpms)Pt^{II} monohydrocarbyl complex being oxidized by O_2 and the subsequent reactivity of the generated (dpms)Pt^{IV} complex

The dpms (when R = H or Me Figure 1.3) scaffold did little to enable the initial C-H activation required to catalytically generate the Pt^{II} hydrocarbyl complex that is required for functionalization. When the (dpms)Pt^{II}(OH)(OH_2) complex was heated in the presence of hydrocarbons, no reaction occurred, instead, formation of **1.1** was observed. Both the oxidation of the Pt^{II} hydrocarbyl complex to yield the reactive Pt^{IV}-R species and the subsequent functionalization of the hydrocarbyl fragment were successfully achieved utilizing (dpms)Pt^{II}-R type systems. Despite this success, the catalytic generation of the Pt^{II}-R fragment under these conditions remained elusive. Therefore, to make this process fully catalytic the Pt^{II} complex that is generated after functionalization must be primed for further reactivity towards the activation of C-H bonds.

Based on some literature precedent,[47] NN ligated Pt^{II} complexes containing at least one labile solvento ligand should be capable of carrying out C-H bond activation. It was speculated that the reason that complex **1.1** was inert towards C-H activation was due to the high energy barrier of dissociation of the dimer into monomeric aqua ligand containing species. Furthermore, it was expected that even if a small amount of the aqua complex could form in equilibrium with **1.1,** then the stabilizing effect of hydrogen bonding to the aqua ligand could still stabilize the complex and disfavor the ligand substitution and hydrocarbon coordination required for C-H activation. This was confirmed by parallel experiments where complexes **1.2** and **1.3** were compared in their abilities to activate R-H bonds (Scheme 1.9).

When C-H activation was attempted in protic solvents with complex **1.2,** no C-H activation was observed for benzene, or methane. Instead, the stabilization granted by the hydrogen bonding to the aqua ligand disfavors the ligand substitution and the complex remains inert towards this difficult to react C-H bonds (Scheme 1.9a). This hydrogen bonding hypothesis was then further supported when complex **1.3** was utilized under anhydrous aprotic reaction conditions (Scheme 1.9b). Complex **1.3** served as a Pt^{IV} precursor species, where with the loss of CH_4 a coordinatively unsaturated Pt^{II} complex is generated. In the presence of $HSiEt_3$, the Si-H bond was cleaved to yield the oxidative addition complex **1.4** (where R = $SiEt_3$). This chemistry was also suitable for the activation of even more inert C-H bonds and has been reported to work for both benzene and methane.

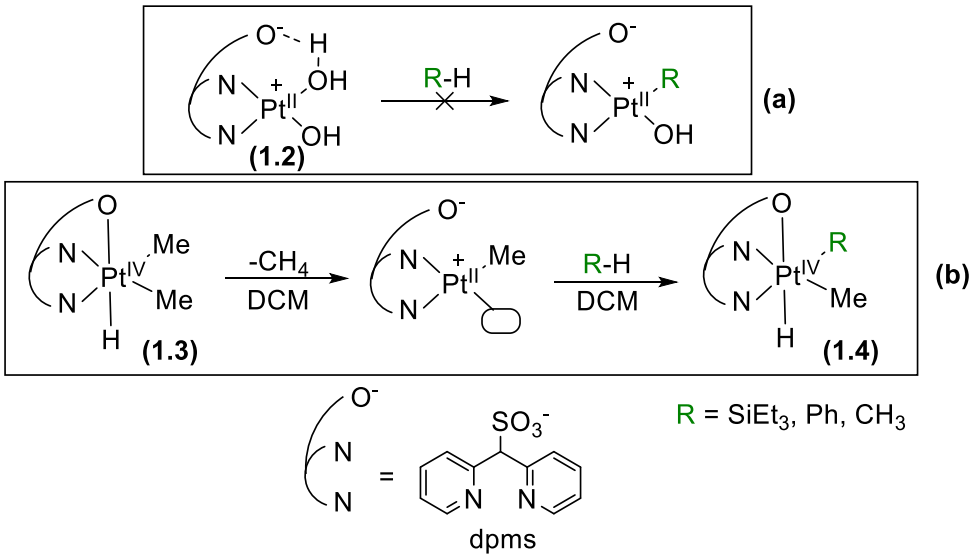

Scheme 1.9. **a)** Complex **1.2** hydrogen bonding stabilization by the pendant sulfonate group and its inability to carry out C-H activation. **b)** Proof of concept that the N,N ligated Pt^{II} center is capable of C-H activation from a coordinatively unsaturated species.

By enhancing the ability of the labile ligand group to efficiently dissociate, the reactivity of the complex was enhanced to effectively activate C-H bonds. This result was among the first indications that the full aerobic Shilov-type cycle may be achievable utilizing (dpms)Pt^{II} type catalysts. Unfortunately, the previously mentioned aerobic oxidation of the dpms bound Pt^{II} complex required the use of protic solvents to facilitate the PCET required for O_2 activation. Therefore, to catalytically activate (and potentially functionalize) C-H bonds under protic conditions, the dissociation of the aqua ligand must become more facile. In other words, the intramolecular hydrogen bonding caused by the pendent sulfonate group must be reduced or eliminated to properly exploit this systems' potential for catalytic C-H activation.

This goal was achieved via the introduction of a phenyl ring to the 6th position of one of the pyridyl fragments on the dpms scaffold, thereby resulting in a new generation of CNN pincer ligand, C_6H_4-dpms. The rationalization behind its design arises from the ligand

binding to the Pt^{II} center in a κ^3-CNN binding mode as opposed to the κ^2-NN observed for dpms. This additional binding group will force more rigidity into the ligand backbone and force the complex to shift towards a square planar arrangement (Scheme 1.10). This shifted geometry of complex **1.5** pushes the sulfonate tail further away from the water molecule bound to Pt and consequently reduces the stabilization caused by the sulfonate ligand. There is an additional consequence of the sulfonate ligand now being positioned further away from the Pt center itself although, not enough to prevent its coordination to stabilize the formation of Pt^{IV} intermediate species.

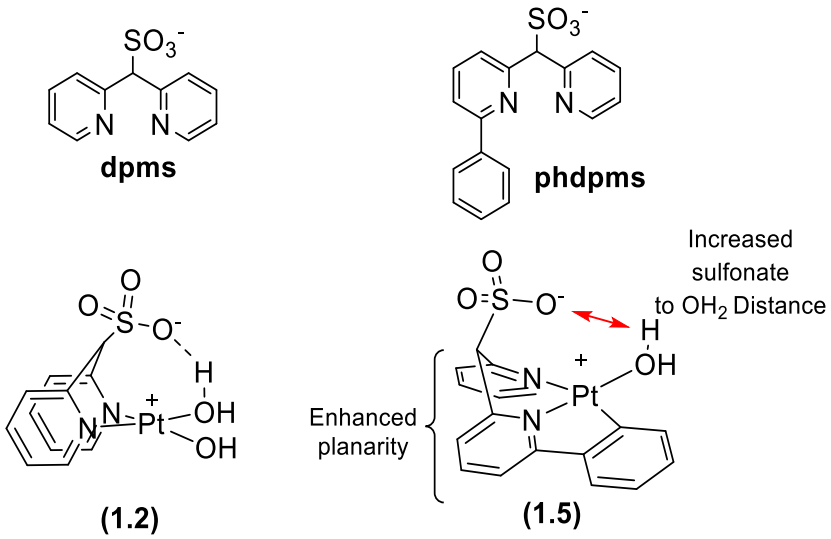

Scheme 1.10. dpms and C_6H_4-dpms structural comparison and a side-on perspective of their corresponding Pt^{II}-OH_2 complexes

This intelligent approach to ligand design was proven to be quite successful. In fact, complex **1.5** proved to be an effective for both C-H and O_2 activation under protic conditions. The derived (C_6H_4-dpms)$Pt^{II}OH_2$ complex was shown both experimentally and computationally to be a kinetically competent catalyst for the H/D exchange of benzene or methylbenzenes in TFE-d_1 or TFE solutions. The reaction turnover numbers exceeded 250 for the H/D exchange of TFE and C_6D_6 with catalyst TOF as high as 0.01 s^{-1} at 80 ^oC. In

solutions of 1:2 Arene:TFE in the presence of 1 atm O_2 complex **1.5** was capable of promoting the consecutive C-H bond of arenes and O_2 activation to yield (C_6H_4-dpms)Pt^{IV}(OH)(Aryl) complexes. This step is ultimately where the reaction ends, since no reductive elimination to yield C-O bonds nor the C-H activation of alkanes were observed with this system.

Further attempts to synthesize more reactive CNN ligated Pt^{II} complexes were made to further expand the scope of hydrocarbon substrates that could be engaged in C-H activation. Specifically, if the C-H activation of alkanes could be promoted by these CNN ligated catalysts, then each independent component of the Shilov cycle would be satisfied with this system. Therefore, other complexes were synthesized with the goal of generating more reactive species towards the activation of C-H bonds. The ligand backbone of the complex was altered to induce a greater planarizing effect and even further reducing the energy barrier for ligand exchange (**Chart 1.1**).

Chart 1.1. Pt^{II}-OH_2 Complexes **1.5**, **1.6**, **1.7** supported by sulfonated CNN-pincer ligands

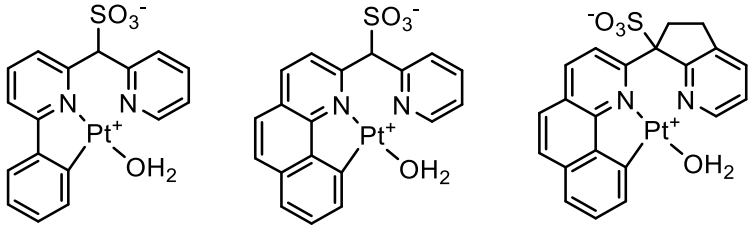

(1.5) **(1.6)** **(1.7)**

If the RDS for the formation of the LPt^{II}-R relies on the ability for the aqua ligand to leave the Pt coordination sphere, then increased planarity will continue to pull the

sulfonate ligand further from the aqua ligand and continue to reduce the stabilizing hydrogen bonding effects. Complex **1.6** differs from **1.5** by the presence of a fused benzoquinolyl fragment. This fused ring system eliminates the free rotation allowed by the phenyl ring and imparts an increased planarity to the complex. The cyclopenteno ring introduced by complex **1.7** tethers the tetrahedral bridging carbon bearing the sulfonate group to the pyridine ring, thus reducing the tetrahedral nature of the sp^3 hybridized carbon and pulling it even further from the aqua ligand. In order to assess how these structural effects influence reactivity, the rate of H/D exchange between benzene and TFE-OD was observed utilizing **1.5-1.7** as catalysts.

Indeed, the increased steric rigidity did play a significant role in the rate of H/D exchange catalysis on benzene, with the rates following the order of **1.5<1.6<<1.7** with the dimerization of **1.7** being observed even in room temperature solutions. The presence of the fused cyclopenteno fragment imparted the greatest effect on the observed rate of H/D exchange for these systems. An unfortunate consequence of this increased reactivity, however, was that the rate of catalyst di(poly)merization also increased with the increasing rigidity of the ligand scaffold, thereby rendering the practical implications of this finding difficult to exploit.

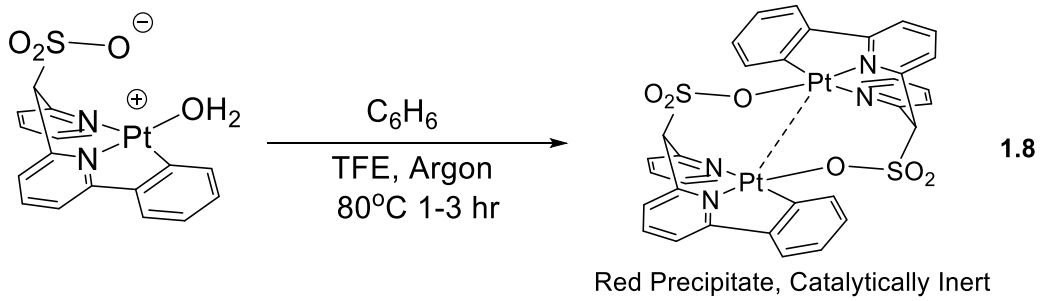

1.8

Scheme 1.11 CNN Ligated Pt^{II} bimolecular deactivation pathway

1.5. Research Goals and Strategy

The aforementioned work utilizing dpms and C_6H_4-dpms ligated Pt^{II} complexes laid the foundation for the specific work described here in this thesis. Despite the success of the complex **1.5** for the consecutive C-H and O_2 activation, there remains a few key challenges for this chemistry to fully satisfy the requirements of the aerobic Shilov inspired cycle. Presently, the C_6H_4-dpms system has superior potential over the dpms ligated complexes for satisfying the requirements of the Shilov cycle utilizing O_2 as an oxidant. This system's limitation is with its low reactivity towards the strong C-H bonds present in some troublesome hydrocarbon substrates such as alkanes and electron poor arenes. Additionally, the prevalence of bimolecular deactivation pathway (Scheme 1.11) has proven to have deleterious effects on catalyst longevity. However, based on results of our DFT calculations, we expect that complexes **1.5-1.7** can activate C-H bonds of arenes and alkanes at low to moderate temperatures. Therefore, in order to access this Pt center's anticipated reactivity, we must overcome the practical limitations through understanding the mechanistic and substrate-dependent behavior of this class of catalysts, as well as exploring the catalysts structure-reactivity relationship.

Accordingly, the goals of this work are to develop more reactive Pt^{II} catalysts for C-H activation chemistry while using catalytic H/D exchange as a probe for catalyst reactivity and achieve a better understanding of underlying structure-reactivity relationship. While doing so, we aim to expand the substrate scope of this class of Pt catalyst to include complex and/or poorly reactive substrates, including some pharmaceutical compounds incorporating multiple reactive sites and functional groups.

In this thesis, we overcome the limitations of C(sp^2)-H bond activation by previously discovered catalytic system **1.5** / TFE-d_1 at 80 ^oC in a multifaceted approach. In Chapter 2, we investigate in detail the substrate scope and current limitations of **1.5** / TFE-d_1 system in catalytic H/D exchange reaction. This allows for a substrate reactivity, selectivity, and heteroatom compatibility profile for this system to be developed. In Chapter 3, we explore covalent immobilization of a CNN-ligated Pt^{II} complex for H/D exchange reaction to eliminate the kinetically competitive catalyst bimolecular deactivation pathway. Finally, in Chapter 4, we explore a series of 4-subsituted C_6H_4-dpms Pt-OH_2 derivatives to assess the substituents' effects on catalysts reactivity and then use the accumulated knowledge of this chemistry to prepare more reactive Pt^{II} complexes that can serve as practically useful catalysts for the H/D exchange of some of the most complex aromatic substrates. Chapter 5 summarizes major results of this work and marks some important benchmark comparisons of our developed systems to the other similar catalysts H/D exchange systems described in the literature, alongside some future directions for this avenue of research.

Chapter 2: **Catalytic Deuteration of C(sp^2)-H Bonds of Substituted (Hetero)Arenes by a Pt^{II} CNN-Pincer Complex in a D_2O - 2,2,2-Trifluoroethanol-d_1 System: the Effect of Substituents on the Reaction Rate and Selectivity**

Reproduced in part from the published article[49] with all experimental work except DFT, MO calculations performed by Morgan Kramer.

2.1. Introduction

Since the discovery of the first homogeneous Pt^{II} complexes capable of hydrocarbon C-H bond activation observed initially as an H/D exchange between hydrocarbon substrates and DCl, AcOD, and D_2O,[10] catalytic H/D exchange experiments have become a prime and simple tool to probe the reactivity of various transition metal species toward C-H bonds. On the practical side, various homogeneous transition metal complexes are now used as catalysts in H/D exchange reactions.[7-8] Our group has previously reported the preparation of Pt^{II} complexes **1.5-1.7** supported by CNN-pincer ligands (Chart 1.1) that appeared to be some of the most active platinum-based homogeneous catalysts for H/D exchange between C(sp^2)-H bonds of arenes (H_nSub) and TFE-d_1 (eq 1),[33] when compared to other reported Pt-based systems:[52-56]

$$H_nSub + nCF_3CH_2OD \rightarrow D_nSub + nCF_3CH_2OH \qquad \textbf{(eq. 2.1)}$$

The above reaction (eq. 2.1) with 10 % vol. benzene as a substrate and complex **1.5** as a catalyst can be observed at 20 ^oC, and the catalysts turnover frequency reaches 46 h^{-1} at 80 ^oC.[33] Our subsequent study of reactivity of complex **1.5** led us to the discovery of Pt-mediated stoichiometric C-H oxidation with O_2 of various arenes ArH and complex **1.5** (eq 2.2).[57] The reaction produces arene-derived Pt^{IV} aryl hydroxo complexes $LPt^{IV}Ar(OH)$ and can involve both electron-rich *ortho*- and *meta*- dialkylbenzenes ArH (alkyl = Me, t-Bu), as well as electron poor *ortho*- dichloro- and difluorobenzenes. Interestingly, except *o*-$F_2C_6H_4$, these oxidation reactions result in >90% selective formation of a single isomer of the derived $LPt^{IV}Ar(OH)$ compounds.[57]

$$2LPt^{II}(H_2O) + ArH + O_2 + CF_3CH_2OH \rightarrow LPt^{IV}Ar(OH) + LPt^{IV}(OCH_2CF_3)(OH) + 2H_2O$$

(eq. 2.2)

Chart 2.1. Pt^{II} aqua complexes **1.5, 1.6** and **1.7** supported by sulfonated CNN-pincer ligands.

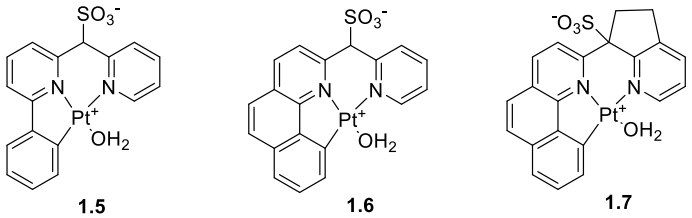

According to a previous kinetics study of reaction (eq 2.2), the arene C-H activation at a Pt^{II} center may be responsible for the selectivity of oxidation of the benzene derivatives above. Hence, a better understanding of the reactivity of complex **1.5** in reaction (**eq 2.1**) with respect to various arene C(sp^2)-H bonds, as well as the effect of arene substitution on such reactivity, may be important for future development of Pt-mediated C-H functionalization chemistry. In this work we focus on the H/D exchange reaction (**2.1**) catalyzed by complex **1.5**. We use a wide range of arenes bearing various electron-donating and electron-withdrawing functional groups, as well as a few heteroarenes, **2.1-2.29** (Charts 2.2-2.3). By using ^{1}H NMR spectroscopy and measuring the initial reaction rate, we were able to determine the reaction kinetic selectivity involving specific types of C(sp^2)-H bonds producing well-resolved ^{1}H NMR signals. The knowledge of the kinetic selectivity of transition metal complexes with respect to various arene C(sp^2)-H bonds is limited,[56-58] which is especially true for Pt-based systems.[12-13, 52-57] Using the rates of H/D exchange at the *meta*- and *para*- positions of monosubstituted benzene derivatives in Chart 2.2 we introduce a new scale of Hammett constants, σ_X^M, for metal-assisted C-H bond activation reactions. An additional result of this study of reactivity of a wide range of substrates shown in Charts 2.2-2.4 is the information about the functional group tolerance of complex **1.5**. Notably, we also tested the performance of catalyst **2.1** in deuteration of a

few pharmaceuticals, Ibuprofen, **2.33**, and Naproxen, **2.34** (Chart 2.4), probing possible application of Pt-catalyzed H/D exchange for deuterium labeling of medicinal compounds.

2.2 Results and Discussion

2.2.1 Experimental setup and expected degree of substrates' deuteration

The catalytic H/D exchange between aromatic substrates H_nSub and wet TFE-d_1 (eq. 2.1) used as a deuterium source was carried out at 80 ^oC using, typically, 0.1-0.5 mol. % of complex **1.5** as a catalyst.[33, 51] In a typical experiment 0.050 mL of H_nSub (or ~50 mg for solids) was dissolved in 0.450 mL of wet TFE-d_1 containing 0.150 M D_2O and 6-12 μmol of catalyst **1.5.** The water additive was shown earlier to slow down the catalyst deactivation caused by the formation of poorly soluble polynuclear species.[4] The reactions were monitored by ^1H NMR spectroscopy using the TFE-d_1 CH_2 group signal as an internal reference. To estimate the initial reaction rate, the conversion of substrates was checked more often in the period of time corresponding to no more than ~10% substrate conversion and minimal catalyst deactivation.[33] Most of the substrates were used in concentration of ~1M which corresponds to 1-6 M concentration of the arene C(sp^2)-H bonds of a specific type. In none of our experiments we were able to observe H/D exchange involving C(sp^3)-H bonds of alkyl groups. The total concentration of exchangeable deuterium from TFE-d_1 was ~12.5M which translates to the expected extent of the substrate's deuteration of ~68-81% upon reaching a hypothetical statistical distribution of deuterium between solvent and all reactive C-H bonds of the substrate. In fact, a ≥67% deuteration was observed for the three most reactive compounds, phenol, **2.9**, N,N-dimethylaniline, **2.10**, and β-CH bonds of indole, **2.17**, by the end of their respective reaction periods (Chart 2.2). Not all of the

compounds **2.5**-**2.34** tested in this work were deuterated under these conditions. The substrates active in the H/D exchange are included in Chart 2.2 and, in part, Chart 2.4 (Naproxen, **2.34**). On the other end of the reactivity series are the substrates shown in Chart 2.3, as well as Ibuprofen **2.33** (Chart 2.4). These compounds either engage in more or less rapid side reactions or decompose in the presence of **2.1** (pyrrole, furan, iodobenzene, styrene and phenylacetylene, **2.18**-**2.22**), or do not change in the presence of **1.5** (trifluoromethylbenzene, benzenesulfonamide, *o*-dichlorobenzene, **2.23**-**2.25**, and Ibuprofen, **2.33**), or are able to strongly coordinate to a Pt^{II} center in complex 1.5 so effectively inhibiting the H/D exchange (e.g., benzonitrile, pyridine, pyrimidine and pyrazole, **2.26**-**2.32**). In practical terms, for substrates **2.23**-**2.33** the extent of deuteration did not exceed ~2%.

Chart 2.2. Aromatic substrates H_nSub studied in this work and the extent of their deuterium incorporation, *x*, observed after the time indicated using ~1M solutions of the substrates in wet TFE-d_1 with complex **1.5** as a catalyst at 80 °C. The values in parentheses show the extent of deuteration *x* observed in the absence of catalyst **1.5** after otherwise identical conditions.

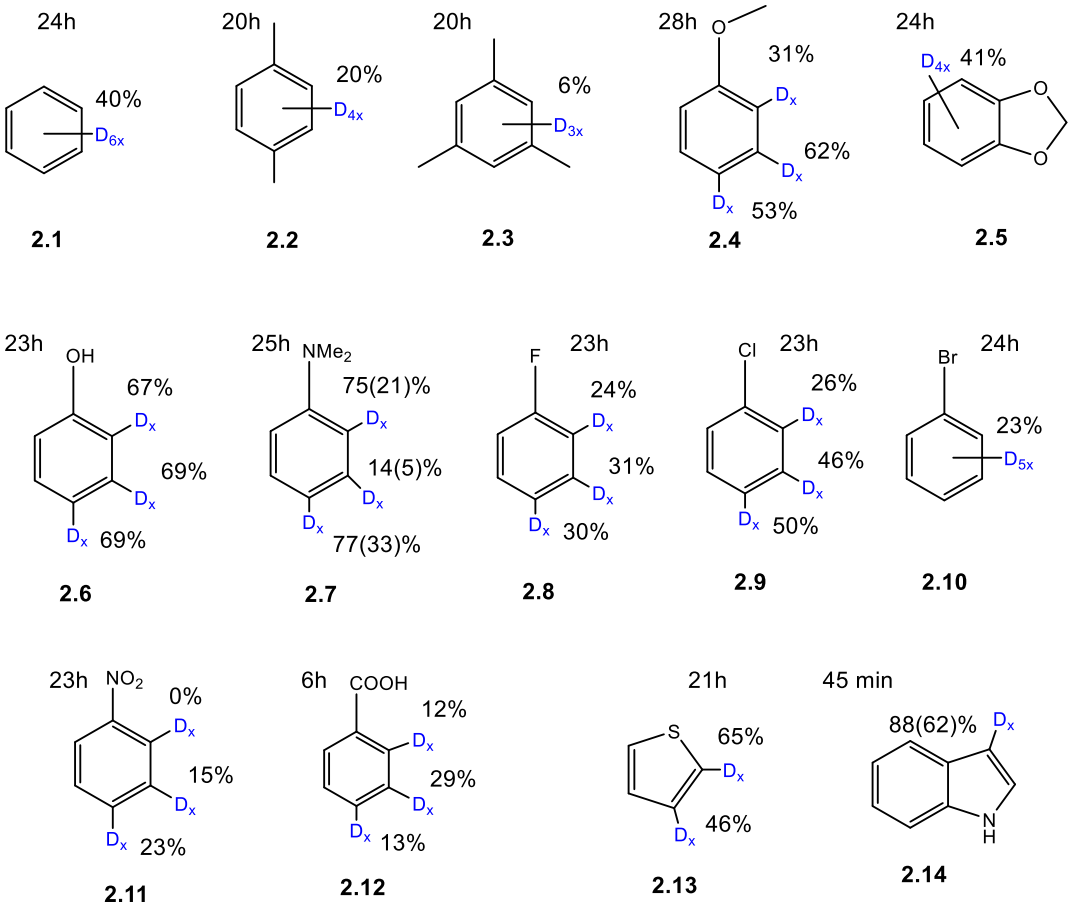

Chart 2.3. Aromatic substrates H_nSub that either engage in side reactions under the conditions indicated in Chart 2.2, or are inactive in the H/D exchange.

Substrates that engage in side reactions

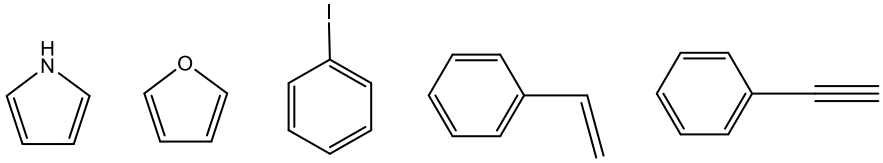

2.15 **2.16** **2.17** **2.18** **2.19**

Inert substrates

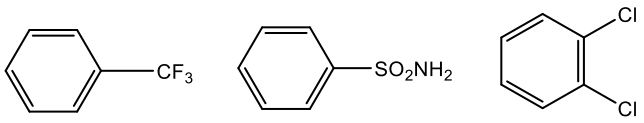

2.20 **2.21** **2.22**

Substrates demonstrating strong coordination to 1.5

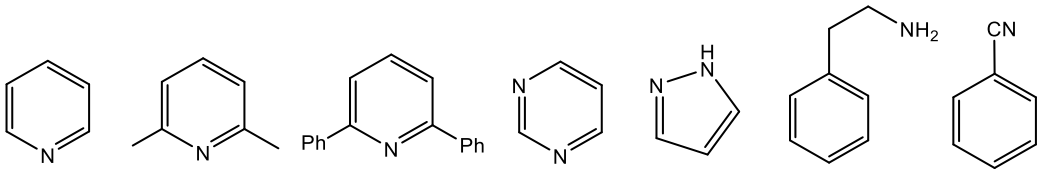

2.23 **2.24** **2.25** **2.26** **2.27** **2.28** **2.29**

Chart 2.4. Pharmaceuticals **2.30** and **2.31** probed in H/D exchange experiments.

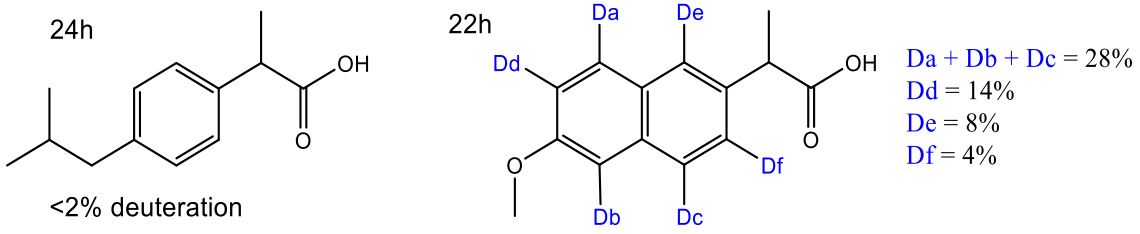

2.30 **2.31**

2.2.2 Stability of catalyst 1.5. Background H/D exchange reactivity with TFE-d_1

The potential issues that may affect our ability to estimates reactivity of **1.5** in reaction (2.1) with respect to specific substrate's C-H bonds may be a strong coordination of a substrate to **1.5**, the catalyst decomposition under our reaction conditions or a background H/D exchange.

Not all Pt^{II}-coordinating substrates may be unreactive in H/D exchange. In particular, N,N-dimethylaniline and thiophene may be expected to form adducts with complex **1.5**. In fact, according to our observations (Chart 2.2), these substrates are very active in this reaction, so suggesting that any secondary adducts with **1.5** are weak. In particular, a dark purple platinum complex **2.32** could be isolated from a solution of **1.5** in 1:1 (vol.) mixture of N,N dimethylaniline and TFE upon precipitation with diethyl ether. The resulting solid is stable under argon atmosphere and in methanol-d_4 solution for at least 72 hours, according to ^{1}H NMR spectroscopy. In the ^{1}H NMR spectrum of the solution two N-CH_3 group signals of equal intensity are observed, along with signals of a Pt-coordinated CNN-pincer ligand of matching intensity, thus suggesting the formation of an adduct LPt($PhNMe_2$), **2.32**. The adduct coexists in an apparent equilibrium with an about equal molar amount of free $PhNMe_2$ and, presumably, a methanol analog of **1.5**, LPt(MeOH), so suggesting that stability of the adduct **2.32** is low. Similar attempts to isolate an adduct of complex **1.5** with thiophene were not successful because of its even lower stability.

A catalyst deactivation due to the formation of a light-yellow precipitate which was not identified was observed for benzoic acid after about 6 h of reaction. Accordingly, the H/D exchange reactivity of this substrate was only analyzed for the first 6 h. For a few other substrates such as chloro- and bromobenzene formation of a red precipitate,

presumably, the dinuclear product of the catalysts **1.5** decomposition,[33, 51] was observed, but only by the end of the monitored reaction (1) period (~24h).

To get a better estimate of the catalyst's **1.5** reactivity, besides considering the catalyst deactivation, the H/D exchange reactions of all studied substrates were analyzed in the absence of **1.5** (Scheme 2.1, a), as well as in the presence of **1.5** (Scheme 1, b). The contribution of the background reaction to the deuteration of substrates' C-H bonds was considered for the initial reaction period (<10% deuteration) and by the end of our experiments (typically, ~24 h); the latter contribution is indicated in parentheses in Chart 2.2.

In fact, the background reaction contribution to the initial rate of reaction (1) was not detected for any of the substrates in Chart 2.2. The background reaction for N,N-dimethylaniline was only noticeable after 24h (Chart 2.2, in parentheses). For indole the background reaction was not noticeable until after ~90 min 'induction period' which is associated, most likely, with the formation of some Pt black that was observed after this time. In turn, the reaction (1) of indole catalyzed by **1.5** is very fast with 3.6% catalyst loading and a close-to-statistical 88% extent of deuteration of indole β-CH bonds is reached after 45 min of reaction, well before the catalyst decomposition and the background reaction become detectable.

Scheme 2.1. Background and Pt-catalyzed H/D exchange between a substrate H_nSub and TFE-d_1.

$$H_nSub + nCF_3CH_2OD \underset{k_{-b}}{\overset{k_b}{\rightleftharpoons}} D_nSub + nCF_3CH_2OH \qquad (a)$$

$$H_nSub + nCF_3CH_2OD \underset{[Pt],\ k_{-c}}{\overset{[Pt],\ k_c}{\rightleftharpoons}} D_nSub + nCF_3CH_2OH \qquad (b)$$

For the rest of the substrates in Chart 2.2 no noticeable H/D exchange was observed in the absence of the catalyst **1.5** and no visible sign of the catalyst decomposition was detected.

2.2.3 Reaction (2.1) kinetics model and initial rates of C-H activation

The reaction (2.1) mechanism with **1.5** as a catalyst and benzene as a substrate was studied earlier by means of kinetics, some mechanistic tests and DFT calculations.[33, 51] It was found that the initial rate of the reaction (b) in Scheme 2.1 is first order in both the substrate C-H bonds concentration, [C-H], and the catalyst **1.5** concentration, [**1.5**], (eq 2.3):

$$\frac{d[C-D]}{dt} = k_c[C-H][\mathbf{1.5}] \qquad \text{(initial rates)} \qquad \text{(eq 2.3)}$$

The proposed reaction sequence responsible for the substrate / TFE-d_1 H/D exchange, slightly modified, as compared to the original publication,[33] is presented in Scheme 2. It involves an arene coordination step *a* to form a σ-arene complex $^{\mathbf{CNN}}\mathbf{1_{ArX}}$ with a CNN-coordinated pincer ligand, an isomerization step *b* to form an isomer $^{\mathbf{CNO}}\mathbf{1_{ArX}}$ with a CNO-coordinated pincer ligand, a rate-limiting C-H bond oxidative addition to a Pt^{II} center at step *c*, via the transition state $\mathbf{TS_{Ar\text{-}X}}$, a redox-isomerization of the resulting Pt^{IV} hydrido complex $\mathbf{1_{(Ar)(X)}}$ at step *d* via a lower-energy transition state $\mathbf{TS_3}$ (Scheme 2) to form a Pt^{II} aryl $\mathbf{1\text{-}X_{Ar}}$ and a facile H/D exchange of the latter with TFE-d_1 or D_2O.

For the purpose of subsequent discussion we assume that the same rate law (2.3) and the same general mechanism are valid for other substrates in Chart 2.2. We will use the effective catalytic rate constants k_c for each specific type of a substrate's C(sp^2)-H bond as a measure of the C-H bond reactivity toward catalyst **1**. The k_c values are calculated using eq 4:

$$k_c = \frac{d[C-D]}{dt}\frac{1}{[C-H]}\frac{1}{[\mathbf{1.5}]} \qquad \text{(initial rates)} \qquad \text{(eq 2.4)}$$

In turn, the initial rate of incorporation of deuterium into a substrate, $\frac{d[C-D]}{dt}$, is determined using the least squares fitting procedure during the reaction period corresponding to the substrate's conversion not exceeding 10% (see Fig. 1 for an example of initial rate calculations for anisole).

Scheme 2.2. A proposed reaction sequence involved in the H/D exchange between arene C(sp^2)-H bonds and TFE-d_1 catalyzed by complex **1.5.** The standard Gibbs energies for individual reaction steps for TFE solutions at 298 K (blue font) are given for benzene, C_6H_6, in kcal/mol. (citation 4)

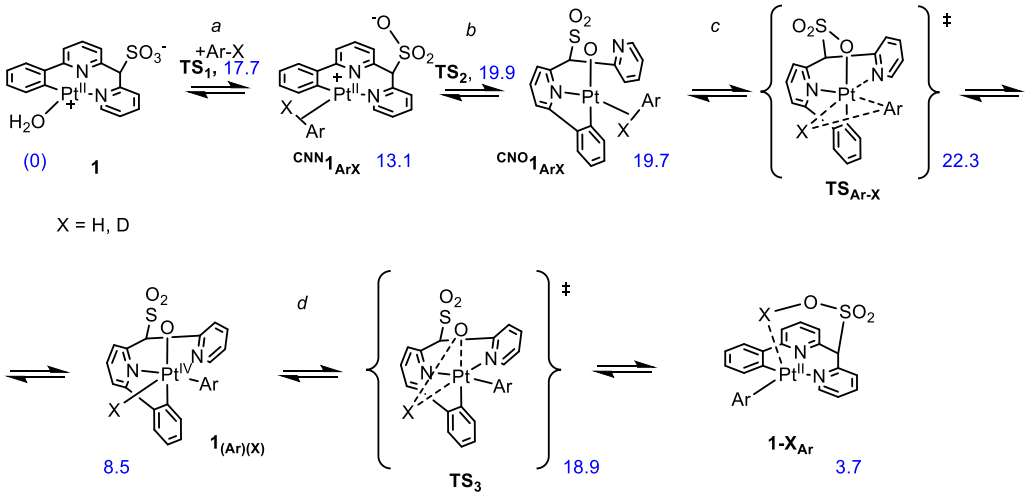

In our experiments involving some monosubstituted benzene derivatives only their *meta*-C(sp^2)-H bonds' ^{1}H NMR signals were resolved well enough to allow for an accurate integration. Accordingly, the corresponding initial rates and rate constants for their *meta*-C(sp^2)-H bonds, $k_{c,m}$, were calculated (Fig. 2.1, right). In turn, the signals produced by *ortho*- and *para*-C-H bonds of these substrates were integrated together, so allowing to calculate the average reaction rates and the average rate constants, $k_{c,o\text{-}p}$, for these C(sp^2)-H bonds (Fig. 2.1, left).

Finally, for substrates containing several types of arene C(sp^2)-H bonds a weighted average value, $k_{c\text{-}all}$, were also calculated. These values can be used for the most general

comparison of substrates' reactivity. The resulting average and individual C-H bonds' k_c values are given in Table 2.1. The k_c value for C_6H_6 will be used as a reference in the following discussion.

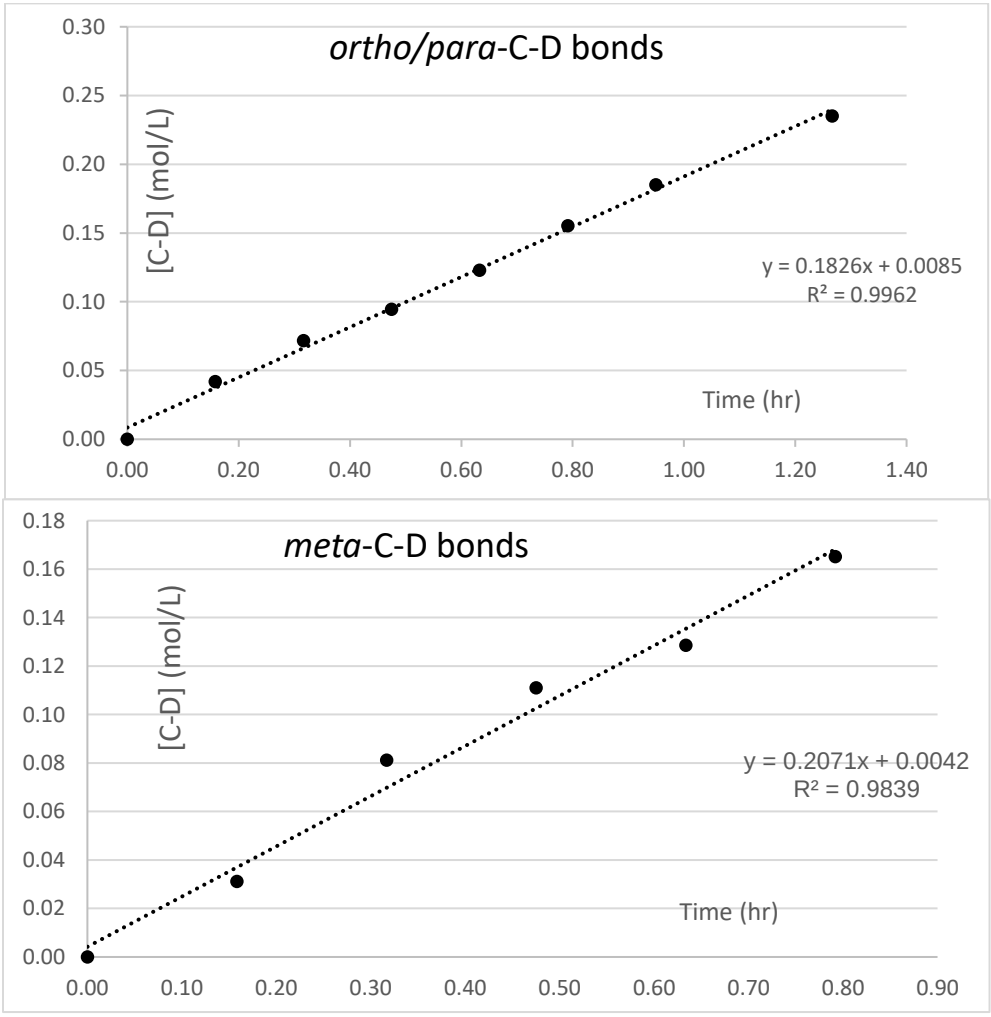

Figure 2.1. Concentration of C(sp^2)-D bonds of anisole-d_x resulting from reaction (2.1) catalyzed by complex **1.5**, as a function of time in the reaction's initial period at 80 °C: a plot for the anisole-d_x *ortho*- and *para*-C-D bonds (left) and a plot for the product's *meta*-C-D bonds (right). The initial concentrations are, $[C_6H_5OCH_3]_0 = 0.87$ M; [**1.5**] = 0.0138M; the resulting rate constants, $k_{c,o\text{-}p}$ =5.1±0.1M^{-1} h^{-1}; $k_{c,m}$ = 8.6±0.5 M^{-1} h^{-1}.

Table 2.1. The H/D exchange rate constants k_c (eq 2.3) and the corresponding Gibbs energies of activation for the H/D exchange between specific C(sp^2)-H bonds of substrates **2.1-2.13** and wet TFE-d_1 catalyzed by **1.5** at 80 °C: $\Delta G_{353}^{\#}$(exp) are the experimental values, $\Delta G_{353}^{\#}$(DFT/gas phase) and $\Delta G_{353}^{\#}$(DFT/TFE) are calculated by DFT for the gas phase and TFE solutions, respectively.

Substrate	C-H bonds	k_c,[a] M^{-1} h^{-1}	Gibbs energy of activation, kcal/mol		
			$\Delta G_{353}^{\#}$(exp), experiment	$\Delta G_{298}^{\#}$(DFT/ gas phase)	$\Delta G_{298}^{\#}$(DFT/ TFE)
Benzene, **2.1**	all	**6.8±0.4**	25.2±0.1	22.5	22.3
p-Xylene**, 2.2**	all C(sp^2)-H	**3.7±0.4**	25.6±0.1	27.5	27.0
Mesitylene, **2.3**	all C(sp^2)-H	**0.52±0.02**			
Anisole, **2.4**	*o*-CH, *p*-CH	5.1±0.1[b]			
	m-CH	8.6±0.5	25.0±0.1	22.8	n/a[c]
	all	**6.5±0.3**[d]			
Benzodioxole, **2.5**	all C(sp^2)-H	**6.5±0.9**[d]			
Phenol, **2.6**	*o*-CH, *p*-CH	4.9±0.7[b]			
	m-CH	7.3±0.4	25.1±0.1	23.1	23.5
	all	**5.9±0.6**[d]			
Dimethylaniline, **2.7**	*o*-CH, *p*-CH	21±1[b]			
	m-CH	3.1±0.3	25.7±0.1	22.4	n/a[c]
	all C(sp^2)-H	**14.0±0.9**[d]			
Fluorobenzene, **2.8**	*o*-CH	0.70±0.12	26.8±0.1	24.6	23.6
	p-CH	1.3±0.22	26.3±0.1	24.0	23.9
	m-CH	1.43±0.06	26.3±0.1	24.2	24.4
	all	**1.1±0.27**[d]			
Chlorobenzene, **2.9**	*o*-CH	2.2±0.3	26.0±0.1	29.4	28.8
	p-CH	2.7±0.8	25.8±0.2	23.6	23.9
	m-CH	3.2±0.2	25.7±0.1	23.6	24.0
	all	**2.7±0.1**[d]			
Bromobenzene, **2.10**	all	**2.4±0.2**[d]			
Nitrobenzene, **2.11**	*o*-CH	0.00			
	p-CH	0.9±0.3	26.6±0.2	25.2	25.1
	m-CH	0.35±0.06	27.3±0.1	24.8	25.2
	all	**0.33±0.04**[d]			
Benzoic acid, **2.12**	*o*-CH, *p*-CH	0.78±0.06			
	m-CH	2.5±0.8	25.9±0.2	24.4	n/a[c]
	all	**1.5±0.4**[d]			
Thiophene, **2.13**	*α*-CH	18±1	24.5±0.1	21.1	20.9
	β-CH	10.±1	24.9±0.1	22.3	22.2
	all	**14.2±0.6**[d]			

[a] Calculated using initial reaction rates at <10% substrate conversion. [b] Weighted-average for *o*- and *p*-C-H bonds, $k_{c,o\text{-}p}$. [c] Not determined due to difficulty of locating **TS$_{Ar\text{-}X}$** in TFE. [d] Weighted-average value for all C(sp^2)-H bonds, $k_{c\text{-}all}$.

2.2.4 Reactivity of benzene derivatives 2.2-2.12

The first two substrates, **2.2** and **2.3**, that follow benzene in Table 2.1, contain one or two methyl substituents in the *ortho*-position to the substrates' C(sp^2)-H bonds. The methyl groups make these substrates electron-richer, as compared to benzene. In addition, in the transition states $\mathbf{TS_{Ar\text{-}X}}$ corresponding to an *ortho*-C-H bond oxidative addition to a Pt^{II} center (Scheme 2.3) a noticeable steric interference is anticipated between these substrates' methyl substituents and the Pt-coordinated oxygen atom of the pincer ligand of the catalyst **1.5**, as shown in Fig. 2.2. These steric interactions destabilize the transition states. Overall, the k_c values for *p*-xylene, **2.2**, and mesitylene, **2.3**, (Table 2.1) decrease in the sequence benzene > *p*-xylene >> mesitylene but it is not clear if the electronic effects of the methyl groups work in the same or in the opposite direction, as compared to the steric interactions in the transition state. To be able to exclude the substituents' steric effect from consideration as the factor affecting substrates' reactivity, and consider the substituents' purely electronic effects, we will focus on the reactions involving substrates' *m*- and *p*-C-H bonds.

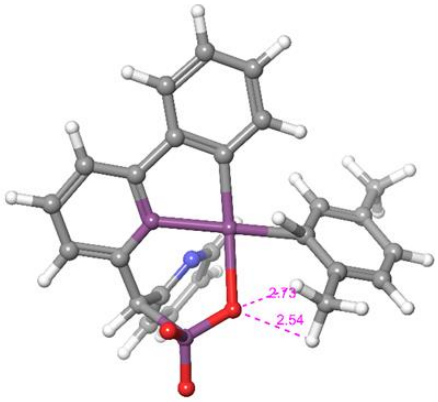

Figure 2.2. A DFT-optimized structure of the transition state $\mathbf{TS_{Ar\text{-}X}}$ for the oxidative addition of a *p*-xylene C(sp^2)-H bond. The shortest distances (Å) between the pincer ligand oxygen atom and two hydrogen atoms of one of the substrate's methyl groups are shown. (Computation performed by Prof. Andrei Vedernikov)

First, we wanted to see if there is any satisfactory correlation between the Gibbs energies of activation of reaction (2.1) involving *m*- and *p*-C-H bonds of monosubstituted benzene derivatives **2.4**, **2.6-2.9**, **2.11-2.12**, and such simple substituents' parameters as the corresponding Hammett σ_X constants.[59, 60] A plot of the experimentally found reaction Gibbs energies of activation, $\Delta G_{353}^{\#}$(exp), vs the substituents' σ_X values is given in Fig. 2.3. The plot shows the absence of any good correlation. Still, one can notice that, overall, the reaction (2.1) tends to be slowed down by electron-withdrawing groups, NO_2, CO_2H and halogens, F and Cl (see also $\sigma_{c\text{-}all}$ values for these substrates and bromobenzene, **2.10**, in Table 2.1), as compared to benzene. In turn, the rate constants for the H/D exchange involving *m*-C-H bonds of phenol, **2.9**, and anisole, **2.7**, are slightly larger than those for benzene and the substrates bearing MeO and OH groups. Similarly to phenol and anisole, benzodioxole, **2.5** (Table 2.1), containing a methylenedioxo fragment, is more reactive than benzene. These observations suggest that the catalyst **1.5** may be weakly electrophilic overall.

The lack of a good correlation in Fig. 2.3 may not be surprising. The regular σ_X constants are determined from proton transfer equilibria (pK_a values) of the corresponding X-substituted benzoic acids where the electron density change on the carboxylic group-bearing arene carbon atom is responsible for the reactivity change ('charge control').[61] In turn, based on the classic mechanistic consideration of concerted C-H oxidative addition to a transition metal center such as one involving **TS$_{Ar\text{-}X}$** (Scheme 2.3), such reactions are orbital-controlled and, ideally, involve a concerted transfer of two electrons from the metal *d*-subshell to the σ* orbital of the substrate C-H bond and a two-electron transfer of the substrate C-H σ-bond electrons onto a suitable empty metal orbital.[62-64] Hence, the C-H

bond oxidative addition to a metal center represents a substantially different reaction type that may require the use of different type of substituents' σ_X constants (*vide infr*a). The involvement of two oppositely directed electron flows in C(sp^2)-H bond oxidative addition reactions may result in the absence of a strong dependence between the reactivity of X-substituted substrates and σ_X constants, as observed in Fig. 2.3. Still, in some situations, the reaction activation energy may be more sensitive to either 'electrophilicity' or 'nucleophilicity' of the engaging C-H bond, depending on the nature and orbital parameters of the reacting species.

In this situation, a DFT modeling of the reaction rate-limiting step and calculation of the Gibbs energy of the corresponding transition states $\mathbf{TS_{Ar\text{-}X}}$ might help account for the experimental observations.

2.2.5 DFT modeling of the effect of substituents on the kinetics of H/D exchange catalyzed by complex 1.5

The Gibbs energies of the formation of the respective transition states $\mathbf{TS_{Ar\text{-}X}}$ from **1.5** and the corresponding substrates (eq 2.5) were calculated in this work using the DFT method employing a PBE functional and a relativistic LACVP** basis set, as implemented in the Jaguar program package,[65] as it was done in our previous DFT analysis of reaction (2.1) with benzene as a substrate:[33]

$$\mathbf{1} + \text{Ar-X} \rightarrow \{\mathbf{TS_{Ar\text{-}X}}\}^{\#} + H_2O \qquad \Delta G_{298}^{\#} \qquad \text{(eq 2.5)}$$

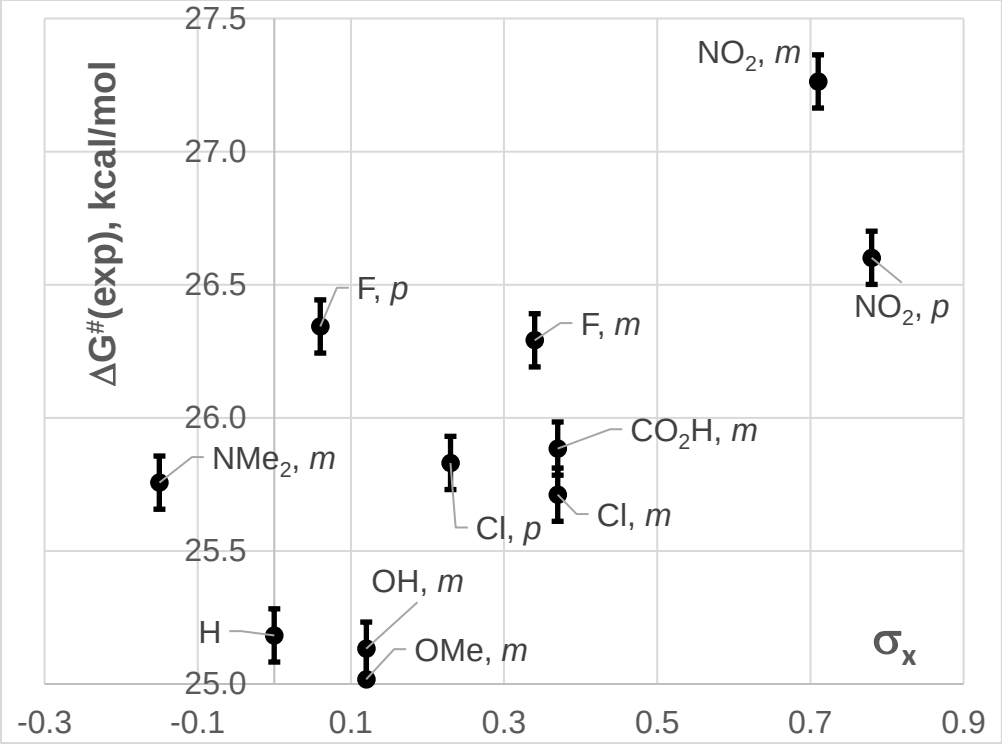

Figure 2.3. A plot of Gibbs energies of activation of reaction (1) involving *m*- and *p*-CH bonds of monosubstituted benzene derivatives **2.4**, **2.6**-**2.9**, **2.11**-**2.12**, and the substituents' Hammett σ_X constants. DFT Calculations performed by Prof. Andrei Vedernikov.

In addition to the gas phase calculations resulting in the corresponding gas phase values $\Delta G_{298}^{\#}$(DFT/gas phase), geometry optimizations were also done for TFE solutions, resulting in the corresponding solution phase values, $\Delta G_{298}^{\#}$(DFT/TFE). Due to some difficulties at geometry optimization of transition states in TFE, some conformationally more flexible substrates were not characterized. The so-produced DFT-calculated Gibbs energies of activation, $\Delta G_{298}^{\#}$(DFT/gas phase) and $\Delta G_{298}^{\#}$(DFT/TFE), are given in Table 2.1 for *m*-C-H and *p*-C-H bonds of monosubstituted benzene derivatives **2.4**, **2.6**-**2.9**, **2.11**-**2.12**, α- and β-CH bonds of thiophene, **2.10**, and *o*-C-H bonds of fluorobenzene, **2.8**, chlorobenzene, **2.9**, and *p*-xylene, **2.2**.

Looking at the calculated gas phase values, $\Delta G_{298}^{\#}$(DFT/gas phase), and the corresponding calculated TFE solutions values, $\Delta G_{298}^{\#}$(DFT/TFE), given in two last columns in Table 2.1, one can note that in most cases they differ only by 0.1-0.4 kcal/mol. Hence, the calculated solvation effects in reaction (2.5) are small. The corresponding higher-temperature values, $\Delta G_{353}^{\#}$(DFT/gas phase) and $\Delta G_{353}^{\#}$(DFT/TFE) have also been found in our calculations. (See Experimental.)

Based on the results of our previous work, our DFT calculations of reaction (2.5) conducted in TFE underestimate the experimental values of the reaction Gibbs energy of activation by ~2-3 kcal/mol. This discrepancy is related to the fact that in neat TFE solutions complex **1.5** produces an adduct with the solvent in a slightly exergonic reaction.[33] Hence, for more accurate results, not complex **1.5** but the TFE adduct should be viewed as a reference state. This consideration suggests that the same small correction parameter needs to be added to each of the DFT-calculated Gibbs energies of activation, $\Delta G_{298}^{\#}$(DFT/gas phase) or $\Delta G_{298}^{\#}$(DFT/TFE), when comparing them with the experimental values. With this idea in mind, a good match of the Gibbs energies of activation calculated for the gas phase reactions, $\Delta G_{298}^{\#}$(DFT/gas phase), and the experimental values, $\Delta G_{353}^{\#}$(exp), can be obtained when the former values are corrected (increased) by 2.3 kcal/mol (Fig. 2.4, *a*; the solid line with slope 1). Two types of C-H bond, *p*-xylene C(sp^2)-H bonds and chlorobenzene *o*-C-H bonds, were not included in this correlation, as the steric effects of the substituents in these substrates, Me and Cl, appear to be overestimated in our DFT calculations of the reaction (2.5) Gibbs energy of activation (*vide infra*). The 2.3 kcal/mol correction allows to attain the root mean square deviation (RMS) of the experimental values from the calculated ones of 0.7 kcal/mol, which is small, as compared to some

typical accuracies attainable currently in DFT calculations of organometallic reactions.[66] In turn, the data points for *p*-xylene and chlorobenzene *o*-C-H bonds deviate from the solid line on the plot in Fig. 2.4, *a* by 4.2 and 5.7 kcal/mol, respectively, both greater than three RMS values

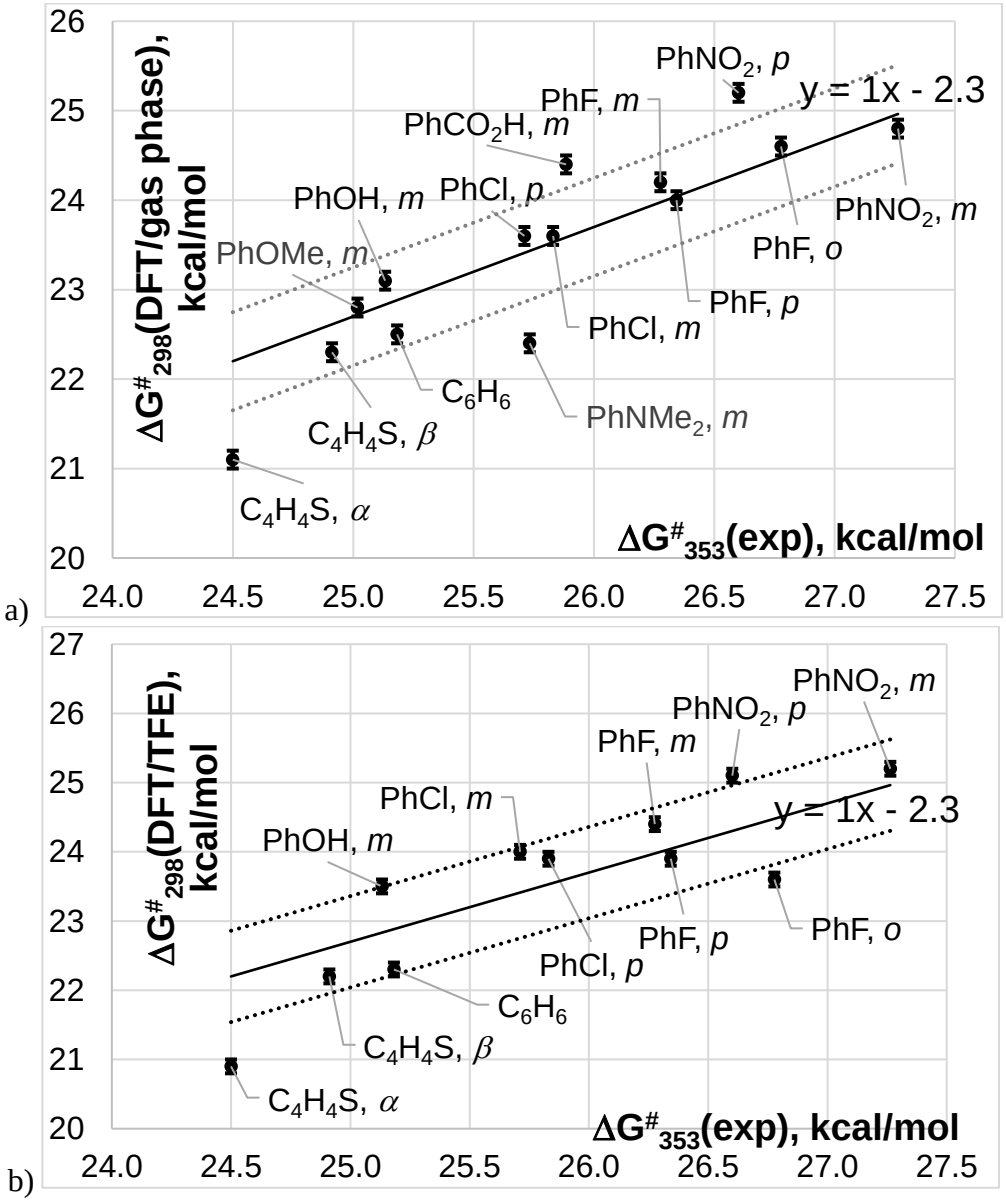

Figure 2.4. Plots of the DFT-calculated values of the Gibbs energies of activation of reaction (2.5) vs. the experimental values $\Delta G_{353}^{\#}$(exp): a) the gas phase-calculated $\Delta G_{298}^{\#}$(DFT/gas phase); b) the TFE-calculated, $\Delta G_{298}^{\#}$(DFT/TFE). Solid lines are shown for minimal root mean square deviation of the 'corrected' DFT-calculated data from the experimental ones with the slope set to 1. Dashed lines are spaced at the RMS value from

the solid lines. Strongly deviating data points for *p*-xylene and chlorobenzene *o*-C-H bonds are not shown.

With the exception of thiophene α-C-H bonds and N,N-dimethylaniline *m*-C-H bonds, the remaining data in Fig. 2.4, *a* fall into a relatively narrow range $\Delta G_{353}^{\#}$(exp) – 2.3 ± RMS (RMS = 0.5 kcal/mol); this range is shown in Fig. 2.4, *a* with two dashed lines with the slope 1 each. The point corresponding to N,N-dimethylaniline may be slightly off of the trend as a consequence of the ability of this compound to become involved in an acid-base equilibrium with TFE and produce the corresponding cation which may have a different reactivity not accounted for in our DFT modeling. Qualitatively, the cation derived from N,N-dimethylaniline should be more electron-poor than the aniline itself and, based on the overall reactivity trend mentioned earlier, be less reactive.

Turning now to the DFT-calculated Gibbs energies of activation of reaction (2.5) in TFE solutions, $\Delta G_{298}^{\#}$(DFT/TFE), and holding in mind small solvation effects calculated for reaction (2.5), as noted earlier, an expected good match of the calculated values and the experimental values, $\Delta G_{353}^{\#}$(exp), can be obtained when the former values are corrected (increased) by 2.3 kcal/mol (Fig. 4, *b*; the solid line with slope 1). The root mean square deviation of the experimental values from the calculated ones in Fig. 2.4, *b* is 0.7 kcal/mol. Once again, a significant deviation from the solid line in Fig. 2.4, *b* of the calculated values $\Delta G_{298}^{\#}$(DFT/TFE) for *p*-xylene and chlorobenzene *o*-C-H bonds, by 4.7 and 5.1 kcal/mol, respectively, may suggest that the DFT model used here overestimates the steric effects of the Me and Cl fragment in these substrates in our calculations of the Gibbs energy of activation of reaction (2.5). Interestingly, a more 'compact' fluorine substituent does not exhibit such issues.

2.2.6 Novel Hammett constants σ_X^M for metal-assisted C-H bond activation reactions

Our inability to describe substituent effects in the organometallic reaction (2.5) using Hammett's σ_X constants and somewhat limited accuracy of modern DFT calculations, as demonstrated in Fig. 2.4 and shown by other researchers,[14] prompted us to introduce a new empirical set of Hammett constants, σ_X^M, for metal-assisted C-H bond activation reactions. Such constants may be useful when analyzing reactivity of various metal complexes and substrates in C-H activation reactions. Our σ_X^M constants are defined by equation (2.6). Since reaction (2.5) is decelerated by electron-withdrawing groups, for the sake of consistency of the sign of σ_X^M and classical σ_X values for the same substituent X, the negative sign is used in front of the logarithmic function:

$$\sigma_X^M = -log(k_c\ (X)/k_c\ (H)) \qquad \text{(eq 2.6)}$$

The corresponding values are given in Table 2. Except the NMe_2 group, the series of σ_X^M constants in Table 2.2 is qualitatively similar to that of σ_X values. The unexpected positive value for the NMe_2 group, 0.34, may be related to the group's partial protonation in TFE solutions, and, therefore, it is not recommended for general use.

Table 2.2. The Hammett-type σ_X^M constants for metal-assisted C-H bond activation reactions based on rate constant k_c data from Table 2.1.

Substituent X	OMe	OH	H	Cl	CO_2H	F	NO_2
σ_X^M, *meta*-	-0.10	-0.03	0	0.33	0.43	0.68	1.29
σ_X^M, *para*-			0	0.40		0.72	0.88

2.2.7 Regioselectivity of H/D exchange (1.5)

Notably, the regioselectivity of the H/D exchange observed in reaction (2.1) is, typically, low, as it follows from the inspection of the rate constant k_c listed in Table 2.1. For example, for chlorobenzene the $k_{c,o}$ (*ortho*-C-H bonds), $k_{c,m}$ (*meta*-C-H bonds) and $k_{c,p}$ (*para*-C-H bonds) values fall in a narrow range of 2.2 – 3.2 M^{-1} h^{-1}. For fluorobenzene the reaction rate constant for *ortho*-C-H bonds, $k_{c,o}$, 0.7 M^{-1} h^{-1}, is only twice lower than the values for its *meta*-C-H bonds, $k_{c,m}$, 1.3 M^{-1} h^{-1}, or *para*-C-H bonds, $k_{c,p}$, 1.43 M^{-1} h^{-1}. There are a few notable exceptions from this picture. In particular, nitrobenzene *ortho*-C-H bonds are virtually unreactive under our reaction conditions, whereas its *para*-C-H bonds, $k_{c,p}$, 0.9 M^{-1} h^{-1}, are somewhat more reactive than *meta*-C-H bonds, $k_{c,m}$, 0.35 M^{-1} h^{-1}. In addition, the relatively low reactivity of *meta*-C-H bonds of *N*,*N*-dimethylaniline makes it possible to carry out a selective deuteration of the C-H bonds in the *ortho*- and *para*-positions of this substrate after 27h or reaction (Fig. 2.5). Finally, an exclusive deuteration of indole β-C-H bonds with a virtually statistical 88% degree of deuterium incorporation was observed in our experiments for indole, **2.14**.

a)

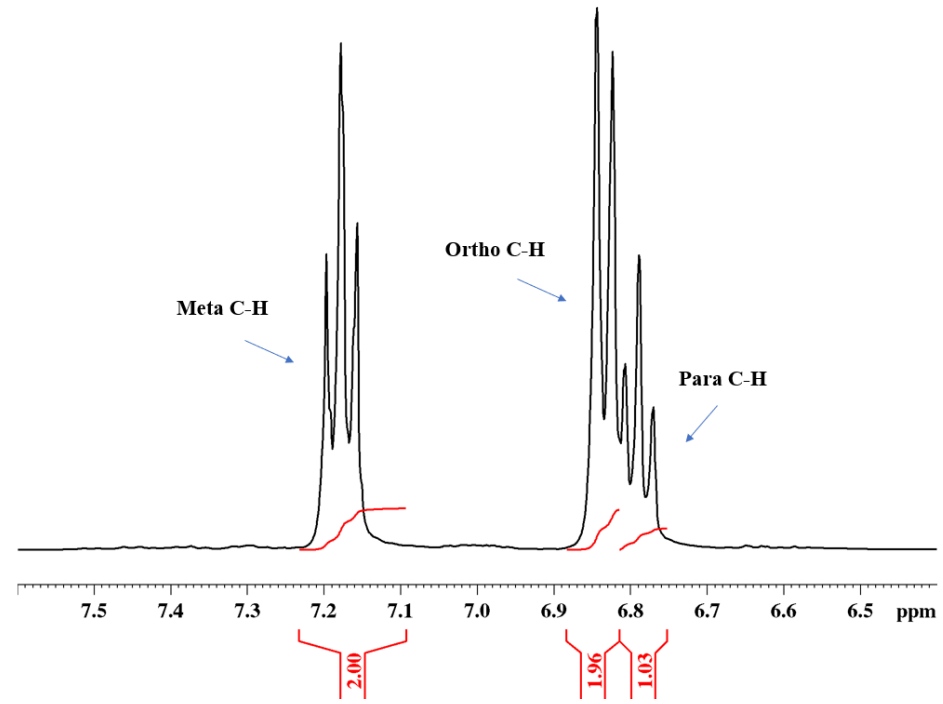

b)

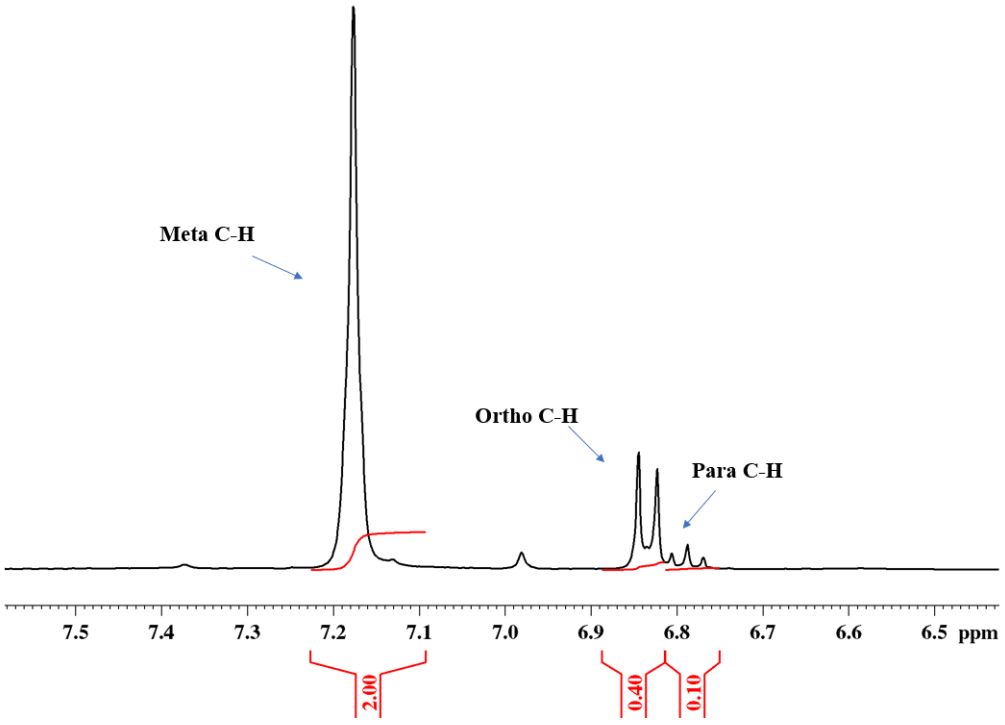

Figure 2.5. ^{1}H-NMR spectra (aromatic region) demonstrating the progress of the H/D exchange between N,N-dimethylaniline and wet TFE-d_1 catalyzed by complex **1.5** at 80 ^{o}C: a) before reaction, b) after 27h.

In contrast to indole and similar to halogenated benzenes, no selective deuteration of thiophene could be achieved (Chart 2.2). This substrate's α-C-H bonds are only 1.8 times more reactive, as compared to its β-C-H bonds (Table 2.1).

To illustrate qualitatively some possible reasons behind the observed regioselectivity of complex **1.5** in the H/D exchange reaction (2.1) that would be consistent with the proposed reaction mechanism (Scheme 2.2), we considered the case of α- vs β-C-H bonds deuteration of thiophene (TP). For this substrate the difference in the reactivity of α- and β-C-H bonds is among the largest, both measured under the conditions used in this work, and according to the DFT-calculated Gibbs energies of activation of reaction (2.5) (Table 2.1, Fig. 2.4). To that end, we considered the frontier molecular orbitals (FMO's) of two fragments, LPt and the corresponding C-H bonds of thiophene that are, formally, engaged in the interaction in the transition state $\mathbf{TS_{Ar\text{-}X}}$. Focusing on the covalent component of such interaction only,[69] a stronger interaction of the FMO's of these fragments, which is proportional to the square of the FMO resonance integral and inversely proportional to their energy difference,[70] would favor a lower activation barrier. Two FMO diagrams are compared in Fig. 2.6, one involving thiophene's α-C-H bonds (Fig. 2.6, *a*) and one involving thiophene's β-C-H bonds (Fig. 2.6, *b*). Qualitatively, two observations can be made using this comparison. First, in both cases the LPt_{LUMO}-TP_{HOMO} gap, ΔE_2, is smaller than the LPt_{HOMO}-TP_{LUMO} gap, ΔE_1, so suggesting that the first interaction is more important and the LPt fragment is somewhat electrophilic. Second, although $\Delta E_{2,a}$ (Fig. 2.6, *a*) corresponding to the cleavage of the thiophene α-C-H bond is slightly greater than $\Delta E_{2,b}$ (Fig. 2.6, *b*) corresponding to the cleavage of thiophene β-C-H bond, the α-C-H HOMO is more localized between the bonded α-C and H atoms, so favoring a stronger

interaction and a lower energy of activation leading to a slightly faster α-C-H bond cleavage

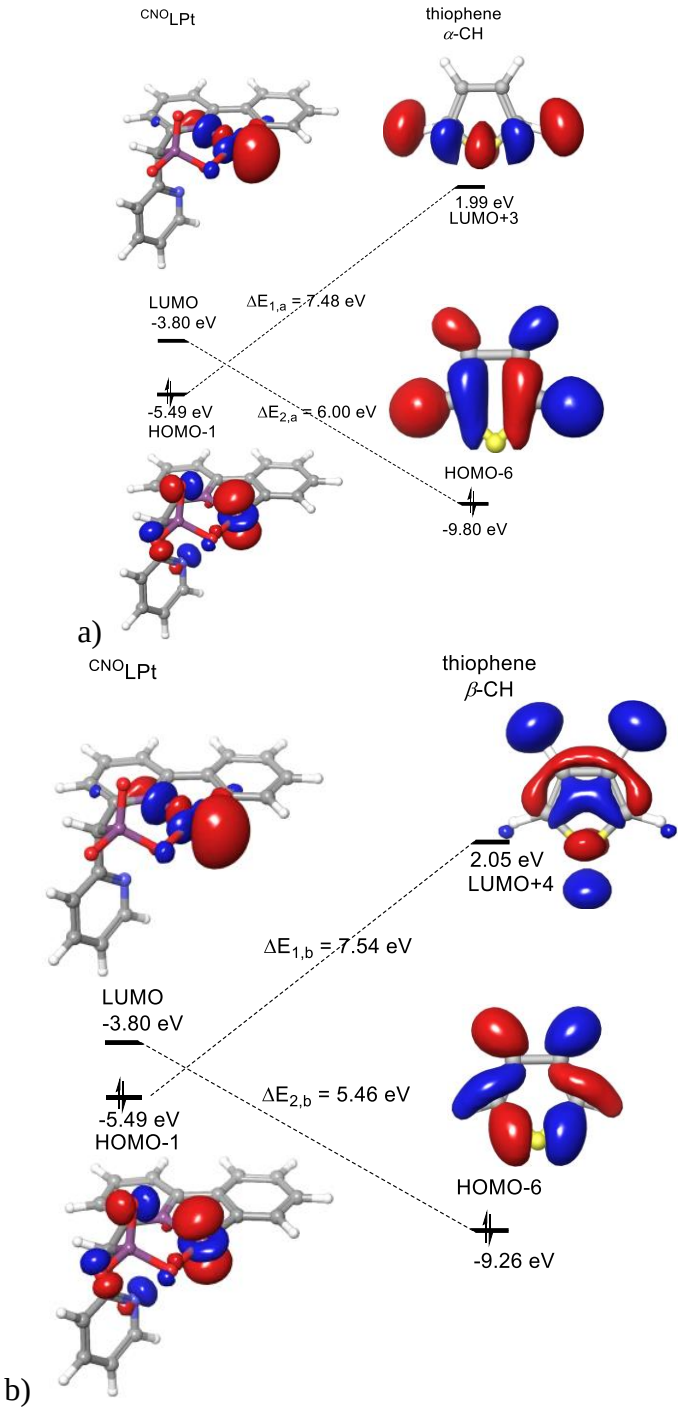

Figure 2.6. A qualitative frontier molecular orbital diagram illustrating FMO interactions between frontier orbitals of the LPt fragment and the corresponding C-H bonds of thiophene: a) α-C-H bonds of thiophene; b) β-C-H bonds of thiophene.

In general, although valuable for some practical applications, [8] the kinetic selectivity of H/D exchange in substituted benzenes has not been systematically analyzed in previous works. In turn, the practically important extent and selectivity of deuteration of aromatic substrates at the late-stage of the reaction have been reported for some catalytic systems[56, 58] and can be compared with our results included in Chart 2.2.

In one of the recent works, an anionic rhodium(III) complex $Na[(bpzmc)RhCl_3]$, **2.33**, (Chart 2.5) in combination with 3 equivalents of AgOTf was used as a catalyst in H/D exchange between a number of aromatic substrates and CF_3CO_2D at 100 °C.[58] The C-H activation in this system was proposed to operate a concerted metallation-deprotonation mechanism which is distinct from C-H bond oxidative addition to a Pt^{II} center considered in this work.

Chart 2.5. Rh^{III} complex **2.33** used in combination with 3 equiv. AgOTf for catalytic H/D exchange between substituted benzene substrates and CF_3CO_2D at 100 °C.[58]

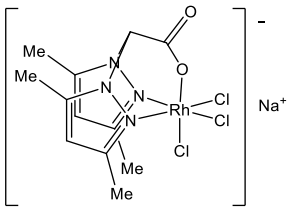

A qualitative comparison of the extent of deuteration *x* in Chart 2.2 with that for identical substrates after 24 h of reaction reported in[9] shows some similarities and some differences. For example, for one of the more reactive substrates, anisole, **2.7**, after 28 h of reaction the catalyst **1.5** allows for a lower extent of *o*-C-H deuteration (31%), as compared to **2.36** / AgOTf (77%), whereas the extent of deuteration of *meta*- and *para*-C-H bonds is about the same, 53-62% in the presence of complex **1.5**/ TFE-d_1 and 64% (on average) in the **2.36** / AgOTf / CF_3CO_2D system.

For another reactive substrate, phenol, **2.6**, after 24 h of reaction both systems show almost identical performance and lack of selectivity with respect to phenol's *ortho*-, *meta*- or *para*-C-H bonds: 67% deuteration for *ortho*-C-H and 69% deuteration for both *meta*- and *para*-C-H bonds for complex **1.5** / TFE-d_1 system vs. 55% (*ortho*-C-H) and 62% (*meta*- and *para*-C-H bonds average) for complex **2.33** / AgOTf / CF_3CO_2D system.

Notably, the reactivity of *N*,*N*-dimethylaniline, **2.7**, is higher when a less acidic system **1.5**/ TFE-d_1 is employed, as compared to the **2.33** / AgOTf / CF_3CO_2D system.[58] In particular, after 25 h of reaction with **1.5** / TFE-d_1 the extent of deuteration of the substrate's *meta*-C-H bonds is 14%, 75% for *ortho*-C-H bonds and 77% for *para*-C-H bonds, which corresponds to 51%, on average, for all substrate's C(sp^2)-H bonds. In turn, a 25% average extent of deuteration was achieved with the **2.35** / AgOTf / CF_3CO_2D. It appears that the protonation of the basic dimethylamino fragment of **2.10** transforms it into an electron-withdrawing ammonium group so causing the reaction to slow.

Interestingly, a higher extent of deuteration by complex **1.5** / TFE-d_1 system, as compared to **35** / AgOTf / CF_3CO_2D, was observed after similar reaction times for electron-poor chlorobenzene. The average degree of deuteration for all arene's C(sp^2)-H bond is 39% in the first system and 2.6% in the second one.

2.2.8. Ibuprofen and Naproxen substrates

Driven by curiosity weather our **1.5** / TFE-d_1 system can be used for deuteration of some pharmaceutical compounds containing C(sp^2)-H bonds, we tested two over-the-counter medications, Ibuprofen, **2.30**, and Naproxen, **2.31** (Chart 2.4). Due to their low solubility in TFE, a 1 : 1 (vol.) mixture of wet TFE-d_1 and $CDCl_3$ was used. The resulting homogeneous solutions containing catalyst **1.5** were subjected to the reaction at 80 ^oC. Similar to the reaction involving benzoic acid, a fine yellow precipitate was observed in Ibuprofen – containing solutions already after 3h. At this time the reaction was stopped to reveal a negligible (<2%) deuterium incorporation. The probable reasons behind this low reactivity are the rapid catalyst deactivation and some steric interference between the catalyst and two substituents which are in the *ortho*-position to the available C(sp^2)-H bonds. In the case of Naproxen the catalyst deactivation was also observed but only after 20h and the reaction resulted in an average 9% deuterium incorporation per C(sp^2)-H bond with a low overall selectivity with respect to six distinct types of C-H bond (Chart 2.4). This result shows some promise of a future possible application of the **1.5** / TFE-d_1 system for deuteration of some pharmaceutical compounds containing aromatic C-H bonds.

2.3. Conclusions

As a result of this work, a wide range of arene substrates were tested in catalytic H/D exchange with wet TFE-d_1 solvent catalyzed by the Pt^{II} pincer complex **1.5** (Charts 2.2-2.4). By monitoring the initial stage of the H/D exchange, we were able to measure the corresponding initial reaction rates and, often, characterize the reaction selectively for different types of C(sp^2)-H bond involved (Table 2.1). A moderate to very high positional H/D exchange selectivity was observed for a few substrates, *N*,*N*-dimethylaniline,

nitrobenzene and indole, whereas for the rest of the substrates the positional selectivity was low. An almost statistical deuterium distribution between substrates' C(sp^2)-H bonds and TFE-d_1 solvent that corresponds to 67-88% deuterium incorporation could be achieved for the most reactive compounds, phenol, indole and *N*,*N*-dimethylaniline. An attempt to use **1.5** / TFE-d_1 / $CDCl_3$ system for deuteration of pharmaceutical compounds, Ibuprofen and Naproxen, was only successful for the latter albeit with a low 9% average deuterium incorporation after 20h. Notably, our attempts to correlate the Gibbs energies of activation of the H/D exchange involving X-monosubstituted benzene derivatives with the corresponding standard Hammett's *meta*- and *para*- σ_X constants resulted in a lack of good correlation and prompted us to introduce a new set of empirical Hammett constants, σ_X^M, which may be useful in the future research of metal-assisted C-H bond activation reactions. Finally, a DFT modeling of the H/D exchange reaction demonstrates a satisfactory match of the experimentally found and calculated Gibbs energies of activation for the reactions involving *meta*- and *para*-C-H bonds of substituted benzenes, as well as C-H bonds of thiophene.

Supporting Information for Chapter 2

I. Materials and Methods

All H/D exchange experiments were carried out under argon atmosphere unless otherwise noted. All reagents were obtained from a commercial vendor (Aldrich, Oakwood, Pressure Chemical, Matrix, Acros Organics, Fischer Chemical, AOB Chem, AK Scientific, or Cambridge Isotope Laboratories). The reagents were used without further purification and were stored under ambient conditions unless otherwise stated. For ligand synthesis, an n-butyl lithium solution in hexane was used and stored at -20 °C. All platinum complexes were synthesized and stored in an argon atmosphere at room temperature. 1H (400 MHz, 500 MHz and 800 MHz) and 13C NMR (125 MHz) spectra were recorded on a Bruker AVANCE 400, Bruker DRX-500 or a Bruker AVANCE III HD 800.

II. Synthesis of Complex 1.5

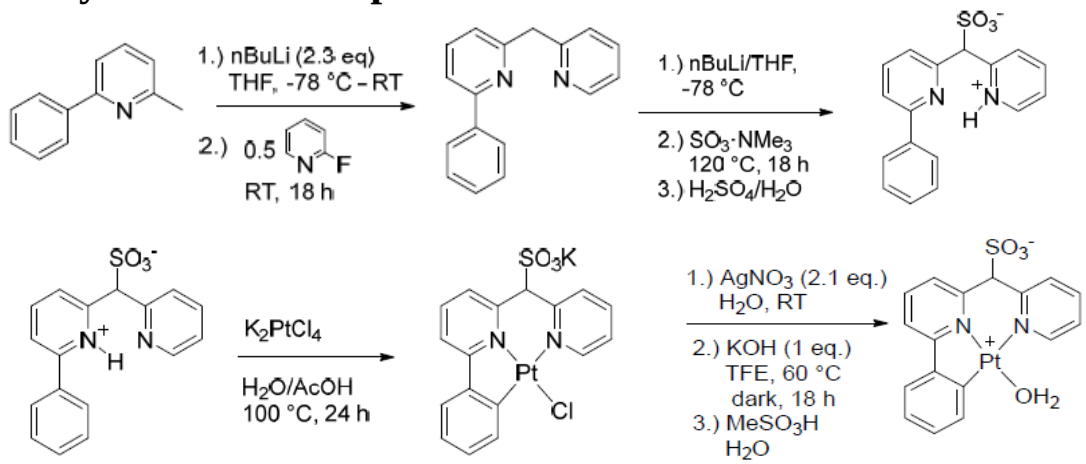

Figure S2.1. Synthesis of (C_6H_4-DPMS)PtOH_2, **1.5**.

Procedure shown in Fig. S1 was slightly modified from our previously described literature method[1] where 2-phenyl-6-methylpyridine is used as a starting material and was purchased from a commercial source. All subsequent transformations are directly in accordance with the previously described methodology shown above.

III. H/D Exchange Overview

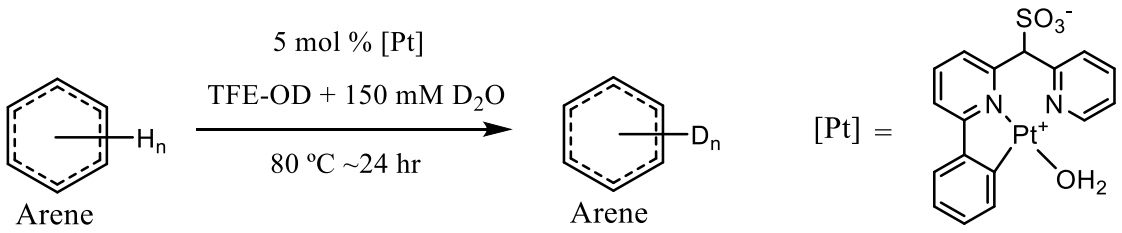

Figure S2.2. H/D exchange reaction scheme for protio-arenes

General Procedure for H/D Exchange

In an argon filled glove box 0.4-0.7 mmol of arene substrate was transferred into a scintillation vial and dissolved in 0.45 mL of a pre-made 150 mM solution of D_2O in TFE-d_1. In a separate scintillation vial ~4.0 mg of complex 1.5 was weighed out and subsequently dissolved in 0.50 mL of the mixture of the substrate and D_2O – TFE solution. The complex was allowed to completely dissolve before finally being transferred into an NMR J. Young tube alongside a D_2O capillary and capped with a pressure tight Teflon seal. The NMR tube was then removed from the glovebox and pressurized under ~20 psi of argon (to prevent reflux) before being placed in an oil bath heated to 80 °C for 24 hours. The sample was periodically removed from the oil bath for NMR measurements to monitor the progress of the reaction. For highly reactive substrates, initial rates were obtained in the NMR probe at 80 °C via sequential ^{1}H-NMR measurements. Deuterium incorporation was only reported if the extent of deuteration exceeded 2% for a given bond type in order to compensate for NMR integration error.

H/D Exchange for Benzene, 2.1

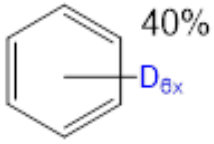

The general procedure outlined above was followed using 0.050 mL of benzene (0.44 mmol) dissolved in 0.45 mL of a pre-made 150 mM solution of D_2O in TFE-d_1 and 4.1 mg (7.6 µmol) of complex 1.5. The resulting solution was a homogeneous yellow color and was heated at 80 °C for 26.0 hours. The reaction proceeded with no color change or precipitate formation. There was no significant background contribution in the H/D exchange.

H/D Exchange for p-Xylene, 2.2

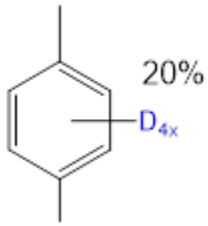

The general procedure outlined above was followed using 0.050 mL of p-xylene (0.41 mmol) dissolved in 0.45 mL of 150 mM solution of D_2O in TFE-d_1 and 4.7 mg (8.7 µmol) of complex 1.5. The resulting solution was a homogeneous yellow color and was heated at 80 °C for 20.0 hours. The reaction proceeded with no color change or precipitate formation. There was no significant background contribution in the H/D exchange.

H/D Exchange for Mesitylene, 2.3

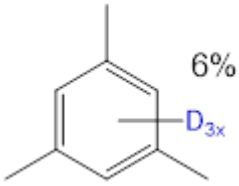

The general procedure outlined above was followed using 0.050 mL of mesitylene (0.36 mmol) dissolved in 0.45 mL of 150 mM solution of D_2O in TFE-d_1 and 5.1 mg (9.4 µmol) of complex 1.5. The resulting solution was a homogeneous yellow color and was heated at 80 °C for 20.0 hours. The reaction proceeded with no color change or precipitate formation. There was no significant background contribution in the H/D exchange.

H/D Exchange for Anisole, 2.4

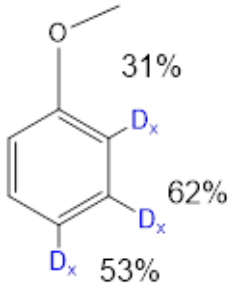

The general procedure outlined above was followed using 0.050 mL of anisole (0.50 mmol) dissolved in 0.45 mL of a pre-made 150 mM solution of D_2O in TFE-$d_1$and 4.0 mg (7.4 µmol) of complex 1.5. The resulting solution was a homogeneous yellow color and was heated at 80 °C for 27.25 hours. The reaction proceeded with no color change or precipitate formation. There was no significant background contribution in the H/D exchange.

H/D Exchange for 1,3-Benzodioxole, 2.5

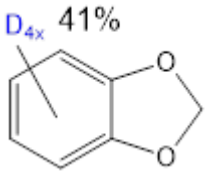

The general procedure outlined above was followed using 0.050 mL of 1,3-benzodioxole (0.43 mmol) dissolved in 0.45 mL of a pre-made 150 mM solution of D_2O in TFE-d_1 and 3.7 mg (6.9 µmol) of complex 1.5. The resulting solution was a homogeneous yellow color and was heated at 80 °C for 24.0 hours. There was no significant background contribution in the H/D exchange. Aromatic signals were not well resolved, and thus total aromatic deuterium incorporation is reported. After 24.0 hours, a light-yellow precipitate was formed on the sides of the NMR tube.

H/D Exchange for Phenol, 2.6

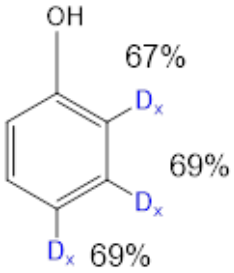

The general procedure outlined above was followed using 41.0 mg of phenol (0.43 mmol) dissolved in 0.45 mL of a pre-made 150 mM solution of D_2O in TFE-d_1 and 5.0 mg (9.3 µmol) of complex 1.5. The resulting solution was a homogeneous yellow color and was

heated at 80 °C for 23.2 hours. The reaction proceeded with no color change or precipitate formation. There was no significant background contribution in the H/D exchange.

H/D Exchange for N,N Dimethylaniline, 2.7

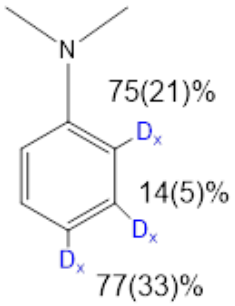

The general procedure outlined above was followed using 0.050 mL of N,N dimethylaniline (0.39 mmol) dissolved in 0.45 mL of a pre-made 150 mM solution of D_2O in TFE-$d_1$and 5.0 mg (9.3 µmol) of complex 1.5. The resulting solution was a homogeneous yellow color and was heated at 80 °C for 25.6 hours. After approximately 3 hours, Pt black was formed. Additionally, there was a significant contribution (shown in parenthesis) to H/D exchange from a background reaction that is shown in the control experiment. Initial rates were probed before Pt black formation is apparent.

H/D Exchange for Fluorobenzene, 2.8

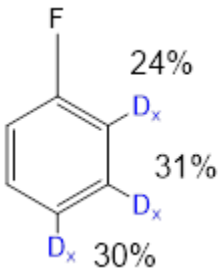

The general procedure outlined above was followed using 0.050 mL of fluorobenzene (0.50 mmol) dissolved in 0.45 mL of a pre-made 150 mM solution of D_2O in TFE-d_1 and 4.9 mg (9.1 µmol) of complex 1.5. The resulting solution was a homogeneous yellow color and was heated at 80 °C for 23.0 hours. The reaction proceeded with no color change or precipitate formation. There was no significant background contribution in the H/D exchange.

H/D Exchange for Chlorobenzene, 2.9

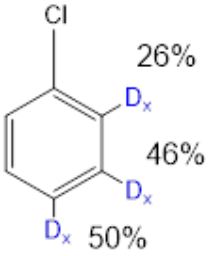

The general procedure outlined above was followed using 0.050 mL of chlorobenzene (0.50 mmol) dissolved in 0.45 mL of a pre-made 150 mM solution of D_2O in TFE-d_1 and 4.0 mg (7.4 µmol) of complex 1.5. The resulting solution was a homogeneous yellow color and was heated at 80 °C for 24 hours. There was no significant background contribution in the H/D exchange. After 25.0 hours a red precipitate formed at the bottom on the NMR tube. This precipitate has been observed previously with this system and is likely the result of catalyst dimerization as described our previous work[1].

H/D Exchange for Bromobenzene, 2.10

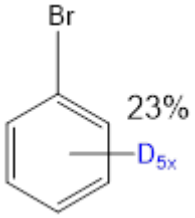

The general procedure outlined above was followed using 0.050 mL of bromobenzene (0.47 mmol) dissolved in 0.45 mL of a pre-made 150 mM solution of D_2O in TFE-d_1 and 4.4 mg (8.2 µmol) of complex 1.5. The resulting solution was a homogeneous yellow color and was heated at 80 °C for 23.6 hours. There was no significant background contribution for H/D exchange. After 24 hours a red precipitate formed at the bottom on the NMR tube. This precipitate has been observed previously with this system and is likely the result of catalyst dimerization as described our previous work[1]. There was not sufficient resolution to distinguish the difference between ortho, meta, and para positions, thus extent of deuteration is reported as total aromatic deuterium incorporation.

H/D Exchange for Nitrobenzene, 2.11

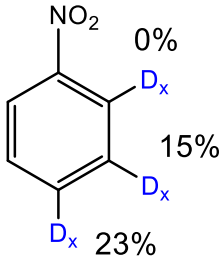

The general procedure outlined above was followed using 0.05 mL of nitrobenzene (0.49 mmol) dissolved in 0.45 mL of a pre-made 150 mM solution of D_2O in TFE-d_1 and 3.7 mg (6.8 µmol) of complex 1.5. The resulting solution was a homogeneous yellow color and was heated at 80 °C for 23.0 hours. There was no significant background contribution in the H/D exchange the reaction proceeded with no color change or precipitate formation. Deuterium incorporation did not exceed the 2% threshold for the ortho position.

H/D Exchange for Benzoic Acid, 2.12

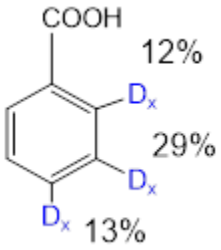

The general procedure outlined above was followed using 22.8 mg of benzoic acid (0.19 mmol) dissolved in 0.45 mL of a pre-made 150 mM solution of D_2O in TFE-d_1 and 4.0 mg (7.4 µmol) of complex 1.5. The resulting solution was a homogeneous yellow color and was heated at 80 °C for 24.4 hours. There was no significant background contribution in the H/D exchange. After ~10 hours a yellow precipitate was formed.

H/D Exchange for Thiophene, 2.13

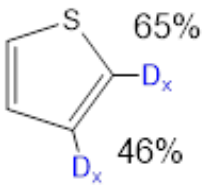

The general procedure outlined above was followed using 0.050 mL of thiophene (0.62 mmol) dissolved in 0.45 mL of a pre-made 150 mM solution of D_2O in TFE-d_1 and 4.0 mg (7.4 µmol) of complex 1.5. The resulting solution was a homogeneous yellow color and was heated at 80 °C for 21.1 hours.

The reaction proceeded with no color change or precipitate formation. There was no significant background contribution in the H/D exchange.

H/D Exchange for Indole, 2.14

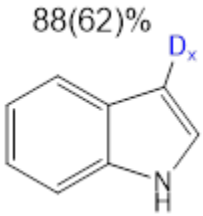

The general procedure outlined above was followed using 55.0 mg of indole (0.46 mmol) dissolved in 0.45 mL of a pre-made 150 mM solution of D_2O in TFE-d_1 and 4.2 mg (7.8 µmol) of complex 1.5. The resulting solution was a homogeneous yellow color and was heated at 80 °C for 24.7 hours. The H/D exchange was only observed in the position β to the pyrrole nitrogen. Pt black formation was visibly present after 60-80 minutes of reaction. However, the reaction approached a statistical incorporation of deuterium after 45 min, prior to Pt black formation. There was a significant contribution (shown in parenthesis) to the H/D exchange from a background reaction as was shown in the control experiment. See **Figure S2.14**.

H/D Exchange for Naproxen, 2.31

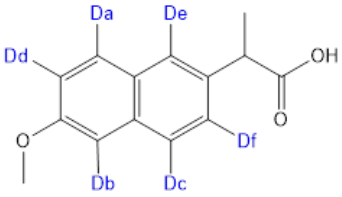

Da + Db + Dc = 28%
Dd = 14%
De = 8%
Df = 4%

In an argon filled glove box 26.0 mg of Naproxen (0.11 mmol) was transferred into a scintillation vial and dissolved in 0.50 mL of $CDCl_3$. In a separate scintillation vial 3.5 mg of complex 1.5 was weighed out and subsequently dissolved into 0.50 mL of a pre-made 150 mM solution of D_2O in TFE-d_1. The complex was allowed to completely dissolve before the two solutions were mixed. Finally, 0.50 mL of the resulting mixture was transferred into a J. Young NMR tube and capped with a pressure tight Teflon seal. The NMR tube was then removed from the glovebox and pressurized under ~20 psi of argon before being placed in an oil bath heated

to 80 °C for 24 hours. After approximately 20 hours, a yellow precipitate formed at the base of the NMR tube.

IV. Functional Group Compatibility Studies

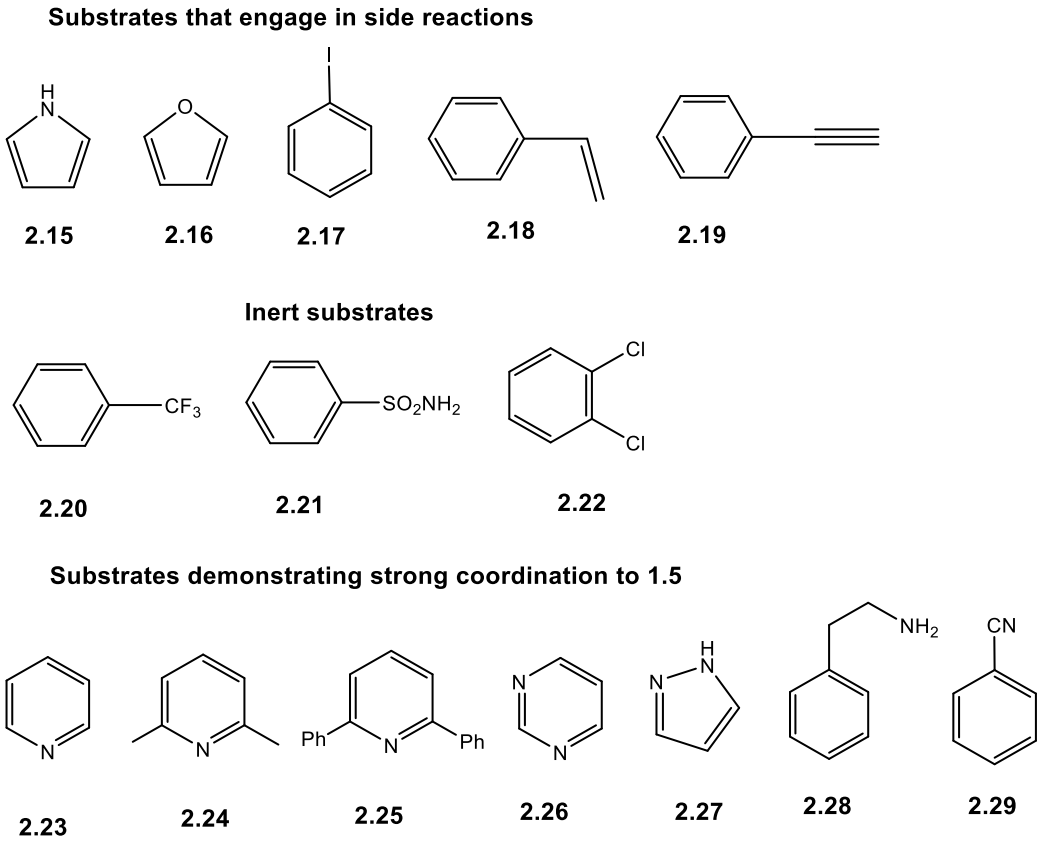

Figure S2.3. List of aromatic substrates inactive in reaction (2.1).

Attempted H/D Exchange for Pyrrole, 2.15

The general procedure outlined above was followed using 0.050 mL of pyrrole (0.73 mmol) dissolved in 0.45 mL of 150 mM solution of D_2O in TFE-d_1 and 4.9 mg (9.1 μmol) of complex 1.5. The resulting solution was a homogeneous orange color and was heated at 80 °C for 24.0 hours. The solution changed coloration after 3 hours to yield a dark blue/green solution. The walls of the NMR tube were coated with a dark grey precipitate. Deuterium incorporation was unable to be determined due to degradation.

Attempted H/D Exchange for Furan, 2.16

The general procedure outlined above was followed using 0.050 mL of pyrrole (0.68 mmol) dissolved in 0.45 mL of 150 mM solution of D_2O in TFE-d_1 and 4.5 mg (8.3 μmol) of complex 1.5. The resulting solution was a homogeneous yellow color and was heated at 80 °C for 24.0 hours. Deuterium incorporation was unable to be determined due to degradation.

Attempted H/D Exchange for Iodobenzene, 2.17

The general procedure outlined above was followed using 0.050 mL of iodobenzene (0.45 mmol) dissolved in 0.45 mL of 150 mM solution of D_2O in TFE-d_1 and 4.9 mg (9.1 μmol) of complex 1.5. The resulting solution was a homogeneous yellow color and was heated at 80 °C for 24.0 hours. Within 2 hrs, a dark red/brown precipitate began to form. This precipitate is different than the previously mention degradation product of the catalyst. Deuterium incorporation did not exceed the 2% threshold.

Attempted H/D Exchange for Styrene, 2.18

The general procedure outlined above was followed using 0.050 mL of styrene (0.44 mmol) dissolved in 0.45 mL of 150 mM solution of D_2O in TFE-d_1 and 4.5 mg (8.3 μmol) of complex 1.5. The resulting solution was a homogeneous yellow color and was heated at 80 °C for 24.0 hours. After ~5 hours Pt black appeared to have formed. Additionally, the walls of the NMR tube were coated with a gray precipitate. Deuterium incorporation did not exceed the 2% threshold.

Attempted H/D Exchange for Phenylacetylene, 2.19

The general procedure outlined above was followed using 0.050 mL of phenylacetylene (0.45 mmol) dissolved in 0.45 mL of 150 mM solution of D_2O in TFE-d_1 and 4.5 mg (8.3 µmol) of complex 1.5. The resulting solution was a homogeneous yellow color and was heated at 80 °C for 24.0 hours. The solution rapidly changed from a homogenous yellow color to a cloudy brown after heating for 10 minutes. After the full 24 hr, the solution was cloudy/yellow with a dark tar-like black/brown precipitate. Deuterium incorporation did not exceed the 2% threshold.

Attempted H/D Exchange for Trifluoromethylbenzene, 2.20

The general procedure outlined above was followed using 0.050 mL of trifluoromethylbenzene (0.55 mmol) dissolved in 0.45 mL of 150 mM solution of D_2O in TFE-d_1 and 3.4 mg (6.3 µmol) of complex 1.5. The resulting solution was a homogeneous yellow color and was heated at 80 °C for 24.0 hours. After 24 hours a red precipitate formed at the bottom on the NMR tube. Deuterium incorporation did not exceed the 2% threshold.

Attempted H/D Exchange for Benzenesulfonamide, 2.21

The general procedure outlined above was followed using 27.5 mg of benzenesulfonamide (0.175 mmol) dissolved in 0.45 mL of 150 mM solution of D_2O in TFE-d_1 and 4.5 mg (8.3 µmol) of complex 1.5. The resulting solution was a homogeneous yellow color and was heated at 80 °C for 24.0 hours. After 24 hours a silty yellow precipitate formed. Deuterium incorporation did not exceed the 2% threshold.

Attempted H/D Exchange for 1,2 Dichlorobenzene, 2.22

The general procedure outlined above was followed using 0.050 mL of 1,2 dichlorobenzene (0.42 mmol) dissolved in 0.45 mL of 150 mM solution of D_2O in TFE-d_1 and 3.4 mg (6.3 μmol) of complex 1.5. The resulting solution was a homogeneous yellow color and was heated at 80 °C for 24.0 hours. After 24 hours a red precipitate formed at the bottom on the NMR tube. Deuterium incorporation did not exceed the 2% threshold.

Attempted H/D Exchange for Pyridine, 2.23

The general procedure outlined above was followed using 0.050 mL of pyridine (0.62 mmol) dissolved in 0.45 mL of 150 mM solution of D_2O in TFE-d_1 and 3.4 mg (6.3 μmol) of complex 1.5. The resulting solution was a homogeneous yellow color and was heated at 80 °C for 24.0 hours. After 24 hours a silty yellow precipitate formed at the bottom on the NMR tube. Deuterium incorporation did not exceed the 2% threshold.

Attempted H/D Exchange for 2,6 Dimethylpyridine, 2.24

The general procedure outlined above was followed using 0.050 mL of 2,6 dimethylpyridine (0.43 mmol) dissolved in 0.45 mL of 150 mM solution of D_2O in TFE-d_1 and 4.1 mg (7.6 μmol) of complex 1.5. The resulting solution was a homogeneous yellow color and was heated at 80 °C for 24.0 hours. No precipitate was observed and deuterium incorporation did not exceed the 2% threshold.

Attempted H/D Exchange for 2,6 Diphenylpyridine, 2.25

The general procedure outlined above was followed using 27.5 mg of 2,6 diphenylpyridine (0.12 mmol) dissolved in 0.45 mL of 150 mM solution of D_2O in TFE-d_1 and 4.1 mg (7.6 µmol) of complex 1.5. The resulting solution was a homogeneous yellow color and was heated at 80 °C for 24.0 hours. No precipitate was observed and deuterium incorporation did not exceed the 2% threshold.

Attempted H/D Exchange for Pyrimidine, 2.26

The general procedure outlined above was followed using 41.0 mg of pyrimidine (0.51 mmol) dissolved in 0.45 mL of 150 mM solution of D_2O in TFE-d_1 and 3.4 mg (6.3 µmol) of complex 1.5. The resulting solution was a homogeneous yellow color and was heated at 80 °C for 24.0 hours. No precipitate was observed, and deuterium incorporation did not exceed the 2% threshold.

Attempted H/D Exchange for Pyrazole, 2.27

The general procedure outlined above was followed using 50.0 mg of pyrazole (0.74 mmol) dissolved in 0.45 mL of 150 mM solution of D_2O in TFE-d_1 and 3.8 mg (7.0 µmol) of complex 1.5. The resulting solution was a homogeneous yellow color and was heated at 80 °C for 24.0 hours. No precipitate was observed, and deuterium incorporation did not exceed the 2% threshold.

Attempted H/D Exchange for Phenylethylamine, 2.28

The general procedure outlined above was followed using 0.05 mL of phenylethylamine (0.4. mmol) dissolved in 0.45 mL of 150 mM solution of D_2O in TFE-d_1 and 4.1 mg (7.6 µmol) of complex 1.5. The resulting solution was a homogeneous yellow color and was heated at 80 °C for 24.0 hours. No precipitate was observed, and deuterium incorporation did not exceed the 2% threshold.

Attempted H/D Exchange for Benzonitrile, 2.29

The general procedure outlined above was followed using 0.050 mL of benzonitrile (0.45 mmol) dissolved in 0.45 mL of 150 mM solution of D_2O in TFE-d_1 and 4.5 mg (8.3 µmol) of complex 1.5. The resulting solution was a homogeneous yellow color and was heated at 80 °C for 24.0 hours. After ~8 hours a red precipitate formed at the bottom on the NMR tube. Deuterium incorporation did not exceed the 2% threshold.

Attempted H/D Exchange for Ibuprofen, 2.30

The general procedure outlined above was followed using 105 mg of ibuprofen (0.48 mmol) dissolved in 0.5 mL $CDCl_3$. The solution was then diluted with 0.5 mL of 150 mM solution of D_2O in TFE-d_1 and 4.1 mg (7.6 µmol) of complex 1.5. The resulting solution was a homogeneous yellow color and was heated at 80 °C for 24.0 hours. A silty yellow precipitate formed after 3 hours and deuterium incorporation did not exceed the 2% threshold.

Attempted Isolation of (C_6H_4-dpms) Pt^{II}-Substrate Adducts

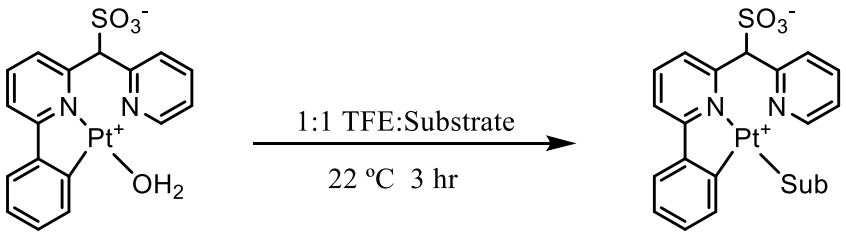

(C_6H_4-dpms) Pt^{II}-N**,N Dimethylaniline adduct formation**

In an argon filled glovebox, 40 mg (74.4 µmol) of complex 1.5 was weighed out into a dry scintillation vial and subsequently dissolved in 10 mL of a 1:1 mixture of N,N dimethylaniline and trifluoroethanol to yield a dark red/purple solution. The solution was allowed to stir for 3 hours before reducing the volume down to ~6 mL. The resulting Pt complex was precipitated out of the solution utilizing Et_2O and was thoroughly washed with additional Et_2O to yield 26 mg of a dark red powder. This powder was then dissolved in MeOD for ^{1}H-NMR analysis. The ^{1}H NMR spectrum of the solution showed no changes after 72 hours. Upon removal of the solvent and exposure of the residue to air for 24 hr, the solid turned black.

In the ^{1}H NMR spectrum of a freshly prepared sample two inequivalent N-CH_3 signals of equal intensity along with matching signals of a Pt-coordinated C_6H_4-dpms ligand, were observed, thus suggesting the formation of a Pt-substrate adduct (C_6H_4-dpms)Pt($PhNMe_2$). The adduct coexisted in an apparent equilibrium with an about equal molar amount of free $PhNMe_2$ and, presumably, a methanol analog of **1**, (C_6H_4-dpms)Pt(MeOH). Hence, the stability of the adduct (C_6H_4-dpms)Pt($PhNMe_2$) is low.

Attempted (C_6H_4-dpms) Pt^{II}-thiophene adduct formation

In an argon filled glovebox, 40 mg (74.4 µmol) of [Pt] was weighed out into a dry scintillation vial and was subsequently dissolved into 10 mL of a 10:1 mixture of thiophene and trifluoroethanol to yield a yellow solution. The solution was allowed to stir for overnight before solvent removal. This yielded a yellow powder which was soluble in methanol. ^{1}H-NMR spectroscopy showed multiple products and was inconclusive as to the nature of the species present.

Attempted (C_6H_4-dpms) Pt^{II}-benzoic acid adduct formation

In an argon filled glovebox, 40 mg (74.4 µmol) of [Pt] was weighed out into a dry scintillation vial and was subsequently dissolved in 2 mL TFE-d_1 containing 9.8 mg (74.4 µmol) of benzoic acid solution. The solution was allowed to thoroughly mix at room temperature. ^{1}H-NMR spectroscopy was inconclusive in showing resolved aromatic signals that could be confidently tied to adduct formation.

V. Initial Rates and Extent of Deuteration

Initial rates of H/D exchange were measured using ^{1}H NMR spectroscopy, by monitoring the change of the integral intensity of specific aromatic C-H bonds of a substrate over time (see an example in Figure. S2.4 below). The integration values were compared against the TFE-d_1 solvent signal at 3.88 ppm (CH_2, quartet) used as an internal standard. Simultaneous control experiments were performed in the absence of complex 1.5. Integration values were used to calculate the concentration of [C-H] bonds as a function of time. The initial rates were calculated for the period of time corresponding to about 10% deuteration of the substrate C-H bonds utilizing LINEST linear regression function on Microsoft Excel.

The ultimate expected 'statistical' extent of deuteration of each specific substrate was calculated as;

$$100\% \times \frac{[TFE - d_1] + 2[D_2O]}{[TFE - d_1] + 2[D_2O] + [C - H]_{arom}}$$

where [TFE-d_1], [D_2O] and $[C\text{-}H]_{arom}$ are the initial molar concentrations of TFE-d_1, D_2O and all aromatic C-H bonds of the substrate, respectively.

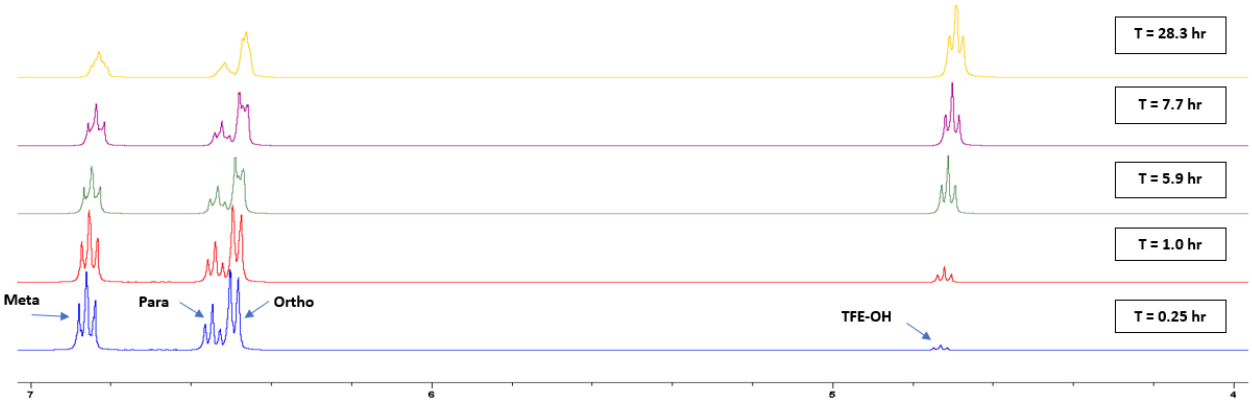

Figure S2.4. Sequential ^{1}H-NMR spectra demonstrating the progress of the H/D exchange between anisole and wet TFE-d_1 catalyzed by complex 1.5 at 80 ^{o}C**.**

T_0-T_4 represent sequential measurements taken over a specific time period. The change in integration over time corresponds to aryl H/D exchange. TFE-OH signal was utilized as a secondary means of confirming H/D exchange was taking place.

An initial round of experiments was performed in order to best estimate initial rates with conditions as described above. The reactions were monitored **by 1.5**H NMR and the integration values for each resolved aromatic peak compared to an internal standard (TFE-d_1, CH_2 quartet at 3.88 ppm). Initial rates were determined within the first 10% conversion of a given C-H bond via the relationship shown below.

$$Initial\ Rate = \frac{d[C-D]}{dt}$$

Initial rates were then used to generate rate constants for each substrate. The specific amounts of reagents used, and reaction windows used to determine initial rates are shown for each substrate in **Figure S2.5-S18.**

Initial Rate Data for Benzene

			Density	Volume	Concentration
[LPt(H2O)], mg			g/mL	mL	M
3.5		TFE + 150 mM D2O	1.384	0.45	12.50
		Benzene	0.876	0.05	1.12

[1.5] = 0.0130 M (0.20% catalyst loading)

SLOPE	0.5922	0.02627	**INT**
(+/-)	0.0344	0.018578	**(+/-)**
r2	0.9867	0.026783	**S(Y)**

Expected statistical extent of deuteration of the substrate aromatic C-H bonds: 65%

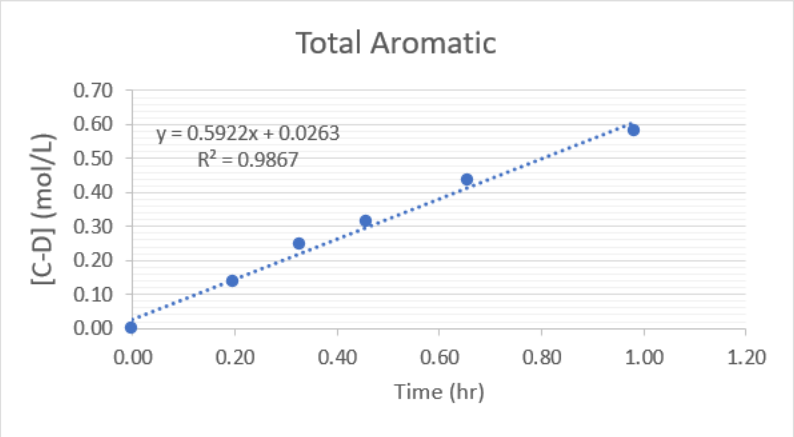

Figure S2.5. Initial rate of reaction (2.1) catalyzed by 1.5 with benzene substrate at 80 °C.

The rate constant for the H/D exchange (2.1) catalyzed by complex 1.5 at 80 °C:
$k_c = 6.8 \pm 0.4\ M^{-1}\ h^{-1}$.

Initial Rate Data for Anisole

			Density	Volume	Concentration
[LPt(H2O)], mg			g/mL	mL	M
3.7		TFE + 150 mM D2O	1.384	0.45	12.50
		Anisole	0.946	0.05	0.87
Temperature (C)	80				

[1.5] = 0.0138 M (0.32% catalyst loading)

Meta C-H				Ortho/Para C-H			
SLOPE	0.20713	0.004	INT	SLOPE	0.182623473	0.00848	INT
(+/-)	0.013261	0.006	(+/-)	(+/-)	0.004607407	0.00321	(+/-)
r2	0.98387	0.009	S(Y)	r2	0.996195516	0.00515	S(Y)

Expected average statistical extent of deuteration of the substrate aromatic C-H bonds: 74%

The rate constants for the H/D exchange (2.1) catalyzed by complex 1.5 at 80 °C:
ortho-, *para*-CH bonds, $k_{c,o\text{-}p}$ =5.1±0.1M^{-1} h^{-1};
meta-CH bonds, $k_{c,m}$ = 8.6±0.5 M^{-1} h^{-1}.

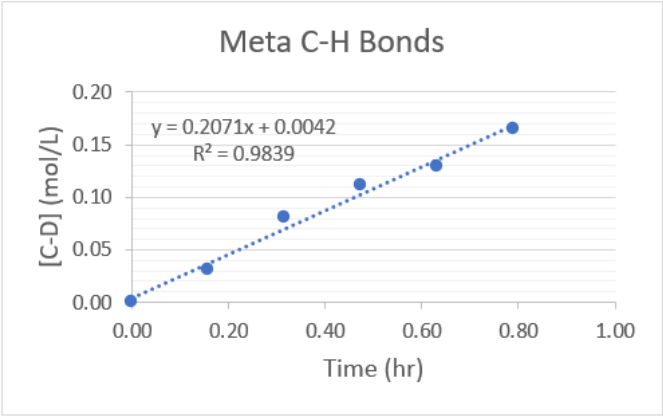

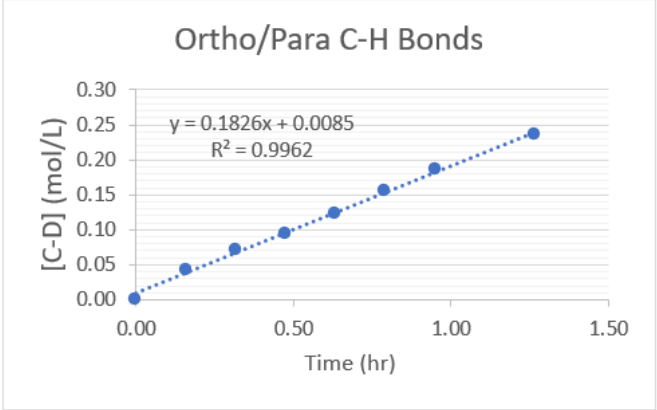

Figure S2.6. Initial rates of reaction (2.1) catalyzed **by 1.5** with anisole substrate at 80 °C.

Initial Rate Data for N,N Dimethylaniline

			Density	Volume	Concentration
[LPt(H2O)], mg			g/mL	mL	M
6		TFE + 150 mM D2O	1.384	0.45	12.50
		N,N Dimethylaniline	0.956	0.05	0.79
Temperature (C)	80				

[1.5] = 0.0223 M (0.56% catalyst loading)

	Meta C-H			Ortho/Para C-H			
SLOPE	0.111705	-9E-04	INT	SLOPE	1.125823958	0.004076528	INT
(+/-)	0.001915	0.001	(+/-)	(+/-)	0.071263193	0.012221112	(+/-)
r2	0.999413	0.002	S(Y)	r2	0.992050254	0.014607023	S(Y)

Expected average statistical extent of deuteration of the substrate aromatic C-H bonds: 74%

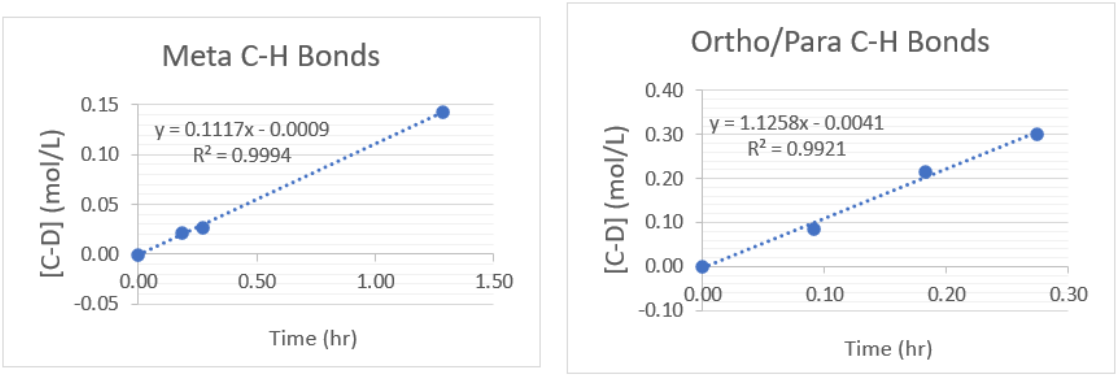

Figure S2.7a. Initial rates of reaction (2.1) catalyzed by 1.5 with N,N dimethylaniline substrate at 80 °C.

The rate constants for the H/D exchange (2.1) catalyzed by complex 1.5 at 80 °C:
ortho-, *para*-CH bonds, $k_{c,o\text{-}p}$ = 21±1.4 M^{-1} h^{-1};
meta-CH bonds, $k_{c,m}$ = 3.1±0.3 M^{-1} h^{-1}.

Initial Rate Data for N,N Dimethylaniline Background Reaction

			Density	Volume	Concentration
[LPt(H2O)], mg			g/mL	mL	M
0		TFE + 150 mM D2O	1.384	0.45	12.46
		Dimethyl Aniline	0.956	0.05	0.789
Temperature (C)	80				

Expected average statistical extent of deuteration of the substrate aromatic C-H bonds: 74%

Meta C-H				Ortho C-H			
SLOPE	-0.0117	1E-03	INT	SLOPE	-6E-04	0.004	INT
(+/-)	0.000972	8E-04	(+/-)	(+/-)	0.004	0.003	(+/-)
r2	0.986388	0.001	S(Y)	r2	0.014	0.004	S(Y)
Para C-H							
SLOPE	0.0073671	0.005	INT				
(+/-)	0.0069011	0.005	(+/-)				
r2	0.3629763	0.007	S(Y)				

*No observed extent of deuteration >2% for any position during the initial rate window

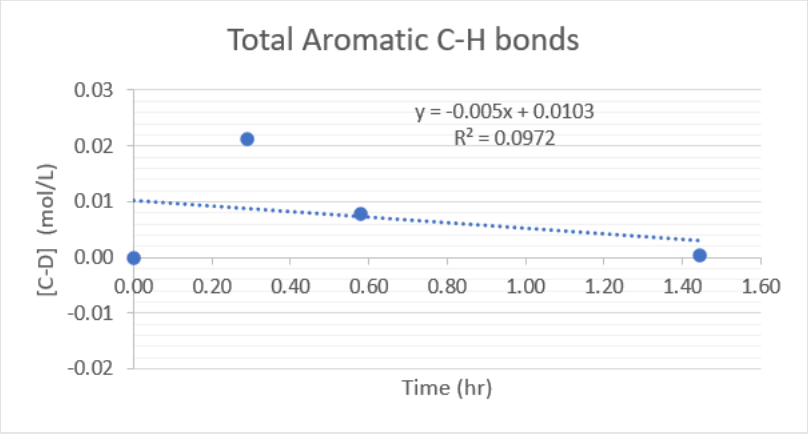

Figure S2.7b. Initial rates of reaction (2.1) in the absence of **1** with N,N dimethylaniline substrate at 80 °C.

Initial Rate Data for Fluorobenzene

			Density	Volume	Concentration
[LPt(H2O)], mg			g/mL	mL	M
4.9		TFE + 150 mM D2O	1.384	0.45	12.50
		Fuorobenzene	1.025	0.05	1.07
Temperature (C)	80				

[1.5] = 0.0182 M (0.34% catalyst loading)

	Meta C-H			Para C-H			
SLOPE	0.055607	0.024329413	INT	SLOPE	0.024350541	0.01121	INT
(+/-)	0.008114	0.026950842	(+/-)	(+/-)	0.004206413	0.013971	(+/-)
r2	0.959153	0.032042603	S(Y)	r2	0.943680159	0.016611	S(Y)

	Ortho-C-H		
SLOPE	0.027199532	0.011392	INT
(+/-)	0.00449918	0.014944	(+/-)
r2	0.948115784	0.017767	S(Y)

Expected average statistical extent of deuteration of the substrate aromatic C-H bonds: 70%

The rate constants for the H/D exchange (2.1) catalyzed by complex 1.5 at 80 °C:
ortho-CH bonds, $k_{c,o}$ = 0.70±0.12 M^{-1} h^{-1};
para-CH bonds, $k_{c,p}$ = 1.3±0.2 M^{-1} h^{-1};
meta-CH bonds, $k_{c,m}$ = 1.43±0.06 M^{-1} h^{-1}.

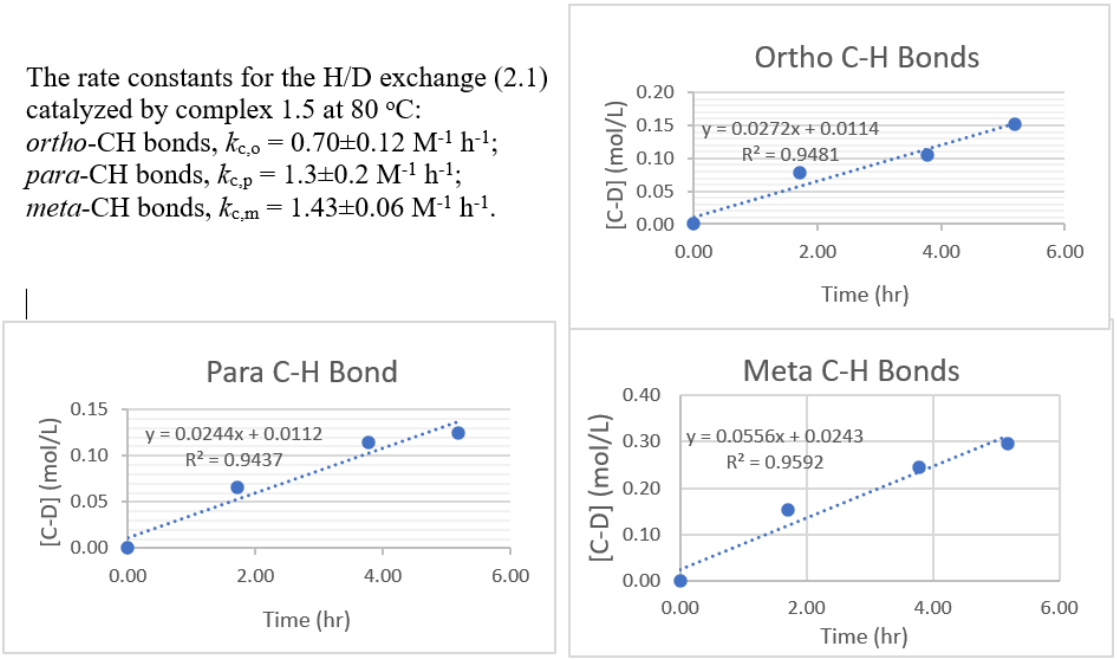

Figure S2.8. Initial rates of reaction (2.1) catalyzed **by 1.5** with fluorobenzene substrate at 80 °C.

Initial Rate Data for Phenol

			Density	Volume	Concentration
[LPt(H2O)], mg			g/mL	mL	M
6.5		TFE + 150 mM D2O	1.384	0.45	12.50
		Phenol	1.070	55.60	1.31
Temperature (C)	80				

[1.5] = 0.0242 M (0.37% catalyst loading)

	Meta C-H			Ortho/Para C-H			
SLOPE	0.464065	0.003032	INT	SLOPE	0.469960272	0.01687	INT
(+/-)	0.026261	0.008442	(+/-)	(+/-)	0.068470039	0.02201	(+/-)
r2	0.990485	0.009934	S(Y)	r2	0.940132752	0.02590	S(Y)

Expected average statistical extent of deuteration of the substrate aromatic C-H bonds: 66%

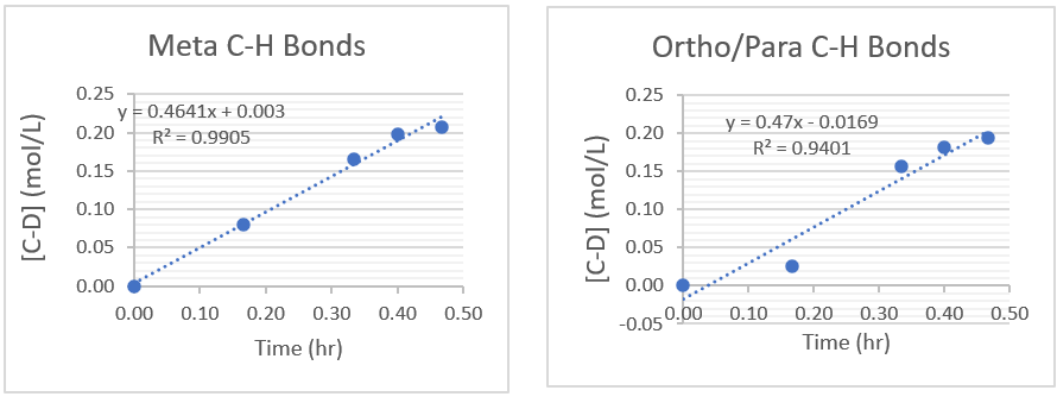

Figure S2.9. Initial rates of reaction (2.1) catalyzed by 1.5 with phenol substrate at 80 °C.

The rate constants for the H/D exchange (2.1) catalyzed by complex 1.5 at 80 °C:
ortho-, *para*-CH bonds, $k_{c,o\text{-}p}$ = 4.9±0.7 M^{-1} h^{-1};
meta-CH bonds, $k_{c,m}$ = 7.3±0.4M^{-1} h^{-1}.

Initial Rate Data for Chlorobenzene

			Density	Volume	oncentratic
[LPt(H2O)], mg			g/mL	mL	M
3.7		TFE + 150 mM D2O	1.384	0.45	12.50
		Chlorobenzene	1.110	0.05	0.99
Temperature (C)	80				

[1.5] = 0.0138 M (0.28% catalyst loading)

Expected average statistical extent of deuteration of the substrate aromatic C-H bonds: 72%

	Ortho C-H				Meta C-H		
SLOPE	0.062190308	0.00726247	INT	SLOPE	0.089307792	-0.00025	INT
(+/-)	0.007670177	0.010612205	(+/-)	(+/-)	0.00530669	0.007342	(+/-)
r2	0.97047567	0.012151374	S(Y)	r2	0.992987986	0.008407	S(Y)

	Para C-H		
SLOPE	0.037508	0.012263	INT
(+/-)	0.011259	0.015577	(+/-)
r2	0.847312	0.017836	S(Y)

The rate constants for the H/D exchange (2.1) catalyzed by complex 1.5 at 80 °C:
ortho-CH bonds, $k_{c,o}$ =2.3±0.3M^{-1} h^{-1};
para-CH bonds, $k_{c,p}$ = 2.7±0.8 M^{-1} h^{-1};
meta-CH bonds, $k_{c,m}$ =3.3±0.2M^{-1} h^{-1}

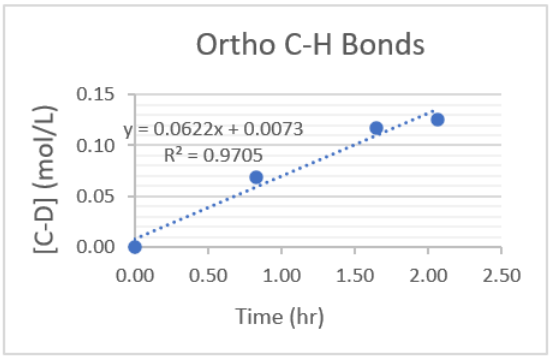

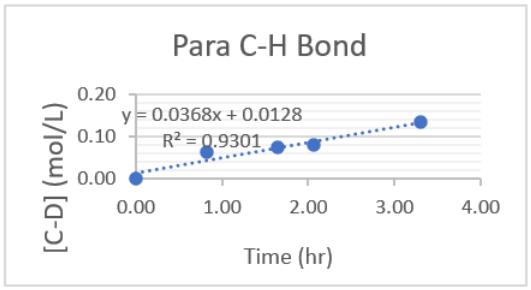

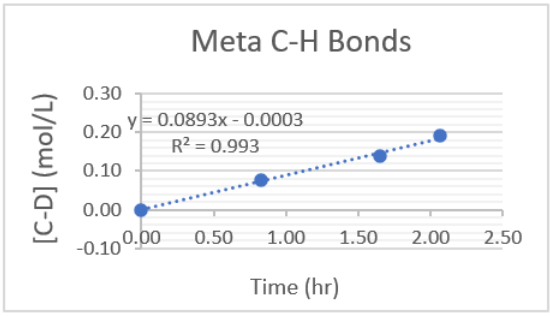

Figure S2.10. Initial rates of reaction (2.1) catalyzed **by 1.5** with chlorobenzene substrate at 80 °C.

Initial Rate Data for Bromobenzene

			Density	Volume	Concentration
[LPt(H2O)], mg			g/mL	mL	M
3.3		TFE + 150 mM D2O	1.384	0.45	12.50
		Bromobenzene	1.500	0.05	0.96
Temperature (C)	80				

[1.5] = 0.0123 M (0.26% catalyst loading)

	Total Aromatic C-H		
SLOPE	0.140064405	0.006635	INT
(+/-)	0.014573858	0.029749	(+/-)
r2	0.968541851	0.038405	S(Y)

Expected average statistical extent of deuteration of the substrate aromatic C-H bonds: 72%

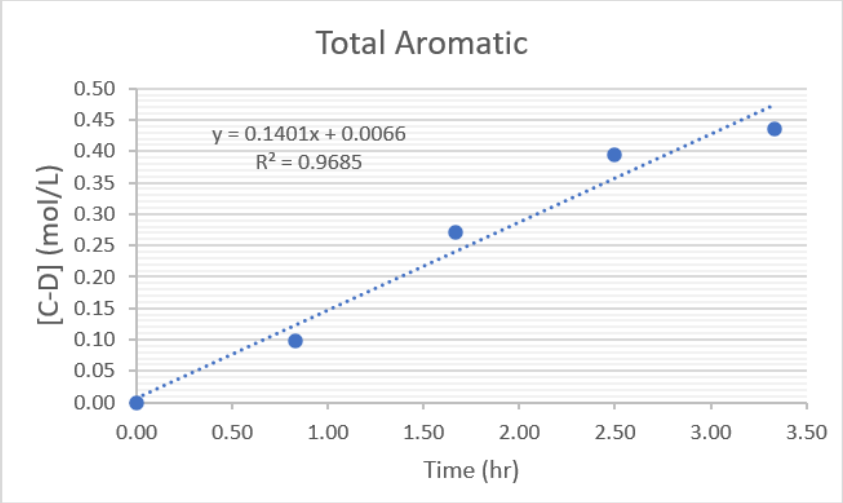

Figure S2.11. Initial rates of reaction (2.1) catalyzed **by 1.5** with bromobenzene substrate at 80 °C.

The average rate constant for the H/D exchange (2.1) catalyzed by complex 1.5 at 80 °C: k_c = 2.4±0.2 M^{-1} h^{-1}.

Initial Rate Data for Nitrobenzene

			Density	Volume	Concentration
[LPt(H2O)], mg			g/mL	mL	M
3.7		TFE + 150 mM D2O	1.384	0.45	12.50
		Nitrobenzene	1.200	0.05	0.98
Temperature (C)	80				

[1.5] = 0.0138 M (0.28% catalyst loading)

Ortho C-H*				Para C-H			
SLOPE	-0.00031	0.005167849	INT	SLOPE	0.012579	0.014079	INT
(+/-)	0.000601	0.006204688	(+/-)	(+/-)	0.004119	0.014517	(+/-)
r2	0.081475	0.010651634	S(Y)	r2	0.823409	0.017899	S(Y)

*No observed H/D exchange

Meta C-H			
SLOPE	0.009338	-0.00611	INT
(+/-)	0.001701	0.005996	(+/-)
r2	0.937743	0.007393	S(Y)

Expected average statistical extent of deuteration of the substrate aromatic C-H bonds: 72%

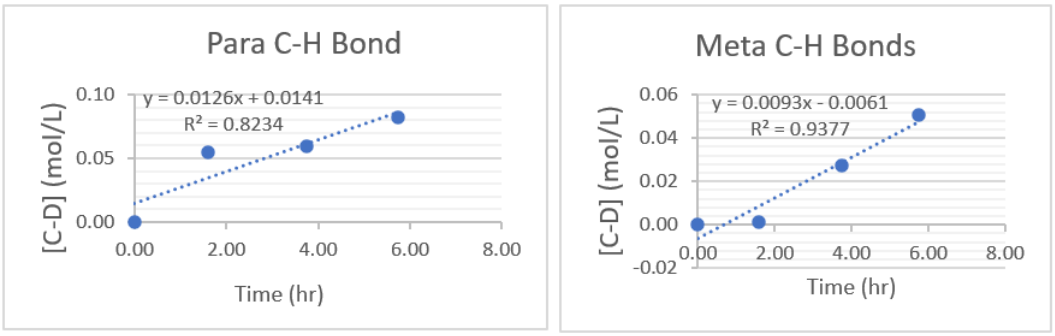

Figure S2.12. Initial rates of reaction (2.1) catalyzed by 1.5 with nitrobenzene substrate at 80 °C.

The rate constants for the H/D exchange (2.1) catalyzed by complex 1.5 at 80 °C:
para-CH bonds, $k_{c,p}$ =0.9±0.3 M^{-1} h^{-1};
meta-CH bonds, $k_{c,m}$ =0.35±0.06M^{-1} h^{-1}.

Initial Rate Data for Benzoic acid

			Density	Volume	Concentration
[LPt(H2O)], mg			g/mL	mL	M
4		TFE + 150 mM D2O	1.384	0.45	12.50
Temperature (C)	80	Benzoic Acid	1.070	22.8 mg	0.41

[1.5] = 0.0149 M (0.73% catalyst loading)

Meta C-H				Ortho/Para C-H			
SLOPE	0.030564906	2E-04	INT	SLOPE	0.014369976	0.00149	INT
(+/-)	0.010237987	0.037	(+/-)	(+/-)	0.001095168	0.003978	(+/-)
r2	0.816729949	0.049	S(Y)	r2	0.988516779	0.005219	S(Y)

Expected average statistical extent of deuteration of the substrate aromatic C-H bonds: 86%

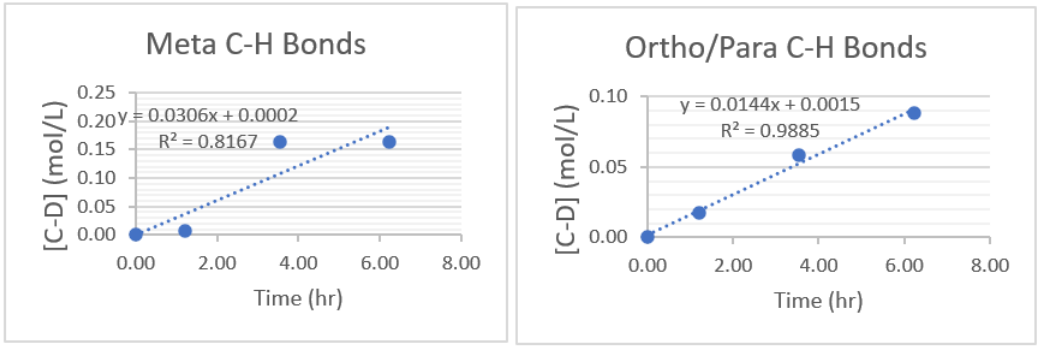

Figure S2.13. Initial rates of reaction (2.1) catalyzed by 1.5 with benzoic acid substrate at 80 °C.

The rate constants for the H/D exchange (2.1) catalyzed by complex 1.5 at 80 °C:
ortho-, *para*-CH bonds, $k_{c,o\text{-}p}$ = 0.78±0.06 M^{-1} h^{-1};
meta-CH bonds, $k_{c,m}$ = 2.5±0.8 M^{-1} h^{-1}.

Initial Rate Data for Thiophene

			Density	Volume	Concentration
[LPt(H2O)], mg			g/mL	mL	M
4.6		TFE + 150 mM D2O	1.384	0.45	12.50
		Thiophene	1.050	0.05	1.25
Temperature (C)	80				

[1.5] = 0.0171 M (0.34% catalyst loading)

Alpha C-H				Beta C-H			
SLOPE	0.781054325	0.0207	INT	SLOPE	0.4300	0.041	INT
(+/-)	0.056242299	0.0188	(+/-)	(+/-)	0.0512	0.021	(+/-)
r2	0.979680725	0.0215	S(Y)	r2	0.9214	0.027	S(Y)

Expected average statistical extent of deuteration of the substrate aromatic C-H bonds: 71%

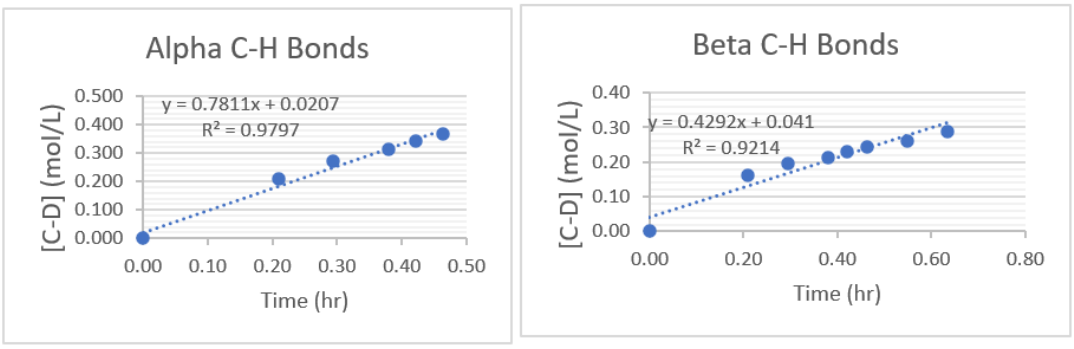

Figure S2.14. Initial rates of reaction (2.1) catalyzed by 1.5 with thiophene substrate at 80 °C.

The rate constants for the H/D exchange (2.1) catalyzed by complex 1.5 at 80 °C:
Alpha-CH bonds, $k_{c,\alpha}$ = 18±1 M^{-1} h^{-1};
Beta-CH bonds, $k_{c,\beta}$ = 10.0±1.2 M^{-1} h^{-1}.

H/D Exchange Data for Indole

			Density	Volume	Concentration
[LPt(H2O)], mg			g/mL	mL	M
4.2		TFE + 150 mM D2O	1.384	0.45	12.50
		Indole	1.170	22.8 mg	0.43
Temperature (C)	80				

[1.5] = 0.0156 M (3.6% catalyst loading)

Expected average statistical extent of deuteration of the substrate β-C-H bonds: 96%

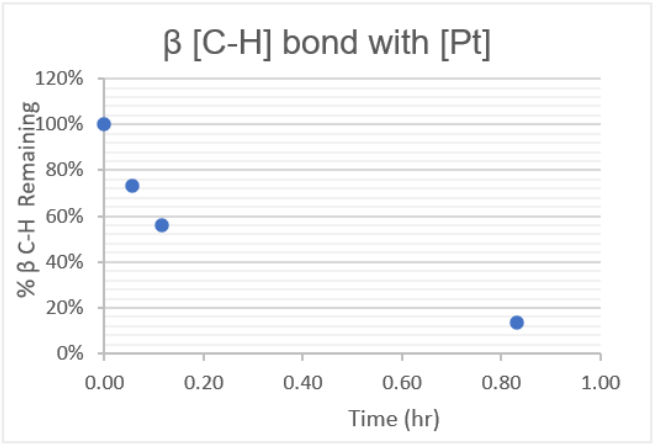

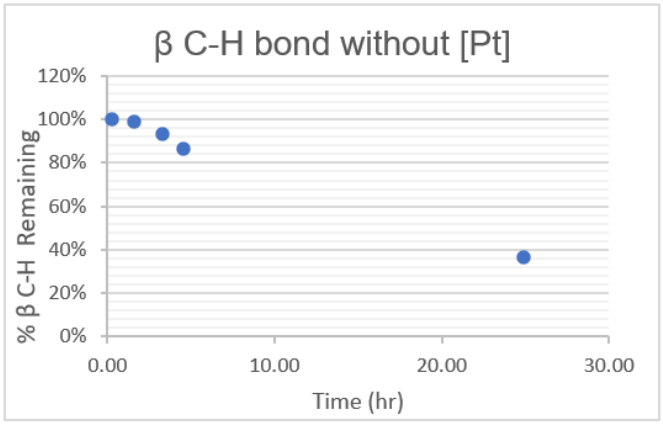

Figure S2.15. β C-H H/D exchange in Indole.

The H/D exchange was observable on indole β C-H in the reaction conditions when **1** was not present. The presence of the catalyst greatly accelerated the rate of reaction. For the reaction catalyzed **by 1.5**, a statistical extent of deuteration was achieved after 0.83 hr, whereas in the system without **1.5** a statistical incorporation of deuterium was not achieved even after 25 hours. An initial rate for the catalyzed system was impossible to calculate due to a very fast reaction / insufficient data points in the initial 10% conversion window.

Initial Rate Data for Benzodioxole

			Density	Volume	Concentration
[LPt(H2O)], mg			g/mL	mL	M
3.5		TFE + 150 mM D2O	1.384	0.45	12.50
		Benzodioxole	1.060	0.05	0.87
Temperature (C)	80				

[1.5] = 0.0130 M (0.37% catalyst loading)

SLOPE	0.292000208	0.022713682	**INT**
(+/-)	0.040659806	0.02221319	**(+/-)**
r2	0.945029354	0.032514439	**S(Y)**

Expected average statistical extent of deuteration of the substrate aromatic C-H bonds: 78%

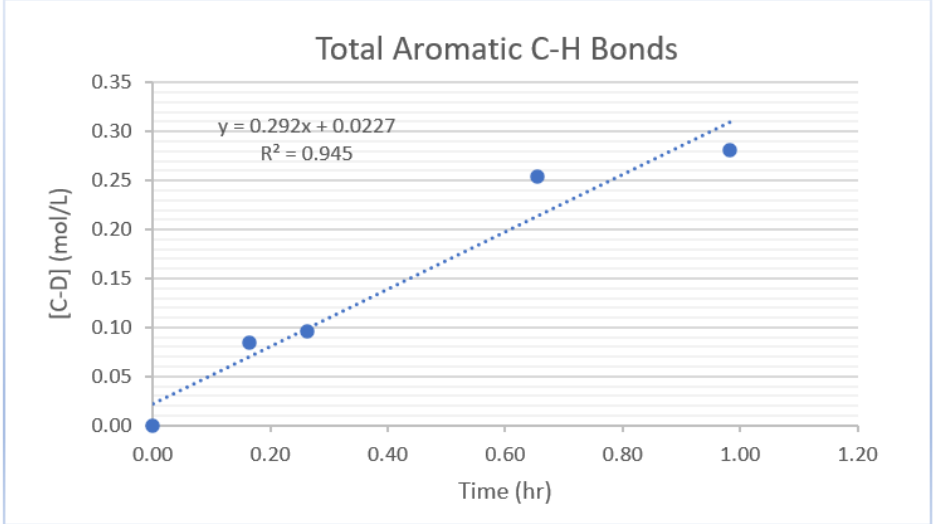

Figure S2.16. Initial rates of reaction (2.1) catalyzed by 1.5 with benzodioxole substrate at 80 °C.

The average rate constant for the H/D exchange (2.1) catalyzed by complex 1.5 at 80 °C: k_c = 6.5±0.9 M^{-1} h^{-1}.

Initial Rate Data for Mesitylene

			Concentration
[LPt(H2O)], mg			M
4		TFE-d1	12.50
		Mesitylene	0.72
Temperature	80		

[1.5] = 0.0149M (0.69% catalyst loading)

	Total Aromatic		
SLOPE	0.016731	0.004351695	INT
(+/-)	0.000503	0.004722057	(+/-)
r2	0.997293	0.008387503	S(Y)

Expected average statistical extent of deuteration of the substrate aromatic C-H bonds: 85%

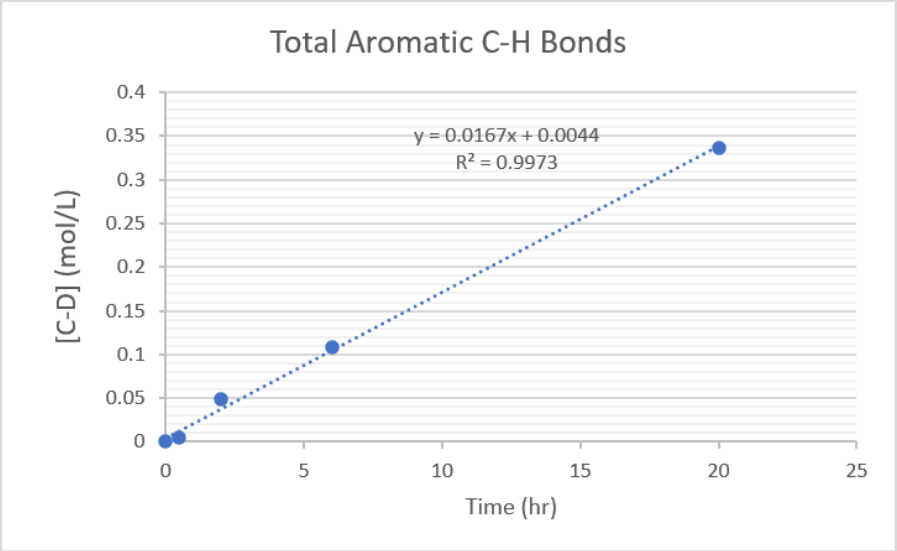

Figure S2.17. Initial rates of reaction (2.1) catalyzed **by 1.5** with mesitylene substrate at 80 °C.

The rate constant for the H/D exchange (2.1) catalyzed by complex 1.5 at 80 °C:
k_c = 0.52±0.02 M^{-1} h^{-1}.

Initial Rate Data for p-xylene

			Concentration
[LPt(H2O)], mg			M
4		TFE-d1	12.50
		p-Xylene	0.81
Temperature (C)	80		

[1.5] = 0.0149 M (0.46% catalyst loading)

	Total Aromatic		
SLOPE	0.181560555	0.07	INT
(+/-)	0.019779069	0.063	(+/-)
r2	0.976814796	0.093	S(Y)

Expected average statistical extent of deuteration of the substrate aromatic C-H bonds: 79%

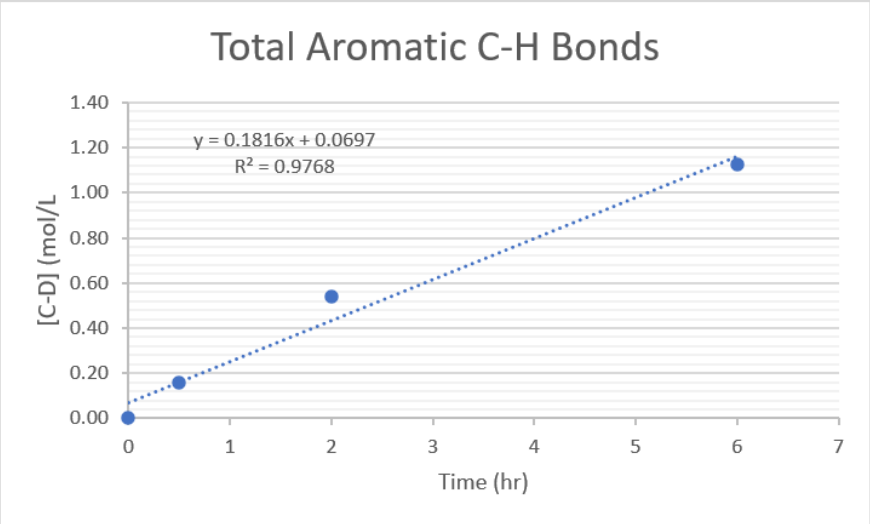

Figure S2.18. Initial rates of reaction (2.1) catalyzed **by 1.5** with *p*-xylene substrate at 80 °C.

The rate constant for the H/D exchange (2.1) catalyzed by complex 1.5 at 80 °C:
$k_c = 3.7 \pm 0.4\ M^{-1}\ h^{-1}$.

Chapter 3: **H/D Exchange Catalysis of Aromatic C-H bonds and TFE-d_1, AcOD-d_4, *and* D_2O Enabled by Covalent Immobilization of a Sterically Rigid Molecular Sulfonated CNN-Pt^{II}-OH_2 Complex**

All experimental work including the original synthetic development of 3.5 and 3.5-FC performed by Morgan Kramer. Crystals of 3.5-FC were obtained by Dr. Jiaheng Ruan and XRD analysis was performed by Dr. Peter Zavalij. Materials characterization including SEM, TEM, and N_2 Sorption was performed by Dr. Matthew Leonard.

3.1. Introduction

There has been steady progress in the field of homogenous transition metal-catalyzed hydrocarbon C-H functionalization over the past 50 years. Specifically, there has been a significant push towards the development of catalysts that are both thermally robust and can provide an economic advantage over their more wide-spread counterparts [75-77] For the case of molecular catalysts, there have been reports of utilizing sterically encumbered diimine ligands for the generation of highly thermally robust Pd^{II} and Pt^{II} dichloro complexes which have a high propensity for the C-H activation of arenes.[24-26] These sterically bulky, and electronically diverse diimine ligands enabled the H/D exchange reaction of arenes under hard reaction conditions with temperatures up to 150^{o}C in TFA-d_1. However, despite this success, these catalysts ultimately still suffer from the same bimolecular deactivation that has been reported for numerous other molecular Pt^{II} catalysts.[33-34,49]

Typically, H/D exchange was used as a mechanistic probe for metal complexes propensity to activate C-H bonds. However, the utilization of transition metal complexes for H/D exchange catalysis has long been neglected, although the synthesis of deuterium enriched materials is often a sought-after process in and of itself. Deuterium enriched materials are often utilized in research as NMR solvents, MS standards, and as chemical mechanistic probes. Expanding outside of the research environment, deuterium labeled substrates are now emerging as the active pharmaceutical ingredients in drugs both in clinical trials and presently on the market.[78] This fact further highlights the importance of the development of more active, economically viable catalysts for the production of deuterium enriched materials.

Presently, there are numerous catalytic systems for the H/D exchange of the C(sp^2)-H bonds which are highly prevalent in pharmaceuticals. [7-8, 80] Previously, our group reported the discovery and the utilization of novel sulfonated CNN-pincer Pt^{II}-OH_2 complexes as the active catalysts for the H/D exchange between TFE-d_1 and aromatic C-H bonds (Figure 1a).

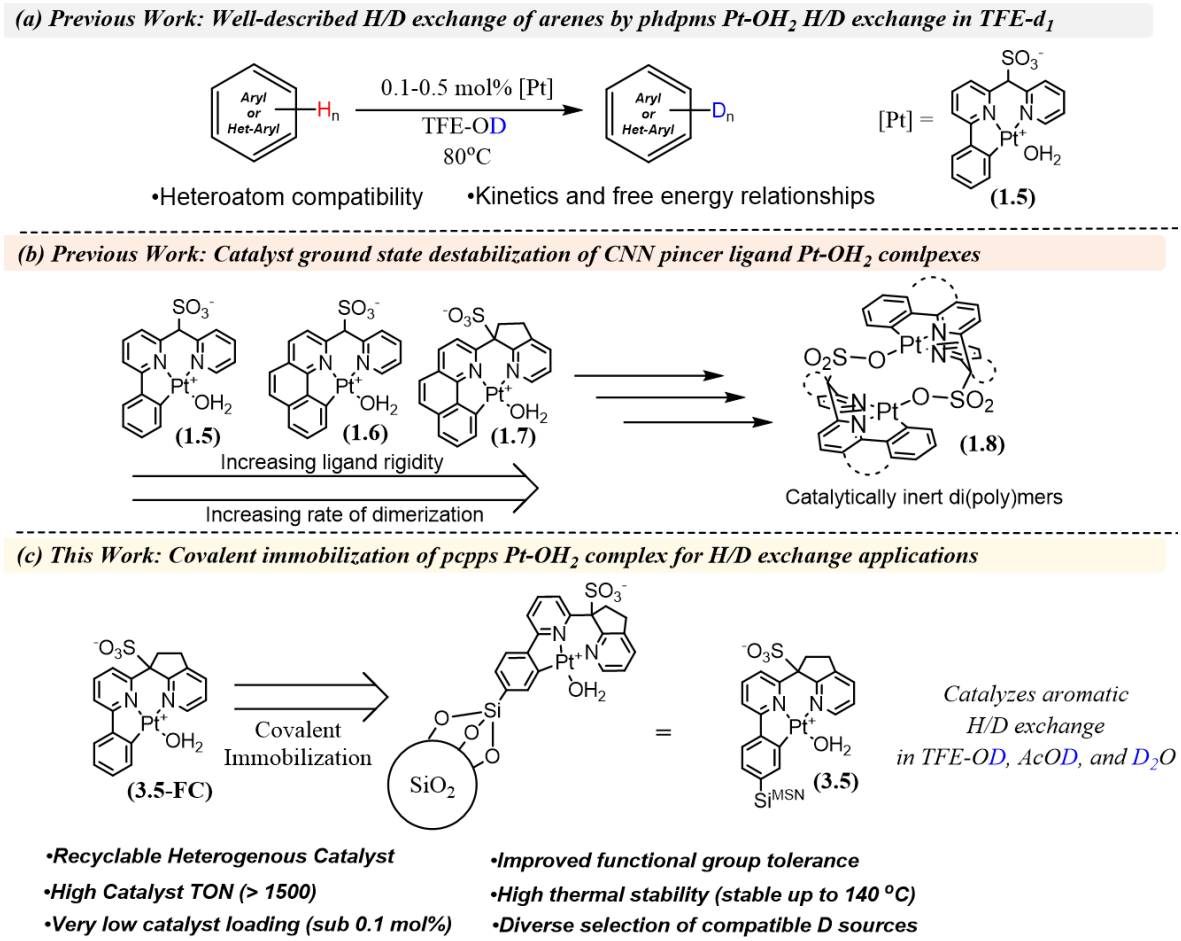

Figure 3.1. Comparison of CNN-Pincer ligand Pt-OH_2 Complexes and the past work motivations for this study.

As described in Chapter 2, our initial efforts utilizing complex **1.5** as a catalyst in reaction (Figure. 3.1, *a*) were focused on the analysis of reactivity of various substituted (hetero)arenes, the reaction regioselectivity with respect to different C(sp^2)-H bonds, and functional group compatibility of this catalytic system.[49] In the course of these studies some

important limitations of the system were revealed: i) strongly coordinating groups such as sulfonamides, pyridines, and nitriles were incompatible with **1.5**, ii) the reactivity of electron poor arenes was very low and iii) at reaction times exceeding a few hours a bimolecular deactivation of **1.5** to yield **1.8** (a proposed structure is shown in Figure 3.1, *b*) greatly inhibited the catalyst's activity.

To accelerate the catalytic H/D exchange, some similar sulfonated CNN pincer ligand complexes **1.6** and **1.7** were designed and their reactivity studied computationally (Figure 3.1, *a* and 3.1, *b*).[33,49] The reactivity of complexes **1.6** and **1.7** in C-H activation of arenes was predicted computationally to increase in the series **1.7 > 1.6 > 1.5**. The addition of the fused benzene **(1.6)** and fused cyclopentane **(1.7)** fragments onto these ligand scaffolds led to a progressive destabilization of the calculated Pt^{II}-OH_2 bond strength, thereby reducing the relative height of the barrier for C-H activation. While the expected reactivity trend was experimentally confirmed in H/D exchange reactions of benzene in TFE-d_1 solutions with **1.5 – 1.7** as catalysts, the rate of a competitive catalyst deactivation to form di(poly)nuclear species such as **1.8** also increased in the same sequence. As a result, a low steady state concentrations of **1.6** and **1.7** in reaction mixtures could only be used so making the application of **1.6** and **1.7** in H/D exchange catalysis even less practical than the use of the parent catalyst **1.5**. Therefore, in order to effectively exploit the enhanced reactivity of **1.7** the bimolecular deactivation pathway to yield catalytically inert **1.8**, must be removed. Our strategy for achieving this goal is a covalent immobilization of one of our Pt^{II} catalysts.

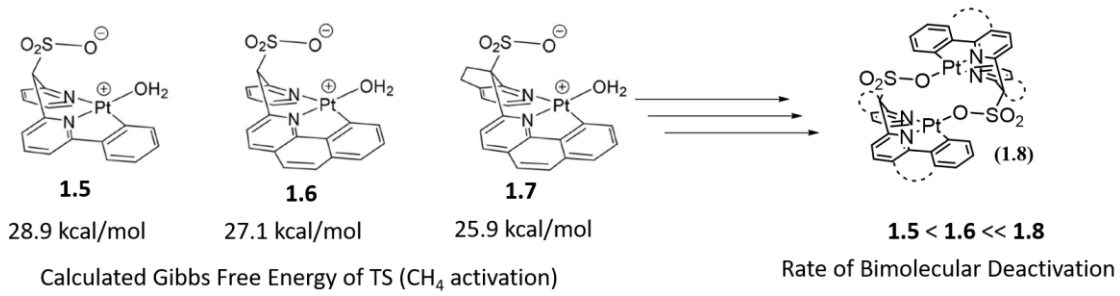

Figure 3.2. Comparison of Pt^{II}-OH_2 complexes computationally predicted $\Delta G^{\#}$ for the C-H activation of CH_4 in the gas phase at 80°C and the corresponding rates of dimerization.

Previously our group has shown that immobilization of a sulfonated dipyridinemethanesulfonate Pt^{II} complex on mesoporous silica nanoparticles (MSN) allowed for an about 1000-fold enhancement of its catalytic activity in olefin epoxidation with O_2.[34] In turn, we anticipated that the immobilization of **1.7** on MSN may be far too challenging synthetically. At the same time, our computational studies showed that the benzoquinolyl fragment in **1.7** was only a minor contributor to the enhancement of a Pt^{II} center reactivity in this complex, as compared to that in **1.5**. [51] In turn, the presence of a fused cyclopentene ring in **1.7** was shown computationally to have the major effect on the rate of H/D exchange. In this Chapter we present the covalent immobilization of a molecular complex, **3.5** that was predicted computationally to be similarly active as **1.7** (Figure. 3.1, *c* and 3.3).

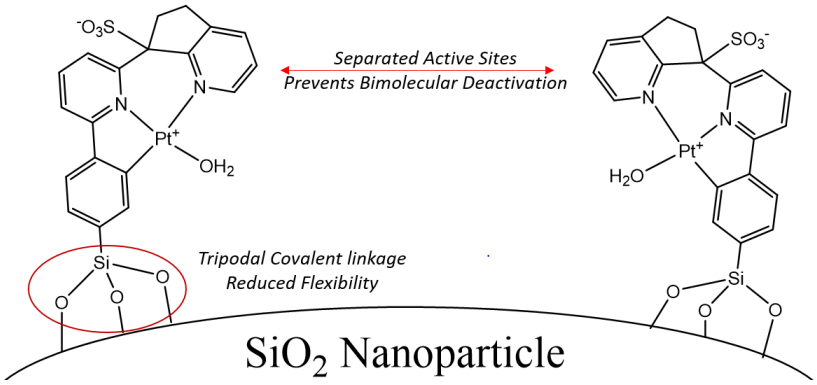

Figure 3.3. Illustration of the surface dilution effect and tripodal immobilization strategy for MSN supported **3.5**.

We speculated that if we preserve the fused cyclopentane fragment present in **1.7** and maintain the modularity of the phenylene fragment from **1.5**, then we will have the necessary combination of enhanced reactivity in the H/D exchange, and synthetic modularity required to covalently immobilize the molecular complex to generate **3.5** (Figure 3.1c). The advantages that complex **3.5** has over the free complexes **1.5-1.7** is that bimolecular deactivation would be eliminated altogether. Based on the concentration of **3.5** on the mesoporous silica nanoparticle surface, there would be virtually no active Pt^{II} centers within an appropriate distance from the sulfonate on the most proximal active site to coordinate to (Figure 3.3). Furthermore, the tripodal silicate functionality at the base of the complex removed additional degrees of freedom that might allow Si(OH)-to-Pt^{II} interactions that may have plagued other similar MSN supported catalysts in the past.[34]

3.2. MSN-immobilization of a Novel Sulfonated Pre-ligand

3.2.1 Synthesis of a Si(OEt)$_3$-substituted Sulfonated Pre-ligand

Our strategy for the synthesis of our new MSN-supported catalyst **3.5** has a similar design to a previous catalyst reported by our group.[34] It has been reported that the -Si(OEt)$_3$ moiety is a useful motif for the anchoring of molecular ligands onto the surface of MSNs (Scheme 3.1). [34, 81-82]

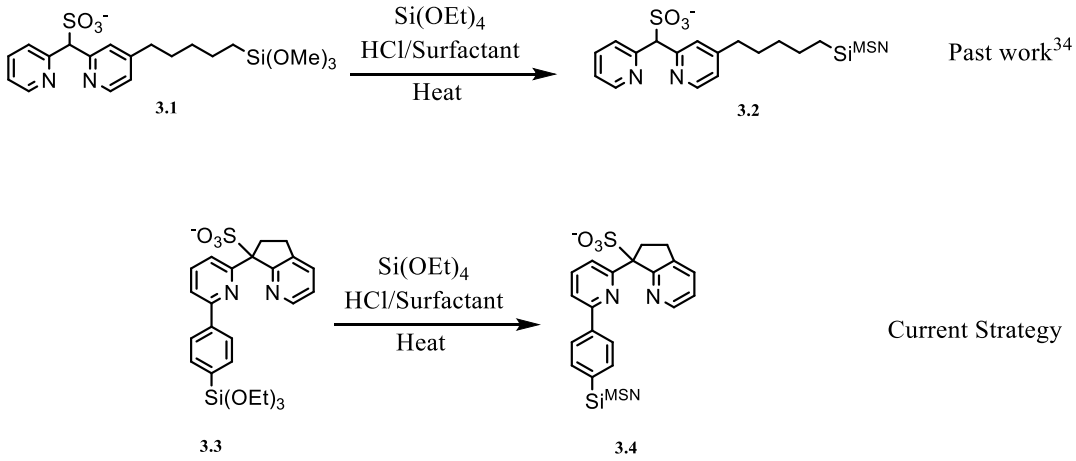

Scheme 3.1. Synthetic strategy for the production of **3.4** and past strategies for covalent ligand immobilization[34]

In a prior report from our group,[34] a 6-(Si,Si,Si-trimethoxy)silahexyl group was used for incorporating a sulfonated dipyridinemethanesulfonate (dpms) ligand **3.1,** into MSN to yield the immobilized ligand, **3.2.** (Scheme 3.1, top). The resulting silahexyl tether is flexible and may have allowed for a Si(OH)-Pt^{II} coordination in the resulting catalyst and the catalyst deactivation. In fact, the catalyst deactivation was experimentally observed, and the catalyst could be used for a single run only. To avoid a potential Si(OH)-Pt^{II} coordination of our new MSN-immobilized Pt^{II} catalyst and the catalyst deactivation, we needed to use a very rigid anchoring group. Hence, instead of using of alkyl chains with

terminal $Si(OR)_3$ groups for tethering of a molecular pre-ligand, we decided to use a direct silicate linkage for this purpose.

With this selection of a tether, we faced another challenge since our past synthetic strategy for the synthesis of pre-ligands necessary for the preparation of **1.7** (shown in Scheme 3.2) was not applicable due to its incompatibility with a $Si(OMe)_3$ group.

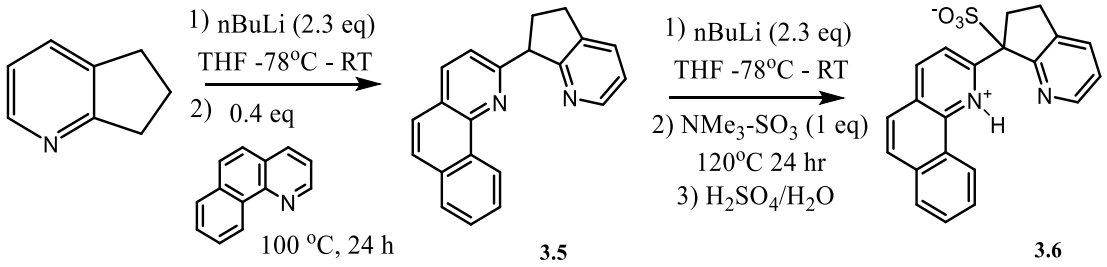

Scheme 3.2. Past synthetic strategy for the generation of cyclopenteno-fused sulfonated CNN pincer ligands

Both the assembly of the pre-ligand core, **3.5** and the sulfonation to yield a pre-ligand **3.6** involve relatively harsh reaction conditions that are not compatible with a -$Si(OR)_3$ functional group pre-installed. With these considerations in mind, a new synthetic approach for the synthesis of our new pre-ligand was developed (Scheme 3.3). Our strategy targets **3.10** as a desired brominated pre-ligand precursor which is next silylated.

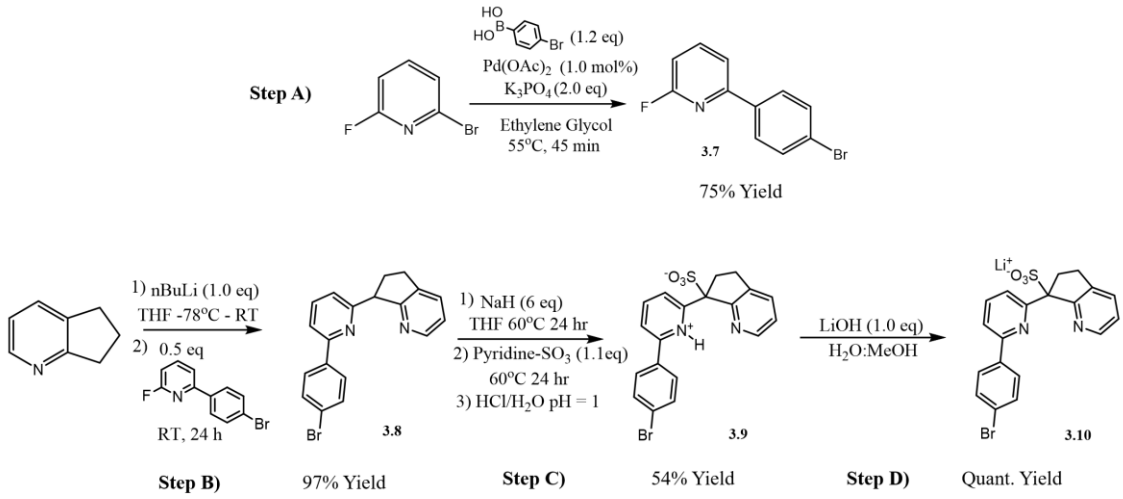

Scheme 3.3. Synthetic scheme for the production of the pre-ligand **3.10. Step A)** Suzuki coupling. **Step B)** Nucleophilic aromatic substitution of a fluoropyridine **Step C)** Reduced temp benzylic sulfonation **Step D)** Cation exchange.

The advantages to the synthetic strategy highlighted in Scheme 3.3 are multifaceted. Step A allows for the installation of a substituted phenyl fragment to the pyridyl core, which is of critical importance for the immobilization step of our pre-ligand, as well as for the preparation of various benzene core-substituted analogs of our pincer ligands that will be explored next in Chapter 4. In the syntheses of **3.1**-**3.3**, the phenylene fragment was not modular, and was already attached to a quinoline or a pyridine core. The assembly of the dipyridyl methane fragment was done via a fluoride nucleophilic substitution involving a pyridylalkyl anion and a fluoropyridine **3.7** (Step B) which is generally high yielding and can be performed at room temperature. Step C is a significant improvement over past syntheses that utilized ^{n}BuLi – deprotonated alkylpyridines. First, the new reaction no longer requires the use of nBuLi, which would engage in a competitive transmetallation reaction that would destroy the Ar-Br moiety in **3.8**. Instead, a suspension of NaH in THF is used to deprotonate **3.8**. As a result of using organosodium intermediates, their sulfonation can be performed at a significantly lower temperature, 60 ^{o}C vs. 120 ^{o}C,

also improving the functional group compatibility of this synthetic approach. The new compounds **3.7 – 3.10** were characterized by means of ^{1}H and ^{13}C NMR spectroscopy and, for the anionic compound **3.10**, by ESI-MS(-). The major ^{1}H-NMR signal used as a diagnostic was *ortho*-pyridyl C-H virtual doublet for compounds **3.8** and **3.9.** For the unsulfonated preligand, **3.8,** the *o*-pyridyl resonance was a doublet at 8.36 ppm in $CDCl_3$ and a doublet at 8.25 ppm in DMSO-d_6. Upon sulfonation, the product, **3.10**, was insoluble in $CDCl_3$ and had an *o*-pyridyl resonance at 8.75 ppm which showed a substantial downfield shift compared to its unsulfonated counterpart. Due to its anionic natures, ESI-MS was used to characterize the product in MeOH. The expected m/z ratio for **3.10** was 428.99 with the characteristic isotopic distributions associated with a Br atom. We found that the experimental m/z for **3.10** to be 428.81 also with strong signals at 430.85 which is characteristic of two roughly equal Br isotopic contributions. For more details on ^{1}H and ^{13}C NMR spectroscopy of **3.10** see the supporting information. The pre-ligand **3.11** was prepared and fully characterized by us in an earlier work.[64] (For more information and specific experimental details see the Supporting Information).

The final step of the preparation of $Si(OR)_3$ – substituted pre-ligand **3.3** was achieved by reacting **3.10** with $^{n}BuLi$ and an *in situ* quenching of a resulting aryllithium intermediate with $Si(OEt)_4$ at -78 ^{o}C to yield a mixture of **3.3**, and **3.13-3.14** with **3.3** being the major product (Scheme 3.4). Notably, **3.11**, a product of dehalogenation of **3.10** is observed in significant amounts.

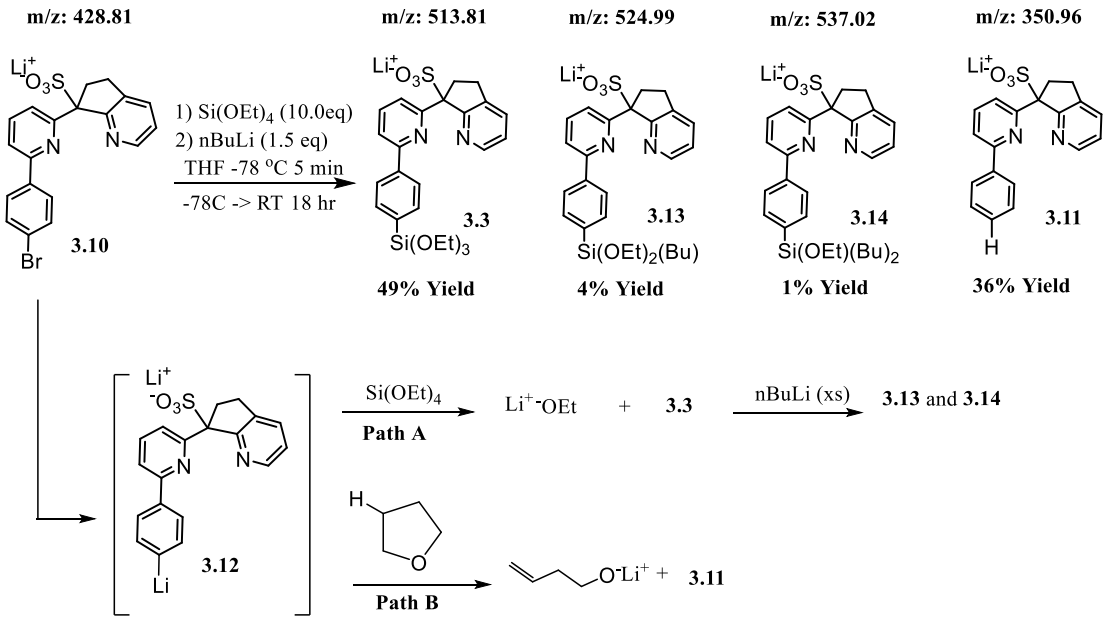

Scheme 3.4. Silylation reaction for the conversion of **3.10** to **3.12-3.14**. Path A) Silylation reaction of **3.12** with $Si(OEt)_4$ to yield **3.3** and side products. Path B) Ring opening alkoxides elimination reaction of THF.

The general silylation reaction was adapted from the published procedure of lithiation of aryl bromides.[83-85] For specific reaction details, see the Supporting Information. The reaction shown in Scheme 3.4 generates **3.3** and **3.13-3.14** from **3.10** in a single pot. Our attempts to carry the silylation stepwise by performing a transmetallation with ^{n}BuLi first, and combining it with $Si(OEt)_4$ next, resulted in comparable yields of the target compound **3.3**. Overall, the solubility of the starting material, **3.10** and the stability of the generated intermediate, **3.12**, were considered when developing these synthetic methods. Generally, these reactions yielded nearly equal quantities of **3.11** and **3.3**. The reaction performance in this case is, most likely, due to a high reactivity of an expected very basic anionic aryllithium intermediate **3.12** that reacted with the solvent (THF) to form **3.11** and a lithium alkoxide (Scheme 3.4, path B). In turn, when 10.0 equ of $Si(OEt)_4$ is

present in the reaction mixture, the intermediate **3.12** can concurrently attack $Si(OEt)_4$ to form **3.3** and the THF solvent to form an elimination product and **3.11**. Our optimization of the reaction conditions showed that the use of 10.0 equ of $Si(OEt)_4$ allows for the best yield of **3.3**. The use of larger amounts of $Si(OEt)_4$ (40.0 eq) leads to the precipitation of **3.10** and the transmetallation of **3.10** to **3.12** does not occur readily.

During our reaction optimization study the products distribution was monitored primarily through ESI-MS(-) using MeOH solutions resulting from MeOH quenching of sampled reaction mixtures. After an allotted reaction time, 5 distinct species were observable. Typically, some amount of the starting material **3.10** was detected even when excess nBuLi was used. This is likely due to the one-pot design, where nBuLi can also act as a nucleophile towards the excess $Si(OEt)_4$ or as a base towards THF. The presence of **3.13** and **3.14** in this reaction pot affirm this possibility. Finally, **3.11** was always detected, and it is the major byproduct of the silylation reaction. The products distribution can be controlled to some extent to favor the **3.3** when the concentration of $Si(OEt)_4$ is sufficiently high. However, **3.10** precipitates from such solutions leading to poor conversions of **3.10**. Alternatively, by using a faster addition of **3.10** / ^{n}BuLi mixture to $Si(OEt)_4$ to minimize possible side-reactions, a two-pot approach for the preparation of **3.3** was shown to be similarly effective (see supporting information for more details).

Separation of **3.3** proved to be quite challenging. Due to its sensitivity to water and bases, our typical aqueous work up methods were not usable. Instead, after removal of THF, **3.3** and **3.13-3.14** and excess $Si(OEt)_4$ were extracted from so-produced residues with Et_2O. The separation of the the salt-like pre-ligands from of $Si(OEt)_4$ was achieved by a

subsequent hexane extraction. The crude **3.3** contaminated with **3.13** and **3.14** was used without further purification in co-condensation with $Si(OEt)_4$.

3.2.2 Immobilization of the novel $Si(OEt)_3$-substituted Pre-ligand on MSN

With a crude **3.3** in hand, we moved to covalently immobilize the target pre-ligand using a condensation reaction between **3.3** and $Si(OEt)_4$ in an aqueous surfactant solution (Scheme 3.5).

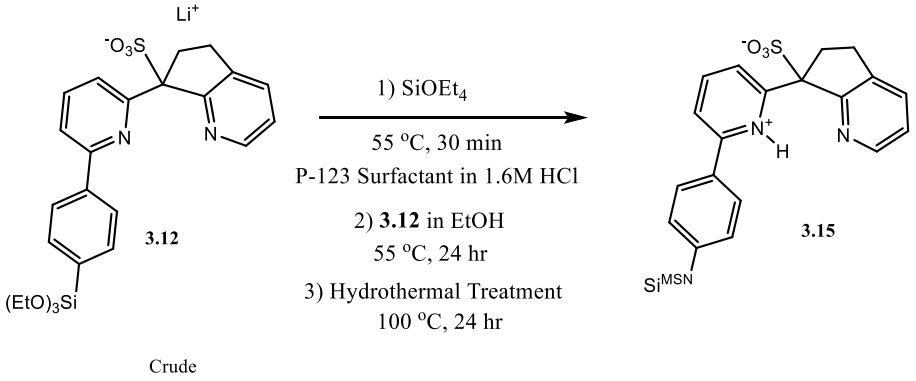

Scheme 3.5. The covalent immobilization of **3.3** on MSNs.

A procedure for co-condensation of various hydrocarbylsilicates and $Si(OR)_4$ to form derived MSNs has been previously reported for similar systems.[34] The process first involves the dissolution of 2.3g of P-123 surfactant (ethylene oxide/propylene oxide co-oligomer) into 100 mL of a solution of 1.6M HCl at 55 °C for 2 hours under rapid stirring and the formation of a well-defined surfactant micelles. Then, 4.8g of a neat $Si(OEt)_4$ is added to the reaction mixture. Due to the hydrophobicity of $Si(OEt)_4$, the compound is solubilized by entering the hydrophobic cavities of the micelles. In turn, the acidic aqueous environment promotes an initial condensation of $Si(OEt)_4$ to form MSN. This condensation reaction is allowed to proceed for an additional 30 minutes in order to allow for the nanoparticle formation to get underway. Then, a solution containing 225 mg of crude **3.3**

in 10 mL EtOH is added to the reaction pot and the solution is allowed to react overnight at 55 ^{o}C. This prolonged reaction time ensures the complete condensation of all alkoxysilane species. After this was complete, the silica-bound product **3.15** was filtered and rinsed thoroughly with water to removed surfactant, then was heated to 100^{o}C in 1.6M HCl for 24 hours. Then, the precipitate was filtered away from the solution and added to 250 mL beaker followed by 100 mL of EtOH. The beaker was then warmed to 60^{o}C and the solution was stirred for 2 hours. The powder was isolated via filtration and the washing procedure was repeated 3 times with 100 mL of EtOH. The powder was collected via filtration and dried in a vacuum oven at 100 ^{o}C for 24 hr to yield 1.78 g of light brown powder. The liquid phase containing all soluble materials was subsequently analyzed via ESI-MS under negative mode conditions. The resulting spectrum showed no silicon containing ligand species, thereby indicating that all silylated compounds **3.12-3.14** became incorporated into the solid.

To further quantitatively evaluate the ligand loading and incorporation of the pincer pre-ligand from **3.3**, **3.13-3.14** into the MSN structure, a KOH digest in D_2O was performed on a small sample to completely homogenize **3.15** and produce water-soluble **3.15-Digest** (Scheme 3.6). First, 22.2 mg of **3.15** was combined with 4.0 mL of a D_2O solution containing 176.1 mg of KOH. The mixture was allowed to stir at room temperature for 30 minutes to form a colorless solution. Then, 2.0 µL of 1,4-dioxane was added as an internal standard for quantitation. The solution was then transferred to an NMR tube for ^{1}H NMR analysis. Based on the NMR data, the material contained immobilized CNN-pincer ligand at a concentration of 0.243 mmol/g. A similar digestion in KOH/H_2O mixture was used to

prepare deuterium-free samples of **3.15-Digest** suitable for ESI-MS(-) analysis. The observed signal matched a software-simulated one for the anionic part of **3.15-Digest**.

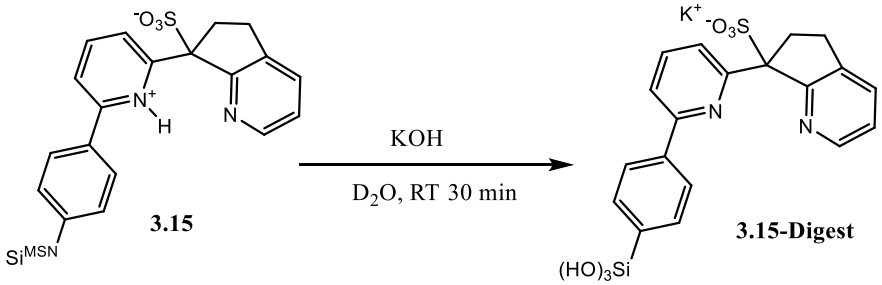

Scheme 3.6. KOH digest of **3.15** for the purpose of quantitation of ligand loading and validation of immobilization.

3.2.3 Synthesis of Molecular and MSN-immobilized Pt^{II} Aqua Complexes

With the success of our immobilization strategy to generate an immobilized pre-ligand species, **3.15**, and our quantitative assessment of the ligand loading now known, we moved towards the metalation of the ligand species. For method validation, the molecular complex **3.5-FC** was prepared first (Scheme 3.7, top), followed by the preparation of its MSN-immobilized analog **3.5** (Scheme 3.7, bottom).

3.2.4 Synthesis of a Novel Molecular Pt^{II} Complex

The preparation of the molecular pre-ligand **3.11** (Scheme 3.7, top), its cyclometallation to form an intermediate Pt^{II} chloro complex **3.16-FC** (Scheme 3.7, bottom) was recently reported by us.[64] The compounds **3.11** and **3.5-FC** were fully characterized by ^{1}H and ^{13}C NMR spectroscopy and ESI-MS(-). The metallation of molecular pre-ligand **3.11** was performed using 1 equivalent of K_2PtCl_4 as a metallating agent dissolved in 3:2 (vol) H_2O : AcOH mixture at 100 ^{o}C; these conditions are similar to those used for the synthesis of **1.5**.[33]

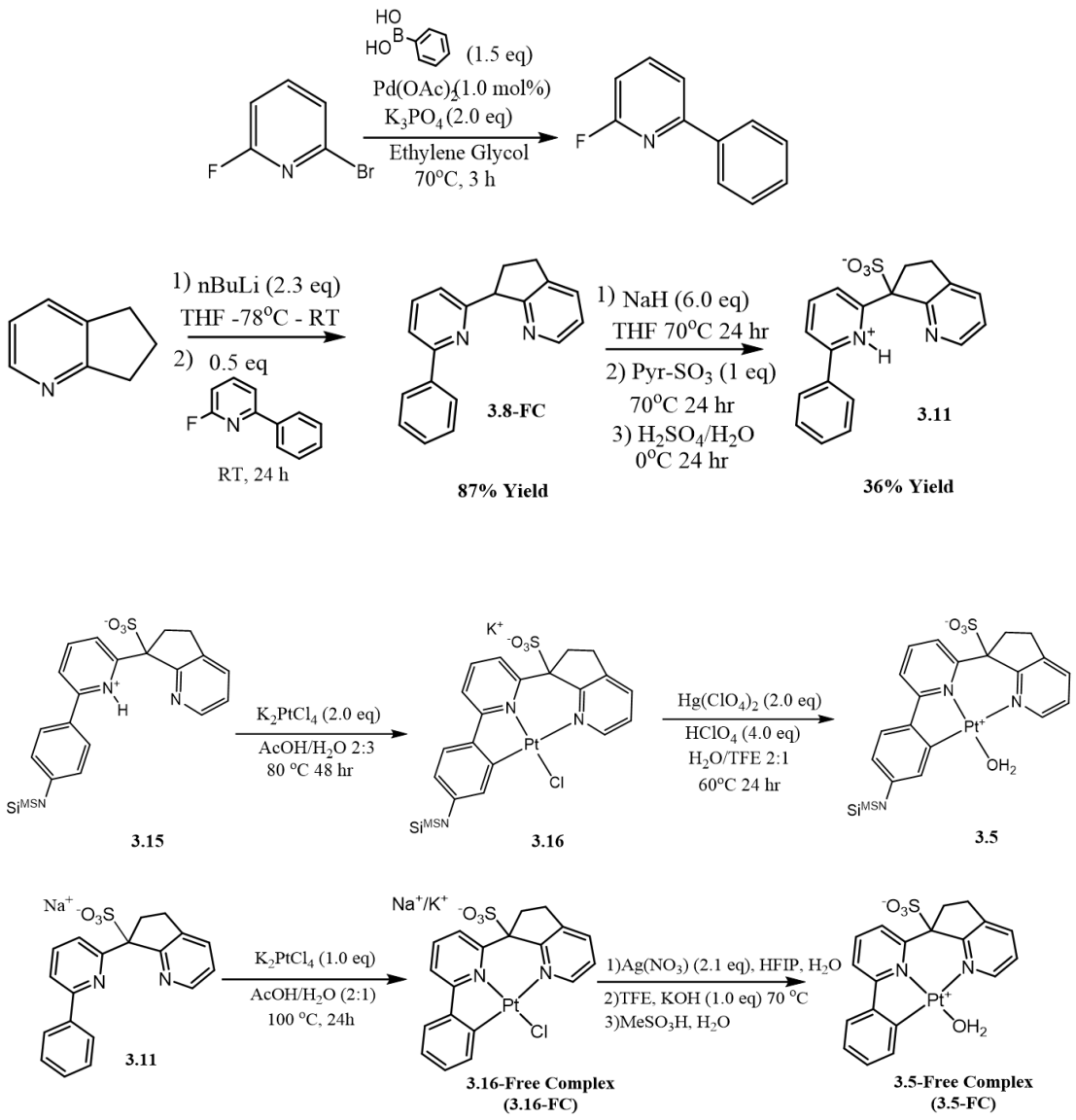

Scheme 3.7 (**Top)** Synthesis of a molecular pre-ligand **3.11. (Bottom)** Metalation and subsequent ligand exchange of free and immobilized complexes.

The synthesis of **3.5-FC** is largely analogous to our previously described synthesis of **1.5** reported in the literature.[33, 49] However there are a few modifications that were made in order to better model the eventual synthesis of the 4-Br substituted ligand species **3.15.** Starting with the initial Suzuki coupling, we generated 2-fluoro-6-phenyl pyridine from the Suzuki coupling reaction between 2-Bromo-6-fluoro pyridine and phenyl boronic acid.

Previously, the synthetic strategy had a methyl group in the 2-postion, which was then deprotonated with nBuLi and coupled to a fluoropyridine. However, in Scheme 3.5, we aimed to minimize the contact time between the phenylene core and nBuLi in attempt to best mimick the ideal reaction conditions when the phenyl core bears a Br atom. Next, 6,7-dihydro-5*H*-cyclopenta[*b*]pyridine was deprotonated with nBuLi/THF which was then used as a nucleophile to attack 2-fluoro-6-phenyl pyridine and generate the unsulfonated pre-ligand **3.8-FC**. Then the new sulfonation procedure that was developed for **3.10** was applied utilizing a two-step synthesis with the deprotonation of the methylidine C-H bond by NaH, followed by the low temperature sulfonation by the pyridine-sulfur trioxide complex. For specific synthetic details and spectroscopic information see the supporting information. The new homogenous Pt complexes **3.16-FC** and **3.5-FC** were synthesized via an identical procedure to the one reported in the literature to produce **1.5**.[34, 49] A single crystal of **3.5-FC** was grown by Jiaheng Ruan, a graduate student in our group, and the crystal was characterized by X-ray diffraction (Figure. 3.4).

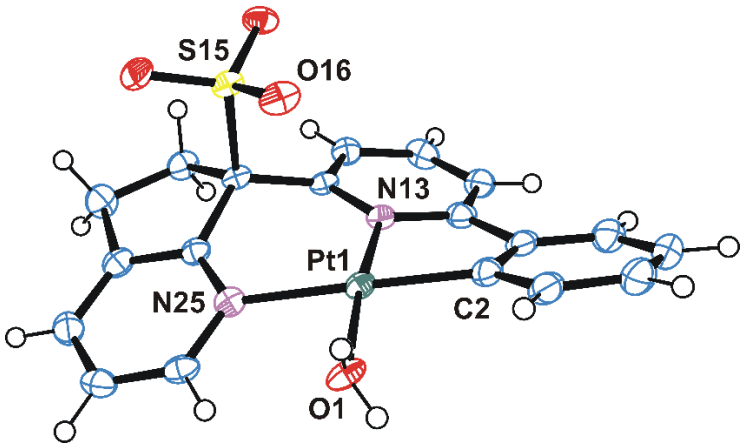

Figure 3.4 ORTEP drawing (50% probability ellipsoids) of **3.5-FC**.

3.2.5 Synthesis of an MSN-immobilized Pt^{II} Aqua Complex

Metalation of **3.15** was performed under conditions that were similar to those used for the preparation of **3.16-FC** (Scheme 3.7),[34, 49] as well as other sulfonated CNN-pincer ligand – supported Pt^{II} complexes.[33,34,51] Due to the heterogeneous nature of the reaction, the cyclometallation step may be expected to be much slower than for **3.11**. In turn, the use of higher than 100 ^{o}C temperatures and/or prolonged reaction times for the cyclometallation of **3.15** could lead to a possible undesirable bimolecular disproportionation of K_2PtCl_4 into Pt(0), KCl and K_2PtCl_6. As such, for the preparation of **3.16** milder reaction conditions were used. The metalation of **3.15**, as compared with that of **3.11** (Scheme 3.7), employed: i) the increase of K_2PtCl_4 amount to 2.0 eq to accelerate the metalation reaction, ii) the use of more dilute solutions of K_2PtCl_4 (~1-2 mM) in order to inhibit Pt^{II} disproportionation, iii) the reduction of reaction temperature to 80^{o}C to suppress the disproportionation of K_2PtCl_4 into Pt^0 and K_2PtCl_6, and iv) the use of a longer reaction time. To monitor the reaction progress, we used an alkaline digestion technique of the resulting MSN-materials that was similar to the one described above (Scheme 3.8). The alkaline digestion was followed by ^{1}H NMR and/or ESI-MS(-) analysis. The large differences in the chemical shifts of the well-resolved resonances of the *o*-pyridyl protons for each of the species, the Pt-free **3.5-Digest** (8.29 ppm) and the cycloplatinated **3.16-Digest** (8.76 ppm), turned out to be a convenient tool for quantitating the outcome of the cycloplatination reaction and the following chloride ligand substitution step. Note that all chloro ligands in **3.16-Digest** were substituted with hydroxo. It is important to note, that if KOH was absent (a pure D_2O sample was used), no digestion/dissolution of MSN materials

occurred and no detectable ^{1}H NMR signals could be observed in the aromatic region in the resulting liquid.

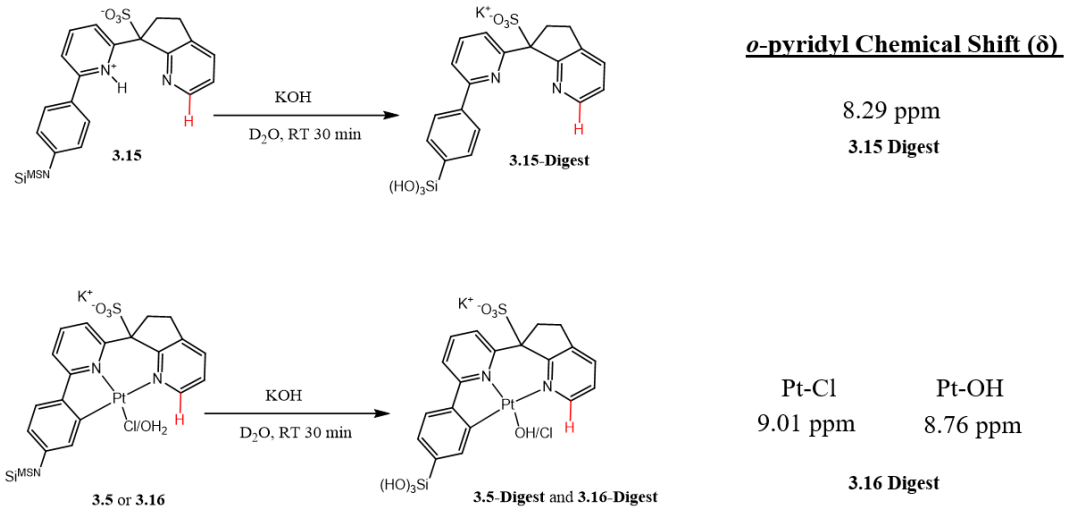

Scheme 3.8. KOH digests of **3.15, 3.16,** and **3.5** and the corresponding *o*-pyridyl signal used for ^{1}H NMR analysis of the extent of metallation of **3.15**

Even under the optimized conditions, according to our observations, the cyclometallation of **3.15** to yield **3.16** was only ~40-50% complete. Additionally, as anticipated, when the reaction was run at a higher temperature of 100-120 ^{o}C or a more concentrated solution of K_2PtCl_4 (>20 mM) was used, the formation of Pt^0 black was observed. Hence, the so-produced solid contained 40-50 mol % **3.16** with the balance of **3.15**.

The next and final step of the preparation of the MSN-immobilized catalyst **3.5** involves the chloride for aqua ligand exchange in **3.16**. Previously the substitution of chloride ligand in some sulfonated CNN-pincer Pt^{II}-chloro complexes to form derived Pt^{II}-alkoxides was performed utilizing mixtures of KOH and either EtOH or TFE.[33,34 49] In some other cases, additives of $Ag(NO_3)$ had been used as well,[33] in order to further facilitate the abstraction of the Pt^{II}-bound chloride.[33,34] However, neither of these strategies previously

reported are suitable for our MSN-based materials. The alkaline solutions would destroy the MSN, and, in the presence of $Ag(NO_3)$, would also yield insoluble AgCl species as a contaminant. In such a situation, to abstract chloride ligand from a Pt^{II} center we utilized 2.0 equivalents of a water soluble $Hg(ClO_4)_2$ in an $HClO_4$ solution in a 2:1 mixture of H_2O/TFE (Scheme 3.7) The acid additive was used to suppress any possible hydrolysis of Hg^{2+} cations that would produce insoluble HgO. The ClO_4^- anion was explicitly chosen as a weakly coordinating species, so that upon ionization of the Pt^{II}-Cl bond, the perchlorate anion would not be sufficiently competitive when it comes to coordination of a solvent molecule at the resulting formally three-coordinate Pt^{II} center.

To monitor the chloride ligand exchange and assess its extent, as well as the degree of cyclometallation of the immobilized pre-ligand, the solids isolated from reaction mixtures of **3.16** and $Hg(ClO_4)_2$ were carefully washed with dilute $HClO_4$ and water and then fully digested in KOH/D_2O solutions followed by ^1H NMR analysis of the resulting liquids (Scheme 3.8). The degree of the cyclometallation of a CNN-pincer ligand was calculated by dividing the integral intensity of ^1H NMR signals originating from the *o*-pyridyl protons of both Pt-OH and Pt-Cl (if any) species over the total integral intensity of the *o*-pyridyl protons originating from all CNN-pincer ligand-derived species and/or using an internal standard technique. Remarkably, using the reaction conditions in Scheme 3.7, the ligand exchange reaction was quantitative, and no signals of the *o*-pyridyl protons originating from the metalacyclic Pt-Cl species were observed in alkaline digests of the resulting solids (Fig. 3.4).

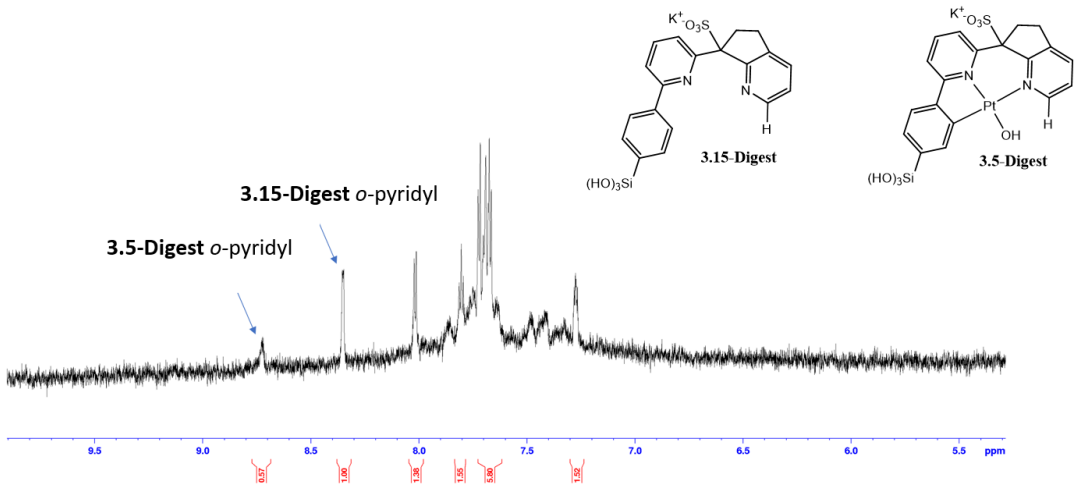

Figure 3.5. ^{1}H-NMR for KOH digest of an isolated MSN-derived product of a reaction of **3.16** and $Hg(ClO_4)_2$ in D_2O.

3.3. MSN Materials Characterization

All scanning electron microscopy (SEM), transmission electron microscopy (TEM), energy-dispersive X-ray spectroscopy (EDX), and N_2 sorption experiments were performed by Dr. Matthew Leonard from the research group of Prof. Efrain Rodriguez.

The core of our immobilized catalyst **3.5** is the MSN framework to which a sulfonated CNN-pincer ligand is covalently linked. Now that we have shown that **3.5** can be prepared by co-condensation of molecular components, $Si(OEt)_4$ and **3.3**, it is important to consider its solid state structure. Mesoporous silica nanoparticles can adopt structures with varying degrees of porosity, particle size, and surface area.[90-91] These parameters may be important for the catalytic performance of **3.5**. The purpose of this Section is to provide some basic characterization of our new MSN-supported catalyst **3.5**.

To characterize MSN-based materials prepared in this work, the MSN-immobilized pre-ligand **3.15**, the derived immobilized cyclometallated Pt^{II}-Cl complex **3.16** and the derived immobilized cyclometallated Pt^{II} aqua complex **3.5**, we used N_2 sorption (Brunauer–Emmett–Teller (BET) and Barrett–Joyner–Halenda (BJH) methods), scanning

electron microscopy (SEM), transmission electron microscopy (TEM), and energy-dispersive X-ray spectroscopy (EDX). We observed that, as soon as the immobilization of the pre-ligand **3.3** is done to produce **3.15**, the subsequent cyclometallation of **3.15** to form **3.16** and ligand substitution at a coordinated Pt^{II} center to form **3.5** had very little effect on the overall morphology of these solids. The major difference in the MSN-materials characteristics was observed when a control synthesis of the MSNs was carried out in the absence of $Si(OEt)_3$-substituted co-reactant **3.3** in EtOH. This difference, in part, may be related to the ability of added EtOH to disrupt micelle formation during condensation of the reaction components, so affecting the particles porosity and size distribution. [89,90] Not less importantly, the bulky pre-ligand **3.3** may interfere with the formation of more ordered MSNs, which was observed by us earlier for the MSN-material in Scheme 3.1, top.[34] None of the chemical modifications of **3.15** leading to **3.16** and **3.5** had any major effects on these MSN materials morphology. For the sake of brevity, the focus of this Section will be primarily on the solid state characterization of the catalyst **3.5** (see Supporting information for the characterization of **3.15** and **3.16**).

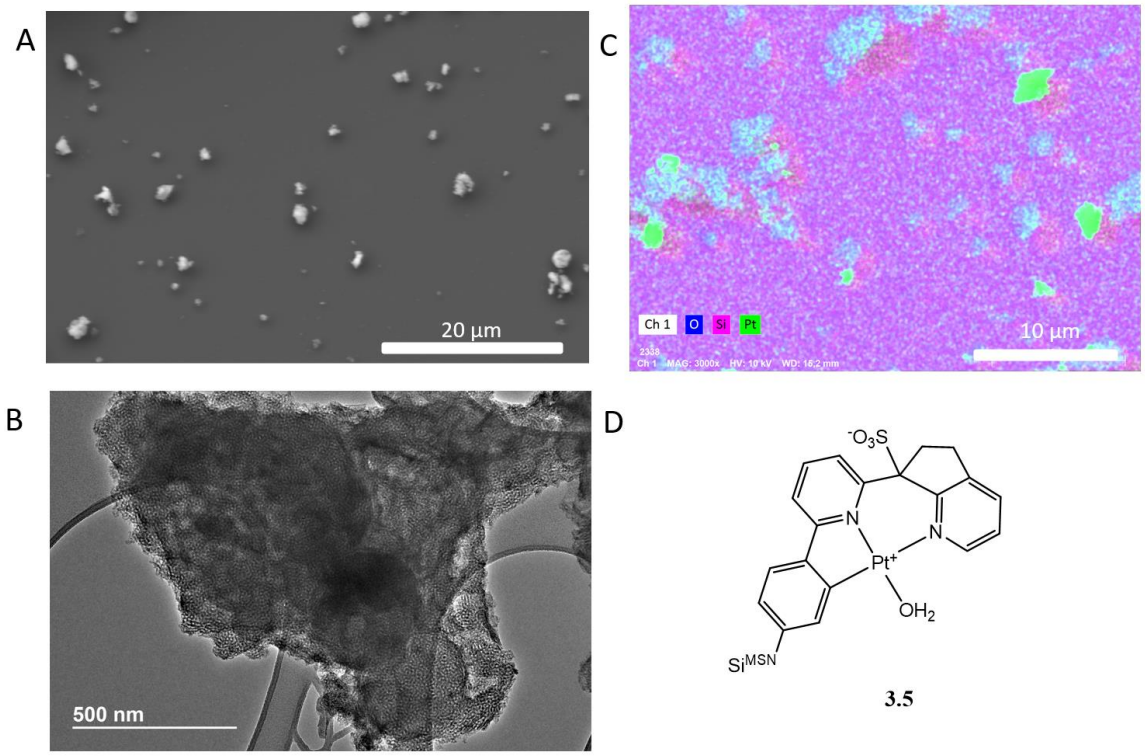

Figure 3.6. (A) SEM Image of **3.5**; (B) TEM image of **3.5** C) EDS image overlay showing O in blue, Si in purple, and Pt in green; and (D) Molecular drawing of **3.5.**

The scanning electron microscopy (SEM) image of the MSN-supported **3.5** (Fig. 3.5, A) shows a powder-like nature of this material where the particle size ranges from <1 µm to ~3 µm. The transmission electron microscopy (TEM) images in Fig. 3.5, B highlight the high porosity of the material. The numerous small almost spherical pores are less ordered, as compared to other similar MSNs such as SBA-16 which has long cylindrical pores.[89] A similar predominance of close to spherically shaped pores was observed by us earlier for similar MSN-materials (Scheme 3.1, top).[34]

The energy-dispersive X-ray spectroscopy (EDX) image of **3.5** (Fig. 3.5, C) allowed to obtain a picture of the Pt atoms distribution within the nanoparticles. While most of Pt atoms are well separated from each other by multiple SiO_2 units, there are some large nanoparticles with a high density of Pt atoms. As one alternative, these Pt atoms may be assigned to particles produced as a result of a predominant condensation of **3.3** involving

little to no $Si(OEt)_4$ which is a result of a stepwise condensation method that we employed to synthesize **3.15** (Scheme 3.5). The condensation reaction of $Si(OEt)_4$ was initiated 30 minutes before the introduction of the pre-ligand **3.3**. Thus, it can be expected that some pincer ligand-free nanoparticles have formed prior to encountering any **3.3**. In turn, protonation of **3.3** in the acidic reaction mixture would produce hydrophobic zwitterionic intermediates that may either react with the pre-formed MSN so resulting in silica-rich co-condensation product **3.15** or form silica-poor nanoparticles resulting from a predominant condensation of **3.3** alone. Such nanoparticles of high pincer ligand density would be responsible for a high Pt atoms density in the resulting metallated products. An alternative assignment of nanoparticles with high density of Pt atoms may be to Pt(0) clusters resulting from the disproportionation of K_2PtCl_4 into Pt(0) and K_2PtCl_6 that may have occurred to some extent during metallation of **3.15**. Section 3.4.5 will address the question if, in such a case, Pt(0) may be responsible for the observed catalytic properties of **3.5**.

Importantly, the TEM-EDX analysis showed no residual Hg present in the **3.5** sample. An energy-dispersive X-ray spectroscopy analysis of **3.5** sample was also performed as a quantitative assay for the pincer ligand incorporation, which was compared with the results of the chemical digestion / ^{1}H NMR method (Scheme 3.8). For the same batch of **3.5** that we analyzed, both methods were in near perfect agreement, with the ligand loading of 0.247 mmol/g, according to EDX, and 0.243 mmol/g, according to the chemical digestion / ^{1}H NMR method.

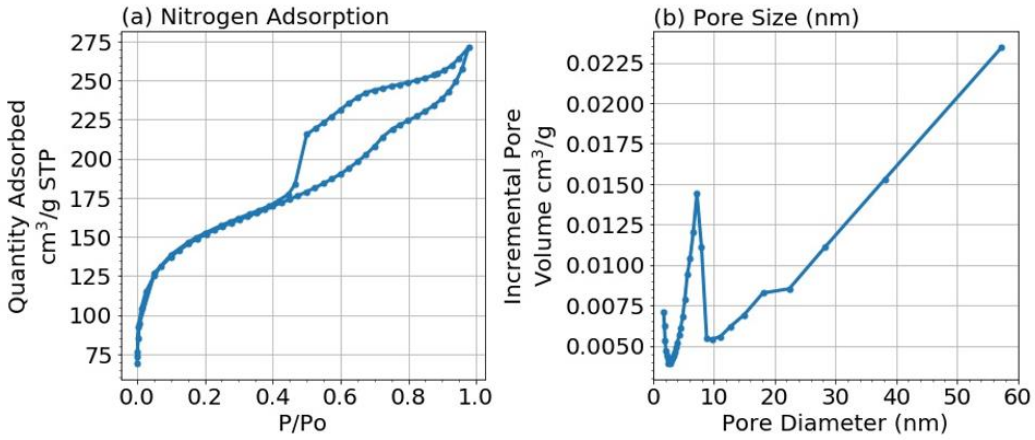

Figure 3.7. (Left) N_2 sorption isotherm displaying historetic behavior of **3.5** (Brunauer–Emmett–Teller (BET) and Barrett–Joyner–Halenda (BJH) methods) (Right) Pore size distribution

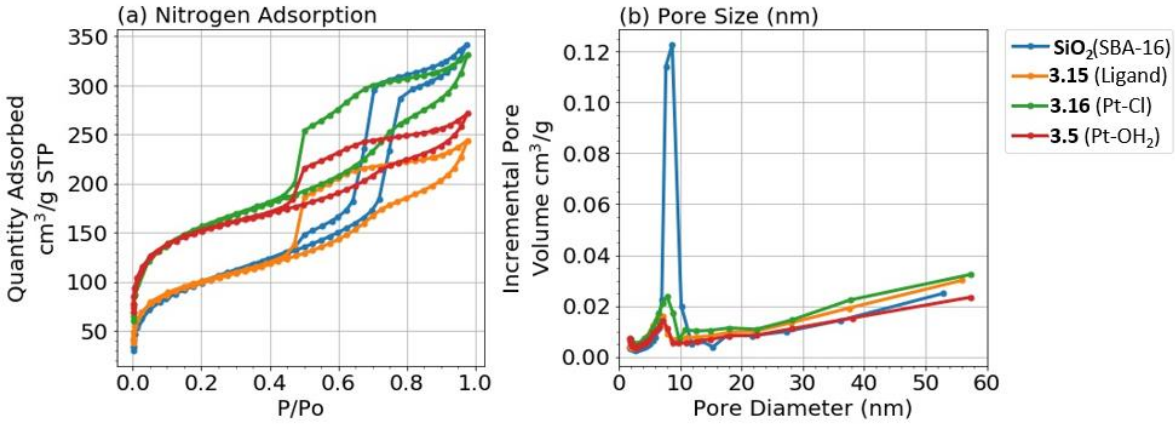

Figure 3.8. Left: an N_2 sorption isotherm overlay of SBA-16, **3.15**, **3.16** and **3.5** (Brunauer–Emmett–Teller (BET) and Barrett–Joyner–Halenda (BJH) methods). Right: an overlay of pore size distribution for each material.

The N_2 sorption data for the immobilized materials **3.5**, **3.15** and **3.16** synthesized in this work are given in Fig. 3.7 and 3.8. Figure 3.7 (left) shows the N_2 sorption isotherm for the hysteresis of N_2 sorption by **3.5**. This profile could be a combination of adsorption profiles typical of spherical pores (H2) and nanoparticles (H3) or slit-like pores (H4).[89-90]

The results of the BET method for N_2 sorption showed that **3.5** had an average surface area of 493 $m^2\ g^{-1}$ (compare with ~700 $m^2\ g^{-1}$ for Scheme 3.1, top), an average pore size of 5.3 nm, and a pore volume of 0.25 cm^3/g (compare with ~0.73 $cm^3\ g^{-1}$ for Scheme 3.1, top[34]. When each material's physical characteristics are compared to one another (Figure 3.8) it can be visually discerned that each of the immobilized materials, **3.5**, **3.15** and **3.16**, have remarkably similar physical characteristics. The major outlier is the standard unfunctionalized SBA-16, which was synthesized independently in the absence of silylated pincer pre-ligand **3.3** and EtOH. Otherwise, there was a slight increase in the pore volume when moving from **3.15** to **3.16** which may be indicative of the $AcOH/H_2O$ solution assisting in removing some adventitious surfactant impurities from the MSNs micropores. In summary, the material characteristics of **3.5** are on par with that of similar covalently immobilized molecular catalysts supported on SiO_2.[34, 90-91]

3.4 Aromatic H/D Exchange Catalyzed by Molecular and MSN-immobilized Pt^{II} Aqua Complexes

3.4.1 Extent of Deuteration for Aromatic H/D Exchange by 3.5 and Comparison to 1.5

As it was discussed in the Introduction, complex **3.5** was synthesized with the primary goal of overcoming some shortcoming of our previously described systems for H/D exchange between arenes and aqueous TFE-d_1 solutions catalyzed by complexes **1.5 – 1.7**. Our aim was to attain a higher reactivity, as compared to **1.5-1.7**, which may result, in part, from the inhibition of the bimolecular deactivation pathway via covalent immobilization. With the successful synthesis and characterization of **3.5** we moved towards benchmarking the performance of **3.5** under the previously developed reaction conditions (Scheme 3.10).

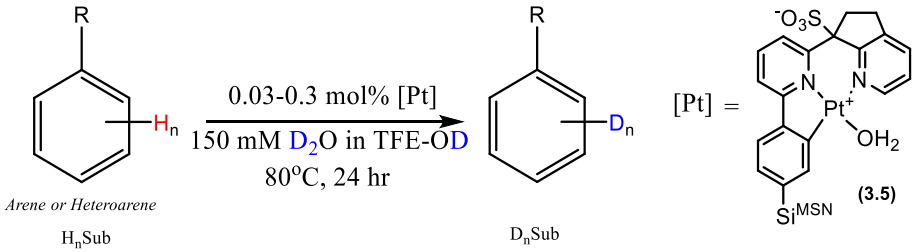

Scheme 3.9. Initial conditions for catalyst screening for aromatic H/D exchange in aqueous TFE-d_1 at 80 °C.

The catalytic H/D exchange between aromatic substrates H_nSub and TFE-d_1 used as a deuterium source was carried out at 80 °C using, typically, 0.1-0.5 mol. % of complex **3.5** as a catalyst.[33, 51] In a typical experiment 0.050 mL of H_nSub (or ~50 mg for solids) was dissolved in 0.450 mL of wet TFE-d_1 containing 0.150 M D_2O and 20-35 mg of MSN **3.5** containing 0.5-2 μmol of Pt^{II}, per its alkaline digestion / ^1H NMR characterization. The water additive has previously been shown to decrease the rate of catalyst deactivation and was kept for this set of experiments in order to develop a comparative profile between **3.5** and **3.1**. The reactions were monitored by ^1H NMR spectroscopy using the TFE-d_1 CH_2 group signal as an internal reference. Most of the substrates were used in concentration of ~1M which corresponds to 1-6 M concentration of the arene C(sp^2)-H bonds of a specific type. In none of our experiments we were able to observe H/D exchange involving C(sp^3)-H bonds of alkyl groups. The total concentration of exchangeable deuterium from D_2O/TFE-d_1 was ~12.5M which translates to the expected extent of the substrate's deuteration of ~68-81% upon reaching a hypothetical statistical distribution of exchangeable deuterium atoms between the solvent and all reactive C-H bonds of the substrate.

The initial screening of the extent of deuteration showed that complex **3.5** (Chart 3.1) is a competitive catalyst for the H/D exchange of arenes when comparing to our

original catalyst **3.1**. The key difference in the reaction conditions, besides the catalyst identity, included the catalysts loading that was ~3-10 times lower in the case of **3.5**. The maximum practical loading of the immobilized complex **3.5** is limited due to the need to allow for a facile mass exchange between the catalyst's surface and solution and, therefore, a limited amount of solid **3.5** that can be used per mL of reaction mixture, and the Pt loading in the MSNs. In a typical NMR J. Young-tube reaction, only 20-30 mg of complex **3.5** can be loaded at a time, which in our experiments corresponded to 0.5-2.0 μmol of Pt content**.** In turn, in the case of the soluble catalyst **1.5**, much higher catalyst loadings were used, ~7-9 μmol. Therefore, despite about 2-fold lower extents of deuteration in Chart 3.1, complex **3.5** still is viewed as a more active H/D exchange catalyst. For example, in the H/D exchange reaction with benzene, **3.17**, catalyzed by **3.5** 21.6% of all exchangeable H atoms were substituted with D. Over the same reaction period, the reaction catalyzed by **1.5**, benzene had an extent of deuteration of 40%. Considering the reaction conditions were identical in all but catalyst identity and loading, this 2-fold difference in the extent of deuteration is less than the 3-fold decrease in catalyst loading. In the absence of **3.5**, no H/D exchange was observed for any of the substrates besides the *ortho/para* position of N,N dimethylaniline, where there was a 14.8% deuteration observed over the 24-hour reaction period. Notably, after a 24 hours reaction period, both the reactions catalyzed by **1.5** and **3.5** would approach their expected statistical incorporation of deuterium of ~67-81%.

In Table 3.1, the respective turnover numbers (TON) of catalysts **1.5** or **3.5** are shown for the H/D exchange reactions of some selected substrates H_nSub.

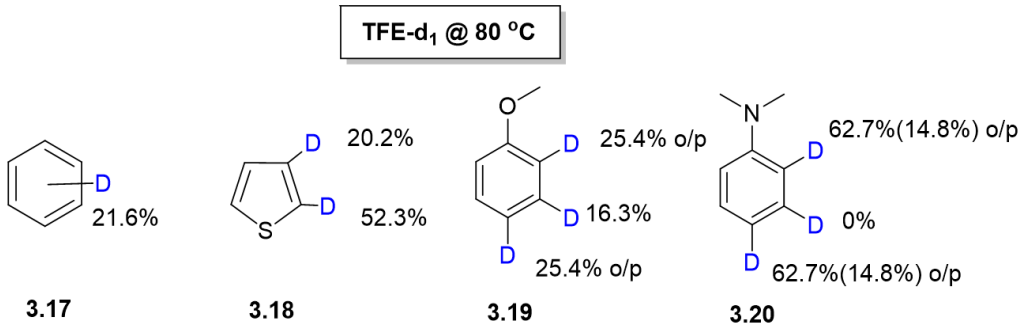

Chart 3.1. The extent of deuteration of substrates used for catalyst performance screening in the H/D exchange with 0.150 M D_2O in TFE-*d*$_1$ catalyzed by 0.03-0.3 mol % **3.5** after 24 hours of reaction at 80 °C.

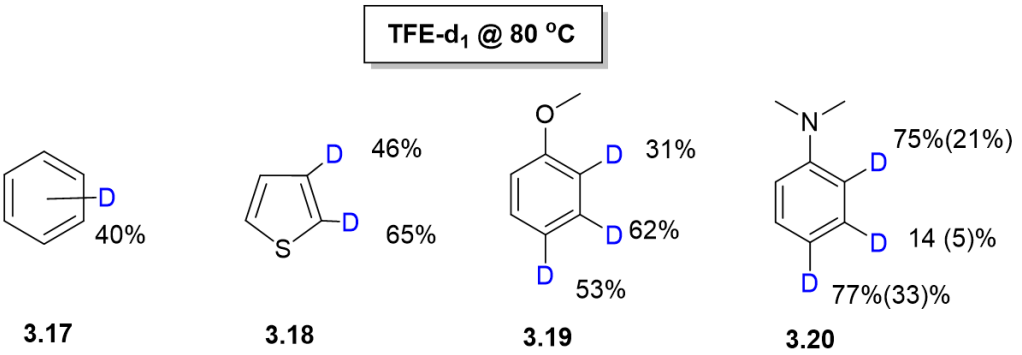

Chart 3.2. The extent of deuteration of substrates used for catalyst performance screening in the H/D exchange with 0.150 M D_2O in TFE-*d*$_1$ catalyzed by 0.03-0.3 mol % **1.5** after 24 hours of reaction at 80 °C.

Table 3.1. TON of catalysts **1.5** and **3.5** for the aromatic H/D exchange of some selected substrates H_nSub and 0.150 M D_2O/TFE-*d*$_1$ after 24 hours at 80 °C.

	TON-24 Hours			
Catalyst	**Benzene**	**Thiophene**	**Dimethylaniline**	**Anisole**
1.5	**139**	**184**	**73**	**161**
3.5	**285**	**429**	**254**	**258**

For each of the aromatic substrates, complex **3.5** outperformed **1.5** in terms of the catalysts TON over a 24 hour reaction period. Complex **1.5** had TON of 139, 184, 73 and 161 for benzene, thiophene, dimethylaniline, and anisole respectively. Whereas complex **3.5** had TON of 285, 429, 254 and 258 for benzene, thiophene, dimethylaniline, and anisole

respectively, thereby indicating that for **3.5** the lower extents of deuteration in Chart 3.1 are due to the increased ratio of H_nSub:[Pt] rather than as a result of a less reactive Pt center. One of the major reasons for the higher activity of **3.5**, as compared to **1.5**, may be a fully suppressed bimolecular deactivation. In turn, for **1.5** such deactivation was observed and documented earlier as the factor responsible for a gradual loss of the catalyst activity.[51] While complex **1.5** experienced bimolecular deactivation to yield catalytically inert dimers over the course of each of these reactions, **3.5** is physically incapable of deactivation via this pathway, leading to an increased catalyst lifetime, which may be a significant practical advantage in employing this system.

Given this success, we looked to explore other practical advantages that **3.5** may have over its predecessor **1.5**. In past studies, it was shown that **1.5** was poorly soluble in mixtures of AcOD and D_2O which both are much cheaper sources of exchangeable deuterium (≤$100/mol D), as compared to TFE-d_1 (~$1000/mol D). Additionally, the H/D exchange reactions catalyzed by **1.5** were much slower in these mixtures, as compared to TFE, at 80 ^oC.[49] In turn, when solutions of **1.5** were exposed to ~90-100^oC to accelerate the reactions, it would result in a rapid formation of catalytically inert dimers (**1.8**). Considering the increased longevity of **3.5** we looked to expand this catalysts' application into new solvent systems and a potential use of temperatures well above 80 ^oC.

3.4.2 Expansion of reaction conditions and substrate scope when using 3.5

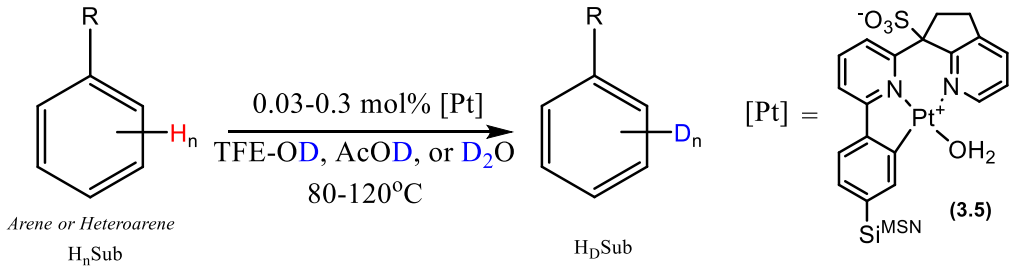

Scheme 3.10. Expanded conditions of H/D exchange reaction involving H_nSub and AcOD or D_2O as deuterium sources and **3.5** as a catalyst**.**

The catalytic H/D exchange between aromatic substrates H_nSub and the described deuterium source was performed using a procedure similar to the one highlighted above. The temperature and a source of deuterium are varied and are explicitly described when used. In a typical experiment 0.050 mL of H_nSub (or ~50 mg for solids) was dissolved in 0.450 mL of the deuterium source and 20-35 mg of MSN containing 0.5-2 μmol of catalyst **3.5**. The reactions were monitored by ^{1}H NMR spectroscopy, and H/D exchange was further qualitatively confirmed utilizing ^{2}H NMR. TFE or 1,4-dioxane was used as an internal reference. Most of the substrates were used in concentration of ~1M which corresponds to 1-6 M concentration of the arene C(sp^2)-H bonds of a specific type. In none of our experiments we were able to observe H/D exchange involving C(sp^3)-H bonds of alkyl groups. The total concentration of exchangeable deuterium from TFE-d_1 was ~12.5M and ranged up to ~25M for 1:1 mixtures of AcOD:D_2O (~55M for neat D_2O in one example) which translates to the expected extent of the substrate's deuteration of ~68-88% upon reaching a hypothetical statistical distribution of deuterium between solvent and all reactive C-H bonds of the substrate. Some representative ^{1}H and ^{2}H NMR spectra are shown in Fig. 3.8 and 3.9.

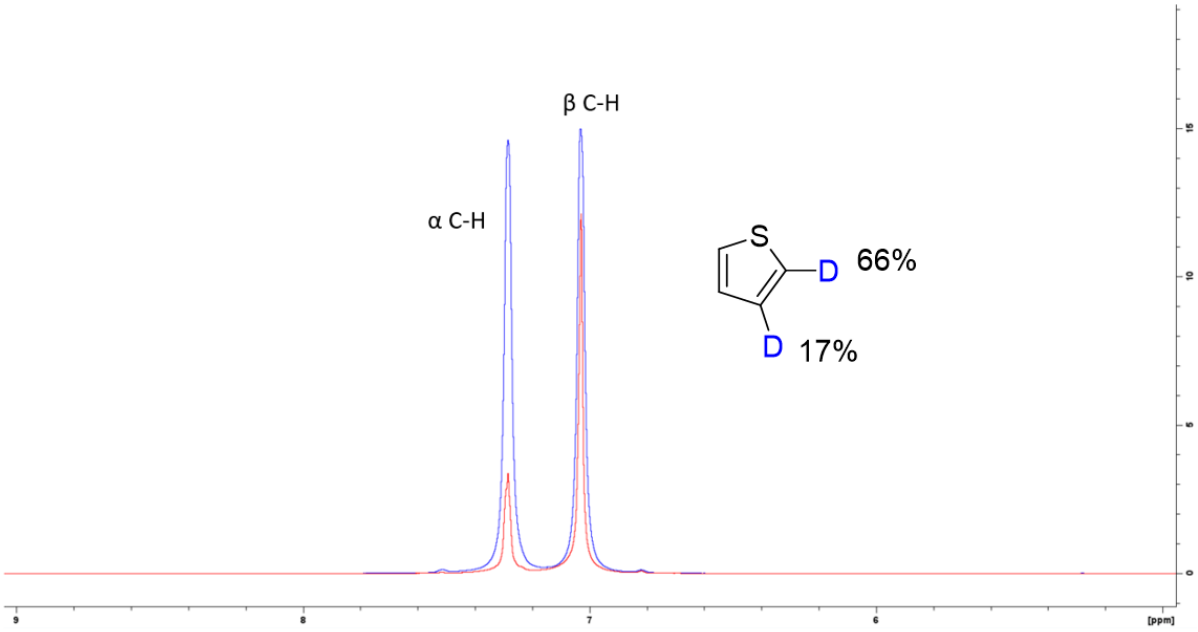

Figure 3.9. Superimposed ^{1}H-NMR spectra for the H/D exchange reaction between thiophene and AcOD-d_4 after 24 hours at 120^{o}C catalyzed by **3.5** Blue trace: 0 hr reaction time Red trace: After 24 hr reaction time.

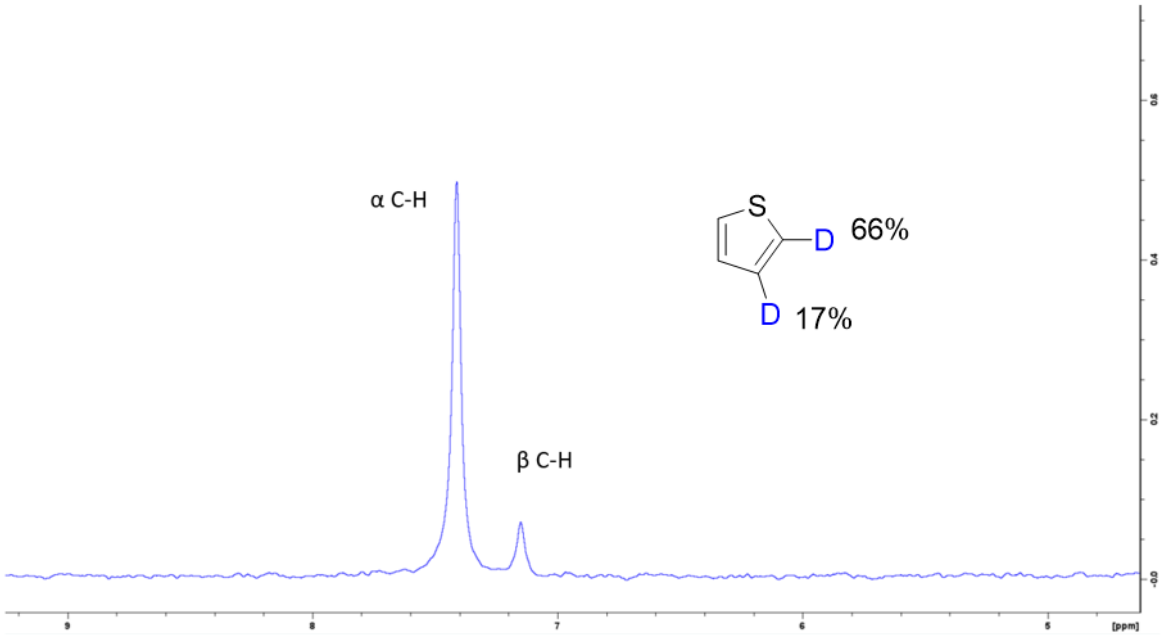

Figure 3.10. Aromatic region of ^{2}H NMR spectra for the H/D exchange reaction between thiophene and AcOD-d_4 after 24 hours at 120^{o}C catalyzed by **3.5.**

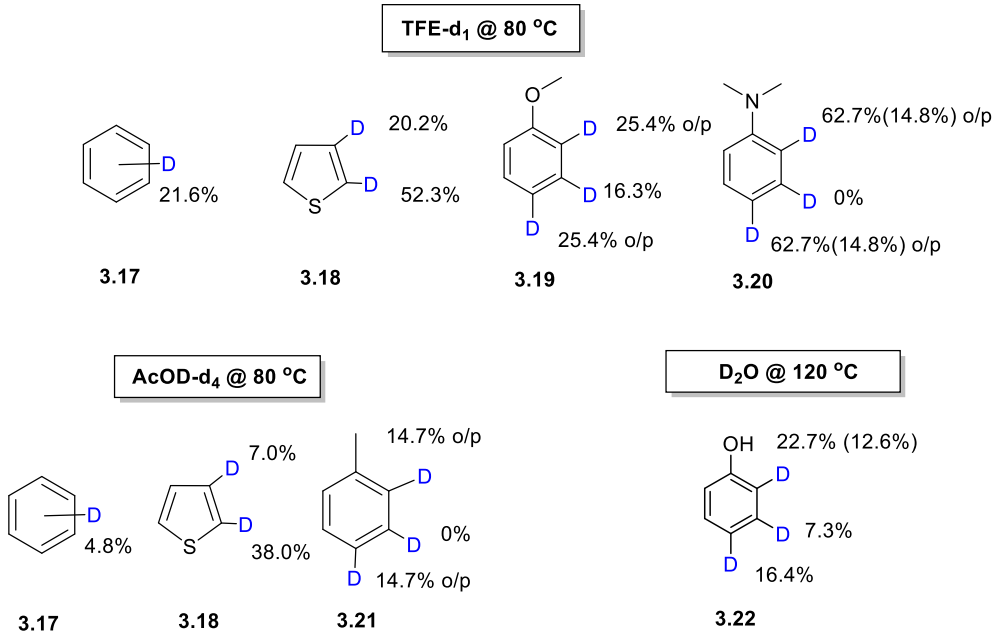

Chart 3.3. 24-hour extent of deuteration results for H_nSub under various conditions catalyzed by **3.5** Values in parentheses represent the contribution of H/D exchange in the absence of **3.5.**

3.4.3. Discussion for Chart 3.3

Chart 3.3 shows a small selection of aromatic substrates and three compatible sources of exchangeable deuterium, TFE-d_1 (~$1000 / mol D), AcOD-$d_1$ (~$120 / mol D) and D_2O (~$18 / mol D), that were screened. As previously mentioned, the H/D exchange of arenes in aqueous TFE-d_1 at 80 °C catalyzed by **3.5** represents the initial starting point for benchmarking the performance of this catalyst. Under these conditions, three electron rich species, **3.18-3.20**, as well as benzene, were noticeably reactive. Benzene, **3.17** had a deuterium incorporation of 21.6% over the 24-hour reaction period. Thiophene, **3.18**, performed better than benzene and showed a total deuterium incorporation of 36.3% with 52.3% and 20.2% deuterium incorporation into the α and β positions respectively. This ~2.5:1 α:β selectivity catalyzed by **3.5** reflects a significant degree of preference for the more electron rich α C-H position, which matches the selectivity observed for **1.5** under

identical reaction conditions.[49] Anisole, **3.19**, had a total deuteration of 21.7% which has no preference for the electron richer *ortho/para* positions with a combined *o/p* deuteration of 25.4% for 3 C-H bonds versus 16.3% for the two *meta* C-H bonds. Accounting for the difference in statistical abundance of the sum of *ortho* and *para* versus *meta,* all positions in anisole are roughly equally reactive. Due to the broad signals in ^{1}H-NMR, resolution of the *ortho/para* positions was not achieved. For N,N-dimethylaniline, **3.20**, a high extent of deuteration was observed in the combined *ortho/para* positions with an overall 62.7% deuteration but 14.8% deuteration was observed in the absence of complex **3.5**. Interestingly, no deuterium incorporation was observed in the *meta* C-H position of **3.20**, making this H/D exchange reaction highly selective for the electron rich *ortho/para* positions of **3.20.**

We expanded these initial screening results in aqueous TFE-d_1 at 80 ^{o}C to neat AcOD-d_4 at 80 ^{o}C in an attempt to assess this catalysts' potential applications in this more economically viable solvent. Benzene, **3.17**, and thiophene, **3.18**, were again subjected to the H/D exchange conditions detailed above, but now with AcOD-d_4 as the deuterium source. Benzene had a dramatically decreased extent of deuteration at only 4.8% over the same 24-hour reaction period. Thiophene, **3.18**, was also less reactive, with a total deuterium incorporation of 22.5% with 38% and 7% deuterium incorporation into the α and β positions, respectively. Despite this reduction in reactivity, we were still able to achieve modest deuterium incorporations with a high regioselectivity under these reaction conditions. This encouraged further expansion into the solvent system at increased temperatures.

Finally, we screened the H/D exchange reaction of D_2O and phenol **3.22**, in neat D_2O solution at 120 ^oC catalyzed by **3.5**. This was done in order to assess if D_2O itself is capable of engaging in H/D exchange. Remarkably, this H/D exchange reaction was successful with the total deuterium incorporation of 15.3% and 22.7%, 7.3% and 16.4% in the *ortho*, *meta*, and *para* C-H positions respectively. A control reaction in the absence of **3.5** showed that the *ortho* C-H position of phenol engaged in H/D exchange to yield 12.6% deuterium incorporation but none of the other positions were engaged. This result serves as a promise for the potential applications of D_2O as the most affordable liquid deuterium source for this system. The major limitation of utilizing neat D_2O for aromatic H/D exchange naturally lies in an often limited solubility of non-polar aromatic substrates in the polar D_2O phase, but this result is encouraging and indicated that some biphasic, or multicomponent solvent systems utilizing D_2O may be useful in future applications.

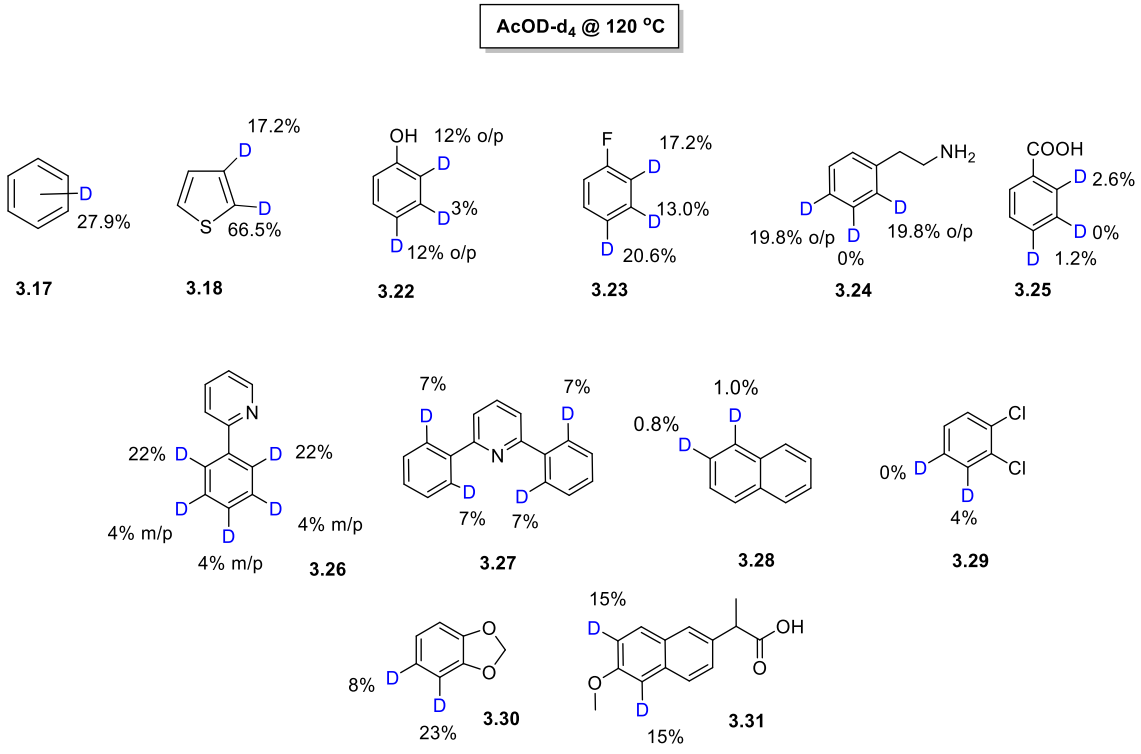

Chart 3.4. 24-hour extent of deuteration results for H_nSub in AcOD-*d*$_4$ catalyzed by **3.5**

3.4.4 Discussion for Chart 3.4 and some mechanistic insight

The rate and extent of deuteration of arenes in AcOD-d_4 catalyzed by **3.5** was decreased in comparison to the aqueous TFE-d_1 system at 80°C. In order to increase the applicability of the AcOD-d_4 system we explored the use of elevated temperatures and attempted the use of substrates that were previously unreactive in the system catalyzed by **1.5** at 80°C. In this screening, the reaction procedure was the same as previously mentioned, now utilizing neat AcOD-d_4 at 120 °C and **3.5** as a catalyst. Upon increasing the reaction temperature, the previously screened substrates benzene, **3.17**, and thiophene, **3.18**, had a dramatic improvement in the extent of deuteration over 24 hours versus the system using AcOD-d_4 at 80 °C. Benzene had an extent of deuteration of 27.9% over a 24 hour reaction period in AcOD-d_4 at 120 °C compared to the 4.8% deuteration observed in same reaction at 80 °C. The reaction in AcOD-d_4 at 120 °C outperforms the reaction utilizing aqueous TFE-d_1 at 80 °C. Considering that AcOD-d_4 is cheaper, more environmentally friendly, and a generally better solvent for arenes, the fact that we can achieve similar performance using this deuterium source is a significant advantage for this catalytic system over its predecessor. Additionally, the difference in rate between the AcOD-d_4 and TFE-d_1 is an indication that the kinetic barrier for H/D exchange is increased when the solvent is changed from TFE-d_1 to AcOD-d_4.

Thiophene, **3.18**, had a similar improvement in performance in AcOD-d_4 system at elevated temperatures. We observed a total extent of deuteration of 41.8% with 66.5% and 17.2% deuterium incorporation into the α and β positions, respectively. The total extent of deuterium incorporation was an improvement over both the TFE-d_1 and AcOD-d_4 systems at 80 °C. Additionally, this reaction showed a higher degree of selectivity for the α position

in thiophene with a 3.8:1 α: β selectivity ratio. The selectivity preference is highlighted in Fig. 3.8, where the blue trace presents the initial measurement of the reaction mixture before heating, and the red trace is the overlay of the reaction after a 24 hour reaction period. The signal at 7.35 ppm corresponds to the α C-H bond of thiophene and the signal at 7.00 ppm corresponds to the β C-H bond. After 24 hours there is a clear decrease in the α C-H relative to the β C-H ^{1}H NMR signals. Furthermore, Fig. 3.9 is a ^{2}H NMR spectrum of the same solution, thereby further affirming the weakening of the α C-H signal at 7.35 ppm in the ^{1}H-NMR corresponds to the formation of α C-D bonds.

Phenol, **3.22,** fluorobenzene, **3.23,** benzoic acid, **3.25**, benzodioxole**, 3.30,** and naproxen, **3.31**, represent substrates that were previously successful in the catalytic of H/D exchange of aromatics and TFE-d_1 by **1.5** at 80 ^{o}C. Given the improvement in terms of both economic viability, and substrate solubility that the use of AcOD-d_4 at 120 ^{o}C presents, we were hopeful that catalyst **3.5** and these substrates would behave well under these new conditions. Phenol, **3.22** performed only modestly, with a total deuteration of 8.4% and 12% deuteration in the combined *ortho* and *para* positions with 3% deuteration in the *meta* position. Considering the electron richness of phenol, it was expected to have a better performance under these conditions. Fluorobenzene, **3.23** performed quite well for an electron deficient aromatic substrate, with a total deuteration of 16% and 17.2%, 13.0%, and 20.6% in the *ortho, para* and *meta* positions, respectively. Benzodioxole, **3.30**, had a significant regioselective preference for the α C-H position, with a 23% and 8% deuteration in the α and β positions respectively, representing a 2.87:1 α:β regioselectivity ratio; previous experiments utilizing catalyst **1.5** in TFE-d_1 at 80 ^{o}C were unable to resolve the α and β C-H ^{1}H NMR signals. Benzoic acid was generally very poorly reactive under the

new conditions despite being modestly reactive in the old reaction setup involving **1.5** in TFE-d_1 at 80 ^{o}C. Finally, a pharmaceutical substrate, Naproxen, **3.31**, was regioselectivity deuterated to 15% exclusively at the *ortho*- positions to the methoxy group. While this value is still low, increasing the reaction time beyond 24h or increasing catalyst loading may enable greater extents of deuteration.

Substrates **3.28** and **3.29** were previously used in the system catalyzed **1.5** in an aqueous TFE-d_1 system at 80 ^{o}C and were shown to be inactive, largely due to their poor solubility in TFE. Hence, we were interested in reinvestigated these substrates utilizing complex **3.5** in AcOD-d_4 at 120 ^{o}C. For naphthalene, **3.28**, there was very little deuterium incorporation observed after 24 h (<1%) despite the substrate being very soluble in AcOD. Similarly, substrate **3.29** showed little engagement in H/D exchange; only 4% of the total α C-H were engaged in H/D exchange. Despite these low values, this still presents an encouraging improvement, that now polycyclic and some electron deficient arenes may be kinetically viable substrates for H/D exchange under improved conditions.

Phenethylamine, **3.24**, 2-phenylpyridine, **3.26**, and 2,6 diphenylpyridine, **3.27**, are all substrates that had previously proven challenging for C-H bond activation by **1.5** in our aqueous TFE-d_1 system at 80 ^{o}C. The presence of 1^{o} amines or strongly coordinating pyridine moieties has previously been demonstrated to deactivate complex **1.5** in aqueous TFE. However, we speculated that with in AcOD, the basic pyridine and amine moieties will be less deactivating due to their participation in acid-base equilibria. In fact, despite their strongly coordinating nature, phenethylamine, **3.24**, had an overall extent of deuteration of 12%, with exclusive deuteration at the *ortho* and *para* positions. No *meta* C-H bonds or alkyl H/D exchange products were observed. Similarly, both 2-phenylpyridine,

3.26, and 2,6-diphenylpyridine, **3.27**, were also reactive. **3.26** had exclusive deuteration on its phenyl fragment and no deuterium was detected in the pyridyl core. Specifically, the *ortho* positions were selectively deuterated with a deuterium incorporation of 22% whereas the *meta/para* combined value was only 4%. This *ortho* preference for H/D exchange is a rather surprising result, considering the *ortho* position is the most sterically encumbered position on the substrate. This selectivity is also seen in 2,6-diphenylpyridine, **3.27**, where again, only the phenyl fragments engage in H/D exchange (presumably, electronically controlled) but the *ortho* C-H bonds are the only ones to be engaged at a value of 7% across all equivalent positions.

There are some significant mechanistic implications for this observed selectivity. If the H/D exchange of substrates **3.26** and **3.27** were only electronically controlled, based on the "electron richness" of the most reactive C-H bonds, then it would be predicted that *ortho/para* positions would react at roughly the same rate. Furthermore, if the reaction were only sterically controlled, we would expect the *meta/para* positions to dominate the reaction. The observation of an exclusive *ortho*-to-directing group (pyridine) selectivity in substrates **3.26** and **3.27** implies that there may be a directing group effect responsible for this selectivity. Typically, we would not expect this avenue to be possible, due to directing group mediated C-H activation requiring two coordination vacancies, while complex **3.5** has only one accessible site after aqua ligand dissociation.[7-8, 92] The observed reaction selectivity indicates that perhaps a coordination vacancy is opened during the reaction sequence. One possible avenue for an additional vacancy to occur is through the protonolysis of the Pt-C bond in the CNN ligand scaffold.

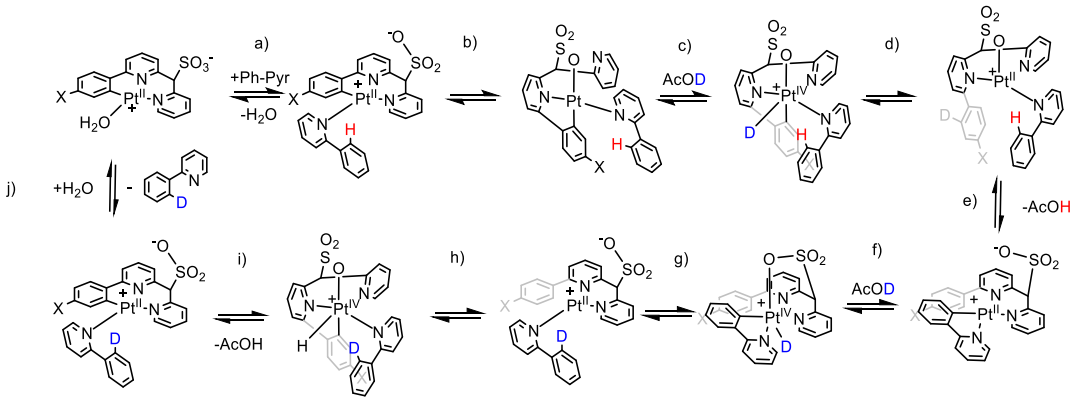

Scheme 3.11. One possible directing group-mediated C-H activation pathway leading to the *ortho* selectivity of **3.26 a)** aqua ligand exchange **b)** CNN to CNO isomerization **c)** Protonation or Deuteration of Pt **d)** RE of phenylene fragment from ligand and hydride **e)** OA of substrate *ortho* C-H bond and isomerization **f)** Deuteration of Pt by AcOD **g)** RE of deuterated substrate **h)** OA of ligand bound phenylene C-H bond **i**) deprotonation at Pt **j)** ligand exchange and expulsion of *ortho*-selective deuterated substrate.

Alternatively, there could be at least two other possible mechanistic pathways to achieve the same directing group mediated effects shown in scheme 3.11. For example, step c may progress via a concerted σ-bond metathesis mechanism, where the *ortho* C-H bond on the substrate is responsible for the protonolysis of the Pt-C bond. Furthermore, the protonolysis of the Pt-C bond may not necessarily be responsible for forming the coordination vacancy necessary for this mechanism to progress. Dissociation of the terminal pyridyl fragment of the complex might also produce a coordination vacancy. However, in some experiments utilizing AcOD and homogenous CNN ligated Pt complexes we have observed intramolecular incorporation of deuterium into the *ortho* C-H bonds of the phenylene fragment of ligand scaffold, thus reinforcing the facile protonolysis of this bond under these H/D exchange conditions.

Additional evidence for these proposed mechanism in Scheme 3.11 comes from Chart 3.5, where a 1:1 mixture of AcOD-d_4:D_2O was used as the H/D exchange medium for substrate **3.26** catalyzed by **3.5.** Through the addition of D_2O to the reaction solution,

the dissociation of AcOD-d_4 is increased via the stabilization of charged intermediates through solvation. Additionally, the formation of the protonated form of **3.26** would also become more favorable for the same reason. Therefore, a larger portion of **3.26** would exist in the fully protonated state in the 1:1 solution of AcOD-d_4:D_2O when compared to the neat AcOD-d_4 solution. This implies that the coordination of **3.26** to Pt would be inhibited, and as a result, we would expect the directing group mediated C-H activation pathway to be inhibited. Accordingly, in the 1:1 solution of AcOD-d_4:D_2O the *ortho*- selectivity of deuteration of **3.26** was less pronounced.

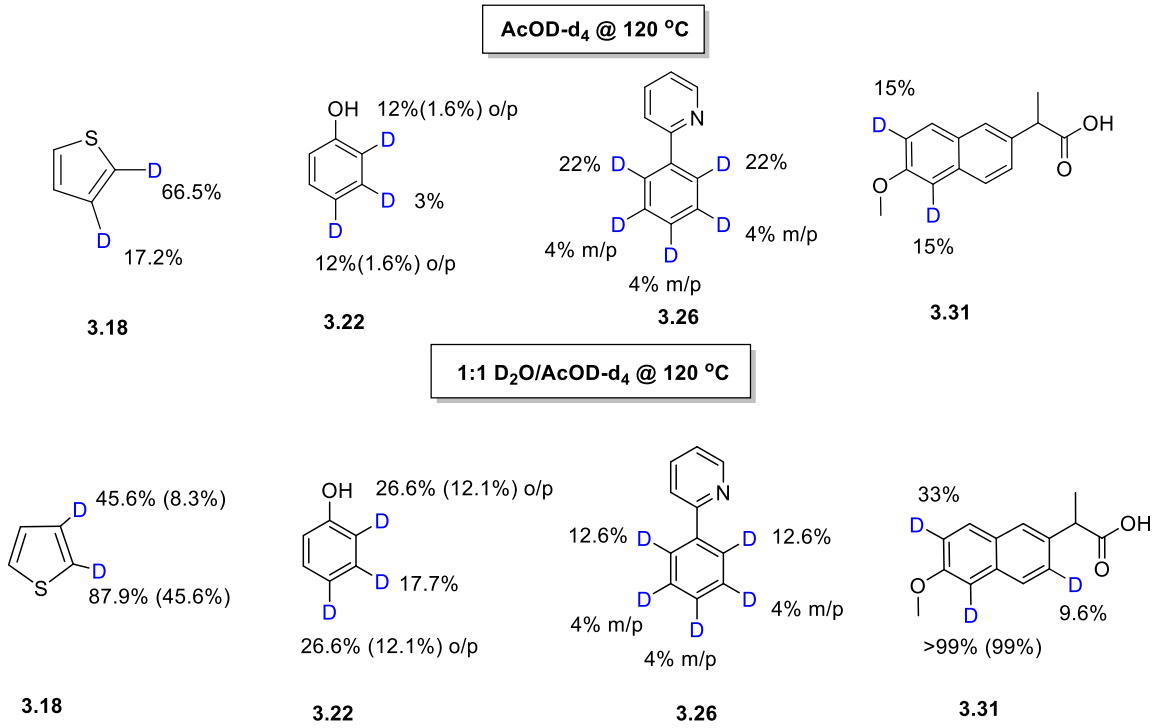

Chart 3.5. 24-hour extent of deuteration results for H_nSub in AcOD-d_4 and 1:1 AcOD-d_4:D_2O solutions catalyzed by **3.5**. Values in parentheses represent a background contribution to the H/D exchange in the absence of **3.5.**

3.4.5 Discussion for Chart 3.5

Chart 3.5 presents a comparison of 4 aromatic substrates and their respective performance in the H/D exchange reaction catalyzed by **3.5** under differing solvent conditions. For Chart 3.5 (top), the 24 hour values for the substrates are shown for the H/D exchange in AcOD-d_4 at 120 ^{o}C, as previously discussed in the last section. Chart 3.5 (bottom) presents the results for the same H/D exchange reactions conditions, however, now with a 1:1 AcOD-d_4:D_2O solution as the relevant deuterium sources. Considering the past success with the H/D exchange of phenol and neat D_2O, it was already established that D_2O is a competent deuterium source for our catalyst and aromatic substrates. Therefore, by using our cheapest liquid deuterium source, D_2O, mixed with AcOD-d_4 which is generally a good solvent for aromatic compounds, we may be able to further expand the practical viability of this system while simultaneously increasing the [exchangeable deuterium] to [H_nSub] ratio.

For thiophene, **3.18**, changing the solvent conditions had rather dramatic effects on the extent of deuteration after 24 hours. The total extent of deuteration increased from 41.8% to 66.8%. As a result of approaching the expected statistical deuterium incorporation, the regioselectivity of the H/D exchange was also decreased with the α C-H position being deuterated at 87.9% and the β position at 45.6%. While neat AcOD-d_4 showed no background contribution to the H/D exchange, with the 1:1 AcOD-d_4:D_2O solution, there is a significant contribution to the reaction, with 45.6% and 8.3% of the α and β C-H positions being deuterated in the absence of **3.5**. An increasing acidity of 1 : 1 AcOD-d_4 / D_2O mixtures may be responsible for this background process involving electrophilic aromatic substitution with D^+ as an electrophile. Therefore, the more electron

rich positions (which are also favored selectively by **3.5**) have a greater background contribution. However, for practical applications, where simple deuterium enrichment is the goal, this background reaction actually presents a meaningful advantage.

For phenol, **3.22**, a similar effect was observed when switching to the 1:1 AcOD-d_4:D_2O solvent mixture. The overall deuterium incorporation after 24 hours increased over the neat AcOD-d_4: reaction from 8.4% to 23% with 26.6% deuteration in the combined *ortho* and *para* positions and 17.7% in the *meta* position. There was an increase in the background contribution for H/D exchange of 12.1% in the combined *ortho* and *para* positions. In turn, 2-phenylpyridine **3.26** had an overall decrease in performance in the 1:1 AcOD-d_4:D_2O solvent mixture. The pyridyl fragment of **3.26** remained untouched, and the *meta*/*para* combined values for deuteration of its phenyl group remained the same under both sets of solvent conditions. However, the *ortho* C-H bond deuteration dropped significantly, from 22% down to 12.6%. This is likely due to the reasons mentioned above surrounding the directing group-mediated mechanism for the H/D exchange of this type of substrate. Under the increasingly acidic conditions, the 2-phenylpyridine has a greater fraction of protonated species than in the neat AcOD-d_4. Therefore, the coordination of the pyridyl fragment to a Pt^{II} center is reduced and the subsequent *ortho* C-H bond activation is inhibited (Scheme 3.11). Finally, Naproxen, **3.31**, saw a 2-fold increase in the extent of deuteration up to 30% from 15% one ortho-to-methoxy and up to 99% deuterium introduction for the other. Albeit with the same extent of deueteration observed for the background reaction. Additionally, the ortho-to-carbxylate C-H position was deuterated now up to 9.6%.

3.4.6 Kinetic performance of MSN-supported Catalyst

When evaluating a catalysts' performance, we considered three major reaction parameters: a catalyst's TON after 24 hours, the observed second order rate constant for the H/D exchange for the reaction period of 24h, $k_{24\text{-}obs}$, and the extent of deuteration after 24 hours. The rationalization behind utilizing "observed" parameters for the rate constant revolves around the heterogenous nature of **3.5**. Upon metalation, there is an incomplete conversion of ligand species to Pt-Cl complex, which implies that not all of the immobilized ligand species are accessible for the metallation. Furthermore, the percentage of "active" Pt sites across the surface of the MSN is unknown. Therefore, a true rate constant for this catalyst cannot be properly determined due to the normalization factor required for Pt concentration.

Additionally, due to the heterogeneity of the catalyst minute changes in ^{1}H NMR signals corresponding to sometimes slight changes in deuteration percentage were difficult to monitor. The experimental design for this system had a large amount of insoluble SiO_2-bound complex present in a J. Young tube during ^{1}H NMR measurements. Thus, the broadened signals affected the sensitivity of our measurements. To make our rate estimates more uniform, we ran each deuteration experiment for 24 hours, periodically taking ^{1}H NMR measurements throughout the experiment and always including the 24 hour data point for calculations of 24h-average reaction rates. As a result, we use 24-hour – average rate constant values when assessing the reactivity H_nSub and **3.5** in our H/D exchange reactions. In calculations of $k_{24\text{-obs}}$ we utilized the total Pt amount present in the added catalyst **3.5** (eq 3.1 – 3.2):

$$rate = -\frac{d[C-H]}{dt} = \frac{d[C-D]}{dt} \qquad \text{(eq. 3.1)}$$

$$k_{24-obs} = \frac{rate}{[C-H]\times[\mathbf{3.5}]} \quad \text{(eq. 3.2)}$$

We use $k_{24\text{-}obs}$ values also to compare the reactivity of individual C-H bonds, provided that all reactions being compared were measured under otherwise identical conditions. Importantly, such a comparison is only meaningful for the extent of deuteration not exceeding 10-20% after 24 h of reaction. As the reaction approaches the statistical deuterium distribution threshold of ~60-80%, the 'initial rates' approximation becomes increasingly invalid and $k_{24\text{-}obs}$ values for different C-H bonds asymptotically approach the same value. The TON values were calculated using equation 3.3 and were evaluated for each C-H bond of interest with NMR-resolved signals:

$$\text{TON} = \frac{[C-D]}{[\mathbf{3.5}]} \quad \text{(After 24 hr)} \quad \text{(eq. 3.3)}$$

The so-produced reaction parameters for different substrates and solvents are collected in Tables 3.2 and 3.3. Table 3.2 reports data produced using various solvents except AcOD-d_4 at 120 ^{o}C whereas Table 3.3 contains data produced exclusively AcOD-d_4 at 120 ^{o}C.

Benzene and thiophene were typically utilized as the reference compounds to see how the catalyst performed kinetically across each of the reaction conditions. Benzene, **3.17**, in aqueous TFE-d_1 at 80 ^{o}C showed a 22% deuteration by **3.5** and had $k_{24\text{-}obs}$ of 2.2 ± 0.4 $M^{-1}Hr^{-1}$ with TON of 290 after 24 hours. For comparison, under similar reaction conditions but with higher catalyst loading, complex **1.5** showed a 40.% deuteration and had $k_{24\text{-}obs}$ of 1.08 ± 0.1 $M^{-1}Hr^{-1}$ with TON of 139 after 24 hours. This ~2-fold increase in $k_{24\text{-}obs}$ indicates that complex **3.5** may be a more practical catalyst to produce deuterated arenes. Admittedly, due to the method in which this value is calculated, the increase in $k_{24\text{-}}$

$_{obs}$ for **3.5** over **1.5** may be due to the inhibition of bimolecular deactivation which plays a significant role in the long-term kinetics of **1.5**.

When the H/D exchange of benzene by complex **3.5** was carried out in AcOD-d_4 at 80 ^{o}C, there was a significant decrease in both the extent of deuteration and $k_{24\text{-}obs}$, down to 4.8% and 0.92 ± 0.2 $M^{-1}Hr^{-1}$, respectively. This result indicates that the energy of the transition state corresponding to the RDS for the H/D exchange of benzene in AcOD is greater than that of the same process in TFE. This may imply that the AcOD solvent binds more strongly to a Pt^{II} center in **3.5**, than TFE, so increasing the overall reaction activation barrier. Alternatively, or in addition, the more acidic medium may be involved in a reversible protonolysis of the Pt-C bond in **3.5**, so decreasing the effective concentration of the intact catalyst.

Table 3.2. A summary of the extent of deuteration, the observed 24-hour – average rate constants, $k_{24\text{-obs}}$, and catalyst TONs for the H/D Exchange of H_nSub catalyzed by **3.5** under various conditions.

TFE-d_1 @80 °C				
Substrates	**Extent of Deuteration**	**3.5 (μmol)**	**$k_{24\text{-obs}}$ ($M^{-1}Hr^{-1}$)**	**TON-24 hr**
Benzene	21.6%	2.0	2.2 ± 0.4	285
Thiophene	36.2%	2.1	3.6 ± 0.5	426
α-C-H	52.3%	2.1	5.1 ± 0.7	307
β-C-H	20.2%	2.1	2.0 ± 0.2	119
Dimethylaniline*	37.6% (7.5%)	2.2	3.0 ± 0.5*	283*
o/p-C-H	62.7% (14.8%)	2.2	4.1 ± 0.03*	233*
Anisole	20.3%	2.1	2.0 ± 0.4	218
o/p-C-H	25.4%	2.1	2.5 ± 0.4	152
m-C-H	16.3%	2.1	1.6 ± 0.4	66
AcOD-d_4 @80 °C				
Substrates	**Extent of Deuteration**	**3.5 (μmol)**	**$k_{24\text{-obs}}$ ($M^{-1}Hr^{-1}$)**	**TON-24 hr**
Benzene	4.8%	1.3	0.92 ± 0.2	145
Toluene	8.9%	1.7	1.1 ± 0.5	124
o/p-C-H	14.7%	1.7	1.8± 0.9	124
Thiophene	22.0%	2.6	2.1 ± 0.1	209
α-C-H	38.0%	2.6	3.6 ± 0.5	177
β-C-H	7.0%	2.6	0.66 ± 0.2	32
D_2O @120 °C				
Substrates	**Extent of Deuteration**	**3.5 (μmol)**	**$k_{24\text{-obs}}$ ($M^{-1}Hr^{-1}$)**	**TON-24 hr**
Phenol*	15.2% (4.3%)	1.6	1.7 ± 0.7	214
o-C-H	22.7% (12.6%)	1.6	1.6 ± 0.4	90
p-C-H	16.4%	1.6	2.4 ± 0.9	66
1:1 AcOD-d_4/D_2O @120 °C				
Substrates	**Extent of Deuteration**	**3.5 (μmol)**	**$k_{24\text{-obs}}$ ($M^{-1}Hr^{-1}$)**	**TON-24 hr**
Thiophene*	66.9% (23.9%)	1.8	5.1 ± 0.5*	612*
α-C-H	87.9% (45.3%)	1.8	4.7 ± 0.3*	284*
β-C-H	45.6%	1.8	5.4 ± 0.7*	325
Phenol*	22.9% (7.6%)	1.5	3.1 ± 0.8	435
o/p-C-H	26.5% (12.6%)	1.5	3.6 ± 0.8	303
m-C-H	17.7%	1.5	2.4 ± 0.7	136
2-Phenylpyridine	5.1%	1.7	0.6 ± 0.3	95
o-phenyl-C-H	12.6%	1.7	1.6 ± 0.7	52
Naproxen	10.0%	1.3	1.7 ± 0.8	116
o-methoxy-C-H	30.6%	1.3	5.9 ± 1.5	116

Entries indicated with * notate a background reaction was observed; the reported values for $k_{24\text{-obs}}$ and TON-24 hr are based on the contribution from **3.5** only. Reactions were performed under the standardized reaction conditions shown in Scheme 3.10.

Table 3.3. The extent of deuteration summary, the observed 24-hour – average rate constants, $k_{24\text{-obs}}$, and catalyst TONs for the H/D Exchange of H_nSub catalyzed by **3.5** in AcOD-d_4 at 120 ^oC. N.D = Not Determined

AcOD-d_4@120 ^oC				
Substrates	**Extent of Deuteration**	**3.5 (μmol)**	$k_{24\text{-obs}}$ **($M^{-1}Hr^{-1}$)**	**TON-24 hr**
Benzene	27.9%	1.3	4.4 ± 0.4	717
Thiophene	41.8%	2.0	4.3 ± 0.4	520
α-C-H	66.5%	2.0	6.9 ± 0.9	413
β-C-H	17.2%	2.0	1.8 ± 0.5	107
Phenol	8.4%	1.1	1.5 ± 0.3	208
o/p-C-H	12.0%	1.1	2.1 ± 1.0	178
m-C-H	3.0%	1.1	0.58 ± N.D.	33
Fluorobenzene	16.3%	1.1	3.1± 1.0	401
o-C-H	17.2%	1.1	3.3± 1.0	170
p-C-H	20.6%	1.1	4.0 ± 1.2	102
m-C-H	13.0%	1.1	2.5 ± 1.3	128
Phenethylamine	10.3%	1.4	1.6 ± 0.6	170
o/p C-H	19.8%	1.4	3.0 ± 0.9	170
Benzoic Acid	1.9%	1.9	0.20 ± N.D.	20
o-C-H	2.6%	1.9	0.28 ± N.D.	12
p-C-H	1.2%	1.9	0.19 ± N.D.	8
2-Phenylpyridine	8.1%	1.5	1.2 ± 0.8	177
o-phenyl-C-H	22.0%	1.5	3.2 ± 0.9	106
m/p-phenyl-C-H	4.0%	1.5	0.57 ± N.D.	29
2,6 Diphenylpyridine	2.3%	1.2	0.40 ± N.D.	53
o-phenyl-C-H	7.1%	1.2	2.0 ± N.D.	53
Naphthalene	0.9%	1.5	0.12 ± N.D.	20
1,2 Dichlorobenzene	2.2%	1.3	0.34 ± N.D.	30
o-C-H	4.3%	1.3	0.69 ± N.D.	30
1,3 Benzodioxole	18.1%	1.6	2.3 ± 0.7	194
o-C-H	23.2%	1.6	3.0 ± 0.8	124
m-C-H	8.3%	1.6	1.1 ± 0.6	70
Naproxen	2.2%	1.2	0.37 ± N.D.	61
o-methoxy-C-H	15.6%	1.2	2.6 ± 1.0	61

The same observation can be made when comparing the reactivity of thiophene **3.19**, across the reaction in AcOD-d_4 at 80 ^oC and aqueous TFE-d_1 at 80 ^oC. In TFE-d_1 at 80 ^oC, thiophene was deuterated up to 36% with $k_{24\text{-}obs}$ of 3.6 ± 0.5 $M^{-1}Hr^{-1}$ and TON of 426 after 24 hours. When the solvent was swapped to AcOD-d_4 at 80 ^oC, the same reaction performed with a total extent of deuteration of 22%, a $k_{24\text{-}obs}$ of 2.1± 0.1 $M^{-1}Hr^{-1}$ and TON of 210 after 24 hours. These results are consistent with the observations made for benzene.

As we continue with the solvent screening series with thiophene, an additional comparison can be made by looking at the 1:1 AcOD-d_4:D_2O solution at 120 ^oC vs neat AcOD-d_4 at 120 ^oC (Tables 3.2 and 3.3). In the 1:1 AcOD-d_4:D_2O solution at 120 ^oC the H/D exchange reaction for thiophene catalyzed by **3.5** had a total extent of deuteration of 67% with a 24% contribution from the background reaction, a $k_{24\text{-}obs}$ of 5.1± 0.5 $M^{-1}Hr^{-1}$ (contribution from **3.5** only) and TON of 610 after 24 hours. When compared to the same reaction conditions in neat AcOD-d_4 at 120 ^oC, no background reaction was observed, and the extent of deuteration by **3.5** was remained about the same at 42% with a $k_{24\text{-}obs}$ of 4.3 ± 0.4 $M^{-1}Hr^{-1}$ and TON of 520 after 24 hours. There was only a rather slight decrease in the $k_{24\text{-}obs}$ across these two sets of reactions. This implies that for longer timescale reactions, the additional D_2O does not have a significant inhibitive effect on catalysis and, in fact it enhances the system's performance. That is an important observation since, in practical terms, D_2O is a much cheaper source of exchangeable deuterium than AcOD. In addition, a high D_2O content would allow for a higher degree of "statistical" deuterium incorporation under otherwise identical conditions. It appears also that D_2O is less binding to a Pt^{II} center than AcOD, which also favors faster H/D exchange.

When considering past systems utilizing aqueous TFE-d_1, the increase of the amounts of D_2O additive inhibited catalysis by suppressing an equilibrium of the aqua ligand substitution with a substrate. Expectedly, the final solvent comparison to be made is in neat AcOD-d_4 at 80 ^oC and 120 ^oC. Unsurprisingly, the increase in temperature results in the increase in reaction rate and extent of deuteration after 24 hours across all substrates screened. Benzene's extent of deuteration increased from 4.8% to 28% with a $k_{24\text{-}obs}$ increasing from 0.92 ± 0.2 to 4.4 ± 0.4 $M^{-1}Hr^{-1}$ which corresponds to a 4.8 times increase in the observed reaction rate constant. A conclusion that follows from this analysis of the solvent effects is that at 80 ^oC 0.150 M D_2O / TFE-d_1 kinetically outperforms neat AcOD-d_4. When the temperature is increased to 120 ^oC there is a significant increase in the rate of reaction for AcOD-d_4. Finally, when moving from neat AcOD-d_4 at 120 ^oC to 1:1 AcOD-d_4:D_2O mixture at 120 ^oC, the substrates that follow the traditional electrophilic aromatic substitution H/D exchange mechanism previously reported in the literature[33,49] have an increase in the extent of deuteration and, generally, a slight increase in the $k_{24\text{-}obs}$. Interestingly, for the strongly coordinating substrates such as 2-phenylpyridine, the rate of reaction decreases and the *ortho*-selectivity is reduced, thereby suggesting inhibition of the directing group - mediated H/D exchange.

Another observation from this kinetic assay concerns the reaction rate sensitivity to substrates' electronic effects when the solvent is AcOD-d_4 at 120 ^oC. From our past studies utilizing **1.5** in aqueous TFE-d_1 at 80 ^oC, the rate of the H/D exchange decreased in the order electron rich (hetero)arenes > benzene >> electron poor (hetero)arenes. However, in AcOD-d_4 at 120^oC with **3.5** as a catalyst, there seems to be a much less pronounced trend among such substrates. For example, for β-C-H bonds of thiophene, $k_{24\text{-}obs}$ is 1.8 ± 0.9 M^-

$^{1}Hr^{-1}$, fluorobenzene *m*-C-H bonds are more reactive with $k_{24\text{-}obs}$ of 2.5 ± 1.3 $M^{-1}Hr^{-1}$, and benzene C-H bonds are a potentially twice more reactive with $k_{24\text{-}obs}$ of 4.4 ± 0.4 $M^{-1}Hr^{-1}$. For the same catalyst in aqueous TFE-d_1 at 80 °C a smaller ratio is found for $k_{24\text{-}obs}$ values of benzene C-H bonds and β-C-H bonds of thiophene, 2.2 : 2.0. Hence, based on this very limited set of data, it appears that in wet TFE-d_1 at 80 °C the reaction is less substrate-selective than in AcOH at 120 °C with the $k_{24\text{-}obs}$ ratio of 4.4 : 1.8. This indicates that the substrate electronic effects in the aqueous TFE-d_1 at 80 °C are less pronounced / less substrate differentiating than in AcOD-d_4 at 120 °C, thus suggesting either a change in the reaction mechanism, or that the solvent significantly affects the reactivity of the Pt^{II} center in **3.5**. For a more reliable conclusion, a larger set of data of relevant substrates is needed.

3.4.7 Catalytic performance of a molecular analog of 3.5

From a practical perspective, the immobilization strategy of complex **3.5** provided enhanced reactivity ($k_{24\text{-}obs}$, TON) over the soluble 1st generation sulfonated CNN-pincer complex **1.5.** Given that the H/D exchange system for H_nSub in aqueous TFE-d_1 at 80 °C catalyzed by **1.5** was our previous benchmark, the immobilization strategy was successful in delivering a more efficient catalyst not suffering from bimolecular deactivation. However, in order to truly evaluate the effect of immobilization of **3.5** we must compare its reactivity with that of its molecular variant, complex **3.5-FC.** Given the past shortcomings of a similarly structured cyclopenteno-fused sulfonated CNN ligated Pt-OH_2 complex, **1.7**, it is expected that **3.5-FC** would be inherently more reactive than **1.5** but suffer from an even faster biomolecular deactivation pathway leading to insoluble, catalytically inert dimers, such as **1.8**. Catalyst **3.5-FC** was subjected to identical reaction

parameters as in the benchmarking of **3.5**. The reaction scheme for the H/D exchange utilizing this complex is shown below (Scheme 3.12). For the benchmarking of catalytic activity of the molecular complex **3.5-FC** two aromatic substrates were chosen, benzene and thiophene, both well characterized in H/D exchange by **3.5**. The results for benzene are summarized in Table 3.4, and the results for thiophene are shown in Table 3.5.

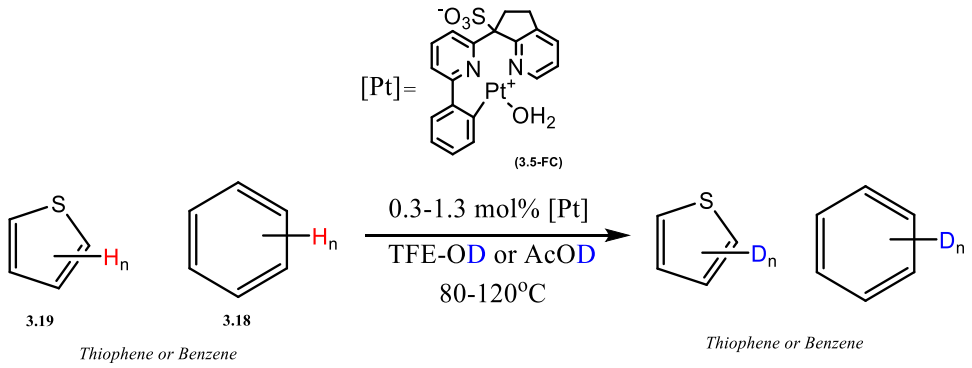

Scheme 3.12. Evaluation of the catalytic activity of a molecular complex **3.5-FC** in H/D exchange reaction between two deuterium sources and selected substrates H_nSub.

Table 3.4. Comparison of the catalytic activity of immobilized catalyst, **3.5**, its molecular variant, **3.5-FC**, and a benchmark complex **1.5**, in H/D exchange of benzene and different sources of exchangeable deuterium. N.R. = No Reaction, N.D. = Not Detemined

H/D Exchange Catalyst Comparison For Benzene					
Catalyst	**Conditions**	**Extent of Deuteration**	**Pt loading (μmol)**	**$k_{24\text{-}obs}$ ($M^{-1}Hr^{-1}$)**	**TON-24 hr**
3.5	**TFE-d_1 @80 °C**	21.6%	2.0	2.2 ± 0.4	360
	AcOD-d_4 @80 °C	4.8%	1.3	0.92 ± 0.2	150
	AcOD-d_4@120 °C	27.9%	1.3	4.4 ± 0.4	720
3.5-FC	**TFE-d_1 @80 °C**	4.1%	10.1	0.46 ± N.D.	15
	AcOD-d_4 @80 °C	0.0%	8.4	N.R.	N.R.
	AcOD-d_4@120 °C	28.0%	8.4	0.70 ± N.D.	57
1.5	**TFE-d_1 @80 °C**	40.0%	7.4	1.1 ± 0.2	180
	AcOD-d_4 @80 °C	14.0%	7.2	0.38 ± N.D.	64
	AcOD-d_4@120 °C	N/A	N/A	N/A	N/A

Table 3.4 shows a comparison of the catalytic performance of three different catalysts in the H/D exchange reaction of benzene under three different reaction conditions. In all cases, complex **3.5** had the best performance in terms of both $k_{24\text{-}obs}$ and the TON achieved over the 24 hour reaction period. Somewhat expectedly the free complex **3.5-FC** was extremely poorly performing. The complex was poorly soluble at room temperature and was only completely dissolved at elevated temperature and after 45 minutes of reaction time in TFE-d_1 at 80 ^{o}C a large amount of yellowish orange precipitate began to form, thus indicating the presumed formation of di(poly)mers similar to **1.8**. Despite this fact, the reaction catalyzed by **3.5-FC** did still manage to deliver 4.1% deuterium incorporation over 24 hours with $k_{24\text{-}obs}$ of 0.46 $M^{-1}hr^{-1}$ and 15 TON. **3.5-FC** was completely inactive in AcOD-d_4 at 80 ^{o}C, and it was not until 120 ^{o}C that the complex was able to engage in H/D exchange, yielding 28% deuteration with $k_{24\text{-}obs}$ of 0.70 $M^{-1}hr^{-1}$ and TON of 57. This is a significant improvement over its performance under reduced temperature, as well as in TFE-d_1 at 80 ^{o}C. However, complex **3.5-FC** failed to outperform either complex **1.5** or **3.5**, based on their reactivity parameters, $k_{24\text{-}obs}$ and TON, shown in Table 3.4. The catalyst **3.5-FC**, expectedly more reactive in H/D exchange, thanks to the increased rigidity of pincer ligand, cannot be efficiently utilized in solutions due to the fast catalyst deactivation.

Table 3.5. Comparison of the catalytic activity of immobilized catalyst, **3.5**, and its molecular variant, **3.5-FC**, in H/D exchange of thiophene and different sources of exchangeable deuterium. Reactions were performed under the standardized conditions shown in Scheme 3.10.

H/D Exchange Catalyst Comparison For Thiophene						
Catalyst	**Conditions**	**C-H Bond Type**	**Extent of Deuteration**	**Pt loading (μmol)**	**$k_{24\text{-}obs}$ ($M^{-1}Hr^{-1}$)**	**TON-24 hr**
3.5	**TFE-d_1 @80 °C**	**All Aromatic**	36%	4.2	3.6 ± 0.5	430
		α-C-H	52%	4.2	5.1 ± 0.7	310
		β-C-H	20.%	4.2	2.0 ± 0.2	120
	AcOD-d_4 @80 °C	**All Aromatic**	22%	2.6	2.1 ± 0.4	210
		α-C-H	38%	2.6	3.6 ± 0.9	180
		β-C-H	7.0%	2.6	0.66 ± 0.5	32
	1:1 AcOD-d_4:D_2O @120C	**All Aromatic**	67% (24%)	1.8	5.1 ± 0.5*	610*
		α-C-H	88% (45%)	1.8	4.7 ± 0.3*	280*
		β-C-H	46%	1.8	5.4 ± 0.7	330
3.5-FC	**TFE-d_1 @80 °C**	**All Aromatic**	52%	8.4	1.3 ± 0.2	150
		α-C-H	66%	8.4	1.7 ± 0.1	100
		β-C-H	36%	8.4	0.90 ± 0.2	54
	AcOD-d_4 @80 °C	**All Aromatic**	18.7%	8.9	0.47 ± 0.2	52
		α-C-H	24%	8.9	0.59 ± 0.2	33
		β-C-H	13.7%	8.9	0.34 ± 0.1	19
	1:1 AcOD-d_4:D_2O @120°C	**All Aromatic**	83% (24%)	8.9	1.5 ± 0.1*	166*
		α-C-H	90.% (45%)	8.9	1.0 ± 0.06*	58*
		β-C-H	77%	8.9	1.9 ± 0.2	108

* A background reaction was observed, reported values for $k_{24\text{-}obs}$ and TON-24 hr are based on the contribution from **3.5** only.

A similar series of experiments were performed utilizing thiophene as a substrate (Table 3.5). By choosing thiophene as a substrate, we speculated that if a higher degree of reactivity were to be achieved utilizing **3.5-FC** then that would be most likely when using

it with a more reactive arene, so that the catalyst deactivation will be less competitive with the faster H/D exchange. In fact, we were able to see H/D exchange catalyzed by **3.5-FC** in AcOD at 80 ^{o}C, under the reaction conditions where benzene was unable to be engaged. The molecular catalysts showed a competitive performance in terms of the practical deuteration extent of the substrate thanks to its higher loading. In turn, considering the reactivity parameters ($k_{24\text{-obs}}$, TON), complex **3.5** outperformed its molecular analog **3.5-FC** kinetically about 3-5-fold. As expected, a comparable, in practical terms, performance (a comparable percent of substrate deuteration) of **3.5-FC** vs. **3.5** may only be expected at higher loading of **3.5-FC** when highly reactive substrates such as thiophene are employed.

3.4.8 Recyclability of MSN-immobilized catalyst 3.5

Some inherent advantage to the use of heterogeneous catalysts in synthetic applications is the easy separation of the catalysts from reaction solutions and, often, the ability to reuse the catalysts several times. Considering that the immobilized catalyst **3.5** outperformed either of the homogenous complexes **1.5** and **3.5-FC**, based on our practical metrics, we wanted to explore the recyclability of **3.5** under a variety of reaction conditions and compare the relevant catalysis parameters, $k_{24\text{-}obs}$ and TON, after each catalyst reuse.

Catalyst recyclability was tested by repeating the H/D exchange reaction of thiophene as the aromatic substrate and different sources of exchangeable deuterium (Scheme 3.10) over multiple 24h reaction cycles. The use of different deuterium sources in the H/D exchange allowed to compare the catalyst recyclability as a function of the solvent and reaction temperature.

Table 3.6. Recyclability study of complex **3.5** under various conditions for the H/D exchange of thiophene. Reactions were performed under the standardized reaction conditions shown in Scheme 3.10. Reaction cycle 1 was run at 2-fold larger reaction scale from the procedure in Scheme 3.10

H/D Exchange Catalyst Comparison for Thiophene					
Conditions	**Cycle #**	**Extent of Deuteration**	**Pt loading (μmol)[a]**	**$k_{24\text{-}obs}$ ($M^{-1}Hr^{-1}$)**	**TON-24 hr**
TFE-d_1 @ 80 °C	**1**	20.%	2.2	3.2 ± 0.4	230
	2	34%	2.2	3.3 ± 0.4	390
	3	30.%	1.6	3.9 ± 0.5	210
	4	10.%	0.9	3.9 ± 0.5	310
Conditions	**Cycle #**	**Extent of Deuteration**	**Pt loading (μmol)**	**$k_{24\text{-}obs}$ ($M^{-1}Hr^{-1}$)**	**TON-24 hr**
AcOD-d_4 @ 120 °C	**1**	42%	4.0	4.4 ± 0.9	520
	2	44%	3.7	2.4 ± 0.2	290
	3	24%	2.3	3.9 ± 0.8	470
	4	22%	1.3	3.5 ± 0.7	420
Conditions	**Cycle #**	**Extent of Deuteration**	**Pt loading (μmol)**	**$k_{24\text{-}obs}$ ($M^{-1}Hr^{-1}$)**	**TON-24 hr**
1:1 AcOD-d_4:D_2O @120C	**1**	67% (24%)	3.6	5.1 ± 0.5 [b]	610
	2	89% (24%)	3.5	3.7 ± 0.4[b]	450
	3	44% (24%)	2.8	2.1 ± 0.2[b]	250
	4	49% (24%)	1.8	2.8 ± 0.3 [b]	340

[a] Pt loading is reported as the μmol of **3.5** used in the reaction per 0.5 mL of reaction solution.

[b] A background reaction was observed. The reported values for $k_{24\text{-}obs}$ and TON-24 hr are based on the contribution from **3.5** only.

To monitor the progress of the reactions, ^{1}H-NMR and ^{2}H-NMR spectra were collected periodically. After 24h the reactions were stopped, the catalyst was collected via filtration and the JY tube was rinsed with methanol to remove as much solid as possible. Then, the catalyst was rinsed with either 2,2,2-trifluoroethanol or acetic acid and was allowed to dry under vacuum. A subsequent drying was done in a vacuum oven at 100 °C

for 2 hrs. Then the catalyst was weighed and used for a subsequent H/D exchange under identical reaction conditions.

Generally, there was a very good recyclability across each of the screened reaction conditions. Aqueous TFE-d_1 at 80 ^{o}C showed generally very good recyclability, where the $k_{24\text{-}obs}$ had very little variation in the reaction cycles 1-4 Additional recycles were not accomplished due to the small scale of the reaction and material loss.

The recyclability of this catalyst remained very good as the reaction conditions changed to AcOD-d_4 at 120 ^{o}C. The extent of deuteration, $k_{24\text{-}obs}$, and TON for this solvent system were improved over the TFE-d_1 at 80 ^{o}C system. The first cycle for this series of experiments had an overall extent of deuteration for thiophene of 42% with 2.0 μmol catalyst loading, with a $k_{24\text{-}obs}$ of 4.3 $M^{-1}hr^{-1}$ and a TON of 520 after the 24 hour reaction cycle. These values fluctuated slightly over the course of the following experiments. The first cycle for the experiments were run at 2x standard scale, in order to produce a large portion of "once" recycled material. This served to allow for more material to be available for subsequent recyclability studies. The 4th reaction cycle had an extent of deuteration of 21.6% because of a decreased catalyst loading of 1.3 μmol associated with a physical loss of **3.5** during separations. After each recycle, there is some inevitable loss of complex that cannot be recovered, as a result the loading of **3.5** in cycle 4 versus cycle 1 is about half, which would lead to a increase in the relative concentration of H_nSub to **3.5** which would result in a decrease in extent of deuteration over the same time period. Nevertheless, $k_{24\text{-}obs}$ of 3.5 $M^{-1}hr^{-1}$ and a TON of 420 matched average values observed in the previous 3 runs, a sign of the catalyst's remarkably steady performance and a high degree of recyclability for complex **3.5** under these reaction conditions.

The use of even harsher / more acidic environment, 1:1 AcOD-d_4:D_2O solution at 120 ^oC, was also tested. Unlike the previous two solvents, there was a noticeable deterioration of the catalyst **3.5** performance when moving from the 1st to the 4th reaction run. Cycle 1 had the highest extent of deuteration of thiophene over the reaction period with 67% with a background contribution of 24%. The values of $k_{24\text{-}obs}$ and TON were calculated by subtracting the contribution of the background reaction with the solvent. The first cycle had the highest overall $k_{24\text{-}obs}$ and TON of any of the first reaction cycles with a $k_{24\text{-}obs}$ of 5.1 ± 0.5 $M^{-1}hr^{-1}$ and 610 total TON after 24 hours. However, as this series of recycles progressed, the $k_{24\text{-}obs}$ and TON steadily decreased, thereby implying a deactivation and/or leeching of **3.5** over time. After 4 reaction cycles, the performance of **3.5** dropped to a $k_{24\text{-}obs}$ of 2.8 ± 0.3 $M^{-1}hr^{-1}$ and the catalyst TON of 340. This final reaction cycle presented a 45% decrease in the performance of catalyst **3.5**.

An impressive metric that should be highlighted in this study is that complex **3.5** was able to maintain its reactivity virtually at the same level across 4 separate 24 hour reaction cycles in both aqueous TFE-d_1 at 80 ^oC and AcOD-d_4 at 120 ^oC. The fluctuations in catalytic performance appear to be associated with potential measurement errors, and a more exhaustive/extensive recyclability study must be performed in order to realize just how robust this catalyst is under these reaction conditions. When the catalyst TONs in these reactions are treated as cumulative values across each reaction cycle for a given set of reaction conditions, the total TONs of the catalyst **3.5** in the H/D exchange of thiophene are 1140, 1700, and 1700 for the TFE-d_1 at 80 ^oC, AcOD-d_4 at 120 ^oC, and the 1:1 AcOD-d_4:D_2O solution at 120 ^oC, respectively. Considering that the homogeneous catalytic systems using **1.5** or **3.5-FC** struggled to achieve catalyst TON of ~180 before succumbing

to bimolecular deactivation, this nearly 10-fold increase in the catalyst efficiency presents a significant advancement.

3.4.9 Evidence of Pt^{II} acting as the active catalyst of the H/D exchange by 3.5

Identifying the active catalytic species in heterogeneous systems is often a complex and difficult task. For the purposes of many catalytic processes, Pt^0 has been utilized in its metallic form, colloidal nanoparticle suspensions, and also supported on substrates such as charcoal, graphene, carbon nanotubes, and simple silica supports.[7-8, 93] Additionally, some of the premier industrial applications for the direct deuteration of hydrocarbons utilize heterogeneous Pt^0 catalysts. This consideration raises some questions about the identity of the active species present in our system including our catalyst **3.5**. One reason for this concern is due to some side reactions that may occur during the metalation step of the immobilized pre-ligand **3.15** with K_2PtCl_4 (Scheme 3.7). The formation of a black precipitate that was presumed to be Pt^0 was observed over the course of reaction optimization experiments. The formation of Pt^0 is likely a result of a well-known thermally driven disproportionation of K_2PtCl_4 to yield $K_2Pt^{IV}Cl_6$ and Pt^0.[94]

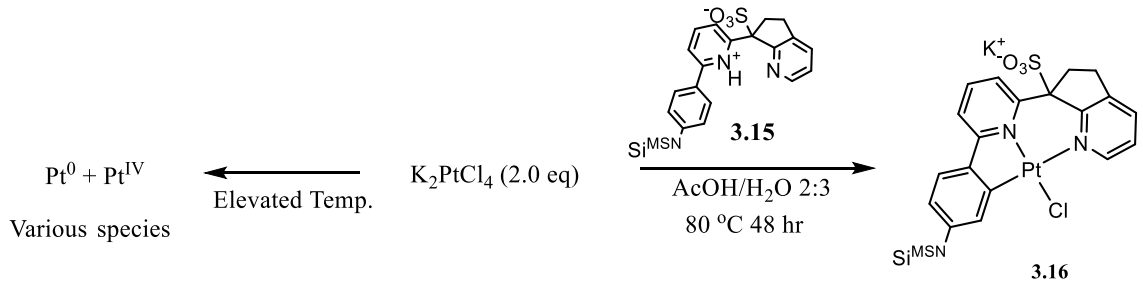

Scheme 3.13. A potentially competitive formation of **3.16** and Pt^0 and Pt^{IV} disproportionation products.

Under the optimized reaction conditions for the metallation of **3.15** with K_2PtCl_4 shown in Scheme 3.13, there was no visual indication of Pt^0 formation. In fact, the reaction conditions highlighted above were chosen specifically to exclude the visually detectable

formation of Pt^0. However, this visual inspection is not sufficient and the presence of small amounts of potentially highly reactive Pt^0 nanoparticles capable of activating C-H bonds cannot be ruled out. Due to the insolubility of the final product **3.5**, we had no way of separating this solid MSN material from other solids potentially Pt^0 containing that may have formed during the reaction. To address this concern, control experiments were designed to test for what the active catalytic species is, Pt^0 particles or the immobilized Pt^{II} complex **3.5**. The experiments utilized two catalysts, the immobilized Pt^{II} aqua complex **3.5**, and its precursor, the immobilized Pt^{II}-Cl complex **3.16**, measured to have an identical Pt^{II} loading of 2.3 µmol using KOH digest / ^{1}H NMR analysis of these solids. The H/D exchange reactions between anisole and TFE-d_1 were run in the presence of **3.5** or **3.16** under the reaction conditions highlighted in Scheme 3.10 at 80 °C.

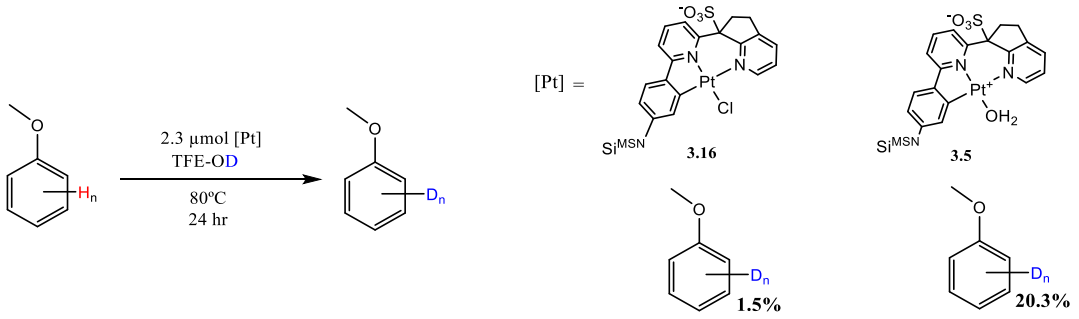

Scheme 3.14. Assessment of a relative activity of **3.16** and **3.5** in catalytic aromatic H/D exchange with TFE-d_1.

As it is shown in Scheme 3.14, **3.5** was more active than **3.16** by at least one order of magnitude. This result suggests that Pt^0 particles (if any present) would not contribute much to the catalytic activity of **3.5**. Indeed, if Pt^0 particles were present in **3.16**, then these Pt^0 particles would be present in **3.5** as well in the same or an even lesser amount because of their possible mechanical losses and/or aggregation/deactivation during the

transformation of **3.16** to **3.5**. As such, if Pt^0 particles were the major contributor to the catalytic activity of **3.5**, we would expect that the catalytic H/D exchange of anisole would yield similar results for both **3.16** and **3.5** utilized as a catalyst. What was observed here is exactly the opposite.

3.5. Conclusions

We have successfully synthesized and characterized a mesoporous silica nanoparticles (MSN) - immobilized sulfonated CNN-pincer Pt^{II}-OH_2 complex **3.5** that can catalyze H/D exchange between arenes and various deuterium sources, TFE-d_1, AcOD and D_2O. When compared to our previous homogenous system utilizing complex **1.5** in D_2O / TFE-d_1 at 80 ^oC, complex **3.5** outperforms **1.5** in each of our "practical" parameters for catalysis ($k_{24\text{-}obs}$ and TON @ 24h). Catalyst **3.5** is capable of overcoming the limitations of our past homogenous systems, and is capable of deuterating aromatic substrates bearing EDGs, some EWGs and some moderately strong coordinating groups such as 1^o amines, and some substituted pyridines. In the course of our substrate screening, we have observed *ortho*-selective deuteration of 2-phenylpyridines which is a strong indication that a directing group-mediated C-H activation mechanism may be possible for this class of catalysts. While the extent of deuteration of most aromatic substrates catalyzed by **3.5** remained modest in most cases, the thermal robustness and the recyclability of the catalyst suggest its potential for achieving higher extents of deuteration over prolonged reaction periods and/or repeated cycles. The recyclability of **3.5** has been shown to be remarkably good over 4 reaction cycles in aqueous solutions of TFE-d_1 at 80 ^oC and in AcOd-d_4 at 120 ^oC leading to the cumulative catalyst TON ~1100 and ~1700, respectively. In summary,

we have synthesized an MSN supported immobilized molecular Pt^{II} complex, **3.5**, that is capable of catalytically propagating the H/D exchange of arenes under various deuterium sources. This complex has proven to be more kinetically reactive and more thermally robust than either homogenous complex of the same class, **1.5** or **3.5-FC**. Finally, on a practical side, complex **3.5** can be consecutively recycled, and is compatible with cheaper deuterium sources such as AcOD and D_2O.

Supporting Information for Chapter 3

I. General Information

Solvents, Reagents and Techniques for Synthesis

All solvents and reagents were purchased directly from commercial sources Aldrich, Oakwood, Pressure Chemical, Matrix, Acros Organics, Fischer Chemical, AOB Chem, AK Scientific, or Cambridge Isotope Laboratories) Tetrahydrofuran was dried with sodium metal and was collected via fractional distillation. All other reagents and solvents were used without further purification unless otherwise noted. All glassware was dried overnight in an oven at 140^{o}C.

Solvents and Reagents for H/D Exchange Experiments

All solvents and reagents were purchased directly from commercial sources Aldrich, Oakwood, Pressure Chemical, Matrix, Acros Organics, Fischer Chemical, AOB Chem, AK Scientific, or Cambridge Isotope Laboratories) and were used without further purification. All solvents and reagents were degassed and stored under and argon atmosphere prior to use. All JY tubes used were dried in overnight in an oven at 140^{o}C prior to use.

Instrumentation

^{1}H-, ^{2}H-, ^{13}C, and ^{19}F NMR Spectra were collected using various Bruker NMR instruments (AVANCE III HD NanoBay 400 MHz, AVANCE NEO 400 MHZ, Bruker DRX-500 MHz, and AVANCE III 600 MHz). All chemical shift (δ) values are reported with respect to an internal standard. NMR-data are reported as follows: chemical shift (δ) (multiplicity [s =singlet, d = doublet, t = triplet, q = quartet, quint = quintet, sept = septet, hept = heptet, m = multiplet], coupling constants (J, Hz) and integration). All data was processed using Bruker Topspin 4.1.1 data processing program. All quantitation involving extent of deuteration was performed by measure the loss ^{1}H-NMR signal intensity and ^{2}H-NMR was

used primarily as a qualitative proof of C-D Bond formation due to the low signal to noise and broad NMR signals.

High resolution mass spectra (HRMS) were recorded on a JEOL AccuTOF ESI-MS. All samples were introduced into the MS via an HPLC line containing an H_2O/MeOH mobile phase.

Tunneling electron microscope (TEM) images were taken on a JOEL-2100 LaB_6 TEM with an accelerating voltage of 200 kV and a beam current of 104 μA. All samples were dispersed in ethanol and drop cast onto a lacey carbon 200-mesh copper grid. Scanning electron microscope (SEM) images were taken using a Hitachi SU-70 Field Emission SEM equipped with a Bruker energy dispersive spectroscopy (EDS) detection model: Flash 6T/60 with a silicon drift detection (no Li dopant) and solid angle of 0.189 sr.

Nitrogen isotherms were recorded with a Micrometrics ASAP 2020 Porosimeter. Samples were degassed in vacuum at 100°C for 6h prior to characterization. The surface area was determined using the Brunauer-Emmett-Teller (BET) method with a relative pressure range (P/P_o) of 0.05-0.30. Pore size and volume was calculated from the adsorption branch using the Barrett, Joyner, and Halenda (BJH) method.

II. Synthesis

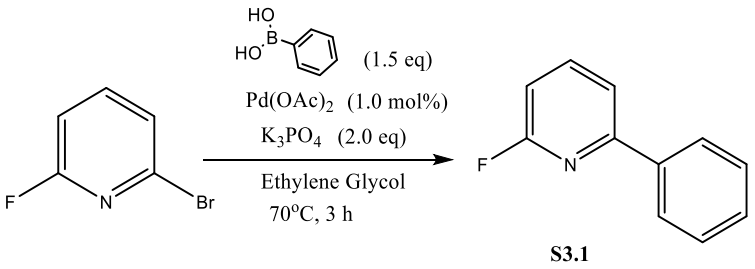

Scheme S3.1. Synthesis of 2-fluoro-6-phenylpyridine **S3.1**.

Synthesis of 2-fluoro-6-phenylpyridine

120 mL of ethylene glycol was added dry round bottom flask and was heated to 70^{o} C. After the solvent reached a homogenous temperature, 10.2 g of K_3PO_4*$7H_2O$ (30.1 mmol 2.0 eq), 3.66 g of phenylboronic acid (30.0 mmol 2.0 eq), and 2.64g of 2-bromo-6-fluoropyridine (15.0 mmol 1.0 eq) were added sequentially to the flask and allowed to fully dissolve. Then 40.0 mg of $Pd(OAc)_2$ (0.178 mmol 1.2 mol%) was added and the solution turned a transparent yellow color and the reaction was allowed to proceed for 3 hrs before quenching with a concentrated brine solution. The progress of the reaction was monitored via TLC using 90:10:0.1 (Hex:EtOAc:TEA) as a mobile phase. When the reaction was complete the solution was extracted with 3x30 mL Et_2O and dried with $MgSO_4$ before removing solvent under vacuum to yield 3.8 g of a crude yellow oil. The product was purified via column chromatography using 90:10:0.1 (Hex:EtOAc:TEA) to yield 2.1 g of a colorless viscous oil (80% isolated yield) of 2-fluoro-6-phenylpyridine.

^{1}H-NMR (400 MHz, $CDCl_3$): δ = 8.01 (m, 2H) 7.81 (q, 1H), 7.60 (dd 1H), 7.46 (m, 3H), 6.84 (dd, 1H) ppm.

^{13}C-NMR (100 MHz, C $CDCl_3$): δ = 164.48, 162.58, 156.39, 141.75, 137.67, 129.74, 128.90, 127.02, 117.40,

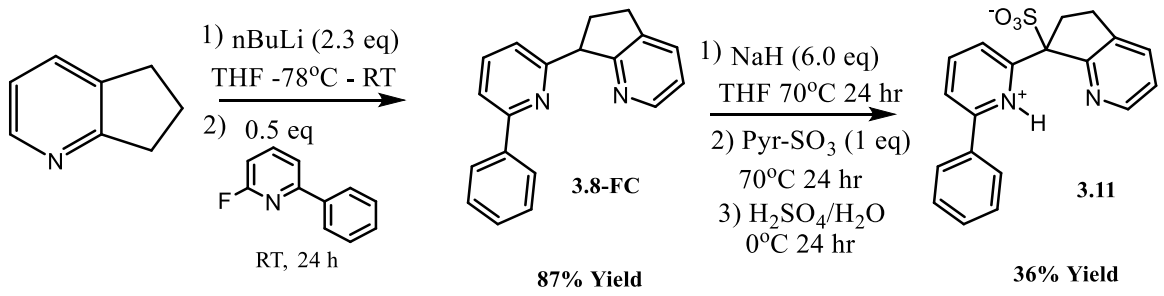

Scheme S3.2. Synthesis of 7-(6-phenylpyridin-1-ium-2-yl)-6,7-dihydro-5*H*-cyclopenta[*b*]pyridine-7-sulfonate **3.11**.

Synthesis of 7-(6-phenylpyridin-2-yl)-6,7-dihydro-5*H*-cyclopenta[*b*]pyridine 3.8-FC

A dry 50 mL Schlenk tube was transferred into an argon filled glove box and was charged with 1.61 g 6,7-dihydro-5*H*-cyclopenta[*b*]pyridine (5.45 mmol 2.3 eq) and was subsequentially dissolved into 15 mL dry THF and the tube was sealed with a Teflon cap. The solution was then transferred onto a Schlenk line and cooled to -78 °C for 30 minutes under rapid stirring. Then, 1.3 mL of 11M nBuLi in hexanes (5.45 mmol, 2.3 eq) was added dropwise over 10 minutes. The resulting dark red solution was then stirred at -78 °C for an additional 30 minutes then was warmed to room temperature and sustained for 2 hours to allow for complete formation of the anion. Next, the solution was cooled back to -78 °C and 5mL of a THF solution containing 934.6 mg 2-fluoro-6-phenyl pyridine, **S3.1** (1.80 mmol, 1.0 eq) was added dropwise over 1 minute. The solution maintained a dark red coloration and was allowed to warm back to room temperature and was allowed to stir at room temperature for 24 hr. The next day, the solution was quenched with 20 mL DI H_2O. The resulting mixture was then extracted with 3x30 mL of Et_2O and the solvent was removed via reduced pressure to yield 2.5g (87% yield by NMR) of an impure viscous red/orange oil and was further purified via column chromatography with a 60:40:0.01:0.01 (Hexane:EtOAc:$CHCl_3$:TEA) mobile phase to yield 1.28 g of a viscous orange oil (82%

isolated yield). The crude material is suitable for sulfonation, though higher yields are achieved with the purified compound.

^{1}H-NMR (400 MHz, $CDCl_3$): δ = 8.37 (m, 1H), 7.97, (m, 2H), 7.68 (t, 1H), 7.57 (m, 2H), 7.41 (m, 3H), 7.18 (dd, 1H), 7.07 (dd, 1H), 4.60 (t, 1H), 3.25 (m, 1H), 3.02 (m, 1H), 2.65 (m, 2H) ppm.

^{13}C-NMR (100 MHz, $CDCl_3$): δ = 166.4, 163.0, 157.0, 148.1, 139.9, 137.9, 137.3, 132.8, 128.8, 127.1, 121.7, 121.3, 118.4, 54.2, 31.5, 30.0 ppm.

Synthesis of Sodium 7-(6-phenylpyridin-2-yl)-6,7-dihydro-5H-cyclopenta[b]pyridine-7-sulfonate, 3.11

A dry 50 mL Schlenk tube was transferred into an argon filled glove box and was charged with 30 mL of A dry THF solution containing 4.2g of 7-(6-phenylpyridin-2-yl)-6,7-dihydro-5*H*-cyclopenta[*b*]pyridine **3.8-FC** (15.4mmol, 1.0 eq). Under heavy stirring, 2.47 g of NaH powder (92.5 mmol, 6.0 eq) was added to the solution (note: not all of NaH will completely dissolve) and the Schlenk flask was sealed with a Teflon cap and was heated to 70 ^{o}C for 24 hr. Periodically, the solution was removed from heat and vented under reduced pressure to allow H_2 gas to be released. The resulting solution is a viscous dark red color indicative of carbanion formation. The solution was then allowed to cool to room temperature and transferred into an argon filled glovebox where 2.45 g of solid pyridine sulfur trioxide complex (15.4 mmol 1.0 eq) was added into the flask (note: rinsing with additional THF may reduce yield) The reaction mixture undergoes a rapid series of color changes starting from a dark red color to a brown/green, and eventually maintains a red/orange color. The flask was then sealed and heated to 70 ^{o}C for an additional 24 hr.

The solution is then placed into an ice bath and quenched with 100 mL of a 3:1 mixture of THF/MeOH added slowly over 30 minutes. The solvent was then removed, and the remaining dark browns solids were reconstituted into 50 mL DI H_2O. insoluble materials were removed from the solution via vacuum filtration. The pH of the solution was adjusted to a pH of ~1 and placed in the refrigerator overnight to yield a silty brown precipitate. The precipitate was filtered off and dried to yield 2.1g of zwitterionic product **3.11**. This zwitterionic product **3.11** can be quantitatively converted to the corresponding alkali salts by combining the zwitterion with a stoichiometric equivalent of the metal hydroxide.

Corresponding spectral data for the sodium salt 3.11

^{1}H-NMR (400 MHz DMSO-*d*$_6$): δ = 8.76 (d, 1H), 8.48 (d, 1H), 7.98 (t, 1H), 7.92 (m, 5H), 7.44 (m, 3H), 3.28 (m, 2H), 3.11 (m, 1H), 2.71 (m, 1H)

^{13}C-NMR (150 MHz, DMSO-*d*$_6$): δ = 158.2, 153.7, 144.6, 139.4, 138.1, 129.1, 128.5, 126.7, 125.2, 122.2, 119.0, 76.5, 64.9, 35.6, 28.6, 15.1

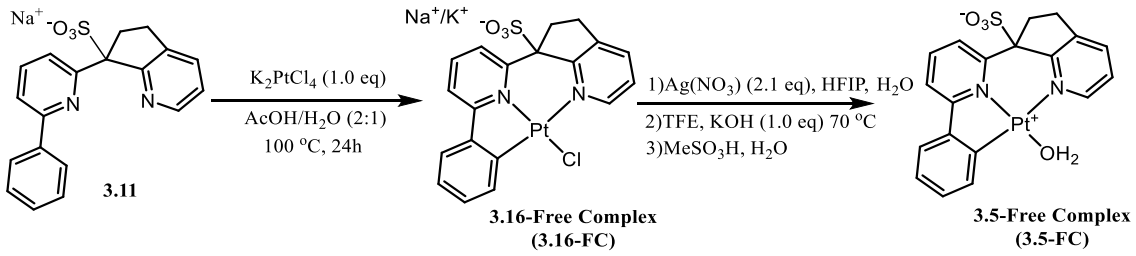

Scheme S3.3. Synthesis of **3.5-FC**

Synthesis of Pt^{II}-Cl Complex 3.16-FC

A dry 50 mL Schlenk tube was charged with 750 mg (2.0 mmol 1.0 eq) Sodium 7-(6-phenylpyridin-2-yl)-6,7-dihydro-5H-cyclopenta[b]pyridine-7-sulfonate (the zwitterion **3.11** may also be used for this step) dissolved in 20 mL of a 1:1 AcOH/H_2O solution. Then, 10 mL of a 1:1 AcOH/H_2O solution containing 840 mg (2.0 mmol, 1.0 eq) K_2PtCl_4 was added and the flask was sealed. Then the flask was headed to 100 ^oC for 18 hr under rapid stirring. The resulting orange solution was dried under vacuum to yield a yellow powder. The powder was extracted 3x10 mL of warm trifluoroethanol and the solution was filtered in order to remove any insoluble salts. The TFE solution was then dried under vacuum to yield 590mg (48.0% yield) of **3.16-FC**.

^{1}H-NMR (400 MHz MeCN-*d_3*): δ = 9.50 (d, 1H), 8.04 (d, 1H), 7.97 (t, 1H), 7.87 (dd, 1H), 7.77 (dd, 1H), 7.61 (m, 1H), 7.48 (m, 1H), 7.41 (m, 1H), 7.10 (m, 2H), 3.57 (m, 2H), 3.11 (m, 1H), .87 (m, 1H) ppm.

ESI-MS (– mode) in H_2O Calculated m/z for [(C_6H_4-pcpps)Pt^{II}(Cl)]: 580.1 Found 580.207

Synthesis of 3.5-FC

400 mg (0.65-0.66 mmol) Pt^{II}-Cl complex **3.16-FC** was placed in a 100 mL round bottom flask (crude material containing K / NaCl may also be used in this synthesis). To the round-bottom flask was added 40 ml HFIP and the contents were stirred until completely dissolved. In a vial, 0.236 g (1.39 mmol, 2.1 equiv.) AgNO3 was dissolved in 5 mL DI H2O and was added to the HFIP solution. The resulting mixture / colloid was rotatory evaporated down to about 10 ml when a large amount of solid formed. The solid was removed via filtration and rinsed with H_2O. The solid material was redissolved in 20 mL TFE and transferred to a 50 mL Schlenk flask. In a separate vial, 44 mg (0.66 mmol, 1

equiv) of 85 % KOH was dissolved in 5 mL TFE which was then transferred to the Schlenk flask. The resulting slurry was wrapped in tin foil and stirred at 70 °C overnight. The next day, the Schlenk flask was removed from the heating bath and the slurry was filtered through Celite to give a yellow-colored filtrate. The filtrate was reduced in volume to ~3 mL and dispersed in 67 mL DI H2O. The mixture was filtered to give a bright yellow solution. The pH was then adjusted to 2 using a 50% $MeSO_3H$ solution which was accompanied by the formation of a silty yellow precipitate. The supernatant solution was decanted off and the precipitate was washed with fresh DI H2O and HFIP. This process was repeated until the washing was colorless. The precipitate was then dried under high vacuum for 24h at room to yield 190 mg of **3.5-FC** (50 % yield).

^{1}H-NMR (400 MHz DMSO-*d_6*): δ = 8.81 (d, ^{3}JHH=5.7 Hz, 1H), 8.21 (d, ^{3}JHH=4.5 Hz, 2H), 8.12 (d, ^{3}JHH=7.7 Hz, 1H), 7.89-7.84 (m, 1H), 7.76 (d, ^{3}JHH=4.5 Hz, 1H), 7.72-7.69 (m, 1H), 7.62 (dd, ^{3}JHH=8.4 Hz, JHH=5.8 Hz, 1H), 7.30-7.22 (m, 2H), 3.15 (dd, 1H), 2.84 (q, ^{3}JHH=10.5 Hz, 1H).

^{13}C-NMR (100 MHz, DMSO-*d_6*): δ = 164.7, 156.8, 156.0, 146.1, 142.3, 141.1, 140.9, 136.6, 134.0, 130.1, 125.4, 125.2, 124.7, 124.4, 119.1, 80.3, 36.1, 29.4.

ESI-MS (– mode) in in HFIP with KOH (aq) added Calculated m/z for [(C_6H_4-pcpps)Pt^{II}(OH)]: 562.04, Found 562.0466

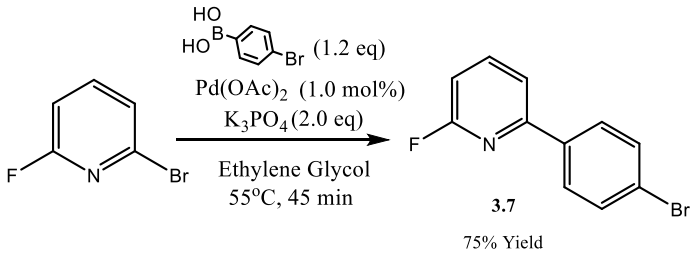

Scheme S3.4. Synthesis of 2-fluoro-6-(4-bromophenyl) pyridine **3.7**

Synthesis of 2-(4-bromophenyl)-6-fluoropyridine 3.7

240 mL of ethylene glycol was added dry round bottom flask and was heated to 55 ^{o}C. After the solvent reached a homogenous temperature, 16.2 g of K_3PO_4*H_2O (70.3 mmol 2.0 eq), 8.4 g of 4-bromophenylboronic acid (41.8 mmol 1.2 eq), and 6.2g of 2-bromo-6-fluoropyridine (35.2 mmol 1.0 eq) were added sequentially to the flask and allowed to fully dissolve. Then 80.0 mg of $Pd(OAc)_2$ (3.2 mmol 1.0 mol%) was added and the solution turned a transparent yellow color and the reaction was allowed to proceed for 45 min before quenching with a concentrated brine solution. A large amount of white precipitate formed during the reaction. The progress of the reaction was monitored via TLC using 90:10:0.1 (Hex:EtOAc:TEA) as a mobile phase. Upon addition of brine, more white precipitate formed, and the solution was allowed to cool in the freezer overnight. The following morning the precipitate was filtered off to yield 12.2 g of a crude off white solid. The product was purified via column chromatography using 90:10:0.1 (Hex:EtOAc:TEA) to yield 6.6 g of a white powder (75% isolated yield) of 2-fluoro-6-(4-bromophenyl)pyridine **3.7** This reaction is prone to side reactions where the cross-coupling can occur multiple times on the substrate to yield poly aryl fluoropyridines.

^{1}H-NMR (400 MHz, $CDCl_3$): δ = 7.85 (m, 3H), 7.58 (m, 3H), 6.88 (dd, 1H) ppm.

^{19}F-NMR (400 MHz, $CDCl_3$): δ = -66.28 ppm

^{13}C-NMR (100 MHz, $CDCl_3$): δ = 164.6, 162.27, 155.2, 141.8, 136.4, 132.0, 128.5, 124.2, 117.2, 108.1 ppm.

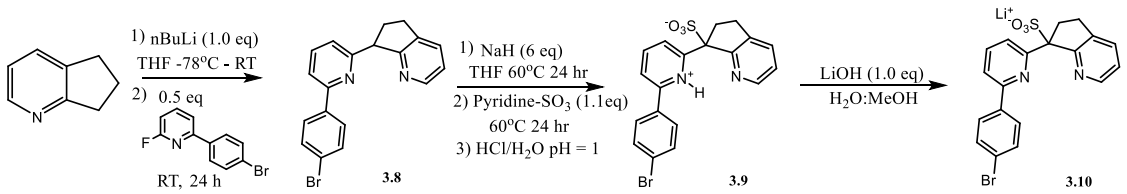

Scheme S3.5. Synthesis of 7-(6-(4-bromophenyl)pyridin-1-ium-2-yl)-6,7-dihydro-5H-cyclopenta[b]pyridine-7-sulfonate **3.10**.

Synthesis of 2-(4-bromophenyl)-6-(2,3 cylcopentenopyridyl) pyridine, 3.8

A dry 50 mL Schlenk tube was transferred into an argon filled glove box and was charged with 972 mg 2,3-Cyclopentenopyridine, (8.0 mmol 2.0 eq) and was subsequentially dissolved into 5 mL dry THF and the tube was sealed with a Teflon cap. The solution was then transferred onto a Schlenk line and cooled to -78 ^{o}C for 30 minutes under rapid stirring. Then, 0.73 mL of 11M nBuLi in hexanes (8.0 mmol, 2.0 eq) was added dropwise over 10 minutes. The resulting dark red solution was then stirred at -78 ^{o}C for an additional 30 minutes then was warmed to room temperature and sustained for 2 hours to allow for complete anion formation. Next, the solution was cooled back to -78 ^{o}C and 5mL of a THF solution containing 1.0 g 2-fluoro-6-(4-bromophenyl) pyridine **3.7** (4.0 mmol, 1.0 eq) was added dropwise over 1 minute. The solution maintained a dark red coloration and was allowed to warm back to room temperature and was held for 24 hr. After the reaction was completed, the solution was quenched with 20 mL DI H_2O. The resulting solution was then extracted with 3x20 mL of Et_2O and the solvent was removed via reduced pressure to yield 3.2g (97% yield by NMR) of an impure viscous red/orange oil and was further was purified via column chromatography with a 70:30:0.01:0.01 (Hexane:EtOAC:$CHCl_3$:TEA) mobile

phase to yield 1.12 g of a viscous orange oil **3.8** (80% isolated yield). The crude material is suitable for sulfonation, though higher yields are achieved with the purified compound. **^{1}H-NMR (400 MHz, $CDCl_3$)**: δ = 8.36 (d, 1H), 7.84 (m, 2H), 7.68 (t, 1H), 7.55 (m 4H), 7.21 (d, 1H), 7.07 (dd, 1H), 4.63 (dd, 1H), 3.23 (m, 1H), 3.02 (m, 1H), 2.64 (m 2H) ppm. **^{1}H-NMR (400 MHz, DMSO-d_6)**: δ = 8.25 (d, 1H), 7.97 (d, 2H), 7.81 (m, 2H), 7.69 (d, 1H), 7.65 (d, 2H), 7.30 (dd, 1H), 7.15, (dd, 1H), 4.58 (t, 1H), 3.17 (m, 1H), 3.00 (m, 1H), 2.54 (m, 2H) ppm

Synthesis of 7-(6-(4-bromophenyl)pyridin-1-ium-2-yl)-6,7-dihydro-5H-cyclopenta[b]pyridine-7-sulfonate, 3.9

A dry 50 mL Schlenk tube was transferred into an argon filled glove box and was charged with 30 mL of A dry THF solution containing 4.8 g of 2-(4-bromophenyl)-6-(2,3 cylcopentenopyridyl) pyridine **3.8** (13.8 mmol, 1.0 eq). Under heavy stirring, 1.99 g of NaH powder (82.8 mmol, 6.0 eq) was added to the flask, and the Schlenk flask was sealed with a Teflon cap and transferred out of the glovebox and placed in an oil bath at 60 ^oC. Periodically, the solution was removed from heat and vented under reduced pressure to allow for H_2 gas to be released. The resulting solution is a viscous dark red color indicative of carbanion formation. The solution was then allowed to cool to room temperature and transferred into an argon filled glovebox where 2.3 g of solid pyridine sulfur trioxide complex (14.1 mmol 1.1 eq) was added into the flask (it is important to not rinse with excess solvent at this step). The reaction mixture quickly changes from a dark red to a red/orange color. The flask was then sealed and heated to 60 ^oC for an additional 24 hr. The resulting mixture is a deep orange color with a white precipitate. The solution is then placed into an ice bath and quenched with 20 mL of cold MeOH added slowly followed by

an additional 20 mL of cold DI H_2O. The mixture was then dried under vacuum and the product was extracted using 3x30 mL of warm MeOH. The ligand containing MeOH fraction was then dried under vacuum and additional impurities were removed via a thorough THF wash. The solid material was then redissolved into 50 mL H_2O and the pH of the solution was reduced to ~1 using HCl pH = 1. The precipitate was then filtered and dried to yield filtered and dried to yield 3.17 g of pure product **3.9.** This zwitterionic compound **3.9** was then subsequently converted to the corresponding lithium salt **3.10** utilizing 1.0 eq LiOH in a 1:1 H_2O:MeOH solution.

^{1}H-NMR (400 MHz, DMSO-*d_6*): δ = 8.75 (d, 1H), 8.51 (d, 1H), 7.96 (m, 4H), 7.87 (m, 2H), 7.63 (m, 2H), 3.28 (m, 2H), 3.13 (m, 1H), 2.68 (m, 1H) ppm.

^{13}C-NMR (150 MHz, DMSO-*d_6*):): δ = 158.6, 155.6, 152.6, 144.7, 142.0, 139.2, 138.1, 137.4, 131.5

ESI-MS (– Mode) in MeOH, calculated m/z for [$C_{19}H_{14}BrN_2SO_3^-$]: 428.99, **Found m/z:** 428.81

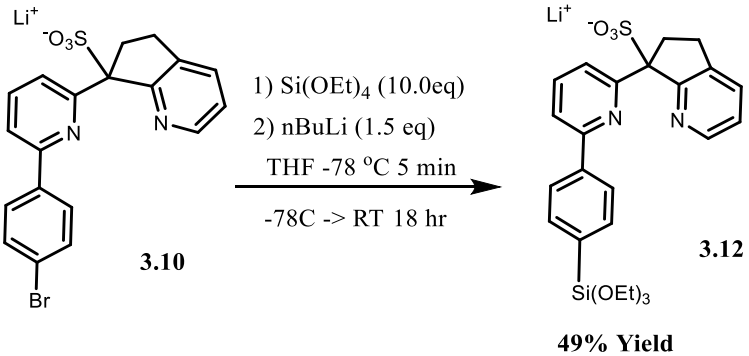

Scheme S3.6. Synthesis of lithium 7-(6-(4-triethoxyphenyl)pyridin-2-yl)-6,7-dihydro-5H-cyclopenta[b]pyridine-7-sulfonate **3.12**.

One-Pot Synthesis

A dry 50 mL Schlenk tube was transferred into an argon filled glove box and was charged with 300 mg of **3.10** (0.68 mmol 1.0 eq) and was subsequentially dissolved in 30 mL dry THF and the solution was added to the Schlenk tube and the tube was sealed with a Teflon cap. The solution was allowed to stir for 30 minutes at room temperature to allow for the solid to dissolve. Then, 3.19 g of $Si(OEt)_4$ (6.8 mmol, 10.0 eq) was added dropwise to the stirring solution. The Schlenk tube was sealed and the transferred out of the glovebox and placed onto a Schlenk line under argon. The tube was then cooled to –78 ^oC and 1.5 mL of 1.6M nBuLi solution was added dropwise over 5 minutes under heavy stirring. Upon addition of the nBuLi solution a slight color change from a light brown to a deep amber/orange color was observed. The solution was allowed to stir at –78 ^oC for 5 minutes before being removed from the dry ice bath and allowed to warm to room temperature. The reaction was allowed to stir overnight at room temperature. The following morning, 10 mL of EtOH was added to the mixture and the volume of the solution was reduced under vacuum to ~ 5 mL. Then, 30 mL of Hexane was added to remove and unreacted $Si(OEt)_4$ and resulted in the precipitation of a light brown powder. The solution was then filtered, and 298.4 mg of crude (49% Yield) product **3.12** was isolated. For larger scale reactions (>300 mg) an alternative, 2 step approach was used.

Two-Step Synthesis

A dry 100 mL Schlenk tube was transferred into an argon filled glove box and was charged with 500 mg of the **3.10** (1.14 mmol 1.0 eq) and was subsequentially dissolved into was dissolved in 45 mL dry THF and the solution was added to the Schlenk tube and the tube

was sealed with a Teflon cap. The solution was allowed to stir for 30 minutes at room temperature to allow for the solid to dissolve. Then, the Schlenk tube was placed into a dry ice/acetone bath and cooled to –78 ^{o}C. Then, 2.25 mL (3.6 mmol, 3.0 eq) was added dropwise to the solution over 30 seconds under heavy stirring. The solution was allowed to stir for 10 minutes at –78 ^{o}C, then 5.2 g of $Si(OEt)_4$ (11.4 mol, 10.0 eq) was quickly added to the solution. The mixture was allowed to stir for an additional 5 minutes at –78 ^{o}C before being removed from the dry ice bath and allowed to react overnight at room temperature. The following morning, 10 mL of EtOH was added to the mixture and the volume of the solution was reduced under vacuum to ~ 5 mL. Then, 30 mL of Hexane was added to remove and unreacted $Si(OEt)_4$ and resulted in the precipitation of 592.8 mg a crude light brown powder containing 299.9 mg (50.6% Yield) of silylated material. Due to difficulty in separating the SM from the silylated product, only crude ^{1}H-NMR data was collected, determination of yield was obtained via ESI-MS.

ESI-MS (– Mode) in MeOH, calculated m/z for $[C_{25}H_{29}SiN_2SO_6^-]$: 513.15, **Found m/z:** 512.91

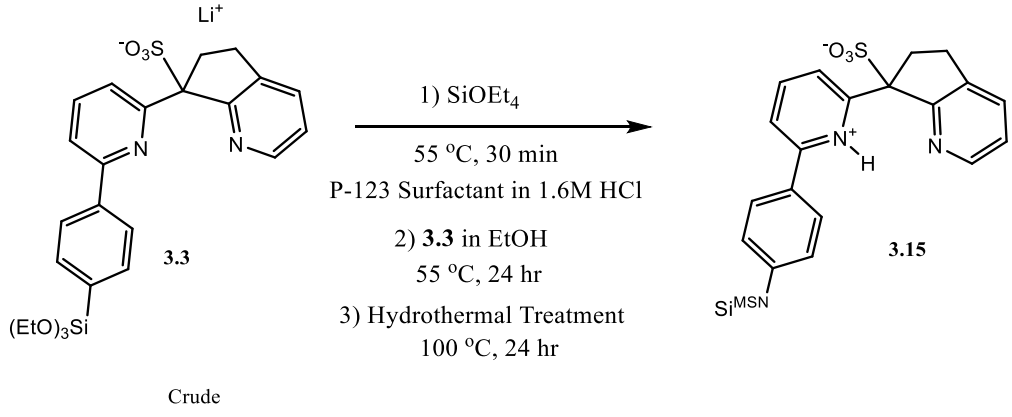

Crude

Scheme S3.7. Immobilization of lithium 7-(6-(4-triethoxyphenyl)pyridin-2-yl)-6,7-dihydro-5H-cyclopenta[b]pyridine-7-sulfonate **3.3**.

Immobilization Procedure

Under open air in a fume hood, a 100 mL round bottom flask was charged with 2.30g of P123 surfactant. Then, 73.5 mL of a 1.6M HCl solution was added to the flask and the solution was warmed to 55^{o}C and was allowed to stir for 2 hr. Then 4.8 g of $Si(OEt)_4$ was added to the solution and it was allowed to stir for an additional 30 minutes. Finally, 225.3 mg (crude) of **3.3** dissolved into 10 mL EtOH was added to the flask and the round bottom was lightly covered with parafilm and was left under rapid stirring at 55^{o}C for 24 hr. The following morning the vessel was then heated to 100^{o}C and allowed to stir for an additional 24 hr. Then, the precipitate was filtered away from the solution and added to 250 mL beaker followed by 100 mL of EtOH. The beaker was then warmed to 60^{o}C and the solution was stirred for 2 hours. The powder was isolate via filtration and the washing procedure was repeated 3 times with EtOH. The powder was collected via filtration and dried under vacuum. The resulting material was then dried in a vacuum oven at 100 ^{o}C for 24 hr to yield 1.78 g of light brown powder of **3.15**.

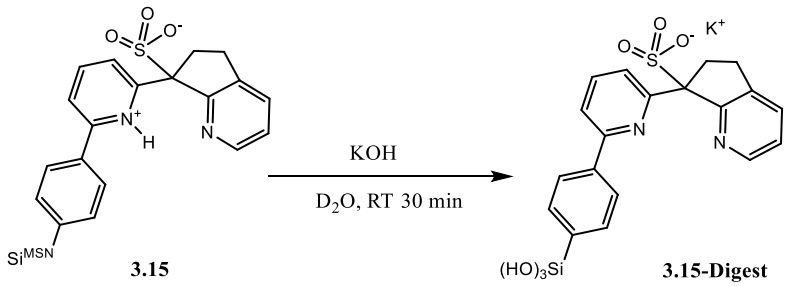

3.15 **3.15-Digest**

Scheme S3.7. KOH Digestion of Immobilized Ligand, **3.15**, to produce 7-(6-(4-trihydroxyphenyl)pyridin-2-yl)-6,7-dihydro-5H-cyclopenta[b]pyridine-7-sulfonate **3.15-Digest**

Quantitation of Ligand Loading

The ligand loading of **3.15** was determined via quantitative digestion of the SiO_2 bound material. First, 22.2 mg of **3.15** was digested by 4 mL of a D_2O solution containing 176.1 mg of KOH. The mixture was allowed to stir at room temperature for 30 minutes and the resulting solution was colorless. Then, 2 µL of 1,4-dioxane was added as an internal standard for quantitation. The solution was then transferred to an NMR tube for analysis. The material contained immobilized ligand at a concentration of 0.243 mmol/g. In order to assess the yield of the immobilization reaction, the non-immobilized washings were concentrated under vacuum and analyzed via negative mode ESI MS. No silicon containing species were detected in the wash, thus indicating a quantitative conversion of all silylated ligand species.

Corresponding Spectral Data for KOH Digested Species 3.15-Digest

^{1}H-NMR (400 MHz, D_2O): δ = 8.46 (d, 1H), 8.15 (d, 1H), 7.92 (t, 2H), 7.81 (m, 5H), 7.39 (dd, 1H), 3.27 (m, 1H), 3.19 (m, 1H), 3.08 (m, 1H), 3.02 (m, 1H) ppm.

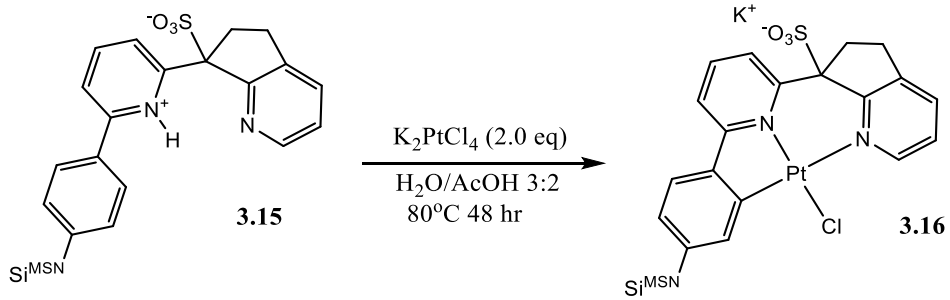

Scheme S3.8. Cyclometallation of immobilized ligand, **3.15** to yield Pt-Cl complex, **3.16**

Cyclometallation of Immobilized Ligand

A dry 50 mL round bottom flask was charged with 500 mg of **3.15** (0.1055 mmol/g Ligand/SiO_2). Then, 50 mL of a 3:2 H_2O:AcOH solution containing 61.8 mg (0.149 mmol, 3.0 eq) of K_2PtCl_4 was added and the flask was lightly sealed. The flask was then heated

to 80 °C and was allowed to react for 48 hr under rapid stirring. The powder was then collected by filtration and washed three times with 30 mL DI H_2O in order to remove any unreacted K_2PtCl_4. The resulting material was a lightly colored brown powder. A KOH digest was performed in order to assess the completion of the reaction. 25.0 mg of the immobilized complex was placed into a scintillation vial. Then, 2.0 mL of a 100mg/mL solution of KOH in D_2O was added and the mixture was allowed to stir for 30 minutes. Quantitation was performed via an internal standard reference and gave a 51.6% yield of immobilized Pt-Cl complex **3.16**.

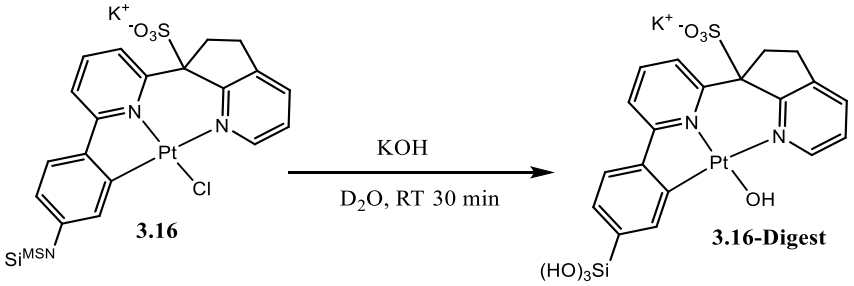

Scheme S3.9. Digestion of Immobilized Complex **3.16** to produce **3.16-Digest**

KOH Digestion Procedure

A KOH digest of **3.16** was performed in order to assess the platinum loading. 25.0 mg of the immobilized complex **3.16** was placed into a scintillation vial. Then, 2.0 mL of a 100mg/mL solution of KOH in D_2O was added and the mixture was allowed to stir for 30 minutes. Quantitation was performed via an internal standard reference and gave a 51.6% yield of immobilized Pt-Cl complex. Only crude ^{1}H-NMR data was collected, combined yield of metallated products **3.16-Digest** was done via comparing the integration values for the *o*-pyridyl signals for the immobilized complex (δ = 8.79 (d, 1H) for Pt–OH and δ = 9.26 (d, 1H) for Pt-Cl) versus the free ligand (δ = 8.49(d, 1H)). In fact, the alkaline digestion yields only Pt-OH complex **3.16-Digest** and non-metallated free ligand **3.16-Digest** no *o*-

pyridyl signals pertaining to complex **3.16** were observed via ^{1}H-NMR. For ESI-MS, a repeated precipitation of silicates was performed using MeOH prior to injection.

ESI-MS (– Mode) in MeOH, calculated m/z for [((p-Si(OH)$_3$ C6H4)-pcpps)Pt^{II}(OH)]: 640.02, **Found m/z:** 640.90

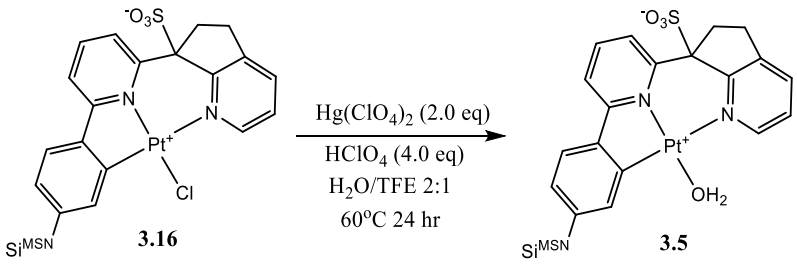

Scheme S3.10. Conversion of immobilized Pt^{II}-Cl complex **3.16** to immobilized Pt^{II} aqua complex **3.5**.

Procedure for aqua for chloro ligand exchange

450 mg of **3.16** was added to a scintillation vial. Then, 4 mL of a premade $Hg(ClO_4)_2$ (2.0 eq based on complex loading) in $HClO_4$ (4.0 eq based on complex loading) solution and 2 mL of TFE was added. The solution was allowed to stir at 60 ^{o}C overnight. The powder was collected via filtration and any remaining Hg salts were extracted with 100 mL of an 80mM $HClO_4$ solution by stirring for 2 hours. The powder was then collected via filtration and subjected to an additional extraction of any other inorganic salts with 100 mL DI H_2O by stirring for 2 hr. The resulting powder was again isolated by filtration and dried under vacuum to yield a light brown colored material **3.5**. Its alkaline digestion yields only Pt-OH complex **3.16-Digest** and free ligand **3.15-Digest** no *o*-pyridyl signals pertaining to Pt^{II} chloro complex **3.16** were observed via ^{1}H-NMR.

III. H/D Exchange Utilizing Immobilized Complex 3.5

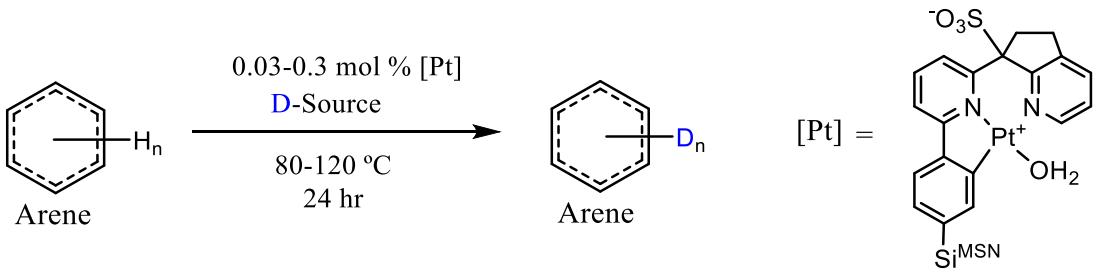

General Procedure A for H/D Exchange utilizing 3.5

In an argon filled glove box 0.4-0.7 mmol of substrate was transferred into a scintillation vial and dissolved in 0.45 mL either AcOD-d_4 or TFE-d_1. Then approximately 40 mg of the immobilized catalyst **3.5** containing 1.5-2.5 µmol [Pt] was added to a dry J Young (JY) NMR Tube. The arene solution was then transferred into the tube and was sealed. Then JY tube was then transferred out of the glovebox and pressurized under ~20 psi argon and was then placed into an oil bath at the designated temperature for 24 hours. The sample was periodically removed from the oil bath for NMR measurements to monitor the progress of the reaction. Deuterium incorporation was measured via the decrease of integration of a given bond type in ^{1}H-NMR. The formation of C-D bonds was subsequently validated qualitatively using ^{2}H-NMR.

Chart S3.1. Summary of aromatic substrates screened for TFE-d_1, AcOD-d_4 and Neat D_2O as solvents and deuterium sources for H/D exchange

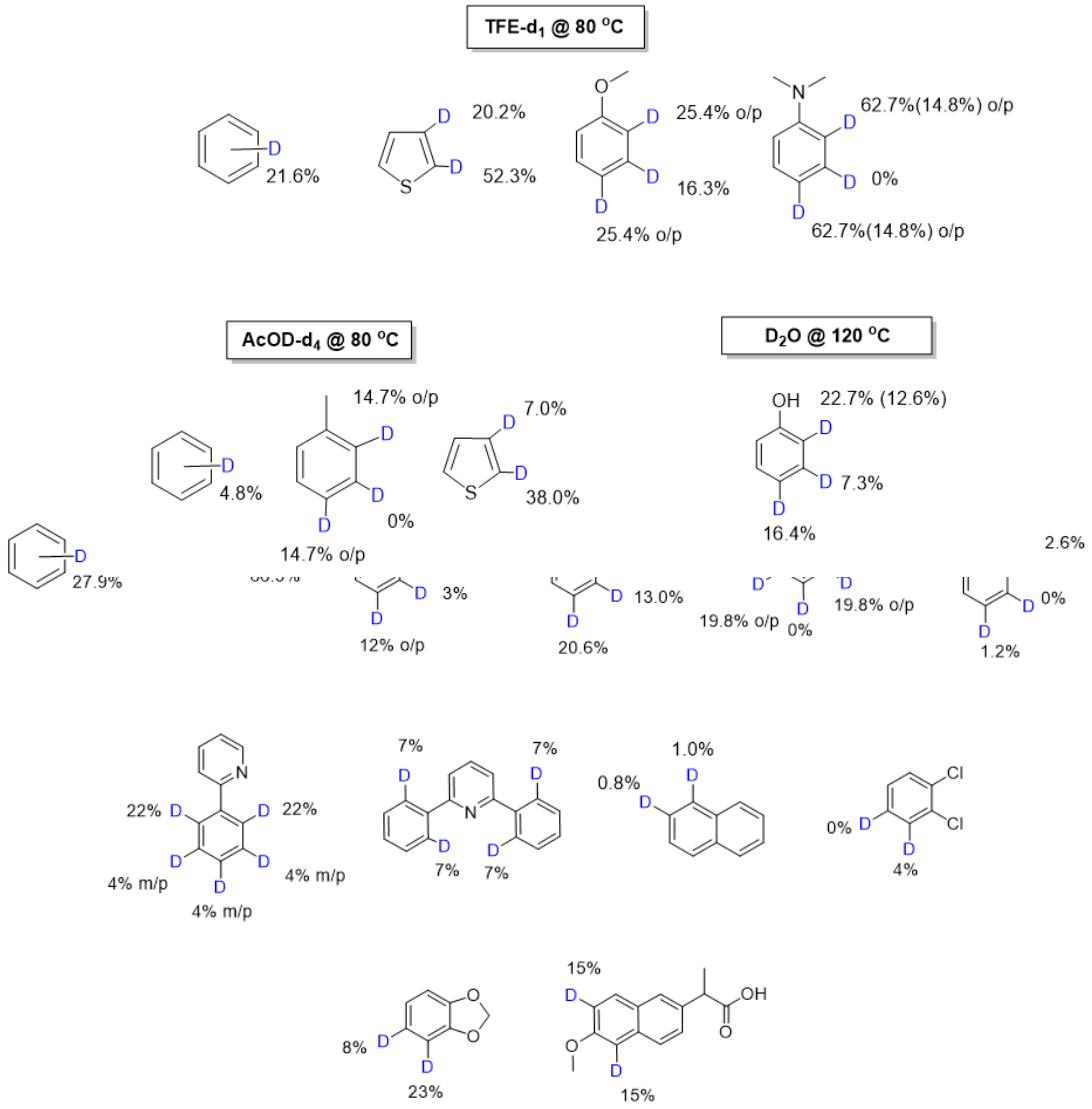

Chart S3.2. Summary of aromatic substrates screened with 1:1 D_2O /AcOD-d_4 mixture as the solvent and deuterium source for H/D exchange

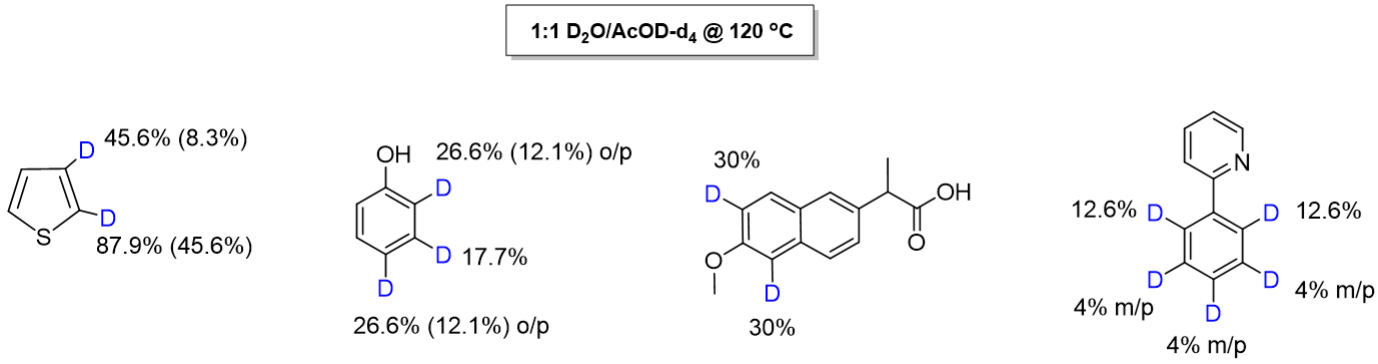

H/D Exchange for Benzene

Standard conditions, TFE-d$_1$ as the solvent @ 80 °C

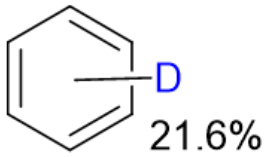

The general procedure outlined above was followed using 0.050 mL of benzene (0.44 mmol) dissolved in 0.45 mL of TFE-d1 and 47 mg of immobilized catalyst **3.5** containing 2.0 µmol of Pt. The resulting solution was colorless, and it was heated at 80 °C for 24 hours. The reaction proceeded with no color change or precipitate formation. There was no significant background contribution in the H/D exchange.

Standard conditions, AcOD-d$_4$ as the solvent @ 80 °C

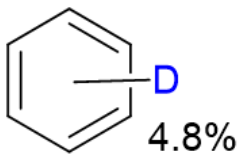

The general procedure outlined above was followed using 0.050 mL of benzene (0.44 mmol) dissolved in 0.45 mL of AcOD-d$_4$ and 32 mg of immobilized catalyst **3.5** containing 1.3 µmol of Pt. The resulting solution was colorless, and it was heated at 80 °C for 24 hours. The reaction proceeded with no color change or precipitate formation. There was no significant background contribution in the H/D exchange.

Standard conditions, AcOD-d_4 as the solvent @ 120 ºC

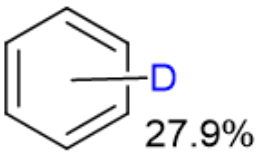

The general procedure outlined above was followed using 0.050 mL of benzene (0.44 mmol) dissolved in 0.45 mL of AcOD-d_4 and 32 mg of immobilized catalyst **3.5** containing 1.3 µmol of Pt. The resulting solution was colorless, and it was heated at 120 °C for 24 hours. The reaction proceeded with no color change or precipitate formation. There was no significant background contribution in the H/D exchange.

H/D Exchange for Thiophene

Standard conditions, TFE-d_1 as the solvent @ 80 ºC

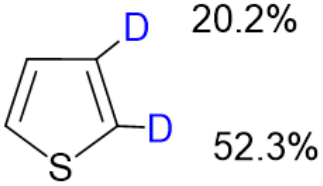

The general procedure outlined above was followed using 0.050 mL of thiophene (0.62 mmol) dissolved in 0.45 mL of TFE-d1 and 51 mg of immobilized catalyst **3.5** containing 2.1 µmol of Pt. The resulting solution was colorless, and it was heated at 80 °C for 24 hours. The reaction proceeded with no color change or precipitate formation. There was no significant background contribution in the H/D exchange.

Standard conditions, AcOD-d_4 as the solvent @ 80 ºC

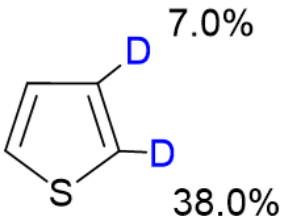

The general procedure outlined above was followed using 0.050 mL of thiophene (0.62 mmol) dissolved in 0.45 mL of AcOD-d_4 and 60 mg of immobilized catalyst **3.5** containing 2.6 µmol of Pt. The resulting solution was colorless, and it was heated at 80 °C for 24 hours. The reaction proceeded with no color change or precipitate formation. There was no significant background contribution in the H/D exchange.

Standard conditions, AcOD-d_4 as the solvent @ 120 °C

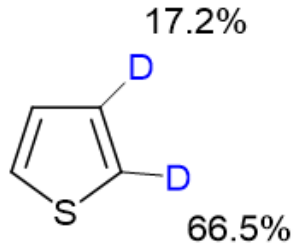

The general procedure outlined above was followed using 0.050 mL of thiophene (0.62 mmol) dissolved in 0.45 mL of AcOD-d_4 and 48 mg of immobilized catalyst **3.5** containing 2.0 µmol of Pt. The resulting solution was colorless, and it was heated at 120 °C for 24 hours. The reaction proceeded with no color change or precipitate formation. There was no significant background contribution in the H/D exchange.

Standard conditions, D_2O/AcOD-d_4 as the solvent @ 120 °C

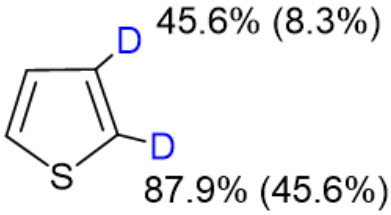

The general procedure outlined above was followed using 0.050 mL of thiophene (0.62 mmol) dissolved in 0.45 mL of a 1:1 v/v D_2O/AcOD-d_4 solution and 48 mg of immobilized catalyst **3.5** containing 2.0 µmol of Pt. The resulting solution was colorless, it was heated at 120 °C for 24 hours. The reaction proceeded with no color change or precipitate formation. There was a significant background contribution in the H/D exchange which is shown in in parenthesis next to the observed extent of deuteration.

H/D Exchange for N,N Dimethylaniline

Standard conditions, TFE-d_1 as the solvent @ 80 °C

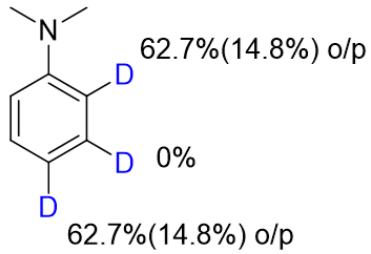

The general procedure outlined above was followed using 0.050 mL of thiophene (0.39 mmol) dissolved in 0.45 mL of TFE-d1 and 53 mg of immobilized catalyst **3.5** containing 2.2 µmol of Pt. The resulting solution was colorless and homogeneous and was heated at 80 °C for 24 hours. The reaction proceeded with no color change or precipitate formation. There was a significant background contribution in the H/D exchange which is shown in in parenthesis next to the observed extent of deuteration.

H/D Exchange for Anisole

Standard conditions, TFE-d_1 as the solvent @ 80 °C

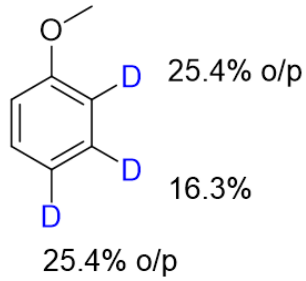

The general procedure outlined above was followed using 0.050 mL of anisole (0.50 mmol) dissolved in 0.45 mL of TFE-d1 and 51 mg of immobilized catalyst **3.5** containing 2.1 µmol of Pt. The resulting solution was colorless, and it was heated at 80 °C for 24 hours. The reaction proceeded with no color change or precipitate formation. There was no significant background contribution in the H/D exchange.

H/D Exchange for Toluene

Standard conditions, TFE-d_1 as the solvent @ 80 °C

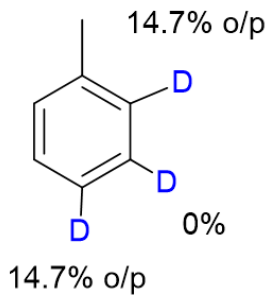

The general procedure outlined above was followed using 0.050 mL of toluene (0.47 mmol) dissolved in 0.45 mL of AcOD-d_4 and 30 mg of immobilized catalyst **3.5** containing 1.7 µmol of Pt. The resulting solution was colorless, and it was heated at 80 °C for 24 hours. The reaction proceeded with no color change or precipitate formation. There was no significant background contribution in the H/D exchange.

H/D Exchange for Phenol

Standard conditions, AcOD-d_4 as the solvent @ 120 °C

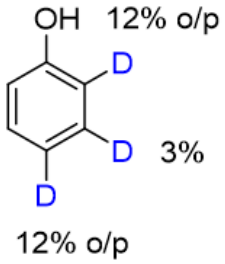

The general procedure outlined above was followed using 55.6 mg of phenol (0.59 mmol) dissolved in 0.5 mL of AcOD-d_4 and 22 mg of immobilized catalyst **3.5** containing 1.1 µmol of Pt. The resulting solution was colorless, and it was heated at 120 °C for 24 hours. The reaction proceeded with no color change or precipitate formation. There was no significant background contribution in the H/D exchange**.**

Standard conditions, D_2O/AcOD-d_4 as the solvent @ 120 °C

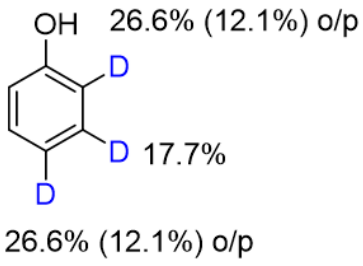

The general procedure outlined above was followed 55.0 mg of phenol (0.59 mmol) dissolved in 0.5 mL of a 1:1 v/v D_2O/AcOD-d_4 solution and 26 mg of immobilized catalyst **3.5** containing 1.5 µmol of Pt. The resulting

solution was colorless, it was heated at 120 °C for 24 hours. The reaction proceeded with no color change or precipitate formation. There was a significant background contribution in the H/D exchange which is shown in in parenthesis next to the observed extent of deuteration.

Standard conditions, D_2O as the solvent @ 120 °C

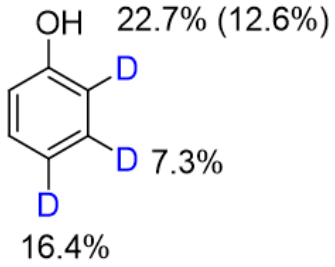

The general procedure outlined above was followed 60.5 mg of phenol (0.64 mmol) dissolved in 0.5 mL of D_2O and 28 mg of immobilized catalyst **3.5** containing 1.6 µmol of Pt. The resulting solution was colorless, it was heated at 120 °C for 24 hours. The reaction proceeded with no color change or precipitate formation. There was a significant background contribution in the H/D exchange which is shown in in parenthesis next to the observed extent of deuteration.

H/D Exchange for Fluorobenzene

Standard conditions, AcOD-d_4 as the solvent @ 120 °C

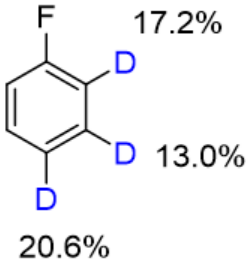

The general procedure outlined above was followed using 0.050 mL of fluorobenzene (0.53 mmol) dissolved in 0.45 mL of AcOD-d_4 and 20 mg of immobilized catalyst **3.5** containing 1.1 µmol of Pt. The resulting solution was colorless, and it was heated at 120 °C for 24 hours. The reaction proceeded with no color change or precipitate formation. There was no significant background contribution in the H/D exchange.

H/D Exchange for Phenethylamine

Standard conditions, AcOD-d_4 as the solvent @ 120 °C

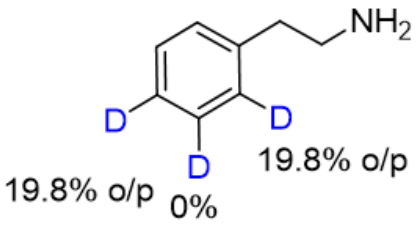

The general procedure outlined above was followed using 0.050 mL of phenethylamine (0.39 mmol) dissolved in 0.45 mL of AcOD-d_4 and 27 mg of immobilized catalyst **3.5** containing 1.4 µmol of Pt. The resulting solution was light yellow color, and it was heated at 120 °C for 24 hours. The reaction proceeded with no color change or precipitate formation. There was no significant background contribution in the H/D exchange.

H/D Exchange for Benzoic Acid

Standard conditions, AcOD-d_4 as the solvent @ 120 °C

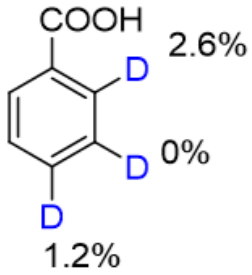

The general procedure outlined above was followed 55.0 mg of benzoic acid (0.41 mmol) dissolved in 0.5 mL of AcOD-d_4 solution and 36 mg of immobilized catalyst **3.5** containing 1.9 µmol of Pt. The resulting solution was colorless, it was heated at 120 °C for 24 hours. The reaction proceeded with no color change or precipitate formation. There was no significant background contribution in the H/D exchange.

H/D Exchange for 2-Phenylpyridine

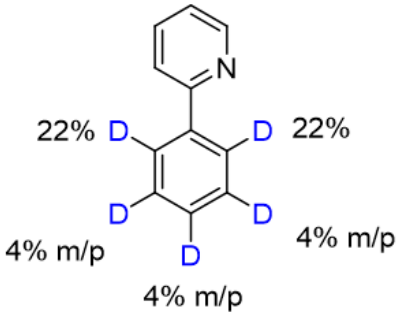

Standard conditions, AcOD-d_4 as the solvent @ 120 °C

The general procedure outlined above was followed using 0.050 mL of 2-phenylpyridine (0.35 mmol) dissolved in 0.45 mL of AcOD-d_4 and 27 mg of immobilized catalyst **3.5** containing 1.4 µmol of Pt. The resulting solution was light yellow color, and it

was heated at 120 °C for 24 hours. The reaction proceeded with no color change or precipitate formation. There was no significant background contribution in the H/D exchange.

Standard conditions, D_2O/AcOD-d_4 as the solvent @ 120 °C

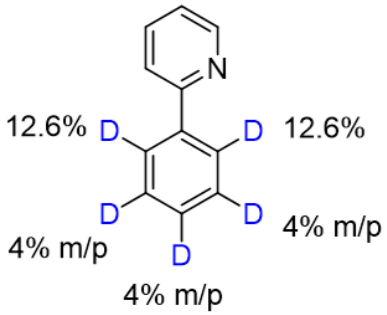

The general procedure outlined above was followed using 0.050 mL of 2-phenylpyridine (0.35 mmol) dissolved in 0.45 mL of a 1:1 v/v D_2O/AcOD-d_4 solution and 30 mg of immobilized catalyst **3.5** containing 1.7 µmol of Pt. The resulting solution was colorless, it was heated at 120 °C for 24 hours. The reaction proceeded with no color change or precipitate formation. There was a significant background contribution in the H/D exchange which is shown in in parenthesis next to the observed extent of deuteration.

H/D Exchange for 2,6-Diphenylpyridine

Standard conditions, AcOD-d_4 as the solvent @ 120 °C

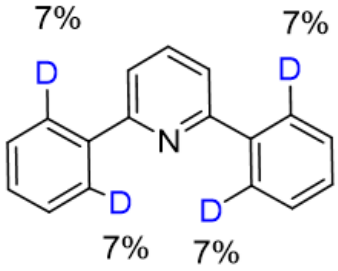

The general procedure outlined above was followed using 32.9 mg of 2,6-Diphenylpyridine (0.14 mmol) dissolved in 0.5 mL of AcOD-d_4 and 23 mg of immobilized catalyst **3.5** containing 1.2 µmol of Pt. The resulting solution was colorless, and it was heated at 120 °C for 24 hours. The reaction proceeded with no color change or precipitate formation. There was no significant background contribution in the H/D exchange.

H/D Exchange for Naphthalene

Standard conditions, AcOD-d_4 as the solvent @ 120 °C

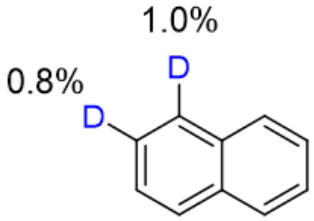

The general procedure outlined above was followed using 57.6 mg of naphthalene (0.45 mmol) dissolved in 0.5 mL of AcOD-d_4 and 23 mg of immobilized catalyst **3.5** containing 1.2 µmol of Pt. The resulting solution was colorless, and it was heated at 120 °C for 24 hours. The reaction proceeded with no color change or precipitate formation. There was no significant background contribution in the H/D exchange

H/D Exchange for 1,2-Dichlorobenzene

Standard conditions, AcOD-d_4 as the solvent @ 120 °C

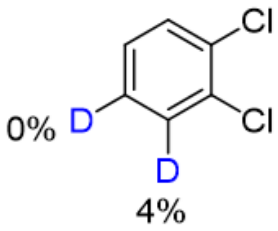

The general procedure outlined above was followed using 0.050 mL of 1,2-dichlorobenzene (0.44 mmol) dissolved in 0.45 mL of AcOD-d_4 and 25 mg of immobilized catalyst **3.5** containing 1.3 µmol of Pt. The resulting solution was colorless, and it was heated at 120 °C for 24 hours. The reaction proceeded with no color change or precipitate formation. There was no significant background contribution in the H/D exchange.

H/D Exchange for 1,2-Dichlorobenzene

Standard conditions, AcOD-d_4 as the solvent @ 160 °C

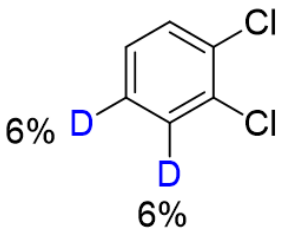

The general procedure outlined above was followed using 0.050 mL of 1,2-dichlorobenzene (0.44 mmol) dissolved in 0.45 mL of AcOD-d_4 and 21 mg of immobilized catalyst **3.5** containing 1.1 µmol of Pt. The resulting solution was colorless, and it was

heated at 160 °C for 24 hours. The reaction proceeded with no color change or precipitate formation. There was no significant background contribution in the H/D exchange.

H/D Exchange for Benzodioxole

Standard conditions, AcOD-d_4 as the solvent @ 120 °C

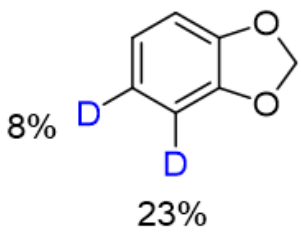

The general procedure outlined above was followed using 0.050 mL of 1,2-benzodioxole (0.43 mmol) dissolved in 0.45 mL of AcOD-d_4 and 31 mg of immobilized catalyst **3.5** containing 1.6 µmol of Pt. The resulting solution was colorless, and it was heated at 120 °C for 24 hours. The reaction proceeded with no color change or precipitate formation. There was no significant background contribution in the H/D exchange.

H/D Exchange for Naproxen

Standard conditions, AcOD-d_4 as the solvent @ 120 °C

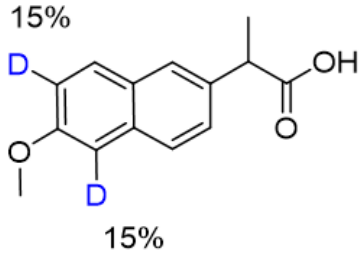

The general procedure outlined above was followed using 55.6 mg of naproxen (0.24 mmol) dissolved in 0.45 mL of AcOD-d_4 and 25 mg of immobilized catalyst **3.5** containing 1.2 µmol of Pt. The resulting solution was colorless, and it was heated at 120 °C for 24 hours. The reaction proceeded with no color change or precipitate formation. There was no significant background contribution in the H/D exchange.

Standard conditions, D_2O/AcOD-d_4 as the solvent @ 120 ºC

The general procedure outlined above was followed using 47.4 mg of naproxen (0.21 mmol) dissolved in 0.45 mL of AcOD-d_4 and 36 mg of immobilized catalyst **3.5** containing 1.3 µmol of Pt. The resulting solution was colorless, and it was heated at 120 °C for 24 hours. The reaction proceeded with no color change or precipitate formation. There was no significant background contribution in the H/D exchange.

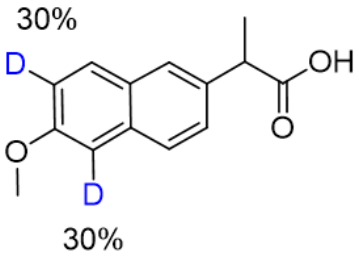

IV. H/D Exchange Utilizing molecular complex 3.5-FC

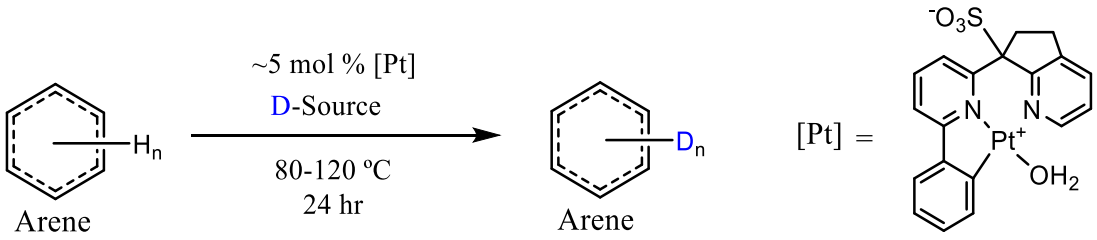

General Procedure B for H/D Exchange utilizing pcpps-Pt-OH_2 (molecular complex)

In an argon filled glove box 0.4-0.7 mmol of substrate was transferred into a scintillation vial and dissolved in 0.45 mL either AcOD-d_4 or TFE-d_1. Then catalyst **3.5-FC** containing approximately 5 mol% [Pt] was added to a dry JYoung (JY) NMR Tube. The arene solution was then transferred into the tube and was sealed. Then JY tube was then transferred out of the glovebox and pressurized under ~20 psi argon and was then placed into an oil bath at the designated temperature for 24 hours. The sample was periodically removed from the oil bath for NMR measurements to monitor the progress of the reaction. Deuterium

incorporation was measured via the decrease of integration of a given bond type in ^{1}H-NMR. The formation of C-D bonds was subsequently validated qualitatively using ^{2}H-NMR.

H/D Exchange for Benzene

Standard conditions, TFE-d$_1$ as the solvent @ 80 °C

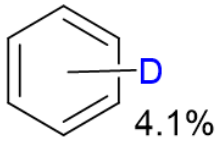

The general procedure outlined above was followed using 0.050 mL of benzene (0.44 mmol) dissolved in 0.45 mL of TFE-d1 and 5.7 mg of Pt catalyst **3.5-FC** (10.1 µmol). The resulting solution was clear yellow color, and it was heated at 80 °C for 24 hours. As the reaction proceeded a large amount of yellow precipitate formed at the bottom of the NMR-Tube. There was no significant background contribution in the H/D exchange.

Standard conditions, AcOD-d$_4$ as the solvent @ 80 °C

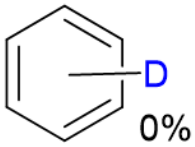

The general procedure outlined above was followed using 0.050 mL of benzene (0.44 mmol) dissolved in 0.45 mL of **,** AcOD-d$_4$ and 4.7 mg of Pt catalyst **3.5-FC** (8.3 µmol). The resulting solution was clear yellow color, and it was heated at 80 °C for 24 hours. As the reaction proceeded a large amount of yellow precipitate formed at the bottom of the NMR-Tube. There was no observable H/D exchange reaction.

Standard conditions, AcOD-d$_4$ as the solvent @ 120 °C

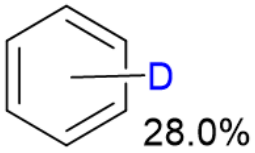

The general procedure outlined above was followed using 0.050 mL of benzene (0.44 mmol) dissolved in 0.45 mL of **,** AcOD-d$_4$ and 4.7 mg of Pt catalyst **3.5-FC** (8.3 µmol). The resulting solution was clear yellow color, and it was heated at 120 °C for 24 hours. As the reaction

proceeded a large amount of yellow precipitate formed at the bottom of the NMR-Tube. Additionally, a dark brown/black precipitate began to form, presumably Pt black.

H/D Exchange for Thiophene

Standard conditions, TFE-d_1 as the solvent @ 80 °C

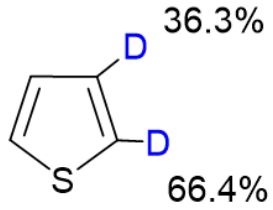

The general procedure outlined above was followed using 0.050 mL of thiophene (0.62 mmol) dissolved in 0.45 mL of TFE-d1 and 4.7 mg of Pt catalyst **3.5-FC** (8.3 µmol). The resulting solution was clear yellow color, and it was heated at 80 °C for 24 hours. As the reaction proceeded a large amount of yellow precipitate formed at the bottom of the NMR-Tube. There was no significant background contribution in the H/D exchange,

Standard conditions, AcOD-d_4 as the solvent @ 80 °C

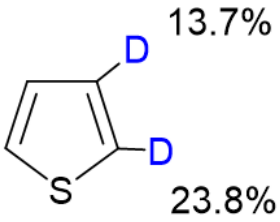

The general procedure outlined above was followed using 0.050 mL of thiophene (0.62 mmol) dissolved in 0.45 mL of **,** AcOD-d_4 and 5.0 mg of Pt catalyst **3.5-FC** (8.9 µmol). The resulting solution was clear yellow color, and it was heated at 80 °C for 24 hours. As the reaction proceeded a large amount of yellow precipitate formed at the bottom of the NMR-Tube.

Standard conditions, D_2O/AcOD-d_4 as the solvent @ 120 °C

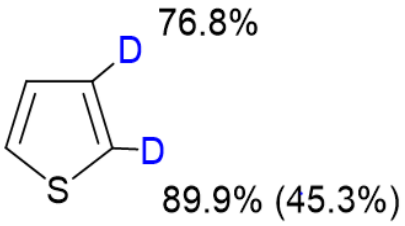

The general procedure outlined above was followed using 0.050 mL of thiophene (0.62 mmol) dissolved in 0.45 mL of a 1:1 v/v D_2O/AcOD-d_4 solution and 5.0 mg of Pt catalyst **3.5-FC** (8.9 µmol). The resulting solution was clear yellow color, and it was heated at 120 °C for 24 hours. There was a significant

background contribution in the H/D exchange which is shown in in parenthesis next to the observed extent of deuteration. As the reaction proceeded a large amount of yellow precipitate formed at the bottom of the NMR-Tube. Additionally, a dark brown/black precipitate began to form, presumably Pt black.

IV. Observed Rates and Extent of Deuteration

Observed rates of H/D exchange were measured via ^{1}H-NMR spectroscopy by monitoring the change of the integral intensity of specific aromatic C-H signals of a given substrate over a 24-hour reaction period. Integration values were compared against an internal standard as reference. Simultaneous control experiments were run under otherwise identical reaction conditions in the absence of any catalyst. In order to properly attribute C-H signal intensity loss to H/D exchange a supplemental ^{2}H-NMR experiment was used qualitatively to detect the formation of C-D bonds (see ***Figure S3.1 and S2***).

$$observed\ rate = -\frac{d[C-H]}{dt} = +\frac{d[C-D]}{dt}$$

The observed rate value was calculated for each of a given substrates aromatic C-H bonds after the allotted 24-hour reaction period. A subsequent normalization for substrate concentration and catalyst loading was applied to calculate a rate constant (k-24-obs).

$$k_{24-obs} = \frac{rate}{[C-H] * [Pt]}$$

This observed rate constant was used as a means of comparing the various regioselective observed rates of H/D exchange for specific bond types across different substrates and reaction conditions.

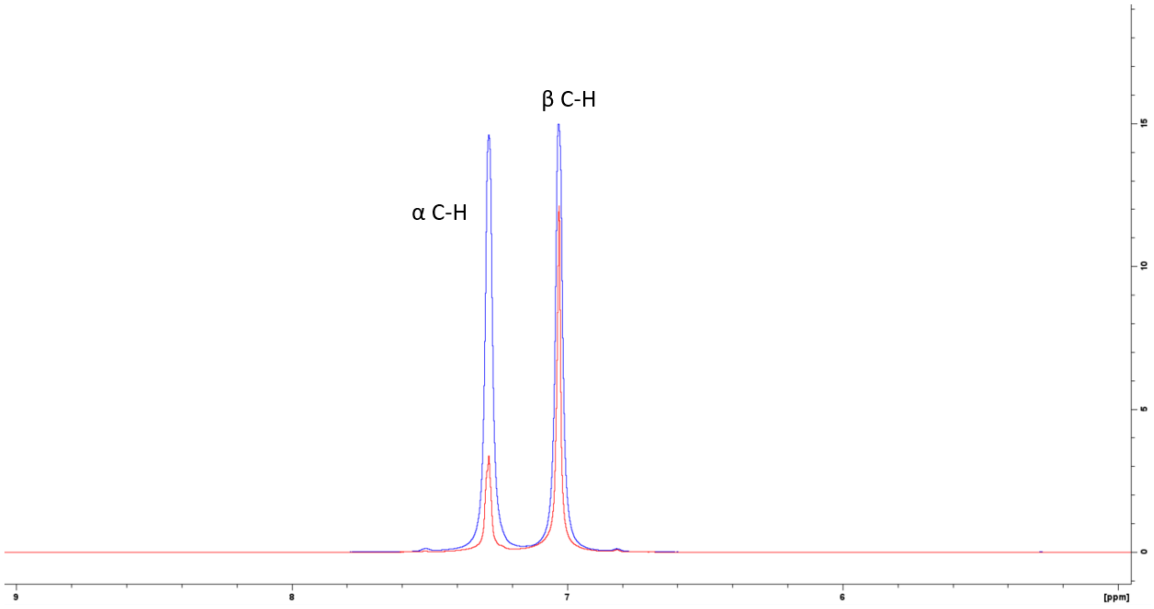

Figure S3.1. Aromatic region overlay of initial and final ^{1}H-NMR spectra for Thiophene in AcOD-d_4
Blue = initial measurement **Red** = final measurement (after 24 Hr)

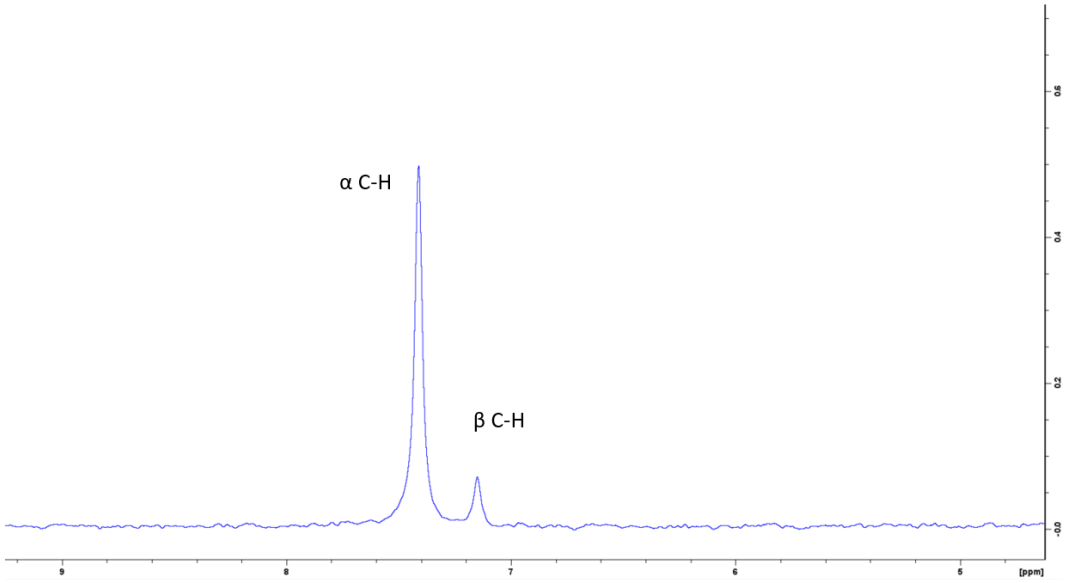

Figure S3.2. Aromatic region ^{2}H-NMR spectra for Thiophene in AcOD-d_4 after 24 hours

V. Immobilized Catalyst 3.5 Recyclability

Procedure for Catalyst Recycling

Catalyst **3.5** recyclability was tested by repeating the general procedure for H/D exchange over multiple reaction cycles. An initial run using thiophene as the aromatic substrate was conducted using the standard procedure outlined above utilizing the highlighted source of deuterium. ^{1}H-NMR and ^{2}H-NMR were collected to monitor the progress of the reaction. The catalyst **3.5** was collected via filtration and the JY tube was rinsed with methanol to remove as much solid as possible. Then, the catalyst **3.5** was rinsed with either 2,2,2 trifluoroethanol or acetic acid and was allowed to dry under vacuum. A subsequent drying was done in a vacuum oven at 100^{o}C for 2 hrs. Then the catalyst **3.5** was weighed and used for a subsequent H/D exchange under identical reaction conditions.

Table S3.1. Immobilized Catalyst Recyclability for Thiophene Under Various Reaction Conditions. Values in parenthesis indicate the extent of deuteration caused in the absence of the Pt catalyst.

H/D Exchange Catalyst Comparison For Thiophene					
Conditions	**Cycle #**	**Extent of Deuteration**	**Pt loading (umol)**	**K-24 Obs (M-1Hr-1)**	**TON-24 hr**
TFE-d1 @80C	**1**	20.1%	2.2	3.55	228
	2	34.4%	2.2	3.26	390
	3	30.0%	1.6	3.89	211
	4	10.0%	0.9	2.59	310
H/D Exchange Catalyst Comparison For Thiophene					
Conditions	**Cycle #**	**Extent of Deuteration**	**Pt loading (umol)**	**K-24 Obs (M-1Hr-1)**	**TON-24 hr**
AcOD-d4 @120C	**1**	41.8%	2.0	4.43	519
	2	43.6%	3.7	2.44	292
	3	23.9%	2.3	3.88	465
	4	21.6%	1.3	3.50	420
H/D Exchange Catalyst Comparison For Thiophene					
Conditions	**Cycle #**	**Extent of Deuteration**	**Pt loading (umol)**	**K-24 Obs (M-1Hr-1)**	**TON-24 hr**
1:1 AcOD-d4/D2O @120C	**1**	66.9% (23.9%)	1.8	5.10*	612
	2	88.7% (23.9%)	3.5	3.68*	454
	3	43.9% (23.9%)	2.8	2.09*	250
	4	49.1% (23.9%)	1.8	2.83*	339

*Indicates that there was a significant background reaction (in the absence of catalyst) reported K-24 Obs is for the Pt complex contribution only.

VI. Evidence supporting Pt^{II} as the active catalyst

The use of K_2PtCl_4 occasionally led to the formation of Pt(0) when metalation was performed under the non-optimized reaction conditions. This led to some concerns that Pt(0) may be responsible for catalyzing the observed H/D Exchange reactions. However, we have performed a series of control experiments, and divergent synthetic avenues in order to disprove the possibility of Pt(0) forming during the synthesis and playing a significant role in catalysis.

General Procedure A was utilized from above for the H/D exchange on Anisole utilizing complexes **3.5** and **3.16.** The purpose of exploring the reactivity of this series of species is to rule out the possibility of whether Pt(0) is responsible for, or contributing meaningfully to the observed catalysis.

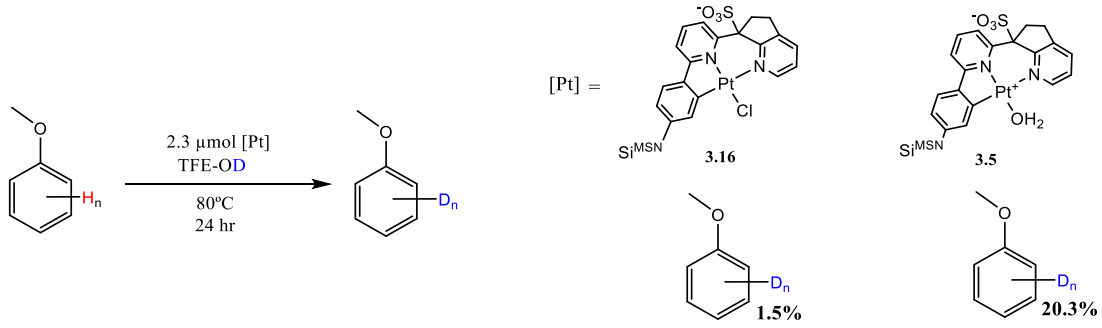

Scheme S3.11. Assessment of a relative activity of **3.16** and **3.5** in catalytic aromatic H/D exchange with TFE-d_1.

In order to properly assess which species is likely responsible for catalysis the 4 immobilized Pt complexes shown above (**Scheme S3.11**) were synthesized independently. The **3.16** is the result after the cyclometallation of the **3.15** and K_2PtCl_4 shown in **Scheme S3.8**. We observed that Pt black would form when the reaction conditions deviated from the optimal reaction conditions (elevated temp, increase Pt loading, impurities present etc.).

So, in order to assess if Pt(0) was responsible for the H/D exchange, then it would be generated via the disproportionation reaction of K_2PtCl_4 during the cyclometallation step. Therefore, if Pt(0) was generated and is responsible for the H/D exchange we observe, the deuteration utilizing **3.16** and **3.5** would be similar. A 24 hour deuteration experiment utilizing anisole was performed. The extent of deuteration was measure via ^1H and ^2D NMR and it showed that **3.16** only demonstrated a minute amount of H/D exchange 1.5% deuterium incorporation after 24 hours. Whereas the **3.5** yielded 20.3% deuterium incorporation over the same reaction period and identical catalyst loading (2.3 μmol Pt, 1.08 M Substrate). Thus indicating that Pt(0) is not the key species responsible for H/D exchange.

VII. Solid Materials Characterization

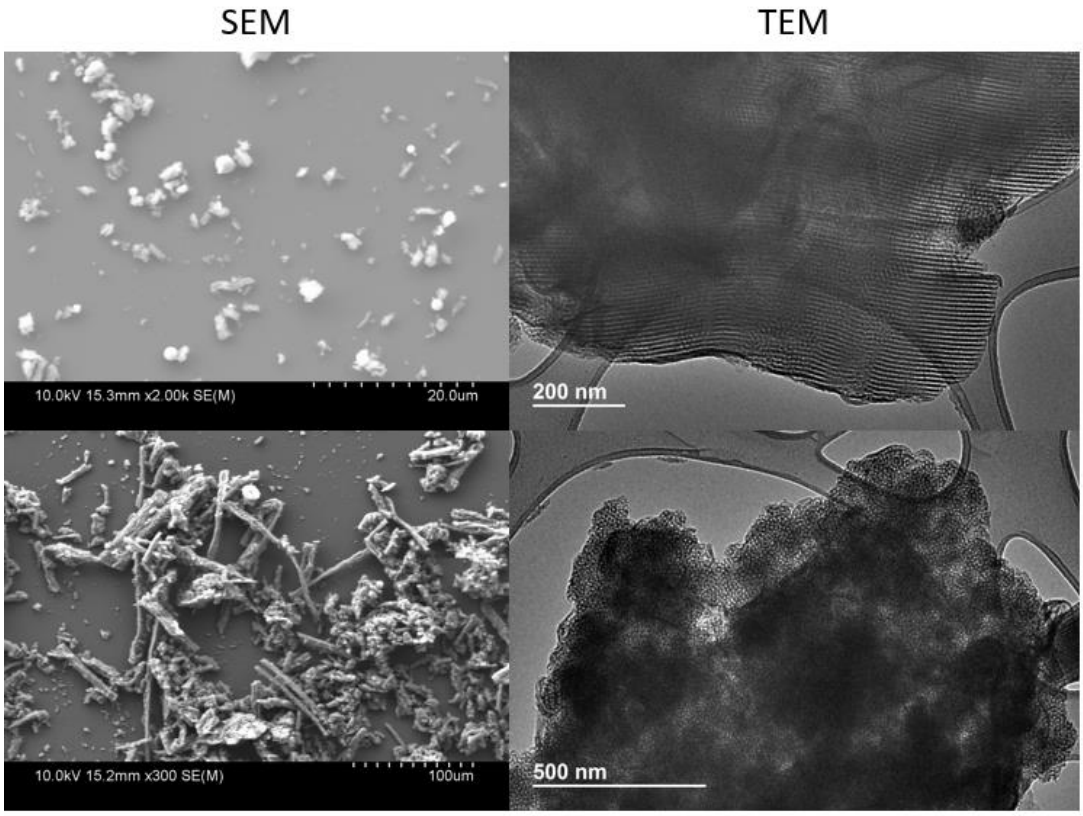

Figure S3.3. SEM and TEM images of SiO_2 nanoparticles synthesized in the absence of added ligand

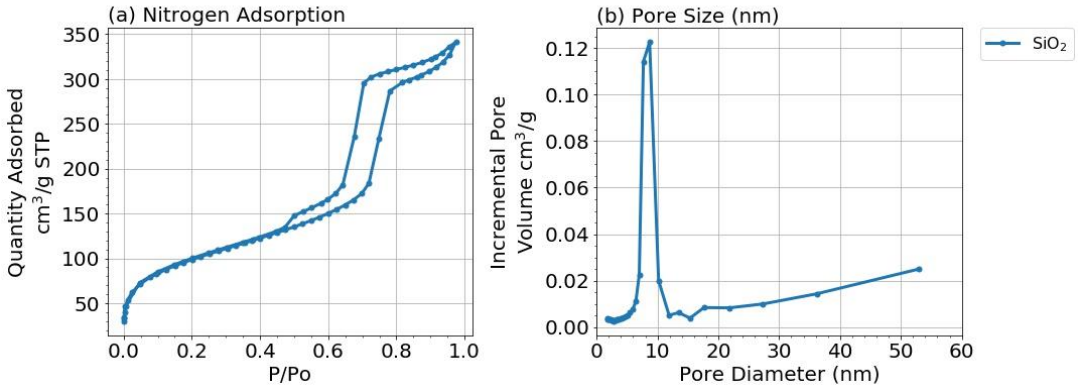

Figure S3.4. N_2 Sorption of SiO_2 nanoparticles synthesized in the absence of added ligand
Surface Area – 347.92 $m^2 g^{-1}$, **Average Pore Size –** 7.09 nm, **Pore Volume** – 0.45 cm^3/g

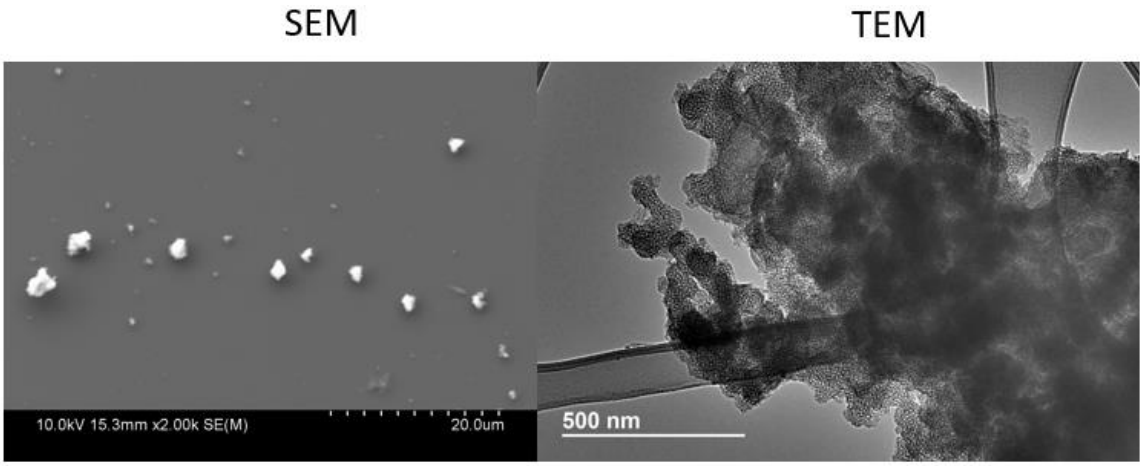

Figure S3.5. SEM and TEM images of immobilized ligand **3.15**

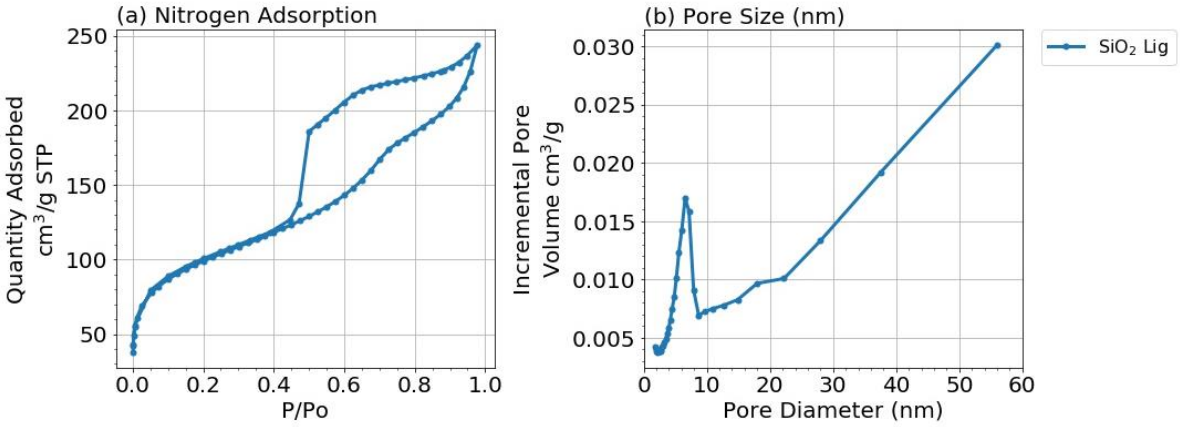

Figure S3.6. N_2 Sorption of immobilized ligand **3.15**
Surface Area – 338.05 $m^2 g^{-1}$, **Average Pore Size** – 6.12 nm, **Pore Volume** – 0.282 cm^3/g

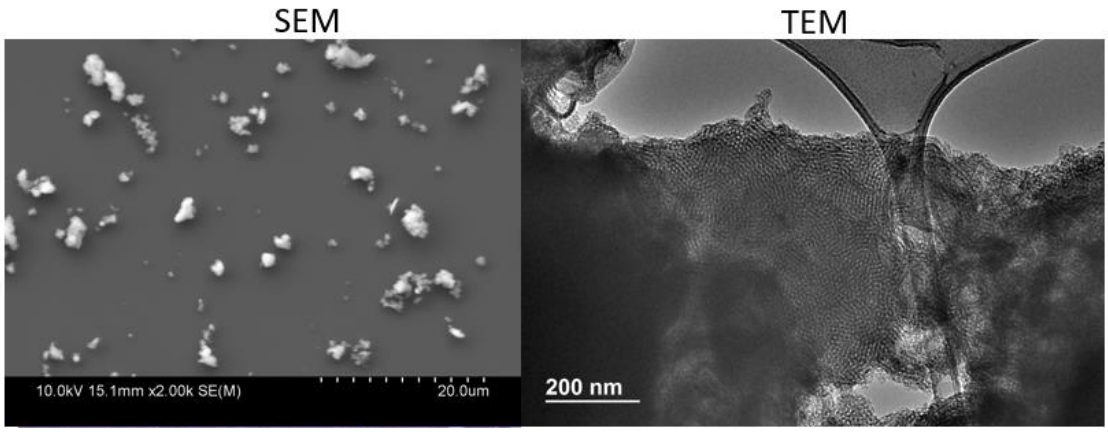

Figure S3.7. SEM and TEM images of **3.16**

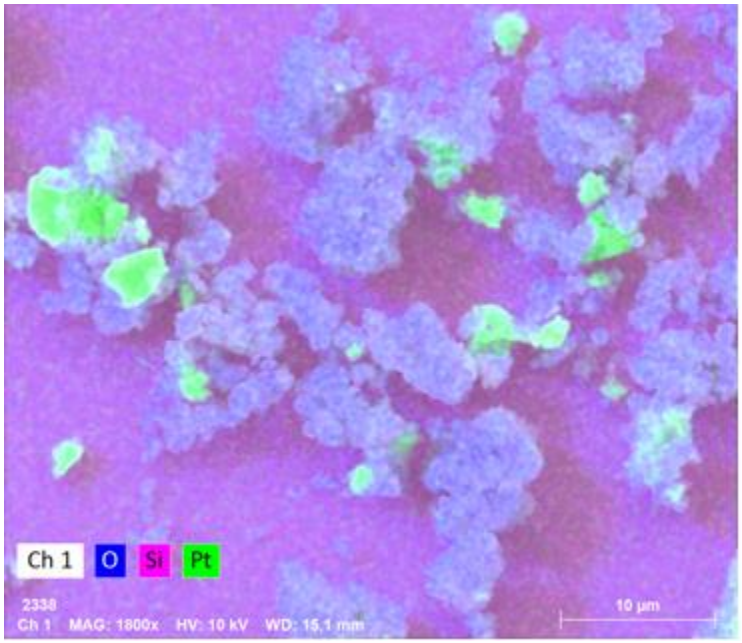

Figure S3.8. EDS images of **3.16,** Blue = Oxygen, Pink = Silicon, Green = Platinum

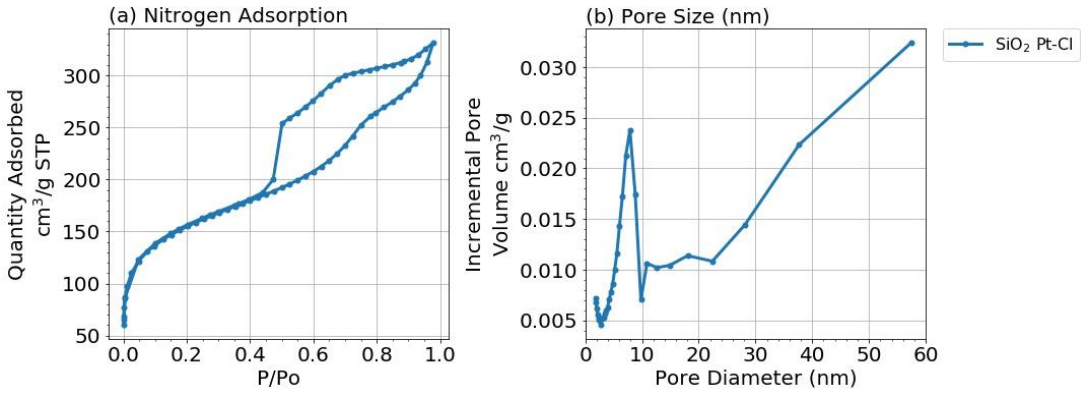

Figure S3.9. N_2 Sorption of immobilized Pt-Cl, **3.16**

Surface Area – 521.33 $m^2 g^{-1}$, **Average Pore Size** – 5.92 nm, **Pore Volume** – 0.35 cm^3/g

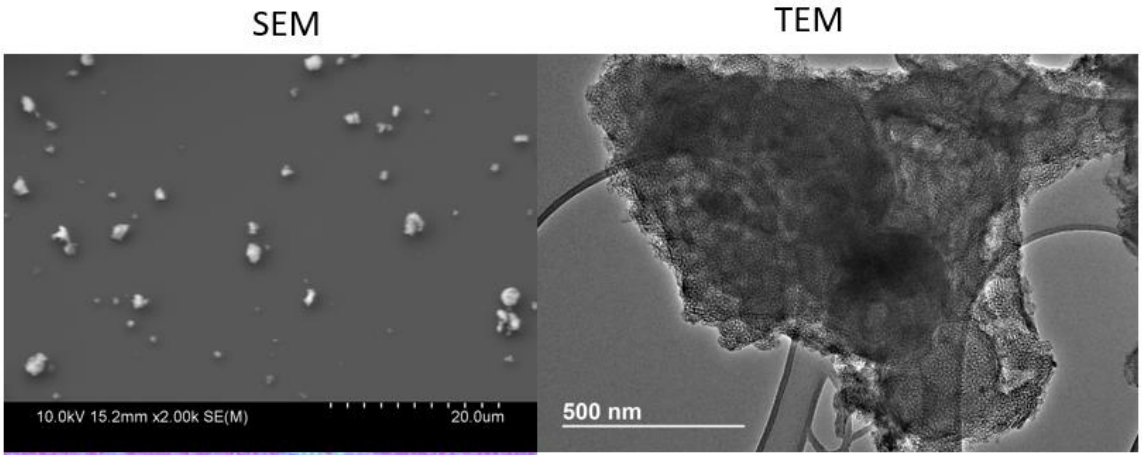

Figure S3.10. SEM and TEM images of **3.5**

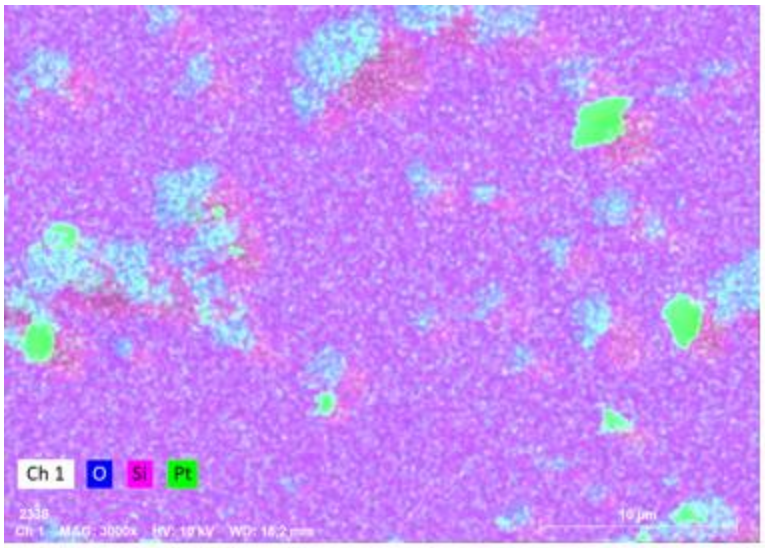

Figure S3.11. EDS images of **3.5**, Blue = Oxygen, Pink = Silicon, Green = Platinum

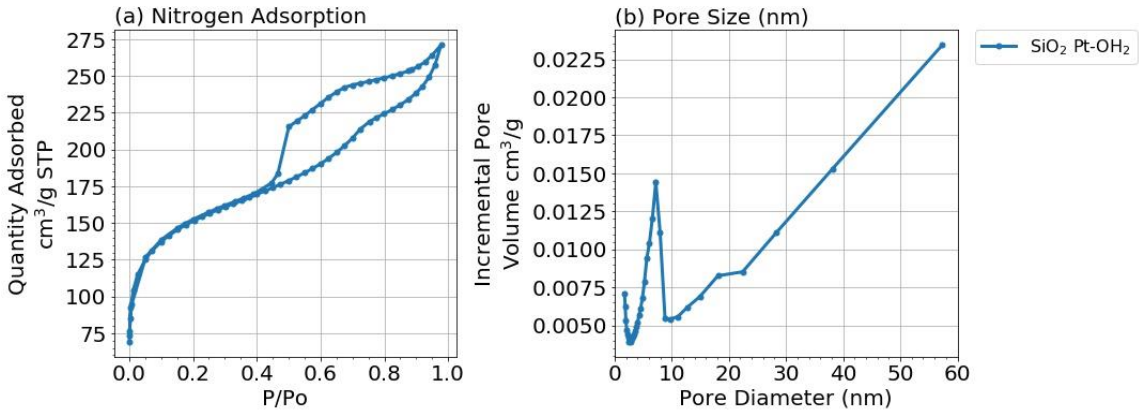

Figure S3.12. N_2 Sorption of immobilized complex **3.5**

Surface Area – 493.18 $m^2 g^{-1}$, **Average Pore Size** – 5.32 nm, **Pore Volume** – 0.25 cm^3/g

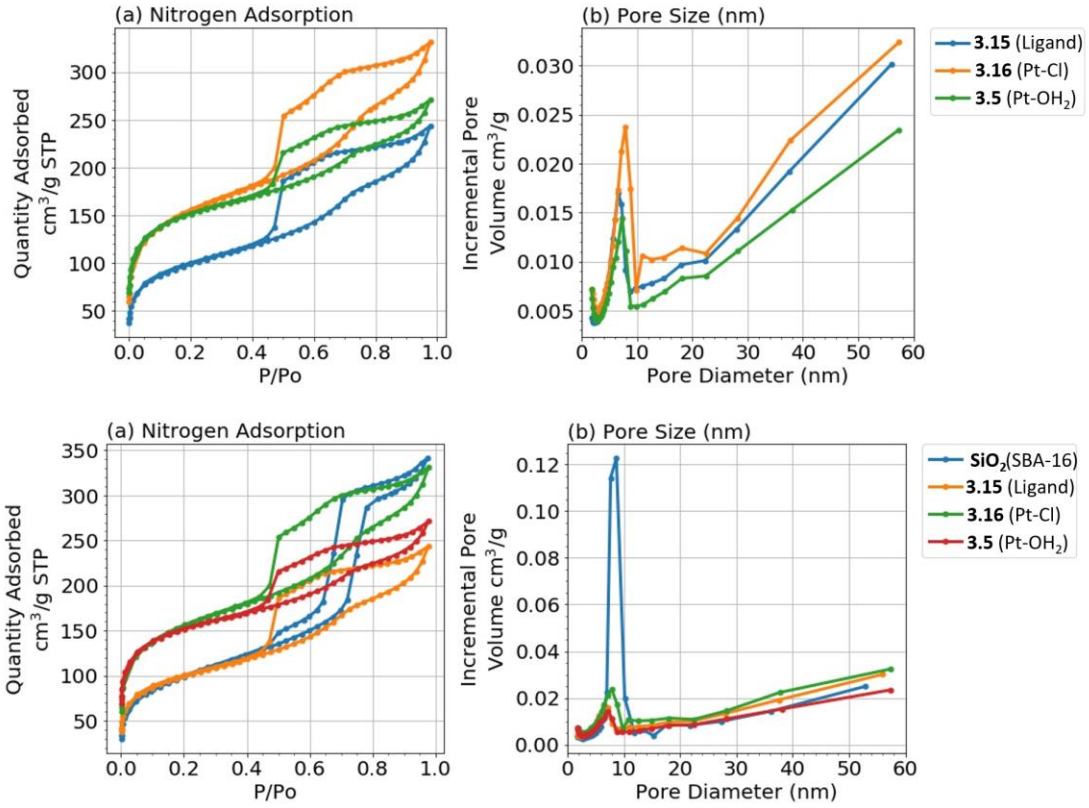

Figure S3.12. N_2 Sorption overlay of all materials

VII. NMR Spectra

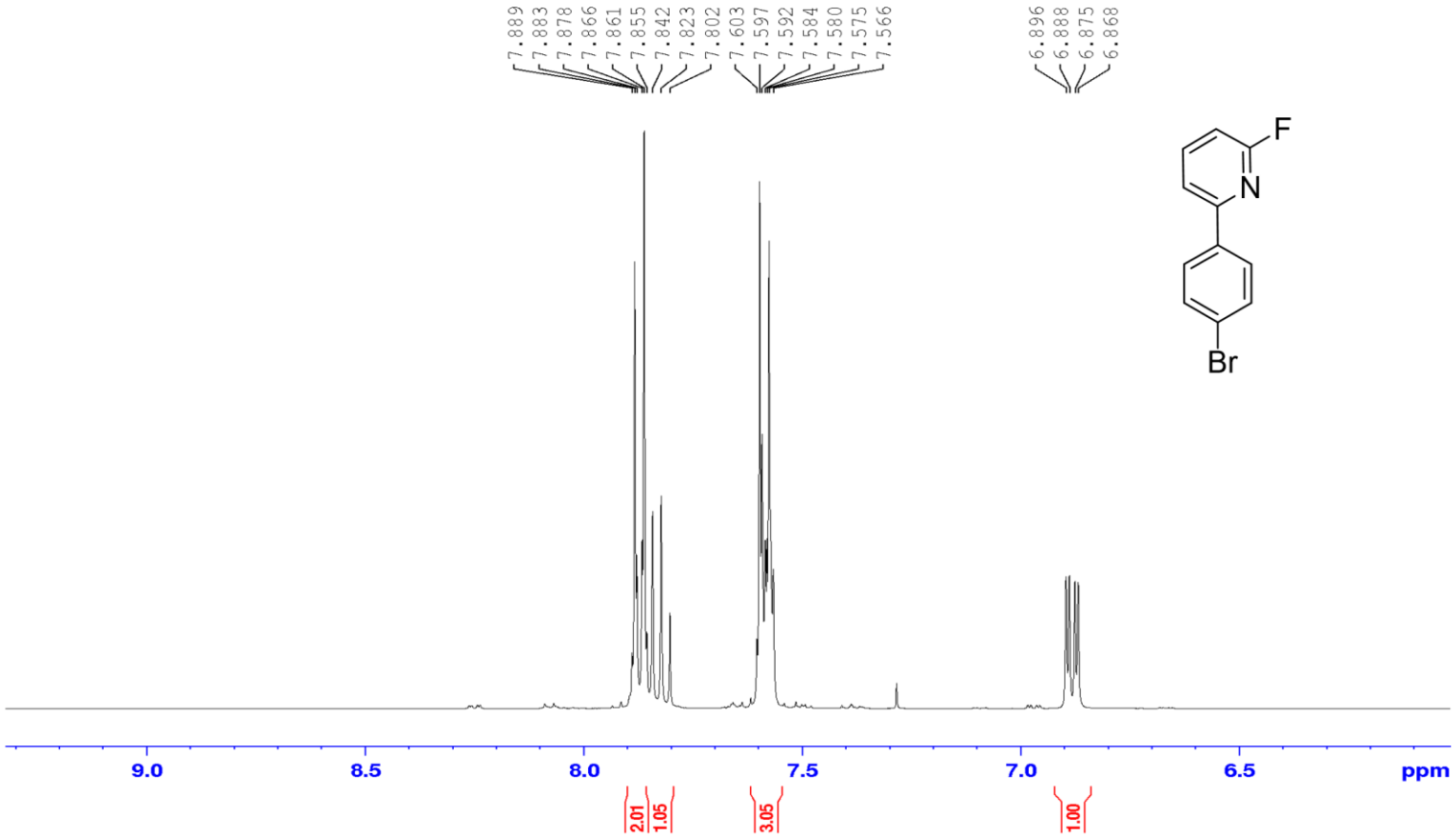

Figure S3.13. ^{1}H-NMR for 2-fluoro-6-(4-bromophenyl) pyridine **3.7** in $CDCl_3$.

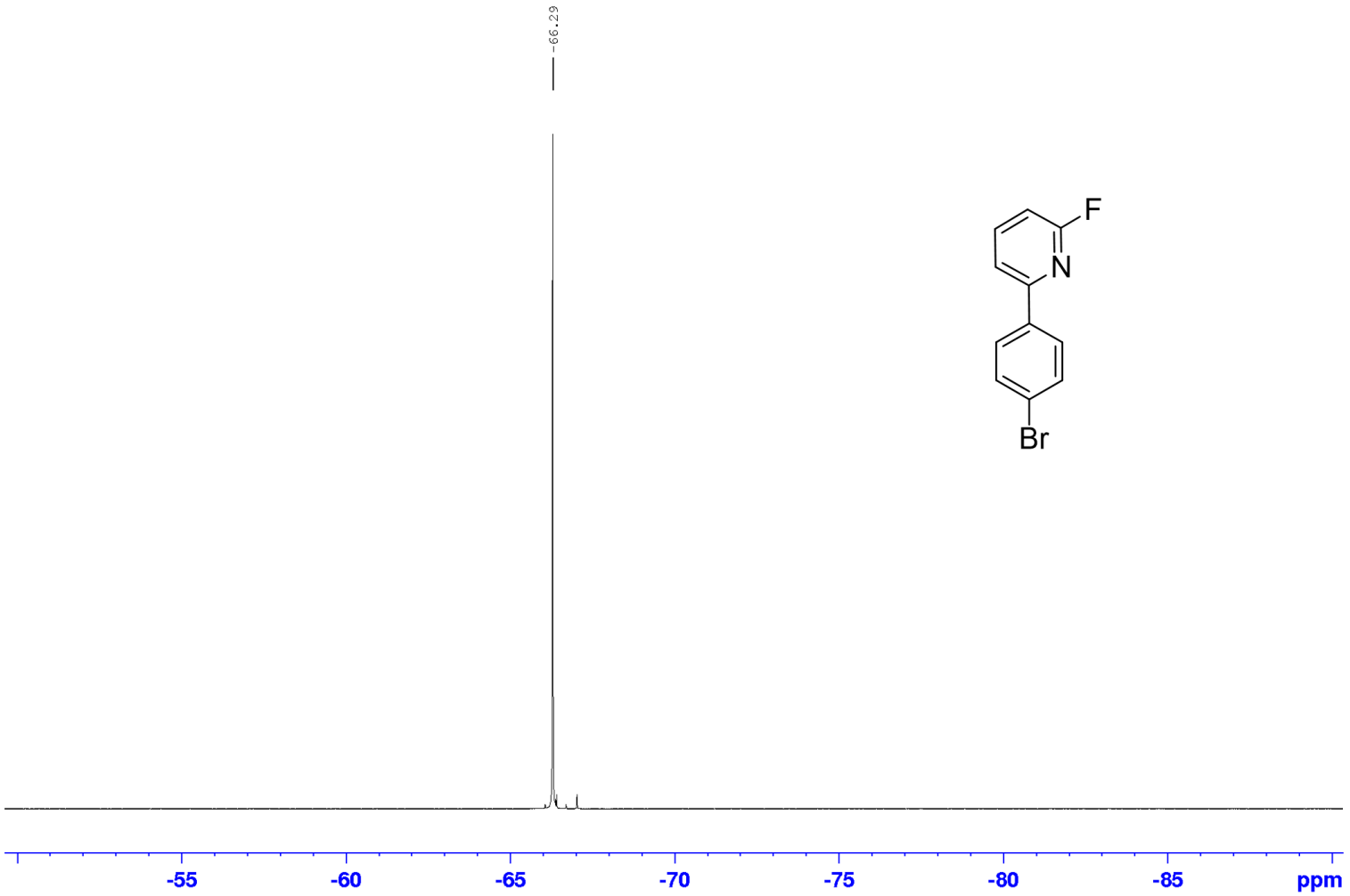

Figure S3.14. ^{19}F-NMR for 2-fluoro-6-(4-bromophenyl) pyridine **3.7** in $CDCl_3$.

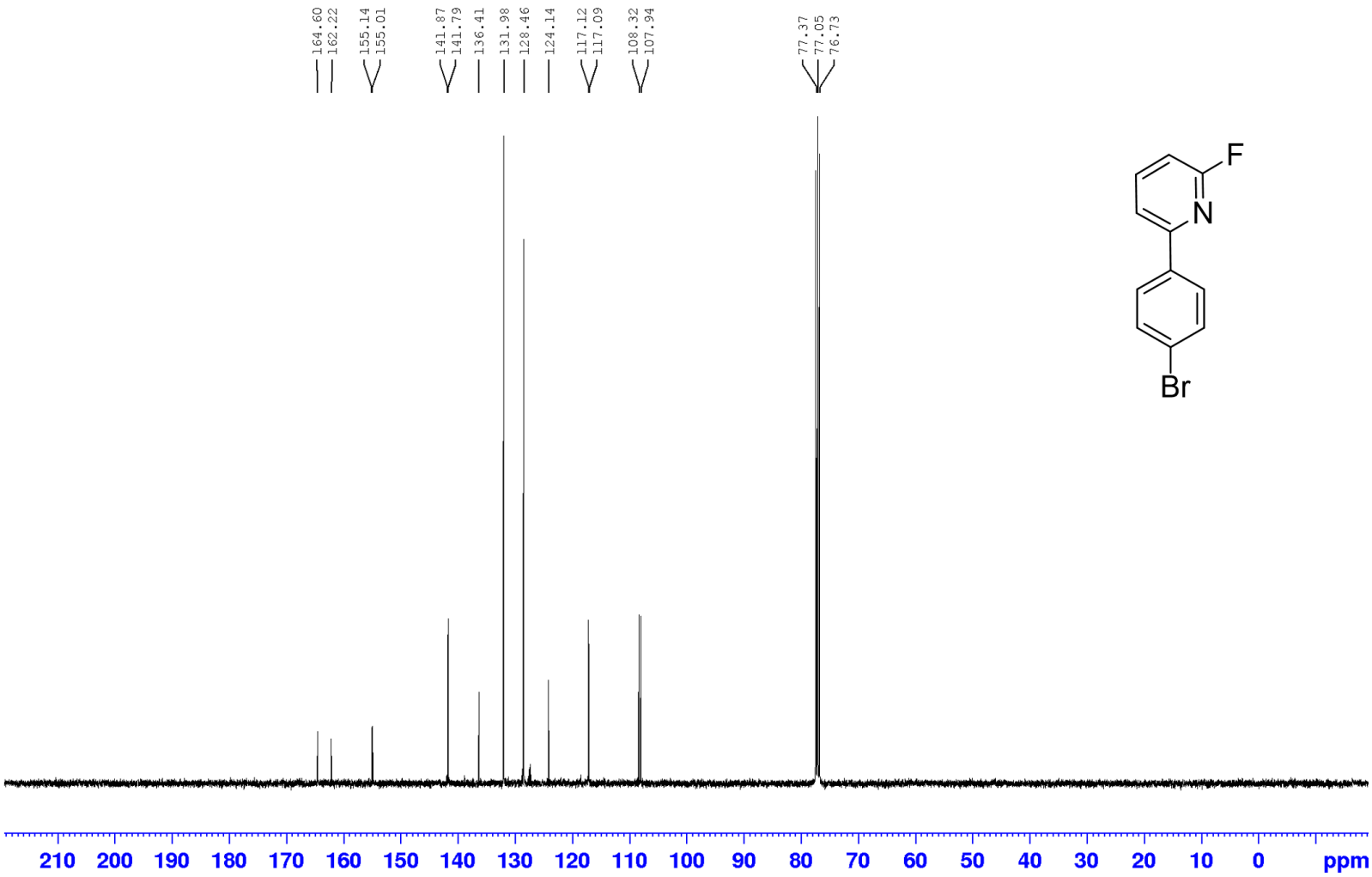

Figure S3.15. ^{13}C-NMR for 2-fluoro-6-(4-bromophenyl) pyridine **3.7** in $CDCl_3$.

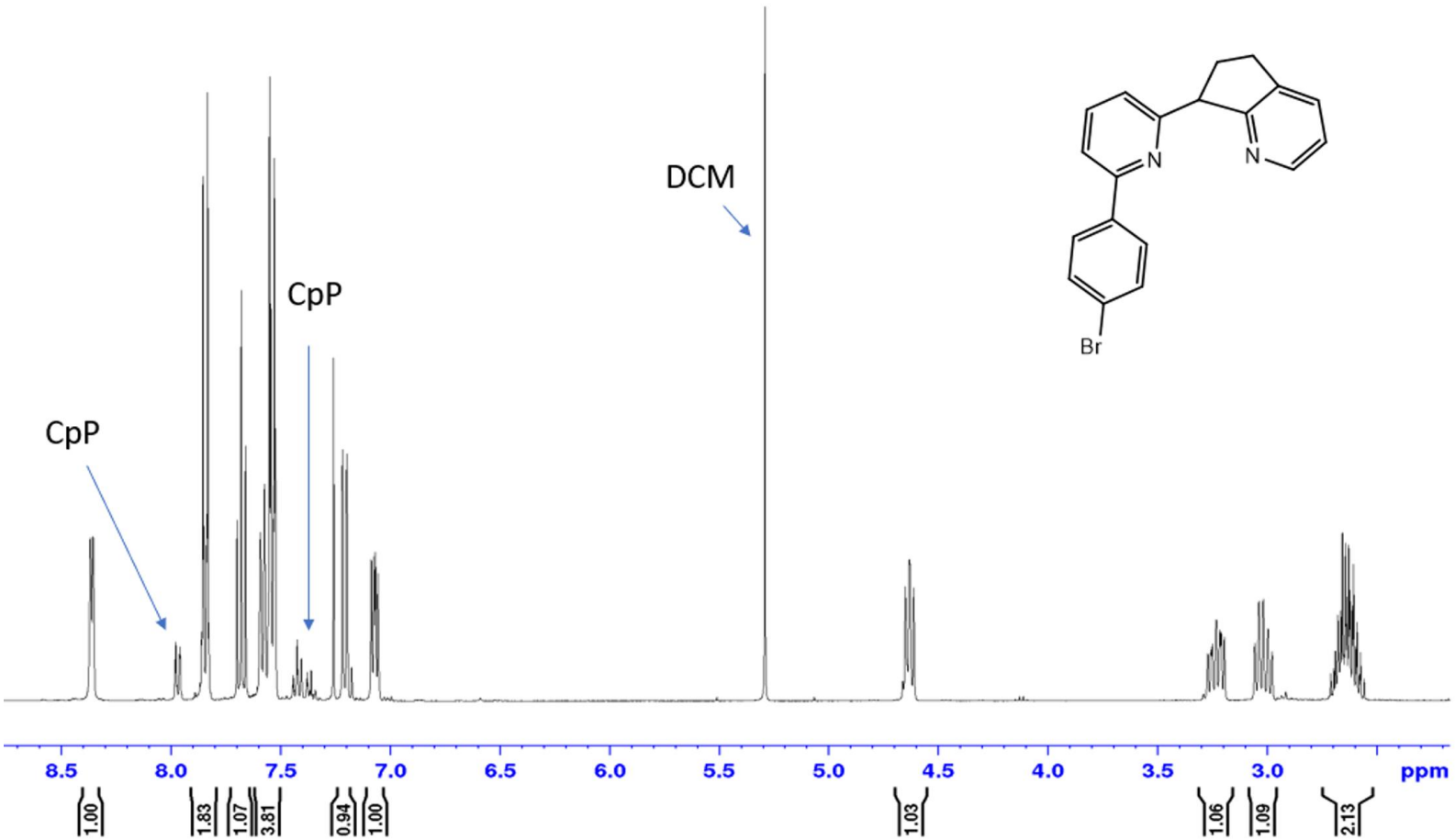

Figure S3.16. ^{1}H-NMR for 2-(4-bromobutylphenyl)-6-(pyridin-2-ylmethyl) pyridine **3.8** in $CDCl_3$

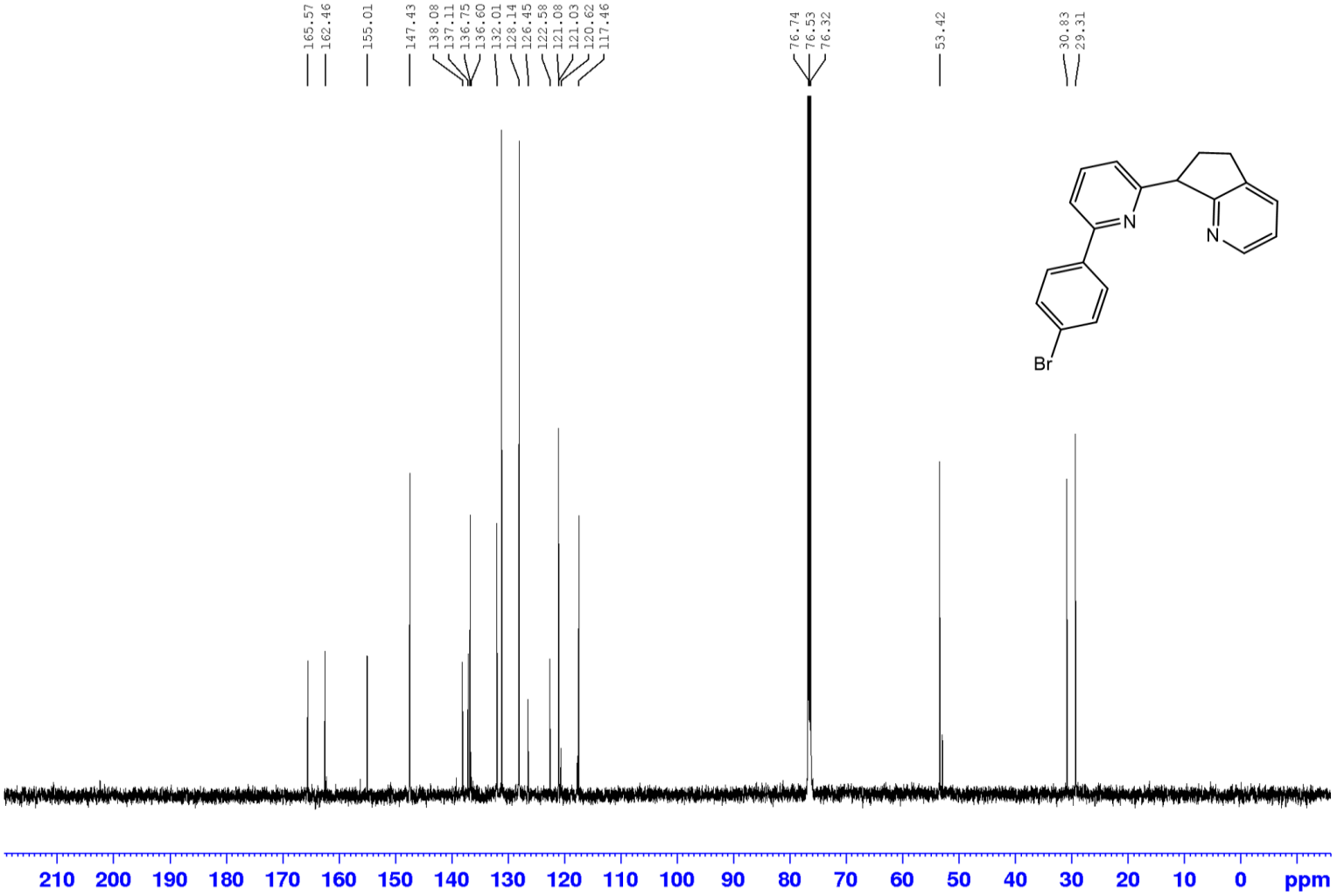

Figure S3.17. ^{13}C-NMR for 2-(4-bromobutylphenyl)-6-(pyridin-2-ylmethyl) pyridine **3.8** in $CDCl_3$.

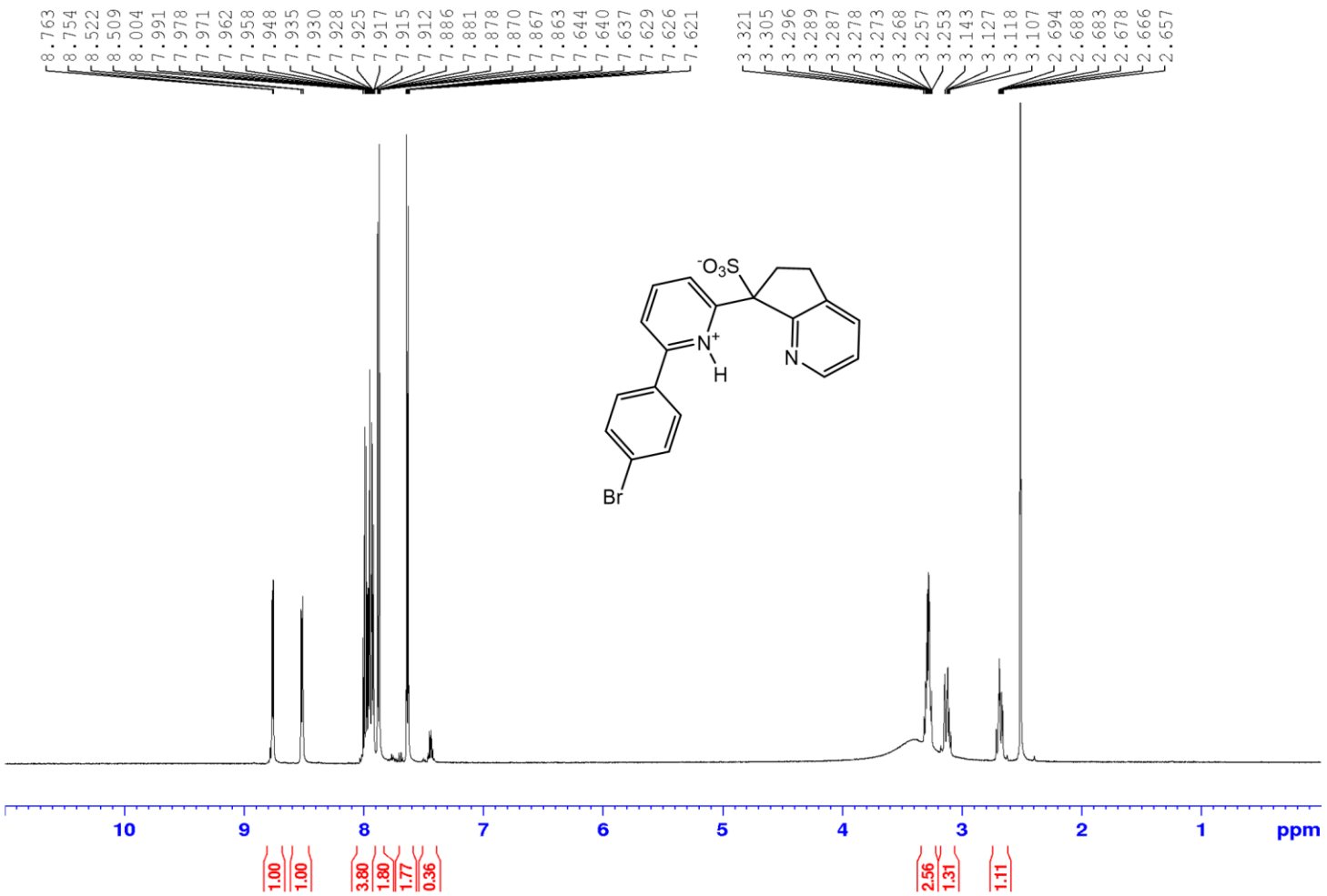

Figure S3.18. ^{1}H-NMR for 2-(4-bromobutylphenyl)-6-(pyridin-2-ylmethyl) pyridinium sulfonate **3.11** in DMSO-d_6.

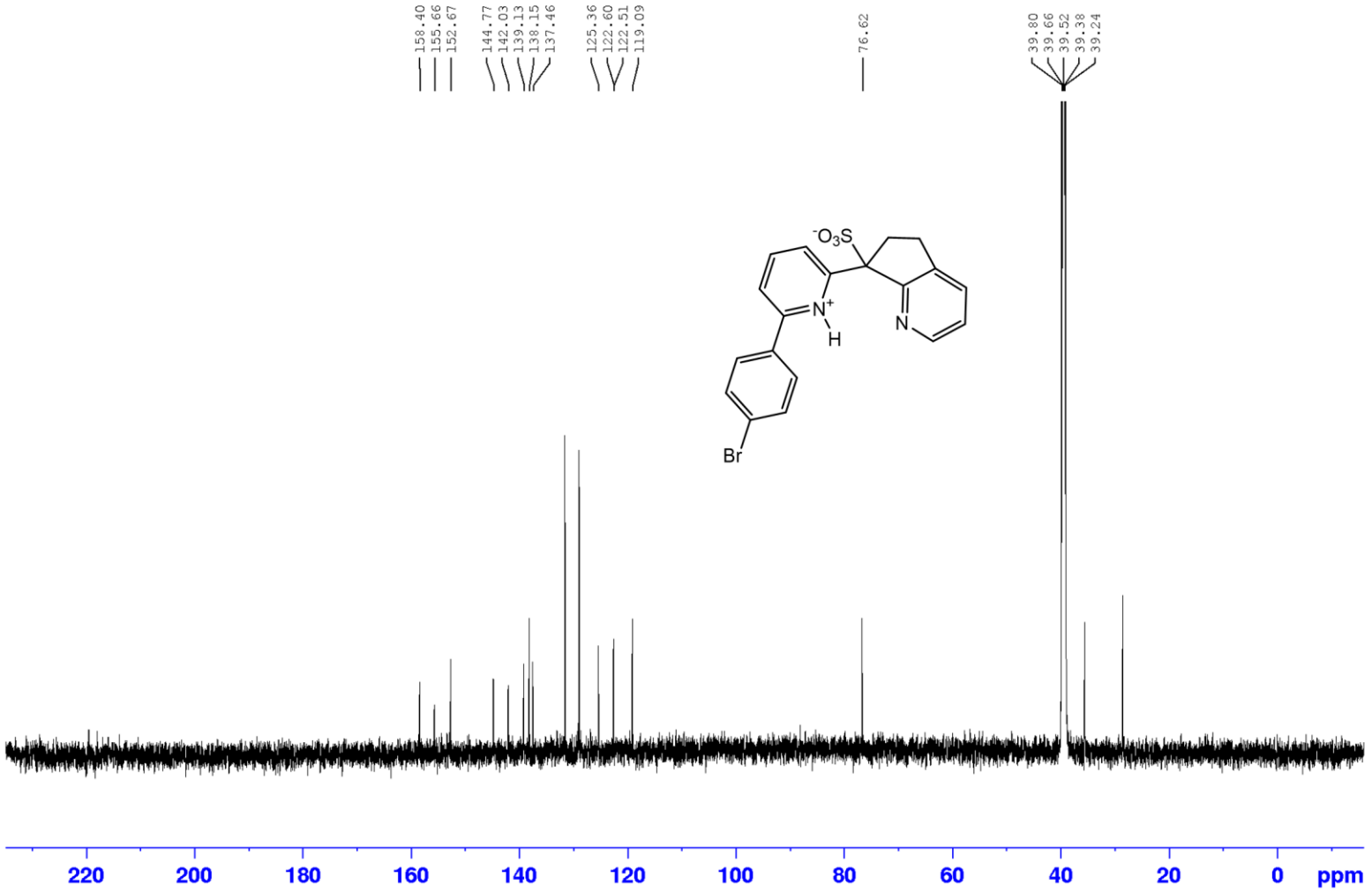

Figure S3.19. ^{13}C-NMR for 2-(4-bromobutylphenyl)-6-(pyridin-2-ylmethyl) pyridinium sulfonate **3.11** in DMSO-*d*.

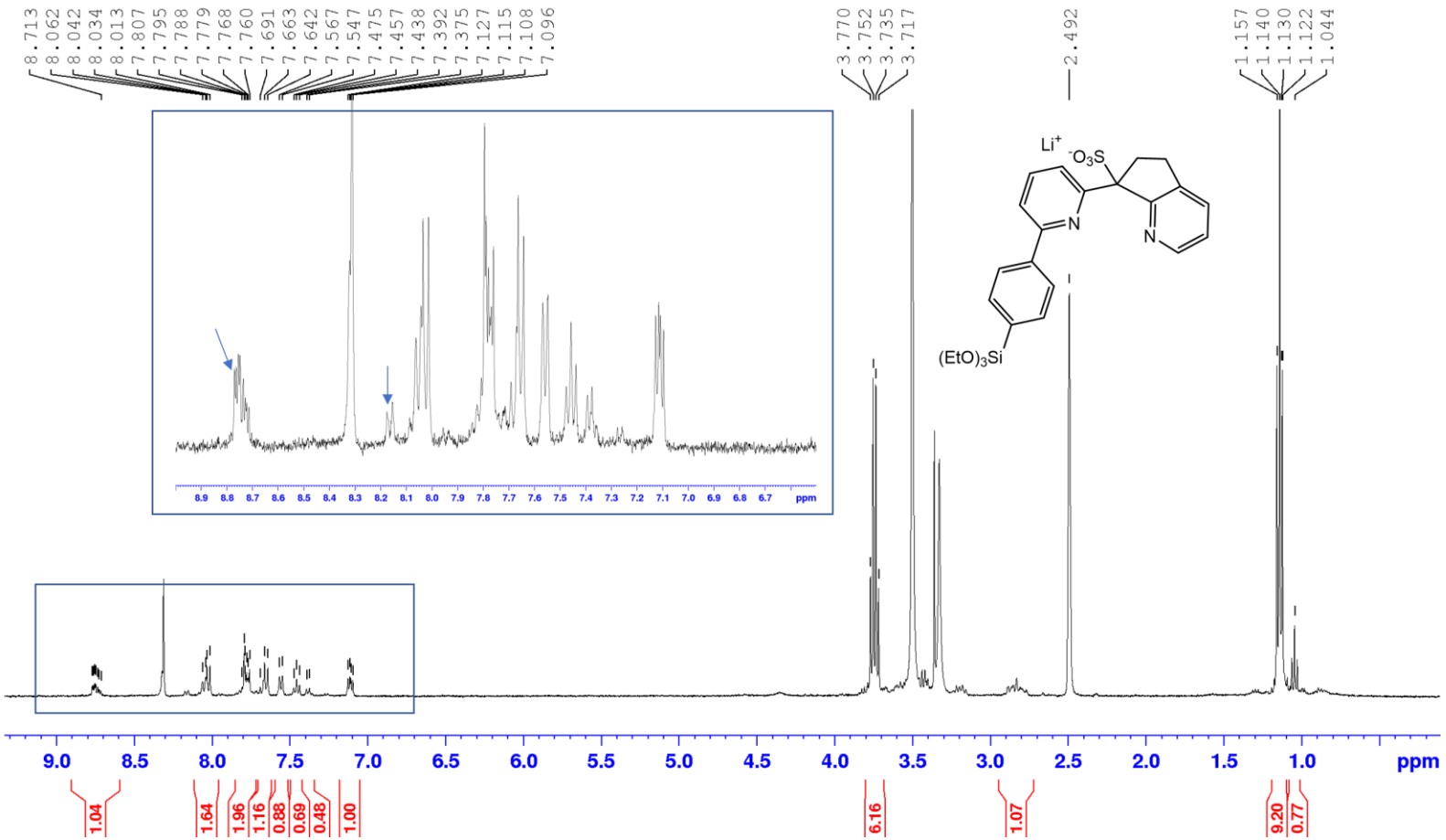

Figure S3.20. ^{1}H-NMR for Crude lithium 2-(4-trimethoxysilylphenyl)-6-(pyridin-2-ylmethyl) pyridine sulfonate **3.3** in DMSO-d_6.

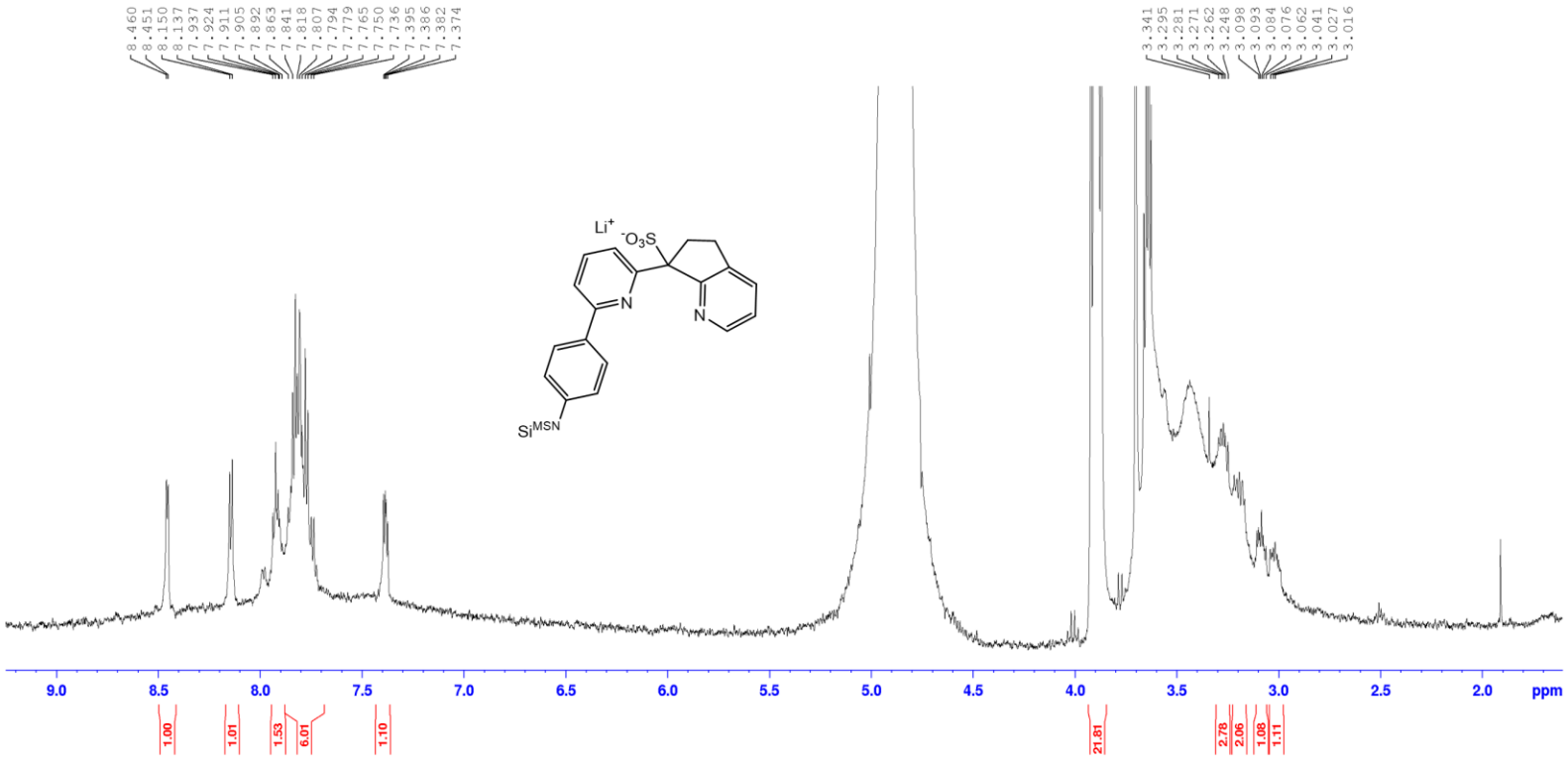

Figure S3.21. ^{1}H-NMR of **3.15-Digest** resulting from KOH digestion of **3.15** in D_2O.

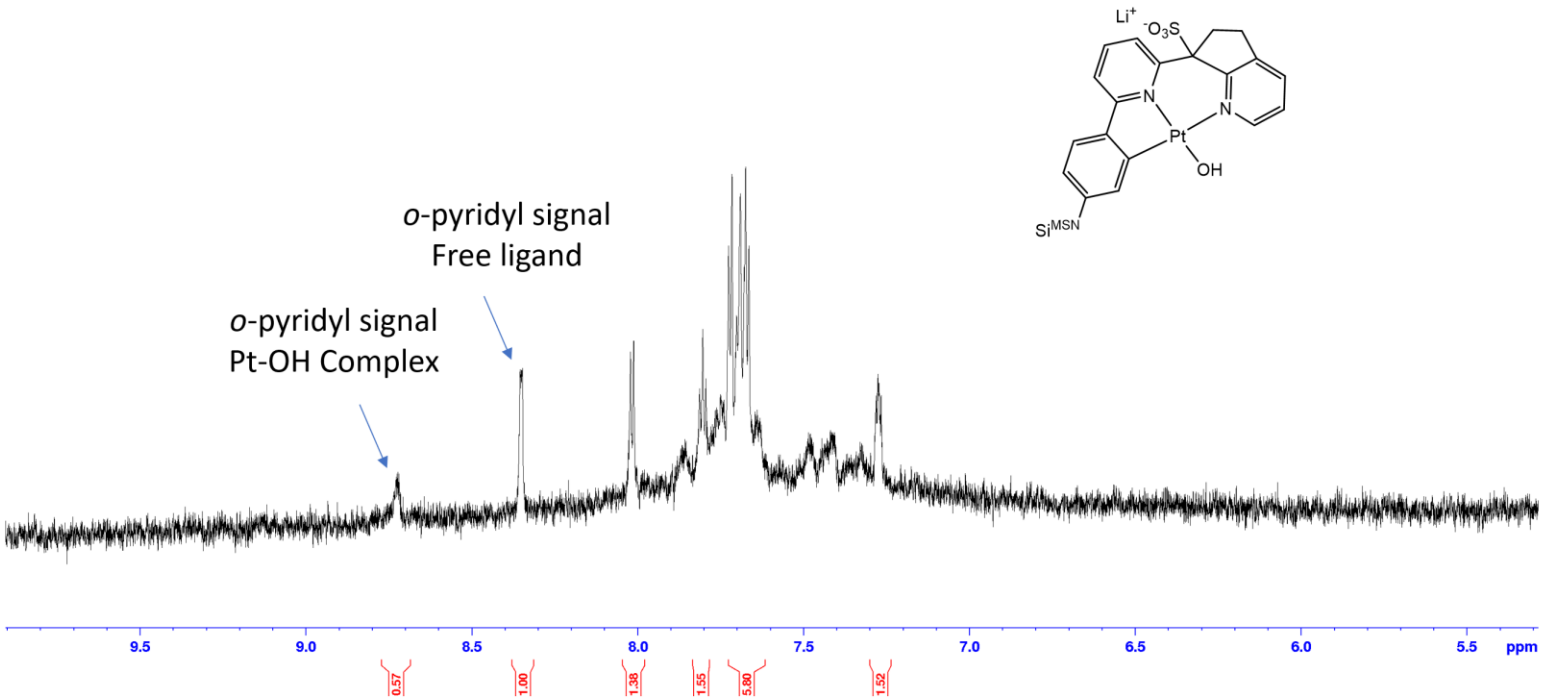

Figure S3.22. ^{1}H-NMR of **3.5-Digest** resulting from KOH Digestion of Immobilized Pt-OH_2 Complex **3.5** in D_2O.

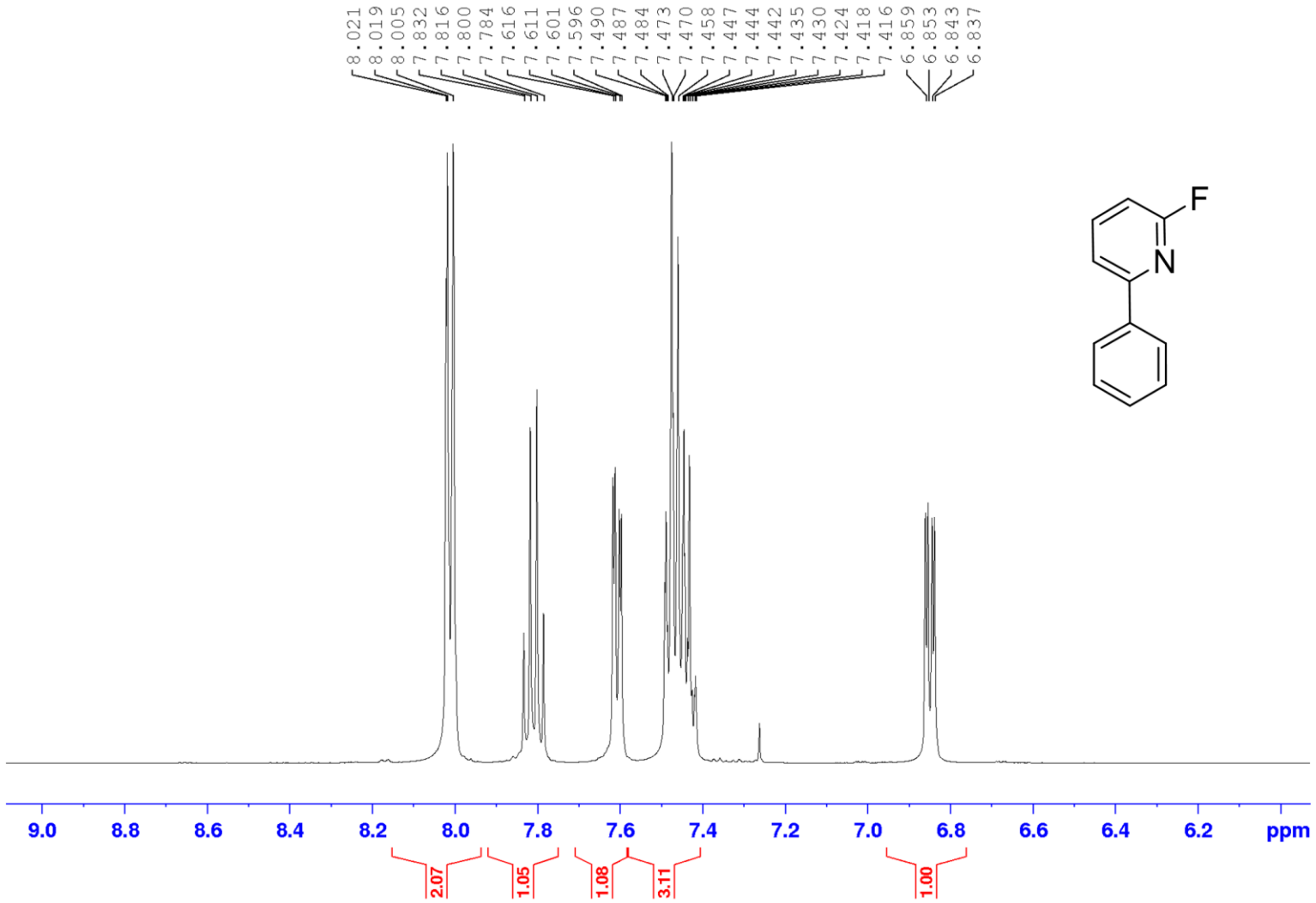

Figure S3.23. ^{1}H-NMR for 2-fluoro-6-phenyl pyridine in $CDCl_3$.

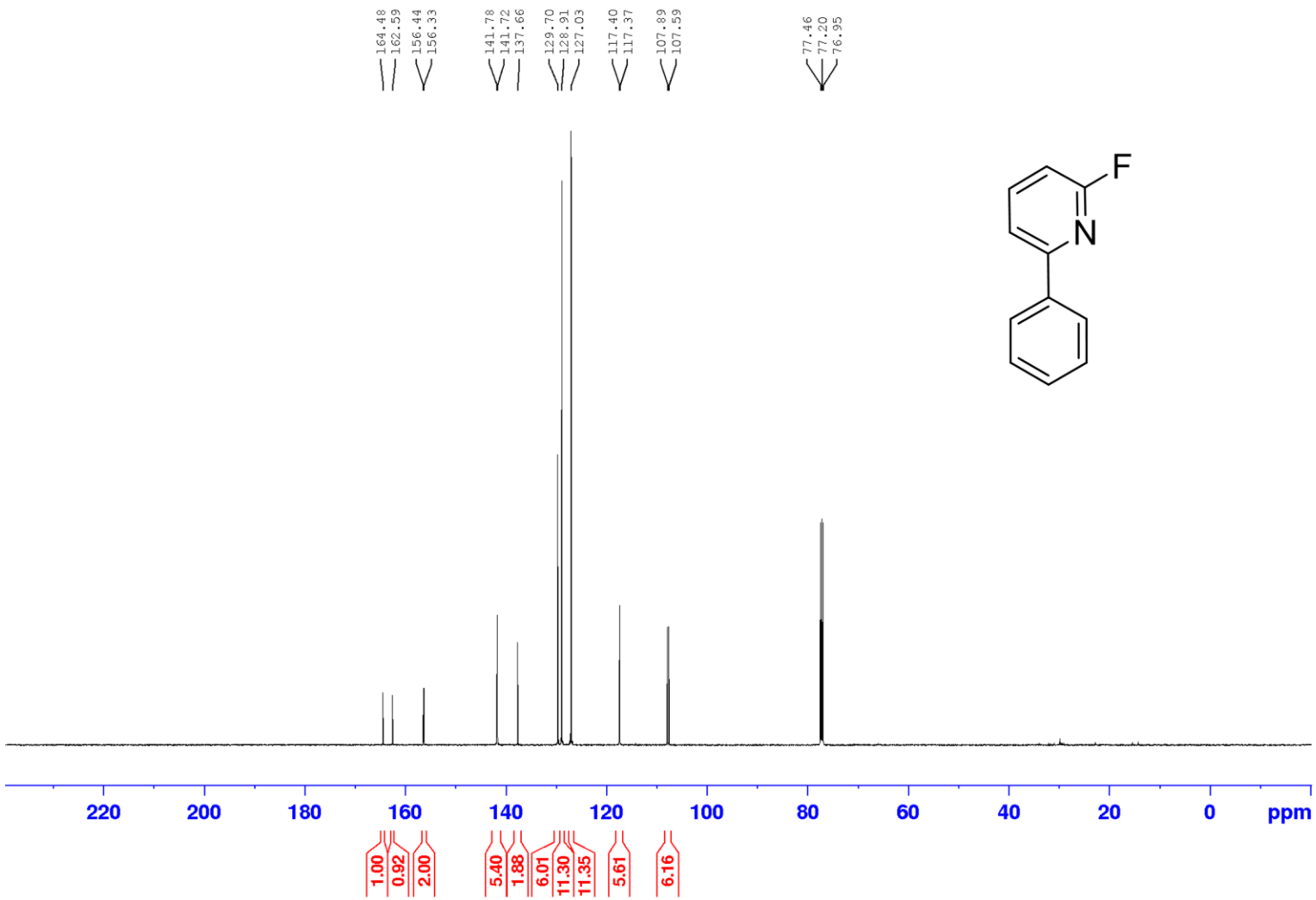

Figure S3.24. ^{13}C-NMR for 2-fluoro-6-phenyl pyridine in $CDCl_3$.

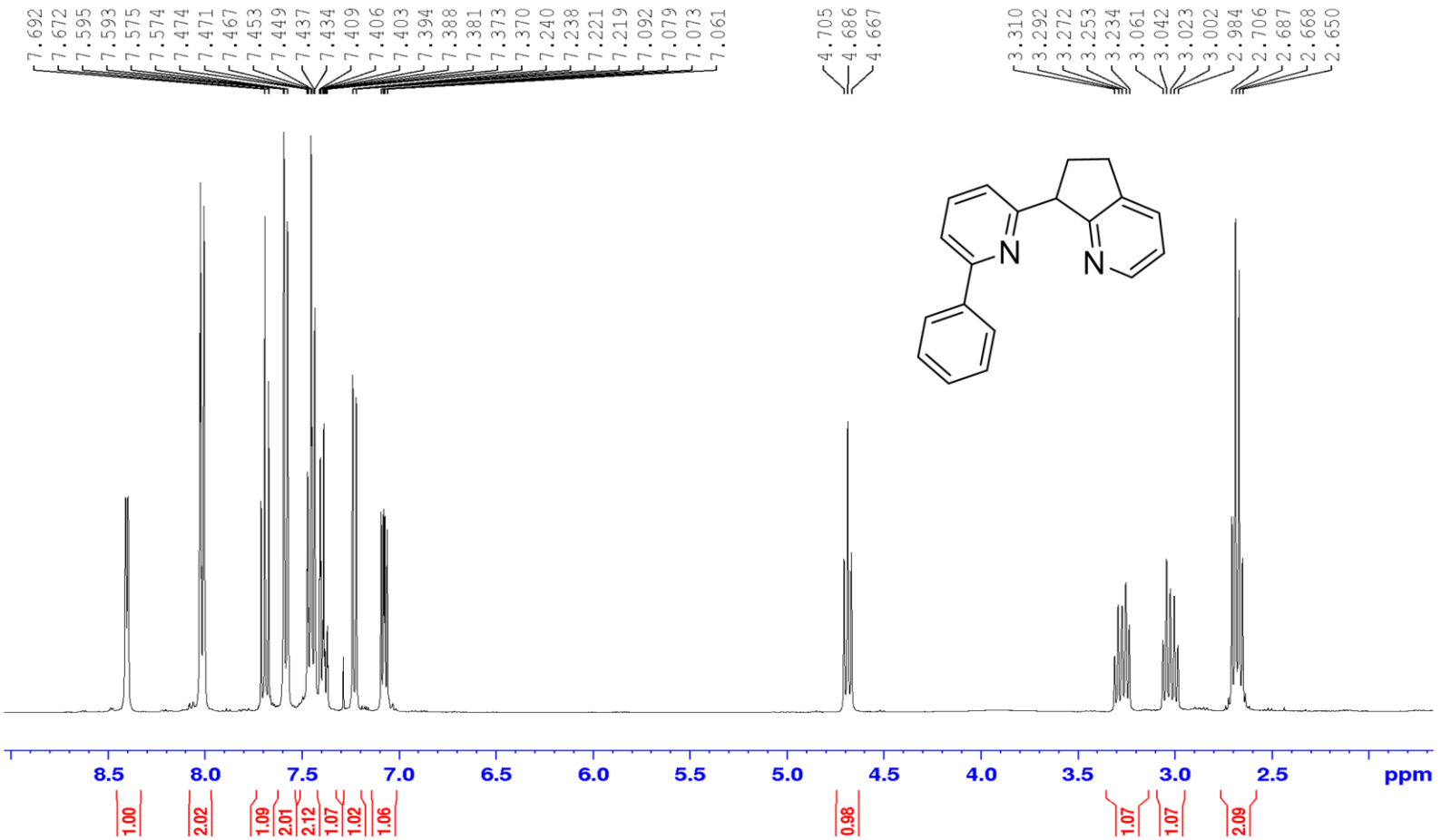

Figure S3.25. ^{1}H-NMR for 2-phenyl-6-(pyridin-2-ylmethyl) pyridine **3.8-FC** in $CDCl_3$.

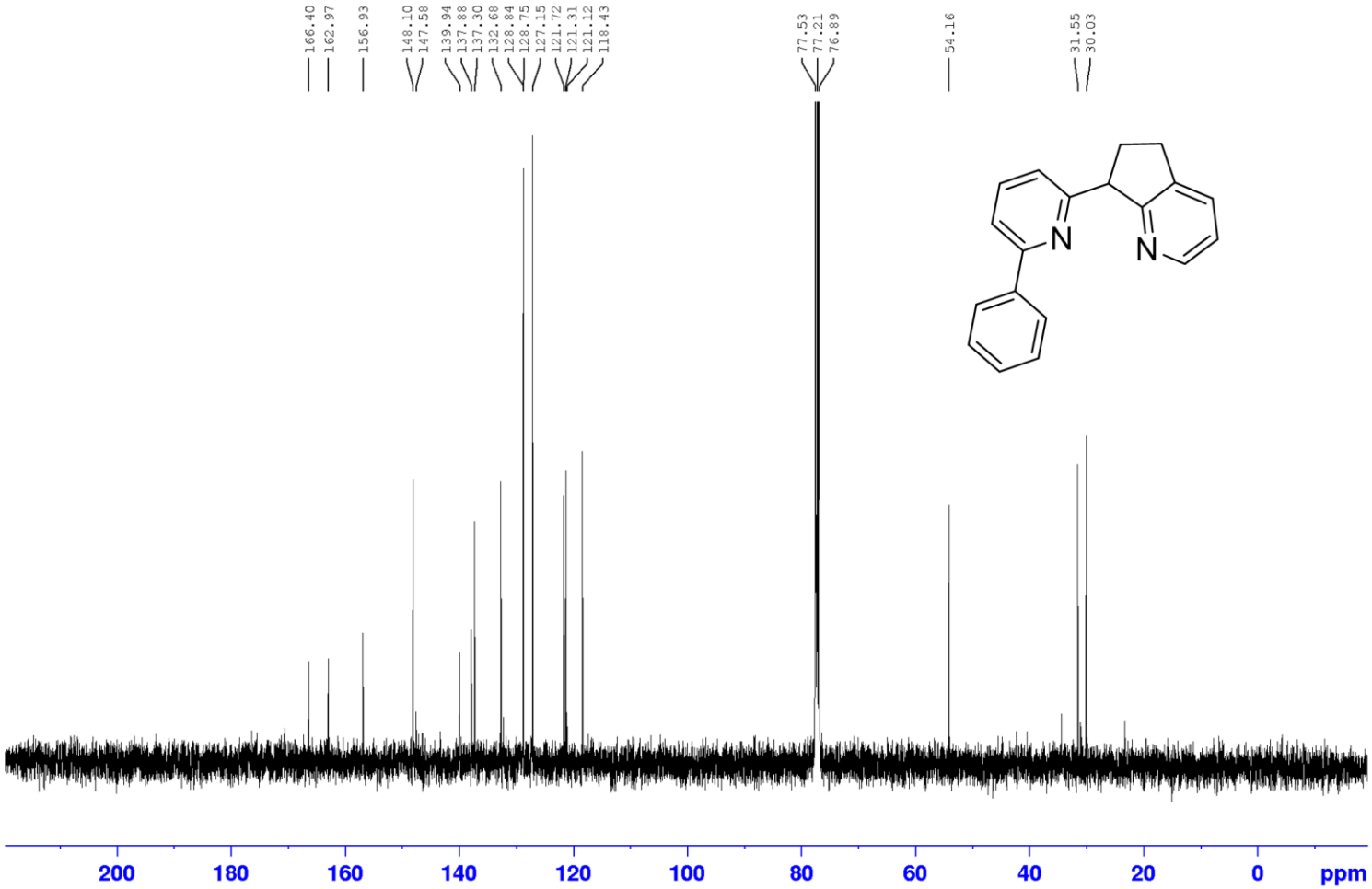

Figure S3.26. ^{13}C-NMR for 2-phenyl-6-(pyridin-2-ylmethyl) pyridine **3.8-FC** in $CDCl_3$.

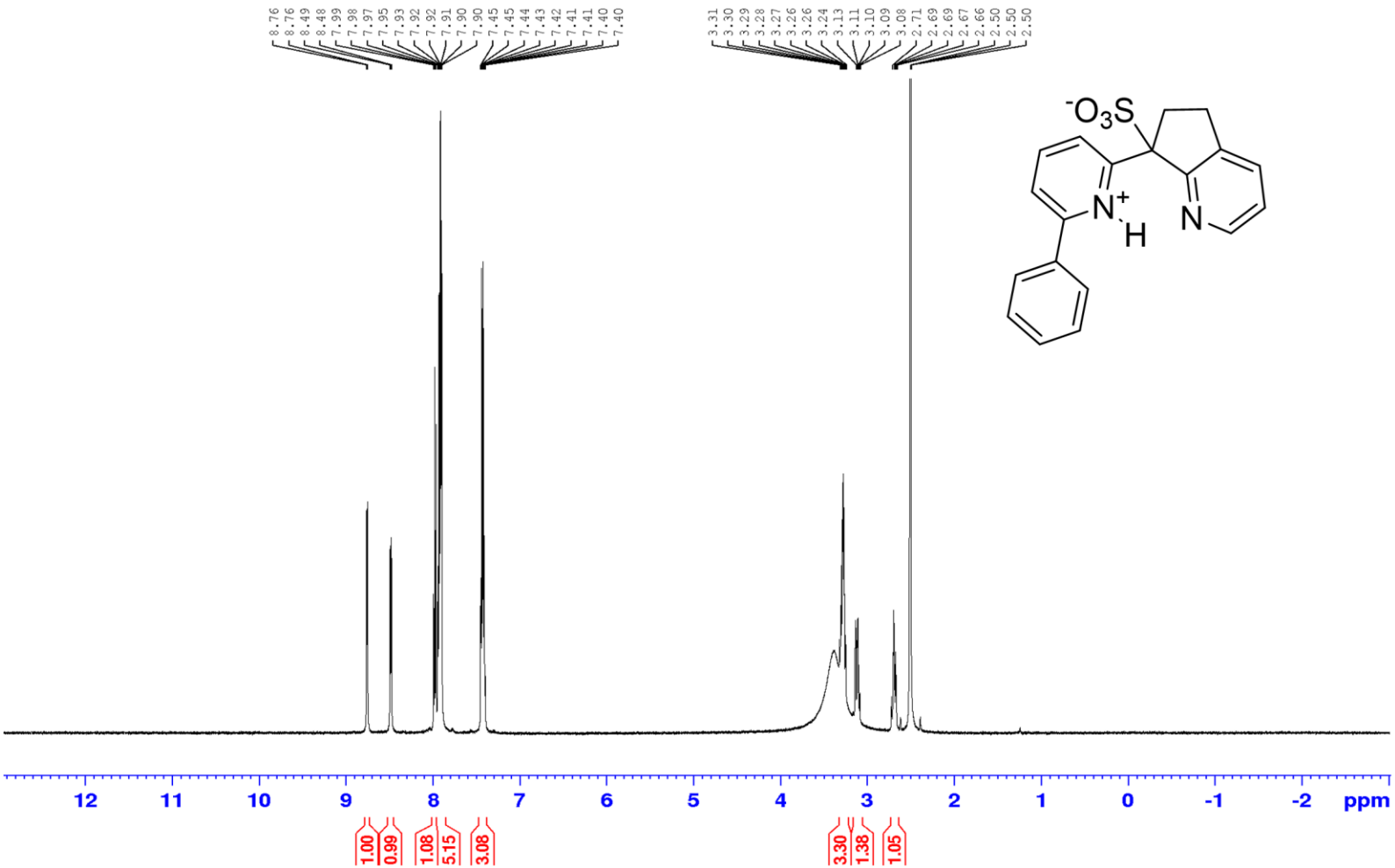

Figure S3.27. ^{1}H-NMR for 2-phenyl-6-(pyridin-2-ylmethyl) pyridinium **3.11** in DMSO-d_6.

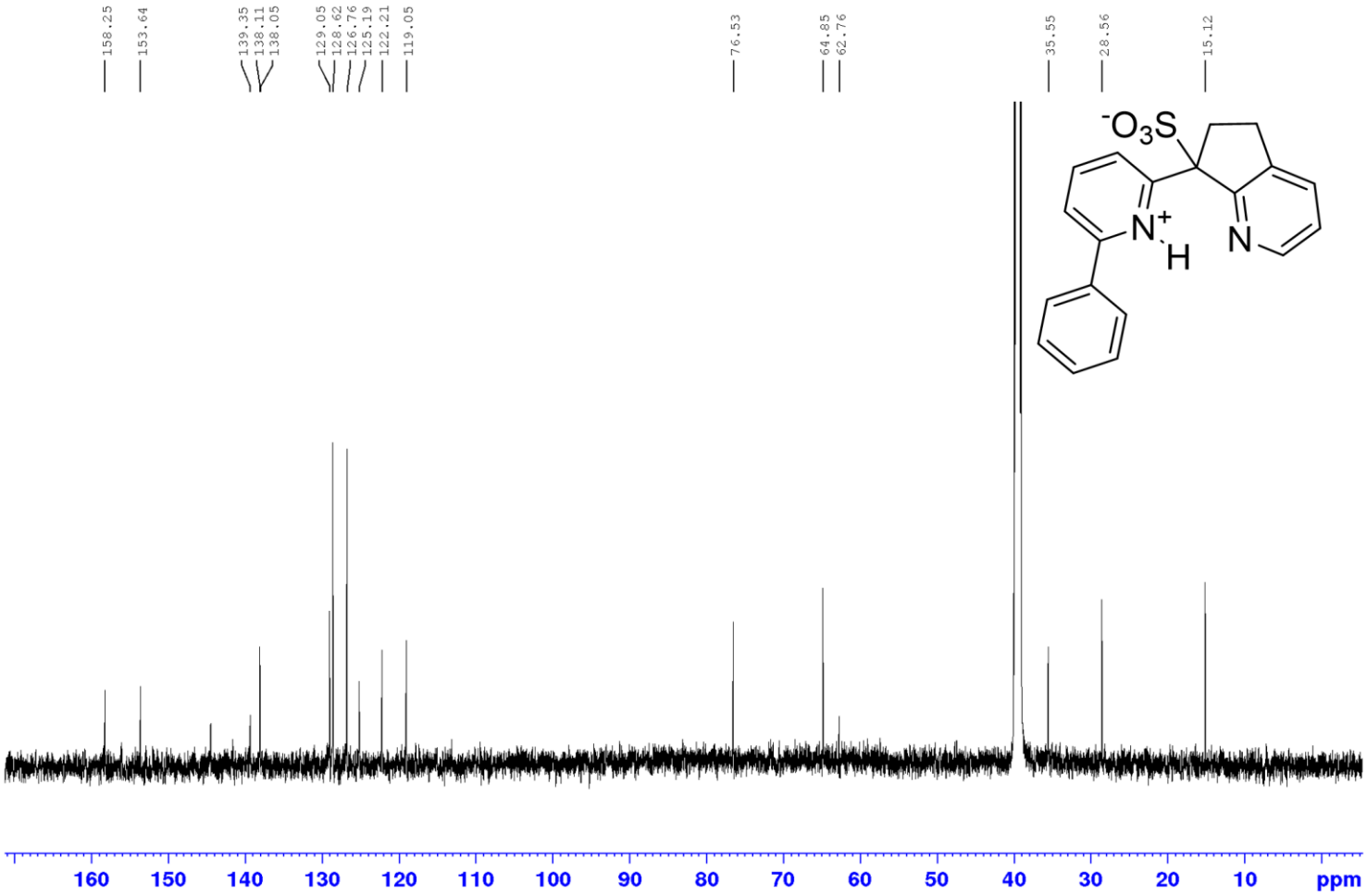

Figure S3.28. ^{13}C-NMR for 2-phenyl-6-(pyridin-2-ylmethyl) pyridinium sulfonate **3.11** in DMSO-d_6.

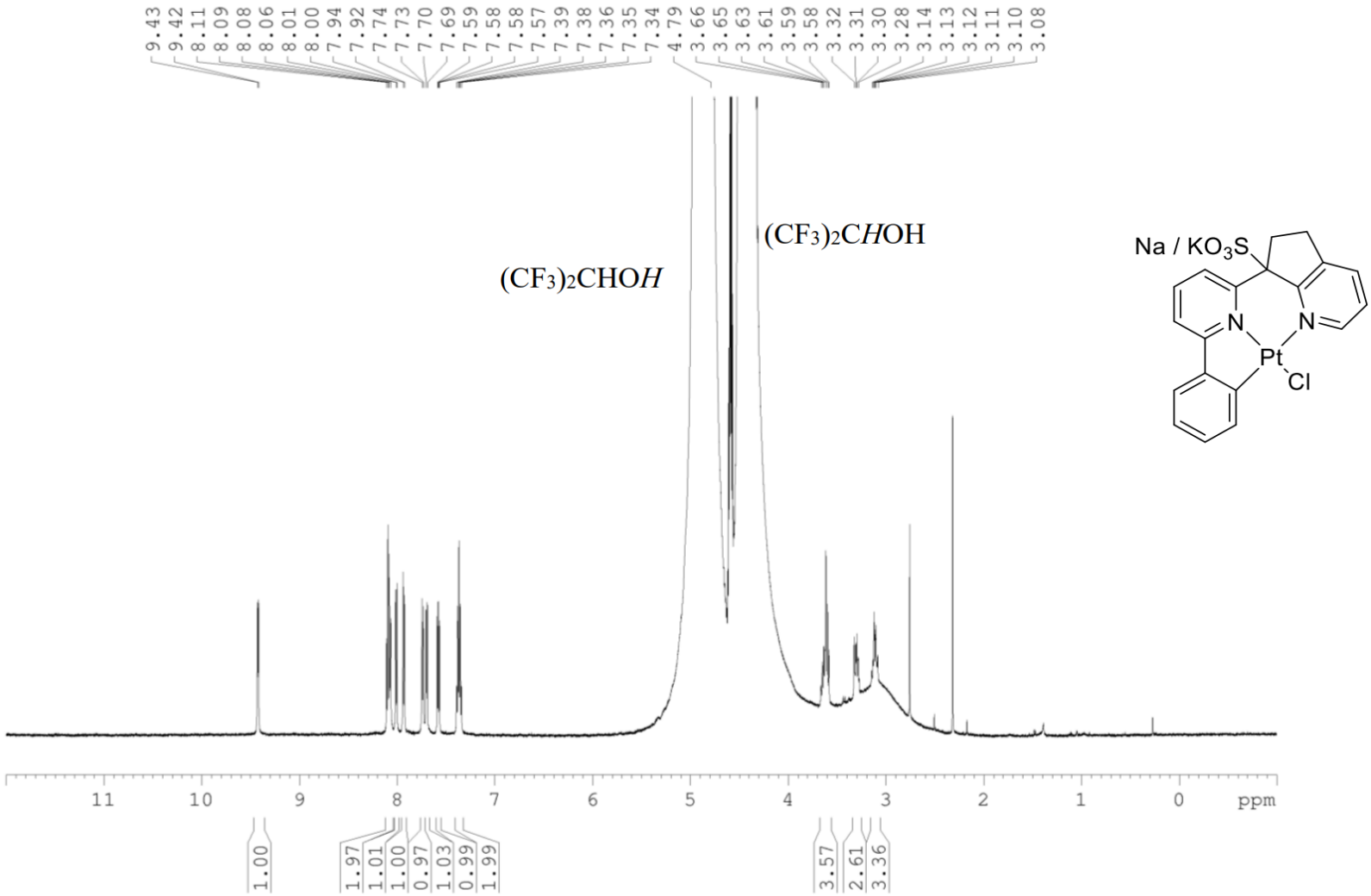

Figure S3.29. ^{1}H-NMR for 2-phenyl-6-(pyridin-2-ylmethyl) pyridine Pt-Cl Complex **3.16-FC** in DMSO-*d*$_6$.

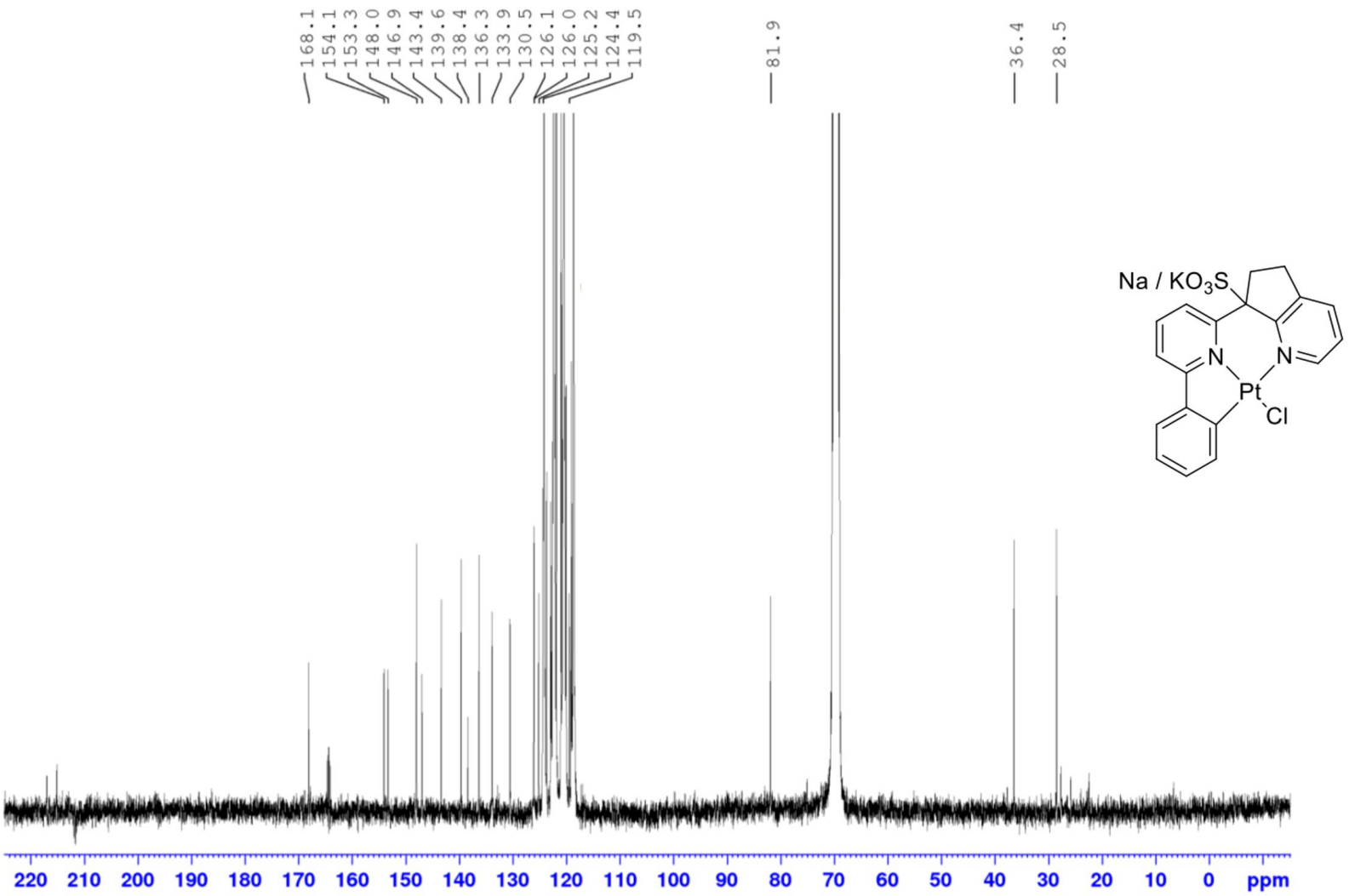

Figure S3.30. ^{13}C-NMR for 2-phenyl-6-(pyridin-2-ylmethyl) pyridine Pt-Cl Complex **3.16-FC** in DMSO-d_6.

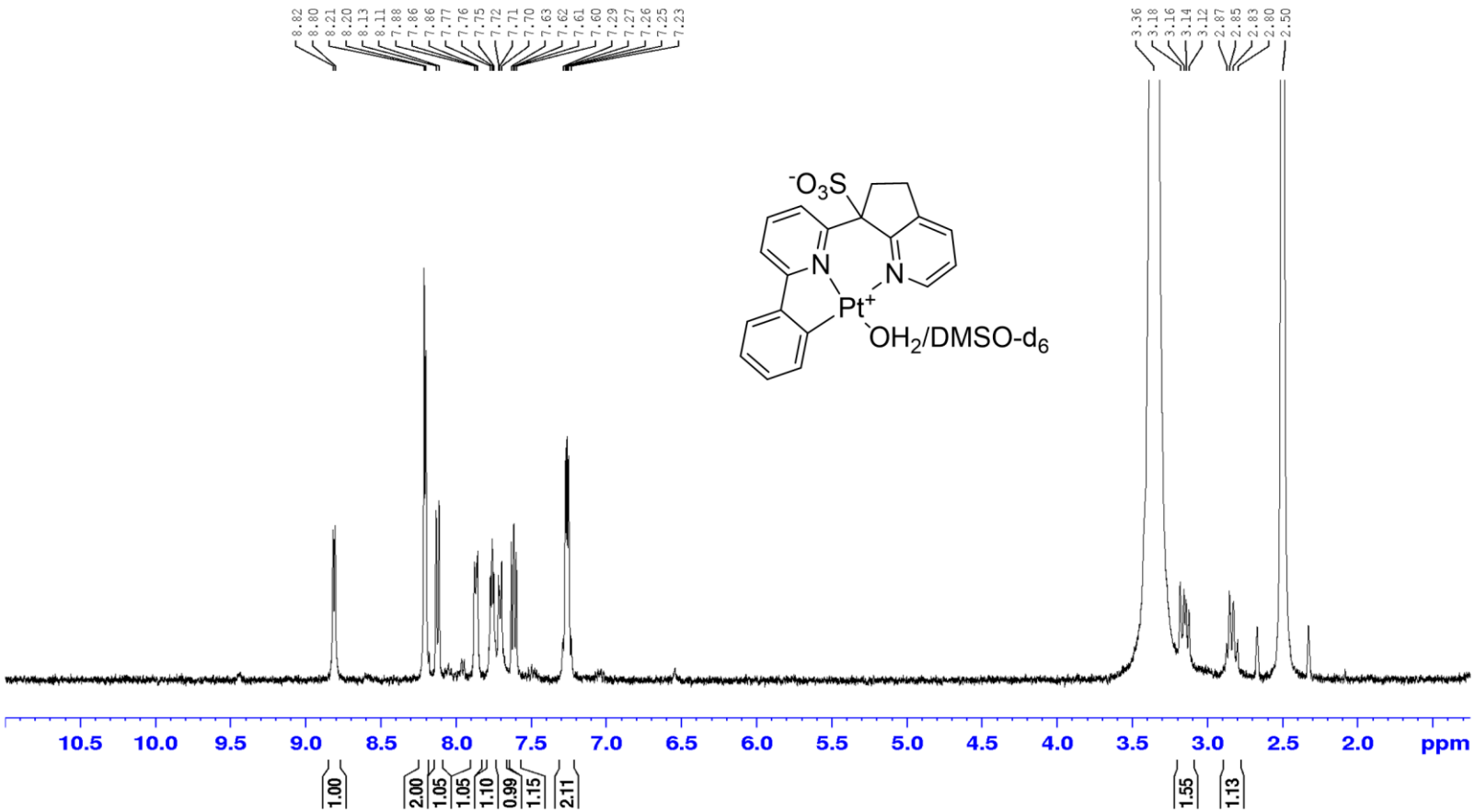

Figure S3.31. ^{1}H-NMR for 2-phenyl-6-(pyridin-2-ylmethyl) pyridine Pt-OH_2 Complex **3.5-FC** dissolved in DMSO-d_6.

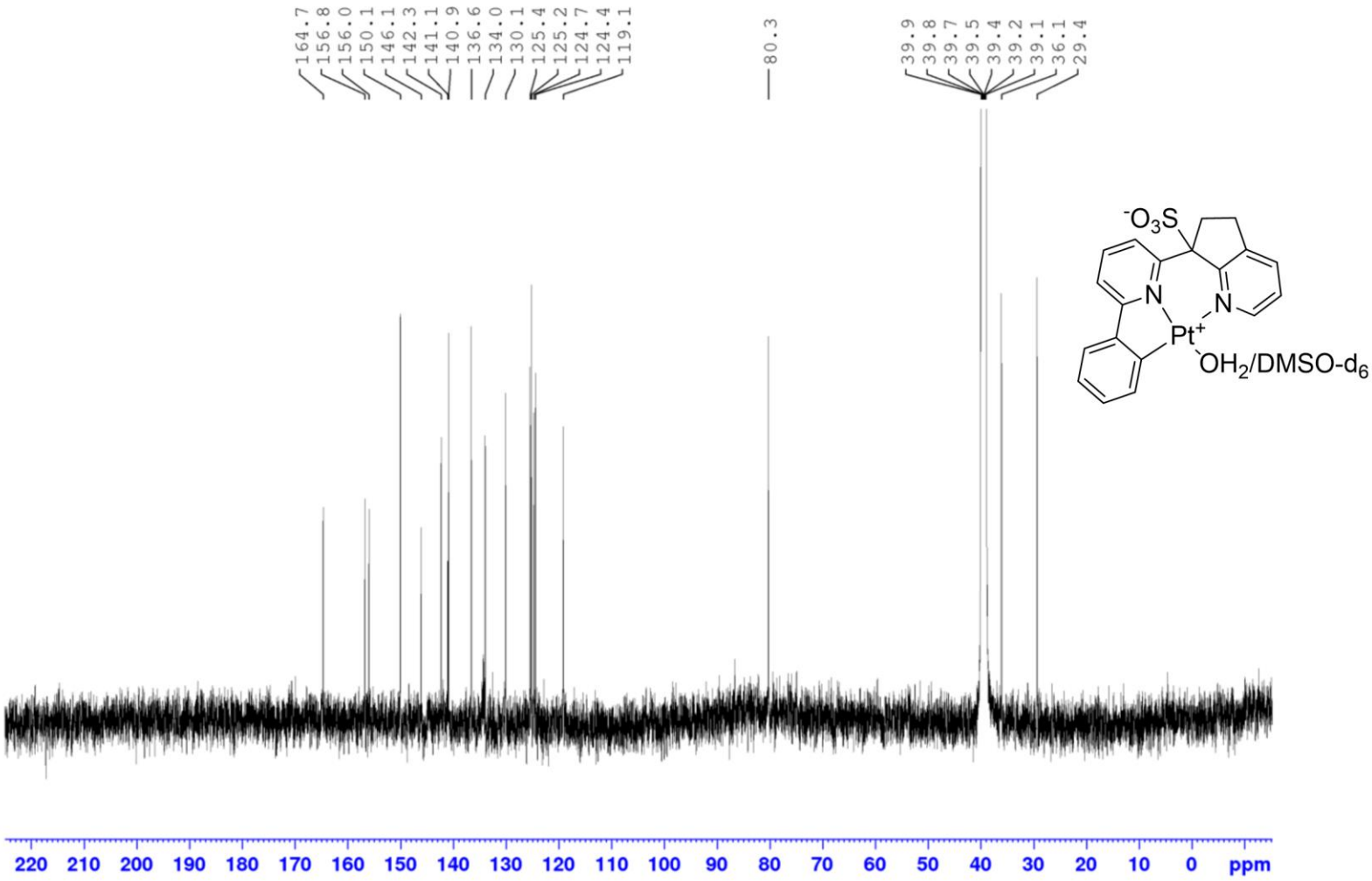

Figure S3.32. ^{13}C-NMR for 2-phenyl-6-(pyridin-2-ylmethyl) pyridine Pt-OH_2 Complex **3.5-FC** dissolved in

Chapter 4: Ligand Structural Effects on H/D Exchange Catalysis: A Thermal and Photochemical Approach

All original synthetic development and experimental work conducted herein was performed by Morgan Kramer; DFT and computational support was performed by Prof. Andrei Vedernikov. Synthesis and Spectroscopic characterization was supported by undergraduate students Derek E. Lai and Andrew B. Norris

4.1. Introduction

Homogenous Pt complexes have long showed promise for practical use in direct C-H functionalization catalysis beginning from the seminal works in the field conducted by Garnett and Hodges in 1967.[10] However, since this discovery, homogenous Pt based catalysts for C-H functionalization,[15,16,] and, more specifically, H/D exchange have remained underdeveloped.[54-56] This is due to many of these systems utilize a cationic Pt^{II} center, and often suffer from slow reaction rates and the related need to use high, 150 – 180 ^{o}C, temperatures, and poor catalytic turnovers.[15, 21, 54-56]

Recently, there has been an increased emphasis on the development of catalytic H/D and H/T exchange reactions involving complex organic substrates that can furnish the respective value added isotopically labeled compounds.[1] Presently, there are over 20 new deuterated pharmaceutical compounds in clinical testing and one drug, deutetrabenzine, that has been approved for patient use. This recent emphasis towards the production of deuterated drugs stems from a natural phenomenon known as the kinetic isotope effect (KIE), where the zero-point energy of a given bond is inversely proportional to the square root of its reduced mass.[1-5] For chemical processes involving the cleavage of a C-H or C-D bond in the rate determining step, this lower ZPE for a C-D bond results in a larger transition state barrier, and consequently a slower rate of reaction. This fact is of practical importance to pharmaceuticals, where deuterium atoms can be strategically placed in order to inhibit the rates of drug metabolism, which could result in longer times between dosing for the patients.[1, 79, 99]

In recent years there have been numerous reports of homogenous transition metal catalyzed H/D exchange of pharmaceutical molecules. A quick overview of some

sufficiently active but arbitrarily chosen homogeneous transition metal-based system used for aromatic H/D exchange catalysis is presented in Fig. 4.1.

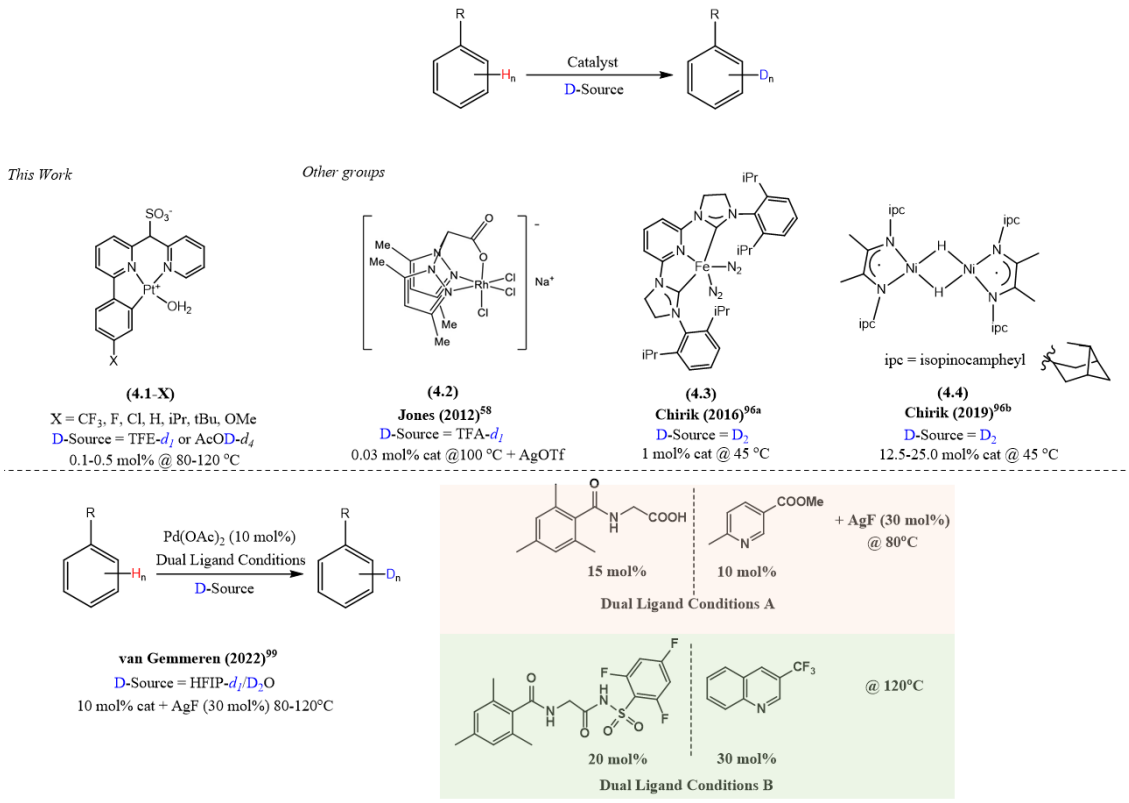

Figure 4.1. Some catalytic systems for aromatic H/D exchange as described in the literature.

Jones *et. al.* developed a Rh^{III} bispyrazolyl complex **4.2** for the H/D exchange of arenes in TFA-d_1 solutions (Figure 4.1). This system was expected to operate a concerted metallation/deprotonation type mechanism and was able to achieve TON up to 120 with relatively low 4 mol % catalyst loading with a AgOTf additive at 100 °C.[58] In a report by MacMillian *et al.* a Rh^{I} /Co^{I} dual metal photocatalytic systems was shown to allow for the use gaseous D_2 for the α-C-H bond-selective labeling of organic amines.[98] Chirik *et al*

presented an Fe-based and a dimeric Ni catalyst for facile deuteration of complex organic substrates.[96] While each of these systems presented a remarkable advancement in the field, the Fe-based system **4.3** shown in Figure 4.1 allowed for a regioselective deuteration exclusively on sterically unencumbered positions, and its deuterium source is limited to D_2 gas. The Ni-based system **4.4** has shown a significant activity for both the tritiation and deuteration of pharmaceutical compounds, but it requires high catalyst loading (12.5-25 mol%) and is restricted to D_2 or T_2 as isotope sources.

These recently reported most prominent homogeneous catalytic systems employing liquid sources of exchangeable deuterium utilized Pt^{II},[33,49] Pd^{II},[99, 100] Rh^{III},[58, 59] among others.[1] A remarkable progress was achieved using D_2O/HFIP-d_1 as a source of deuterium with homogeneous state-of-the-art Pd complexes as catalysts (Fig. 4.1, bottom). At the same time, no similarly active Pt^{II} complexes were reported that would allow for equally efficient deuteration of complex organic substrates, including pharmaceuticals. In this regard, we hypothesized that our own recent work[49] may pave the way to the development of such competitive or even more active and efficient homogeneous Pt^{II}-based catalysts.

Previously we introduced a Pt^{II} aqua complex **1.5** as an active catalyst for H/D exchange between aromatic substrates and aqueous 2,2,2-trifluoroethanol-d_1 (TFE-d_1).[49] This system demonstrated good functional group tolerance. An extensive study of the kinetics and the regioselectivity of this system was conducted (see Chapter 2). The catalytic system allowed to achieve some modest to good extent of deuteration (30 – 70%) of various (hetero)aromatic substrates after 24h reaction at 80 ^{o}C under argon atmosphere with 0.1-0.5 mol % catalysts loading (Figure. 4.2, a). The development of more reactive catalysts was also attempted in our group (Figure. 4.2, b). The reactivity of complexes **1.6** and **1.7**

in C-H activation of arenes was predicted computationally (DFT) to increase in the series **1.7** > **1.6** > **1.5**.[51] The addition of the fused benzene **(1.6)** and fused cyclopentene **(1.7)** fragments onto these ligand scaffolds was expected to lead to a progressive destabilization of the Pt^{II}-OH_2 bond, thereby reducing the relative height of the barrier for C-H activation.

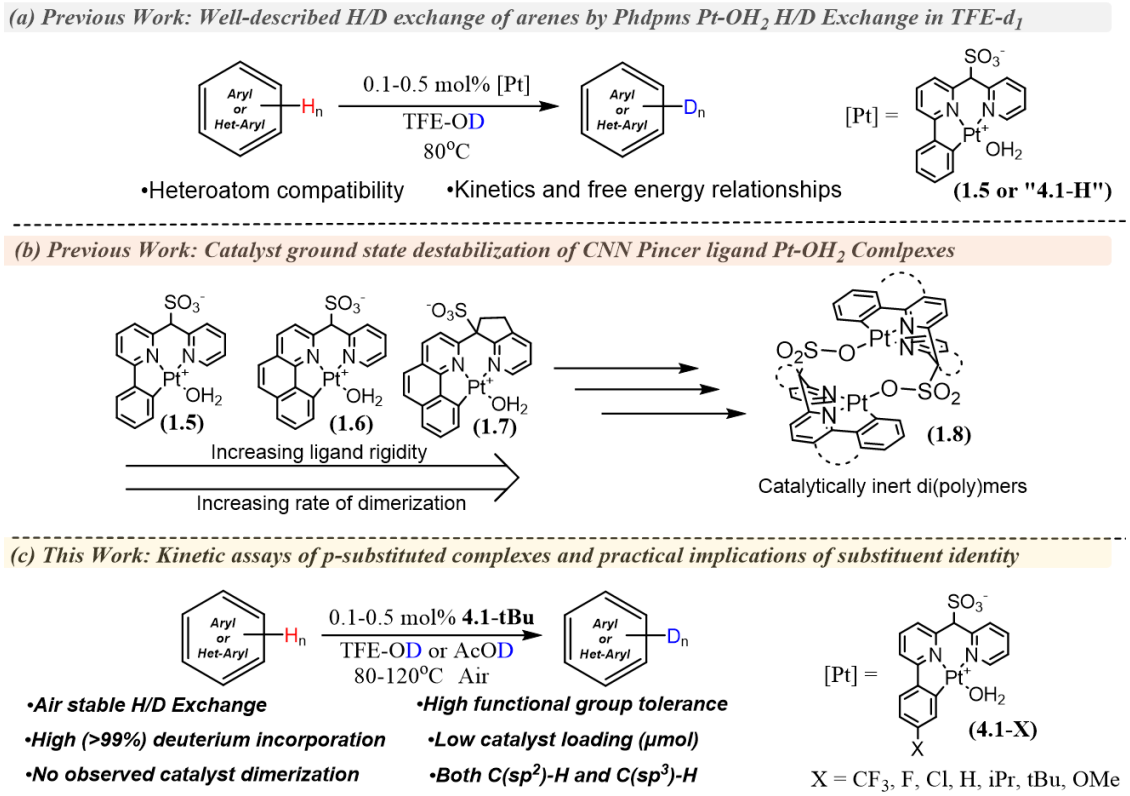

Figure 4.2. Comparison of CNN-Pincer ligand Pt-OH_2 Complexes and the past work motivations for this study.

While the expected reactivity trend was experimentally confirmed in H/D exchange reactions in dilute TFE-d_1 solutions with **1.5 – 1.7** as catalysts, the rate of a competitive catalyst deactivation to form di(poly)mers (**1.8**) also increased in the same sequence. As a result, a low steady state concentrations of **1.6** and **1.7** in reaction mixtures could only be used, so making the application of **1.6** and **1.7** in H/D exchange catalysis even less practical than the use of the parent complex **1.5**. While pursuing the same goal of enhancing catalytic

activity of **1.5**, in this work we decided to retain its pincer ligand core but to explore the structure-reactivity relationship while introducing various substituents in the 4th position of the phenyl fragment of **1.5** (Figure. 4.2, c). Such structure – reactivity relationship is currently unique when it comes to the reactivity study of Pt^{II}-based systems in C-H activation. As a result of our work described below, we discovered new H/D exchange catalysts of superior activity than **1.5** itself. The new catalysts allowed to achieve close to 100% extent of deuteration of a series of substrates in Schemes 4.1 and 4.2 while using cheaper than TFE-d_1 sources of exchangeable deuterium such as CD_3CO_2D and D_2O. Even more, the new catalysts allowed us to carry out efficient H/D exchange reactions under air, which constitutes a significant practical improvement over the previous reaction protocol.[49]

4.2. Results and Discussion

4.2.1 Preparation of Ligands 4.7-X

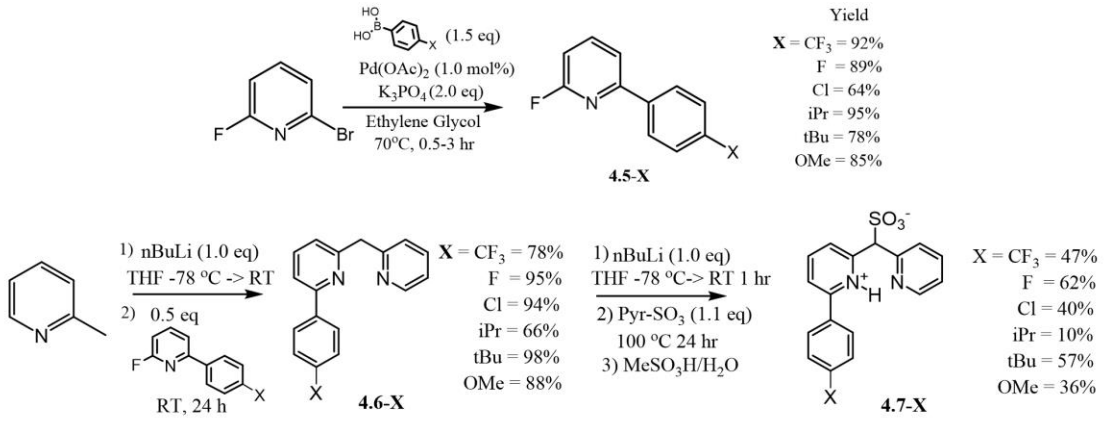

Scheme 4.1. Synthetic scheme to produce the series of ligands **4.7-X**. All reported yields are determined after isolation.

4.2.1.1 Preparation of Pre-Ligand 4.5-X (Suzuki coupling)

The preparation of the **4.1-X** series of catalysts was performed starting from a Suzuki coupling of 2-bromo-6-fluoropyridine to produce 2-fluoro-6-aryl pyridines **4.5-X** which was modified from a literature procedure.[108] 120-240 mL of ethylene glycol was added dry round bottom flask and was heated to 70 ^{o}C. After the solvent reached temperature, 10- 40g of K_3PO_4 (mono, tri or heptahydrate) (29-120 mmol 2.0 eq), 3.0-12.0 g of arylboronic acid (20-80 mmol 2.0 eq), and 2.5-10.0 g of 2,6 bromofluoropyridine (15-60 mmol 1.0 eq) were added sequentially to the flask and allowed to fully dissolve. Then 40-100 mg of $Pd(OAc)_2$ (0.15-0.4 mmol ~1.2 mol%) was added and the solution turned a transparent yellow color and the reaction was allowed to proceed for 2-3 hrs before quenching with a concentrated brine solution. The progress of the reaction was monitored via TLC using 90:10:0.1 (Hex:EtOAc:TEA) as a mobile phase. When the reaction was complete the solution was extracted with 3x30 mL Et_2O and dried with $MgSO_4$ before removing solvent under vacuum to yield the product, which depending on the substituent ranges from a colorless oil (**4.5-iPr** or **4.5-H**), to a while crystalline solid (**4.5-tBu, 4.5-CF_3, 4.5-F, 4.5-Cl, 4.5-OMe**). The product was monitored via TLC and was purified via column chromatography using 90:10:0.1 (Hex:EtOAc:TEA). Typical product R_f range 0.4-0.6. All yields are reported after the column chromatography purification step, and typically, we were able to recover 60-95% of the product. The identity and purity of the **4.5-X** materials were determined via ^{1}H-NMR, ^{19}F-NMR and ^{13}C-NMR spectroscopy. Occasionally, for the synthesis of **4.5-Cl**, the presence of overreacted species were observed, where an additional phenylene fragment could be introduced at the 4-position. The yields for this reaction were generally quite good, with the series **4.5-CF_3, 4.5-F, 4.5-**

Cl, 4.5-iPr, 4.5-tBu, and **4.5-OMe**, giving isolated yields of 92%, 89%, 64%, 95%, 78%, and 85% respectively. The appearance of the purified products varied as a function of the 4-substitent. For **4.5-CF_3, 4.5-F, 4.5-Cl,** and **4.5-OMe** the purified compounds are white crystalline powders. **4.5-tBu** is a white waxy solid, and **4.5-iPr** is a colorless oil. For specific reaction conditions and scale, see the supporting the supporting information.

A version of these reaction conditions was previously developed by Liu *et. al.* for the direct Suzuki coupling of pyridyl halides and heteroaryl halides to aryl boronic acids. This procedure diverges only slightly from our previous Suzuki coupling methodology for the synthesis of **1.5**[33] where we start from 2-bromo-6-fluoropyridine instead of the 6-bromo-2-picoline analogous procedure. This was done strategically, so in the next step, the formation of a carbon nucleophile (Figure 4.1), the 4-substituent on the phenyl ring has minimized contact time with the nBuLi solution. Thereby enhancing the heteroatom compatibility and reducing the possibility of undesirable side reactions in this procedure.

4.2.1.2 Preparation of 4.6-X (S_NAr)

This step of the reaction procedure to yield 2-(4-X-phenyl)-6-(pyridin-2-ylmethyl) pyridines **4.6-X** is expected to proceed through a typical nucleophilic aromatic substitution mechanism (S_NAr) where a benzylic carbanion generated by mixing 2-picoline with nBuLi can act as a nucleophile towards the 2-fluoropyridine derivative **4.5-X.** Upon work-up, a new C-C bond is formed through a methylene bridge between the two aromatic cores. This strategy has been previously utilized in Chapter 3 and also in our published works with a procedure utilizing 2-methyl-6-phenyl pyridine and 2-fluoropyridine.[33,49,51]

A dry 50 mL Schlenk tube was transferred into an argon filled glove box and was charged with 1-5 g of 2-methylpyridine (10-50 mmol, 2.0 eq) and was subsequentially

dissolved into 5-25 mL dry THF and the tube was sealed with a Teflon cap. The solution was then transferred onto a Schlenk line and cooled to -78 ^{o}C for 30 minutes under rapid stirring. Then, 11M nBuLi in hexanes (10-50 mmol, 2.0 eq) was added dropwise over 10 minutes under an argon atmosphere. The resulting dark red solution was then stirred at -78 ^{o}C until homogenous then was warmed to room temperature for 1 hour to allow for complete formation of the carbanion. Next, the solution was cooled back to -78 ^{o}C and 5-10 mL of a THF solution containing 1-5 g **4.5-X** (5-25 mmol, 1.0 eq) was added dropwise over 1 minute. The solution maintained a dark red coloration and was allowed to warm back to room temperature and allowed to react over 18-24 hr. The next day, the solution was quenched with 20 mL DI H_2O. The resulting mixture was then extracted with 3x30 mL of Et_2O and the solvent was removed via reduced pressure to yield viscous red/orange oil. The compounds were further purified via column chromatography with a 60:40:0.01 (Hex:EtOAc:TEA) mobile phase to yield a viscous orange oil. Rf values for these compounds range from 0.2-0.4. The identity and purity of the **4.6-X** materials were determined via ^{1}H-NMR, ^{19}F-NMR (when valid) and ^{13}C-NMR spectroscopy. The yields for this reaction were generally quite good, with the series **4.6-CF$_3$, 4.6-F, 4.6-Cl, 4.6-iPr, 4.6-tBu,** and **4.6-OMe**, giving isolated yields of 78%, 95%, 94%, 66%, 98%, and 88%, respectively. The appearance of the purified products varied only slightly across this series where all purified **4.6-X** derivatives presented as an orange oil, except **4.6-tBu** which was a waxy orange solid. For specific reaction conditions and spectral information see the supporting the supporting information.

4.2.1.3 Preparation of Pre-Ligands 2-(4-X-phenyl)-6-(pyridin-2-ylmethyl) pyridine sulfonates 4.7-X (Sulfonation)

Sulfonation of **4.6-X** derivatives was performed under a modified version of the sulfonation conditions described in Chapter 2 and in our published work.[33, 49, 64] The dibenzyllic methylene bridgehead carbon on compound **4.6-X** is deprotonated by nBuLi to yield another carbanion nucleophile. After formation, a pyridine-sulfur trioxide complex is utilized as a soluble source of SO_3. The carbanion is responsible for a nucleophilic attack at S to form a new C-S bond after heating for a dew hours. Upon acid work-up, the zwitterionic **4.7-X** can be isolated via precipitation from aqueous media. The complete procedure for the synthesis of **4.7-X** is shown below.

A dry 50-100 mL Schlenk tube was transferred into an argon filled glove box and was charged with 30 mL of a dry THF solution containing 1-5 g of **4.6-X** (1-10 mmol, 1.0 eq) and a stir bar the tube was sealed with a Teflon cap. The solution was then transferred onto a Schlenk line and cooled to -78 ^{o}C. Then, 11M nBuLi in hexanes (1-10 mmol, 1.0 eq) was added dropwise over 10 minutes under rapid stirring. The resulting dark red solution was then stirred at -78 ^{o}C until homogenous then was warmed to room temperature for 1 hour to allow for complete formation of the carbanion. After the anion formation was complete (indicated by a deep red coloration) the tube was then transferred back into an argon-filled glove box and 0.5-3 g pyridine-sulfur trioxide complex (1.1-11 mmol 1.1 eq) was added to the tube. The tube was again sealed with a Teflon cap, removed from the glove box, and then heated in a hot oil bath to 100 ^{o}C for 24 hours. The coloration of the solution should slowly change from a deep red to a light transparent red color alongside the formation of a large amount of white or off-white precipitate. After 24 hours, the

reaction was quenched with 30 mL DI H2O and the aqueous phase was washed with an additional 3x15 mL Et_2O. The organic phase often contained up to 50% unreacted starting material that was able to be reused for the sulfonation reaction.

The aqueous phase was then acidified using a 50% $MeSO_3H/H_2O$ ($MeSO_3H$ was used for an NMR handle, H_2SO_4 has also been used successfully) solution to a pH ~1-2. A large amount of white/off-white precipitate formed, and the solution was placed in the refrigerator to allow precipitation to occur over night. The following morning, the solution was filtered and rinsed with copious amounts of cold DI H_2O. The powder was then removed from the filter paper and dried in a desiccator oven at 80 ^oC overnight and yielded 1-5 g of a light brown/off white powder. The yields for this reaction were generally from moderately to good, with the series **4.7-CF3, 4.7-F, 4.7-Cl, 4.7-iPr, 4.7-tBu,** and **4.7-OMe**, giving isolated yields of 47%, 62%, 40%, 10%, 57%, and 36%, respectively. The identity and purity of the **4.7-X** materials were determined via ^{1}H-NMR, ^{19}F-NMR (when valid) and ^{13}C-NMR spectroscopy and the anionic fragment was analyzed via ESI-MS (- mode) via injection via HPLC line.

4.2.2 Preparation of Pt^{II}-Cl Complexes 4.8-X and Pt^{II}-OH_2 Complexes 4.1-X

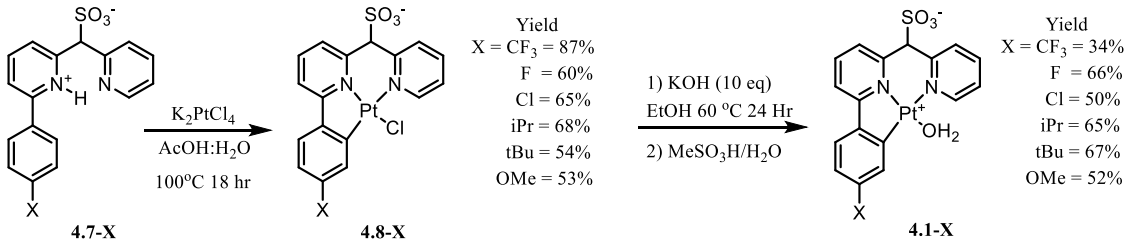

Scheme 4.2. Synthetic scheme for the synthesis of Pt complexes **4.8-X** and **4.1-X**

4.2.2.1 Preparation of Pt^{II}-Cl Complexes 4.8-X

Synthesis of **4.1-X** complexes proceeded first through the cyclometallation reaction of **4.7-X** using K_2PtCl_4 in aqueous acetic acid to yield the corresponding Pt^{II}-Cl complex in accordance with the described literature procedures.[33, 49, 51] Synthesis of complexes **4.8-X** were performed via the following procedure. A dry 50 mL Schlenk tube was charged with 300-750 mg (1-2 mmol 1.0 eq) zwitterionic preligand **4.7-X** (the salt form may also be used for this step) and 415-830 mg (1-2 mmol, 1.0 eq) K_2PtCl_4 and a stir bar. The tube was then rinsed with a 2:1 $AcOH/H_2O$ solution in order to dissolve any remaining solids on the walls of the tube. Then the tube was filled with 20 mL of the $AcOH/H_2O$ solution and sealed with a Teflon cap and placed into a hot oil bath set to 100 ^oC for 24 hours. After the reaction was complete, the solvent was removed, and the remaining crude solid was dissolved in hot methanol and filtered through a Celite plug to remove any remaining KCl. After removing solvent again, the **4.8-X** series of complexes were all isolated as fine yellow crystalline powders. The identity and purity of the **4.8-X** materials were determined via ^{1}H-NMR, ^{19}F-NMR (wh valid) and ^{13}C-NMR spectroscopy and the anionic fragment was analyzed via ESI-MS (- mode) via injection via HPLC line. For specific information about product characterization see the supporting information.

4.2.2.2 Preparation of Pt-OH_2 Complexes 4.1-X

Converting to Pt^{II}-Cl complexes to Pt^{II}-OH_2 derivatives was done by loading 500-1000 mg (1-2 mmol 1.0 eq) of a Pt^{II}-Cl **4.8-X** complex into a 100 mL round bottom flask containing a stir bar (crude **4.8-X** containing KCl may also be used for this step). The

complex was then dissolved into 50 mL EtOH and 0.6-1.2 g of KOH (10-20 mmol, 10 eq) was added to the solution. The flask was then lightly sealed with a rubber stopper and placed into an oil bath heated to 60 ^{o}C for 24 hours under heavy stirring. After the reaction was complete, the solvent was removed via vacuum and the deeply red colored intermediate, a Pt^{II}-OEt complex, was extracted with 30 mL of acetone. The solution was filtered through Celite, and the solvent was again removed via vacuum to yield a dark red crystalline solid. The solid was then redissolved into 30-50 mL H_2O and the pH of the solution was adjusted to ~1-2 using a 50% $MeSO_3H/H_2O$ solution. A large amount of tan/yellow precipitate formed upon acidification and the solution was placed in the refrigerator overnight to allow the complex to fully precipitate. The following morning, there was a large amount of precipitate present at the bottom of the beaker and the solution was only faintly yellow colored. The product was then isolated via vacuum filtration and washed with copious amounts of cold DI H_2O to remove any remaining acid. The isolated Pt^{II}-OH_2 complex was then dried at room temperature under vacuum for 24-48 hours (heating under vacuum must be avoided to prevent decomposition) to yield 100-600 mg of a tan/yellow powder. The identity and purity of the **4.1-X** materials were determined via ^{1}H-NMR, ^{19}F-NMR (when valid) and ^{13}C-NMR spectroscopy.

4.2.3 Kinetic Screening and Catalysis by 4.1-X

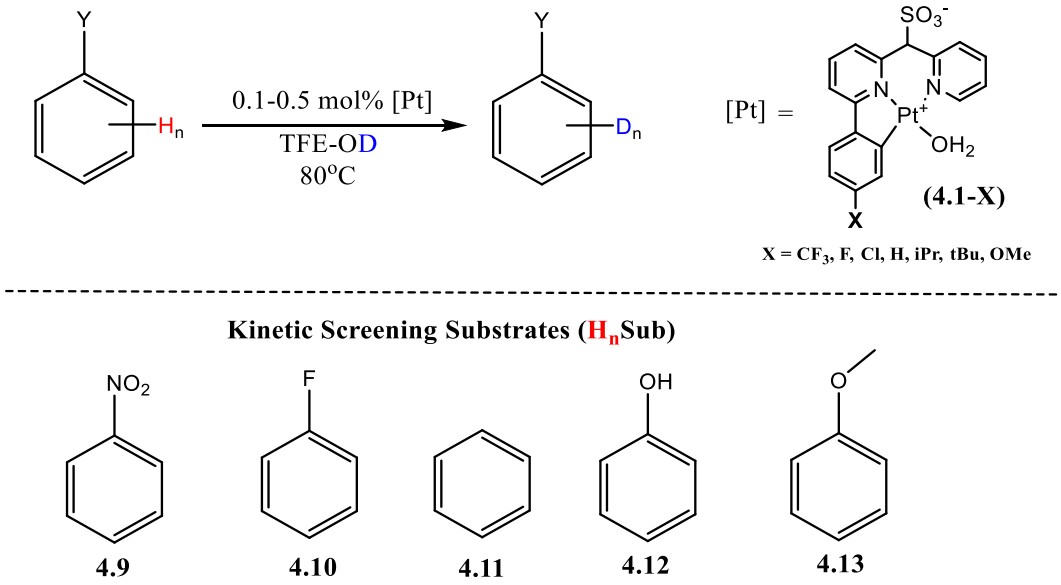

Figure 4.3. Kinetic screening assay for aromatic H/D exchange catalyzed by complexes **4.1-X.**

Our initial experiments on catalytic H/D exchange between aromatic substrates H_nSub and TFE-d_1 were carried out at 80 °C using 0.1–0.5 mol % (depending on catalyst solubility) of complexes **4.1-X**. Typical reaction conditions utilized 0.050 mL H_nSub (~0.5-1 mmol scale) dissolved into 0.45 mL TFE-d_1 containing 150 mM D_2O and 2-10 μmol of **4.1-X** (Figure 4.3). The addition of water has been previously noted to slow down the rate of catalyst deactivation through the formation of insoluble di(poly)mers. The initial reaction rates were measured using ^{1}H-NMR and ^{2}H-NMR spectroscopy using suitable internal standards as described earlier.[33, 49] To compare the catalytic activity of different substrates C_6H_5Y and catalysts **4.1-X** the observed reaction rate constants k_Y were calculated using the experimentally measured initial reaction rates d[C-D]/dt (eq. 4.1), where $[C\text{-}H]_0$ is the initial concentration of aromatic C-H bonds observed in a reaction and $[\mathbf{4.1\text{-}X}]_0$ is the catalyst concentration.

$$k_Y = \frac{d[C-D]}{dt}\frac{1}{[C-H]_0}\frac{1}{[\mathbf{4.1}-\boldsymbol{X}]_0} \qquad \text{(eq. 4.1)}$$

^{1}H NMR spectroscopy was also used to monitor for signs of a catalyst's deactivation during an initial reaction period. The results of our kinetics screening are summarized in Tables 4.1 and 4.2. All aromatic C-H bonds present in a substrate were used to calculate the total [C-H]$_0$ using eq (4.1) resulting in the average observed rate constant $k_{Y,all}$. Our calculations of k_Y values corresponding to specific types of C-H bond were only possible for *meta*-C-H bonds of substrates C_6H_5Y, **4.6 - 4.10**, whose signals are typically well-resolved in the ^{1}H NMR spectra of reaction mixtures (Table 4.2). Considering past observations with catalyst dimerization[33,49,51] all measurements were taken during the reaction window in which no visible precipitation occurred. The reaction period in which no dimerization was observed varies for the **4.1-X** derivatives**. 4.1-CF$_3$** deactivated the fastest, with precipitate becoming visible after only 30 minutes in TFE at 80^{o}C. Uinder the same conditions, **4.1-F** and **4.1-Cl** also rapidly formed precipitates after ~1.5 hours, and **4.1-iPr** and **4.1-OMe** showed visible precipitates after 3 hours of reaction time. **4.1-tBu** was unique in that no visible precipitation of inert dimers was observed under any of our H/D exchange reaction conditions. However, the potential for the formation of soluble, reversible dimers was not evaluated in this initial screening. That means the subsequent Hammett – type analysis of the observed rate constants should be interpreted with great caution.

There are two types of trends to analyze in these two-dimensional assays: i) the effect of the catalyst **4.1-X** identity (the effect of a substituent X in the catalyst) on the relative rates of H/D exchange for each given substrate C_6H_5Y and ii) the sensitivity of k_Y

to the electronic effects of a substituent present in a substrate C_6H_5Y for each complex **4.1-X** (substrate or regioselectivity).

Considering the effect of the catalyst identity, overall, there was no dramatic difference in the average C-H bond values $k_{Y,all}$ of **4.1-X** with respect to benzene as a reference substrate. Still, the electron-poor catalyst **4.1-CF$_3$** (entry 1, Table 4.1) was the most active among all **4.1-X**. It was also least discriminating / least selective with respect to any given **4.9 – 4.13** with $k_{Y,all}$ increasing from electron-poorer **4.9** to electron-richer **4.12** only about 9-fold.

In turn, the halogenated complexes, **4.1-F** and **4.1-Cl** (entries 2 and 3, Table 4.1) were universally less reactive than the parent complex **1.5** despite also being electron-poor (compare to **4.1-CF$_3$**). Complexes **4.1-iPr** and **4.1-OMe** (entries 5, 7, Table 4.1) both also showed an overall slightly lower catalytic activity than the parent **1.5** with the reaction rate constants for benzene of 2.1 and 3.3 $M^{-1}Hr^{-1}$, respectively.

Notably, **4.1-tBu** was the only catalyst to not show any visible formation of insoluble di(poly)mers **1.8** throughout the 24 hour reaction period. In addition, **4.1-tBu** (entry 6, Table 4.1) was almost as reactive as the parent catalyst **1.5** for the H/D exchange reaction on nitrobenzene, fluorobenzene, and benzene in TFE-d_1 at 80 ^oC.

Table 4.1. Substrates C_6H_5Y, **4.9** – **4.13**, C(sp^2)-H bond-averaged values $k_{Y,all}$ resulting from kinetics screening of catalysts **4.1-X** in TFE-d_1 at 80 °C.

		Total Aromatic C-H ($k_{Y,all}$) R-Ph Sub ($M^{-1}Hr^{-1}$)				
Entry	**4.1-X**	**NO_2 4.9**	**F 4.10**	**H 4.11**	**OH 4.12**	**OMe 4.13**
1	**CF_3**	**1.0 ± 0.4**	**4.5 ± 0.8**	**8.1 ± 0.4**	**9 ± 4**	**8 ± 2**
2	**F**	**0.0 ± N.D.**	**0.24 ± 0.01**	**5.8 ± 1.0**	**2.8 ± 0.2**	**4.0 ± 0.1**
3	**Cl**	**0.0 ± N.D.**	**0.50 ± N.D.**	**2.8 ± 0.1**	**3.1 ± N.D.**	**1.9 ± 0.1**
4	**H**	**0.3 ± 0.04**	**1.1 ± 0.3**	**6.8 ± 0.4**	**5.9± 0.6**	**6.5± 0.3**
5	**iPr**	**0.1 ± N.D.**	**0.2 ± N.D.**	**2.1 ± 0.5**	**1.2 ± 0.5**	**1.5 ± 0.2**
6	**tBu**	**0.5 ± 0.1**	**1.1 ± 0.1**	**6.8 ± 0.8**	**13 ± 2**	**10. ± 1**
7	**OMe**	**0.03 ± N.D.**	**0.08 ± 0.01**	**3.3 ± 0.3**	**4.8 ± 0.3**	**5 ± 1**

N.D. = Not Determined

Table 4.2. Substrates C_6H_5Y, **4.9** – **4.13**, *meta*-C(sp^2)-H bond values $k_{Y,meta}$ resulting from kinetics screening of catalysts **4.1-X** in TFE-d_1 at 80 °C.

		Meta C-H ($k_{Y,meta}$) R-Ph Sub (M^{-1} Hr^{-1})				
Entry	**4.1-X**	**NO_2 4.9**	**F 4.10**	**H 4.11**	**OH 4.12**	**OMe 4.13**
1	**CF_3**	**1.8 ± 0.5**	**4 ± 1**	**8.1 ± 0.4**	**10 ± 3**	**6 ± 1**
2	**F**	**0.0 ± N.D.**	**0.5 ± 0.1**	**6 ± 1**	**3.0 ± 0.2**	**4.9 ± 0.1**
3	**Cl**	**0.0 ± N.D.**	**0.6 ± N.D.**	**2.8 ± 0.1**	**2.6 ± N.D.**	**2.3 ± 0.5**
4	**H**	**0.4 ± 0.1**	**1.4 ± 0.1**	**6.8 ± 0.4**	**7.3 ± 0.4**	**8.6 ± 0.5**
5	**iPr**	**0.2 ± N.D.**	**0.2 ± N.D.**	**2.1 ± 0.5**	**1.1 ± 0.6**	**1.3 ± 0.5**
6	**tBu**	**0.8 ± 0.1**	**1.2 ± 0.1**	**6.8 ± 0.8**	**8 ± 1**	**13 ± 2**
7	**OMe**	**0.02 ± N.D.**	**0.08 ± 0.07**	**3.3 ± 0.3**	**5.0 ± 0.3**	**5 ± 1**

N.D. = Not Determined

Based on the first observation, we presume that the catalyst's 4-tBu group, the bulkiest of all groups X in complexes **4.1-X** studied, efficiently interferes with the bimolecular catalyst deactivation. If so, catalysts longevity may be improved via steric protection of their Pt^{II} center from coordination of another catalyst sulfonate group leading to the formation of catalytically less active polynuclear species.

Notably, **4.1-tBu** showed larger $k_{Y,all}$ values for phenol and anisole, as compared to those of catalyst **1.5** (entry 4, Table 4.1). Phenol and anisole can, potentially, weakly coordinate to a Pt^{II} center in **1.5** and other complexes **4.1-X**, so decreasing the corresponding $k_{Y,all}$ values. But, once again, the 4-tBu group in **4.1-tBu** may interfere with such coordination of PhOH and PhOMe to its Pt^{II} center, so making it a bit more active than **1.5**.

Finally, **4.1-OMe** was the most substrate-discriminating with respect to any given benzene derivative **4.9 – 4.13** with $k_{Y,all}$ increasing from electron-poorer **4.9** to electron-richer **4.12** by about two orders of magnitude. Overall, because of some involvement of catalysts' bimolecular deactivation (see Section 4.2.4), the accuracy of determining $k_{Y,all}$ values for all catalysts **4.1-X** except, perhaps, **4.1-tBu**, may depend on the time period it took to measure the initial rate which was different for different substrates. As a result, a more in-depth analysis of data in Table 4.1 appears to be impossible at this time. The same consideration applies to the analysis of data in Table 4.2 given next.

The sensitivity of k_Y to the electronic effects of a substituent Y present in a substrate C_6H_5Y for each complex **4.1-X** (substrate or regioselectivity) was explored via the kinetic study of the sterically decongested *meta* C-H bonds (Table 4.2) of the screening substrates **4.9 – 4.13**. Their subsequent Hammett-type analysis was attempted to calculate the

parameter ρ for each complex **4.1-X**. To do so, we used our previously developed Hammett parameters, σ_Y^M, for metal-assisted C-H activation where the $-\log(k_{meta}(Y)/k(H)) = \sigma_Y^M$ for *meta* C-H bonds of Y-substituted benzenes C_6H_5Y in their H/D exchange reactions catalyzed by **1.5**.[49] This metric serves as a useful tool for assessing the sensitivity of catalysts **4.1-X** towards the electronic effects of substituents Y in substrates C_6H_5Y in comparison to the benchmark catalyst **1.5**. We generated a Hammett-type plot of $\log(k_{meta})$ vs σ_Y^M meta (Figure 4.4) for each of the **4.1-X** in order to work out the overall catalyst sensitivity to substrate electronic effects. If we assume that the rate of catalyst deactivation for a specific **4.1-X** complex is negligible during the reactions initial periods, then we can consider extract the sensitivity parameter (ρ) from the slope of the Hammett plot.

As it follows from analysis of Fig. 4.4 and Table 4.3, in general, there was no clear trend in the electronic effects of catalysts' **4.1-X** substituents X on the parameter ρ. The ρ values fall into the range -0.8 … -1.0 (the value for **4.1-F** has a large error) and are statistically indistinguishable for all **4.1-X** except **4.1-OMe**. The latter, the most electron-rich complex, demonstrated a statistically significant greater kinetic preference for electron-rich substrates (ρ = -1.8), as compared to the rest of catalysts **4.1-X**. Some possible mechanistic implications of these findings will be explored further in Section **4.4,** where we perform some mechanistic tests for H/D exchange reactions.

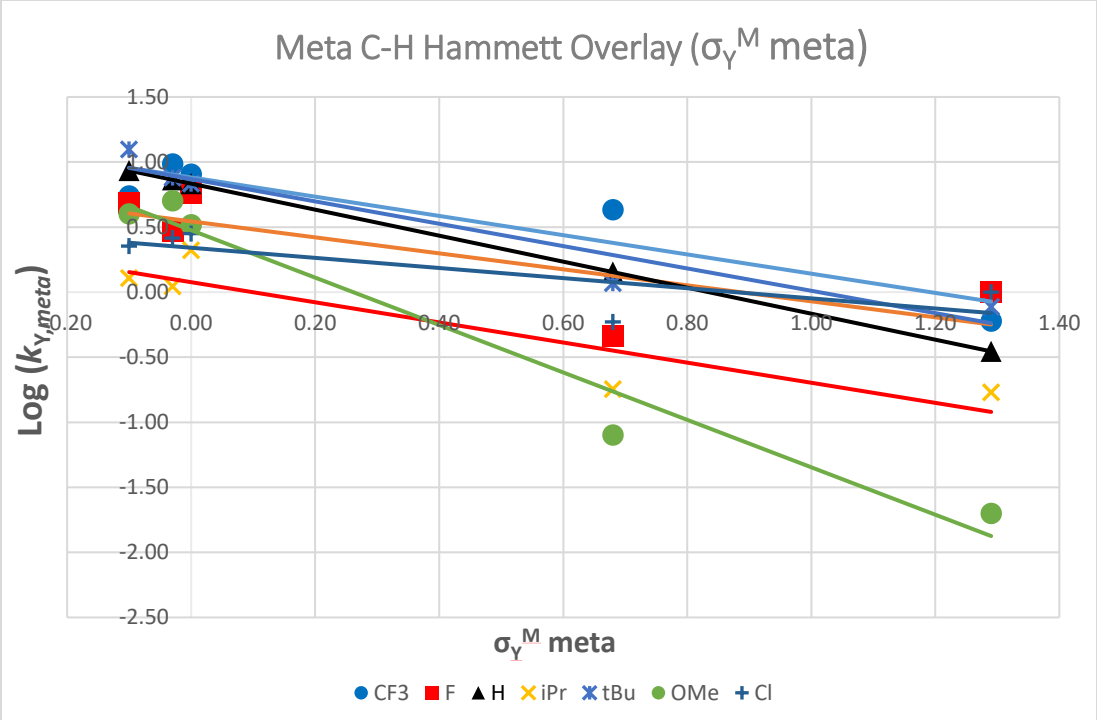

Figure 4.4. Hammett Plot of Log (k_{meta}) vs σ_Y^M meta, C_6H_5Y substituent Y effects on rate for catalysts **4.1-X**. See the slope errors in Table 4.3.

Table 4.3. Hammett Plot slopes (ρ) of the *meta* C-H positions for catalysts **4.1-X** in TFE-d_1 at 80°C

Meta C-H Hammett Plot Slopes	
4.1-X	**Slope (ρ)**
CF_3	**-0.74 ± 0.18**
F	**-1.3 ± 0.3**
Cl	**-0.85 ± 0.15**
H	**-1.0 ± 0.1**
iPr	**-0.77 ± 0.20**
tBu	**-0.86 ± 0.14**
OMe	**-1.8 ± 0.2**

Values are reported with standard errors as ± additions to the slope (ρ). The ρ value for **4.1-H (1.5)** is -1.0±0.1 which serves as a reference for catalysts comparison.

4.2.4 Comparison of the Performance of Catalysts 1.5 and 4.1-X with various sources of exchangeable deuterium

To demonstrate the catalysts **4.1-X** viability for practical applications in the generation of deuterium-labeled aromatic substrates we assessed their TON in deuteration of the parent substrate, benzene, and calculated the average number of deuterium atoms *n* incorporated in one benzene molecule after a 24-hour reaction. These experiments were performed under conditions summarized in Table 4.3 (See supporting information for more details). Expected statistical deuterium incorporations were typically 70-95% and vary from system to system. To get a metric characterizing an H/D reaction completeness under a given reaction conditions, in subsequent discussion we will be reporting observed vs expected statistical deuterium incorporation ratios (OSDR's). A substrate's OSDR represents the observed deuterium incorporation of the substrate divided by the substrate's expected statistical deuterium incorporation, in the percent scale.

Table 4.4. A summary of catalysts **4.1-X** performance, k_X (M^{-1} h^{-1}), using benzene as a substrate (1.12 M), catalysts loading 0.05-0.2 mol%, and various deuterium sources at 80 °C or 120 °C.

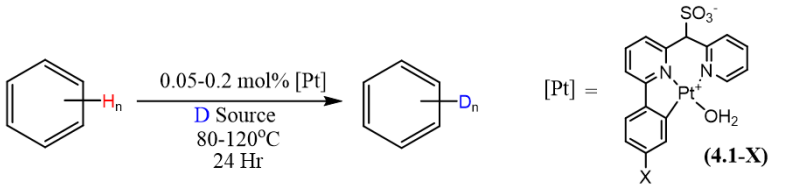

Entry	4.1-X	TON 24hr	OSDR(%)	D-Source	Temp. (°C)	Avg. Rate Constant ($k_{Y,\,All}$)
1	CF_3	28	9	TFE-d_1	80	8.1 ± 0.4
2	F	301	64	TFE-d_1	80	5.8 ± 1.0
3	Cl	188	26	TFE-d_1	80	2.8 ± 0.1
4	H	144	40	TFE-d_1	80	6.8 ± 0.4
5	iPr	240	89	TFE-d_1	80	2.1 ± 0.5
6	tBu	392	91	TFE-d_1	80	6.8 ± 0.8
7	OMe	285	99	TFE-d_1	80	3.3 ± 0.3
8	tBu	31	6	MeOD-d_4	80	0.2 ± 0.06
9	tBu	163	40	MeOD-d_4	120	1.8± 0.3
10	tBu	124	42	TFA-d_1	80	3.2 ± 0.3
11	tBu	301	99	TFA-d_1	120	5.1± 0.1
12	tBu	49	8	AcOD-d_4	80	0.3 ± 0.01
13	tBu	468	>99	AcOD-d_4	120	3.5 ± 0.1
14*	tBu*	491	>99	AcOD-d_4	120	5.1 ± 0.4

Typical catalyst loading of **4.1-X** was 4.0-10.0 mg (0.05-0.2 mol%) depending on complex solubility. Observed vs expected statistical deuterium incorporation ratios (OSDRs) are reported as the ratio of the observed deuterated extent versus the expected equilibrium statistical value. Expected statistical deuterium incorporations were typically 70-95%.* The reaction was run under air.

First, we will consider reactions in entries 1 - 7 where TFE-d_1 serves as a source of exchangeable deuterium. Based on an estimated rate constant value k_{CF3} for complex **4.1-CF3** 8.1 M^{-1} h^{-1} (entry 1) which is about 20% larger than k_H for the parent complex **1.5**, 6.8 M^{-1} h^{-1} (entry 4), we might have assumed that complex **4.1-CF3** is the most active H/D exchange catalyst. In fact, in spite of the fastest initial rate of H/D exchange observed over the period of time of about 20 min, **4.1-CF3** is the worst performing catalyst overall, allowing for only 28 catalyst turnovers (9% deuterium incorporation vs the statistical value), as compared to **1.5** that exhibited TON of 144 (entry 4). The reason behind this

poor performance of the catalyst **4.1-CF$_3$** over a 24h reaction period is its fast deactivation leading to the rapid formation of poorly soluble / catalytically low active di(poly)meric species. The formation of a dark red precipitate of this deactivation product was visually observed after only 30-45 minutes.

The rate constants k_X could not be estimated reliably for complexes **4.1-F** and **4.1-Cl** (entries 2 and 3) because of their visually detectable decomposition leading to di(poly)meric precipitates occurring with different rates over different reaction periods Accordingly, the practical efficiency and activity of complexes **1.5** and **4.1-X** will be analyzed using their TONs. Complexes **4.1-F** and **4.1-Cl** were more efficient than both **4.1-CF$_3$** (entry 1) and **2.1** (entry 4), in terms of their TONs, 301 (**4.1-F**) and 188 (**4.1-Cl**) vs. 144 (**2.1**) and 28 (**4.1-CF$_3$**), respectively. Taking into account the visible signs of decomposition of **4.1-F** and **4.1-Cl**, the formation of di(poly)meric precipitates, these observations suggest that di(poly)mer formation in solutions of **4.1-F** and **4.1-Cl** results in some sufficient steady-state concentrations of these highly catalytically active species. After some initial burst of H/D exchange, the activity of such solutions is expected to decrease due to catalyst deactivation but remain proportional to k_X[**4.1-X**]$_{steady}$. In turn, we assume that the initial burst of H/D exchange in the presence of **1.5** and the residual activity proportional to k_H[**1.5**]$_{steady}$ are lower for the parent catalyst **1.5.** In practical terms, complexes **4.1-F** and **4.1-Cl** are less soluble in TFE than **1.5** and, in spite of their higher activity than **1.5**, one might expect that the limited solubility would not allow for a better extent of deuteration of organic substrates when these catalysts are used. In fact, the low solubility is a real issue for **4.1-Cl** which allowed for only 26% deuterium incorporation into benzene with respect to the statistical value after 24h. By contrast, in spite of a

relatively low solubility of **4.1-F**, its higher reactivity allowed to achieve the 64% deuterium incorporation vs statistical.

Next in Table 4.4, **4.1-iPr** (entry 5), **4.1-tBu** (entry 6), and **4.1-OMe** (entry 7) turned out to be even more practically appealing in terms of their observed vs statistical percent deuterium incorporation, OSDR, which was > 89%, than either of the catalysts in entries 1 – 4. These electron-richer catalysts exhibited a relatively high TON of ≥240, with **4.1-tBu** being the absolute winner in terms of its activity among all catalysts, **2.1** and **4.1-X**, with TON of 392. Complexes **4.1-iPr** and **4.1-OMe** both formed poorly soluble di(poly)mers after ~2.5 and ~6 hours, respectively. However, **4.1-OMe** achieved a virtually statistical deuterium incorporation over the 24h reaction period despite visible catalyst deactivation, so suggesting that the corresponding k_X[**4.1-OMe**]$_{steady}$ value is the highest among all catalysts.

4.1-tBu (entry 6) is another very promising catalyst, with the highest overall TON of 392 over 24 hours. Although the estimated reaction initial rate constant k_{tBu} for the H/D exchange of benzene with TFE-d_1 at 80 ^{o}C by **4.1-tBu** was virtually identical to the catalyst **1.5** with a value of 6.8 $M^{-1}Hr^{-1}$, no catalyst deactivation was observed over the reaction period for **4.1-tBu**. Since catalysts **1.5** and **4.1-X** (except X = Cl, F) were used at same initial concentration, this observation distinguishes **4.1-tBu** among other catalysts. We speculate that the presence of the *tert*-butyl group serves as a steric shield that prevents the formation of stable enough poly/dinuclear species of the type of complex **4.4**. This deactivation pathway has historically been problematic for catalysts that utilize sulfonated dipyridinealkane ligand motif. Hence, the use of 4-*tert*-butyl or other bulky enough groups

appears to be a promising avenue for the future development of even more long living, and practical catalytic systems.

To explore the limits of catalytic activity of **4.1-tBu**, we attempted the use of other, cheaper sources of exchangeable deuterium, MeOD-d_4, TFA-d_1 and AcOD-d_4. We explored this avenue using benzene as a substrate and each of the deuterium sources at 80 ^{o}C and 120 ^{o}C (entry 8 – 14). The kinetic performance of this catalyst and the percent of deuterium incorporation were dramatically reduced at 80 ^{o}C with TON of 49 for the reaction with AcOD-d_4 (entry 12). A similarly poor performance was observed when utilizing MeOD-d_4 under the same conditions with TON of 31 (entry 8). The reaction utilizing TFA-d_1 at 80 ^{o}C (entry 10) showed some promise but the catalyst was still much less reactive than when utilizing TFE-d_1 at the same temperature (entry 6). When the temperature was elevated to 120 ^{o}C, there was a dramatic improvement in performance for all the solvents screened, however for the MeOD-d_4 and TFA-d_1 reactions the precipitation of Pt^0 was observed early on. AcOD-d_4 proved to be different in this regard. No catalyst decomposition leading to the formation of a free pre-ligand and Pt back were detected after 24 hours. This system allowed to achieve an OSDR >99% and 468 catalyst's turnovers (entry 9). Finally, we explored the necessity of an inert argon atmosphere and ran the same reaction under air (entry 14). Excitingly, the reaction parameters were virtually unchanged with the extent of deuterium incorporation virtually matching the statistical value. Hence, the **4.1-tBu** / AcOD-d_4 / 120 ^{o}C system proved to be the most promising and cost-effective alternative to other **1.5** or **4.1-X** TFE-d_1 / 80 ^{o}C systems.

4.2.5 Substrate Scope and Extent of Deuteration Experiments using 4.1-tBu as a Catalyst

With the past success of catalyst **1.5** for the H/D exchange of aromatic compounds with TFE-d_1 we were interested in elucidating the practical implications of our new longer lived, air-stable, and AcOD-d_4 - compatible catalyst, **4.1-tBu,** in the catalytic deuteration of arenes. In particular, we aimed to exploit this improved catalyst's lifetime and solvent compatibility to engage previously poorly reactive/unreactive aromatic substrates. These reactions were carried out utilizing ~0.5-2.0 mmol substrate dissolved into 0.50 mL AcOD-d_4 alongside 4-7 μmol **4.1-tBu** (0.05-2.0 mol %). Substrate loading sometimes varied depending on the solubility of the compounds but typically corresponded to ~1M which translates to a ~1-6M concentration of the arene C-H bonds (see Supporting Information for specific details). In general, the reactions were run under an argon or air atmosphere for up to 72 hours in order to allow for maximum deuterium incorporation. Under these reaction conditions, typical expected extent of deuteration ranged from 65-90%. In Scheme 4.3 and subsequent discussion we will be reporting observed vs expected statistical deuterium incorporation ratios (OSDR's). An OSDR can serve as an indication of the reaction completeness under a given reaction conditions. The percentages at each individual carbon atom will also be given, as they indicate the measured values of deuterium incorporation for the specific site and can be used to analyze reaction regioselectivity. Finally, D_{Total} is another practical parameter that shows the average number of deuterium atoms incorporated per molecule. This parameter may be a useful indicator for this systems' potential practical use for labeling applications.

4.2.5.1 Monosubstituted Benzene Derivatives (4.9 – 4.20)

For substrates **4.9** through **4.13** (Scheme 4.1), reactions were run side by side under argon and under an air atmosphere that led to virtually identical deuterium incorporation (for more details on the comparison of the performance of argon and air reactions see Section VI of Supporting information).

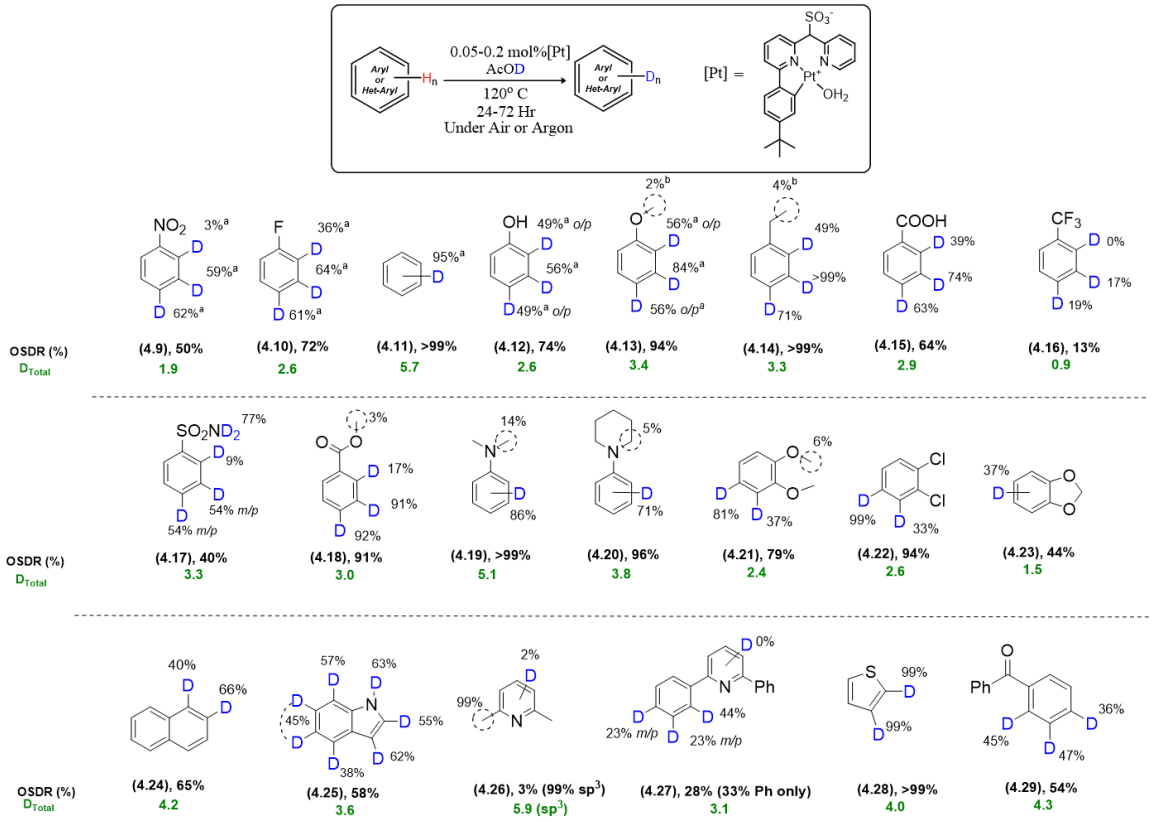

Scheme 4.3. Aromatic substrate scope for catalytic C(sp^2)-H H/D exchange reaction catalyzed by **4.1-tBu**. Values are reported as % D incorporation after 72 hr @ 120 °C in AcOD-d_4. D_{Total} is the average number of D atoms incorporated per molecule. *o/p* and *m/p* are combined *ortho/para* and *meta/para* values, respectively. Observed vs expected statistical deuteration incorporation ratios (OSDRs) are reported as the ratios of the deuterium incorporation in the aromatic fragment vs the expected statistical values.
[a] %D incorporation after 24 Hr heating at 120 °C.
[b] %D incorporation after 120 Hr heating at 120 °C.

The screening set of substrates **4.9** through **4.13** showed a trend consistent with our previous kinetic experiments based on **1.5** / TFE-d_1 @ 80 ^{o}C system. The more electron poor substrate, nitrobenzene (**4.9**), had a reduced OSDR, when compared to the electron rich phenol (**4.12**) or anisole (**4.13**). Despite this trend, the *meta*- and *para*- positions of nitrobenzene (**4.9**) and fluorobenzene (**4.10**) were well deuterated and approached the expected statistical values with the OSDRs ~80%. The more sterically encumbered *ortho*-positions were almost unreactive. This is a trend that is highlighted across the whole series of mono-substituted benzene derivatives **4.9** through **4.20**. The more sterically congested C-H positions appear to become deuterated at a slower rate than their unencumbered counterparts.

Trifluoromethylbenzene (**4.16**) and benzenesulfonamide (**4.17**) were inactive in H/D exchange with catalyst **1.5** in TFE-d_1 @ 80^{o}C. In turn, with **4.1-tBu** as a catalyst, trifluoromethylbenzene (**4.16**) showed ~13% average OSDR in AcOD at 120 ^{o}C after 72 h. This substrate (**4.16**) was selectively deuterated at the *meta*- and *para*- positions with 17% and 19% extent of deuteration, respectively. These values are low but demonstrate an overall improvement in the catalytic system effectiveness. For benzenesulfonamide (**4.17**) we observed the formation of a large amount of bright yellow precipitate. In spite of that, benzenesulfonamide (**4.17**) was engaged in H/D exchange with the extent of deuteration of 9% and 54% for the *ortho*- and *meta-/para*-positions, respectively. The sulfonamide -NH_2 group was deuterated up to 77% which matches the expected statistical extent of deuterium incorporation (OSDR 100%). Overall, these results demonstrate a substantial improvement of reactivity of the catalytic system and good tolerance of sulfonamide group. In fact, the electron poor substrates **4.16** and **4.17** had their OSDR and reactivity universally

improved, when compared to our previous catalytic system based on **1.5** / TFE-d_1 at 80 ^{o}C. Other electron deficient substrates, fluorobenzene (**4.10**), benzoic acid (**4.15**), methylbenzoate **(4.18**), all showed quite good reactivity, with the OSDRs of 72%, 64% and 91%, respectively.

Electron-neutral and electron rich arenes, benzene (**4.11**), ethylbenzene (**4.14**), dimethylaniline (**4.19**), and N-phenylpiperidine (**4.20**), all exhibited very good OSDRs ranging from 94-99%. Interestingly, for ethyl benzene (**4.14**) the terminal -CH_3 was 4% deuterated, and the -O-CH_3 group on anisole (**4.13**) was 2% deuterated after 5 days. After only 72 hours of reaction time, the C(sp^3)-H positions on methyl benzoate (**4.18**), dimethylaniline (**4.19**) and N-phenylpiperidine (**4.20**) were engaged in H/D exchange as well, with low OSDRs of 3%, 14%, and 5%, respectively. It is notable that the only secondary C(sp^3)-H bonds that could be partially deuterated are those of N-phenylpiperidine (**4.20**), in the α-position to its nitrogen atom.

4.2.5.2 Polysubstituted and fused arenes, and heteroaromatics (4.21 – 4.29)

1,2-Dimethoxybenzene (**4.21**) and 1,2-dichlorobenzene (**4.22**) were both efficiently deuterated with the OSDRs of 79% and 94%, respectively. There is a clear, probably, steric in origin, preference for deuteration in the β-C-H vs α-C-H position at ~3:1 ratio for **4.21**. The C(sp^3)-H bonds on the -OCH_3 group of 1,2-dimethoxybenzene (**4.21**) were also engaged in H/D exchange with an OSDR of 6% across both groups. For 1,2-dichlorobenzene (**4.22**), there is a ~3:1 preference for the deuteration of the more sterically accessible *meta*- C-H bonds *vs ortho*-C-H bonds. Benzodioxole (**4.23**) was not as reactive as one could expect, as compared with the **1.5** / TFE-d_1 @ 80 ^{o}C system (Chart 2.2), with a total aromatic deuterium incorporation of 37% and an OSDR of 44%, despite its structural

similarity to 1,2-dimethoxybenzene (**4.21**). Formation of Pt black was observed in this reaction after 24 h, and the low system performance is likely the result of substrate decomposition to yield formaldehyde thereby killing the catalyst. Naphthalene (**4.24**) showed some slight site selectivity for the more sterically accessible C2-position and was overall modestly deuterated with OSDR of 65%. The indole (**4.25**) motif was chosen due to its prevalence in pharmaceutical compounds. Indole was well tolerated and was unselective for H/D exchange, leading to an OSRD of 58%.

Two pyridine derivatives, **4.26** and **4.27**, were also screened, due to our interest to the inhibitive effects of pyridine fragments on transition metal catalysts. Previous attempts utilizing complex **2.1** in TFE-d_1 @ 80^{o}C led to the formation of catalytically inert pyridine adducts that were not engaged in H/D exchange. Here, both 2,6-lutidine (**4.26**) and 2,6-diphenylpyridine (**4.27**) participated in the reaction. For 2,6-lutidine (**4.26**) there was very little engagement of the aromatic C-H bonds of the molecule demonstrating only 2% deuteration in to the pyridyl fragment with an OSDR of only 3%. However, the C(sp^3)-H methyl groups were quantitatively deuterated. Similarly, 2,6-diphenylpyridine (**4.27**) had no measurable deuterium incorporation into C-H bonds of the pyridine core, but the phenyl groups were deuterated with an OSDR of 28%. There was a significant site selectivity for the *ortho*-C-H position of the phenyl rings with 44% deuteration versus the *meta/para* combined value of 23%. These results indicate a possible involvement of a pyridine-directed *ortho*-C-H activation. Thiophene (**4.28**) was an exceptionally well-performing substrate with 99% total deuterium incorporation.

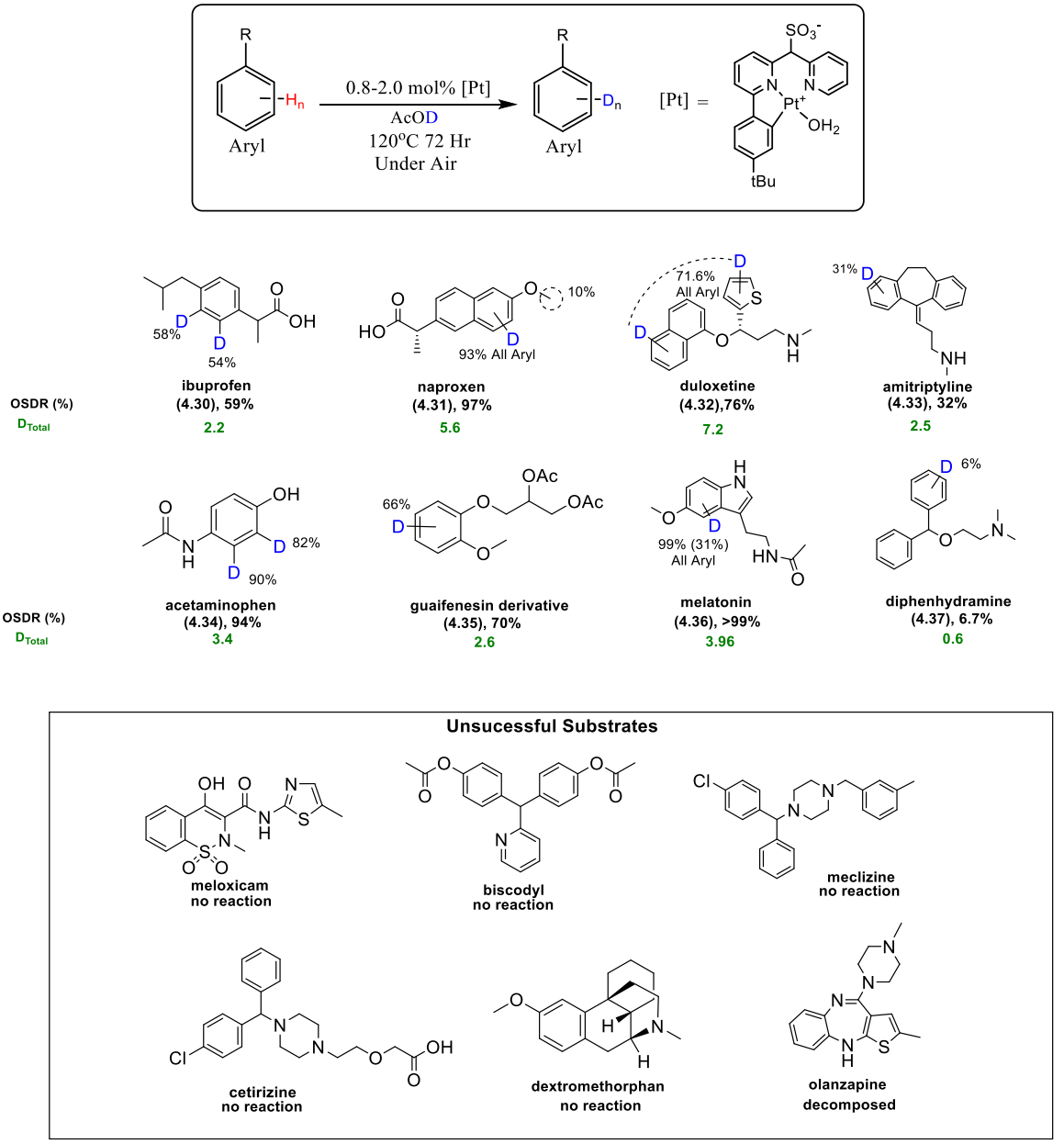

Scheme 4.4. Summary of catalytic H/D exchange on some pharmaceutical compounds catalyzed by **4.1-tBu** in AcOD-d_4 @ 120 °C.
Values are reported as %D incorporation after 72 hr @ 120 °C in AcOD-d_4.
[a] Indicates the % deuterium incorporation after 24 hours.

4.2.5.3 Deuteration of Selected Pharmaceutical Substrates 4.30 – 4.37

Pharmaceutical substrates **4.30 – 4.37** (Scheme 4.4) were selected to be explored as H/D exchange substrates as relatively readily available OTC or prescription-based medications containing aromatic C-H bonds and various functional groups. We wanted to probe the applicability of our new catalytic system, **4.1-tBu** in AcOH-d_4 @ 120 ^{o}C, for some potentially challenging but valuable practical applications. Ibuprofen (**4.30**) was virtually unreactive in H/D exchange in our **2.1** / TFE-d_1 @ 80 ^{o}C system (Chart 2.4). This lack of observed reactivity was attributed to its poor solubility and steric encumbrance leading to very slow reaction rates. Now, with the new active catalytic system in hand, it seemed reasonable to re-explore this substrate under our improved reaction conditions with complex **4.1-tBu**. Ibuprofen (**4.30**) was reasonably well engaged in H/D exchange giving an overall OSDR of 59%, so suggesting that 1,4-disubstituted arenes are reactive in our new catalytic system. Naproxen (**4.31**) was extremely successful with an overall OSDR of 97% and a D_{total} or 5.6 deuterium atoms per molecule. Acetaminophen (**4.34**) was also highly reactive, achieving deuterium incorporations that approached the expected statistical values despite its 1,4-disubstituted aromatic core.

The aromatic C-H bonds in melatonin (**4.36)** were exhaustively deuterated with an OSDR of 99%. Some background reactivity was also observed, but the presence of **4.1-tBu** greatly enhanced the extent of deuteration and the rate of reaction. For duloxetine (**4.32**) the individual aromatic signals were not resolvable, but the total extent of aromatic deuteration was 72% with an OSDR of 76%. There were no observed side reactions, and no C(sp^3)-H H/D exchange was observed. Amitriptyline (**4.33**) had a modest average extent of deuteration of 31% across all arene positions with an OSDR of 32%. While this extent

of deuteration is a bit low, further reaction optimization might lead to more acceptable results. Similarly, diphenhydramine (**4.37**) proved to be a poorly reactive substrate and was only deuterated to 6% over a 24 hour reaction period. Some more structurally complex pharmaceuticals, meloxicam, bisacodyl, cetirizine, dextromethorphan, meclizine, and olanzapine (see Scheme 4.4, bottom) were also screened under these conditions, however, no deuteration was observed for any of these compounds. For the cases of cetirizine, meclizine, and olanzapine, we suspect that the piperidine moiety may be strongly coordinating to the Pt center and inhibiting catalysis via the formation of catalytically inactive coordination complexes. Similarly, bisacodyl bears a sterically accessible pyridine fragment that is likely serving the same purpose. For meloxicam, the presence of several coordinating fragments may also lead to catalytically inactive Pt^{II}-Sub adducts, which inhibits H/D exchange. Finally, the inability for our catalyst to engage dextromethorphan is likely due to a combination of some crowding around the aromatic C-H bonds, which has previously been demonstrated to reduce the rate of H/D exchange for di and tri-substituted arene substrates.[33,49]

4.2.5.4 Olefin Substrates (4.38-4.42)

We wanted to expand the applications of our new **4.1-tBu** / AcOH-d_4 system beyond the scope of aromatic deuteration reactions. Some other similar homogenous Pt^{II} complexes that can catalyze the activation of aromatic C-H bonds have been reported to also catalyze hydroarylation reactions in the presence of a cleavable aromatic C-H bonds and suitably reactive olefins.[102] Given that the deuteration of 2,6-diphenylpyridine (**4.27**) resulted in a selective deuteration in the *ortho* positions of the phenyl fragment, we suspected that there may be some mechanistic contribution to the reaction involving the

coordination of pyridine to Pt, resulting in a directing group - mediated C-H activation. This implies that despite the fact that **4.1-tBu** has three facially chelating donor atoms, two of the four Pt^{II} coordination sites may still be accessible under the H/D exchange conditions shown above. Therefore, other catalytic reactions that require two adjacent coordination vacancies may be accessible within this system (Scheme 4.5).

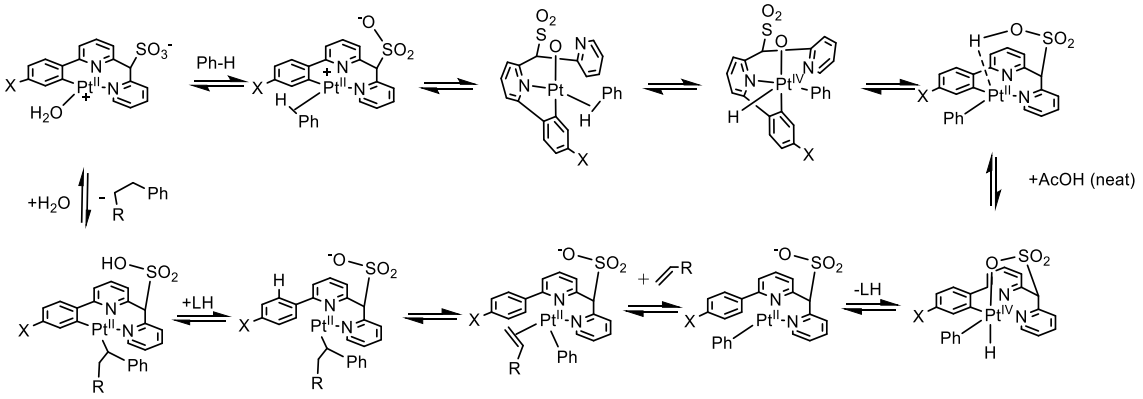

Scheme 4.5. A proposed mechanism for the hydroarylation of olefins.

From past studies,[33,49] it is known that the Pt-C bond within our CNN-pincer Pt complexes can be involved in a number of transformations, e.g., a reductive C-C elimination of some derived Pt^{IV} aryl derivatives yielded C-C coupled products (David). However, no experiments had been done up to this point evaluating the protonolysis of the Pt-C bond under the reaction conditions used for H/D exchange reactions. So, we probed an intramolecular H/D exchange reactivity of **4.1-tBu** under the same reaction conditions that were used for aromatic H/D exchange by **4.1-tBu** in AcOD-d_4 (Scheme 4.6).

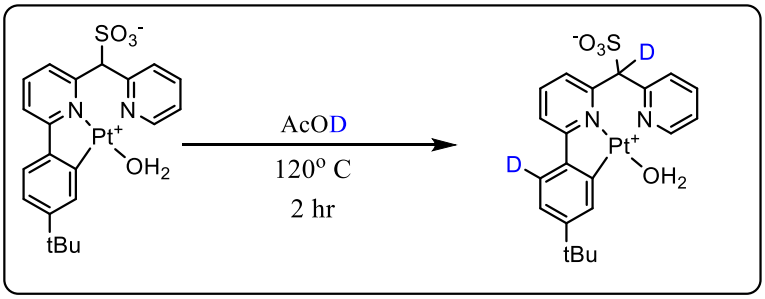

Scheme 4.6. Intramolecular deuteration of 4.1-tBu in AcOD-d_4

It was observed that the *ortho* C-H bonds on the phenylene fragment and the methine C-H bonds of **4.1-tBu** were quantitatively deuterated after 2 hours in AcOD-d_4 at 120 ^{o}C. The phenylene deuteration provides further evidence for the reversible intramolecular C-H activation and Pt-C bond deuterolysis (or protonolysis) under these reaction conditions, thereby strengthening the argument that acidic conditions may generate a coordination vacancy at a Pt^{II} center that could be useful for further chemistry.

With this evidence in hand, several hydrophenylation reactions were attempted but no new products were observed (Schemes 4.7 and 4.8). With styrene, instead only H/D exchange products of both benzene and styrene were detected by ^{1}H NMR. Interestingly, both the olefinic and the aryl C-H bonds in styrene became deuterated after 24 h at 110 ^{o}C (Scheme 4.7).

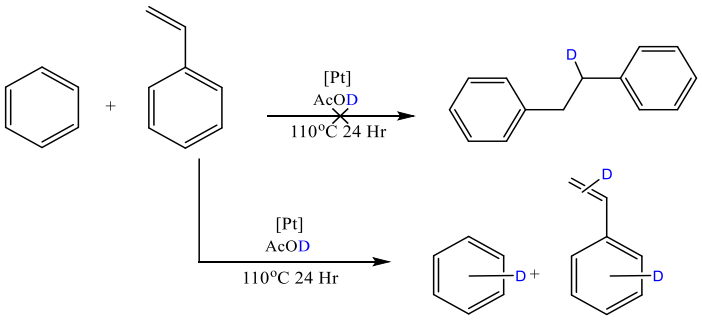

Scheme 4.7. Attempted Hydroarylation of styrene catalyzed by **4.1-tBu**

Previously, when styrene was utilized as a substrate for thermal aromatic H/D Exchange catalyzed by **1.5** in TFE-d_1 at 80 ^oC[49] the substrate underwent an unintended polymerization reaction. It appears that in our new system **4.1-tBu** / AcOH-d_4, the polymerization side reaction was not promoted, and therefore H/D exchange on both the olefin fragment and the aromatic core was possible. This inspired us to explore a series of some other commercially available and structurally diverse olefins to determine if **4.1-tBu** was a generally useful catalyst for olefin deuteration (Scheme 4.8).

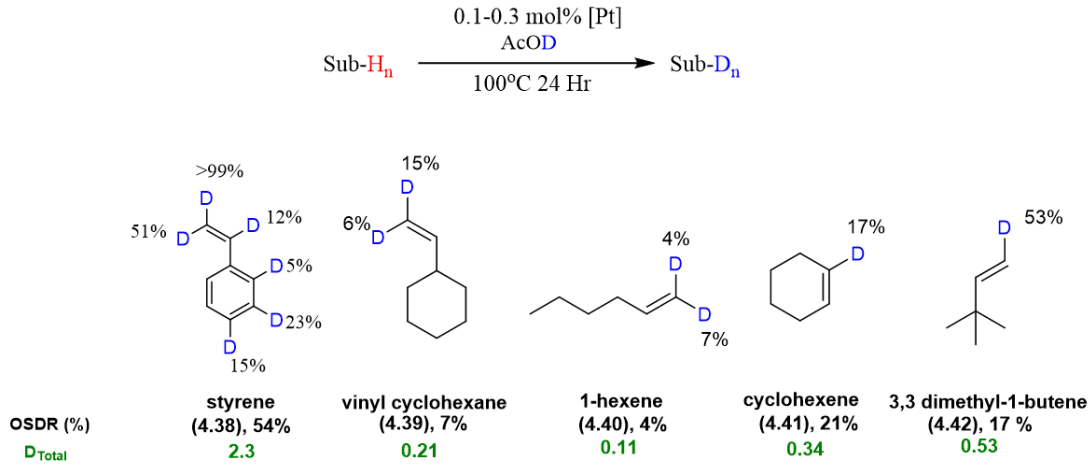

Scheme 4.8. Catalytic H/D exchange of some olefins catalyzed by **4.1-tBu** / AcOH-d_4 at 100 ^oC after 24h. Values is the drawings show %D incorporation. OSDR is reported as the ratio of the observed deuteration vs expected deuteration of all exchangeable protons.

These reactions were carried out utilizing 0.050 mL of olefin substrate dissolved into 0.50 mL AcOD-d_4 alongside 4-7 mg **4.1-tBu** (0.1-0.3 mol %). Substrate loading sometimes varied depending on the density of the olefin but was typically ~0.5-1.0M (see Supporting Information for specific details). The reaction was run exclusively under argon and at a reduced temperature of 100 ^oC to slow down any unwanted potential polymerization reactions. Five olefins were screened as part of this deuteration study.

Notably, there was a clear preference for the olefins terminal *vs* internal vinylic C(sp^2)-H bonds, and an even further preference for the least sterically encumbered *E*- C(sp^2)-H bond of monosubstituted olefins. Remarkably, for the case of styrene (**4.38**) the terminal vinylic *E*- C-H bond was completely deuterated and the Z- C-H bond was deuterated to a lower extent of 51% representing an approximately 2:1 selectivity preference for the vinylic *E*-C-H bond. It is also interesting to note that, when compared to the aromatic C-H bond activation, the olefin fragment was deuterated to a higher extent and this may suggest a greater steric accessibility of vinylic C-H bonds to a Pt^{II} center. Vinylcylohexene (**4.39**) and 1-hexene (**4.40**) were both lightly deuterated, but still demonstrated the same approximate 2:1 selectivity preference for the *E* terminal C-H bond. Cyclohexene (**4.41**) was also compatible with this system and was modestly deuterated to 21%. The low deuteration extents for **4.39** to **4.41** and is likely related to the lower reaction temperature used in these experiments, as compared to arene deuteration, chosen, in turn, because of low boiling points of our olefin substrates. Notably, no allylic C-H bond deuteration was observed for any of these substrates. 3,3-Dimethyl-1-butene (**4.42**) demonstrated exclusive deuteration of the terminal vinylic *E*- C-H bond and was efficiently deuterated to a reasonable 53% after 24 hours of reaction. The high regioselectivity of this deuteration reaction is an especially exciting observation, as it indicates that our new catalyst has a potential in the development of highly regioselective reactions for olefin functionalization. Finally, at this point we presume that the mechanism of the vinylic C(sp^2)-H bond deuteration is similar to that for aromatic C(sp^2)-H bonds (Scheme 2.2).

4.2.5.5 Deuteration of Substrates' C(sp^3)-H Bonds

Given the overwhelming success of **4.1-tBu** as a catalyst for the H/D exchange of aromatic C-H bonds, we were interested in expanding the substrate scope to include more inert C-H bonds such as those in alkanes. Previous attemptes utilzing complex **1.5**, **4.2**, and **4.3** for the C-H activation of simple alkanes and methane led exclusively to catalyst deactivation; no H/D exchange between these catalysts and alkanes was observed. Given that the initial rationale behind the design of our CNN ligated Pt complexes was to enable the consecutive C(sp^2)-H and/or C(sp^3)-H and O_2 activation in order to complete an aerobic Shilov cycle, the only step still proving troublesome for akane substrates is the activation of their C(sp^3)-H bonds. In particualr, the aerobic conversion of Pt^{II}-Me supported by our CNN pinceer ligands to the derived Pt(IV)Me derivatives and the subsequent S_N2-like Me-X reductive elimination have been recently demonstrated.[64] We were inspired by our initial results of the screening of aromatic substrates shown above in Scheme 4.4. Many of these substrates contained C(sp^3)-H bonds, and in many cases, these bonds became deuterated over the course of the reaction (**4.13, 4.14, 4.18-18**, and **4.26**; Scheme 4.4). These observations are the first examples of C(sp^3)-H activation using our sulfonated CNN-pincer Pt^{II} complexes. This fact motivated us to screen a few other C(sp^3)-H bond containing substrates to see if some simple alkanes or their derivatives were compatible with our system.

For the cases of the arene substrates bearing C(sp^3)-H bonds, compounds bearing heteroatoms (such as O or N) adjacent to the C(sp^3)-H showed the greatest reactivity in terms of total deuterium incorporation over the 24h reaction period. For example, N,N-dimethylaniline (**4.19**) showed up to 14% deuteration in the C(sp^3)-H positions.

Remarkably, even secondary C-H bonds were engaged when they were adjacent to donor atoms, as indicated by the 5% deuterium incorporation seen in N-phenylpiperidine (**4.20**). Oxygen was also a suitable α-heteroatom, and the adjacent C(sp^3)-H bonds were deuterated for anisole (**4.13**), methylbenzoate (**4.18**) and 1,2-dimethoxybenzene (**4.21**). This was also observed in complex pharmaceutical substrates where the C(sp^3)-H bonds in the methoxy group of naproxen (**4.31**) was deuterated up to 10% over 24 hours in the presence of air. 2,6-Dimethylpyridine demonstrated the greatest extent of C(sp^3)-H deuteration with 99% deuterium incorporation on the methyl groups. No background reaction was observed in the absence of **1.5**. However, a substantial amount of Pt black was observed for this reaction, and it is unclear whether the homogeneous Pt^{II} catalyst or Pt^0 species are responsible for this H/D exchange. Even C(sp^3)-H bonds in the donor atoms – free substrates were also engaged in H/D exchange, but at a much slower rate. E.g., in the case of ethylbenzene (**4.14**) the terminal CH_3 group was engaged in H/D exchange after 120 hours with 4% deuteration. These findings are significant because these are the first indications of our sulfonated CNN Pt^{II} pincer ligand complexes being able of reacting with C(sp^3)-H bonds. We expanded the scope of substrates to be tested to include some simple alkanes and their derivatives, as shown below in Scheme 4.9.

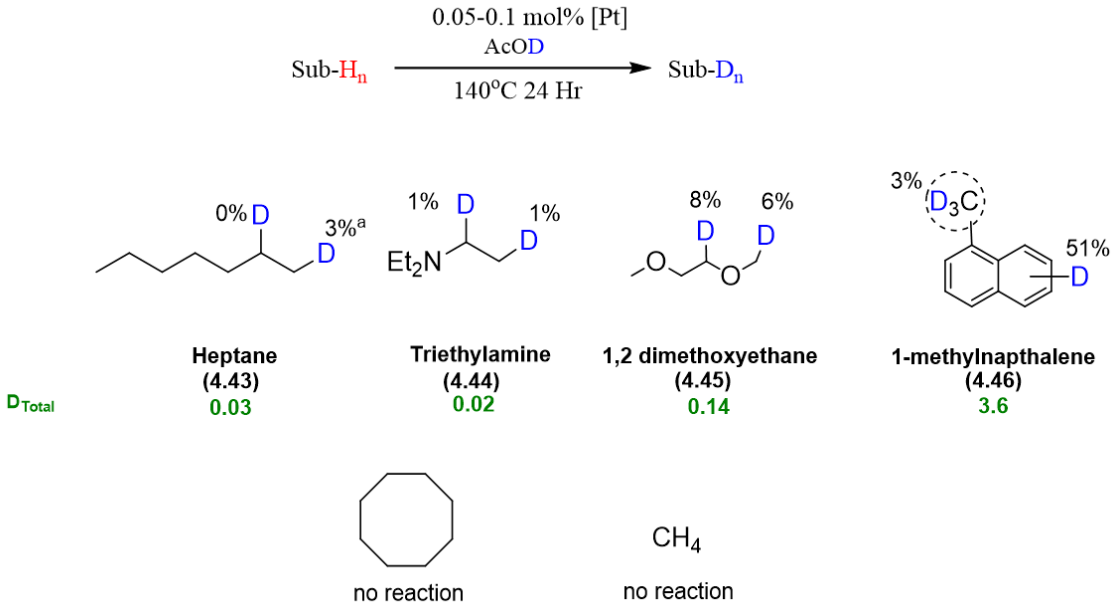

Scheme 4.9. Catalytic H/D exchange of C(sp^3)-H bonds of some simple alkanes and their derivatives by **4.1-tBu** / AcOH-d_4 at 140 °C after 24. Values are reported as %D incorporation.

a) %D incorporation after 72 hr of heating.

Even when we used a higher temperature of 140 °C, these experiments yielded overall low percent of deuteration, as compared to the aromatic and vinylic H/D exchange experiments. Heptane (**4.43**) showed some interesting selectivity, where only the terminal CH_3 was engaged in the H/D exchange. However, the H/D exchange reaction was only detectable via ^2H NMR after 72 hours of heating at 140 °C. While this result is academically interesting, it holds little practical significance for this specific system. Triethylamine (**4.44**) was rather poorly deuterated with 1% total deuteration across all C-H bonds. Additionally, Pt^0 was observed after 24 hours which implies that our catalyst is incompatible with this substrate under given conditions. Similarly, 1,2-dimethoxyethane (**4.45**) was deuterated to 8% for the bridging CH_2 fragment and 6% for the methoxy CH_3 group but after 24 hours of reaction time Pt^0 was observed to form. 1-Methylnapthalene

(**4.46**) was chosen in order to assess how specifically the primary benzylic C-H bonds would engage in H/D exchange under these conditions, and 3% of the methyl C(sp^3)-H bonds were deuterated after 24 hours with 51% of the total aromatic core C-H bonds also engaged. Cyclooctane and methane were also explored as potential substrates for H/D exchange, but no H/D exchange was observed. These results show that our catalyst may be capable of catalytically activating some relatively inert C(sp^3)-H bonds, but to do so effectively may require changing the reaction conditions or further fine-tuning of the catalyst thereby leaving open a potential research avenue.

4.3 Development of More Reactive Thermal Catalysts for Aromatic H/D Exchange

The initial motivation behind this work was to develop catalysts that would be more reactive towards C-H bonds than **1.5**. We hoped that by exploring a range of electronically donating and withdrawing substituents of the series of complexes **4.1-X**, a reactivity trend could be revealed and the electronic effects of substituents X on the catalysts' reactivity could be estimated. However, most of the time, this task was complicated due to the catalysts' bimolecular deactivation. Still, the latter effect was not observed in the sterically encumbered **4.1-tBu** which allowed for its excellent performance as a general H/D exchange catalyst for aromatic substrates and some pharmaceutical compounds. The presence of the 4-tBu suppressed the catalyst bimolecular deactivation reaction and improved solubility of the complex, allowing for AcOD, TFA, and MeOD to be used as solvents. Hence, we speculated that we could utilize a 4-tBu motif to enhance the performance of some other catalysts, such as **4.5-H**, that had previously proven to be inefficient (Scheme 4.10).

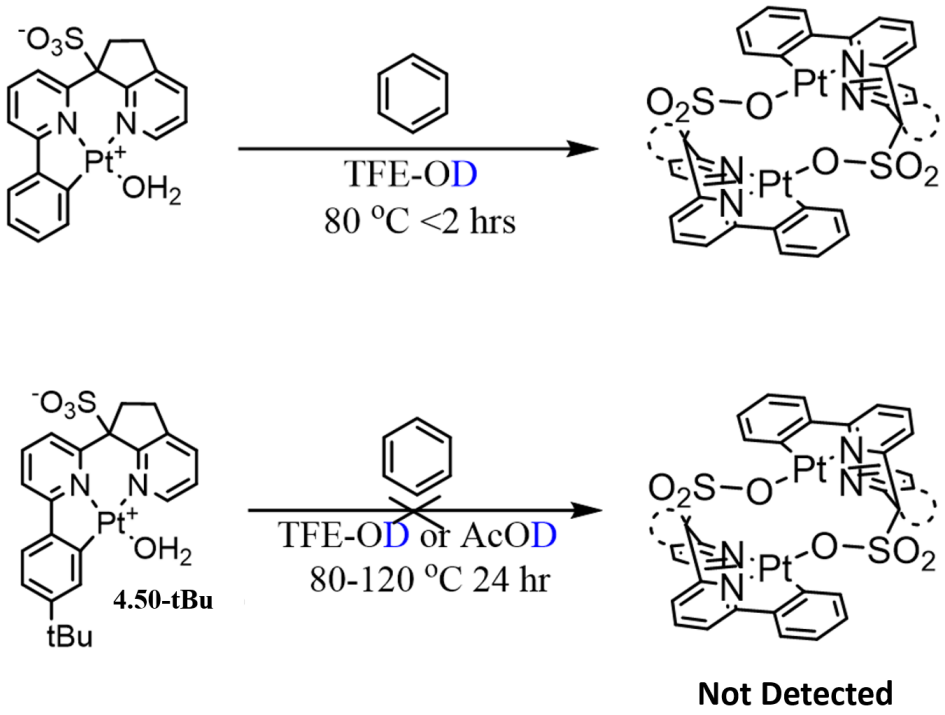

Scheme 4.10. Comparison of stability of **3.5-FC** and **4.50-tBu** under thermal H/D exchange conditions.

4.3.1 Preparation of 4.50-tBu

We hypothesized that by introducing the tBu fragment into **3.5-FC** we could overcome the solubility and dimerization issues we faced with this complex (see Chapter 3, Section 3.5.4). With this idea in mind, we engaged in the preparation of a new complex **4.50-tBu**, a tBu - substituted derivative of **3.5-FC** (Scheme 4.11).

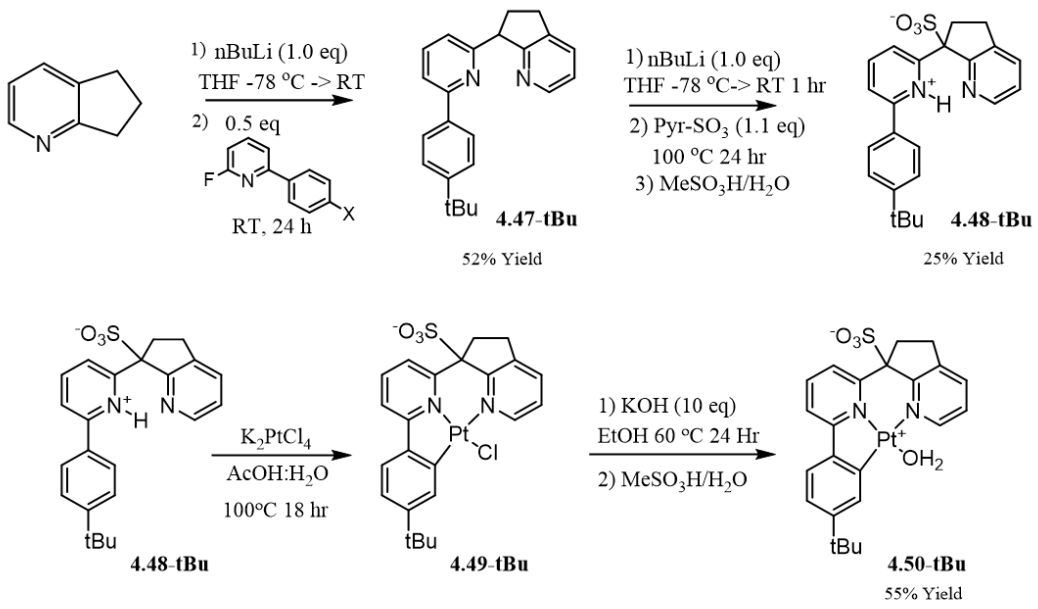

Scheme 4.11. Preparation of complex **4.50-tBu**.

The synthesis for complex **4.50-tBu** was performed under virtually identical conditions to the **4.1-tBu** analogue described above, however, instead of utilizing 2-picoline, 2,3-cyclopentenopyridine was utilized as the pyridyl containing bridgehead.

4.3.1.1 Preparation of Pre-Ligand 4.47-tBu (S_NAr)

A dry 50 mL Schlenk tube was transferred into an argon filled glove box and was charged with 5.9 g 6,7-dihydro-5*H*-cyclopenta[*b*]pyridine (49.7 mmol, 2.0 eq) and was subsequentially dissolved into 30 mL dry THF and the tube was sealed with a Teflon cap. The solution was then transferred onto a Schlenk line and cooled to -78 °C for 30 minutes under rapid stirring. Then, 11M nBuLi in hexanes (49.7 mmol, 2.0 eq) was added dropwise over 10 minutes under an argon atmosphere. The resulting dark red solution was then stirred at -78 °C and was then was warmed to room temperature for 1 hour to allow for complete formation of the carbanion. Next, the solution was cooled back to -78 °C and 5

mL of a THF solution containing 5.7 g **4.5-tBu** (prepared as previously described in 4.2.1.1) (24.8 mmol, 1.0 eq) was added dropwise over 1 minute. The solution maintained a dark red coloration and was allowed to warm back to room temperature and allowed to react over 24 hr. The next day, the solution was quenched with 20 mL DI H_2O. The resulting mixture was then extracted with 3x30 mL of Et_2O and the solvent was removed via reduced pressure to yield 4.2 g (52% yield) viscous red/orange oil. The compounds were further purified via column chromatography with a 60:40:0.01 (Hex:EtOAc:TEA) mobile phase to yield a viscous orange oil. The identity and purity of the **4.47-X** materials were determined via ^{1}H-NMR and ^{13}C-NMR spectroscopy. Typically, some residual 6,7-dihydro-5*H*-cyclopenta[*b*]pyridine (~5%) remained even after subsequent columns, however, this did not seriously affect the sulfonation step.

4.3.1.2 Preparation of Pre-Ligand 4.48-tBu (Sulfonation)

A dry 50-100 mL Schlenk tube was transferred into an argon filled glove box and was charged with 30 mL of a dry THF solution containing 4.2 g of **4.47-tBu** (12.8 mmol, 1.0 eq) and a stir bar the tube was sealed with a Teflon cap. The solution was then transferred onto a Schlenk line and cooled to -78 ^{o}C. Then, 11M nBuLi in hexanes (12.8 mmol, 1.0 eq) was added dropwise over 10 minutes under rapid stirring. The resulting dark red solution was then stirred at -78 ^{o}C until homogenous then was warmed to room temperature for 1 hour to allow for complete formation of the carbanion. After the anion formation was complete (indicated by a deep red coloration) the tube was then transferred back into an argon-filled glove box and 2.2 g pyridine-sulfur trioxide complex (14 mmol 1.1 eq) was added to the tube. The tube was again sealed with a Teflon cap, removed from the glove box, and then heated in a hot oil bath to 100 ^{o}C for 24 hours. The coloration of

the solution should slowly change from a deep red to a light transparent red color alongside the formation of a large amount of white or off-white precipitate. After 24 hours, the reaction was quenched with 30 mL DI H_2O and the aqueous phase was washed with an additional 3x15 mL Et_2O. The organic phase often contained up to 50% unreacted starting material that was able to be reused for the sulfonation reaction.

The aqueous phase was then acidified using a 50% $MeSO_3H/H_2O$ ($MeSO_3H$ was used for an NMR handle, H_2SO_4 has also been used successfully) solution to a pH ~1-2. A large amount of brown precipitate formed, and the solution was placed in the refrigerator to allow precipitation to occur over night. The following morning, the solution was filtered and rinsed with copious amounts of cold DI H_2O. The powder was then removed from the filter paper and dried in a desiccator oven at 80 ^oC overnight and yielded 1.3 g (25% Yield) of a light brown/off white powder. The identity and purity of **4.47-tBu** was determined via ^1H-NMR and ^{13}C-NMR spectroscopy and the anionic fragment was analyzed via ESI-MS (- mode) via injection via HPLC line.

4.3.1.3 Preparation of Pt^{II}-Cl Complex 4.49-tBu

Synthesis of **4.50-tBu** complex proceeded first through the cyclometallation reaction of **4.48-tBu** and K_2PtCl_4 in aqueous acetic acid to yield the intermediate Pt^{II}-Cl complex, **4.49-tBu,** in accordance with the described literature procedures.[33, 49, 51] Synthesis of complex **4.49-tBu** was performed via the following procedure. A dry 50 mL Schlenk tube was charged with 408 mg (1.0 mmol 1.0 eq) **4.48-tBu** (the salt form may also be used for this step) and 415 mg (1 mmol, 1.0 eq) K_2PtCl_4 and a stir bar. The tube was then rinsed with a 2:1 $AcOH/H_2O$ solution in order to dissolve any remaining solids on the

walls of the tube. Then the tube was filled with 20 mL of the AcOH/H_2O solution and sealed with a Teflon cap and placed into a hot oil bath set to 100 ^oC for 24 hours. After the reaction was complete, the solvent was removed, and the remaining crude solid was dissolved in hot methanol and filtered through a celite plug to remove any remaining KCl. After removing solvent again, **4.49-tBu** was isolated as a fine yellow crystalline powder. The identity and purity of the **4.49-tBu** materials were determined via ^{1}H-NMR and ^{13}C-NMR spectroscopy and the anionic fragment was analyzed via ESI-MS (- mode) via injection via HPLC line. For specific information about product characterization see the supporting information.

4.3.1.4 Preparation of Pt^{II}-OH_2 Complex 4.50-tBu

Converting to the Pt^{II}-Cl complex **4.49-tBu** to Pt^{II}-OH_2 **4.50-tBu** was done by loading 670 mg (1 mmol 1.0 eq) of **4.49-tBu** into a 100 mL round bottom flask containing a stir bar (crude **4.49-tBu** containing KCl may also be used for this step). The complex was then dissolved into 50 mL EtOH and ~0.6 g of KOH (10 mmol, 10 eq) was added to the solution. The flask was then lightly sealed with a rubber stopper and placed into an oil bath heated to 60 ^oC for 24 hours under heavy stirring. After the reaction was completed, the solvent was removed via vacuum and the deeply red colored intermediate, a Pt^{II}-OEt complex, was extracted with 30 mL of acetone. The solution was filtered through Celite, and the solvent was again removed via vacuum to yield a dark red crystalline solid. The solid was then redissolved into 30-50 mL H_2O and the pH of the solution was adjusted to ~1-2 using a 50% $MeSO_3H$/H_2O solution. A large amount of tan/yellow precipitate formed upon acidification and the solution was placed in the refrigerator overnight to allow the

complex to fully precipitate. The following morning, there was a large amount of precipitate present at the bottom of the beaker and the solution was only faintly yellow colored. The product was then isolated via vacuum filtration and washed with copious amounts of cold DI H_2O to remove any remaining acid. The isolated Pt^{II}-OH_2 complex was then dried at room temperature under vacuum for 24-48 hours (heating under vacuum must be avoided to prevent decomposition) to yield 375 mg (55% yield) of a brown powder. The identity and purity of **4.50-tBu** was determined via ^{1}H-NMR and ^{13}C-NMR spectroscopy. Interestingly, **4.50-tBu** demonstrated fluxional behavior when dissolved in solutions of DMSO-d_6 in ^{1}H-NMR. Broad signals were observed across the entire spectrum at room temperature and persisted even when heating to 50^{o}C in the NMR probe. Integration values suggest a single product, and the most downfield shifted signal, which we assign as the *ortho*-pyridyl resonance, was shown to be at 8.83 ppm. Thereby suggesting that there was complete conversion of the Pt-Cl complex, which has an *ortho*-pyridyl resonance at 9.45 ppm in DMSO-d_6. When the solvent was changed to AcOD-d_4 the resolution of the ^{1}H-NMR sharpened and a new downfield shifted signal associated with either the native Pt-OH_2 complex or the derived Pt^{II}-AcOD complex was found at 8.40 ppm.

4.3.2 Reactivity of 4.50-tBu in H/D exchange reactions

To our delight, **4.50-tBu** was far more soluble and thermally robust than the parent **3.5-FC** complex. The parent complex **3.5-FC** was poorly soluble in most solvents including TFE and AcOH, and its catalytic activity toward C-H bonds was also quite low due to its fast deactivation, as it was described in Chapter 3 (Section 3.5.4). Importantly, the situation has changed with the introduction of the tBu group and the transition from

3.5-FC to **4.50-tBu**. The new complex **4.50-tBu** is well soluble in TFE and AcOH, which allowed us to use catalyst loadings as high as ~10 mg/mL in AcOD-d_4, and was able to be dissolved at room temperature as compared to ~7 mg/mL for **3.5-FC** at elevated temperatures only. Unlike **3.5-FC** and similar to **4.1-tBu**, **4.50-tBu** does not show signs of dimerization that would be detectable visually (precipitation) and by ^{1}H NMR under the reaction conditions that we use for H/D exchange. Still, on the downside, in some experiments with prolonged heating for more than 4 hours at 120 ^{o}C, **4.50-tBu** showed signs of decomposition leading to a visible Pt^0 precipitate, whereas **4.1-tBu** was stable under the same conditions for over 72 hours.

Previously, in a series of experiments it was estimated that the introduction of an ethylene fragment between the bridging carbon of a CNN-pincer ligand and a C3-position of an attached pyridine ring in complex **1.5** and/or the use of benzoquinoline moiety instead of a phenylpyridine fragment results in an increased reactivity of the derived Pt^{II} aqua complexes **1.5** and **4.3** (Chart 2.1) with respect to C-H bonds of benzene.[51] However, past attempts at comparing and properly exploring the reactivity of these complexes had proven difficult given their rapid deactivation. Given the successful synthesis of **4.1-tBu** and its cyclopenteno-fused variant **4.50-tBu**, now we are not limited in this respect and can assess quantitatively the effects that the fused ring and solvent have on the reactivity of a Pt^{II} center.

Chart 4.1. The average observed rate constants, $k_{Y\text{-all}}$, for Y-substituted benzene substrates C_6H_5Y (Y = NO_2, F, H, OH, OMe) with **4.1-tBu** and **4.50-tBu** as catalysts under various conditions.

Entry	Catalyst	Reaction Conditions	Total Aromatic C-H ($ky_{,all}$), M^{-1} h^{-1}				
			NO_2	**F**	**H**	**OH**	**OMe**
4	**4.1-tBu**	**AcOD-d_4 @120°C (Air)**	1.5 ± 0.14	3.2 ± 0.5	5.1 ± 0.4	7.3 ± 0.6	9.4 ± 0.7
5	**4.50-tBu**	**AcOD-d_4 @120°C (Air)**	2.9 ± 0.03	4.9 ± 0.5	18.9 ± 0.9	21.0 ± 1.8	13.5 ± 0.7
3	**4.1-tBu**	**AcOD-d_4 @120°C (Argon)**	2.3 ± 0.16	3.4 ± 0.2	8.5 ± 0.1	9.8 ± 1.7	6.0 ± 0.2
4	**4.1-tBu**	**AcOD-d_4 @120°C (Air)**	1.5 ± 0.14	3.2 ± 0.5	5.1 ± 0.4	7.3 ± 0.6	9.4 ± 0.7
5	**4.50-tBu**	**AcOD-d_4 @120°C (Air)**	2.9 ± 0.03	4.9 ± 0.5	18.9 ± 0.9	21.0 ± 1.8	13.5 ± 0.7

To that end, the average observed rate constants, $k_{Y\text{-all}}$, for Y-substituted benzene derivatives (Y = NO_2, F, H, OH, OMe) for **4.1-tBu** and **4.50-tBu** – catalyzed H/D exchange are given above in Chart 4.1. Entries 1-4 represent the previously discussed kinetic screening results showing the differences in the reactivity of **4.1-tBu** in TFE-d_1 and AcOH-d_4 at 80 °C and/or 120 °C. The results in entries 4 and 5 allow to compare complexes **4.1-**

tBu and **4.50-tBu** under the most practically appealing reaction conditions, in AcOH-d_4 at 120 ^{o}C under air. A comparison of $k_{Y\text{-}all}$ in these entries shows that the latter complex is about two times more reactive in the catalytic H/D exchange of the arene C-H bonds than **4.1-tBu**. A possible origin of the higher activity of **4.50-tBu** vs **4.1-tBu** is discussed next.

Based on computational (DFT) analysis done in our group earlier for the reaction of Pt^{II} aqua complex **1.5** with benzene in weakly coordinating TFE,[33] the reaction involves two key steps, a benzene – for aqua ligand exchange step at a Pt^{II} center and a subsequent C-H bond cleavage in the transient Pt^{II} (σ-H-Ph) complex. The Gibbs energy of the transition state corresponding to benzene – for aqua ligand exchange is 4.6 kcal/mol lower than that of the transition state for the subsequent C-H bond cleavage, both in TFE solutions. Hence, for **1.5** reacting with benzene in TFE solutions, the substrate C-H bond cleavage is the RDS of the overall reaction of benzene and **1.5**. Based on these results, as a starting point, we presume that the reactions involving **4.1-tBu** in TFE that are reported in Table 4.4 also have the C-H activation step as the RDS of the overall H/D exchange reactions.

Considering now the differences between **4.1-tBu** and **4.50-tBu**, the only modification to **4.1-tBu** leading to **4.50-tBu** is the introduction of a fused cyclopenteno fragment. As it was experimentally (XRD) observed for a cyclopenteno-fused **4.3** vs the parent complex **1.5**,[49,51] such modification resulted in a flatter metal coordination unit and an increased ligand rigidity. Using DFT, it was shown that these changes lead to a 3.0 kcal/mol lower Pt^{II}-OH_2 bond Gibbs energy in **4.3** vs **1.5** and a 1.9 kcal/mol lower Gibbs activation energy for the C-H activation step of benzene reacting with **4.3** vs **1.5**. Getting back to a comparison of **4.50-tBu** vs **4.1-tBu**, we hypothesize that the increased reactivity

of **4.50-tBu** is also due to a more rigid geometry and a resulting weaker Pt^{II}-OH_2 bond in **4.50-tBu**, as compared to **4.1-tBu**. In confirmation of this hypothesis, the DFT-calculated Gibbs energy of dissociation of Pt^{II}-OH_2 bond in gas phase is 25.1 kcal/mol for **4.50-tBu** which is 3.7 kcal/mol lower than 28.8 kcal/mol for **4.1-tBu**. Accordingly, the DFT-calculated Gibbs activation energy of the benzene C-H bond cleavage with **4.50-tBu** is 1.7 kcal/mol lower than with **4.1-tBu** in gas phase. A similar trend may be expected for Pt^{II}-AcOH adducts derived from **4.50-tBu** and **4.1-tBu** (Figure. 4.5). In fact, the Gibbs energy of AcOH dissociation from an AcOH adduct derived from **4.1-tBu** (**4.1-tBu-AcOH**) is 33.3 kcal/mol; the corresponding Gibbs energy for an AcOH adduct derived from **4.50-tBu** (**4.50-tBu-AcOH**) is 31.4 kcal/mol, 1.9 kcal/mol lower (both values are for gas phase). Finally, the Gibbs energy of activation of benzene C-H bond cleavage by the AcOH adduct **4.1-tBu-AcOH** is 29.2 kcal/mol in AcOH solutions and for a similar reaction of **4.50-tBu-AcOH** the Gibbs activation energy is 27.8 kcal/mol, 1.4 kcal/mol lower.

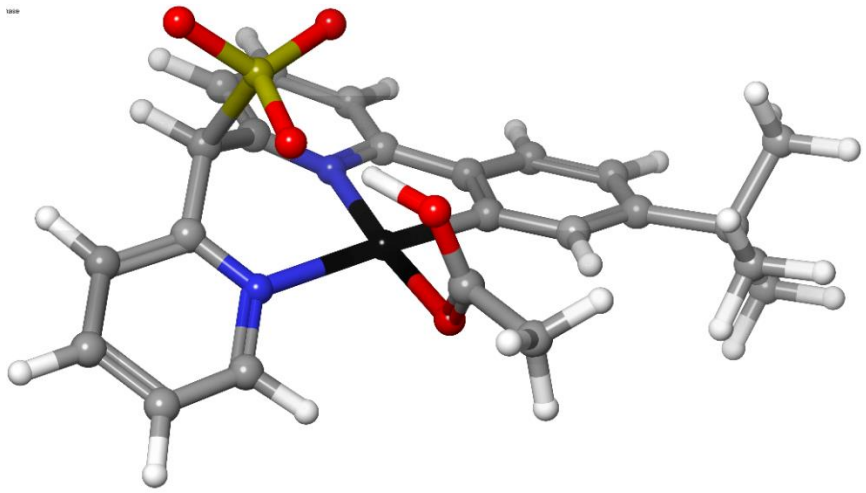

Figure 4.5. A DFT-optimized geometry of an AcOH adduct derived from **4.1-tBu** via aqua ligand substitution.

In addition to looking into the reactivity difference of **4.1-tBu** vs **4.50-tBu** observed in our experiments (Table 4.4), the substrate selectivity of both complexes was analyzed using Hammett-type correlations. The results are given in Figure 4.6 and Table 4.5.

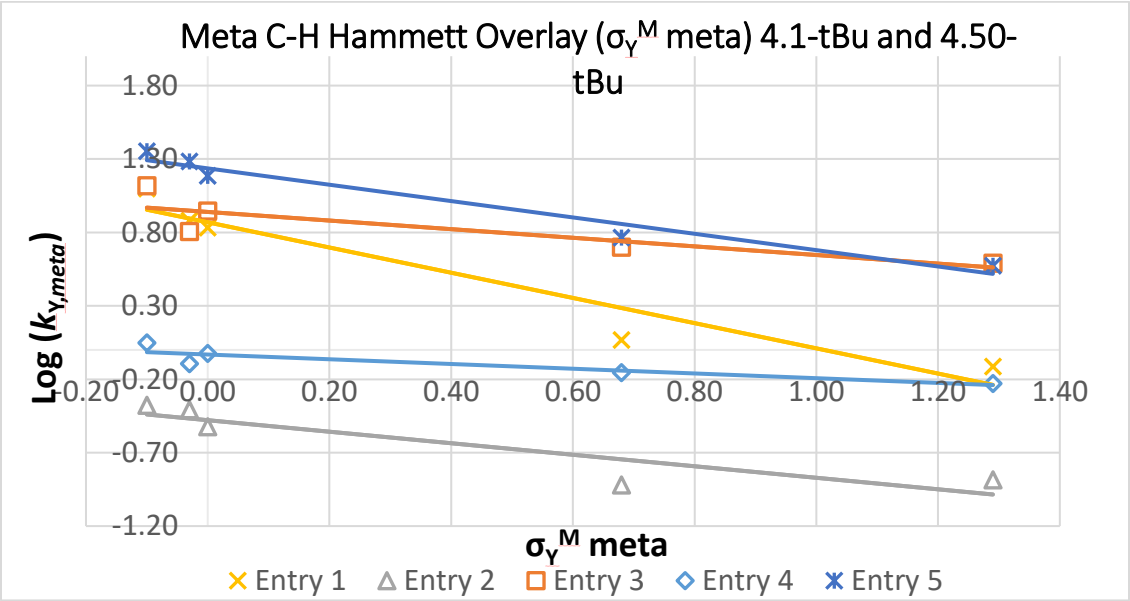

Figure 4.6. Hammett Overlay of Log($k_{Y,meta}$) vs σ_Y^M meta for H/D exchange of C_6H_5Y catalyzed by **4.1-tBu** and **4.50-tBu** under various conditions. Entries refer to the data input in their respective rows in Table 4.4.

Table 4.5. Hammett Plot slopes (ρ) of the *meta*-C-H bonds of Y-substituted benzene derivatives for catalysts **4.1-tBu** and **4.50-tBu** under various conditions.

Entry	Catalyst	Reaction Conditions	Slope (ρ)
1	**4.1-tBu**	TFE-d_1 @ 80°C (Argon)	-0.86 ± 0.14
2	**4.1-tBu**	AcOD-d_4 @ 80°C (Argon)	-0.39 ± 0.10
3	**4.1-tBu**	AcOD-d_4 @ 120°C (Argon)	-0.29 ± 0.10
4	**4.1-tBu**	AcOD-d_4 @ 120°C (Air)	-0.16 ± 0.05
5	**4.50-tBu**	AcOD-d_4 @ 120°C (Air)	-0.56 ± 0.07

Starting with the effect of the reaction conditions on the reactivity of **4.1-tBu**, first, we note a decrease in the magnitude of the reaction parameter ρ, as the deuterium source

is changed from TFE-d_1 to AcOD-d_4 while maintaining the reaction temperature at 80 ^{o}C (entries 1 and 2). When the reaction was carried out in TFE-d_1, the slope of the Hammett plot was -0.86 ± 0.14. The negative ρ values of the same or greater magnitude were observed for the whole series of complexes **4.1-X** in TFE-d_1 at 80 ^{o}C (Table 4.3). However, when switching the solvent to AcOD-d_4, while keeping the same temperature of 80 ^{o}C, the magnitude of the slope decreased with the ρ parameter becoming -0.39 ± 0.10. This statistically significant change in the slope value suggests a decreased substrate selectivity for **4.1-tBu** in AcOH solutions and, potentially, a change in the reaction RDS, when changing solvent from TFE to AcOH. Note also that the reaction rates are much slower in AcOH than in TFE at the same temperature (entry 1 and 2, Table 4.4).

Overall, AcOH is a more strongly Pt^{II}-coordinating ligand than either TFE or H_2O and in AcOH solutions the catalyst **4.1-tBu** may be fully transformed to an AcOH adduct (Figure. 4.5). The stronger Pt^{II}-AcOH coordination may be responsible for the observed overall slower reaction rates and, potentially, for the change in the RDS from the C-H activation step in TFE solutions to a ligand substitution step in AcOH. This change of the RDS may lead to a different substrate selectivity for **4.1-tBu**.

Notably, as the temperature of solutions of **4.1-tBu** in AcOH was increased to 120 ^{o}C (entry 3), the Hammett parameter ρ value remained virtually unchanged. In turn, as the argon atmosphere was changed for air (entry 4), while keeping the deuterium source and temperature the same, the magnitude of the resulting slope was calculated to be -0.16 ± 0.05, which is still statistically undistinguishable from the ρ value in entry 3.

Interestingly, when comparing **4.1-tBu** to **4.50-tBu** (entries 4 and 5), while keeping all other reaction conditions the same, AcOH at 120 ^{o}C, there is a noticeable statistically

significant difference in the magnitude of the Hammett reaction parameters ρ, -0.16 ± 0.05 for **4.1-tBu** and -0.56 ± 0.07 for **4.50-tBu**.

Based on our hypothesis that **4.50-tBu** is more reactive than **4.1-tBu** in AcOH because of the lower Pt^{II}-(solvento ligand) bond energy of the adducts derived from **4.50-tBu**, we can further assume that the lower Pt^{II}-(solvento ligand) bond energy may be responsible for a change from a substrate coordination step being the reaction RDS for **4.1-tBu** to the C-H bond cleavage step being the reaction RDS for **4.50-tBu**. Finally, **4.50-tBu** proved to be relatively unstable at higher temperatures and prolonged reaction times producing a dark precipitate that is presumed to be Pt^0 after ~4 hours of reaction time thereby limiting its potential for long-term experiments.

4.4 Mechanistic Insight and Photo-induced Catalytic C-H Activation

Despite the success of complexes **4.1-tBu** and **4.50-tBu** for the thermally mediated H/D exchange of a wide range of substrates, it became clear that the reaction conditions required to activate these C-H bonds were incompatible with the reaction conditions required to simultaneously activate O_2, as indicated by the high stability of **4.1-tBu** under air at elevated temperatures. This practically useful property of the new catalyst's limits, at the same time, the potential for their application in Shilov-type C-H bond functionalization utilizing O_2 as an oxidant. Previously, work done in our group demonstrated that **1.5** was capable of the consecutive activation of aromatic C-H bonds and O_2 at room temperature is aqueous solutions of TFE (David OM) and this was reviewed previously in Chapter 1. The limitations of this system were i) the system's inertness when it comes to reductive elimination to yield Ar-OH and ii) inability to react with alkane C-H bonds under these conditions. Therefore, in order to maintain our catalysts potential for completing the

aerobic Shilov cycle, we need to enable activation of substrates' C-H bonds at lower temperatures that allow for adequate O_2 solubility and aerobic oxidation of the generated Pt^{II}-R to Pt^{IV}-R species. Additionally, we learned from our previous kinetic catalyst screening of the class of complexes **4.1-X**, that virtually every catalyst, except **4.1-tBu**, underwent a bimolecular deactivation in solutions of TFE which was fast at elevated temperatures, but they were more kinetically stable in TFE solutions at room temperature. With these ideas in mind, we aimed to revisit this room temperature C-H activation regime, however now with the focus lying on explicitly exploring the complexes reactivity towards C-H bonds and utilizing blue (435-445 nm) or violet (405-415 nm) light to promote the reaction.

The series of complexes **4.1-X** have different electronic properties because of the electronic characteristics of their substituent group, X. While this electronic difference played little role in the thermal catalysis, it is expected to play a much more substantial role for the light-driven H/D exchange reactions due to the effect the p-X group has on the HOMO-LUMO gap of the complex. Before accounting for each of the variable the substituent groups may have on the reactivity, we first explored the reactivity of the base complex **2.1** on the photo-induced H/D exchange of benzene in TFE-d_1 (Scheme 4.12).

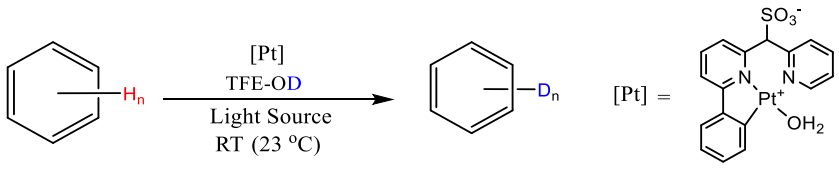

Scheme 4.12. Photo-induced H/D exchange of benzene catalyzed by **1.5 (4.1-H)**.

Our expectation was that a visible or near-UV light absorbed by a CNN-pincer Pt^{II} aqua complex **2.1** would induce an electron transition from a Pt-centered HOMO of the complex to its Pt-O σ* orbital. If the resulting excited singlet state can undergo an

intersystem crossing to produce a long-enough living excited triplet species with an one-electron-populated Pt-O σ* MO that would weaken dramatically the Pt-OH_2 bond and allow for a facile aqua ligand loss and a competitive coordination of an arene substrate, so enabling a facile C-H activation and H/D exchange. Presently, our MO calculations (performed by Prof. Andrei Vedernikov (Figure 4.7)) show that **4.1-OMe** has an appropriate absorption in the violet range that may allow for the promotion of an electron from the HOMO (predominantly a Pt d_{xz} orbital) to the LUMO+3 (predominantly Pt-O σ^* orbital). This electronic excitation would effectively reduce the Pt-O bond order via populating the Pt-OH_2 σ-antibonding orbital, thereby reducing the required barrier for aqua ligand exchange. From the context of the diagram shown above, this would result in a dramatically decreased energy of the TS_1 and the TS_2 becoming a product-determining step.

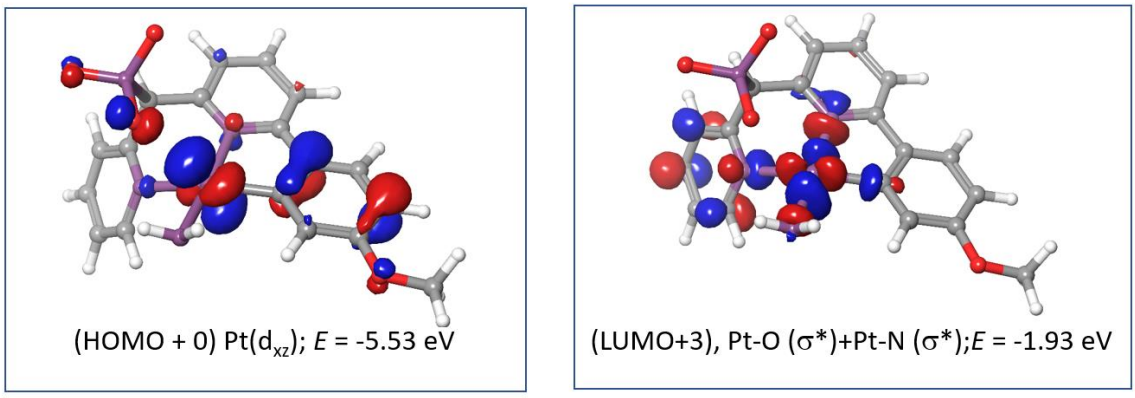

Figure 4.7. Visualizations of the HOMO (predominantly a Pt d_{xz} orbital) and LUMO+3 (predominantly Pt-O σ^* orbital) for **4.1-OMe** that are involved in an electronic transition resulting in a weakened Pt-OH_2 σ-bond. A DFT calculated energy gap is 2.94 eV (421.46 nm) (calculations performed by Prof. Andrei Vedernikov).

To test this idea, our initial approach was an empirical one, as we were interested in first demonstrating a proof of concept for the photo-induced C-H bond activation at a Pt^{II} center in our system. The reactions were performed in Teflon-sealed J. Young NMR

tubes under argon that were placed in the Aldrich MicroPhotochemical Reactors containing a 6W circular LED strip with a spectral range of 435 – 445 nm (blue LEDs)or 405-415 nm (violet LEDs). In some experiments a 23W broad spectrum CFL or two 45W Kessil lamps (390 nm) were used. TFE-d_1 was utilized as the deuterium source and the reactions temperature was regularly monitored to ensure no heating was induced by the light source. Catalyst loading was typically 0.1–0.5 mol % with 0.050 mL benzene dissolved into 0.45 mL TFE-d_1 containing 150 mM D_2O and 2-10 μmol of **2.1**. The NMR tube was then clamped in place and placed into the direct path of the light source. When possible, the tube was placed into a reflective box containing the light source directly. Fans were utilized in order to ensure the maintenance of temperature control. The reactions temperature typically fluctuated around 23-25 ^oC but never exceeded 25 ^oC. Initial rates were recorded utilizing the same method, as reported in Chapter 2. Control experiments were performed in tandem utilizing identical reaction mixtures in the absence of light. No background H/D exchange was observed over a 24-hour reaction period when the samples were not exposed to light. However, when the samples were exposed to a light source for 24h, H/D exchange was detected via ^1H and ^2H-NMR. The initial results are summarized in Table 4.5.

Table 4.6. Light source comparison and effects on the observed rate constant $k_{Y,all}$ for the H/D exchange of benzene catalyzed by **1.5**.

Entry	Rate Constant, $k_{Y,all}$ ($M^{-1}Hr^{-1}(W^{-1})$), for Photochemical H/D Exchange			
	Blue LED (435-445 nm)	Violet LED (405-415 nm)	CFL (Broad)	Kessil Lamp (390 nm)
1	0.05	0.32	0.03	2.76
2	0.01*	0.05*	-	0.03*

*Values are adjusted per watt of power supplied by the light source

The intensity and the wavelength of the light source appeared to have a profound effect on the rate of the reaction. Entry 1 (Table 4.6) shows the apparent reaction rate

constants and entry 2 shows the rate constants normalized for the power of the light source. As shown in Table 4.6, blue LEDs, violet LEDs, a compact fluorescent lamp bulb, and 390 nm Kessil lamps were all able to induce this H/D exchange reaction between benzene and TFE-d_1 catalyzed by **2.1**. In fact, when utilizing 390 nm Kessil lamps, we were able to observe a rate constant as high as 2.76 $M^{-1}Hr^{-1}$, which is only ~2.5 times slower than that measured in our original experiments utilizing **2.1** at 80 °C (Table 2.1). However, when we account for the power applied by the high energy Kessil Lamps, the power-adjusted rate constantly drops to 0.03 $M^{-1}Hr^{-1}W^{-1}$. This value indicates that the 390 nm Kessil lamps are likely not operating in the optimal wavelength range for the photoexcitation of **1.5** under these reaction conditions, despite an overall significantly faster observed H/D exchange rate. However, higher power light sources could prove to be an effective method of improving this system, provided they operate at the optimal wavelength.

The 405-415 nm violet LED rings proved to be the most energy-efficient light sources from this screening. The power-adjusted value of k_{tot} was shown to be 0.05 $M^{-1}Hr^{-1}W^{-1}$ which is a 66% improvement over the 390 nm Kessil lamp. The blue LED and compact fluorescent bulbs were shown to not be the optimal light sources for this reaction, as indicated by their overall weaker performance. With these results in hand, we moved to explore the reactivity of our series of **4.1-X** complexes under these standardized photochemical reaction conditions (Scheme 4.13).

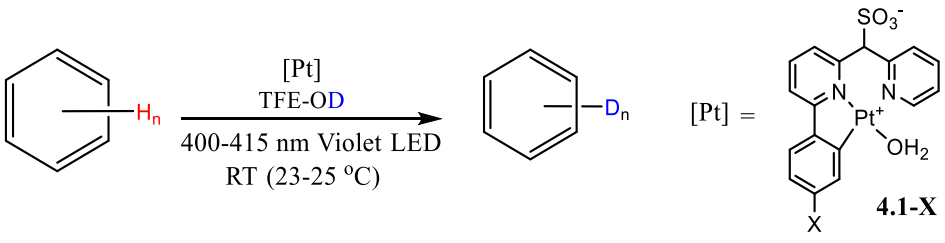

Scheme 4.13. Photo-induced H/D exchange of benzene in TFE-d_1 catalyzed by **4.1-X**.

Table 4.7. Catalyst performance comparison and the observed rate constant $k_{Y,all}$ for the H/D exchange of benzene under photochemical conditions in TFE-d_1 at 25 °C.

4.1-X	$k_{Y,\,all}$ M^{-1} h^{-1}	% Deuteration (24 hr)	TON
CF_3	**0.06**	**2.4**	**2**
F	**0.11**	**1.1**	**12**
H	**0.32**	**12**	**54**
iPr	**0.09**	**1.5**	**7**
tBu	**0.22**	**2.8**	**15**
OMe	**0.89**	**15.3**	**59**

The best performing catalyst was **4.1-OMe** with a $k_{Y,\,all}$ value of 0.89 $M^{-1}Hr^{-1}$ that allowed to achieve 15.3% deuteration of benzene over a 24-hour reaction period. This represents a significant improvement of the rate of the reaction, as compared to the catalyst **2.1**. The other catalysts screened were generally less reactive, and lost reactivity over time much more quickly than **2.1** or **4.1-OMe**. The high efficiency of the latter is likely due to methoxy group, which enhances the molar absorptivity and raises the energy of the catalyst HOMO, thereby reducing the HOMO-LUMO band gap and shifting the corresponding absorption to the wavelengths better matching the violet LEDs emission spectrum. Furthermore, the absorption profile of this catalyst (a shoulder with $\lambda_{max} \sim 404$ nm), and MO calculations support this hypothesis (See supporting information for more details). Two other electron rich species, **4.1-iPr** and **4.1-tBu**, were performing not as well, presumably, due to the fact that the alkyl substituents in them are weaker donors than OMe and do not have a large enough effect on the absorption of these complexes, as compared to OMe group. **4.1-CF_3** and **4.1-F** were expected to have a blue-shifted absorption maximum with a poorer overlap with the spectral range provided by violet LEDs, due to their electron withdrawing nature. With the optimal catalyst **4.1-OMe** in hand, we moved

forward in an attempt to assess extent of deuteration and catalyst longevity. We extended reaction time from 24 hours to 72 hours utilizing our standardized reaction conditions outlined above (Scheme 4.13). According to our observations, the extended reaction times did not yield a linear response in the catalyst's TON and a gradual decrease in the reaction rate was seen as the reaction time increased (Fig. 4.6). A maximum deuteration of 22% (1.6M C-D bonds) was achieved after 72 hours. This relationship suggests that catalyst deactivation is taking place. There were no obvious visual signs of catalyst decomposition, similar to what we the previously observed when running the reaction at 80 °C in the absence of light. Furthermore, the photochemical reaction between benzene and **4.1-OMe** proceeded even in the presence of Hg^0. Thereby suggesting that Pt^0 particles are not responsible for the observed H/D exchange reaction. This further suggests that a parallel decomposition pathway may be operational that is unique to this photochemically induced process.

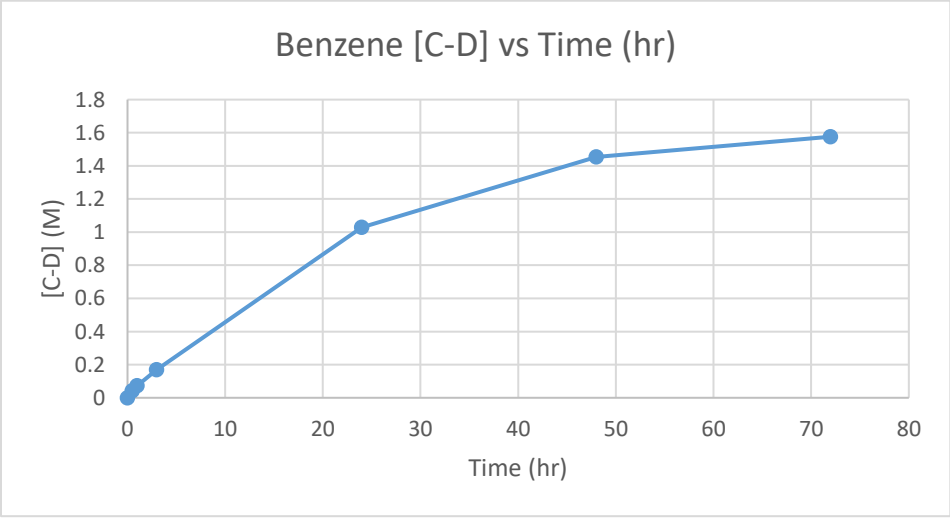

Figure 4.8. Benzene C-D bond formation vs time for the photo-induced H/D exchange reaction in TFE-d_1 catalyzed by **4.1-OMe**.

Since the loss in catalytic activity was slow, we were able to estimate the initial rate of the H/D exchange during first 24 hours of the reaction when a reasonably good linear relationship between [C-D] and the reaction time was observed. The degradation of catalyst **4.1-OMe** only becomes apparent at some time between 24hr to 48hr. We used this fact to explore the substrate selectivity of our photocatalyst in the H/D exchange reactions.

To exclude other possible factors that affect the observed reaction rates, we performed competitive H/D exchange reaction experiments where fluorobenzene or anisole mixtures with benzene were used. To that end, in an argon filled glovebox 0.025 mL of a competing substrate, fluorobenzene or anisole, and 0.025 mL of benzene were combined with 0.45 mL TFE-d_1. This solution was then used to dissolve 7.5 mg of **4.1-OMe** and the resulting mixture was placed into a J. Young Tube. The tube was then removed out of the glovebox and placed in our violet LEDs ring photoreactor. Simultaneous control experiments were also performed in the absence of light, as well as a side-by-side comparison of the reaction under thermal (80 ^{o}C) conditions.

The goal of this experiment was to assess the role that substrate identity has on the rate of H/D exchange catalyzed by **4.1-OMe** under thermal and photochemical conditions. Our previous, studies of the thermally driven H/D exchange of aromatic substrates catalyzed by **2.1** in TFE-d_1 at 80 ^{o}C (Chapter 2, Table 2.1) and by **4.1-OMe** (Table 4.2) showed that fluorobenzene *meta*-C-H bonds reacted at about 2-5 times slower rate than benzene C-H bonds, whereas anisole *meta*-C-H bonds were about 25-50% more reactive, as compared to benzene. For the case of our photochemically induced reactions, we were curious to determine whether this trend was maintained for our new catalyst **4.1-OMe**. Table 4.7 shows a direct comparison of relative rates of H/D exchange of the competing

substrates and benzene in reaction solutions of the same composition. In an argon filled glovebox, 6-8 mg of **4.1-OMe** was weighed out into a scintillation vial and dissolved into 0.9 mL TFE-d_1 solution containing 150 mM D_2O. Then 0.05 mL benzene and 0.05 mL fluorobenzene or anisole were added to the solution. The solution was then thoroughly mixed and 0.5 mL of the solution was transferred into JY Tubes with containing D_2O capillary insert. One tube was used as a thermal competitive reactive probe and the other was used under out photochemical conditions. Reaction were allowed to run for 24 hours and the relative intensity of ^{2}H-NMR resonance for a given C-H bond was then compared to the corresponding C-D resonance for benzene all measured using ^{2}H NMR spectroscopy. The relative rates of thermally driven reactions catalyzed by **4.1-OMe** determined in competition reaction (Table 4.8) matched the trends observed previously in the parallel experiments (Table 4.2). In the thermal reaction, fluorobenzene had a relative reactivity of 0.62±0.01 for its *meta*-C-H bonds 0.57±0.00 for the *para*-C-H bonds and 0.37±0.01 for the *ortho*-C-H bonds with benzene H/D exchange rate set as a reference (1.00) all values were calculated with a statistical correction for the total number of available C-H bonds of a given bond type.

Table 4.8. Relative reactivity of PhF, PhOMe and C_6H_6 in their H/D exchange reactions with TFE-d_1 catalyzed by **4.1-OMe** under thermal and photochemical conditions. Relative rates are normalized to account for variable C-H bond concentration.

Reaction Conditions	Benzene Rel. Rate.	R-Ph, Meta C-H	R-Ph, Para C-H	R-Ph, Ortho C-H
PhF:Benzene @80 °C	**1.00**	**0.62 ± 0.01**	**0.57 ± 0.0**	**0.37 ± 0.01**
PhF:Benzene Violet *hv*	**1.00**	**0.80 ± 0.1**	**0.86 ± 0.01**	**0.59 ±0.02**
PhOMe:Benzene @80 °C	**1.00**	**1.94 ± 0.04**	**1.90 ± 0.02**	**0.97 ± 0.00**
PhOMe:Benzene Violet hv	**1.00**	**0.72 ± 0.01**	**0.98 ± 0.02**	**0.37 ± 0.03**

All values shown here are relative integrations of a given C-H bond type compared to the C-D bonds of benzene for the competitive reaction. ± values are reported as the standard deviation of the integration value over two experiment trials.

However, when the solution of the same composition was reacted under photochemical conditions, the relative rate for the *meta*, *para*, and *ortho* positions of fluorobenzene changed to 0.80 ± 0.1, 0.86 ± 0.01, and 0.59 ± 0.02, respectively. This statistically significant increase in the relative reactivity suggests a decrease in the catalysts selective preference towards more electron rich aromatics than for the thermally driven system.

A more significant difference in the relative reactivity can be seen in the competition experiments involving anisole and benzene. For the thermal reactions, the relative rates of reaction for anisole *meta*-, *para*-and *ortho*-C-H bonds *vs* those of benzene are 1.94±0.04, 1.90±0.02, and 0.97±0.00, respectively. These observations suggest that the *meta*- and *para*-C-H bonds in anisole are roughly twice as reactive as C-H bonds in benzene under the thermal conditions at 80 ^{o}C. However, when the solution of the same composition was reacted under violet light, the selectivity preference changed dramatically, where now the *meta*, *para*, and *ortho*-C-H bonds of anisole have relative rates of 0.72±0.01, 0.98±0.02, and 0.37±0.03, respectively. The statistically significant change suggests that the *meta*- and *para*-C-H bonds of anisole are now slightly less reactive than benzene C-H bonds and anisole *ortho*-C-H binds are much less reactive than benzene C-H bonds, which represents a complete flip in the relative reactivity observed under thermal conditions.

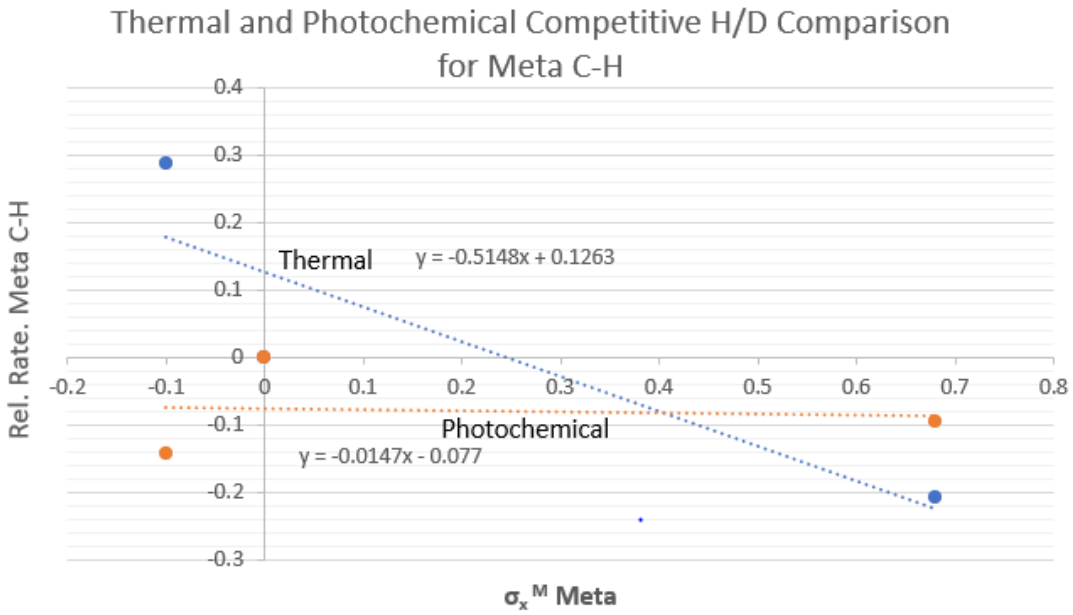

Figure 4.9. Hammett-Type plot for the relative rates of H/D exchange with TFE-d_1 for *meta*-C-H bonds of anisole and fluorobenzene vs benzene C-H bonds catalyzed by **4.1-OMe** at 80 °C and under violet LEDs. Thermal slope (blue): -0.51 ± 0.28; Photochemical slope (orange): -0.015 ± 0.17

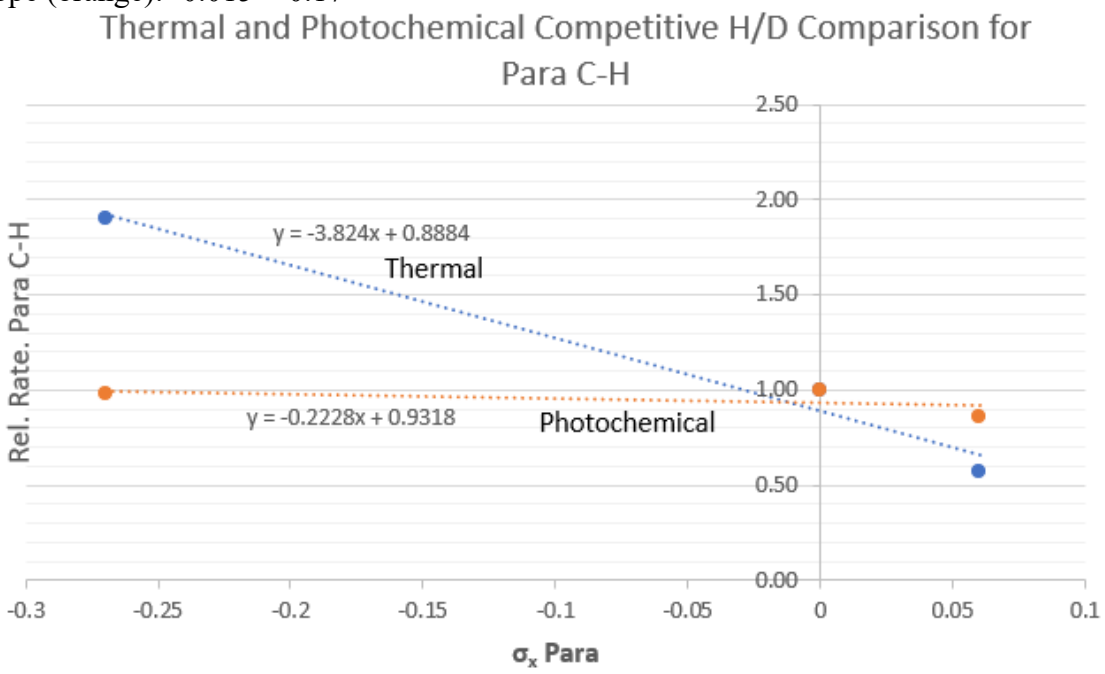

Figure 4.10. Hammett-Type plot for the relative rates of H/D exchange with TFE-d_1 for *meta*-C-H bonds of anisole and fluorobenzene vs benzene C-H bonds catalyzed by **4.1-OMe** at 80 °C and under violet LEDs. Thermal slope (blue): -3.82 ± 0.58; Photochemical slope (orange): -0.22 ± 0.36

When plotted against the respective σ_x^M *meta* and σ_x *para* values, a statistically significant difference in slopes of the thermal process vs the photochemical process can be easily visualized (Figures 4.9 and 4.10). It is notable that the C-H bonds in both benzene derivatives were less reactive than benzene C-H bonds under photochemical conditions. This observation may have significant implications on the potential RDS for the H/D exchange reaction mechanism catalyzed by complexes **4.1-X**.

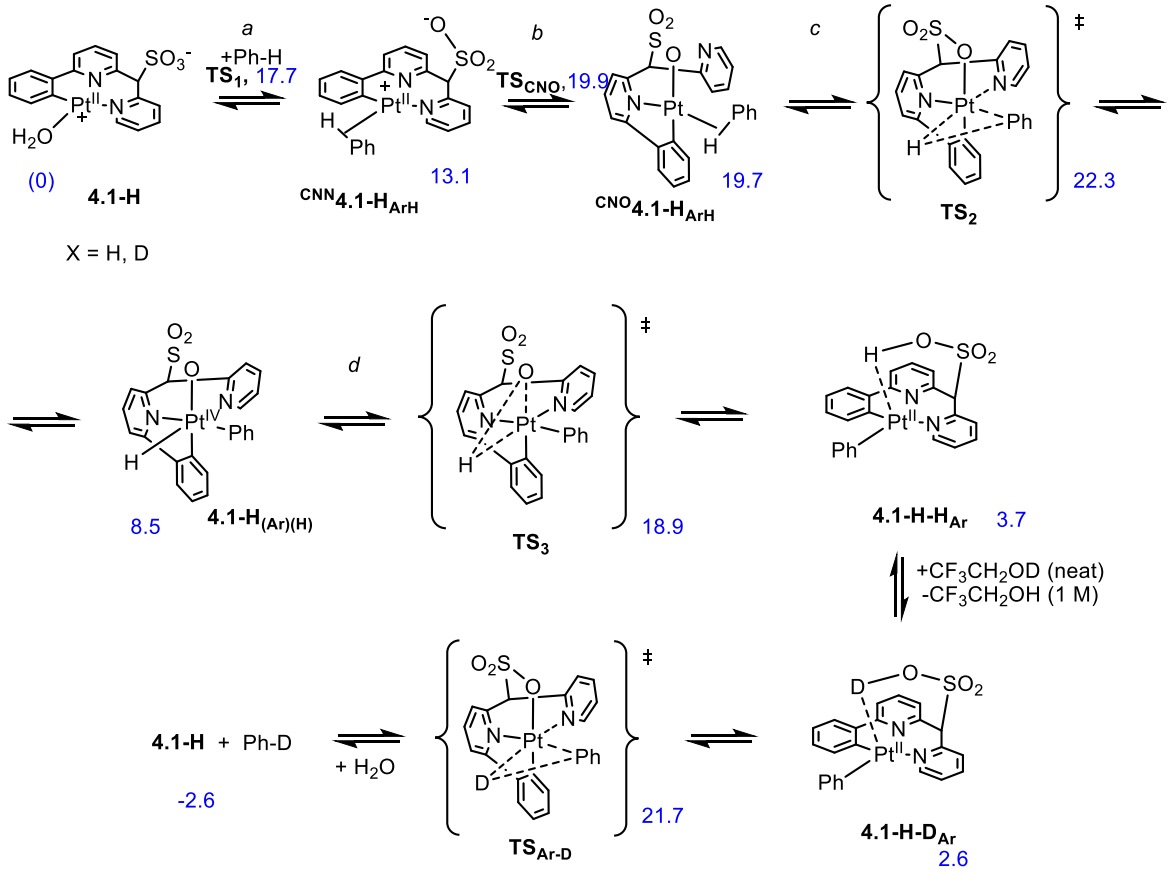

Scheme 4.14. Previously reported reaction sequence for the H/D exchange between arene C(sp^2)–H bonds and TFE-d_1 catalyzed by **1.5**. The standard Gibbs energies for individual reaction steps for TFE solutions at 298 K (blue font) are given for benzene (C_6H_6) in kcal/mol. (Computation performed by Prof. Andrei Vedernikov)[33,4]

Up to this point, we assumed that the RDS of the H/D exchange between benzene and TFE-d_1 catalyzed by **4.1-OMe** was the cleavage of a Pt^{II}-coordinated C-H bond in the σ-complex that is structurally similar to ^{CNO}**1.5**$_{ArH}$ (Scheme 4.14, step *c*).[49] This hypothesis was validated through computational support as well as an indirect experimental evidence

showing that the KIE (k_H/k_D) for this reaction is 1.7. Other research groups have had similar KIE observations in C-H activation of benzene with $Pt^{II}Me$ α-diimine complexes that corroborated their assumption that C-H bond cleavage is rate determining.[105] However, our data in Table 4.8 may suggest that at least for **4.1-OMe** the transition state TS_1 corresponding to arene coordination to a Pt^{II} center may not be much different energetically from the transition state TS_2 that corresponds to the arene C-H bond cleavage (Figure. 4.11, left).

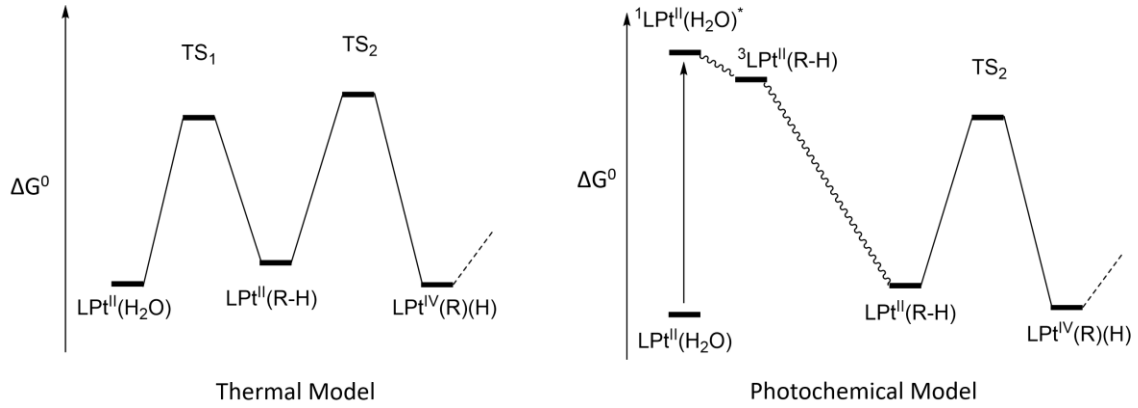

Figure 4.11. Simplified diagram depicting the relative energy levels of the transition state TS_1 corresponding to arene coordination to a Pt^{II} center and the transition state TS_2 that corresponds to the arene C-H bond cleavage under thermal conditions (left) and under photochemical conditions (right).

Figure 4.11 shows a simplified energy diagram representing two TS's that are of similar energy levels. These barriers notated TS_1 and TS_2 represent ligand exchange and C-H bond activation respectively, and they are the two potentially rate-determining steps for the H/D exchange reaction catalyzed by **4.1-X** complexes.

Under violet LED's light, a dramatic decrease of the energy of the TS_1 may be expected as a result of population of a Pt-O σ*-orbital. (Figure. 4.7, right). Under such conditions, the C-H bond cleavage TS_2 (Figure. 4.11, right) will become the product-determining step. The possible consequences of that change for the reaction selectivity

depend on whether TS_1 and TS_2 are of similar energy under thermal conditions / in the absence of light. If TS_1 is of about the same or a higher energy as TS_2, then the result of such dampening of the TS_1 would be that the RDS of the H/D exchange reaction will now be the TS_2. This change, likely, would lead to a change of the substrate selectivity that is now dictated purely by the TS_2. If the TS_1 is lower in energy than the TS_1, the H/D exchange reaction selectivity would remain unchanged due to the same TS_1 being the RDS.

Our experimental results (Table 4.8) indicate the first option is the most likely case in our system. The results of the competitive H/D exchange study show a dramatic change in substrate selectivity as a result of dampening the TS_1 barrier under photochemical conditions. This implies that there is a change in the RDS of the H/D exchange reaction when going from thermal to photochemical conditions. This implies that our initial assumption[33,49] of the RDS for the thermal reactions should be corrected. Since we observed a noticeable deuterium isotope effect in reaction (2.1), TS_2 contributes substantially to the to the overall reaction rate, and since the reaction selectivity changed upon switching from thermal to photochemical conditions, the difference in the energy of TS_1 and TS_2 is not big. As such, the RDS for thermal reactions is not clearly defined and both the TS_1 and the TS_2 are close in energy; it is impossible to say which one is a bit higher than the other and, therefore, is a formal RDS. In line with this explanation, the H/D exchange selectivity observed under thermal conditions favored electron rich aromatic compounds, as opposed to electron deficient aromatics or aliphatic C-H bond donors, which is consistent with the importance of the substrates donicity for the substrate coordination to a Pt^{II} center a noticeable contribution to the overall reaction rate.

4.5. Conclusions

This work has demonstrated that the reactivity of complexes of the **4.1-X** type in the H/D exchange involving C-H bonds of aromatic substrates is affected by the electronic effects of their substituent group, X. However, this effect is relatively weak and most of these catalysts suffer from bimolecular deactivation that limits their practical value. Unexpectedly, when X is a tBu group (complex **4.1-tBu**), the catalyst bimolecular deactivation is not observed, and the catalyst can exhibit an equally robust performance both under argon and under air. High catalyst turnover numbers exceeding 400 can be achieved using this thermally robust complex. That allows one to expand the selection of donors of exchangeable deuterium from a relatively exotic TFE-d_1, which is effective at 80 ^{o}C, to a much cheaper and widely accessible AcOD, although at an elevated temperature of 120 ^{o}C needed to overcome a stronger coordination of this solvent to a Pt^{II} center. As a result, **4.1-tBu** outperforms the original catalyst **2.1** in terms of the practical value in H/D exchange reactions, both due to its resistance to bimolecular deactivation, its increased solubility in most common solvents and stability under air. By using **4.1-tBu** we were able to achieve high deuterium incorporations up to 95-99% across a wide range of complex substrates including a series of polyfunctional pharmaceutical compounds, with low catalyst loadings ranging from 0.05-2.0 mol %. As an extension of what a "steric protection" with a 4-tBu group allows to achieve, a similar but an expectedly more active complex **4.50-tBu** was designed *in silico* and synthesized. Its reactivity was characterized to show that the presence of a fused cyclopenteno ring does, in fact, increase the reactivity of the Pt^{II} complex, and that the tBu group is an effective tool for the prevention of bimolecular catalyst deactivation which enhances catalyst lifetime and solubility. Overall,

we developed a practical, air stable, and essentially heteroatom tolerant system for the aromatic H/D exchange of complex aromatic molecules. Preliminary results have been gathered that suggest that our sulfonated CNN ligated Pt^{II} complexes may also be useful in the deuteration of alkenes and even show some reactivity toward donors of non-activated $C(sp^3)$-H bonds.

Photochemically propagated H/D exchange reactions utilizing **4.1-OMe** in TFE-d_1 utilizing violet LEDs have shown that low to moderate deuterium incorporation into aromatic substrates can be achieved at room temperature during the same timeframe as when using TFE-d_1 at 80 ^oC or AcOD at 120 ^oC. Importantly, a comparative analysis of our H/D exchange experiments ran under thermal and photochemical conditions provided preliminary evidence for a noticeable contribution of the substrate coordination to a Pt^{II} center to the overall rate of H/D exchange reactions under thermal conditions with **4.1-X** as catalysts. This contribution, apparently, is fully eliminated in the H/D exchange reactions set up under photochemical conditions.

Supporting Information for Chapter 4

I. General Information

Solvents, Reagents and Techniques for Synthesis

All solvents and reagents were purchased directly from commercial sources Aldrich, Oakwood, Pressure Chemical, Matrix, Acros Organics, Alfa Aesar, Fischer Chemical, AOB Chem, AK Scientific, or Cambridge Isotope Laboratories) Tetrahydrofuran was dried with sodium metal and was collected via fractional distillation. All other reagents and solvents were used without further purification unless otherwise noted. All glassware was dried overnight in an oven at 140^{o}C.

Solvents and Reagents for H/D Exchange Experiments

All solvents and reagents were purchased directly from commercial sources Aldrich, Oakwood, Pressure Chemical, Matrix, Acros Organics, Alfa Aesar, Fischer Chemical, AOB Chem, AK Scientific, or Cambridge Isotope Laboratories) and were used without further purification. All solvents and reagents were degassed and stored under and argon atmosphere prior to use. All JY tubes used were dried in overnight in an oven prior to use.

Instrumentation

^{1}H-, ^{2}H-, ^{13}C-, and ^{19}F- NMR Spectra were collected using various Bruker NMR instruments (AVANCE III HD NanoBay 400 MHz, AVANCE NEO 400 MHZ, Bruker DRX-500 MHz, and AVANCE III 600 MHz). All chemical shift (δ) values are reported with respect to an internal standard. NMR-data are reported as follows: chemical shift (δ) (multiplicity [s = singlet, d = doublet, t = triplet, q = quartet, quint = quintet, sept = septet, hept = heptet, m = multiplet, br = broad signal], coupling constants (J, Hz) and integration). All data was processed using Bruker Topspin 4.1.1 data processing program. All

quantitation involving extent of deuteration was performed by measure the loss ^{1}H-NMR signal intensity or the accumulation of C-D signals via ^{2}H-NMR.

High resolution mass spectra (HRMS) were recorded on a JEOL AccuTOF ESI-MS. All samples were introduced into the MS via an HPLC line containing an H_2O/MeOH mobile phas

II. Synthesis

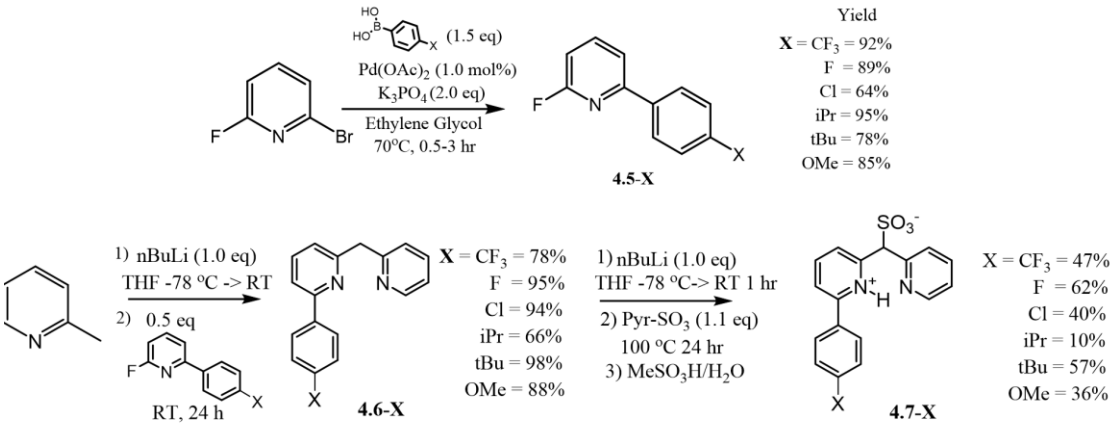

Scheme S4.1. Generalized ligand synthesis

Synthesis of 2-fluoro-6-aryl pyridines. 4.5-X (General Procedure A)

This Suzuki coupling procedure was modified from the literature method.[1] 120-240 mL of ethylene glycol was added dry round bottom flask and was heated to 70° C. After the solvent reached temperature, 10- 40g of K_3PO_4 (mono, tri or heptahydrate) (29-120 mmol 2.0 eq), 3.0-12.0 g of arylboronic acid (20-80 mmol 2.0 eq), and 2.5-10.0 g of 2,6 bromofluoropyridine (15-60 mmol 1.0 eq) were added sequentially to the flask and allowed to fully dissolve. Then 40-100 mg of $Pd(OAc)_2$ (0.15-0.4 mmol ~1.2 mol%) was added and the solution turned a transparent yellow color and the reaction was allowed to proceed for 2-3 hrs before quenching with a concentrated brine solution. The progress of the reaction was monitored via TLC using 90:10:0.1 (Hex:EtOAc:TEA) as a mobile phase. When the

reaction was complete the solution was extracted with 3x30 mL Et_2O and dried with $MgSO_4$ before removing solvent under vacuum to yield 3.8 g of a crude yellow oil. The product was purified via column chromatography using 90:10:0.1 (Hex:EtOAc:TEA). Typical product Rf range 0.4-0.6.

Alternative Procedure

65 mL of DI H_2O and 135 mL of isopropanol was added to a dry round bottom flask and heated to 80 ^oC. After the solvent reached temperature, 8.2 g of Na_3PO_4 (50.0 mmol, 2.0 eq), 5-8g of a 4-substituted phenylboronic acid derivative (~37.5 mmol, 1.5 eq), and 4.4g of 2,6-bromofluoropyridine (25.0 mmol, 1 eq) were added sequentially to the flask and allowed to fully dissolve. Then 84.2 mg of $Pd(OAc)_2$ (0.375 mmol, 1.5 mol%) was added and the solution briefly turned a transparent yellow color before quickly turning black. The reaction was allowed to proceed for 10-15 minutes before quenching with a concentrated brine solution. The progress of the reaction was monitored via TLC using 90:10:0.1 (Hex:EtOAc:TEA) as a mobile phase. Upon addition of brine, a white precipitate formed, and the solution was allowed to cool in the freezer for roughly 30 to 45 minutes or until room temperature was reached. Afterwards, the precipitate was filtered off to yield ~5-6g of a crude off-white viscous oil. The product was purified via column chromatography using 90:10:0.1 (Hex:EtOAc:TEA).

Synthesis of 2-fluoro-6-phenyl pyridine, 4.5-H

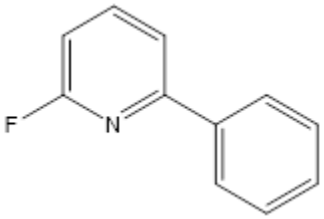

General procedure A was followed, utilizing 10.2 g of $K_3PO_4*7H_2O$ (30.1 mmol 2.0 eq), 3.66 g of phenylboronic acid (30.0 mmol 2.0 eq), 2.64g of 2,6 bromofluoropyridine (15.0

mmol 1.0 eq) and 40.0 mg of $Pd(OAc)_2$ (0.178 mmol 1.2 mol%) in 120 mL ethylene glycol. The reaction was allowed to run for 3 hours. After extraction with Et_2O and removing solvent under vacuum 3.8 g of a crude yellow oil was isolated. The product was purified via column chromatography using 90:10:0.1 (Hex:EtOAc:TEA) to yield 2.1 g (93% Yield) of a colorless viscous oil.

^{1}H-NMR (400 MHz, $CDCl_3$): δ (ppm) = 8.01 (m, 2H) 7.81 (q, 1H), 7.60 (dd 1H), 7.46 (m, 3H), 6.84 (dd, 1H)

^{19}F-NMR (400 MHz, $CDCl_3$): δ (ppm) = -66.28

^{13}C-NMR (100 MHz, $CDCl_3$): δ (ppm) = 164.48, 162.58, 156.39, 141.75, 137.67, 129.74, 128.90, 127.02, 117.40

Synthesis of 2-fluoro-6-(4-trifluoromethylphenyl) pyridine, 4.5-CF_3

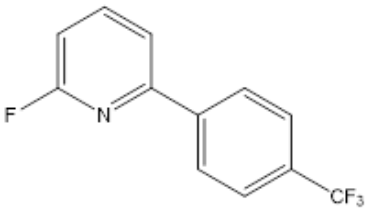

General procedure A was followed, utilizing 22.1g of K_3PO_4*$3H_2O$ (96 mmol 2.0 eq), 13.7 g of 4-trifluoromethylphenyl boronic acid (72 mmol 1.5 eq), and 8.4 g of 2,6 bromofluoropyridine (48 mmol 1.0 eq) and 80 mg of $Pd(OAc)_2$ (0.74 mol%) all dissolved into 240 mL ethylene glycol. The reaction was allowed to run for 3 hours. After extraction with Et_2O and removing solvent under vacuum 13.8 g of a crude yellow waxy solid was isolated. The product was purified via column chromatography using 90:10:0.1 (Hex:EtOAc:TEA) to yield 10.8 g (92% Yield) of a white solid.

^{1}H-NMR (400 MHz, $CDCl_3$): δ (ppm) = 8.13 (d, 2H), 7.90 (q, 1H), 7.73 (d, 2H), 7.68 (dd, 1H), 6.95 (dd, 1H)

^{19}F-NMR (400 MHz, $CDCl_3$): δ (ppm) = -62.69, 66.02

^{13}C-NMR (100 MHz, $CDCl_3$): δ (ppm) = 164.30, 162.62, 154.64, 142.0, 140.7, 127.4, 126.4, 117.9, 109.0

Synthesis of 2-fluoro-6-(4-fluorophenyl) pyridine, 4.5-F

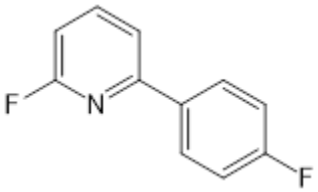

General procedure A was followed, utilizing 21.1 g of K_3PO_4*H_2O (96.0 mmol 2.0 eq), 10.1 g of 4-fluorophenylboronic acid (72.0 mmol 1.5 eq), 8.44g of 2,6 bromofluoropyridine (48.0 mmol 1.0 eq) and 120.0 mg of $Pd(OAc)_2$ (0.535 mmol 1.1 mol%) all dissolved into 240 mL ethylene glycol. The reaction was allowed to run for 2 hours. After extraction with Et_2O and removing solvent under vacuum 10 g of a crude yellow solid was isolated. The product was purified via column chromatography using 90:10:0.1 (Hex:EtOAc:TEA) to yield 8.2g (89% Yield) of a white solid.

^{1}H-NMR (400 MHz, $CDCl_3$): δ (ppm) = 7.93 (q, 2H), 7.73 (q, 1H), 7.46 (dd, 1H), 7.08 (t, 2H), 6.78, (dd, 1H)

^{19}F-NMR (400 MHz, $CDCl_3$): δ (ppm) = -66.62, -111.8

^{13}C-NMR (100 MHz, $CDCl_3$): δ (ppm) = 165.0, 162.5, 155.0, 154.9, 133.6, 128.8, 116.8, 115.7, 107.3

Synthesis of 2-fluoro-6-(4-chlorophenyl) pyridine, 4.5-Cl

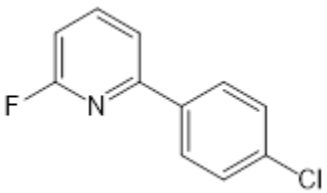

General procedure A was followed, utilizing 14 g of K_3PO_4*H_2O (64.0 mmol 2.0 eq), 5.1 g of 4-chlorophenylboronic acid (32.6 mmol 1.5 eq), 3.8 g of 2,6 bromofluoropyridine (22.0 mmol 1.0 eq) and 40.0 mg of

$Pd(OAc)_2$ (0.178 mmol 0.8 mol%) all dissolved into 240 mL ethylene glycol. The reaction was allowed to run for 1 hour. After extraction with Et_2O and removing solvent under vacuum 3.5 g of a crude yellow solid was isolated. The product was purified via column chromatography using 90:10:0.1 (Hex:EtOAc:TEA) to yield 2.9 g (64% Yield) of a colorless viscous oil.

^{1}H-NMR (400 MHz, $CDCl_3$): δ (ppm) = 7.96 (d, 2H), 7.86 (q, 1H), 7.61 (dd, 1H), 7.45 (m, 2H), 6.89 (dd, 1H)

^{19}F-NMR (400 MHz, $CDCl_3$): δ (ppm) = -66.3

^{13}C-NMR (100 MHz, $CDCl_3$): δ (ppm) = 164.2, 162.6, 155.1, 141.7, 135.8, 129.0, 128.2, 117.1, 108.0

Synthesis of 2-fluoro-6-(4-isopropylphenyl) pyridine, 4.5-iPr

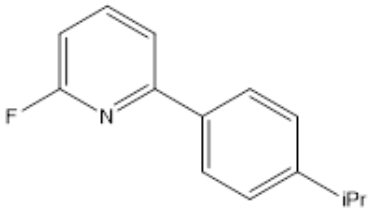

General procedure A was followed utilizing, 7.0 g of K_3PO_4*$3H_2O$ (33.1 mmol 2.0 eq), 4.2 g of 4-isopropylphenyl boronic acid (24.8 mmol 1.5 eq), and 2.9 g of 2,6 bromofluoropyridine (16.5 mmol 1.0 eq) and 40.0 mg of $Pd(OAc)_2$ (1.0 mol%) all dissolved into 120 mL ethylene glycol. The reaction was allowed to run for 2 hours. After extraction with Et_2O and removing solvent under vacuum 3.8 g of a crude yellow liquid was isolated. The product was purified via column chromatography using 90:10:0.1 (Hex:EtOAc:TEA) to yield 3.6 g (95% yield) of a colorless liquid

^{1}H-NMR (400 MHz, $CDCl_3$): δ (ppm) = 8.00 (d, 2H), 7.74 (q, 1H), 7.57 (dd, 1H), 7.36 (d, 2H), 6.80 (dd, 1H), 2.99 (sept, 1H), 1.32 (d, 6H)

^{19}F-NMR (400 MHz, $CDCl_3$): δ (ppm) = -66.5

^{13}C-NMR (100 MHz, $CDCl_3$): δ (ppm) = 164.6, 162.2, 156.4, 150.9, 141.8, 135.4, 127.0, 117.1, 107.2, 34.0, 24.0

Synthesis of 2-fluoro-6-(4-tert-butylphenyl) pyridine, 4.5-tBu

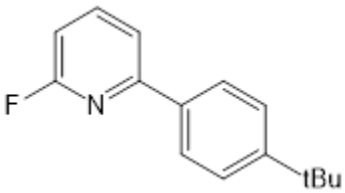

General procedure A was followed, utilizing 21.1 g of K_3PO_4*H_2O (96.0 mmol 2.0 eq), 10.8 g of 4-tert-butylphenylboronic acid (60.0 mmol 1.5 eq), 8.4 g of 2,6 bromofluoropyridine (47.0 mmol 1.0 eq) and 120.0 mg of $Pd(OAc)_2$ (0.535 mmol 1.1 mol%) all dissolved into 240 mL ethylene glycol. The reaction was allowed to run for 2 hours. After extraction with Et_2O and removing solvent under vacuum 12 g of a waxy off-white solid was isolated. The product was purified via column chromatography using 90:10:0.1 (Hex:EtOAc:TEA) to yield 8.5 g (78% Yield) of a colorless white solid.

^{1}H-NMR (400 MHz, $CDCl_3$): δ (ppm) = 7.96 (d, 2H), 7.82 (q, 1H), 7.61 (dd, 1H), 7.51 (d, 2H), 1.38 (s, 9H)

^{19}F-NMR (400 MHz, $CDCl_3$): δ (ppm) = -66.8

^{13}C-NMR (100 MHz, $CDCl_3$): δ (ppm) = 164.2, 162.6, 156.3, 152.9, 141.4, 134.7, 126.6, 125.7, 116.9, 107.2, 34.7, 31.2

Synthesis of 2-fluoro-6-(4-methoxy-butylphenyl) pyridine, 4.5-OMe

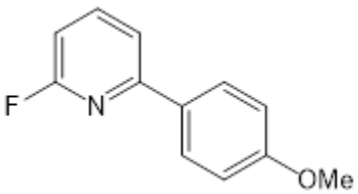

General procedure A was followed, utilizing 22 g of K_3PO_4*H_2O (96.0 mmol 2.0 eq), 10.9 g of 4-methoxyphenylboronic acid (72.0 mmol 1.5 eq), 8.44 of 2,6 bromofluoropyridine (48.0 mmol 1.0 eq) and 120.0 mg of $Pd(OAc)_2$ (0.535 mmol 1.1 mol%) all dissolved into 240 mL ethylene glycol. The reaction was allowed to run for 3

hours. After extraction with Et_2O and removing solvent under vacuum a crude yellow solid was isolated. The product was purified via column chromatography using 90:10:0.1 (Hex:EtOAc:TEA) to yield 8.2 g (85% Yield) of a white solid.

^{1}H-NMR (400 MHz, $CDCl_3$): δ (ppm) = 7.97 (d, 2H), 7.77 (q, 1H), 7.53 (dd, 1H), 6.98 (d, 2H), 6.79 (dd, 1H), 3.85 (s, 3H)

^{19}F-NMR (400 MHz, $CDCl_3$): δ (ppm) = -66.94

^{13}C-NMR (100 MHz, $CDCl_3$): δ (ppm) = 164.2, 162.6, 160.9, 156.0, 141.5, 130.1, 128.3, 116.4, 106.6, 55.4

Synthesis of 2-(4-X-phenyl)-6-(pyridin-2-ylmethyl) pyridines, 4.6-X (General Procedure B)

A dry 50 mL Schlenk tube was transferred into an argon filled glove box and was charged with 1-5 g 2-methylpyridine (10-50 mmol, 2.0 eq) and was subsequentially dissolved into 5-25 mL dry THF and the tube was sealed with a Teflon cap. The solution was then transferred onto a Schlenk line and cooled to -78 ^oC for 30 minutes under rapid stirring. Then, 11M nBuLi in hexanes (10-50 mmol, 2.0 eq) was added dropwise over 10 minutes under an argon atmosphere. The resulting dark red solution was then stirred at -78 ^oC until homogenous then was warmed to room temperature for 1 hour to allow for complete formation of the carbanion. Next, the solution was cooled back to -78 ^oC and 5-10 mL of a THF solution containing 1-5 g **4.5-X** (5-25 mmol, 1.0 eq) was added dropwise over 1 minute. The solution maintained a dark red coloration and was allowed to warm back to room temperature and allowed to react over 18-24 hr. The next day, the solution was quenched with 20 mL DI H_2O. The resulting mixture was then extracted with 3x30 mL of

Et_2O and the solvent was removed via reduced pressure to yield viscous red/orange oil. The compounds were further was purified via column chromatography with a 60:40:0.01 (Hex:EtOAc:TEA) mobile phase to yield a viscous orange oil. Rf values for these compounds range from 0.2-0.4.

Synthesis of 2-(4-trifluoromethylphenyl)-6-(pyridin-2-ylmethyl) pyridine, 4.6-CF_3

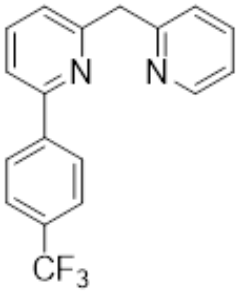

General procedure B was followed, utilizing 346 mg 2-methylpyridine (3.72 mmol, 2.0 eq), 450 mg 2-fluoro-6-(4-trifluoromethylphenyl) pyridine, **4.5-CF_3** (1.86 mmol, 1.0 eq) and 0.34 mL of 11 M nBuLi in hexanes. The reaction was allowed to run for 24 hr before quenching. After extraction and column purification 530 mg of a light orange oil was isolated (78% yield).

^{1}H-NMR (400 MHz, $CDCl_3$): δ (ppm) = 8.58 (dd, 1H) 8.12 (d, 2H), 7.72 (m, 3H), 7.65 (dt, 1H), 7.62 (d, 1H), 7.37 (d, 1H), 7.26 (d, 1H), 7.17 (dd, 1H), 4.44 (s, 2H)

^{19}F-NMR (400 MHz, $CDCl_3$): δ (ppm) = -62.53

^{13}C-NMR (100 MHz, $CDCl_3$): δ (ppm) = 159.6, 159.4, 155.31, 149.3, 142.8, 137.4, 136.6, 127.3, 125.6, 125.5, 123.8, 122.7, 121.5, 118.5, 47.4

Synthesis of 2-(4-fluorophenyl)-6-(pyridin-2-ylmethyl) pyridine, 4.6-F

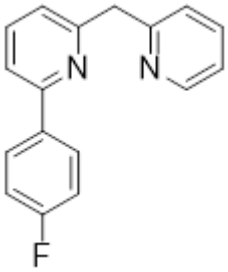

General procedure B was followed, utilizing 2.9 g 2-methylpyridine (31.6 mmol, 2.0 eq), 3.0 g 2-fluoro-6-(4-trifluoromethylphenyl) pyridine, **4.5-F** (15.7 mmol, 1.0 eq) and 2.9 mL of 11 M nBuLi in hexanes. The reaction was allowed to run for 24 hr before quenching. After extraction and column purification 3.9 g of a light orange oil was isolated (95% yield).

^{1}H-NMR (400 MHz, $CDCl_3$): δ (ppm) = 8.57 (d, 1H), 7.98 (q, 2H), 7.62 (m, 2H), 7.49 (d, 1H), 7.33 (d, 1H) , 7.13 (m, 4H), 4.42 (s, 2H)

^{19}F-NMR (400 MHz, $CDCl_3$): δ (ppm) = -113.3

^{13}C-NMR (100 MHz, $CDCl_3$): δ (ppm) = 164.6, 162.2, 159.6, 159.3, 155.8, 149.3, 137.3, 136.7, 135.6, 128.8, 123.8, 121.4, 117.7, 115.5, 47.7

Synthesis of 2-(4-chlorophenyl)-6-(pyridin-2-ylmethyl) pyridine, 4.6-Cl

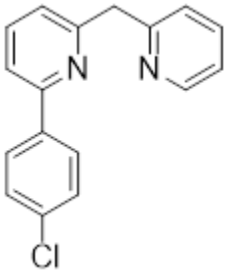

General procedure B was followed, utilizing 3.68 g 2-methylpyridine (39.6 mmol, 2.0 eq), 3.3 g 2-fluoro-6-(4-trifluoromethylphenyl) pyridine, **4.5-Cl** (19.8 mmol, 1.0 eq) and 3.6 mL of 11 M nBuLi in hexanes. The reaction was allowed to run for 24 hr before quenching. After extraction and column purification 5.2 g of a light orange oil was isolated (94% yield).

^{1}H-NMR (400 MHz, $CDCl_3$): δ (ppm) = 8.49 (d, 1H), 7.85 (d, 2H), 7.48 (m, 2H), 7.36 (d, 1H), 7.30 (d, 2H), 7.24 (d, 1H), 7.09 (d, 1H), 7.00 (dd, 1H), 4.35 (s, 2H)

^{13}C-NMR (100 MHz, $CDCl_3$): δ (ppm) = 159.5, 155.4, 137.8, 137.2, 136.4, 135.0, 128.7, 128.1, 124.6, 122.0, 121.4, 117.7, 47.46

Synthesis of 2-(4-isopropylphenyl)-6-(pyridin-2-ylmethyl) pyridine, 4.6-iPr

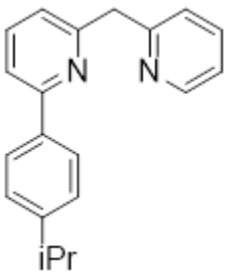

General procedure B was followed, utilizing 6.5 g 2-methylpyridine (69.6 mmol, 2.0 eq), 7.5 g 2-fluoro-6-(4-isopropylphenyl) pyridine, **4.5-iPr** (34.8 mmol, 1.0 eq) and 6.3 mL of 11 M nBuLi in hexanes. The reaction was allowed to run for 24 hr before quenching. After extraction and column purification 6.6 g of a light orange oil was isolated (66% yield).

^{1}H-NMR (400 MHz, $CDCl_3$): δ (ppm) = 8.56 (d, 1H), 7.96 (d, 2H), 7.60 (t, 1H), 7.56 (td, 1H), 7.53 (d, 1H), 7.35 (d, 1H), 7.33 (d, 2H), 7.14 (d, 1H), 7.09 (dd, 1H), 4.44 (s, 2H), 2.56 (sept, 1H), 1.29 (d, 6H)

^{13}C-NMR (100 MHz, $CDCl_3$): δ (ppm) = 159.8, 159.1, 156.9, 149.7, 149.2, 137.2, 137.1, 136.4, 126.9, 126.7, 123.8, 121.5, 121.4, 117.9, 47.6, 33.9, 22.9

Synthesis of 2-(4-tert-butylphenyl)-6-(pyridin-2-ylmethyl) pyridine, 4.6-tBu

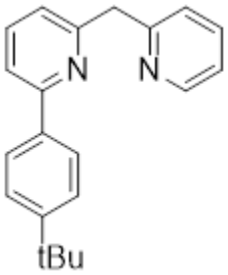

General procedure B was followed, utilizing 4.0 g 2-methylpyridine (43.6 mmol, 2.0 eq), 5.0 g 2-fluoro-6-(4-tert-butylphenyl) pyridine, **4.5-tBu** (21.8 mmol, 1.0 eq) and 4.0 mL of 11 M nBuLi in hexanes. The reaction was allowed to run for 24 hr before quenching. After extraction and column purification 6.5 g of a light orange waxy solid was isolated (98% yield).

^{1}H-NMR (400 MHz, $CDCl_3$): δ (ppm) = 8.59 (d, 1H), 7.95 (d, 2H), 7.65 (q, 2H), 7.57 (d, 1H), 7.50 (d, 2H), 7.39 (d, 1H), 7.12 (d, 2H), 4.45 (s, 2H), 1.38 (s, 9H)

^{13}C-NMR (100 MHz, $CDCl_3$): δ (ppm) = 159.7, 159.1, 156.9, 151.9, 149.1, 137.1, 136.8, 136.6, 126.6, 125.6, 123.9, 121.5, 118.0, 47.4, 31.3

Synthesis of 2-(4-methoxyphenyl)-6-(pyridin-2-ylmethyl) pyridine, 4.6-OMe

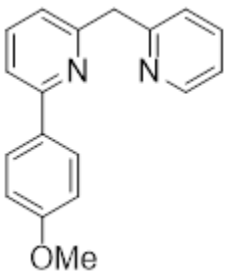

General procedure B was followed, utilizing 4.3 g 2-methylpyridine (46.2 mmol, 2.0 eq), 3.5 g 2-fluoro-6-(4-tert-butylphenyl) pyridine, **4.5-OMe** (22.4 mmol, 1.0 eq) and 4.2 mL of 11 M nBuLi in hexanes. The reaction was allowed to run for 24 hr before quenching. After

extraction and column purification 5.6 g of a light orange waxy solid was isolated (88% yield).

^{1}H-NMR (400 MHz, $CDCl_3$): δ (ppm) = 8.56 (d, 1H), 7.96 (d, 2H), 7.60 (m, 2H), 7.50 (d, 1H), 7.35 (d, 1H), 7.12 (m, 2H), 6.98 (d, 2H), 4.41 (s, 2H), 3.85 (s, 3H)

^{13}C-NMR (100 MHz, $CDCl_3$): δ (ppm) = 160.3, 159.7, 159.0, 156.5, 149.2, 137.1, 136.4, 132.2, 128.1, 123.4, 121.4, 121.1, 117.4, 114.1, 55.3, 47.5

Synthesis of 2-(4-X-phenyl)-6-(pyridin-2-ylmethyl) pyridine sulfonates (General Procedure C)

A dry 50-100 mL Schlenk tube was transferred into an argon filled glove box and was charged with 30 mL of a dry THF solution containing 1-5 g of 2-(4-X-phenyl)-6-(pyridin-2-ylmethyl) pyridine (1-10 mmol, 1.0 eq) and a stir bar the tube was sealed with a Teflon cap. The solution was then transferred onto a Schlenk line and cooled to -78 ^{o}C. Then, 11M nBuLi in hexanes (1-10 mmol, 1.0 eq) was added dropwise over 10 minutes under rapid stirring. The resulting dark red solution was then stirred at -78 ^{o}C until homogenous then was warmed to room temperature for 1 hour to allow for complete formation of the carbanion. After the anion formation was complete (indicated by a deep red coloration) the tube was then transferred back into an argon-filled glove box and 0.5-3 g pyridine-sulfur trioxide complex (1.1-11 mmol 1.1 eq) was added to the tube. The tube was again sealed with a Teflon cap, removed from the glove box, and then heated in a hot oil bath to 100 ^{o}C for 24 hours. The coloration of the solution should slowly change from a deep red to a light transparent red color alongside the formation of a large amount of white or off-white precipitate. After 24 hours, the reaction was quenched with 30 mL DI H_2O and the aqueous

phase was washed with an additional 3x15 mL Et_2O. The organic phase often contained up to 50% unreacted starting material that was able to be reused for the sulfonation reaction. The aqueous phase was then acidified using a 50% $MeSO_3H/H_2O$ ($MeSO_3H$ was used for an NMR handle, H_2SO_4 has also been used successfully) solution to a pH ~1-2. A large amount of white/off-white precipitate formed, and the solution was placed in the refrigerator to allow precipitation to occur over night. The following morning, the solution was filtered and rinsed with copious amounts of cold DI H_2O. The powder was then removed from the filter paper and dried in a desiccator oven at 80 ^oC overnight and yielded 1-5 g of a light brown/off white powder.

Synthesis of 2-(4-trifluoromethylphenyl)-6-(pyridin-2-ylmethyl) pyridine sulfonate,

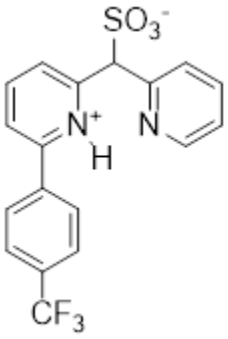

4.7-CF_3

General procedure C was followed, utilizing 3.1 g 2-(4-trifluoromethylphenyl)-6-(pyridin-2-ylmethyl) pyridine, **4.5-CF_3** (9.8 mmol, 1.0 eq), 1.7 g pyridine-sulfur trioxide complex (10.7 mmol, 1.1 eq) and 0.89 mL of 11 M nBuLi in hexanes. 2.2 g of unreacted starting material was isolated, and 532.0 mg of a light brown powder was isolated at the product (30% conversion, 47% Yield).

^{1}H-NMR (400 MHz, DMSO-*d_6*): δ (ppm) = 9.0 (d, 1H), 8.62 (t, 1H), 8.38 (d, 1H), 8.18 (d, 2H), 8.03 (m, 3H), 7.86 (t, 1H), 7.81 (d, 2H), 5.97 (s, 1H)

^{19}F-NMR (400 MHz, DMSO-*d_6*): δ (ppm) = -61.05

^{13}C-NMR (100 MHz DMSO-*d_6*): δ (ppm) = 154.37, 153.7, 151.9, 146.2, 142.5, 141.8, 138.6, 129.51, 127.9, 126.0, 125.3, 120.4, 69.24

ESI-MS in MeOH with KOH (- Mode): [$C_{18}H_{12}F_3N_2SO_3^-$] Calculated: 393.05 **Found:** 393.87

Synthesis of 2-(4-fluorophenyl)-6-(pyridin-2-ylmethyl) pyridine sulfonate, 4.7-F

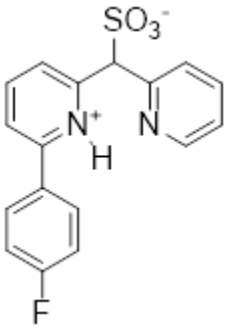

General procedure C was followed, utilizing 4.6 g 2-(4-fluorophenyl)-6-(pyridin-2-ylmethyl) pyridine, **4.5-F** (17.5 mmol, 1.0 eq), 3.1 g pyridine-sulfur trioxide complex (19.2 mmol, 1.1 eq) and 1.6 mL of 11 M nBuLi in hexanes. 3.8 g of a light brown powder was isolated at the product (62% Yield).

^{1}H-NMR (400 MHz, DMSO-*d*$_6$): δ (ppm) = 8.9 (d, 1H), 8.61 (t, 1H), 8.4 (d, 1H), 8.0 (m, 2H), 7.97 (t, 1H), 7.91 (d, 1H), 7.80 (d, 1H), 7.29 (t, 1H), 5.95 (s, 1H)

^{19}F-NMR (400 MHz, DMSO-*d*$_6$): δ (ppm) = -112.8

ESI-MS in MeOH with KOH (- Mode): [$C_{17}H_{12}FN_2SO_3^-$] Calculated: 343.06 **Found:** 343.77

^{13}C-NMR (100 MHz, DMSO-*d*$_6$): δ (ppm) = 164.5, 162.7, 154.1, 152.2, 146.0, 141.9, 138.5, 135.0, 129.4, 125.9, 124.3, 119.5, 116.5, 69.2

Synthesis of 2-(4-chlorophenyl)-6-(pyridin-2-ylmethyl) pyridine sulfonate, 4.7-Cl

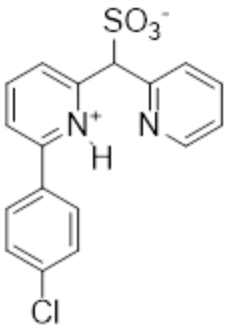

General procedure C was followed, utilizing 1.5 g 2-(4-chlorophenyl)-6-(pyridin-2-ylmethyl) pyridine, **4.5-Cl** (5.3 mmol, 2.0 eq), 843 mg pyridine-sulfur trioxide complex (5.8 mmol, 1.1 eq) and 0.5 mL of 11 M nBuLi in hexanes. 770 mg of a light brown powder was isolated at the product (40% Yield).

^{1}H-NMR (400 MHz, DMSO-*d*$_6$): δ (ppm) = 8.96 (d, 1H), 8.6 (dt, 1H), 8.37 (d, 1H), 7.97 (m, 5H), 7.82 (d, 1H), 7.51 (d, 2H), 5.94 (s, 1H)

^{13}C-NMR (100 MHz, DMSO-*d*$_6$): δ (ppm) = 154.0, 152.2, 146.1, 142.1, 138.8, 137.6, 134.4, 128.9, 126.0, 124.6, 119.7, 69.3

ESI-MS in MeOH with KOH (- Mode): [$C_{17}H_{12}ClN_2SO_3^-$] Calculated: 359.03 **Found:** 359.76

Synthesis of 2-(4-isopropylphenyl)-6-(pyridin-2-ylmethyl) pyridine sulfonate, 4.7-iPr

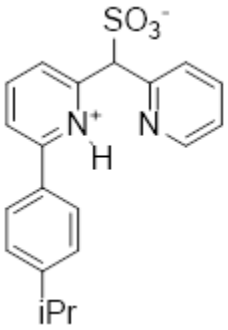

General procedure C was followed, utilizing 6.6 g 2-(4-chlorophenyl)-6-(pyridin-2-ylmethyl) pyridine, **4.5-iPr** (23.1 mmol, 1.0 eq), 4.4 g pyridine-sulfur trioxide complex (25.0 mmol, 1.1 eq) and 2.1 mL of 11 M nBuLi in hexanes. 1.0 g of a light brown powder was isolated at the product. ~4.0 g of unreacted starting material was isolated from the reaction.

^{1}H-NMR (400 MHz, DMSO-*d*$_6$): δ (ppm) = 8.94 (d, 1H), 8.56 (t, 1H), 8.33 (d, 1H), 7.95 (m, 2H), 7.86 (br, 3H), 7.76 (d, 1H), 7.32 (d, 2H), 5.93 (s, 1H), 2.91 (sept, 1H), 1.20 (d, 6H)

^{13}C-NMR (100 MHz, DMSO-*d*$_6$): δ (ppm) = 154.9, 153.8, 152.3, 150.5, 145.5, 142.2, 138.6, 136.0, 129.3, 127.2, 125.8, 124.1, 119.5, 69.2, 33.6, 24.2

ESI-MS in MeOH with KOH (- Mode): [$C_{20}H_{19}N_2SO_3^-$] Calculated: 367.11 **Found:** 367.85

Synthesis of 2-(4-tert-butylphenyl)-6-(pyridin-2-ylmethyl) pyridine sulfonate, 4.7-tBu

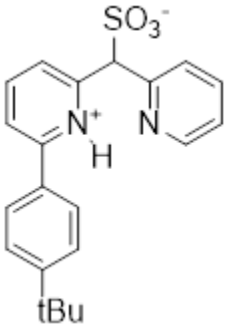

General procedure C was followed, utilizing 3.6 g 2-(4-tert-butylphenyl)-6-(pyridin-2-ylmethyl) pyridine, **4.5-tBu** (11.9 mmol, 1.0 eq), 2.0 g pyridine-sulfur trioxide complex (13.0 mmol, 1.1 eq) and 1.1 mL of 11 M nBuLi in hexanes. 2.6 g of a light brown powder was isolated at the product (57% Yield)

^{1}H-NMR (400 MHz, DMSO-*d*$_6$): δ (ppm) = 8.99, (d, 1H), 8.60 (t, 1H), 8.36 (d, 1H), 7.99 (m, 2H), 7.88 (d, 2H), 7.80 (d, 1H), 7.48 (d, 2H), 5.96 (s, 1H), 1.30 (s, 9H)

^{13}C-NMR (100 MHz, DMSO-*d*$_6$): δ (ppm) = 155.0, 153.2, 151.7, 145.8, 141.9, 138.7, 135.5, 129.4, 126.4, 125.4, 125.3, 123.69, 119.1, 68.5, 34.4, 31.2

ESI-MS in MeOH with KOH (- Mode): [$C_{21}H_{21}N_2SO_3^-$] Calculated: 381.13 **Found:** 381.90

Synthesis of 2-(4-methoxyphenyl)-6-(pyridin-2-ylmethyl) pyridine sulfonate, 4.7-OMe

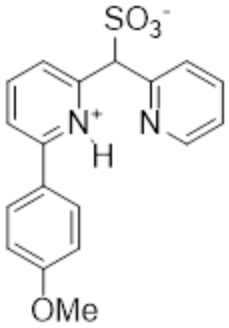

General procedure C was followed, utilizing 5.6 g 2-(4-methoxyphenyl)-6-(pyridin-2-ylmethyl) pyridine, **4.5-OMe** (20.2 mmol, 1.0 eq), 3.5 g pyridine-sulfur trioxide complex (22.4 mmol, 1.1 eq) and 1.8 mL of 11 M nBuLi in hexanes. 2.6 g of a light brown powder was isolated at the product (36% Yield)

^{1}H-NMR (400 MHz, DMSO-*d*$_6$): δ (ppm) = 8.97 (d, 1H), 8.57 (t, 1H), 8.33 (d, 1H), 7.96 (m, 4H), 7.88 (d, 1H), 7.75 (d, 1H), 7.03 (d, 1H), 5.92 (s, 1H), 3.81 (s, 3H)

^{13}C-NMR (100 MHz, DMSO-*d*$_6$): δ (ppm) = 160.8, 154.6, 153.7, 152.5, 145.4, 142.2, 138.7, 130.5, 129.2, 128.6, 125.7, 123.7, 119.1, 114.6, 69.2, 55.7

ESI-MS in MeOH with KOH (- Mode): [$C_{18}H_{15}N_2SO_3^-$] Calculated: 355.08 **Found:** 354.99

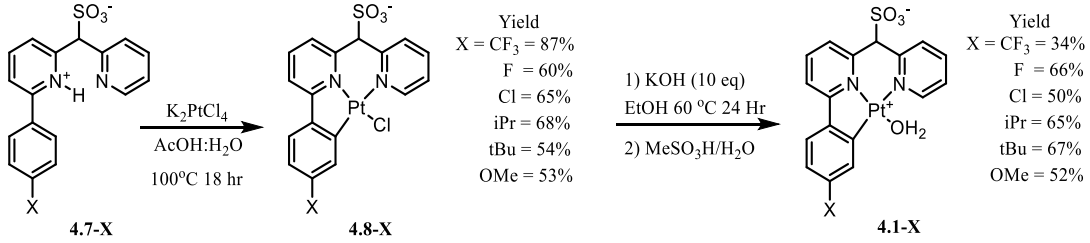

Scheme S4.2. Generalized Pt-OH_2 complex synthesis

<u>Synthesis p-X Ph(dpms) Pt-Cl Complexes (General Procedure D.1)</u>

A dry 50 mL Schlenk tube was charged with 300-750 mg (1-2 mmol 1.0 eq) zwitterionic ligand (the salt form may also be used for this step) and 415-830 mg (1-2 mmol, 1.0 eq) K_2PtCl_4 and a stir bar. The tube was then rinsed with a 2:1 AcOH/H_2O solution in order to dissolve any remaining solids on the walls of the tube. Then the tube was filled with 20 mL of the AcOH/H_2O solution and sealed with a Teflon cap and placed into a hot oil bath set

to 100 ^{o}C for 24 hours. After the reaction was complete, the solvent was removed, and the remaining crude solid was dissolved in hot methanol and filtered through a celite plug to remove any remaining KCl. After removing solvent again, the Pt-Cl complex product was isolated as a fine yellow powder.

Synthesis p-X Ph(dpms) Pt-OH_2 Complexes (General Procedure D.2)

Converting to the Pt-Cl complex to Pt-OH_2 was done by loading 500-1000 mg (1-2 mmol 1.0 eq) of Pt-Cl complex into a 100 mL round bottom flask containing a stir bar (crude **4.8-X** containing KCl may also be used for this step). The complex was then dissolved into 50 mL EtOH and 0.6-1.2 g of KOH (10-20 mmol, 10 eq) was added to the solution. The flask was then lightly sealed with a rubber stopper and placed into an oil bath heated to 60 ^{o}C for 24 hours under heavy stirring. After the reaction was completed, the solvent was removed via vacuum and the intermediate Pt-OEt complex was extracted with 30 mL of acetone. The solution was filtered through celite, and the solvent was again removed via vacuum and yielded a deep red solid. The solid was then redissolved into 30-50 mL H_2O and the pH of the solution was adjusted to ~1-2 using a 50% $MeSO_3H/H_2O$ solution. A large amount of tan/yellow precipitate formed upon acidification and the solution was placed in the refrigerator overnight to allow the complex to fully precipitate. The following morning, there was a large amount of precipitate present at the bottom of the beaker and the solution was only faintly yellow colored. The product was then isolated via vacuum filtration and washed with copious amounts of cold DI H_2O to remove any remaining acid. The isolated Pt-OH_2 complex was then dried at room temperature under vacuum for 24-48

hours (heating under vacuum must be avoided to prevent decomposition of the Pt-OH_2 bond) to yield 100-600 mg of a tan/yellow powder.

Synthesis of p-CF_3 Ph(dpms) Pt – Cl Complex, 4.8-CF_3

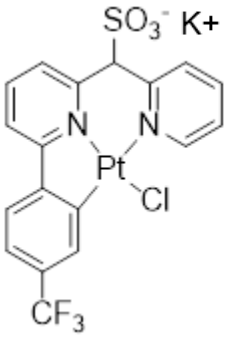

General procedure D.1 was followed, utilizing 447 mg **4.7-CF_3** (1.1 mmol, 1.0 eq), 470 mg K_2PtCl_4 (1.1 mmol, 1.0 eq) dissolved into 25mL 2:1 AcOH/H_2O solution. 651 mg of a light brown powder was isolated at the product (87% Yield).

^{1}H-NMR (400 MHz, DMSO-*d_6*): δ (ppm) = 9.58 (dd, 1H), 8.29 (s, 1H), 8.15 (t, 1H), 8.10 (m, 2H), 7.84 (t, 2H), 7.65 (d, 1H), 7.58 (t, 1H), 7.37 (dd, 1H), 6.02 (s, 1H)

^{19}F-NMR (400 MHz, DMSO-*d_6*): δ (ppm) = -61.0

ESI-MS in MeOH (- Mode): [$PtC_{18}H_{11}ClF_3N_2SO_3^-$] Calculated: 621.98 **Found:** 622.25

Synthesis of p-F Ph(dpms) Pt – Cl Complex, 4.8-F

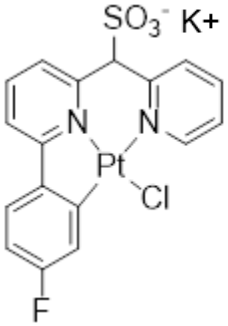

General procedure D.1 was followed, utilizing 340 mg **4.7-F** (0.98 mmol, 1.0 eq), 409 mg K_2PtCl_4 (0.98 mmol, 1.0 eq) dissolved into 25 mL 2:1 AcOH/H_2O solution. 360 mg of a yellow powder was isolated at the product (60% Yield).

^{1}H-NMR (400 MHz, DMSO-*d_6*): δ (ppm) = 9.58 (d, 1H), 8.07 (m, 2H), 7.93 (d, 1H), 7.82 (d, 1H), 7.73 (q, 1H), 7.63 (dd, 1H), 7.55 (q, 2H), 6.87 (dt, 1H), 5.96 (s, 1H)

^{19}F-NMR (400 MHz, DMSO-*d_6*): δ (ppm) = -110.8

^{13}C-NMR (100 MHz, DMSO-*d*$_6$): δ (ppm) = 165.6, 153.11, 152.31, 138.4, 129.7, 126.6, 125.9, 124.26, 120.45, 118.0, 110.3, 76.5, 59.6

ESI-MS in MeOH (- Mode): [$PtC_{17}H_{11}ClFN_2SO_3^-$] Calculated: 571.98 **Found:** 572.14

Synthesis of p-Cl Ph(dpms) Pt – Cl Complex, 4.8-Cl

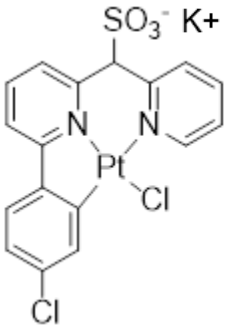

General procedure D.1 was followed, utilizing 680 mg **4.7-Cl** (1.8 mmol, 1.0 eq), 747 mg K_2PtCl_4 (1.8 mmol, 1.0 eq) dissolved into 35 mL 2:1 AcOH/H_2O solution. 731 mg of a yellow powder was isolated at the product (65% Yield).

^{1}H-NMR (400 MHz, DMSO-*d*$_6$): δ (ppm) = 9.56 (d, 1H), 8.08 (q, 2H), 7.96 (d, 1H), 7.91 (br, 1H), 7.82 (d, 1H), 7.67 (d, 1H), 7.56 (d, 2H), 7.11 (d, 1H), 5.98 (s, 1H)

ESI-MS in MeOH (- Mode): [$PtC_{17}H_{11}Cl_2N_2SO_3^-$] Calculated: 587.95 **Found:** 588.12

Synthesis of p-iPr Ph(dpms) Pt – Cl Complex, 4.8-iPr

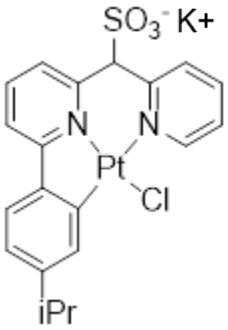

General procedure D.1 was followed, utilizing 775 mg **4.7-iPr** (2.1 mmol, 1.0 eq), 872 mg K_2PtCl_4 (2.1 mmol, 1.0 eq) dissolved into 35mL 2:1 AcOH/H_2O solution. 900 mg of a light brown powder was isolated at the product (68% Yield). Crude Material was used for ESI MS and for conversion to aqua complex

ESI-MS in MeOH (- Mode): [$PtC_{20}H_{18}ClN_2SO_3^-$] Calculated: 596.04 **Found:** 596.19

Synthesis of p-tBu Ph(dpms) Pt – Cl Complex, 4.8-tBu

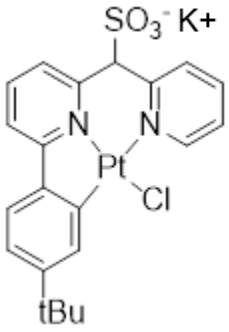

General procedure D.1 was followed, utilizing 380 mg **4.7-tBu** (0.98 mmol, 1.0 eq), 411 mg K_2PtCl_4 (0.98 mmol, 1.0 eq) dissolved into 25 mL 2:1 AcOH/H_2O solution. 345 mg of a yellow powder was isolated at the product (54% Yield).

^{1}H-NMR (400 MHz, DMSO-*d*$_6$): δ (ppm) = 9.61 (d, 1H), 8.04 (m, 3H), 7.86 (d, 1H), 7.80 (d, 1H), 7.55 (t, 1H), 7.49 (m, 2H), 7.06 (dd, 1H), 5.93 (s, 1H), 1.32 (s, 9H)

^{13}C-NMR (100 MHz, DMSO-*d*$_6$): δ (ppm) = 166.8, 153.1, 152.1, 150.9, 149.8, 143.0, 142.5, 138.1, 131.8, 129.7, 126.2, 124.0, 123.5, 120.4, 117.6, 76.5, 35.1, 31.7

ESI-MS in MeOH (- Mode): [$PtC_{21}H_{20}ClN_2SO_3^-$] Calculated: 610.05 **Found:** 610.26

Synthesis of p-OMe Ph(dpms) Pt – Cl Complex, 4.8-OMe

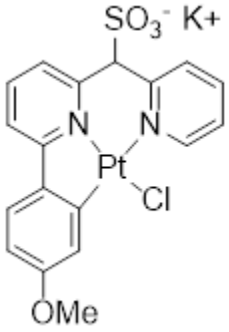

General procedure D.1 was followed, utilizing 600 mg p-OMe Ph(dpms) (1.7 mmol, 1.0 eq), 699 mg K_2PtCl_4 (1.7 mmol, 1.0 eq) dissolved into 35 mL 2:1 AcOH/H_2O solution. 553 mg of a light brown powder was isolated at the product (53% Yield).

^{1}H-NMR (400 MHz, DMSO-*d*$_6$): δ (ppm) = 9.59 (d, 1H), 8.07 (t, 1H), 7.97 (t, 1H), 7.79 (t, 2H), 7.54 (m, 3H), 7.41 (d, 1H), 6.62 (d, 1H), 5.89 (s, 1H), 3.77 (s, 3H)

^{13}C-NMR (100 MHz DMSO-*d*$_6$): δ (ppm) = 172.4, 166.7, 159.2, 153.2, 151.9, 149.9, 145.1, 138.5, 138.0, 129.7, 125.4, 124.0, 119.4, 117.1, 109.6, 76.4, 59.5, 21.5

ESI-MS in MeOH (- Mode): [$PtC_{18}H_{14}ClN_2SO_4^-$] Calculated: 584.00 **Found:** 584.20

Synthesis of p-CF_3 Ph(dpms) Pt – OH_2 Complex, 4.1-CF_3

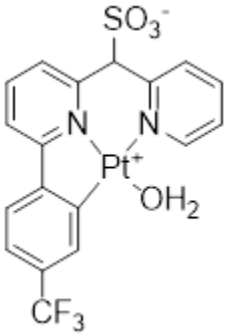

General procedure D.2 was followed, utilizing 575 mg p-CF_3 Ph(dpms) Pt-Cl (1.25 mmol, 1.0 eq), 840 mg KOH dissolved into 50 mL EtOH. After reaction work up, 260 mg of a fine light brown powder was isolated (34% Yield).

^{1}H-NMR (400 MHz TFE-d_1): δ (ppm) = 8.80 (d, 1H), 8.25-6.9 (br, 9 H), 5.79, (s, 1H)

^{1}H-NMR (400 MHz DMSO-*d_6*): δ (ppm) = 9.07 (d, 1H), 8.35 (m, 1H), 8.30 (t, 1H), 8.27 (t, 1H), 8.0 (m, 4H), 7.89 (d, 1H), 7.69 (t, 1H), 7.6 (d, 1H), 6.35 (s, 1H)

^{19}F-NMR (400 MHz, DMSO-*d_6*): δ (ppm) = -61.3

^{13}C-NMR (100 MHz, DMSO-*d_6*): δ (ppm) = 169.3 153.9, 153.1, 152.4, 150.1, 142.5, 141.8, 140.7, 130.4, 129.4, 128.2, 126.3, 125.6, 122.6, 120.9, 75.5

Synthesis of p-F Ph(dpms) Pt – OH_2 Complex, 4.1-F

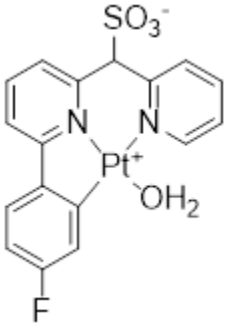

General procedure D.2 was followed, utilizing 366 mg p-F Ph(dpms) Pt-Cl (0.6 mmol, 1.0 eq), 660 mg KOH dissolved into 50 mL EtOH. After reaction work up, 222 mg of a fine yellow powder was isolated (66% Yield).

^{1}H-NMR (400 MHz, DMSO-*d_6*): δ (ppm) = 9.08 (d, 1H), 8.21 (m, 3H), 8.0 (d 1H), 7.97 (t, 1H), 7.76 (d, 1H), 7.67 (t, 1H), 7.46 (d, 1H), 7.11 (t, 1H), 6.28 (s, 1H)

^{19}F-NMR (400 MHz, DMSO-*d_6*): δ (ppm) = -108.0

^{13}C-NMR (100 MHz, DMSO-*d_6*): δ (ppm) = 164.2, 153.9, 152.4, 143.3, 142.4, 141.5, 129.3, 127.6, 127.0, 126.0, 120.7, 119.7, 112.8, 75.2

Synthesis of p-Cl Ph(dpms) Pt – OH_2 Complex, 4.1-Cl

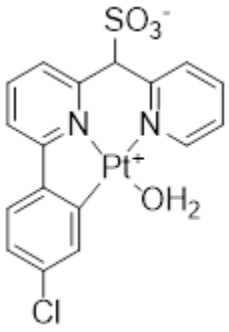

General procedure D.2 was followed, utilizing 382 mg p-Cl Ph(dpms) Pt-Cl (0.65 mmol, 1.0 eq), 660 mg KOH dissolved into 50 mL EtOH. After reaction work up, 120 mg of a fine light brown powder was isolated (34% Yield).

^{1}H-NMR (400 MHz, DMSO-*d_6*): δ (ppm) = 9.05 (d, 2H), 8.22 (m, 3H), 8.01 (d, 1H), 7.91 (d 1H), 7.80 (d, 1H), 7.67 (m, 2H), 7.33 (d, 1H), 6.29 (s, 1H)

^{13}C-NMR (100 MHz, DMSO-*d_6*): δ (ppm) = 164.0, 154.0, 152.7, 152.5, 145.0, 142.3, 141.6, 135.0, 133.6, 129.4, 127.2, 126.8, 126.2, 125.6, 120.0, 75.2,

Synthesis of p-iPr Ph(dpms) Pt – OH_2 Complex, 4.1-iPr

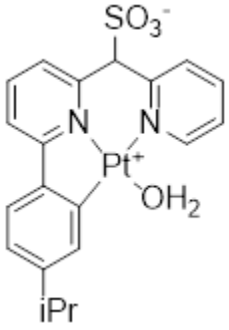

General procedure D.2 was followed, utilizing 413 mg p-iPr Ph(dpms) Pt-Cl (0.65 mmol, 1.0 eq), 660 mg KOH dissolved into 50 mL EtOH. After reaction work up, 245 mg of a fine light brown powder was isolated (65% Yield).

^{1}H-NMR (400 MHz, TFE-d_1): δ (ppm) = 9.03 (br, 1H), 8.23-7.10 (br, 10H), 5.88 (br, 1H)

^{1}H-NMR (400 MHz, DMSO-*d_6*): δ (ppm) = 9.05 (d, 1H), 8.16 (m, 3H), 7.68 (m, 4H), 7.13 (d, 1H), 6.2 (s, 1H), 2.93 (br, 1H), 1.25 (br, 6H)

Synthesis of p-tBu Ph(dpms) Pt – OH_2 Complex, 4.1-tBu

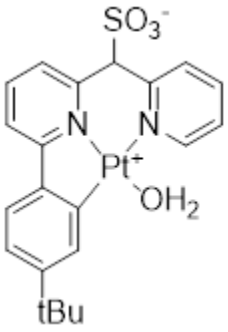

General procedure D.2 was followed, utilizing 1.0 g p-tBu Ph(dpms) Pt-Cl (1.66 mmol, 1.0 eq), 1.0g KOH dissolved into 50 mL EtOH. After reaction work up, 660 mg of a fine light brown powder was isolated (67% Yield).

^{1}H-NMR (400 MHz, TFE-d_1): δ (ppm) = 8.88 (d, 1H), 8.04 (t, 1H), 7.88 (t, 1H), 7.81 (d, 1H), 7.68 (d, 1H), 7.58 (t, 1H), 7.46 (d, 1H), 7.39 (d, 1H), 7.36 (s, 1H), 7.30 (d, 1H), 5.74 (s, 1H), 1.37 (s, 9H)

^{1}H-NMR (400 MHz, DMSO-*d_6*): δ (ppm) = 9.06 (d, 1H), 8.24 (dt, 1H), 8.17 (t, 1H), 8.12 (dd, 1H), 8.00 (d, 1H), 7.79 (d, 1H), 7.76 (d, 1H), 7.72 (dd, 1H), 7.66 (m, 1H), 6.22 (s, 1H), 1.33 (s, 9H)

^{13}C-NMR (100 MHz, DMSO-*d_6*): δ (ppm) = 165.3, 153.7, 153.5, 152.7, 152.6, 143.2, 141.9, 141.2, 140.3, 131.4, 129.3, 129.3, 126.4, 126.0, 125.0, 122.6, 119.1, 75.3, 35.2, 31.4

Synthesis of p-OMe Ph(dpms) Pt – OH_2 Complex, 4.1-OMe

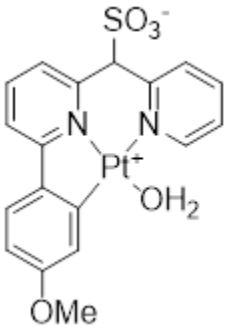

General procedure D.2 was followed, utilizing 623 mg p-OMe Ph(dpms) Pt-Cl (1.0 mmol, 1.0 eq), 660 mg KOH dissolved into 50 mL EtOH. After reaction work up, 305 mg of a fine yellow powder was isolated (52% Yield).

^{1}H-NMR (400 MHz, DMSO-*d_6*): δ (ppm) = 9.05 (d, 1H), 8.24 (t, 1H), 8.12 (t, 1H), 8.05 (d, 1H), 8.00 (d, 1H), 7.82 (d, 1H), 7.66 (m, 2H), 7.26 (s, 1H), 6.84 (dd, 1H), 6.19 (s, 1H), 3.83 (s, 3H)

^{13}C-NMR (100 MHz, DMSO-d_6): δ (ppm) = 165.3, 160.6, 153.8, 152.7, 152.18, 142.3, 141.8, 141.3, 138.4, 129.3, 126.9, 125.8, 120.1, 118.7, 110.7, 75.2, 55.

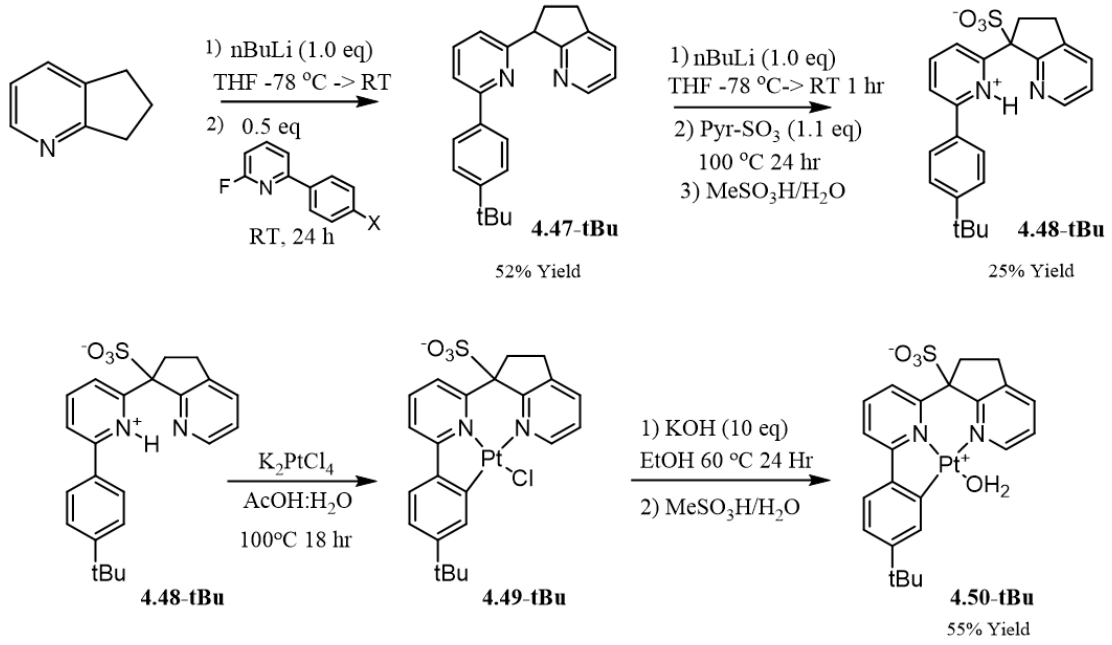

Scheme S4.3. Synthetic scheme for the production of **4.50-tBu**

General procedures **A-D2** were directly utilized in the production 4.50-tBu without any major deviations. These procedures proved to be compatible when utilizing 2,3 cyclopentenopyridine as a nuceleophile and bridging moiety.

Synthesis of pre-ligand, 4.47-tBu

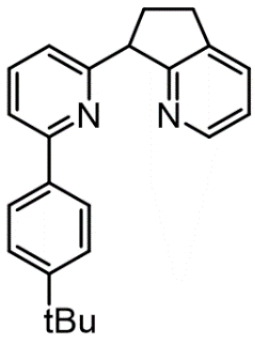

General procedure B was followed, utilizing 5.9 g 2,3-cyclopentenopyridine (49.6 mmol, 2.0 eq), 5.7 g 2-fluoro-6-(4-tert-butylphenyl) pyridine (24.8 mmol, 1.0 eq) and 2.0 eq of 11 M nBuLi in hexanes. The reaction was allowed to run for 24 hr before quenching. After extraction and column purification 4.2 g of a light red/orange oil was isolated (52% yield).

^{1}H-NMR (400 MHz, $CDCl_3$): δ (ppm) = 8.35 (d, 1H), 7.90 (d, 2H), 7.62 (t, 1H), 7.53 (m, 2H), 7.16 (d, 1H), 7.00 (dd, 1H), 4.62 (t, 1H), 3.01 (t, 3H) 2.6 (t, 3H), 1.33 (s, 9H)

Synthesis of sulfonated pre-ligand, 4.48-tBu

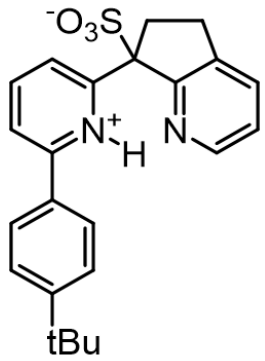

General procedure C was followed, utilizing 4.2 g of 4.47-tBu (12.8 mmol, 1.0 eq), 2.2 g pyridine-sulfur trioxide complex (14.0 mmol, 1.1 eq) and 1.1 mL of 11 M nBuLi in hexanes. 1.3 g of a light brown powder was isolated at the product (25% Yield)

^{1}H-NMR (400 MHz, DMSO-*d_6*): δ (ppm) = 8.76 (d, 1H), 8.49 (d, 1H), 7.95 (m, 2H), 7.82 (m, 4H), 7.64 (d, 2H), 3.29 (m, 2H), 3.11 (m, 1H), 2.66 (m, 1H), 1.30 (s, 9H)

^{13}C-NMR (100 MHz, DMSO-*d_6*): δ (ppm) = 158.5, 156.4, 154.1, 152.3, 145.1, 142.3, 139.8, 139.8, 138.9, 135.6, 127.1, 125.9, 122.4, 119.4, 76.87, 36.1, 34.9, 31.5, 29.1, 25.9

ESI-MS in MeOH (- Mode): [$C_{23}H_{23}N_2SO_3^-$] Calculated: 407.14 **Found:** 407.25

Synthesis of Pt – Cl Complex, 4.49-tBu

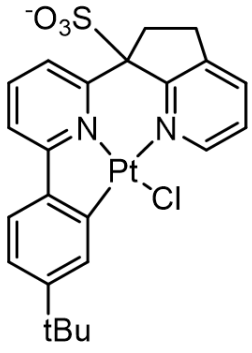

General procedure D.1 was followed, utilizing 408 mg 4.48-tBu (1.0 mmol, 1.0 eq), 415 mg K_2PtCl_4 (1.0 mmol, 1.0 eq) dissolved into 25 mL 2:1 AcOH/H_2O solution. 674 mg of a yellow powder was isolated as the product (99% yield).

^{1}H-NMR (400 MHz, DMSO-*d*$_6$): δ (ppm) = 9.45 (d, 1H), 8.06 (d, 1H), 8.01 (t, 1H), 7.96 (d, 1H), 7.88 (d, 1H), 3.40 (m, 1H), 3.30 (m, 1H), 3.00 (dd, 1H), 2.76 (m, 1H), 1.30 (s, 9H)

^{13}C-NMR (100 MHz, DMSO-*d*$_6$): δ (ppm) = 172.47. 166.70. 157.01, 150.72, 146.70, 143.86, 143.38, 142.50, 137.85, 134.59, 131.75, 127.20, 124.23, 123.85, 123.51, 120.46, 117.66, 80.87, 37.47, 35.14, 31.71, 29.26, 21.50,

ESI-MS in MeOH (- Mode): [$PtC_{23}H_{22}ClN_2SO_3^-$] Calculated: 636.07 **Found:** 636.90

Synthesis of Pt – OH_2 Complex, 4.49-tBu

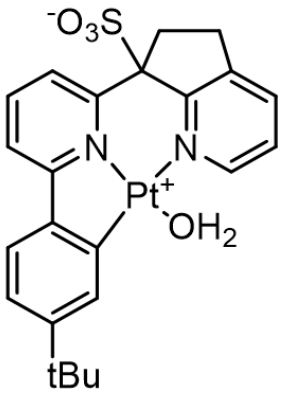

General procedure D.2 was followed, utilizing 677 mg **4.49-tBu** (1.0 mmol, 1.0 eq), 600 mg KOH (10 eq) dissolved into 50 mL EtOH. After reaction work up, 375 mg of a fine light brown powder was isolated (55% Yield).

^{1}H-NMR (400 MHz, AcOD-*d*$_4$): δ (ppm) = 8.40 (d, 1H), 7.99 (m, 3H), 7.79 (d, 1H), 7.65 (d, 1H), 7.50 (m, 3H), 7.19 (d, 1H), 7.02 (br, 1H), 3.15 (br, 2H), 2.91 (br, 2H), 1.34 (s, 9H)

^{1}H-NMR (400 MHz, DMSO-*d*$_6$): δ (ppm) = 8.84 (br , 1H), 8.15 (br, 3H), 7.69 (br m, 4H), 7.27 (br, 1H), 1.33 (br s, 9H). (ethylene bridge hydrogens obscured by H_2O peak)

III. Experimental Conditions for Catalytic H/D Exchange (Kinetics)

Scheme S4.4. Reaction scheme for kinetic studies for H/D exchange catalyzed by **4.1-X**

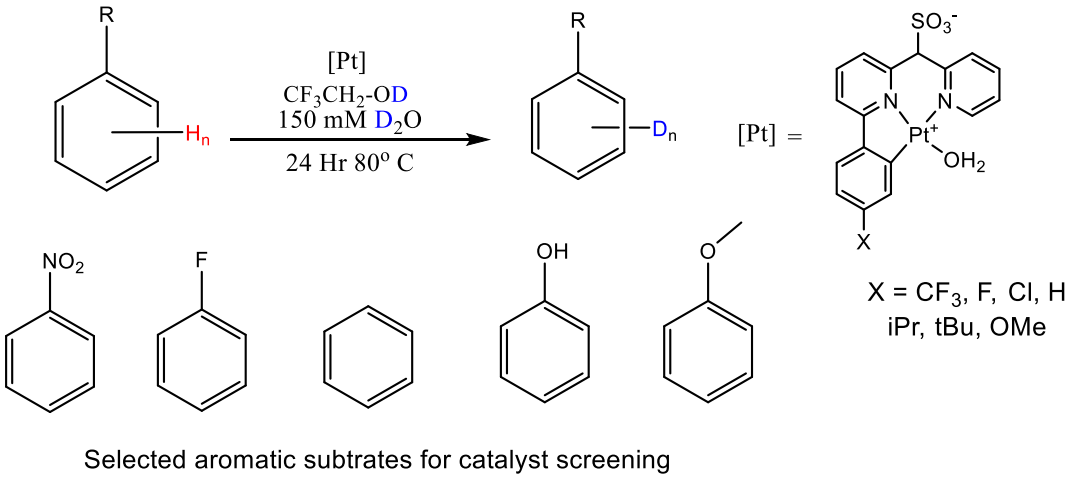

Selected aromatic subtrates for catalyst screening

General Procedure E for Kinetic H/D Exchange Experiments

In an argon filled glove box 0.4-0.7 mmol of substrate was transferred into a scintillation vial and dissolved in 0.45 mL in TFE-d_1 solution containing 150 mM D_2O. Then 2-7 mg of the **4.1**-X catalyst was weighed out and the TFE-d_1 solution was used to dissolve the catalyst and the mixture was then transferred into a dry JYoung (JY) NMR Tube and subsequently sealed with a Teflon cap. Then JY tube was then transferred out of the glovebox and pressurized under ~20 psi argon (to prevent reflux) and was then placed into an oil bath at the designated temperature for 24 hours. The sample was periodically removed from the oil bath for NMR measurements to monitor the progress of the reaction. Deuterium incorporation was measured via the evolution of signals (**Figure S4.1**) of a given bond type in ^{2}H-NMR. For quickly reacting substrate/catalyst combinations elevated temperature NMR experiments were performed instead of heating in an oil bath in order to ensure accurate reactivity profiles. All data points collected for generating rate constants were collected within the first 10% conversion of the substrate and allowed to fully react

for 24 hours to assess catalyst lifetime. For specific catalyst loading and substrate loading values see Tables S4.1-S4.6.

Table S4.1. Experimental Parameters for **4.1-CF$_3$** 0.45 mL TFE-d_1 solution at 80 °C

p-CF3	Cat. Loading (mg)	Cat. Loading (umol)	Substrate Loading (M)
Nitrobenzene	8.4	13.9	0.97
Fluorobenzene	6.1	10.1	1.31
Benzene	6.1	10.1	1.12
Phenol	4.7	7.8	0.94
Anisole	4.0	6.6	0.92

Table S4.2. Experimental Parameters for **4.1-F** in 0.45 mL TFE-d_1 solution at 80 °C

p-F	Cat. Loading (mg)	Cat. Loading (umol)	Substrate Loading (M)
Nitrobenzene	2.6	4.6	0.97
Fluorobenzene	2.6	4.7	1.31
Benzene	2.6	4.7	1.12
Phenol	2.9	5.1	1.18
Anisole	2.6	4.6	0.92

Table S4.3. Experimental Parameters for **4.1-Cl** in TFE-d_1 solution at 80 °C

p-Cl	Cat. Loading (mg)	Cat. Loading (umol)	Substrate Loading (M)
Nitrobenzene	0.3	0.5	0.97
Fluorobenzene	0.4	0.7	1.31
Benzene	1.8	3.1	1.12
Phenol	0.3	0.5	1.14
Anisole	0.3	0.5	0.92

Table S4.4. Experimental Parameters for **4.1-iPr** in 0.45 mL TFE-d_1 solution at 80 °C

p-iPr	Cat. Loading (mg)	Cat. Loading (umol)	Substrate Loading (M)
Nitrobenzene	3.2	5.4	0.97
Fluorobenzene	4.7	8.1	1.31
Benzene	4.7	8.1	1.12
Phenol	3.6	6.2	1.22
Anisole	3.6	6.2	0.92

Table S4.5. Experimental Parameters for **4.1-tBu** OH_2 in 0.45 mL TFE-d_1 solution at 80 ^oC

p-tBu	Cat. Loading (mg)	Cat. Loading (umol)	Substrate Loading (M)
Nitrobenzene	3.9	6.2	0.97
Fluorobenzene	4.4	7.0	1.31
Benzene	3.2	5.1	1.12
Phenol	4.9	7.8	1.14
Anisole	4.4	7.0	0.92

Table S4.6. Experimental Parameters for **4.1-OMe** in 0.45 mL TFE-d_1 solution at 80 ^oC

p-OMe	Cat. Loading (mg)	Cat. Loading (umol)	Substrate Loading (M)
Nitrobenzene	3.6	5.3	0.97
Fluorobenzene	3.1	4.6	1.31
Benzene	3.3	4.9	1.12
Phenol	3.6	5.3	0.48
Anisole	5.7	8.4	0.92

IV. Observed Rates and Extent of Deuteration

Observed rates of H/D exchange were measured via ^{1}H-NMR and ^{2}H-NMR spectroscopy by monitoring the change of the integral intensity of specific aromatic C-D signals of a given substrate over a 24-hour reaction period. Integration values were compared against an internal standard as reference. Simultaneous control experiments were run under otherwise identical reaction conditions in the absence of any catalyst. To properly attribute C-H signal intensity loss to H/D exchange a supplemental ^{2}H-NMR experiment was used as the primary method for quantitation and identification for the formation of C-D bonds (see **Figure S4.1**).

$$rate = -\frac{d[C-H]}{dt} = +\frac{d[C-D]}{dt}$$

The rate was calculated for each of a given substrates aromatic C-H bonds after during the 24-hour reaction period before a full 10% conversion. ^{2}H-NMR integration values were used to calculate the concentration of [C-H] bonds as a function of time. The initial rates were calculated for the period corresponding to ~10% deuteration of the substrate C-H bonds utilizing LINEST linear regression function on Microsoft Excel. A subsequent normalization for substrate concentration and catalyst loading was applied to calculate a rate constant (k_x).

$$k_x = \frac{rate}{[C-H] * [Pt]}$$

This observed rate constant was used as a means of comparing the various regioselective rates of H/D exchange for specific bond types across different substrates and reaction conditions.

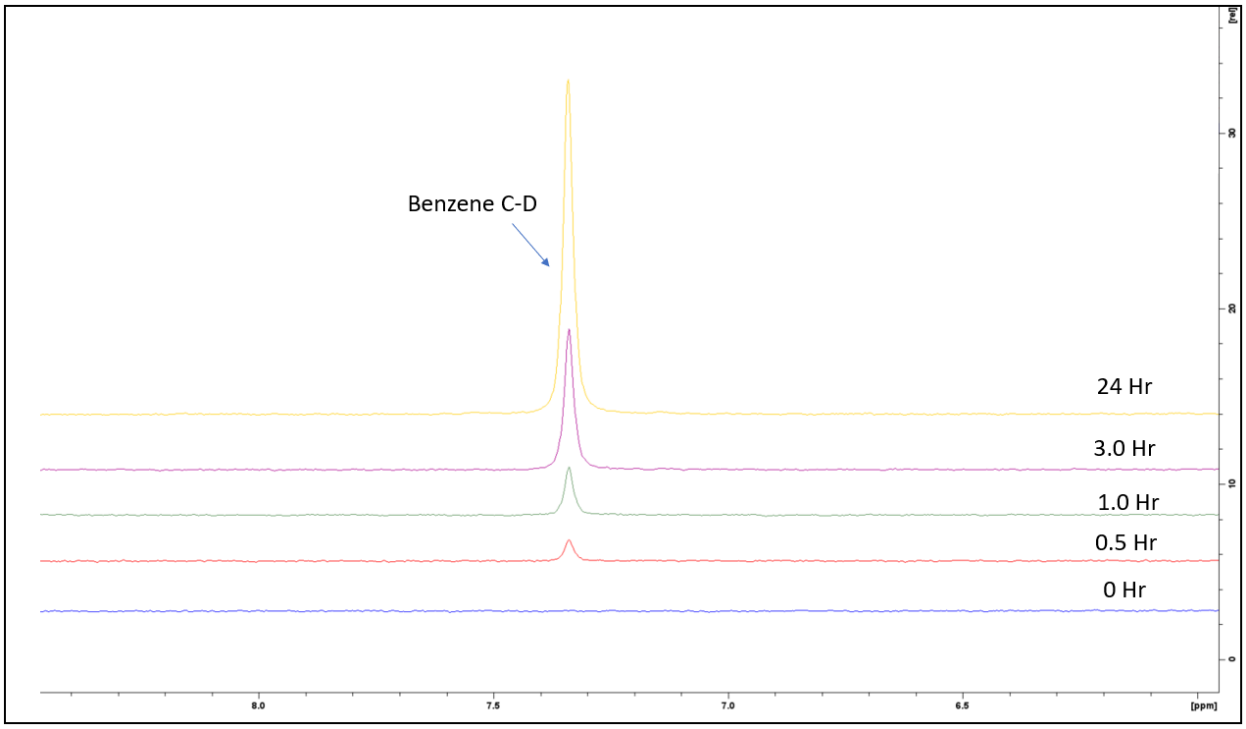

Figure S4.1. ^{2}H NMR Overlay for the H/D exchange reaction of Benzene in TFE-d_1 by p-tBu DPMS Pt-OH_2 at 80 ^{o}C.

Table S4.6. Substrate C(sp^2)-H bond-averaged values $k_{X,all}$ resulting from kinetics screening of catalysts **4.1-X** using substrates **6 - 10** in TFE-d_1 at 80 °C.

		Total Aromatic C-H ($k_{X,all}$) R-Ph Sub (M^{-1} Hr^{1})				
Entry	**4.1-X**	**NO_2**	**F**	**H**	**OH**	**OMe**
1	**CF_3**	**1.0 ± 0.4**	**4.5 ± 0.8**	**8.1 ± 0.4**	**9 ± 4**	**8 ± 2**
2	**F**	**0.0 ± N.D.**	**0.20 ± 0.01**	**5.8 ± 1.0**	**2.8 ± 0.2**	**4.0 ± 0.1**
3	**Cl**	**0.0 ± N.D.**	**0.50 ± 0.05**	**2.8 ± 0.1**	**3.1 ± N.D.**	**1.9 ± 0.1**
4	**H**	**0.3 ± 0.04**	**1.1 ± 0.3**	**6.8 ± 0.4**	**5.9± 0.6**	**6.5± 0.3**
5	**iPr**	**0.1 ± N.D.**	**0.2 ± N.D.**	**2.1 ± 0.5**	**1.2 ± 0.5**	**1.5 ± 0.2**
6	**tBu**	**0.5 ± 0.1**	**1.1 ± 0.1**	**6.8 ± 0.8**	**13 ± 2**	**10. ± 1**
7	**OMe**	**0.03 ± N.D.**	**0.08 ± 0.01**	**3.3 ± 0.3**	**4.8 ± 0.3**	**5 ± 1**

N.D. = Not Determined

Table S4.7. Substrate *meta*-C(sp^2)-H bond values $k_{X,meta}$ resulting from kinetics screening of catalysts **4.1-X** using substrates **4.6 – 4.10** in TFE-d_1 at 80 °C.

		Meta C-H ($k_{X,meta}$) R-Ph Sub (M^{-1} Hr^{-1})				
Entry	**4.1-X**	**NO_2**	**F**	**H**	**OH**	**OMe**
1	**CF_3**	**0.6 ± 0.4**	**4 ± 1**	**8.1 ± 0.4**	**10 ± 3**	**6 ± 1**
2	**F**	**0.0 ± N.D.**	**0.5 ± 0.1**	**6 ± 1**	**3.0 ± 0.2**	**4.9 ± 0.1**
3	**Cl**	**0.0 ± N.D.**	**0.6 ± 0.1**	**2.8 ± 0.1**	**2.6 ± N.D.**	**2.3 ± 0.5**
4	**H**	**0.4 ± 0.1**	**1.4 ± 0.1**	**6.8 ± 0.4**	**7.3 ± 0.4**	**8.6 ± 0.5**
5	**iPr**	**0.2 ± N.D.**	**0.2 ± N.D.**	**2.1 ± 0.5**	**1.1 ± 0.6**	**1.3 ± 0.5**
6	**tBu**	**0.8 ± 0.1**	**1.2 ± 0.1**	**6.8 ± 0.8**	**8 ± 1**	**13 ± 2**
7	**OMe**	**0.02 ± N.D.**	**0.08 ± 0.07**	**3.3 ± 0.3**	**5.0 ± 0.3**	**5 ± 1**

N.D. = Not Determined

Table S4.8. Substrate *para*-C(sp^2)-H bond values $k_{X,meta}$ resulting from kinetics screening of catalysts **4.1-X** using substrates **4.6 – 4.10** in TFE-d_1 at 80 °C.

		Para C-H ($k_{X,meta}$) R-Ph Sub (M^{-1} Hr^{-1})				
Entry	**4.1-X**	**12**	**F**	**H**	**OH**	**OMe**
1	**CF_3**	**1.5**	**4.8**	**8.1**	**11.3**	**15.3**
2	**F**	**0.0**	**0.3**	**5.8**	**2.7a**	**3.4a**
3	**Cl**	**0.0**	**0.7**	**2.8**	**3.29a**	**2.3**
4	**H**	**0.9**	**1.3**	**6.8**	**4.9a**	**5.1a**
5	**iPr**	**0.15**	**0.17**	**2.1**	**1.18a**	**1.2**
6	**tBu**	**0.72**	**1.00**	**6.8**	**16.9**	**11.6**
7	**OMe**	**0.04a**	**0.09**	**3.3**	**4.5**	**3.2a**

N.D. = Not Determined. a) notates combined *ortho/para* combined values

Table S4.9 Substrate *ortho*-C(sp^2)-H bond values $k_{X,meta}$ resulting from kinetics screening of catalysts **4.1-X** using substrates **4.6 – 4.10** in TFE-d_1 at 80 °C.

		Ortho C-H ($k_{X,meta}$) R-Ph Sub (M^{-1} Hr^{-1})				
Entry	**4.1-X**	**NO_2**	**F**	**H**	**OH**	**OMe**
1	**CF_3**	**1.7**	**4.6**	**8.1**	**7.8**	**7.0**
2	**F**	**0.0**	**0.2**	**5.8**	**2.7a**	**3.4a**
3	**Cl**	**0.0**	**0.4**	**2.8**	**3.29a**	**1.4**
4	**H**	**0.0**	**0.7**	**6.8**	**4.9a**	**5.1a**
5	**iPr**	**0.0**	**0.15**	**2.1**	**1.18a**	**0.6**
6	**tBu**	**0.0**	**0.96**	**6.8**	**13.6**	**3.7**
7	**OMe**	**0.04a**	**0.05**	**3.3**	**4.6**	**3.2a**

N.D. = Not Determined . a) notates combined *ortho/para* combined values

24 Hour H/D Exchange Experiments

As a compliment to the kinetic assays outlined above, each of the catalyst/substrate pairs were allowed to react for a full 24 hours. After which, the extent of deuterium incorporation

was measured for each distinctly resolvable C-H position. The extent of deuteration was then compared to the expected statistical values (calculation shown below) to allow for the determination of yield. The concentration of the generated C-D bonds over the reaction period was also used to determine the TON for the respective catalyst/substrate combination.

$$\%Yield = \frac{Measured\ \%D\ incorporation}{Exp.Statistical}\ x\ 100$$

$$Exp.Statistical\ Deuteration\ = \frac{[Exchangable\ D]}{[Exchangeable\ D] + [C-H]} x100$$

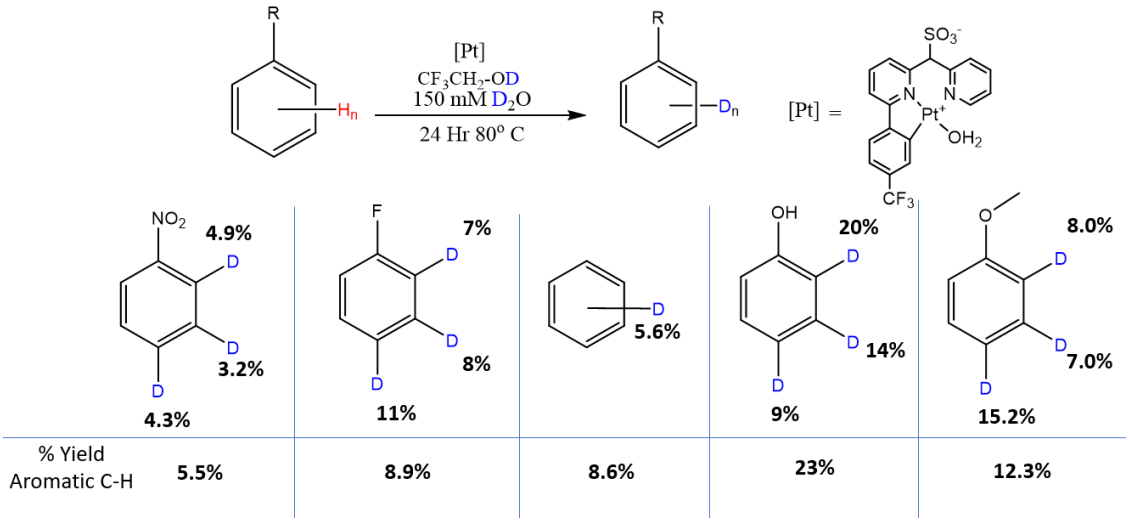

Figure S4.2. 24 Hour Yields for Arene Screening of **4.1-CF$_3$** in 0.45 mL TFE-d$_1$ solution at 80°C (Conditions shown in Table S4.1)

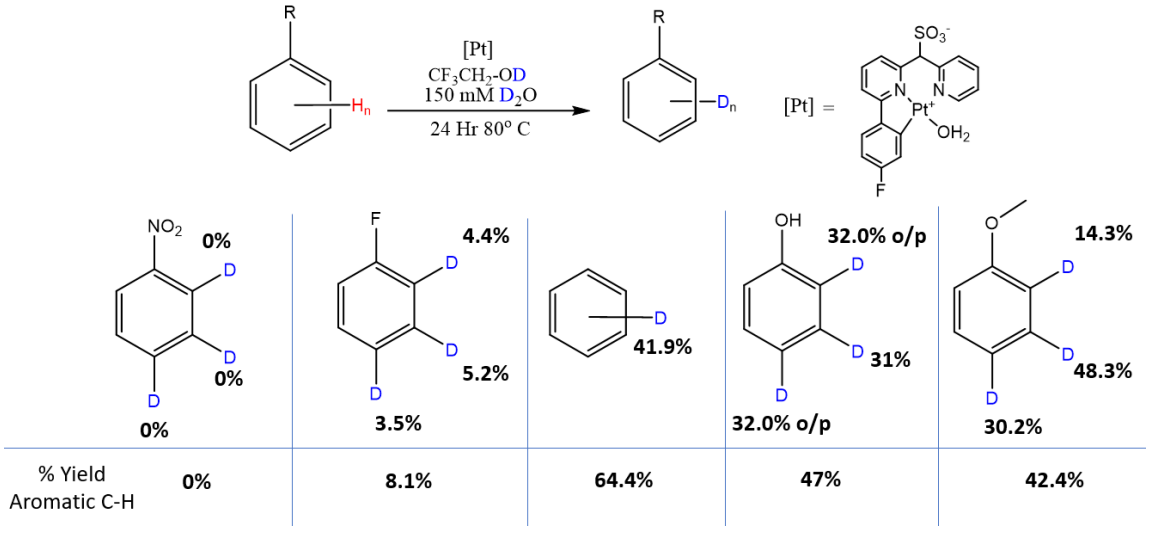

Figure S4.3. 24 Hour Yields for Arene Screening of **4.1-F** in 0.45 mL TFE-d_1 solution at 80°C (Conditions shown in Table S4.2)

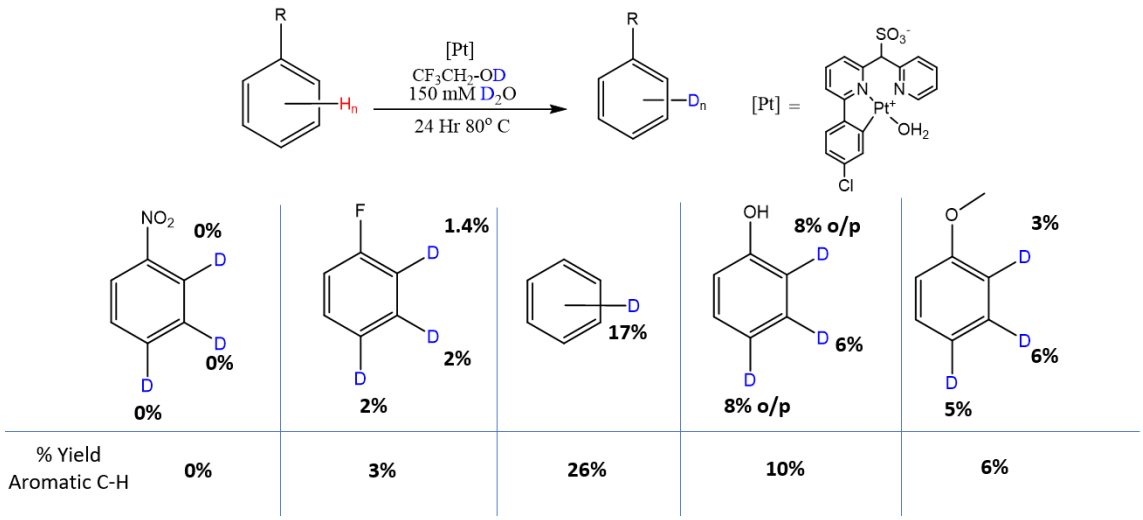

Figure S4.4. 24 Hour Yields for Arene Screening of **4.1-Cl** in 0.45 mL TFE-d_1 solution at 80°C (Conditions shown in Table S4.3)

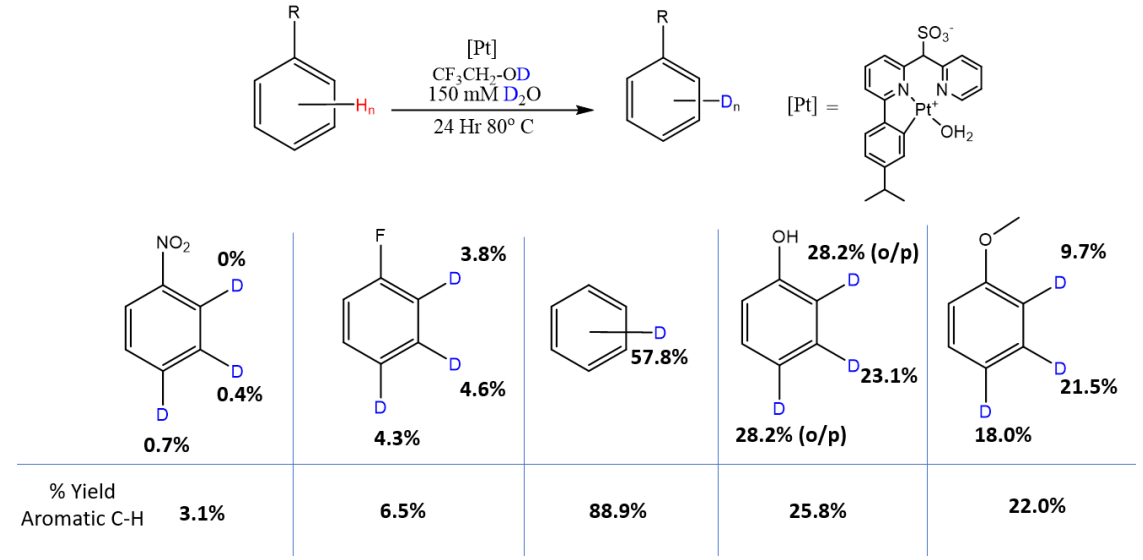

Figure S4.5. 24 Hour Yields for Arene Screening of **4.1-iPr** in 0.45 mL TFE-d_1 solution at 80°C (Conditions shown in Table S4.4)

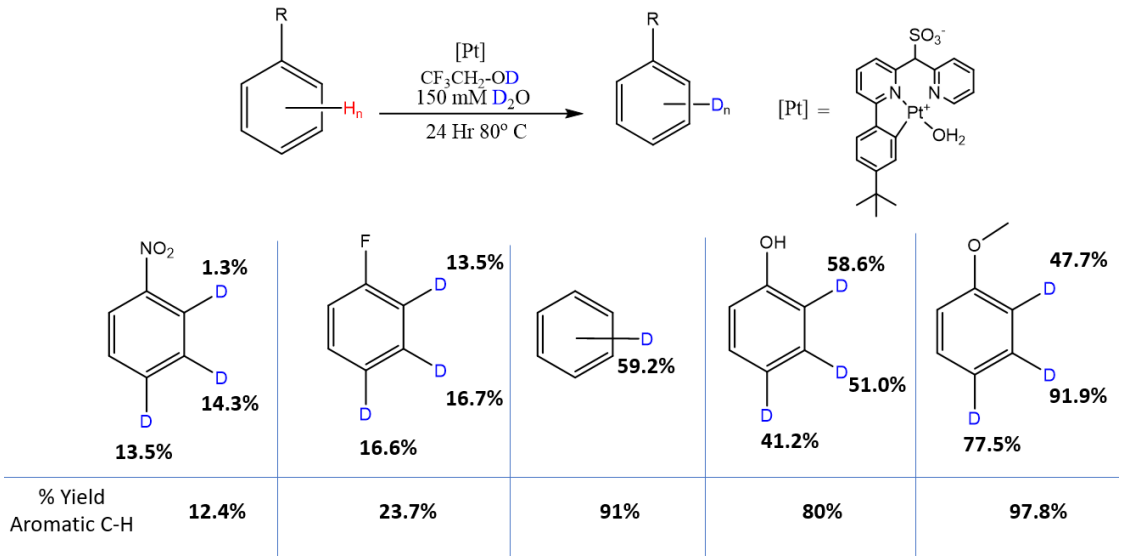

Figure S4.6. 24 Hour Yields for Arene Screening of **4.1-tBu** in 0.45 mL TFE-d_1 solution at 80°C (Conditions shown in Table S4.5)

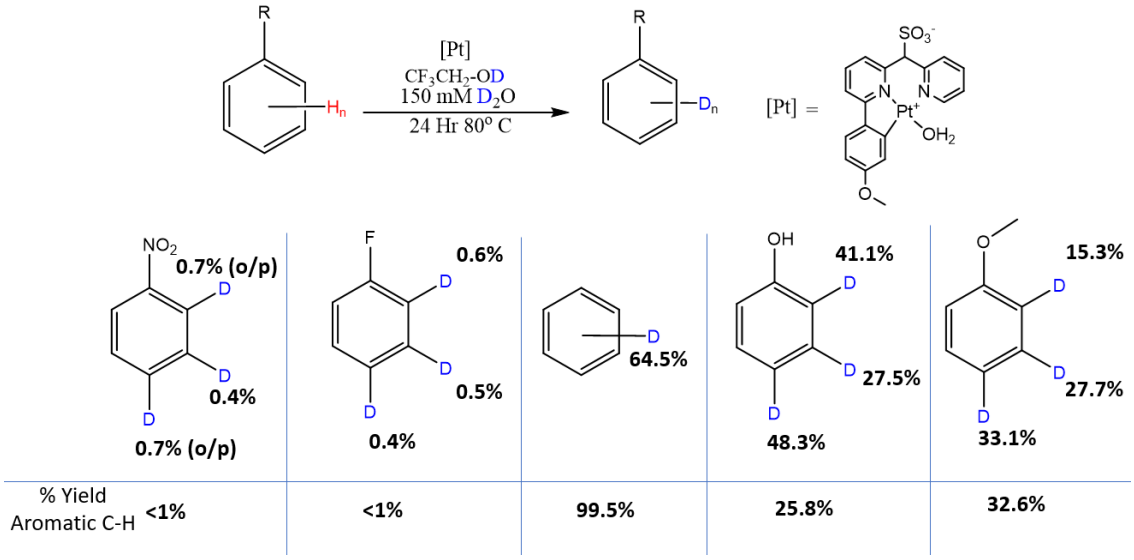

Figure S4.7. 24 Hour Yields for Arene Screening of **4.1-OMe** in 0.45 mL TFE-d_1 solution at 80°C (Conditions shown in Table S4.6)

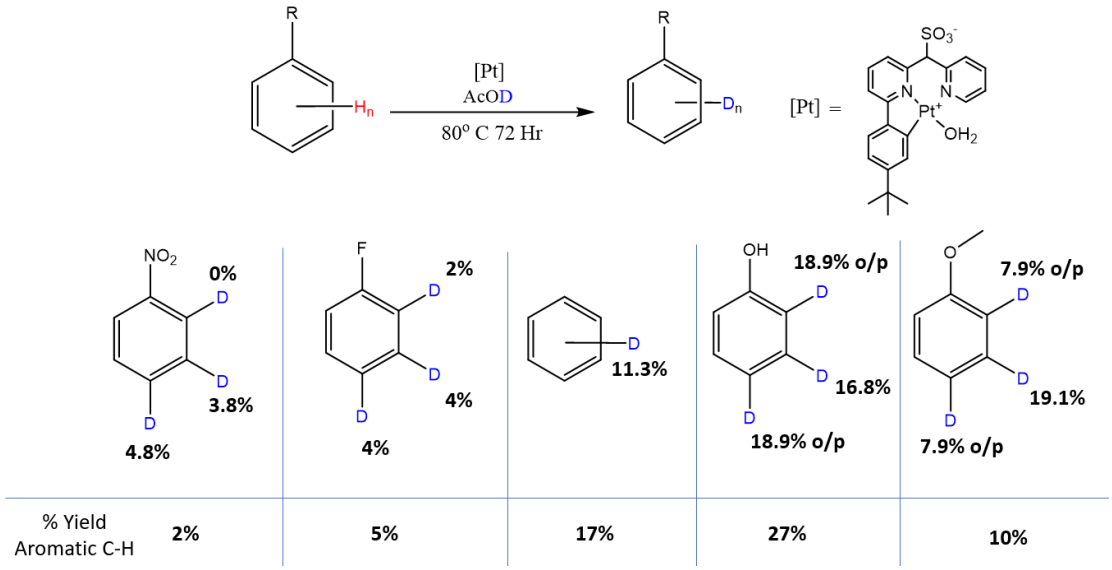

Figure S4.8. 24 Hour Yields for Arene Screening of **4.1-tBu** in 0.5 mL AcOD-d_4 solution at 80°C

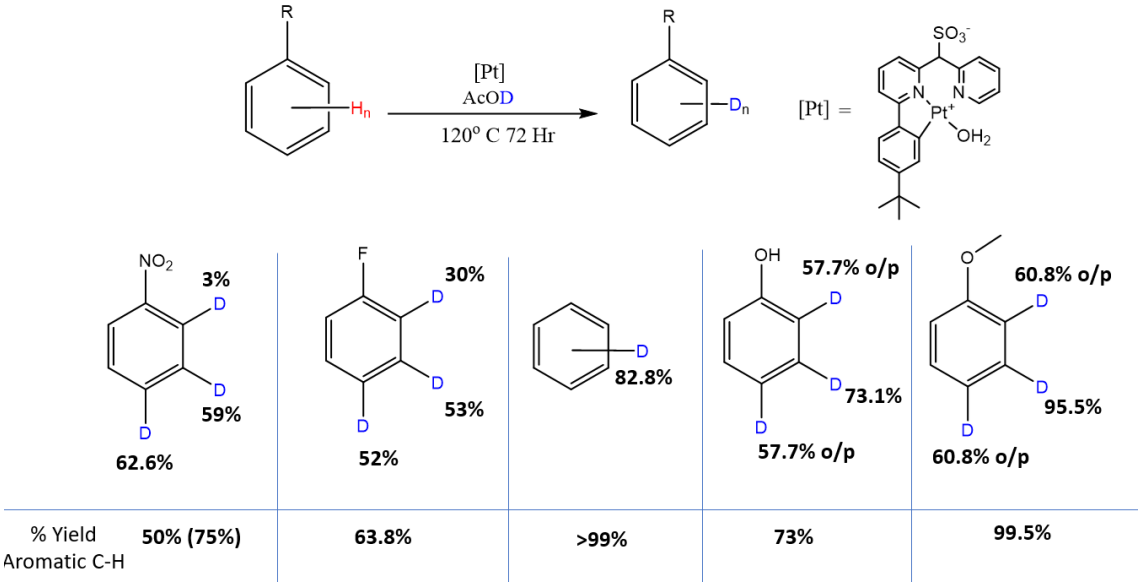

Figure S4.9. 24 Hour Yields for Arene Screening of **4.1-tBu** in 0.5 mL AcOD-d_4 solution at 120°C

Table S4.10. TON-24 for **4.1-X** complex screening profile in 0.45 mL TFE-d_1 solution at 80°C For the reactions shown in Figures S.4.2-4.7.

		TON-24 Hr for R-Ph Sub				
Entry	**4.1-X**	**NO_2**	**F**	**H**	**OH**	**OMe**
1	**CF_3**	**13**	**4**	**28**	**6**	**16**
2	**F**	**0**	**37**	**301**	**179**	**155**
3	**Cl**	**0**	**84**	**188**	**411**	**212**
4	**H**	**23**	**81**	**144**	**161**	**131**
5	**iPr**	**11**	**17**	**240**	**85**	**75**
6	**tBu**	**35**	**72**	**392**	**190**	**235**
7	**OMe**	**3**	**39**	**285**	**84**	**65**

*p-Cl and p-F both were poorly soluble in TFE and have lower catalyst loading (see Tables S4.2 and S4.3)

V. High %D Incorporation Experiments with p-tBu PhDPMS Pt OH_2

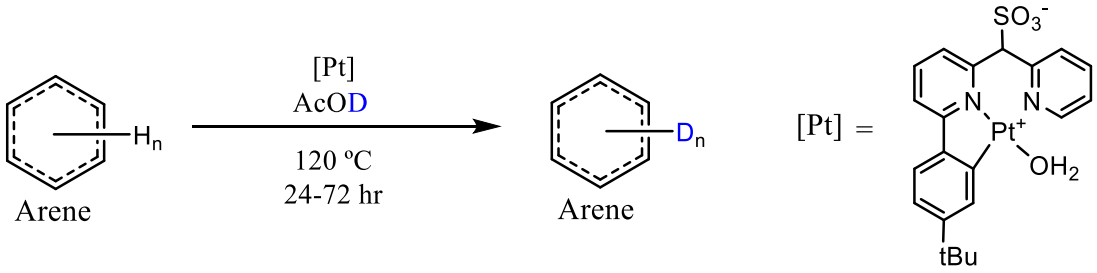

General Procedure F for High %D incorporation H/D Exchange Experiments

Under air or Argon, 0.25-1.5 mmol of substrate was transferred into a scintillation vial and dissolved in 0.5 mL of AcOD-d_4 solution containing 5-7 mmol [Pt]. The scintillation vial was then sealed with an airtight cap and transferred out of the glovebox. The vial was then additionally sealed with electrical tape and placed into a hot oil bath at 120 °C for 1-3 days. At the end of the allotted reaction time, the vials were allowed to cool to room temperature and the contents were transferred into a dry NMR tube. Deuterium incorporation was measured via the increase of integration of a given bond type in ^{2}H-NMR.

H/D Exchange for Nitrobenzene

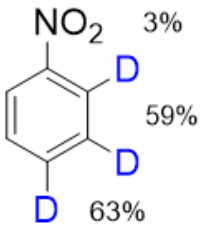

General procedure F outlined above was followed using 0.05 mL of nitrobenzene (0.48 mmol) dissolved in 0.5 mL of AcOD-d_4 containing 3.1 mg **4.1-tBu** (4.6 µmol). The resulting solution was a light orange color, and it was heated at 120 °C for 72 hours. The reaction proceeded with no color change or precipitate formation. There was no observed background contribution in the H/D exchange.

H/D Exchange for Fluorobenzene

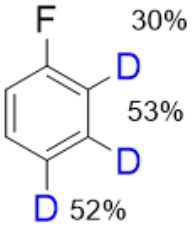

General procedure F outlined above was followed using 0.05 mL of fluorobenzene (0.66 mmol) dissolved in 0.5 mL of AcOD-d_4 containing 3.1 mg **4.1-tBu** (4.6 µmol). The resulting solution was a light orange color, and it was heated at 120 °C for 72 hours. The reaction proceeded with no color change or precipitate formation. There was no observed background contribution in the H/D exchange.

H/D Exchange for Benzene

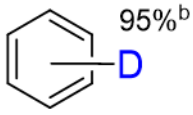

General procedure F outlined above was followed using 0.05 mL of benzene (0.66 mmol) dissolved in 0.5 mL of AcOD-d_4 containing 3.1 mg **4.1-tBu** (4.6 µmol). The resulting solution was a light orange color, and it was heated at 120 °C for 24 hours. The reaction proceeded with no color change or precipitate formation. There was no observed background contribution in the H/D exchange.

H/D Exchange for Phenol

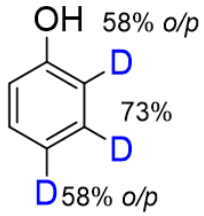

General procedure F outlined above was followed using 33.8 mg of phenol (0.36 mmol) dissolved in 0.5 mL of AcOD-d_4 containing 3.2 mg **4.1-tBu** (4.7 µmol). The resulting solution was a light orange color, and it was heated at 120 °C for 72 hours. The reaction proceeded with no color change or precipitate formation. There was no observed background contribution in the H/D exchange.

H/D Exchange for Anisole

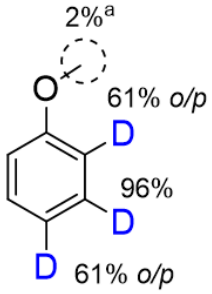

General procedure F outlined above was followed using 0.05 mL of anisole (0.46 mmol) dissolved in 0.5 mL of AcOD-d_4 containing 3.1 mg **4.1-H** (4.6 µmol). The resulting solution was a light orange color, and it was heated at 120 °C for 72 hours. The reaction proceeded with no color change or precipitate formation. There was no observed background contribution in the H/D exchange.

H/D Exchange for Ethylbenzene

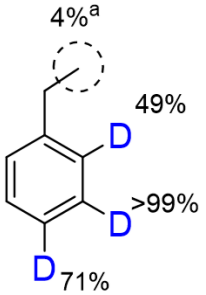

General procedure F outlined above was followed using 0.05 mL of ethylbenzene (0.54 mmol) dissolved in 0.5 mL of AcOD-d_4 containing 4.75 mg (7.0 µmol) **4.1-tBu**. The resulting solution was a light orange color, and it was heated at 120 °C for 72 hours. The reaction proceeded with no color change or precipitate formation. There was no observed background contribution in the H/D exchange.

H/D Exchange for Benzoic acid

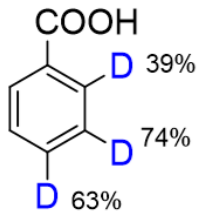

General procedure F outlined above was followed using 18.8 mg of benzoic acid (0.16 mmol) dissolved in 0.5 mL of AcOD-d_4 containing 3.4 mg (5.4 µmol) **4.1-tBu**. The resulting solution was a light orange color, and it was heated at 120 °C for 72 hours. The reaction proceeded with no color change or precipitate formation. There was no observed background contribution in the H/D exchange.

H/D Exchange for α,α,α Trifluorotoluene

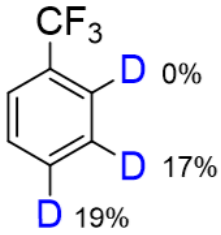

General procedure F outlined above was followed using 0.05 mL of α,α,α trifluorotoluene (0.41 mmol) dissolved in 0.5 mL of AcOD-d_4 containing 3.4 mg (5.4 µmol) **4.1-tBu**. The resulting solution was a light orange color, and it was heated at 120 °C for 72 hours. The reaction proceeded with no color change or precipitate formation. There was no observed background contribution in the H/D exchange.

H/D Exchange for Benzenesulfonamide

General procedure F outlined above was followed using 25.8 mg of Benzenesulfonamide (0.17 mmol) dissolved in 0.5 mL of AcOD-d_4 containing 3.4 mg 5.4 µmol) **4.1-tBu**. The resulting solution was a light orange color, and it was heated at 120 °C for 72 hours. The reaction proceeded with a slight darkening of the solution after 72 hours. There was no observed background contribution in the H/D exchange.

H/D Exchange for Benzodioxole

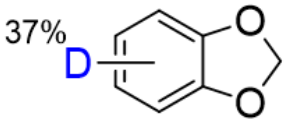

General procedure F outlined above was followed using 0.05 mL of benzodioxole (0.49 mmol) dissolved in 0.5 mL of AcOD-d_4 containing 3.4 mg (5.4 µmol) **4.1-tBu**. The resulting solution was a light orange color, and it was heated at 120 °C for 72 hours. Over the course of the reaction period a significant amount of Pt black was observed, additionally, the solution darkened substantially. There was no observed background contribution in the H/D exchange.

H/D Exchange for N,N Dimethylaniline

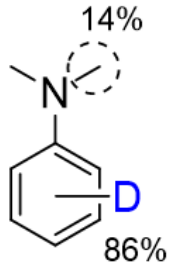

General procedure F outlined above was followed using 0.10 mL of N,N dimethylaniline (1.58 mmol) dissolved in 0.5 mL of AcOD-d_4 containing 4.7 mg (7.4 µmol) **4.1-tBu**. The resulting solution was a light orange color, and it was heated at 120 °C for 72 hours. Over the course of the reaction period the solution darkened slightly to a red/orange color. There was no observed background contribution in the H/D exchange.

H/D Exchange for N-Phenyl piperidine

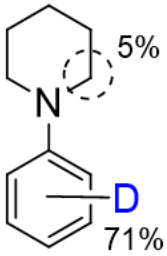

General procedure F outlined above was followed using 0.10 mL of N-phenyl piperidine (1.19 mmol) dissolved in 0.5 mL of AcOD-d_4 containing 4.7 mg (7.4 µmol) **4.1-tBu**. The resulting solution was a light orange color, and it was heated at 120 °C for 72 hours. Over the course of the reaction period the solution darkened slightly to a red/orange color. There was no observed background contribution in the H/D exchange.

H/D Exchange for 1,2 Dimethoxybenzene

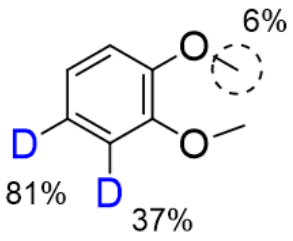

General procedure F outlined above was followed using 52.0 mg of 1,2 Dimethoxybenzene (0.38 mmol) dissolved in 0.5 mL of AcOD-d_4 containing 4.7mg (7.4 µmol) **4.1-tBu**. The resulting solution was a light orange color, and it was heated at 120 °C for 72 hours. The reaction proceeded no significant color change. There was no observed background contribution in the H/D exchange.

H/D Exchange for 1,2 Dichlorobenzene

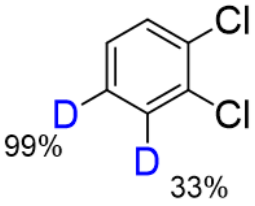

General procedure F outlined above was followed using 0.10 mL of 1,2 Dichlorobenzene (1.77 mmol) dissolved in 0.5 mL of AcOD-d_4 containing 4.7 mg (7.4 µmol) **4.1-tBu**. The resulting solution was a light orange color, and it was heated at 120 °C for 72 hours. The reaction proceeded no significant color change. There was no observed background contribution in the H/D exchange.

H/D Exchange for Methylbenzoate

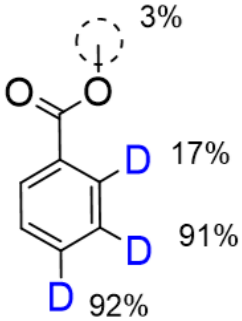

General procedure F outlined above was followed using 0.10 mL of methylbenzoate (1.59 mmol) dissolved in 0.5 mL of AcOD-d_4 containing 4.7 mg (7.4 µmol) **4.1-tBu**. The resulting solution was a light orange color, and it was heated at 120 °C for 72 hours. The reaction proceeded no significant color change. There was no observed background contribution in the H/D exchange.

H/D Exchange for Naphthalene

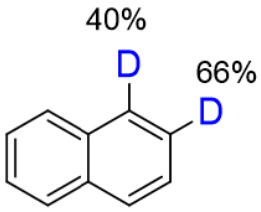

General procedure F outlined above was followed using 27.2 mg of naphthalene (0.21 mmol) dissolved in 0.5 mL of AcOD-d_4 containing 3.4 mg (5.4 µmol) **4.1-tBu**. The resulting solution was a light orange color, and it was heated at 120 °C for 72 hours. The reaction proceeded no significant color change. There was no observed background contribution in the H/D exchange.

H/D Exchange for Indole

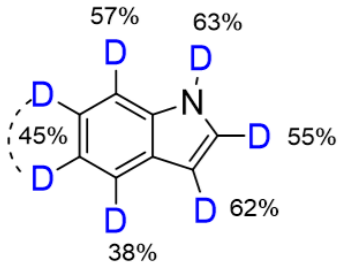

General procedure F outlined above was followed using 22.0 mg of Indole (0.19 mmol) dissolved in 0.5 mL of AcOD-d_4 containing 3.4 mg (5.4 µmol) **4.1-tBu**. The resulting solution was a light brown color, and it was heated at 120 °C for 72 hours. The reaction proceeded no significant color change. There was no observed background contribution in the H/D exchange.

H/D Exchange for 2,6 Dimethylpyridine

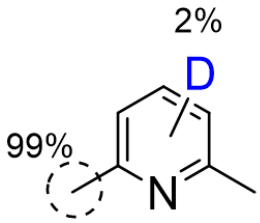

General procedure F outlined above was followed using 0.05 mL of 2,6 dimethylpyridine (0.87 mmol) dissolved in 0.5 mL of AcOD-d_4 containing 4.7 mg (7.4 µmol) **4.1-tBu**. The resulting solution was a light brown color, and it was heated at 120 °C for 72 hours. After the 72 hour reaction period a significant amount of Pt(0) was observed. There was no observed background contribution in the H/D exchange.

H/D Exchange for 2,6 Diphenylpyridine

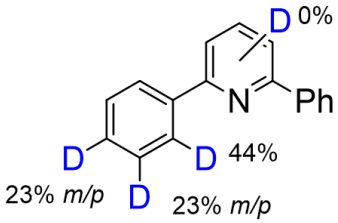

General procedure F outlined above was followed using 52.0 mg of 2,6 diphenylpyridine (0.23 mmol) dissolved in 0.5 mL of AcOD-d_4 containing 4.7 mg (7.4 µmol) **4.1-tBu**. The resulting solution was a light brown color, and it was heated at 120 °C for 72 hours under air. The reaction proceeded with no obvious color change. There was no observed background contribution in the H/D exchange.

H/D Exchange for Ibuprofen

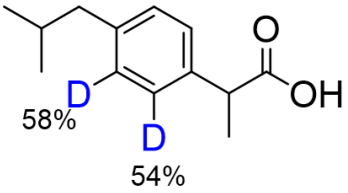

General procedure F outlined above was followed using 22.5 mg of ibuprofen (0.11 mmol) dissolved in 0.5 mL of AcOD-d_4 containing 4.7 mg (7.4 µmol) **4.1-tBu**. The resulting solution was a light orange color, and it was heated at 120 °C for 72 hours under air. The reaction proceeded no significant color change. There was no observed background contribution in the H/D exchange.

H/D Exchange for Naproxen

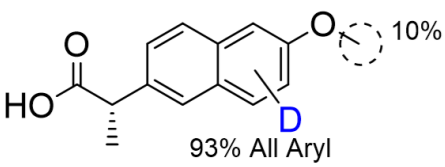

General procedure F outlined above was followed using 13.5mg of Naproxen (0.06 mmol) dissolved in 0.5 mL of AcOD-d_4 containing 4.7 mg (7.4 µmol) **4.1-tBu**. The resulting solution was a light orange color, and it was heated at 120 °C for 72 hours under

air. The reaction proceeded no significant color change. There was no observed background contribution in the H/D exchange.

H/D Exchange for Duloxetine

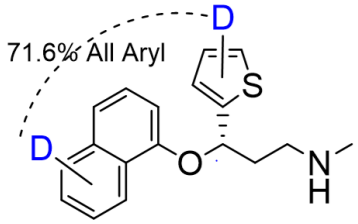

General procedure F outlined above was followed using 17.8 mg of duloxetine (0.06 mmol) dissolved in 0.5 mL of AcOD-d_4 containing 4.7 mg (7.4 µmol) **4.1-tBu**. The resulting solution was a light orange color, and it was heated at 120 °C for 72 hours under air. The reaction proceeded no significant color change. There was no observed background contribution in the H/D exchange.

H/D Exchange for Nortriptyline

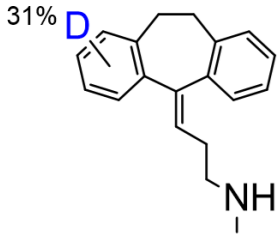

General procedure F outlined above was followed using 16.8 mg of nortriptyline (0.07 mmol) dissolved in 0.5 mL of AcOD-d_4 containing 4.7 mg (7.4 µmol) **4.1-tBu**. The resulting solution was a light orange color, and it was heated at 120 °C for 72 hours under air. The reaction proceeded no significant color change. There was no observed background contribution in the H/D exchange.

H/D Exchange for Acetaminophen

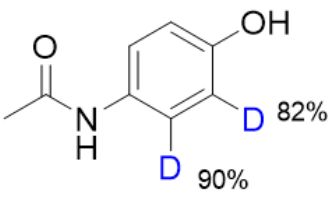

General procedure F outlined above was followed using 23.2 mg of acetaminophen (0.15 mmol) dissolved in 0.5 mL of AcOD-d_4 containing 4.7 mg (7.4 µmol) **4.1-tBu**. The resulting solution was a light orange color, and it was heated at 120 °C for 72 hours under air. The reaction

proceeded no significant color change. There was no observed background contribution in the H/D exchange.

H/D Exchange for Guaifenesin Derivative

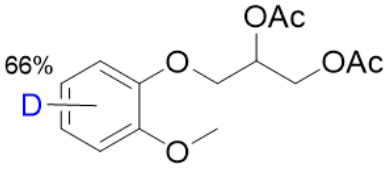

General procedure F outlined above was followed using 27.6 mg of guaifenesin (0.14 mmol) dissolved in 0.5 mL of AcOD-d_4 containing 5.2 mg (8.2 µmol) **4.1-tBu**. The resulting solution was a light orange color, and it was heated at 120 °C for 24 hours under air. The reaction proceeded no significant color change. Guaifenesin underwent a condensation reaction under the reaction conditions to yield the diacylated guaifenesin derivative. Deuterium incorporations percentages are reported as the aromatic contribution to H/D exchange only. There was no observed background contribution in the H/D exchange.

H/D Exchange for Melatonin

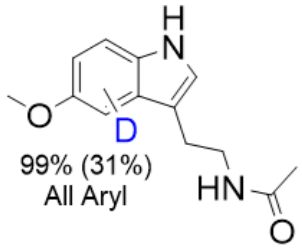

General procedure F outlined above was followed using 22.7 mg of melatonin (0.1 mmol) dissolved in 0.5 mL of AcOD-d_4 containing 5.2 mg (8.3 µmol) **4.1-tBu**. The resulting solution was a light orange color, and it was heated at 120 °C for 72 hours under air. The reaction proceeded no significant color change. There was some background reaction observed in the absence of catalyst leading to 31% deuterium incorporation.

H/D Exchange for Diphenhydramine

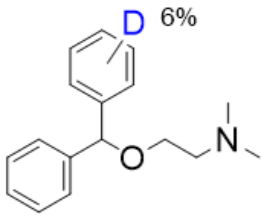

General procedure F outlined above was followed using 26.4 mg of diphenhydramine (0.10 mmol) dissolved in 0.5 mL of AcOD-d_4 containing 5.2 mg (8.3 µmol) **4.1-tBu**. The resulting solution

was a light orange color, and it was heated at 120 °C for 72 hours under air. The reaction proceeded no significant color change. There was no observed background contribution in the H/D exchange.

Chart S4.1. List of unsuccessful Substrates for H.D Exchange catalyzed by **4.5-tBu**

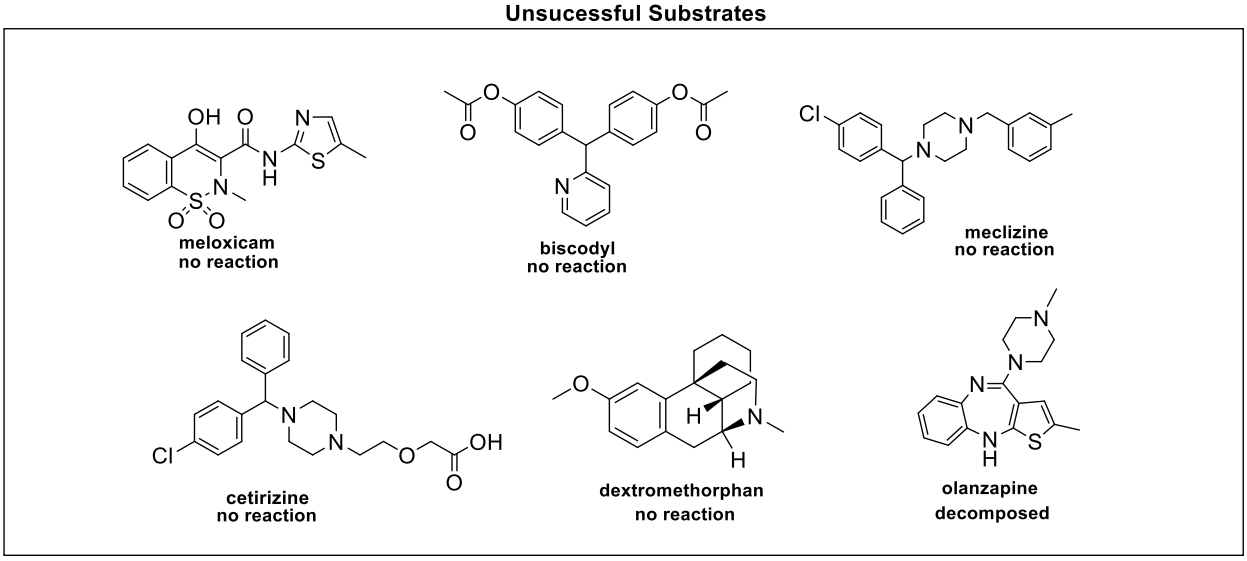

VI. H/D Exchange Experiments on Olefins and C(sp^3)-H Substrates

General Procedure G for High %D incorporation H/D Exchange Experiments

Under Argon, 0.05 mL of substrate was transferred into a scintillation vial and dissolved in 0.5 mL of AcOD-d_4 solution containing 5-7 mmol [Pt]. The solution was then transferred into a JYoung tube and sealed with a teflon cap, then it was transferred out of the glovebox into a hot oil bath at 100°C (for olefins) or 140°C (for C(sp^3)-H substrates) for 24 hours. The tubes were periodically removed from the oil bath for NMR analysis. Deuterium

incorporation was measured via the increase of integration of a given bond type in ^{2}H-NMR.

H/D Exchange for Styrene

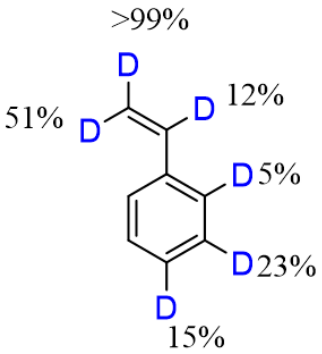

General procedure G outlined above was followed using 0.05 mL of Styrene (0.86 mmol) dissolved in 0.5 mL of AcOD-d_4 containing 3.4 mg (5.4 µmol) **4.1-tBu**. The resulting solution was a light orange color, and it was heated at 100 °C for 24 hours under argon. The reaction proceeded no significant color change. There was no observed background contribution in the H/D exchange.

H/D Exchange for Vinylcyclohexane

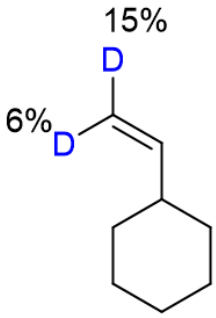

General procedure G outlined above was followed using 0.05 mL of Vinylcyclohexane (0.76 mmol) dissolved in 0.5 mL of AcOD-d_4 containing 3.4 mg (5.4 µmol) **4.1-tBu**. The resulting solution was a light orange color, and it was heated at 100 °C for 24 hours under argon. The reaction proceeded no significant color change. There was no observed background contribution in the H/D exchange.

H/D Exchange for 1-Hexene

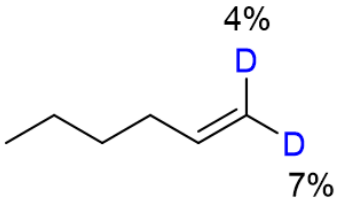

General procedure G outlined above was followed using 0.05 mL of 1-hexene (0.79 mmol) dissolved in 0.5 mL of AcOD-d_4 containing 3.4 mg (5.4 µmol) **4.1-tBu**. The resulting solution was a light orange color, and it was heated at 100 °C for 24 hours under argon. The reaction proceeded no significant color change. There was no observed background contribution in the H/D exchange.

H/D Exchange for Cyclohexene

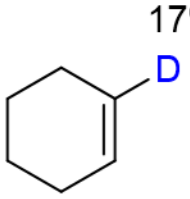

General procedure G outlined above was followed using 0.05 mL of cyclohexene (0.98 mmol) dissolved in 0.5 mL of AcOD-d_4 containing 3.4 mg (5.4 µmol) **4.1-tBu**. The resulting solution was a light orange color, and it was heated at 100 °C for 24 hours under argon. The reaction proceeded no significant color change. There was no observed background contribution in the H/D exchange.

H/D Exchange for 3,3 dimethyl-1-butene

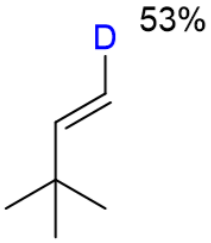

General procedure G outlined above was followed using 0.05 mL of 3,3 dimethyl-1-butene (0.77 mmol) dissolved in 0.5 mL of AcOD-d_4 containing 3.4 mg (5.4 µmol) **4.1-tBu**. The resulting solution was a light orange color, and it was heated at 100 °C for 24 hours under argon. The reaction proceeded no significant color change. There was no observed background contribution in the H/D exchange.

H/D Exchange for Heptane

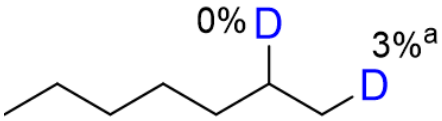

General procedure G outlined above was followed using 0.05 mL of heptane (0.68 mmol) dissolved in 0.5 mL of AcOD-d_4 containing 4.3 mg (6.4 µmol) **4.1-tBu**. The resulting solution was a light orange color, and it was heated at 140 °C for 72 hours under argon. The reaction proceeded no significant color change. There was no observed background contribution in the H/D exchange.

H/D Exchange for Heptane

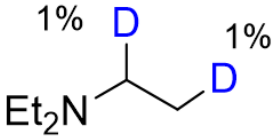

General procedure G outlined above was followed using 0.05 mL of triethylamine (0.71 mmol) dissolved in 0.5 mL of AcOD-d_4 containing 4.3 mg (6.4 µmol) **4.1-tBu**. The resulting solution was a light orange color, and it was heated at 140 °C for 24 hours under argon. The reaction proceeded no significant color change. There was no observed background contribution in the H/D exchange. Pt black was observed after 24 hours.

H/D Exchange for 1,2 dimethoxyethane

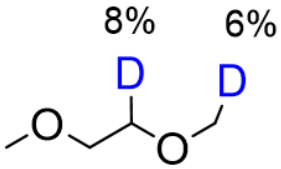

General procedure G outlined above was followed using 0.05 mL of 1,2 dimethoxyethane (0.96 mmol) dissolved in 0.5 mL of AcOD-d_4 containing 4.3 mg (6.4 µmol) **4.1-tBu**. The resulting solution was a light orange color, and it was heated at 140 °C for 24 hours under argon. The reaction proceeded no significant color change. There was no observed background contribution in the H/D exchange. Pt black was observed after 24 hours.

H/D Exchange for 1-Methylnapthalene

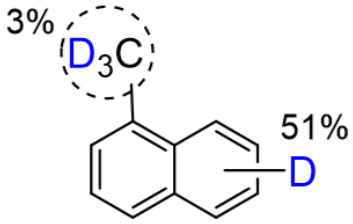

General procedure G outlined above was followed using 0.05 mL of 1-methylnapthalene (0.70 mmol) dissolved in 0.5 mL of AcOD-d_4 containing 4.3 mg (6.4 µmol) **4.1-tBu**. The resulting solution was a light orange color, and it was heated at 140 °C for 24 hours under argon. The reaction proceeded no significant color change. There was no observed background contribution in the H/D exchange. Pt black was observed after 24 hours.

Initial Rate Data for the H/D Exchange Reaction of 4.1-CF_3 and Nitrobenzene in TFE-*d_1*

Mass [Pt] (mg)			Density g/mL	Volume mL	Conc. M
8.4		TFE-OD	1.384	0.45	12.46
[Pt] MW 605.45		Nitrobenzene	1.200	0.05	0.97
Temp. (°C)	80			Substrate MW	123.11

Meta C-H				Para C-H			
SLOPE	0.095029	0.004572	INT	SLOPE	0.037431	0.005942	INT
(+/-)	0.026397	0.01333	(+/-)	(+/-)	0.010311	0.007346	(+/-)
r2	0.928365	0.014092	S(Y)	r2	0.868238	0.008498	S(Y)
F	12.95963	1	DOF	F	13.17883	2	DOF
Reg.SS	0.002574	0.000199	Res. SS	REGRESSION SS	0.000952	0.000144	Res. SS

Ortho C-H				Total Aromatic			
SLOPE	0.02108	-0.00026	INT	SLOPE	0.104002	0.019185	INT
(+/-)	0.00149	0.000753	(+/-)	(+/-)	0.033697	0.024009	(+/-)
r2	0.995027	0.000796	S(Y)	r2	0.826479	0.027771	S(Y)
F	200.0833	1	DOF	F	9.525984	2	DOF
REGRESSION SS	0.000127	6.33E-07	Res. SS	REGRESSION SS	0.007347	0.001542	Res. SS

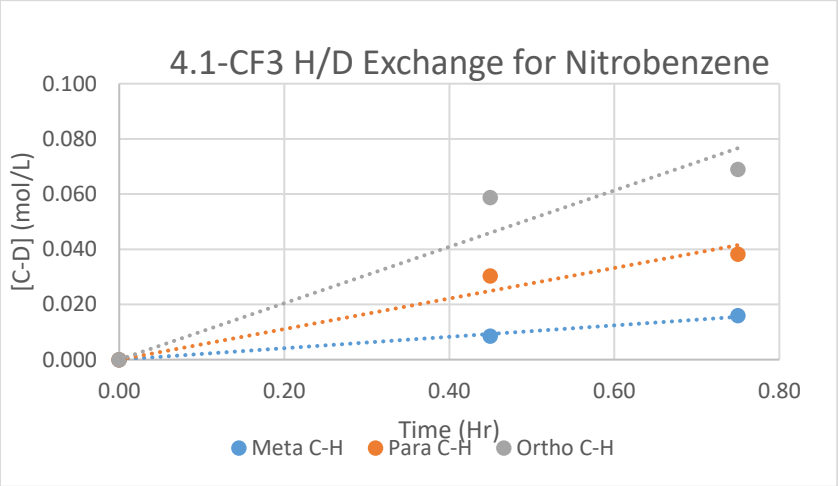

Chart S4.2 Initial rates for the H/D exchange reaction catalyzed by **4.1-CF_3** with Nitrobenzene substrate at 80 °C.

The rate constants for the H/D exchange catalyzed by complex **4.1-CF_3** at 80 °C: *ortho*-, *para*-, *meta*-, CH bonds, $k_{c,}$ = 0.4±0.03 M^{-1} h^{-1};1.4±0.4 M^{-1} h^{-1}; 1.8±0.5 M^{-1} h^{-1}; *Average* CH bond, $k_{c,}$ = 1.0±0.4 M^{-1} h^{-1}

Initial Rate Data for the H/D Exchange Reaction of 4.1-CF_3 and Fluorobenzene in TFE-d_1

Mass [Pt] (mg)			Density g/mL	Volume mL	Conc. M
6.1		TFE-OD	1.384	0.45	12.46
[Pt] MW 605.45		Fluorobenzene	1.025	0.05	1.31
Temp. (°C)	80			Substrate MW	78.11

Meta C-H				Para C-H			
SLOPE	0.2251	0.0162	INT	SLOPE	0.1259	0.0249	INT
(+/-)	0.0551	0.0175	(+/-)	(+/-)	0.0533	0.0169	(+/-)
r2	0.8478	0.0245	S(Y)	r2	0.6506	0.0237	S(Y)
F	16.7047	3	DOF	F	5.5859	3	DOF
Reg.SS	0.0101	0.0018	Res. SS	Reg.SS	0.0031	0.0017	Res. SS

Ortho C-H				Total Aromatic			
SLOPE	0.2451	0.0053	INT	SLOPE	0.5960	0.0463	INT
(+/-)	0.0141	0.0045	(+/-)	(+/-)	0.1161	0.0369	(+/-)
r2	0.9901	0.0063	S(Y)	r2	0.8978	0.0517	S(Y)
F	300.5237	3	DOF	F	26.34	3	DOF
Reg.SS	0.0119	0.0001	Res. SS	Reg.SS	0.0705	0.0080	Res. SS

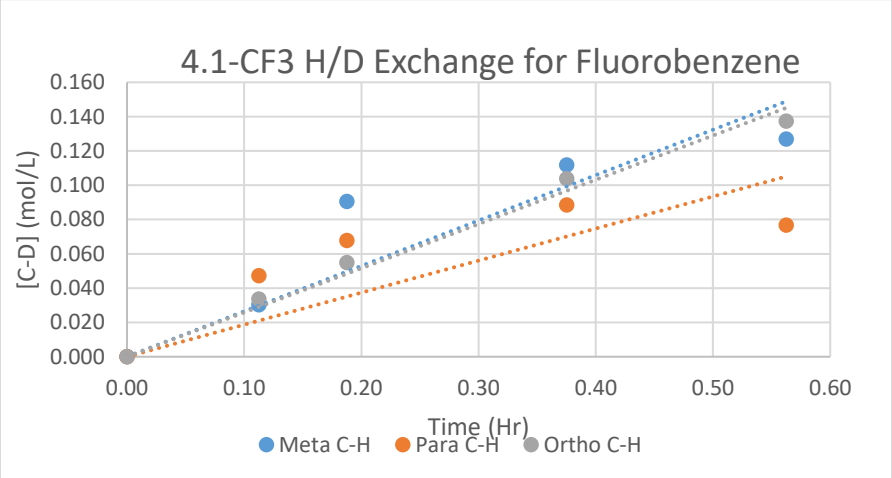

Chart S4.3. Initial rates for the H/D exchange reaction catalyzed by **4.1-CF_3** with Fluorobenzene substrate at 80 °C.

The rate constants for the H/D exchange catalyzed by complex **4.1-CF_3** at 80 °C: *ortho*-, *para*-, *meta*-, CH bonds, k_c = 4.6±0.3M^{-1} h^{-1}; 4.8±2.0 M^{-1} h^{-1}; 4.3±1.0 M^{-1} h^{-1}; *Average* CH bond, k_c = 4.5±0.8 M^{-1} h^{-1}

Initial Rate Data for the H/D Exchange Reaction of 4.1-CF_3 and Benzene in TFE-d_1

			Density	Volume	Conc.
Mass [Pt] (mg)			g/mL	mL	M
3.5		TFE-OD	1.384	0.45	12.46
[Pt] MW		Benzene	0.876	0.05	1.12
605.45					
				Substrate	
Temp. (°C)	80			MW	78.11

SLOPE	1.1067	-0.0051	INT
(+/-)	0.0515	0.008074	(+/-)
r2	0.9957	0.008844	S(Y)
F	462.3515	2	DOF
REGRESSION			
SS	0.0362	0.000156	Res. SS

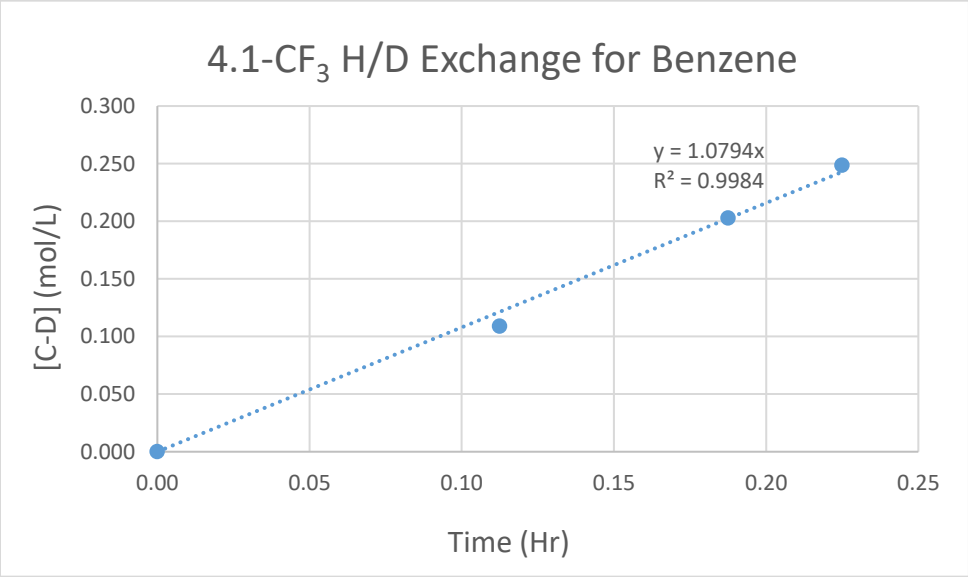

Chart S4.4. Initial rates for the H/D exchange reaction catalyzed by **4.1-CF_3** with benzene substrate at 80 °C.

The rate constants for the H/D exchange catalyzed by complex **4.1-CF_3** at 80 °C: *Average* CH bond, $k_{c,}$ = 8.2±0.4 M^{-1} h^{-1}

Initial Rate Data for the H/D Exchange Reaction of 4.1-CF_3 and Phenol in TFE-d_1

				Density	Volume/Mass	Conc.		
Mass [Pt] (mg)				g/mL	mL or mg	M		
4.7			TFE-OD	1.384	0.45	12.46		
[Pt] MW 605.45			Phenol		44.00	0.94		
Temp. (°C)	80				Substrate MW	94.11		
Meta C-H					Para C-H			
SLOPE	0.2821	-0.01696	INT		SLOPE	0.1644	-0.01853	INT
(+/-)	0.1068	0.032832	(+/-)		(+/-)	0.1066	0.032786	(+/-)
r2	0.7773	0.03729	S(Y)		r2	0.5432	0.037237	S(Y)
F	6.9797	2	DOF		F	2.3785	2	DOF
REGRESSION SS	0.0097	0.002781	Res. SS		REGRESSION SS	0.0033	0.002773	Res. SS
Ortho C-H					Total Aromatic			
SLOPE	0.2272	-0.01226	INT		SLOPE	0.6737	-0.04775	INT
(+/-)	0.0617	0.018961	(+/-)		(+/-)	0.2736	0.084148	(+/-)
r2	0.8716	0.021536	S(Y)		r2	0.7519	0.095572	S(Y)
F	13.5744	2	DOF		F	6.0609	2	DOF
REGRESSION SS	0.0063	0.000928	Res. SS		REGRESSION SS	0.0554	0.018268	Res. SS

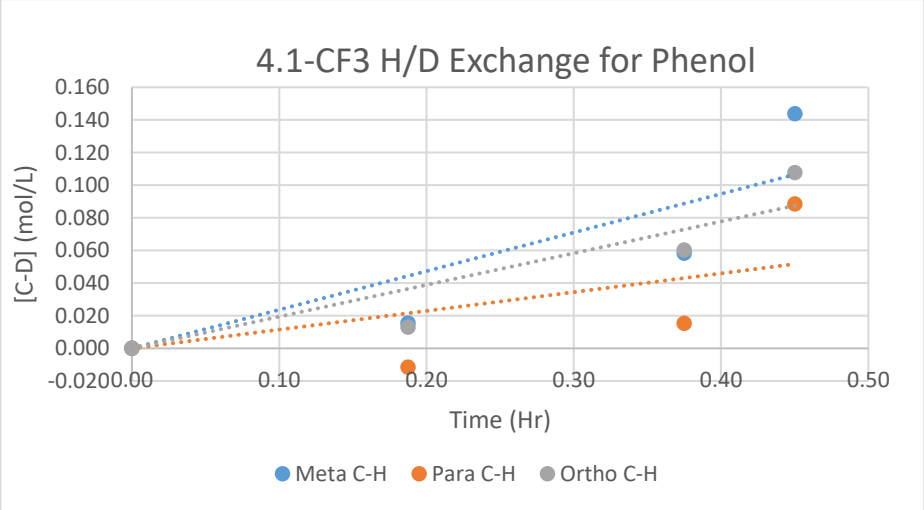

Chart S4.5. Initial rates for the H/D exchange reaction catalyzed by **4.1-CF_3** with Phenol substrate at 80 °C.

The rate constants for the H/D exchange catalyzed by complex **4.1-CF_3** at 80 °C: *ortho-*, *para-*, *meta-*, CH bonds, $k_{c,}$ = 7.8±2.1 M^{-1} h^{-1}; 11.3±6.0M^{-1} h^{-1}; 10.±3.M^{-1} h^{-1}; *Average* CH bond, $k_{c,}$ = 9.±4. M^{-1} h^{-1}

Initial Rate Data for the H/D Exchange Reaction of 4.1-CF_3 and Anisole in TFE-d_1

		Density	Volume	Conc.
Mass [Pt] (mg)		g/mL	mL	M
4	TFE-OD	1.384	0.45	12.46
[Pt] MW	Anisole	0.995	0.05	0.92
605.45				
			Substrate	
Temp. (°C)	80		MW	108.14

Meta C-H			
SLOPE	0.132815	0.021199	INT
(+/-)	0.033151	0.015507	(+/-)
r2	0.842527	0.020728	S(Y)
F	16.05085	3	DOF
REGRESSION SS	0.006896	0.001289	Res. SS

Para C-H			
SLOPE	0.18534	0.017906	INT
(+/-)	0.02530	0.011834	(+/-)
r2	0.94706	0.015818	S(Y)
F	53.67140	3	DOF
REGRESSION SS	0.01343	0.000751	Res. SS

Ortho C-H			
SLOPE	0.170763	-0.00563	INT
(+/-)	0.074512	0.034855	(+/-)
r2	0.636455	0.046589	S(Y)
F	5.252067	3	DOF
REGRESSION SS	0.0114	0.006512	Res. SS

Total Aromatic			
SLOPE	0.48892	0.033475	INT
(+/-)	0.10372	0.048516	(+/-)
r2	0.88106	0.064849	S(Y)
F	22.22212	3	DOF
REGRESSION SS	0.09345	0.012616	Res. SS

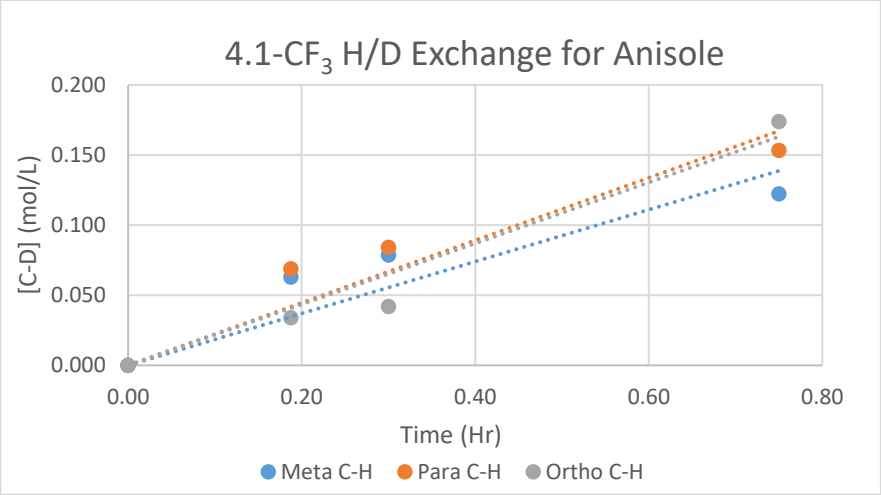

Chart S4.6. Initial rates for the H/D exchange reaction catalyzed by **4.1-CF_3** with anisole substrate at 80 °C.

The rate constants for the H/D exchange catalyzed by complex **4.1-CF_3** at 80 °C: *ortho*-, *para*-, *meta*-, CH bonds, k_c = 9.7±1.2 M^{-1} h^{-1}; 15.8±2.7 M^{-1} h^{-1}; 6.1±1.6 M^{-1} h^{-1}; *Average* CH bond, k_c = 9.5±1.0 M^{-1} h^{-1}

Initial Rate Data for the H/D Exchange Reaction of 4.1-F and Fluorobenzene in

Mass [Pt] (mg)		Density g/mL	Volume mL	Conc. M
2.6	TFE-OD	1.384	0.45	12.46
[Pt] MW 555.44	Fluorobenzene	1.025	0.05	1.31
Temp. (°C) 80			Substrate MW	78.11

Meta				Para			
SLOPE	0.005682	0.000845	INT	SLOPE	0.004083	-0.0059	INT
(+/-)	0.000716	0.007782	(+/-)	(+/-)	0.000262	0.002845	(+/-)
r2	0.954486	0.014506	S(Y)	r2	0.987805	0.005303	S(Y)
F	62.91422	3	DOF	F	243	3	DOF
REG. SS	0.013239	0.000631	Res. SS	REG. SS	0.006835	8.44E-05	Res. SS

Ortho C-H				Total Aromatic			
SLOPE	0.005115	-0.00739	INT	SLOPE	0.01488	-0.01244	INT
(+/-)	0.000328	0.003564	(+/-)	(+/-)	0.000641	0.006959	(+/-)
r2	0.987805	0.006644	S(Y)	r2	0.99447	0.012971	S(Y)
F	243	3	DOF	F	539.5344	3	DOF
REG. SS	0.010725	0.000132	Res. SS	REG. SS	0.09078	0.000505	Res. SS

TFE-*d*$_1$

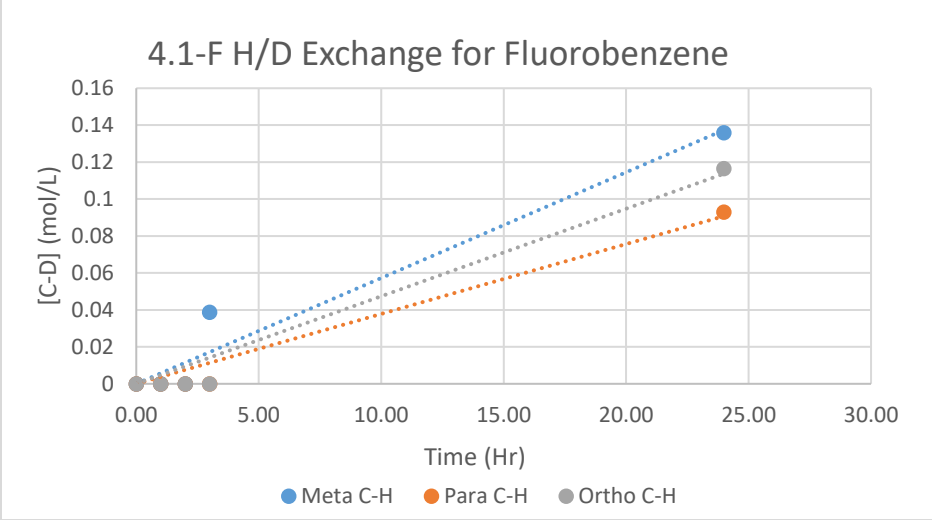

Chart S4.7 Initial rates for the H/D exchange reaction catalyzed by **4.1-F** with fluorobenzene substrate at 80 °C.

The rate constants for the H/D exchange catalyzed by complex **4.1-F** at 80 °C:
ortho-, *para*-, *meta*-, CH bonds, $k_{c,}$ = 0.21±0.01 M^{-1} h^{-1}; 0.33±0.02 M^{-1} h^{-1}; 0.5±0.06 M^{-1} h^{-1};
Average CH bond, $k_{c,}$ = 0.24±0.01M^{-1} h^{-1}

Initial Rate Data for the H/D Exchange Reaction of 4.1-F and Benzene in TFE-d_1

Mass [Pt] (mg)			Density g/mL	Volume mL	Conc. M
2.6		TFE-OD	1.384	0.45	12.46
[Pt] MW		Benzene	0.876	0.05	1.12
555.44					
Temp. (°C)	80			Substrate MW	78.11

SLOPE	0.362589	-0.01524	INT
(+/-)	0.065601	0.030067	(+/-)
r2	0.938555	0.03817	S(Y)
F	30.5496	2	DOF
REG. SS	0.044509	0.002914	Res. SS

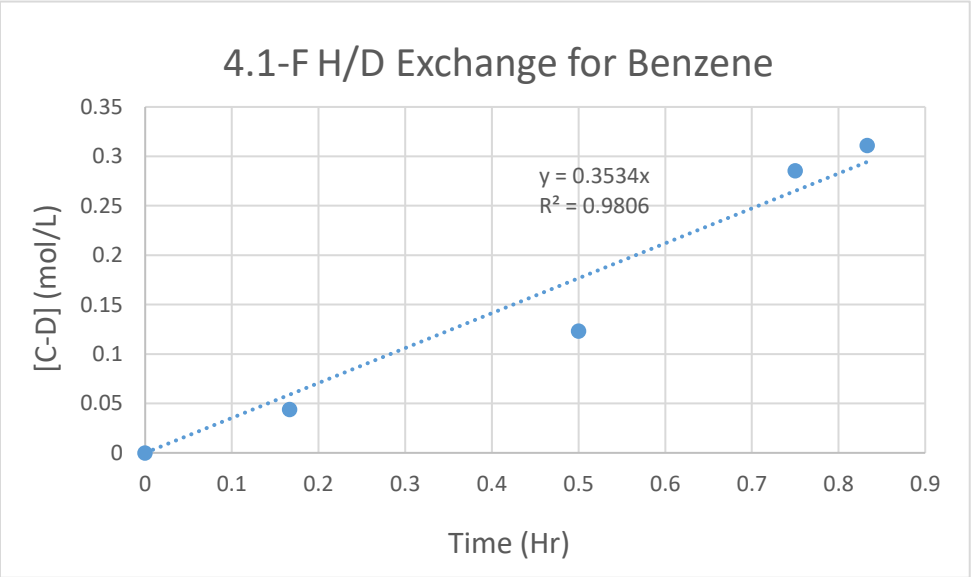

Chart S4.8 Initial rates for the H/D exchange reaction catalyzed by **4.1-F** with benzene substrate at 80 °C.

The rate constants for the H/D exchange catalyzed by complex **4.1-F** at 80 °C: *Average* CH bond, $k_{c,}$ = 5.8±1.0 M^{-1} h^{-1}

Initial Rate Data for the H/D Exchange Reaction of 4.1-F and Phenol in TFE-d_1

			Density	Volume or mass	Conc.
Mass [Pt] (mg)			g/mL	mL/mg	M
2.85		TFE-OD	1.384	0.45	12.46
[Pt] MW		Phenol		55.30	1.18
555.44					
Temp. (°C)	80			Substrate MW	94.11

Meta C-H			
SLOPE	0.07189	-0.00252	INT
(+/-)	0.00436	0.00909	(+/-)
r2	0.99632	0.00943	S(Y)
F	270.992	1	DOF
REG. SS	0.02412	8.9E-05	Res. SS

Ortho/Para C-H			
SLOPE	0.09824	-0.00487	INT
(+/-)	0.00843	0.01756	(+/-)
r2	0.99267	0.01822	S(Y)
F	135.571	1	DOF
REGRESSION SS	0.04504	0.00033	Res. SS

Total Aromatic			
SLOPE	0.17013	-0.00739	INT
(+/-)	0.01280	0.02665	(+/-)
r2	0.99437	0.02766	S(Y)
F	176.540	1	DOF
REG. SS	0.13508	0.00076	Res. SS

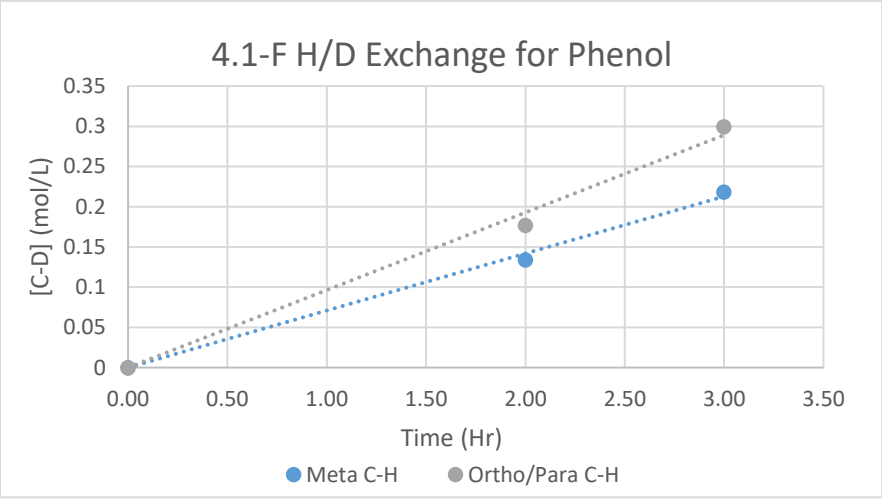

Chart S4.9. Initial rates for the H/D exchange reaction catalyzed by **4.1-F** with Phenol substrate at 80 °C.

The rate constants for the H/D exchange catalyzed by complex **4.1-F** at 80 °C:
ortho/*para*-, *meta*-, CH bonds, $k_{c,}$ = 2.7±0.2 M^{-1} h^{-1}; 3.0±0.2 M^{-1} h^{-1};
Average CH bond, $k_{c,}$ = 2.8±0.2M^{-1} h^{-1}

Initial Rate Data for the H/D Exchange Reaction of 4.1-F and Anisole in TFE-d_1

			Density	Volume	Conc.
Mass [Pt] (mg)			g/mL	mL	M
2.56		TFE-OD	1.384	0.45	12.46
[Pt] MW 555.44		Anisole	0.995	0.05	0.92
Temp. (°C)	80			Substrate MW	108.14

Meta C-H			
SLOPE	0.08277	-0.00069	INT
(+/-)	0.000671	0.000967	(+/-)
r2	0.999869	0.001097	S(Y)
F	15221.85	2	DOF
REG. SS	0.018304	2.41E-06	Res. SS

Ortho/Para C-H			
SLOPE	0.085392	0.005022	INT
(+/-)	0.00613	0.008837	(+/-)
r2	0.989798	0.01002	S(Y)
F	194.0393	2	DOF
REG. SS	0.019483	0.000201	Res. SS

Total Aromatic			
SLOPE	0.168161	0.004333	INT
(+/-)	0.005512	0.007947	(+/-)
r2	0.997856	0.00901	S(Y)
F	930.6189	2	DOF
REG. SS	0.075556	0.000162	Res. SS

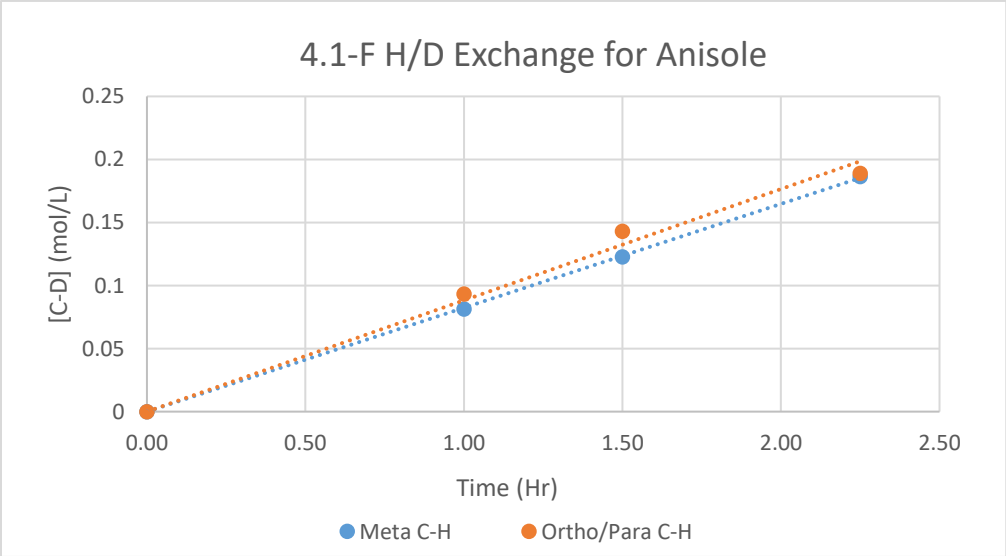

Chart S4.10. Initial rates for the H/D exchange reaction catalyzed by **4.1-F** with Anisole substrate at 80 °C.

The rate constants for the H/D exchange catalyzed by complex **4.1-F** at 80 °C:
ortho/*para*-, *meta*-, CH bonds, k_c, = 3.4±0.2 M^{-1} h^{-1}; 4.9±0.1 M^{-1} h^{-1};
Average CH bond, k_c, = 4.0±0.1 M^{-1} h^{-1}

Initial Rate Data for the H/D Exchange Reaction of 4.1-Cl and Benzene in TFE-d_1

Mass [Pt] (mg)			Density g/mL	Volume mL	Conc. M
1.8		TFE-OD	1.384	0.45	12.46
[Pt] MW		Benzene	0.876	0.05	1.12
571.9					
Temp. (°C)	80			Substrate MW	78.11

SLOPE	0.1195	-0.00343	INT
(+/-)	0.005947	0.007677	(+/-)
r2	0.99753	0.00841	S(Y)
F	403.8152	1	DOF
REG. SS	0.028561	7.07E-05	Res. SS

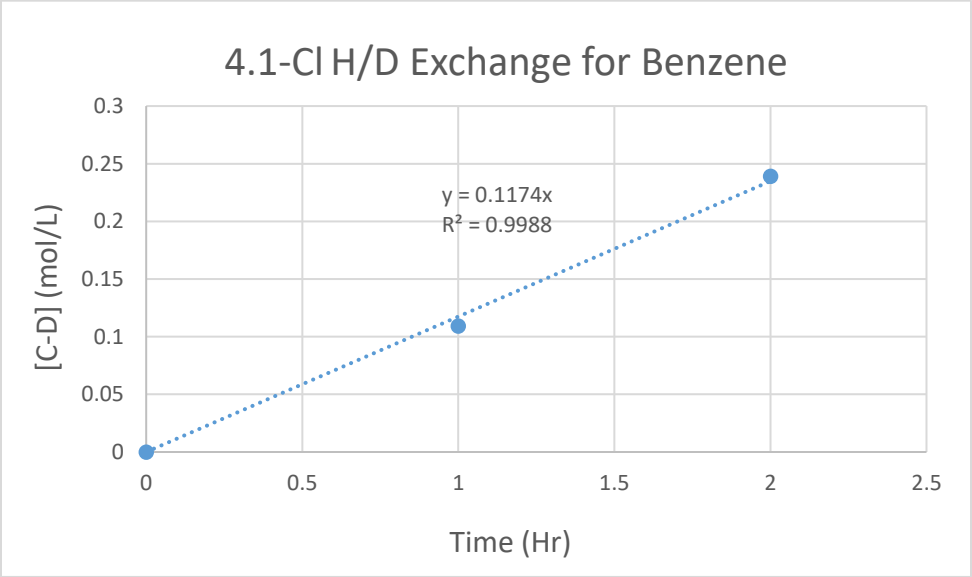

Chart S4.11. Initial rates for the H/D exchange reaction catalyzed by **4.1-Cl** with benzene substrate at 80 °C.

The rate constants for the H/D exchange catalyzed by complex **4.1-Cl** at 80 °C: *Average* CH bond, $k_{c,}$ = 2.8±0.1 M^{-1} h^{-1}

Rate Data for the H/D Exchange Reaction of 4.1-iPr and Fluorobenzene in TFE-d_1

Mass [Pt] (mg)			Density g/mL	Volume mL	Conc. M
3.15		TFE-OD	1.384	0.45	12.46
[Pt] MW		Fluorobenzene	1.025	0.05	1.31
579.53					
Temp. (°C)	80			Substrate MW	78.11

Meta C-H			
SLOPE	0.005336	-0.01049	INT
(+/-)	0.000724	0.008893	(+/-)
r2	0.96448	0.013942	S(Y)
F	54.30696	2	DOF
Reg. SS	0.010556	0.000389	Res. SS

Para C-H			
SLOPE	0.002567	-0.00504	INT
(+/-)	0.000348	0.004277	(+/-)
r2	0.96448	0.006705	S(Y)
F	54.30696	2	DOF
Reg. SS	0.002442	8.99E-05	Res. SS

Ortho C-H			
SLOPE	0.004387	-0.00862	INT
(+/-)	0.000595	0.00731	(+/-)
r2	0.96448	0.01146	S(Y)
F	54.30696	2	DOF
Reg. SS	0.007133	0.000263	Res. SS

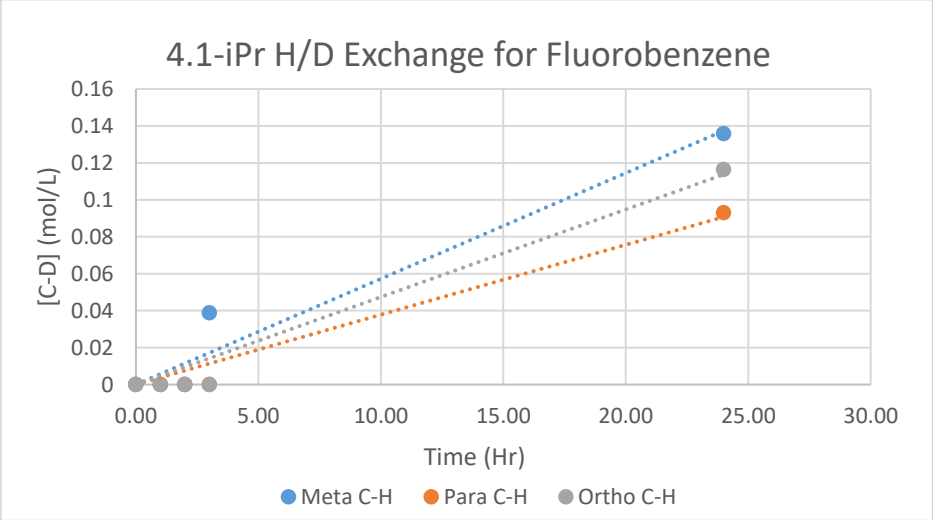

Chart S4.12 Initial rates for the H/D exchange reaction catalyzed by **4.1-iPr** with Fluorobenzene substrate at 80 °C.

The rate constants for the H/D exchange catalyzed by complex **4.1-iPr** at 80 °C:
Ortho-, *para-*, *meta-*, CH bonds, $k_{c,}$ = 0.2±0.03 M^{-1} h^{-1}; 0.2±0.02 M^{-1} h^{-1}; 0.2±0.04 M^{-1} h^{-1};
Average CH bond, $k_{c,}$ = 0.16±0.03 M^{-1} h^{-1}

Initial Rate Data for the H/D Exchange Reaction of 4.1-iPr and Benzene in TFE-d_1

			Density	Volume	Conc.
Mass [Pt] (mg)			g/mL	mL	M
5		TFE-OD	1.384	0.45	12.46
[Pt] MW		Benzene	0.876	0.05	1.12
579.53					
Temp. (°C)	80			Substrate MW	78.11

SLOPE	0.237691	0.068245	INT
(+/-)	0.055504	0.034802	(+/-)
r2	0.859414	0.055032	S(Y)
F	18.33918	3	DOF
Reg. SS	0.05554	0.009085	Res. SS

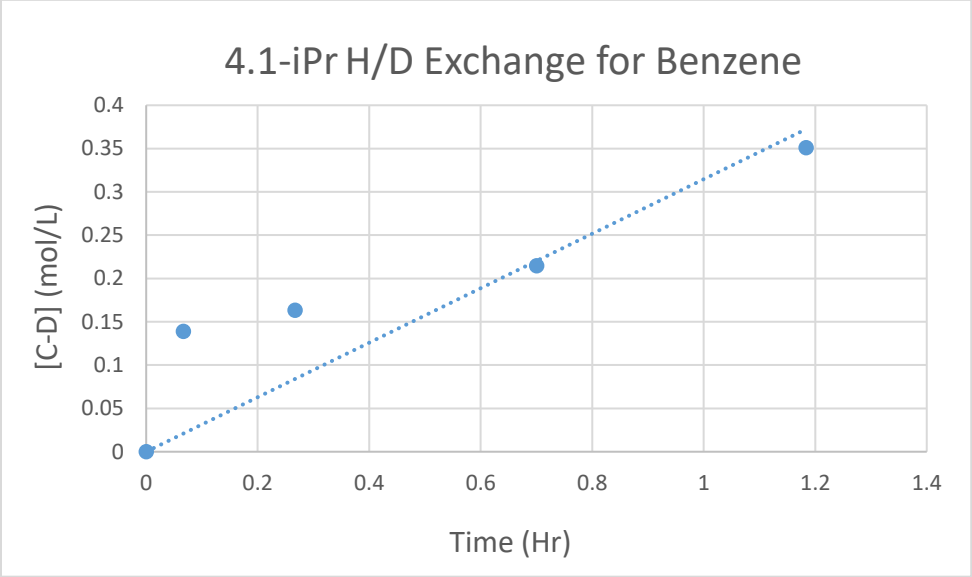

Chart S4.13. Initial rates for the H/D exchange reaction catalyzed by **4.1-iPr** with benzene substrate at 80 °C.

The rate constants for the H/D exchange catalyzed by complex **4.1-iPr** at 80 °C: *Average* CH bond, $k_{c,}$ = 2.1±0.5M^{-1} h^{-1}

Initial Rate Data for the H/D Exchange Reaction of 4.1-iPr and Phenol in TFE-d_1

			Density	Volume/mass	Conc.
Mass [Pt] (mg)			g/mL	mL/mg	M
3.6		TFE-OD	1.384	0.45	12.46
[Pt] MW		Phenol		57.50	1.22
579.53					
Temp. (°C)	80			Substrate MW	94.11

Ortho/Para C-H			
SLOPE	0.053793	0.039252	INT
(+/-)	0.020797	0.057486	(+/-)
r2	0.76986	0.076545	S(Y)
F	6.690374	2	DOF
Reg. SS	0.0392	0.011718	Res. SS

Meta C-H			
SLOPE	0.033552	0.05667301	INT
(+/-)	0.017261	0.047711263	(+/-)
r2	0.653898	0.063529587	S(Y)
F	3.778647	2	DOF
Reg. SS	0.015251	0.008072017	Res. SS

Total Aromatic			
SLOPE	0.087345	0.09592526	INT
(+/-)	0.035839	0.09906472	(+/-)
r2	0.748104	0.131908911	S(Y)
F	5.939778	2	DOF
Reg. SS	0.103352	0.034799921	Res. SS

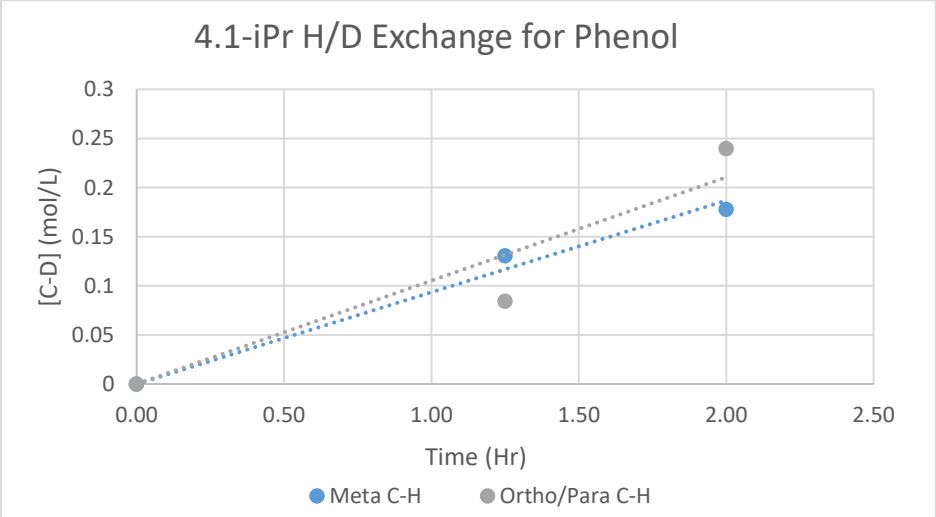

Chart S4.14. Initial rates for the H/D exchange reaction catalyzed by **4.1-iPr** with Phenol substrate at 80 °C.

The rate constants for the H/D exchange catalyzed by complex **4.1-iPr** at 80 °C:
ortho/*para*-, *meta*-, CH bonds, $k_{c,}$ = 1.2±0.4 M^{-1} h^{-1}; 1.1±0.3 M^{-1} h^{-1}
Average CH bond, $k_{c,}$ = 1.2±0.5 M^{-1} h^{-1}

Initial Rate Data for the H/D Exchange Reaction of 4.1-iPr and Anisole in TFE-d_1

Mass [Pt] (mg)			Density g/mL	Volume mL	Conc. M
3.6		TFE-OD	1.384	0.45	12.46
[Pt] MW		Anisole	0.995	0.05	0.92
579.53					
Temp. (°C)	80			Substrate MW	108.14

Meta C-H				Para C-H			
SLOPE	0.0459	0.0057	INT	SLOPE	0.0208	0.0011	INT
(+/-)	0.0117	0.0360	(+/-)	(+/-)	0.0009	0.0029	(+/-)
r2	0.8854	0.0421	S(Y)	r2	0.9960	0.0034	S(Y)
F	15.4589	2	DOF	F	494.7306	2	DOF
Reg. SS	0.0274	0.0035	Res. SS	Reg. SS	0.0056	0.0000	Res. SS

Ortho C-H				Total Aromatic			
SLOPE	0.0203	0.0142	INT	SLOPE	0.0870	0.0210	INT
(+/-)	0.0055	0.0171	(+/-)	(+/-)	0.0135	0.0416	(+/-)
r2	0.8704	0.0200	S(Y)	r2	0.9540	0.0487	S(Y)
F	13.4300	2	DOF	F	41.4847	2	DOF
Reg. SS	0.0054	0.0008	Res. SS	Reg. SS	0.0983	0.0047	Res. SS

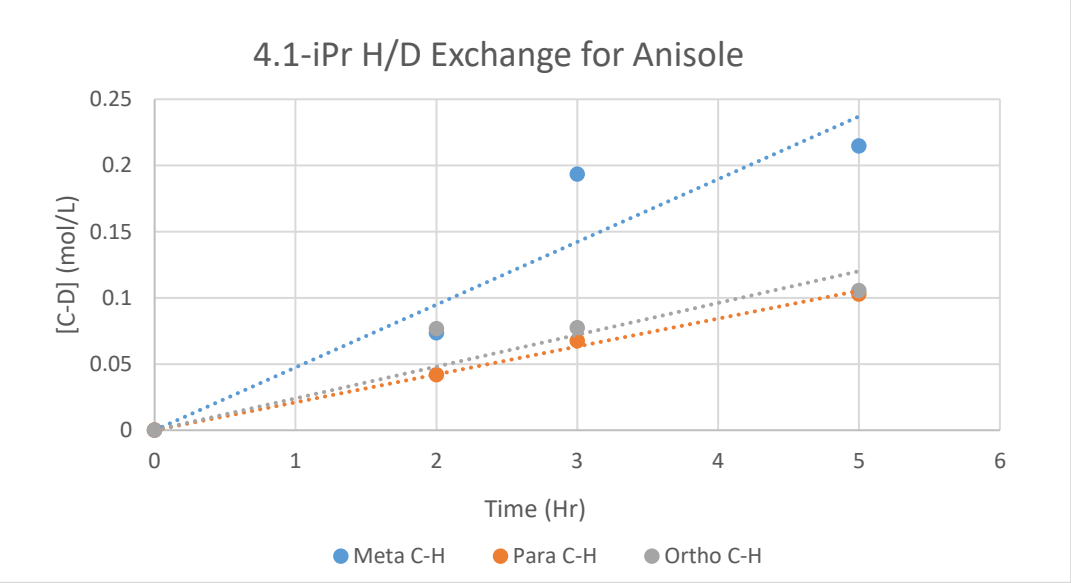

Chart S4.15. Initial rates for the H/D exchange reaction catalyzed by **4.1-iPr** with Anisole substrate at 80 °C.

The rate constants for the H/D exchange catalyzed by complex **4.1-iPr** at 80 °C:
Ortho-, *para-*, *meta-*, CH bonds, k_c = 0.9±0.2 M^{-1} h^{-1}; 1.8±0.1 M^{-1} h^{-1}; 2.0±0.5 M^{-1} h^{-1}
Average CH bond, k_c = 1.5±0.2 M^{-1} h^{-1}

Initial Rate Data for the H/D Exchange Reaction of 4.1-OMe and Fluorobenzene in TFE-d_1

		Density g/mL	Volume mL	Conc. M
Mass [Pt] (mg)	TFE-OD	1.384	0.45	12.46
3.1	Fluorobenzene	1.025	0.05	1.31
[Pt] MW + 7 H2O				
675.48			Substrate MW	78.11

Meta C-H				Para C-H			
SLOPE	0.0020	0.0047342	INT	SLOPE	0.0011	0.001841646	INT
(+/-)	0.0004	0.0056011	(+/-)	(+/-)	0.0002	0.00217888	(+/-)
r2	0.9607	0.0073338	S(Y)	r2	0.9799	0.002852924	S(Y)
F	24.4558	1	DOF	F	48.745	1	DOF
Reg. SS	0.0013	5.379E-05	Res. SS	Reg. SS	0.0004	8.13918E-06	Res. SS

Ortho C-H				Total Aromatic			
SLOPE	0.0013	0.0061917	INT	SLOPE	0.0048	-0.00040451	INT
(+/-)	0.0005	0.0073255	(+/-)	(+/-)	3E-05	0.000478584	(+/-)
r2	0.8611	0.0095916	S(Y)	r2	0.9999	0.000626636	S(Y)
F	6.2012	1	DOF	F	19908	1	DOF
Reg. SS	0.0006	9.2E-05	Res. SS	Reg. SS	0.0078	3.92672E-07	Res. SS

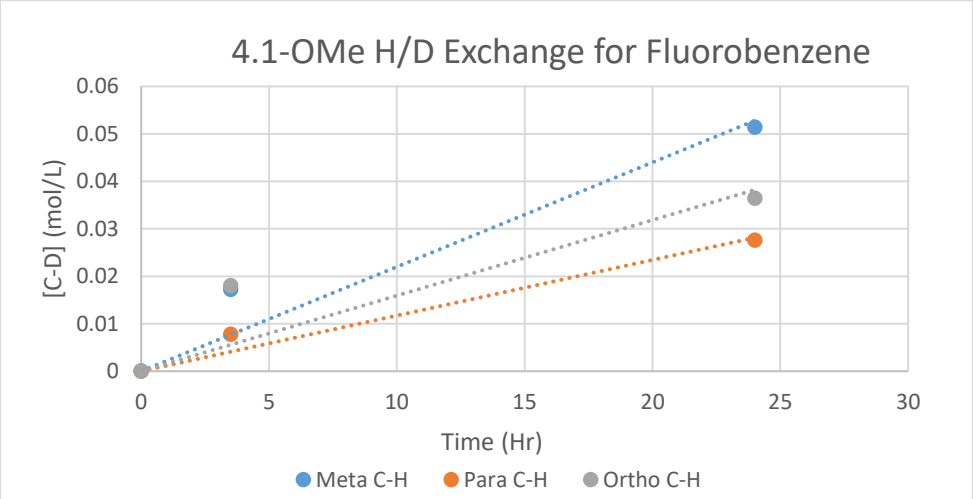

Chart S4.16. Initial rates for the H/D exchange reaction catalyzed by **4.1-OMe** with Fluorobenzene substrate at 80 °C.

The rate constants for the H/D exchange catalyzed by complex **4.1-OMe** at 80 °C:
Ortho-, *para-*, *meta-*, CH bonds, k_c, = 0.05±0.002 M^{-1} h^{-1}; 0.1±0.02 M^{-1} h^{-1}; 0.08±0.02 M^{-1} h^{-1}
Average CH bond, k_c, = 0.08±0.01 M^{-1} h^{-1}

Initial Rate Data for the H/D Exchange Reaction of 4.1-OMe and Benzene in TFE-d_1

			Density	Volume	Conc.
Mass [Pt] (mg)			**g/mL**	**mL**	**M**
3.1		**TFE-OD**	1.384	0.45	12.46
[Pt] MW + 7 H2O		**Benzene**	0.876	0.05	1.12
675.48					
Temp. (°C)	**80**			**Substrate MW**	78.11

SLOPE	0.200627	0.030818	**INT**
(+/-)	0.018797	0.025981	**(+/-)**
r2	0.97434	0.034043	**S(Y)**
F	113.9147	3	**DOF**
Reg. SS	0.132016	0.003477	**Res. SS**

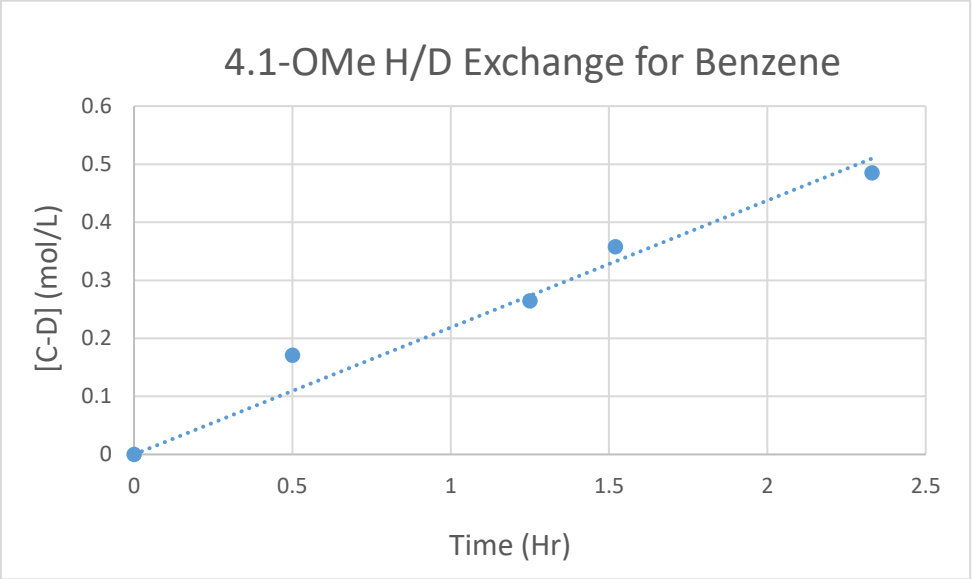

Chart S4.17. Initial rates for the H/D exchange reaction catalyzed by **4.1-OMe** with benzene substrate at 80 °C.

The rate constants for the H/D exchange catalyzed by complex **4.1-OMe** at 80 °C: *Average* CH bond, $k_{c,}$ = 3.3±0.3 M^{-1} h^{-1}

Initial Rate Data for the H/D Exchange Reaction of 4.1-OMe and Phenol in TFE-d_1

			Density	Volume/mass	Conc.
Mass [Pt] (mg)			g/mL	mL/mg	M
3.55		TFE-OD	1.384	0.45	12.46
[Pt] MW + 7 H2O		Phenol		22.5	0.48
675.48					
Temp. (°C)	80			Substrate MW	94.11

Meta C-H				Para C-H			
SLOPE	0.0507	0.0008	INT	SLOPE	0.0226	0.0056	INT
(+/-)	0.0032	0.0086	(+/-)	(+/-)	0.0036	0.0096	(+/-)
r2	0.9919	0.0097	S(Y)	r2	0.9512	0.0108	S(Y)
F	245.6029	2	DOF	F	38.9463	2	DOF
Reg. SS	0.0229	0.0002	Res. SS	Reg. SS	0.0046	0.0002	Res. SS

Ortho C-H				Total Aromatic			
SLOPE	0.0464	0.0095	INT	SLOPE	0.1197	0.0159	INT
(+/-)	0.0057	0.0152	(+/-)	(+/-)	0.0085	0.0224	(+/-)
r2	0.9703	0.0172	S(Y)	r2	0.9901	0.0253	S(Y)
F	65.2531	2	DOF	F	199.5491	2	DOF
Reg. SS	0.0192	0.0006	Res. SS	Reg. SS	0.1279	0.0013	Res. SS

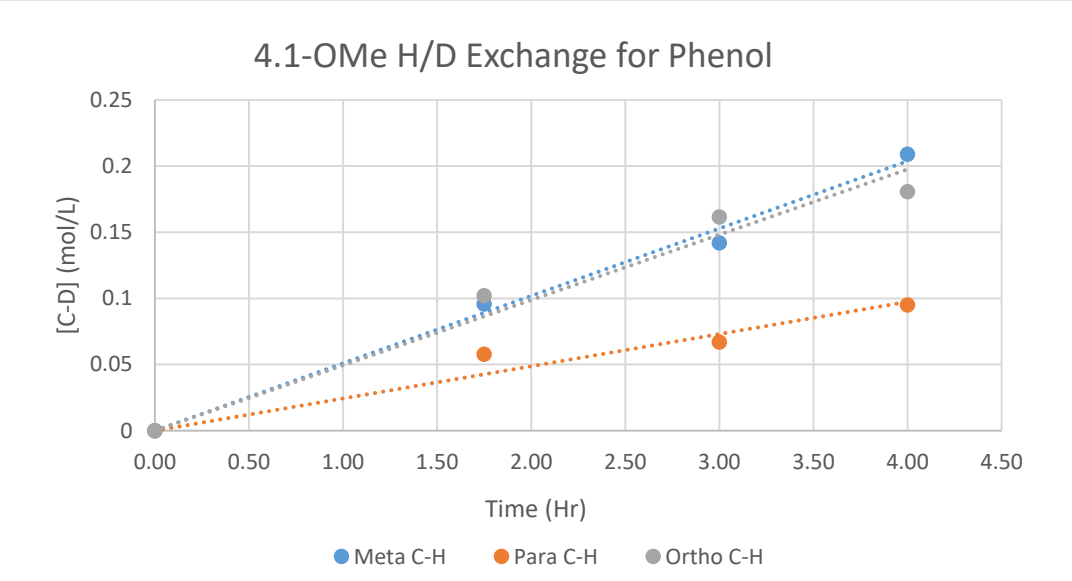

Chart S4.18. Initial rates for the H/D exchange reaction catalyzed by **4.1-OMe** with Phenol substrate at 80 °C.

The rate constants for the H/D exchange catalyzed by complex **4.1-OMe** at 80 °C:
Ortho-, *para-*, *meta-*, CH bonds, $k_{c,}$ = 4.6±0.6 M^{-1} h^{-1}; 4.5±1.7 M^{-1} h^{-1}; 5.0±0.3 M^{-1} h^{-1}
Average CH bond, $k_{c,}$ = 4.8±0.3 M^{-1} h^{-1}

Initial Rate Data for the H/D Exchange Reaction of 4.1-OMe and Anisole in TFE-d_1

Mass [Pt] (mg)		Density g/mL	Volume mL	Conc. M
5.7	TFE-OD	1.384	0.45	12.46
[Pt] MW + 7 H2O	Anisole	0.995	0.05	0.92
675.48				
Temp. (°C)	80		Substrate MW	108.14

Meta C-H				Ortho/Para C-H			
SLOPE	0.084652	-0.00105	INT	SLOPE	0.130630676	0.009823	INT
(+/-)	0.023658	0.011505	(+/-)	(+/-)	0.027126237	0.013192	(+/-)
r2	0.810167	0.016273	S(Y)	r2	0.885454911	0.018658	S(Y)
F	12.80336	3	DOF	F	23.1905598	3	DOF
Reg. SS	0.00339	0.000794	Res. SS	Reg. SS	0.008073345	0.001044	Res. SS

Total Aromatic			
SLOPE	0.215282	0.008774	INT
(+/-)	0.048474	0.023573	(+/-)
r2	0.867983	0.033342	S(Y)
F	19.72436	3	DOF
Reg. SS	0.021927	0.003335	Res. SS

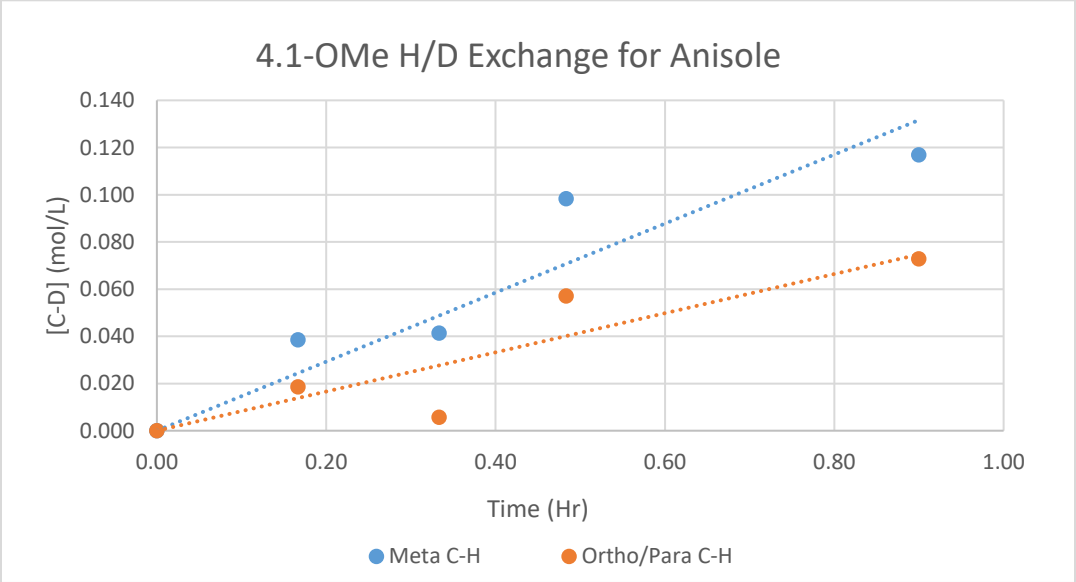

Chart S4.19. Initial rates for the H/D exchange reaction catalyzed by **4.1-OMe** with Anisole substrate at 80 °C.

The rate constants for the H/D exchange catalyzed by complex **4.1-OMe** at 80 °C:
ortho/*para*-, *meta*-, CH bonds, $k_{c,}$ = 5.2±1.1 M^{-1} h^{-1}; 5.0±1.4 M^{-1} h^{-1}
Average CH bond, $k_{c,}$ = 5.1±1.1 M^{-1} h^{-1}

Initial Rate Data for the H/D Exchange Reaction of 4.1-tBu and Nitrobenzene in TFE-d_1

Mass [Pt] (mg)			Density g/mL	Volume mL	Conc. M
3.9		TFE-OD	1.384	0.45	12.46
[Pt] MW + 2 H2O		Nitrobenzene	1.200	0.05	0.97
629.56					
Temp. (°C)	80			Substrate MW	123.11

Ortho C-H				Para C-H			
SLOPE	0.001107	-0.00182	INT	SLOPE	0.008674	-0.00389	INT
(+/-)	9.14E-05	0.00111	(+/-)	(+/-)	0.00586	0.012624	(+/-)
r2	0.986538	0.001776	S(Y)	r2	0.686618	0.01321	S(Y)
F	146.5701	2	DOF	F	2.190997	1	DOF
Reg. SS	0.000462	6.31E-06	Res. SS	Reg. SS	0.000382	0.000175	Res. SS

Meta C-H				Total Aromatic			
SLOPE	0.01866	0.002001	INT	SLOPE	0.027334	-0.00189	INT
(+/-)	0.003013	0.006491	(+/-)	(+/-)	0.002847	0.006134	(+/-)
r2	0.974589	0.006792	S(Y)	r2	0.989267	0.006418	S(Y)
F	38.35347	1	DOF	F	92.16891	1	DOF
Reg. SS	0.001769	4.61E-05	Res. SS	Reg. SS	0.003797	4.12E-05	Res. SS

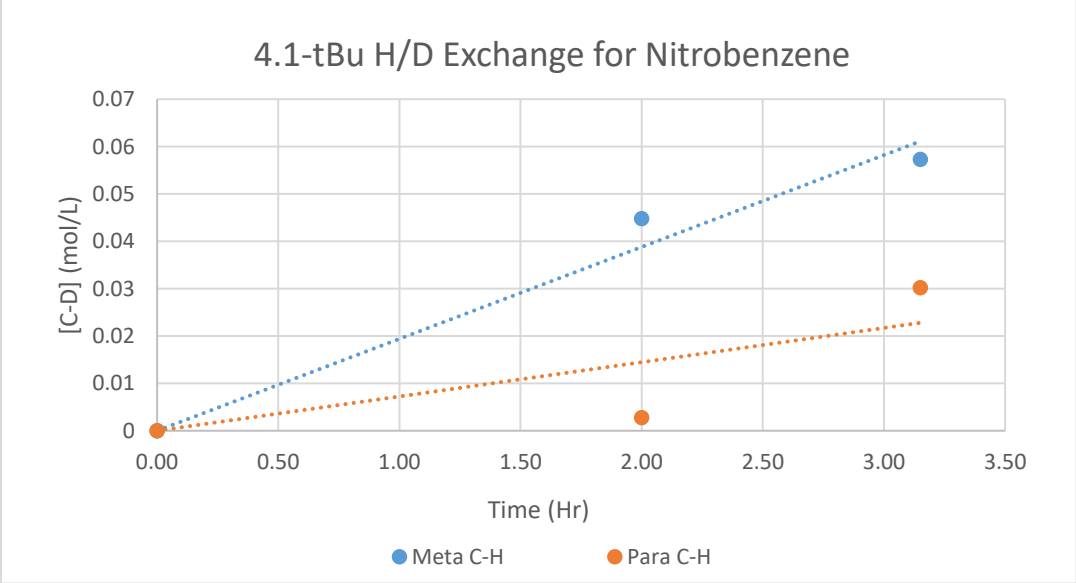

Chart S4.20. Initial rates for the H/D exchange reaction catalyzed by **4.1-tBu** with Nitrobenzene substrate at 80 °C.

The rate constants for the H/D exchange catalyzed by complex **4.1-tBu** at 80 °C:
para-, *meta-*, CH bonds, k_c = 0.7±0.5M^{-1} h^{-1}; 0.8±0.1M^{-1} h^{-1}
Average CH bond, k_c = 0.5±0.05 M^{-1} h^{-1}

Ortho-, C-H bond rate estimated from 24 hour deuteration: $k_{c,\,obs}$ = 0.04 M^{-1} h^{-1}

Initial Rate Data for the H/D Exchange Reaction of 4.1-tBu and Fluorobenzene in TFE-d_1

		Density	Volume	Conc.
Mass [Pt] (mg)		g/mL	mL	M
4.4	TFE-OD	1.384	0.45	12.46
[Pt] MW + 2 H2O	Fluorobenzene	1.025	0.05	1.31
629.56				
			Substrate	
Temp. (°C)	80		MW	78.11

Meta				Para			
SLOPE	0.042935693	0.002579941	INT	SLOPE	0.01859	0.003752	INT
(+/-)	0.002635988	0.004853816	(+/-)	(+/-)	0.002652	0.004883	(+/-)
r2	0.992517989	0.006066711	S(Y)	r2	0.960895	0.006103	S(Y)
F	265.3078099	2	DOF	F	49.14419	2	DOF
Reg. SS	0.00976465	7.361E-05	Res. SS	Reg. SS	0.001831	7.45E-05	Res. SS

Ortho				Total Aromatic			
SLOPE	0.035327434	0.004716814	INT	SLOPE	0.096853	0.011049	INT
(+/-)	0.002447784	0.004507263	(+/-)	(+/-)	0.007232	0.013317	(+/-)
r2	0.990489535	0.005633559	S(Y)	r2	0.988972	0.016644	S(Y)
F	208.2946675	2	DOF	F	179.3601	2	DOF
Reg. SS	0.006610646	6.3474E-05	Res. SS	Reg. SS	0.049687	0.000554	Res. SS

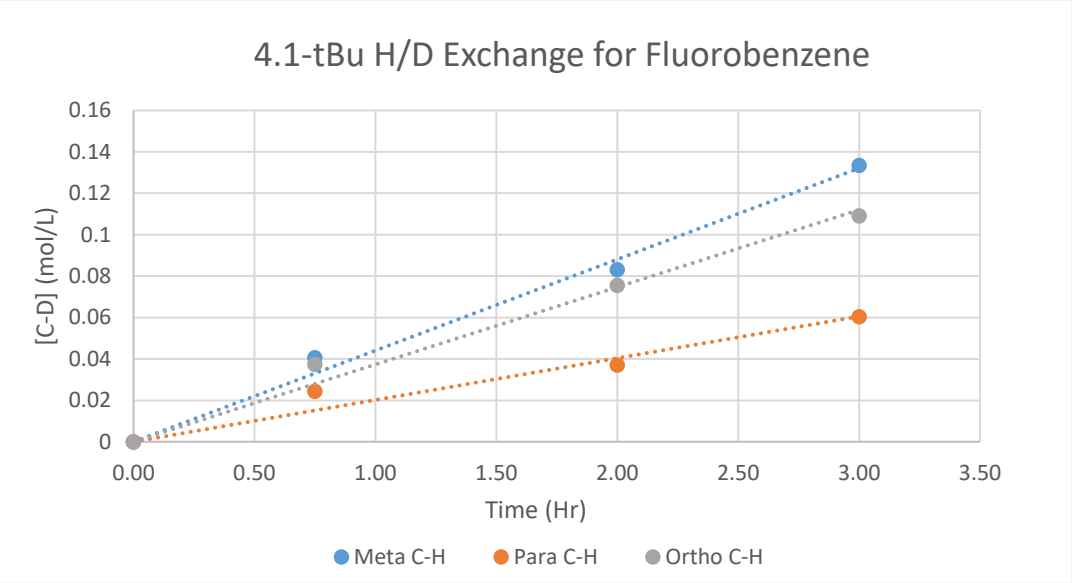

Chart S4.21. Initial rates for the H/D exchange reaction catalyzed by **4.1-tBu** with Fluorobenzene substrate at 80 °C.

The rate constants for the H/D exchange catalyzed by complex **4.1-tBu** at 80 °C:
Ortho-, *para*-, *meta*-, CH bonds, k_c = 1.0±0.1 M^{-1} h^{-1}; 1.0±0.1 M^{-1} h^{-1}; 1.2±0.1 M^{-1} h^{-1}
Average CH bond, k_c = 1.1±0.1 M^{-1} h^{-}

Initial Rate Data for the H/D Exchange Reaction of 4.1-tBu and Benzene in TFE-d_1

			Density	Volume	Conc.
Mass [Pt] (mg)			g/mL	mL	M
3.2		TFE-OD	1.384	0.45	12.46
[Pt] MW + 2 H2O		Benzene	0.876	0.05	1.12
629.56					
Temp. (°C)	80			Substrate MW	78.11

SLOPE	0.46164	-0.012671	INT
(+/-)	0.00758	0.0121279	(+/-)
r2	0.99946	0.0172557	S(Y)
F	3712.8	2	DOF
Reg. SS	1.10552	0.0005955	Res. SS

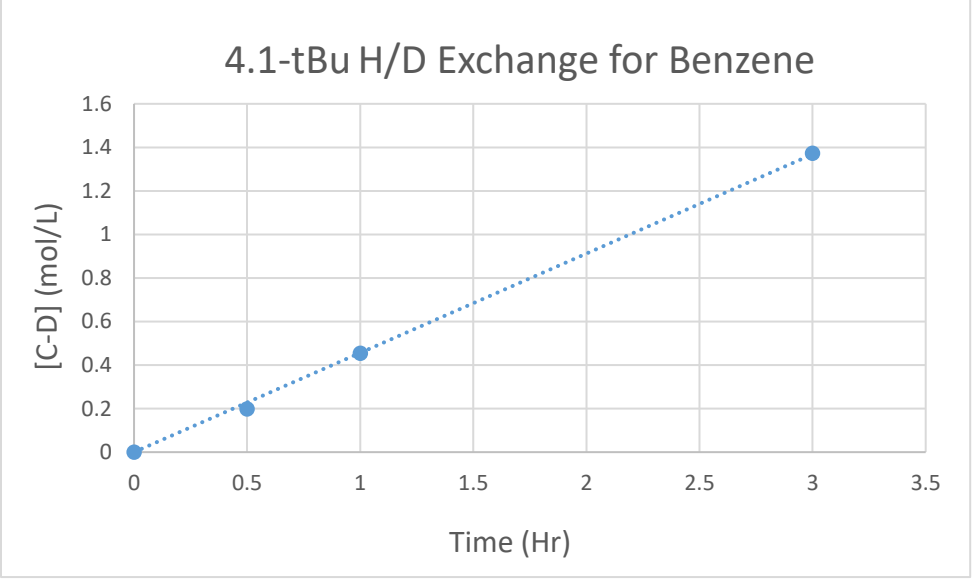

Chart S4.22. Initial rates for the H/D exchange reaction catalyzed by **4.1-tBu** with benzene substrate at 80 °C.

The rate constants for the H/D exchange catalyzed by complex **4.1-tBu** at 80 °C: *Average* CH bond, $k_{c,}$ = 6.8±0.1 M^{-1} h^{-1}

Initial Rate Data for the H/D Exchange Reaction of 4.1-tBu and Phenol in TFE-d_1

				Density	Volume/mass	Conc.
Mass [Pt] (mg)				g/mL	mL/mg	M
4.9			TFE-OD	1.384	0.50	13.84
[Pt] MW + 2 H2O			Phenol		53.50	1.14
629.56						
Temp. (°C)	80				Substrate MW	94.11

Meta C-H				Para C-H			
SLOPE	0.2701	0.0324	INT	SLOPE	0.2998	0.0058	INT
(+/-)	0.0420	0.0208	(+/-)	(+/-)	0.0307	0.0101	(+/-)
r2	0.9322	0.0284	S(Y)	r2	0.9795	0.0120	S(Y)
F	41.2714	3	DOF	F	95.5213	2	DOF
Reg. SS	0.0334	0.0024	Res. SS	Reg. SS	0.0138	0.0003	Res. SS

Ortho C-H				Total Aromatic			
SLOPE	0.4809	0.0236	INT	SLOPE	1.1578	0.0399	INT
(+/-)	0.0371	0.0183	(+/-)	(+/-)	0.1567	0.0518	(+/-)
r2	0.9824	0.0251	S(Y)	r2	0.9647	0.0613	S(Y)
F	167.5655	3	DOF	F	54.6157	2	DOF
Reg. SS	0.1058	0.0019	Res. SS	Reg. SS	0.2055	0.0075	Res. SS

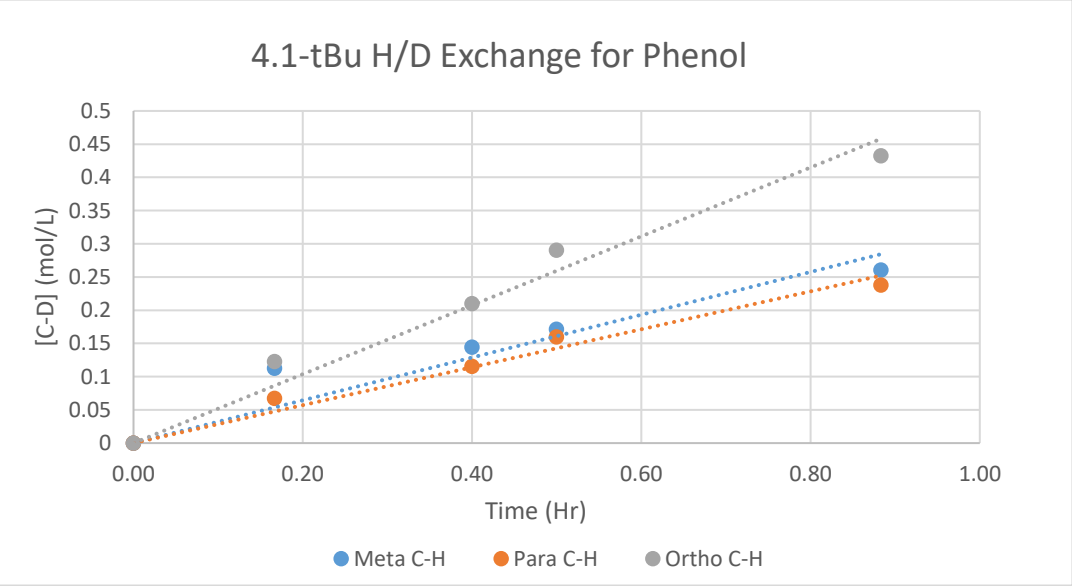

Chart S4.23. Initial rates for the H/D exchange reaction catalyzed by **4.1-tBu** with Phenol substrate at 80 °C.

The rate constants for the H/D exchange catalyzed by complex **4.1-tBu** at 80 °C:
ortho-, *para*-, *meta*-, CH bonds, $k_{c,}$ = 13.6±1.1 M^{-1} h^{-1}; 17.±1.7 M^{-1} h^{-1}; 7.6±1.2 M^{-1} h^{-1}
Average CH bond, $k_{c,}$ = 13.1±1.8 M^{-1} h^{-1}

Initial Rate Data for the H/D Exchange Reaction of 4.1-tBu and Anisole in TFE-d_1

			Density	Volume	Conc.
Mass [Pt] (mg)			g/mL	mL	M
4.4		TFE-OD	1.384	0.45	12.46
[Pt] MW + 2 H2O		Anisole	0.995	0.05	0.92
629.56					
Temp. (°C)	80			Substrate MW	108.14

Meta C-H				Para C-H			
SLOPE	0.322544	0.013987	INT	SLOPE	0.148842	0.001622	INT
(+/-)	0.039955	0.015046	(+/-)	(+/-)	0.00635	0.002391	(+/-)
r2	0.970224	0.018188	S(Y)	r2	0.996373	0.00289	S(Y)
F	65.16918	2	DOF	F	549.48	2	DOF
Reg. SS	0.021558	0.000662	Res. SS	Reg. SS	0.004591	1.67E-05	Res. SS

Ortho C-H				Total Aromatic C-H			
SLOPE	0.095529	0.030812	INT	SLOPE	0.642072	0.022578	INT
(+/-)	0.009415	0.01085	(+/-)	(+/-)	0.062421	0.023506	(+/-)
r2	0.953687	0.019514	S(Y)	r2	0.981448	0.028415	S(Y)
F	102.9612	5	DOF	F	105.8034	2	DOF
Reg. SS	0.039209	0.001904	Res. SS	Reg. SS	0.085429	0.001615	Res. SS

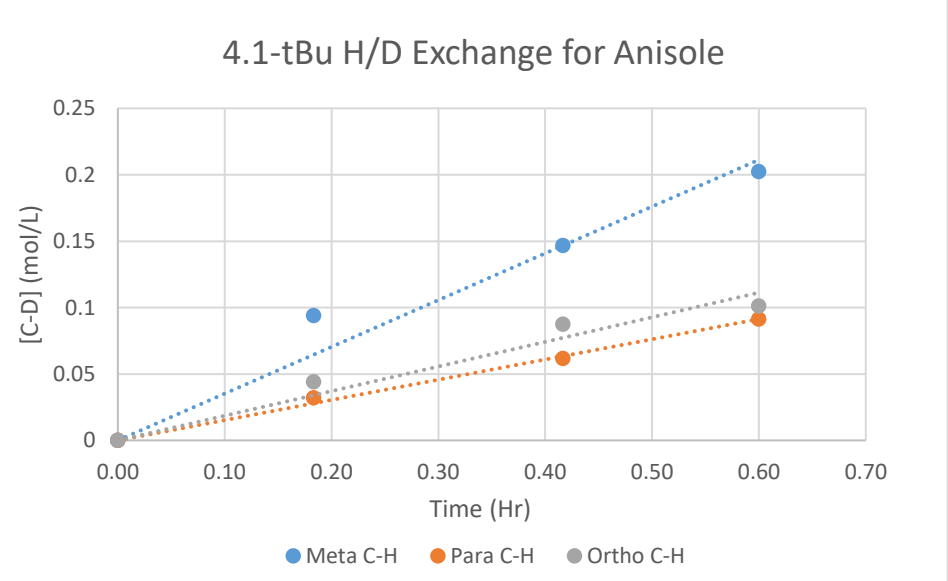

Chart S4.24. Initial rates for the H/D exchange reaction catalyzed by **4.1-tBu** with Anisole substrate at 80 °C.

The rate constants for the H/D exchange catalyzed by complex **4.1-tBu** at 80 °C:
ortho-, *para-*, *meta-*, CH bonds, k_c, = 3.7±0.4 M^{-1} h^{-1}; 11.±0.5 M^{-1} h^{-1}; 13±1.5 M^{-1} h^{-1}
Average CH bond, k_c, = 10±1 M^{-1} h^{-1}

VII. Spectral Data

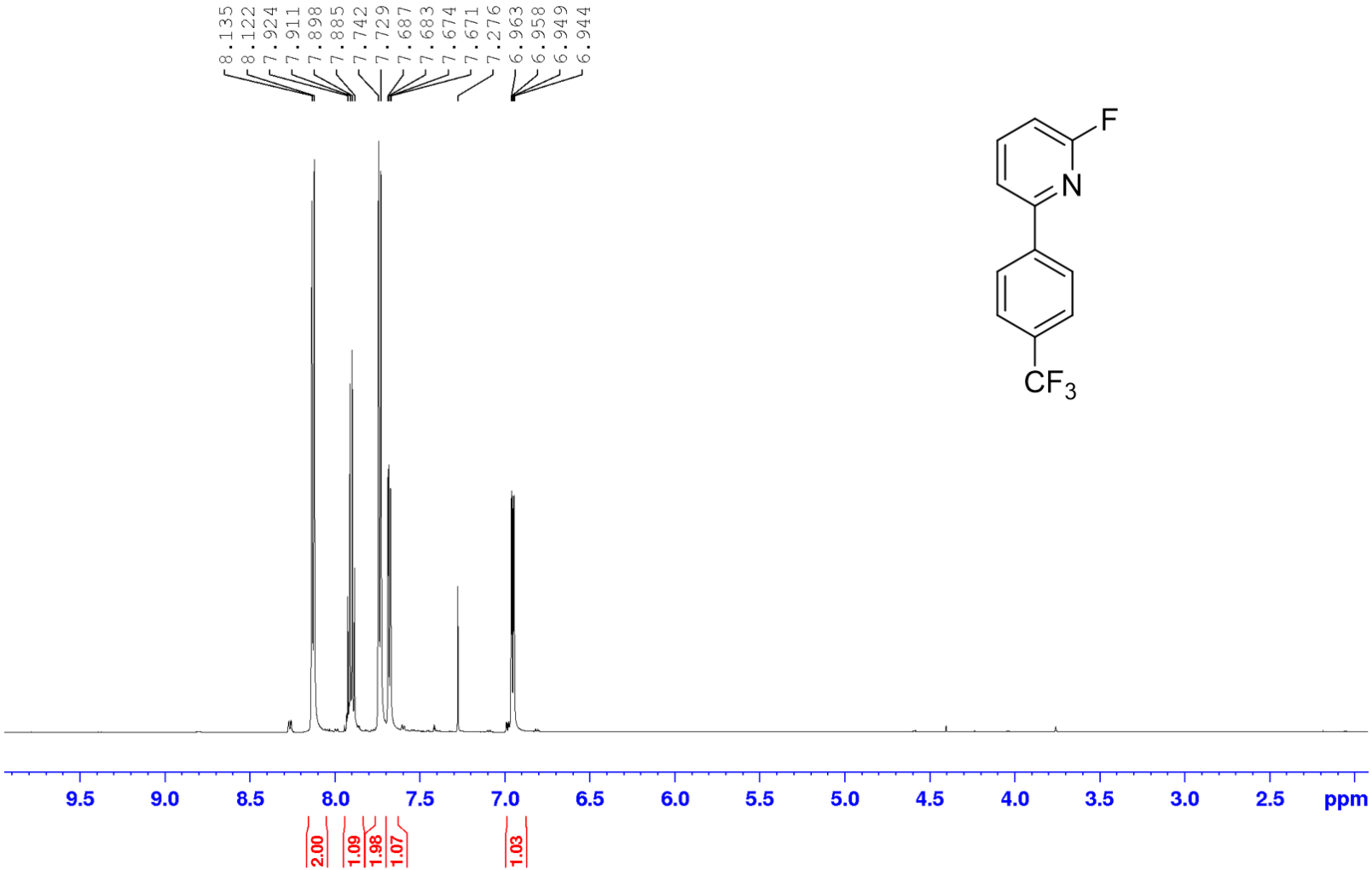

Figure S4.13. ^{1}H-NMR for 2-fluoro-6-(4-trifluoromethylphenyl) pyridine, **4.5-CF$_3$** in $CDCl_3$

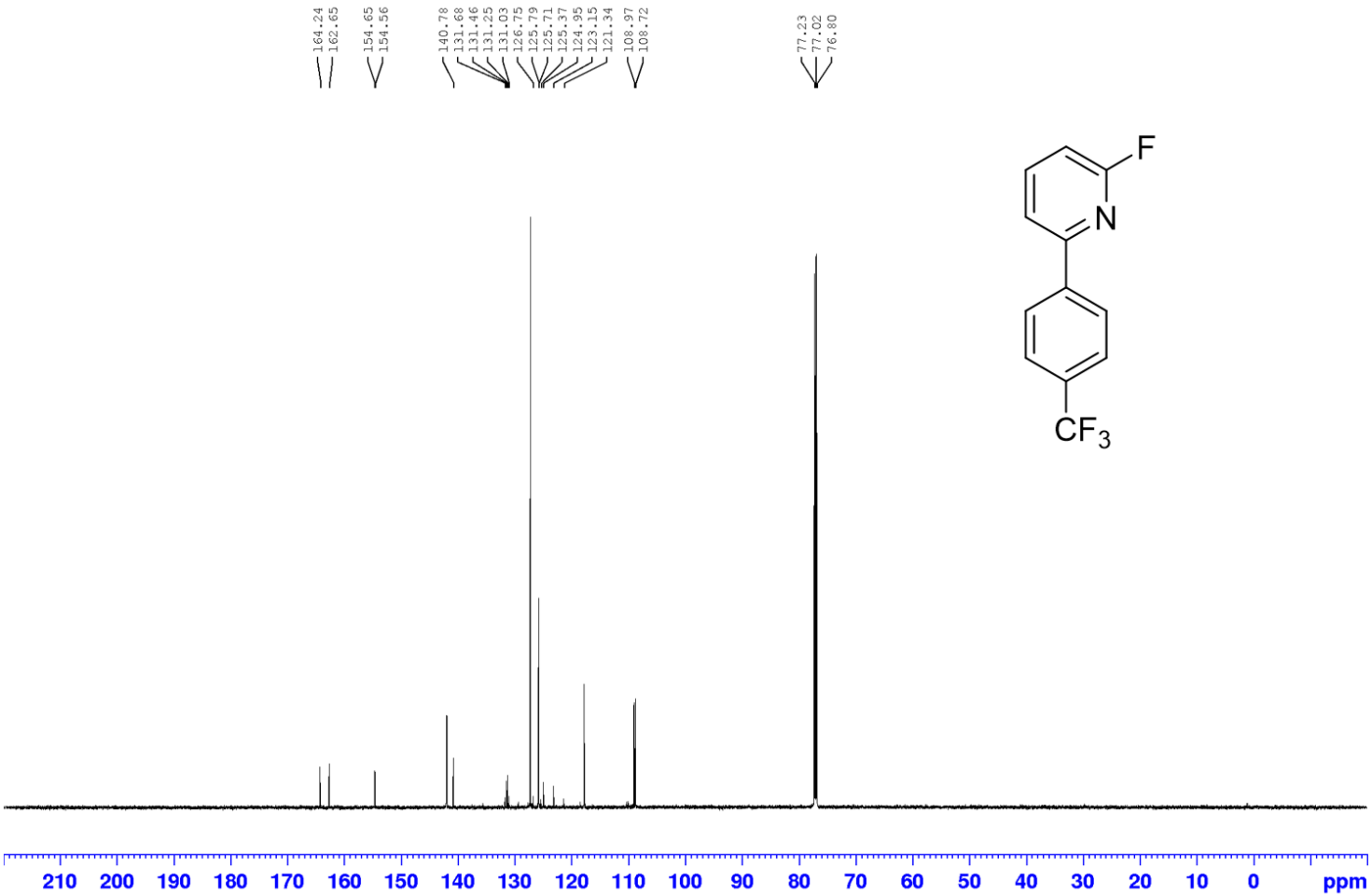

Figure S4.14. ^{13}C-NMR for 2-fluoro-6-(4-trifluoromethylphenyl) pyridine, **4.5-CF$_3$** in $CDCl_3$

Figure S4.15. ^{19}F-NMR for 2-fluoro-6-(4-trifluoromethylphenyl) pyridine, **4.5-CF$_3$** in $CDCl_3$

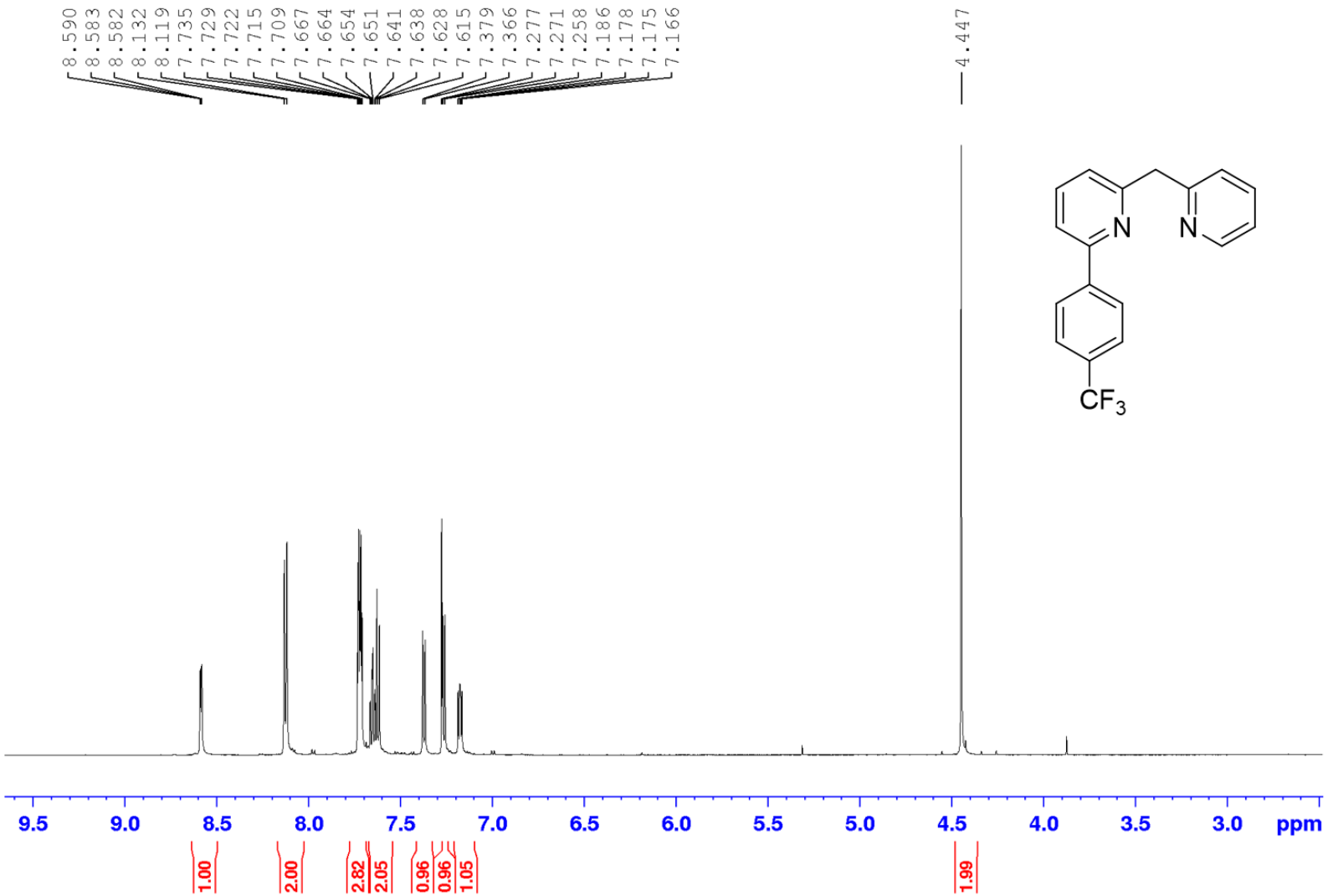

Figure S4.16. ^{1}H-NMR for 2-(4-trifluoromethylphenyl)-6-(pyridin-2-ylmethyl) pyridine, **4.6-CF$_3$** in $CDCl_3$

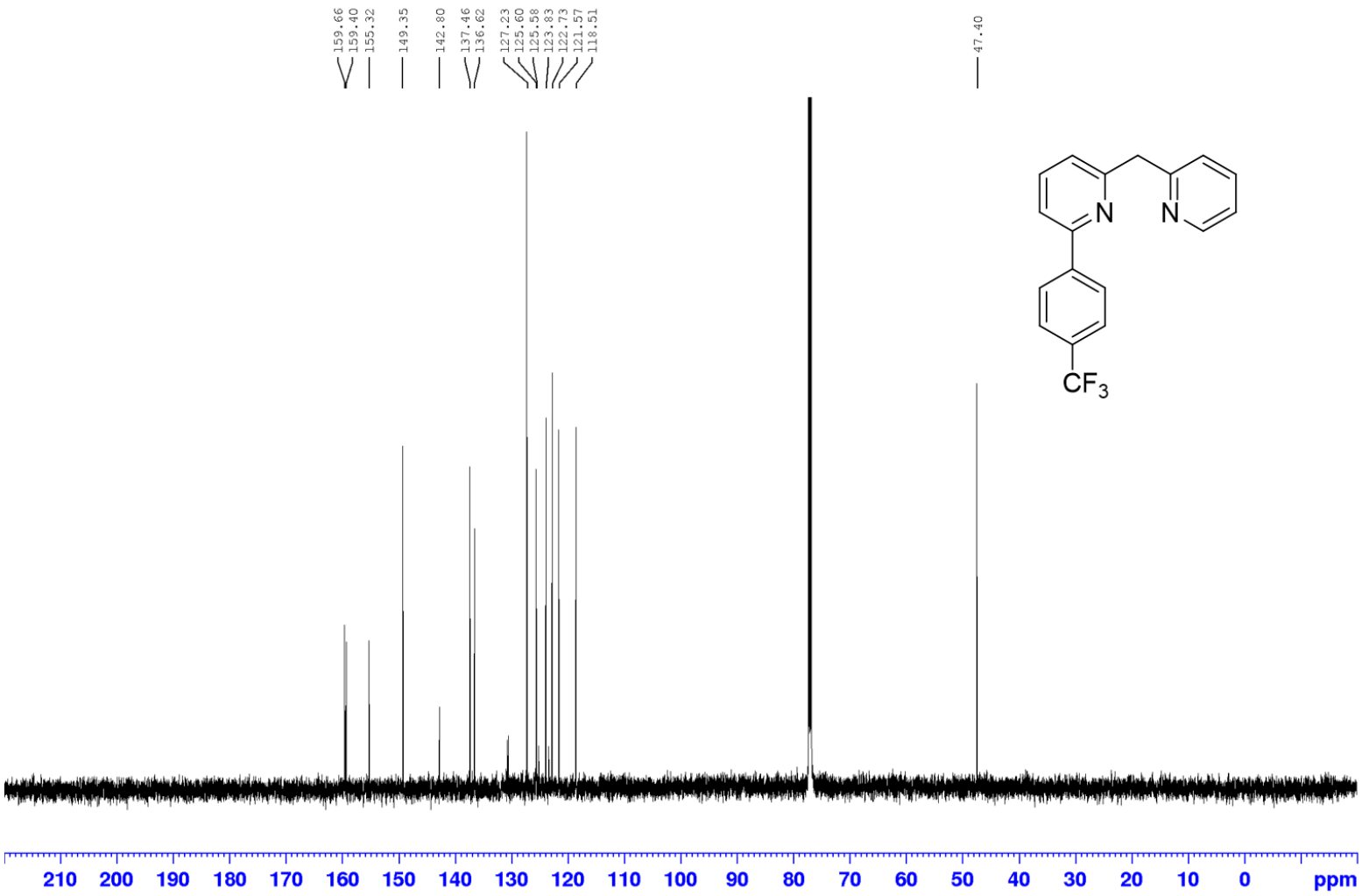

Figure S4.17. ^{13}C-NMR for 2-(4-trifluoromethylphenyl)-6-(pyridin-2-ylmethyl) pyridine, **4.6-CF$_3$** in $CDCl_3$

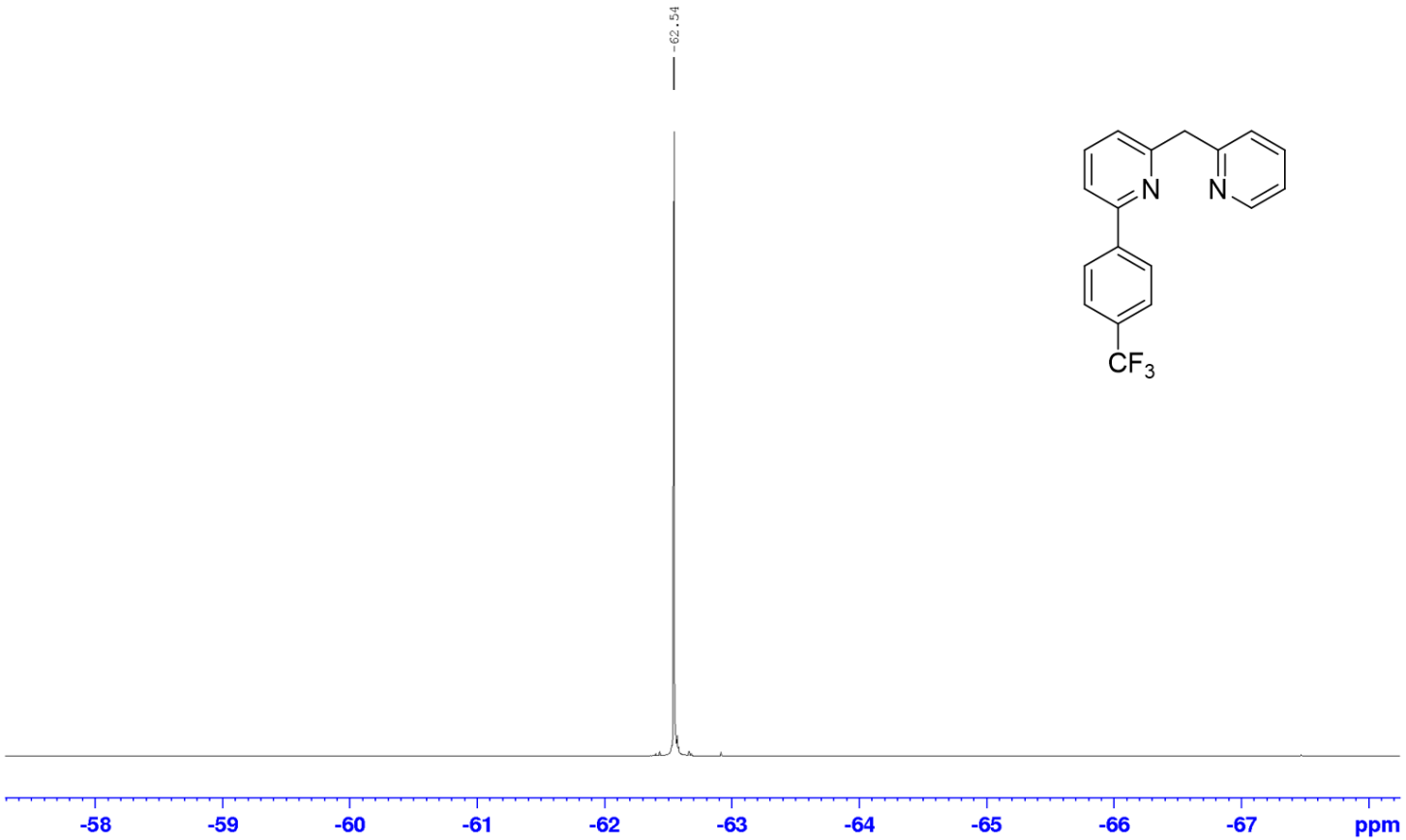

Figure S4.18. ^{19}F-NMR for 2-(4-trifluoromethylphenyl)-6-(pyridin-2-ylmethyl) pyridine, **4.6-CF$_3$** in $CDCl_3$

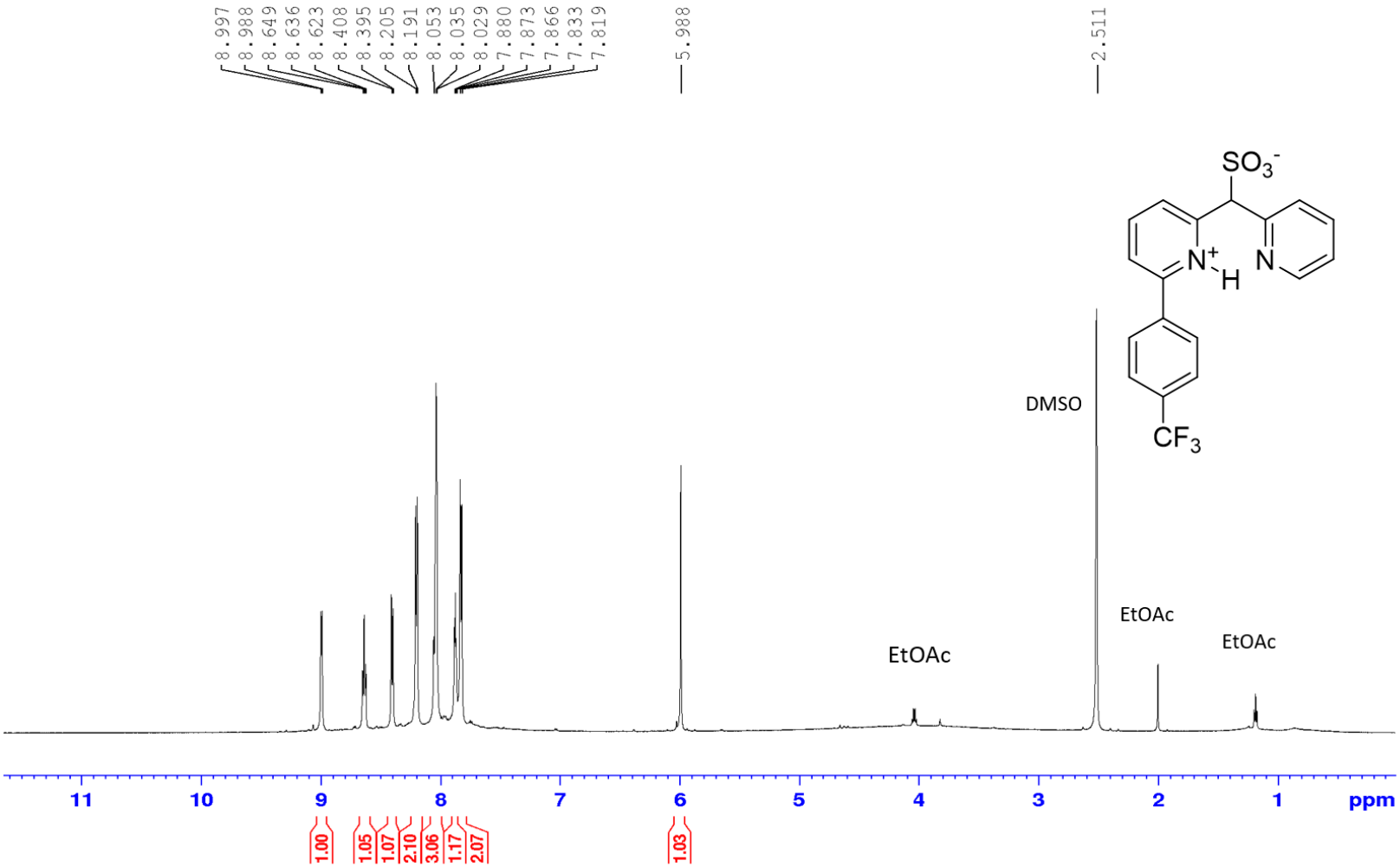

Figure S4.19. ^{1}H-NMR for 2-(4-trifluoromethylphenyl)-6-(pyridin-2-ylmethyl) pyridinium sulfonate, **4.7-CF$_3$** in DMSO-d_6

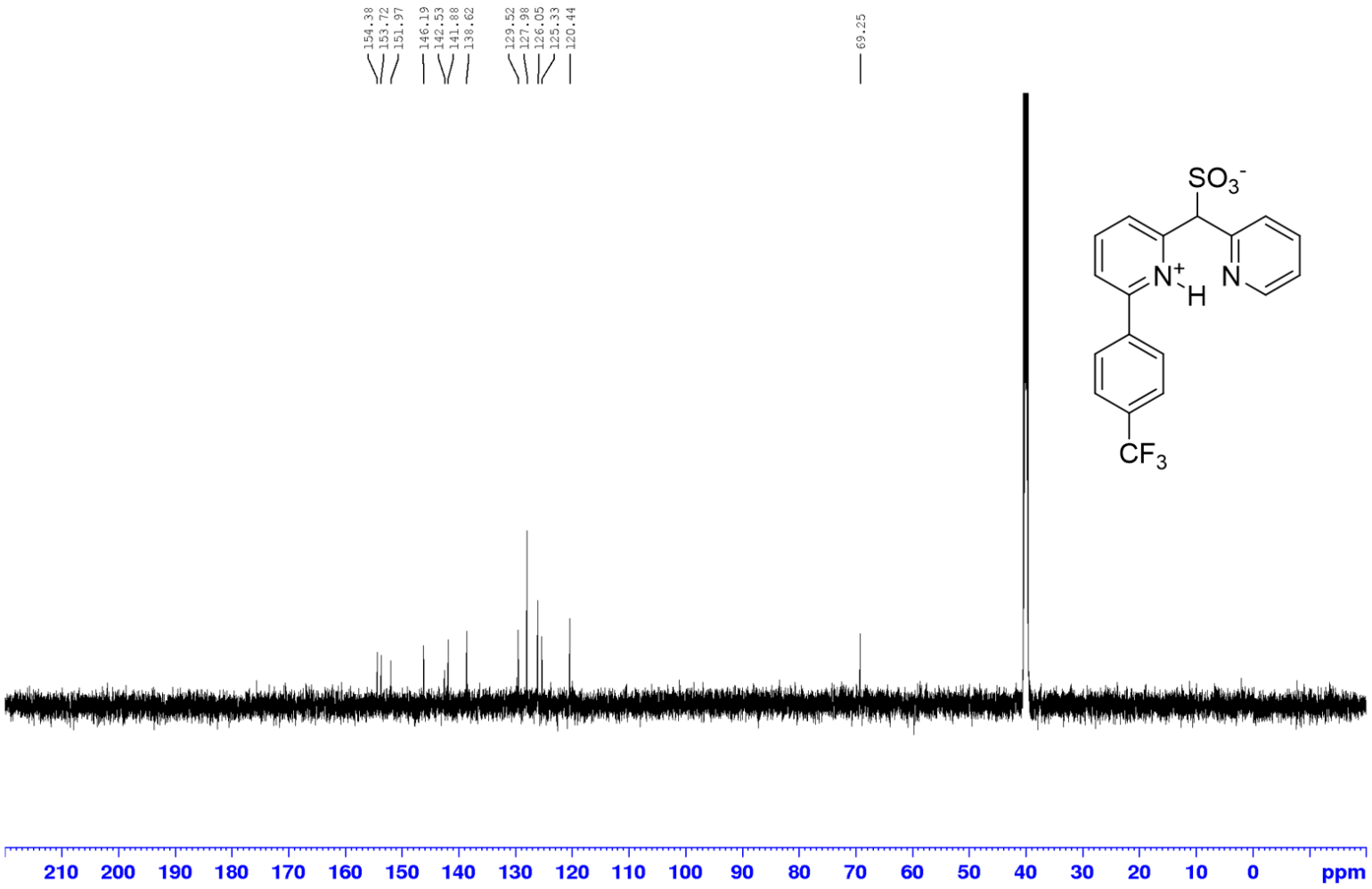

Figure S4.20. ^{13}C-NMR for 2-(4-trifluoromethylphenyl)-6-(pyridin-2-ylmethyl) pyridinium sulfonate, **4.7-CF$_3$** in DMSO-*d*$_6$

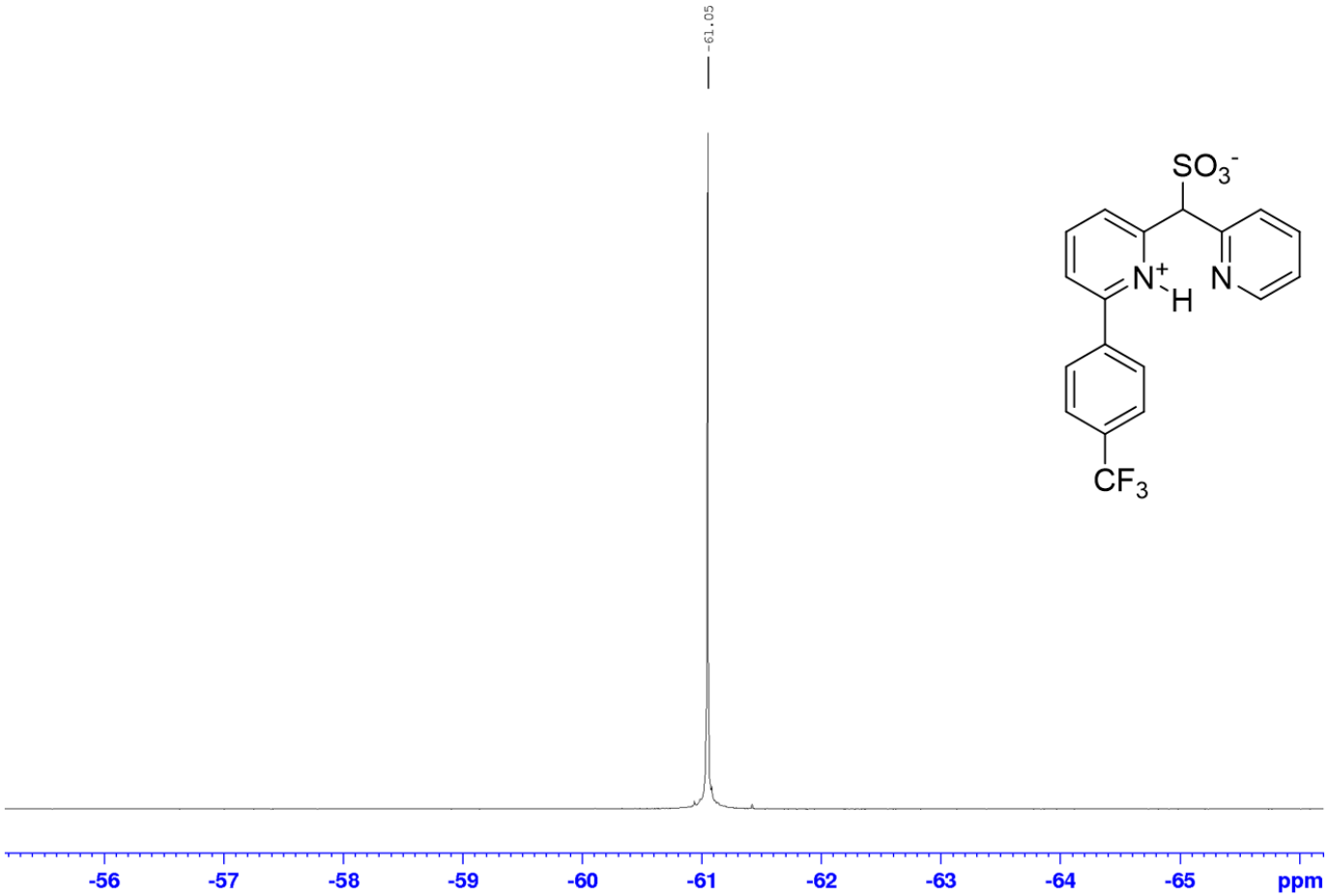

Figure S4.21. ^{19}F-NMR for 2-(4-trifluoromethylphenyl)-6-(pyridin-2-ylmethyl) pyridinium sulfonate, **4.7-CF$_3$** in DMSO-d_6

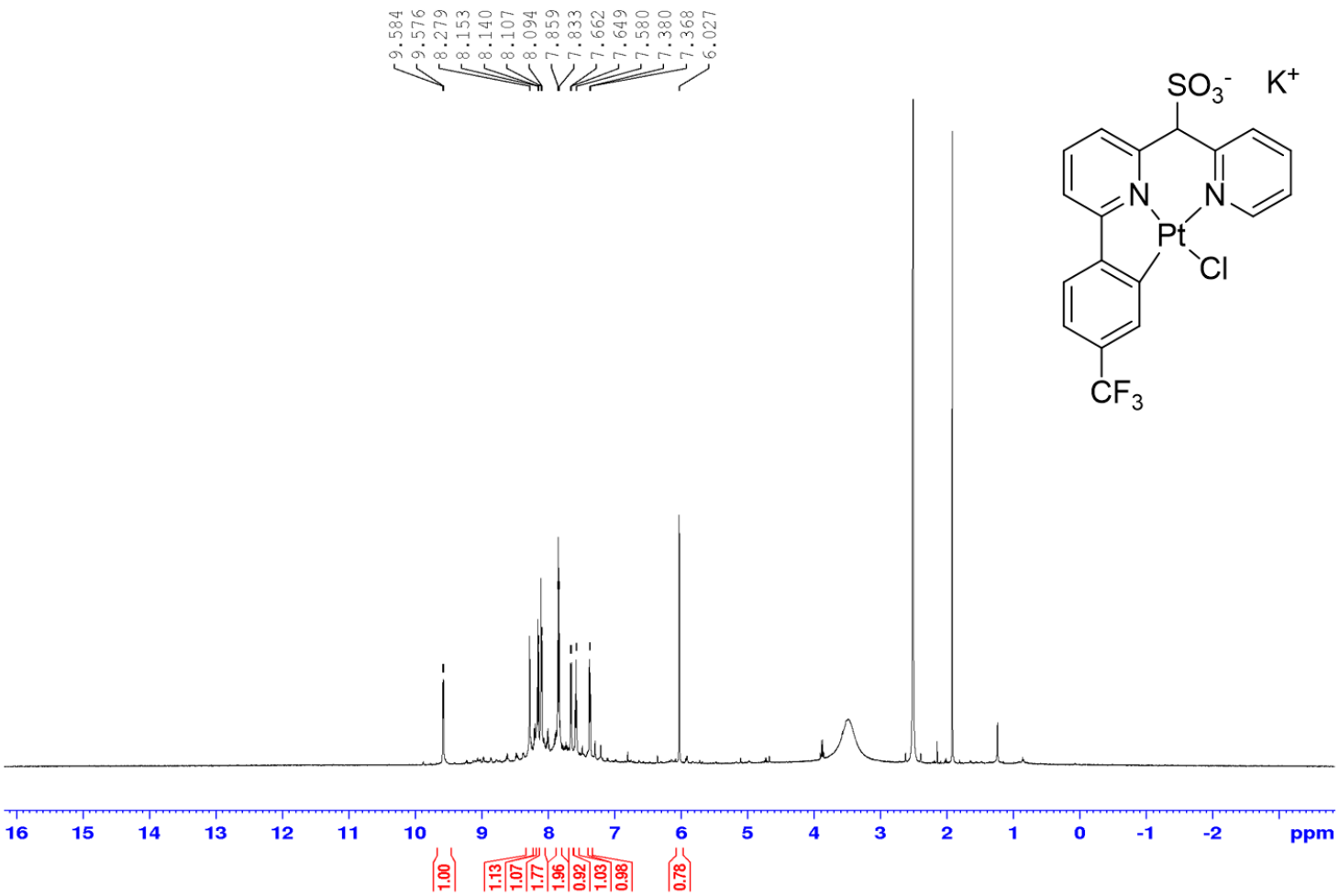

Figure S4.22. ^{1}H-NMR for 2-(4-trifluoromethylphenyl)-6-(pyridin-2-ylmethyl) pyridine Pt-Cl Complex, **4.8-CF$_3$** in DMSO-*d*$_6$

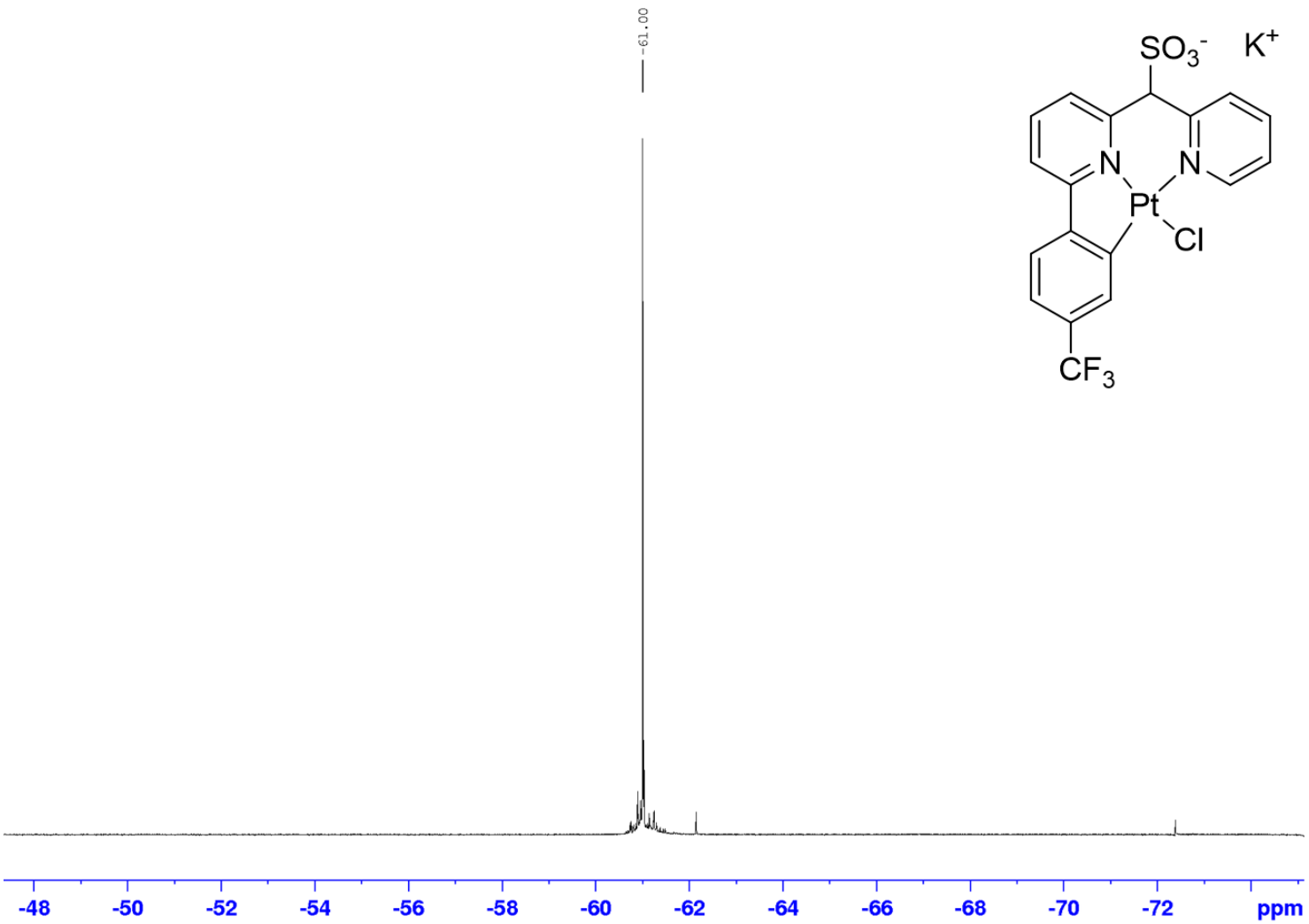

Figure S4.23. ^{19}F-NMR for 2-(4-trifluoromethylphenyl)-6-(pyridin-2-ylmethyl) pyridine Pt-Cl Complex, **4.8-CF$_3$** in DMSO-d_6

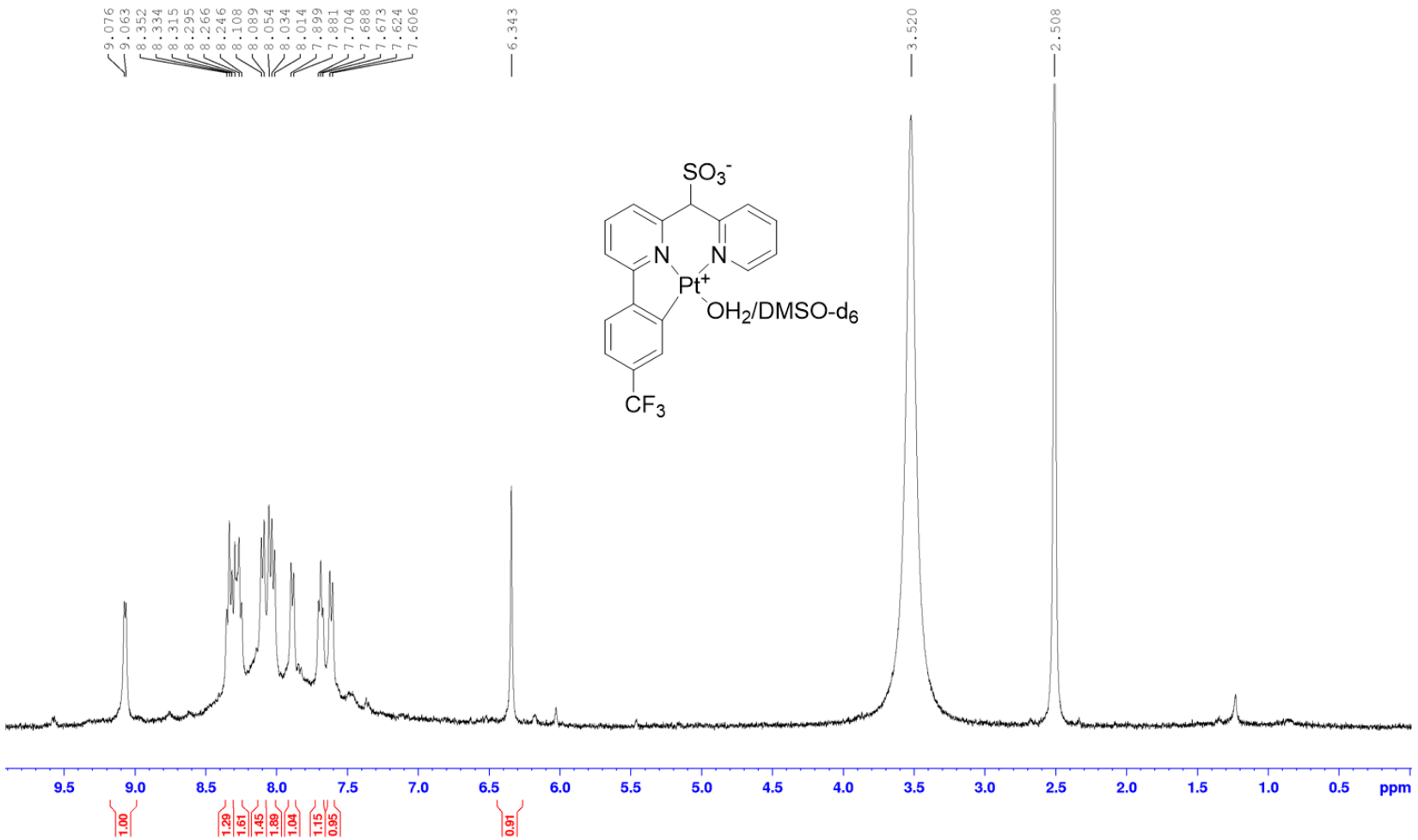

Figure S4.24. ^{1}H-NMR for **4.1-CF$_3$** Complex in DMSO-*d*$_6$

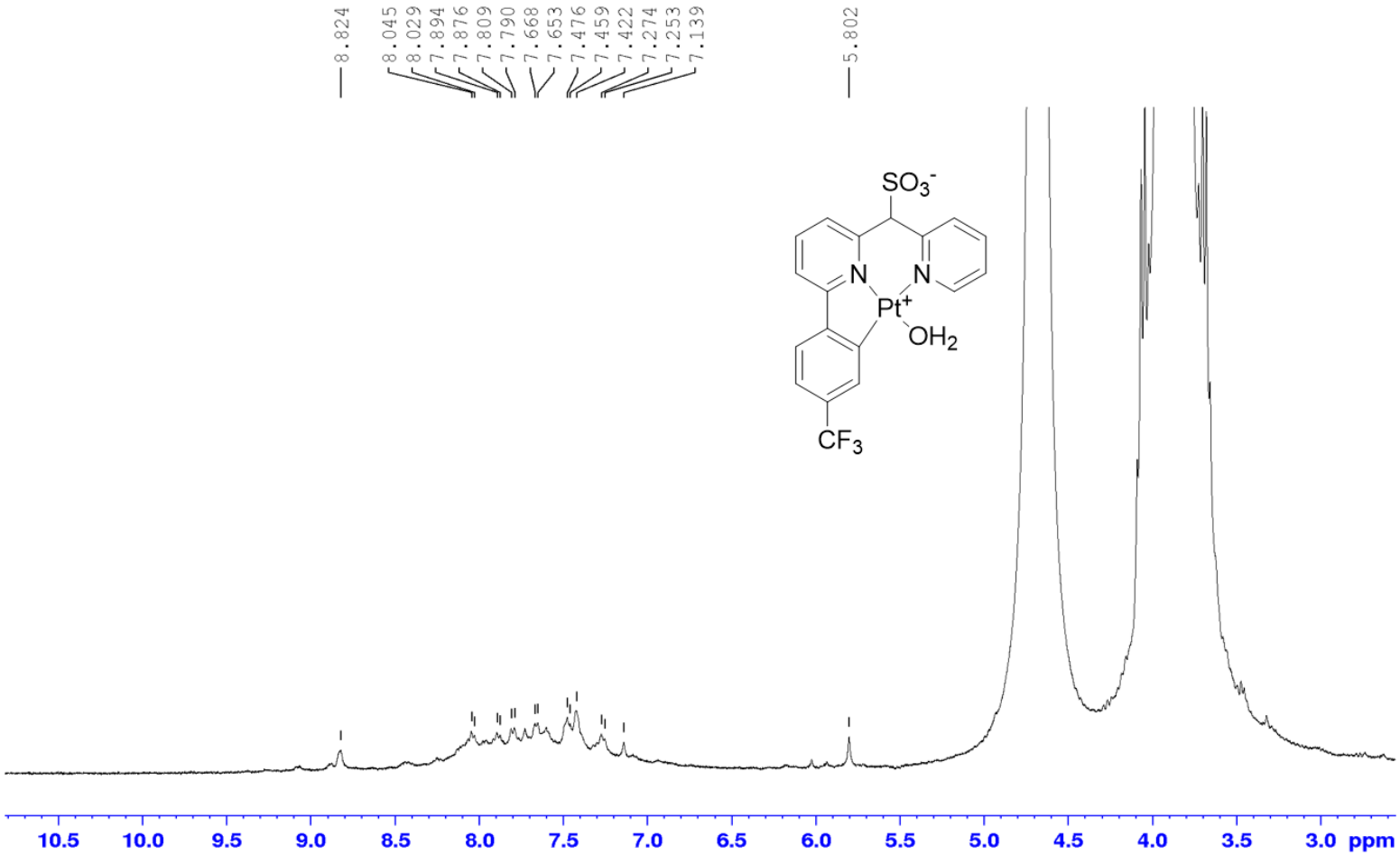

Figure S4.25. ^{1}H-NMR for **4.1-CF$_3$** Complex in TFE-*d*$_1$

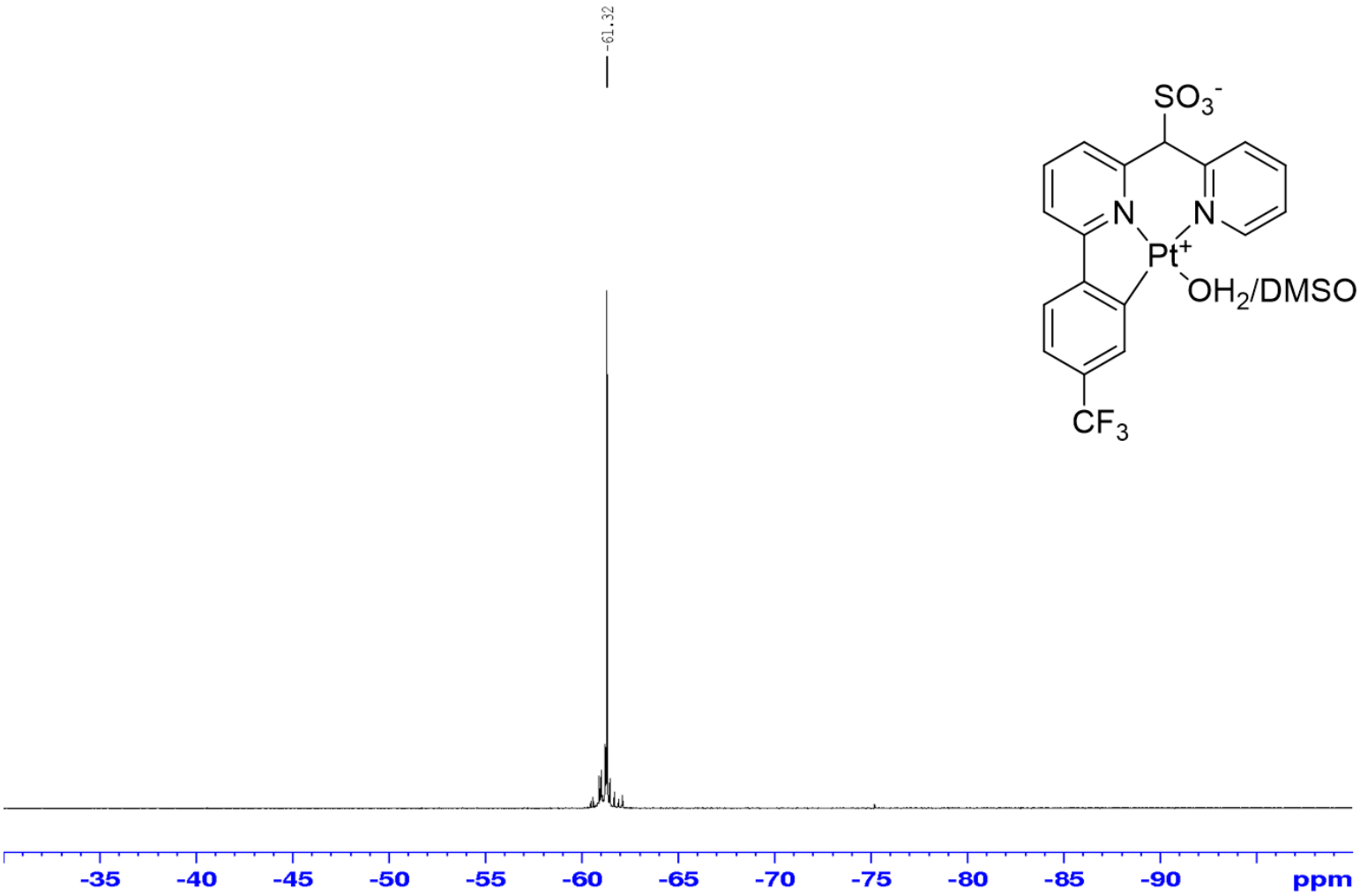

Figure S4.26. ^{19}F-NMR for **4.1-CF$_3$** Complex in DMSO-*d*$_6$

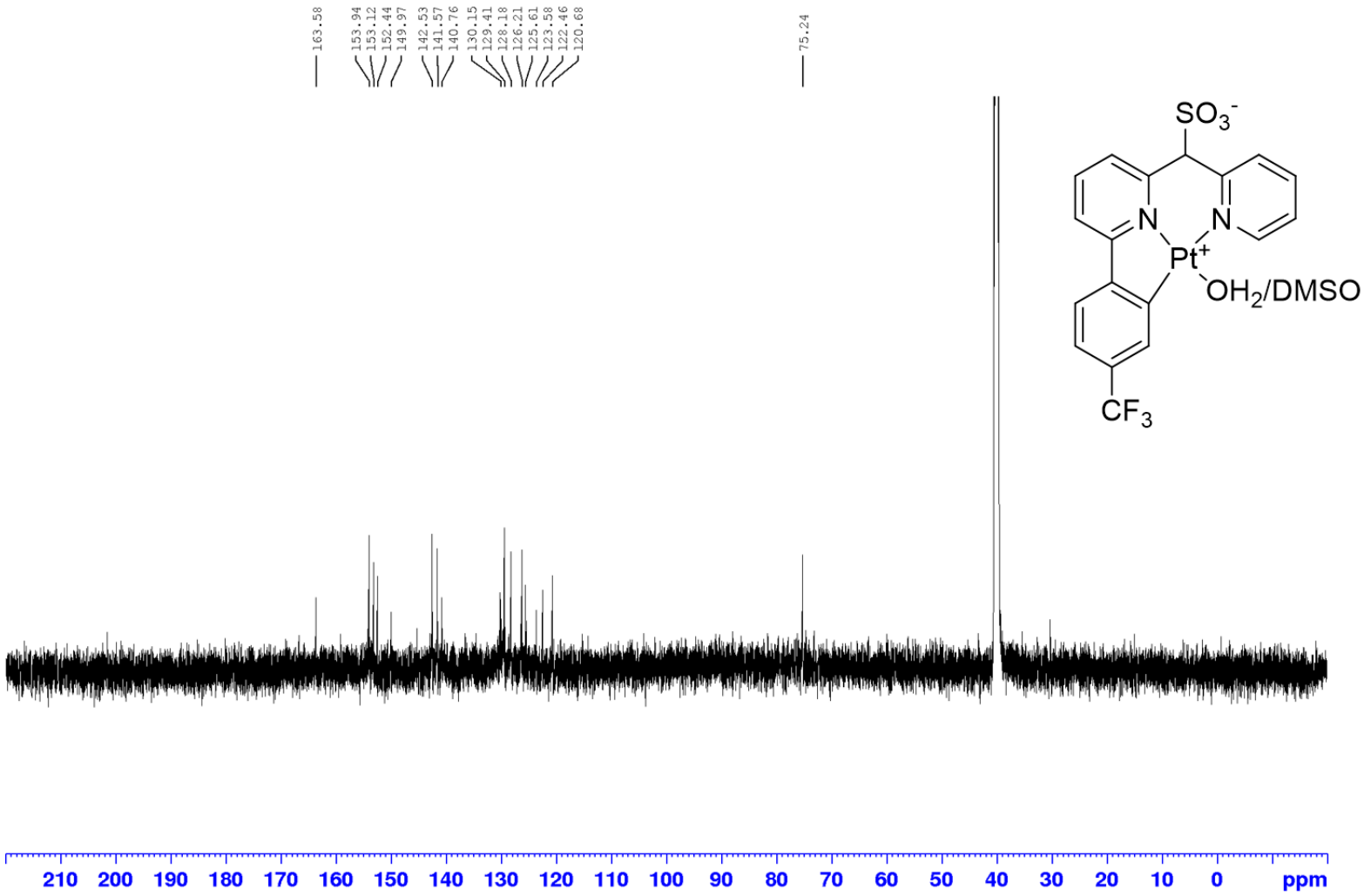

Figure S4.27. ^{13}C-NMR for **4.1-CF$_3$** Complex in DMSO-d_6

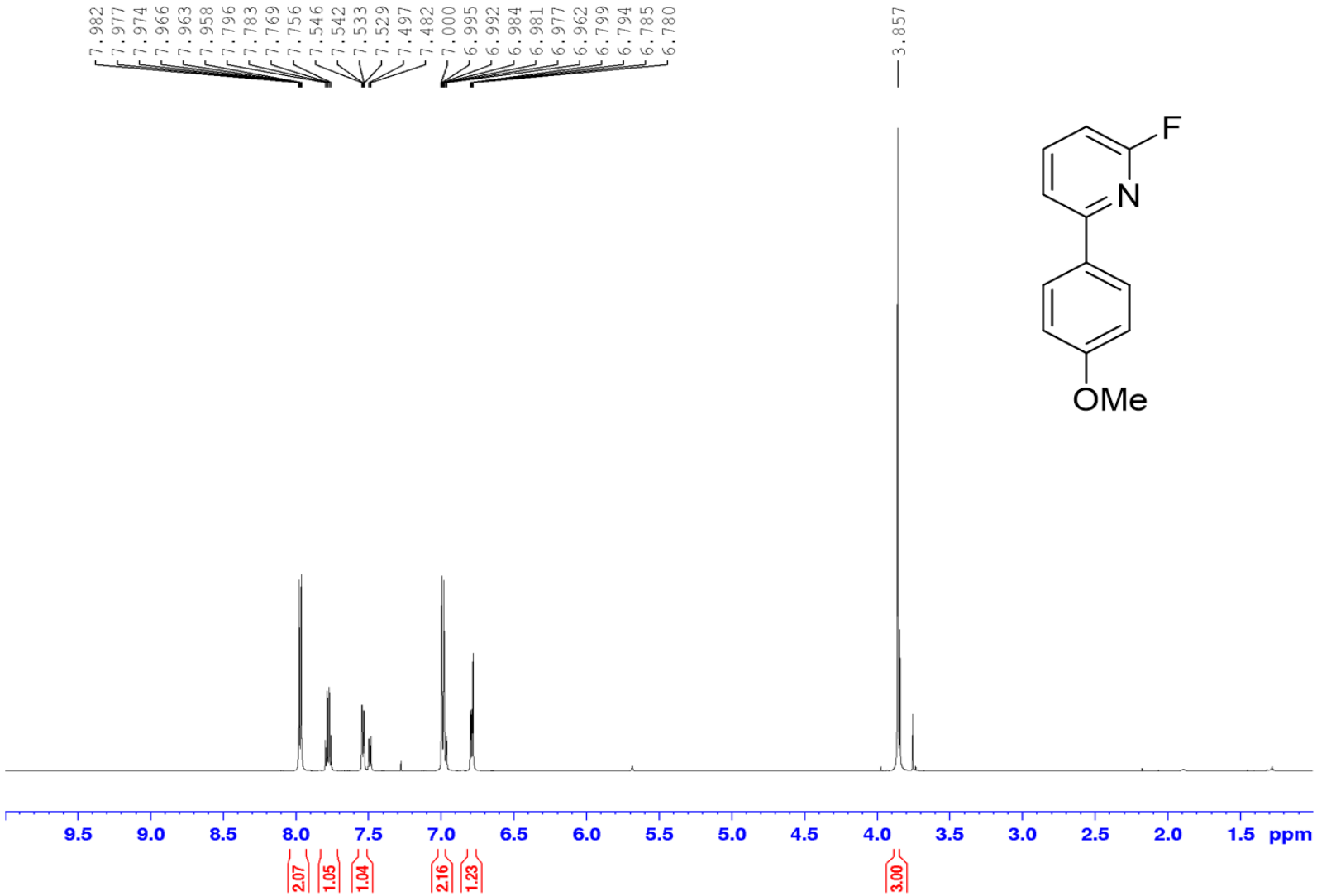

Figure S4.28. ^{1}H-NMR for 2-fluoro-6-(4-methoxyphenyl) pyridine, **4.5-OMe** in $CDCl_3$

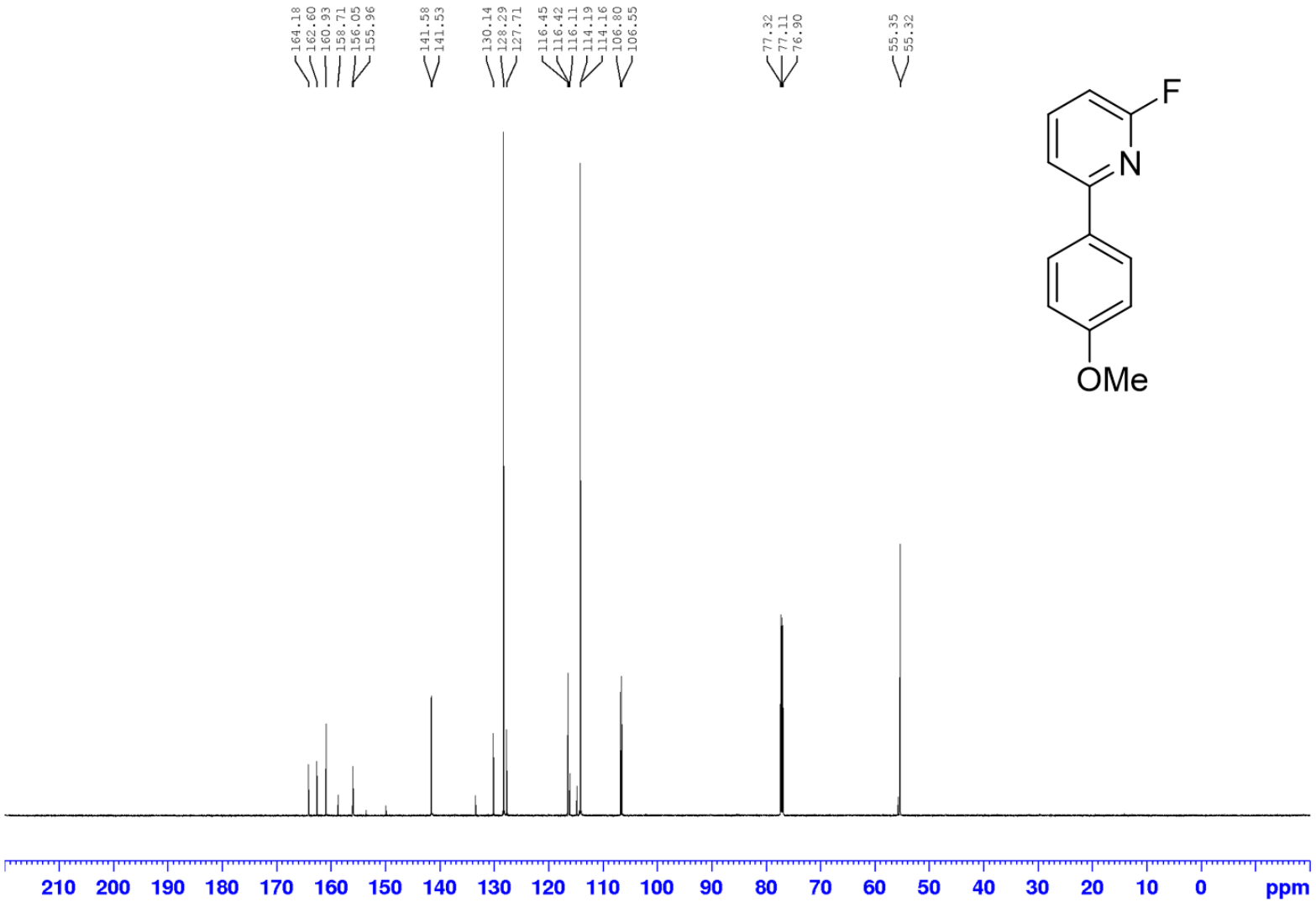

Figure S4.29. ^{13}C-NMR for 2-fluoro-6-(4-methoxyphenyl) pyridine, **4.5-OMe** in $CDCl_3$

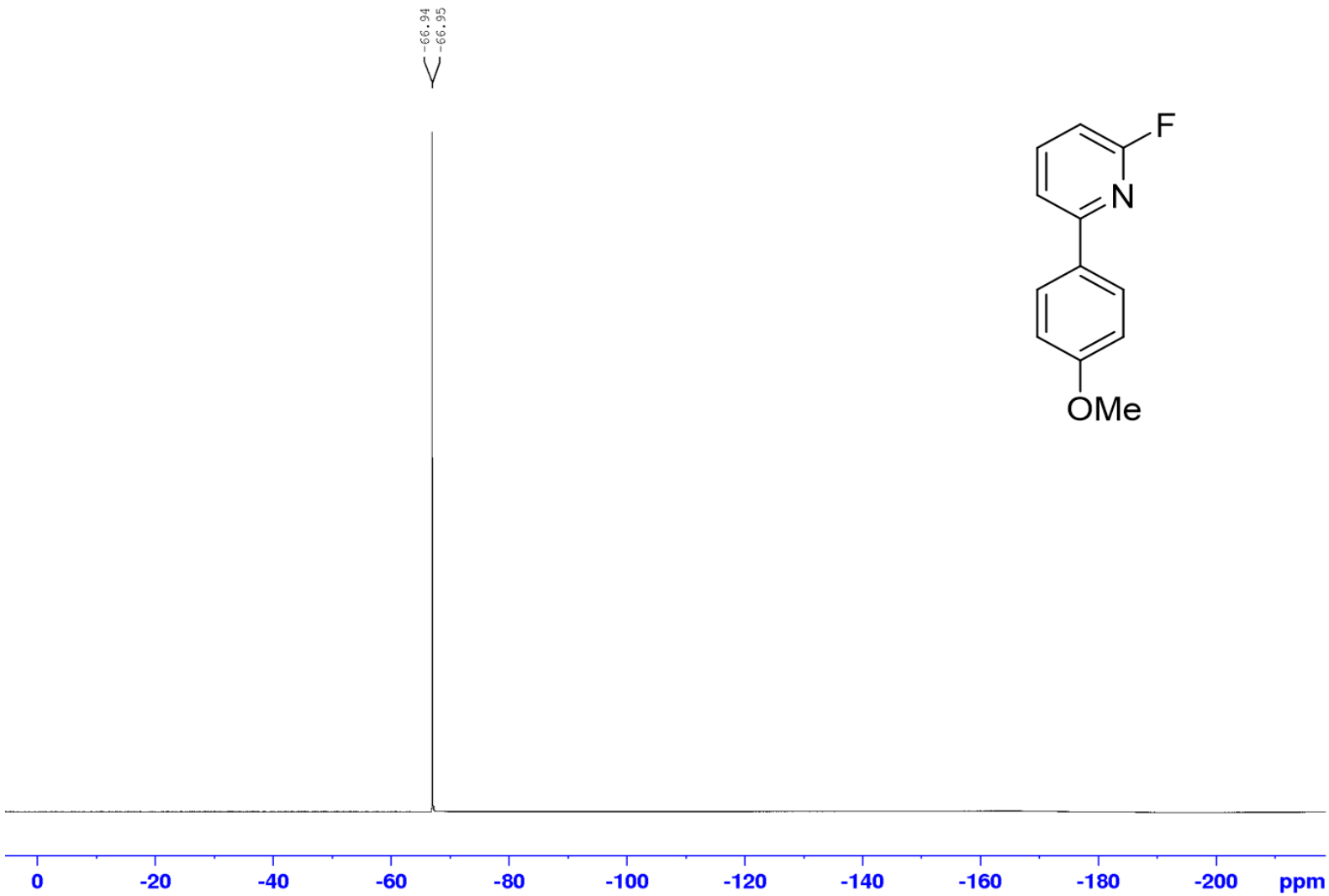

Figure S4.30. ^{19}F-NMR for 2-fluoro-6-(4-methoxyphenyl) pyridine, **4.5-OMe** in $CDCl_3$

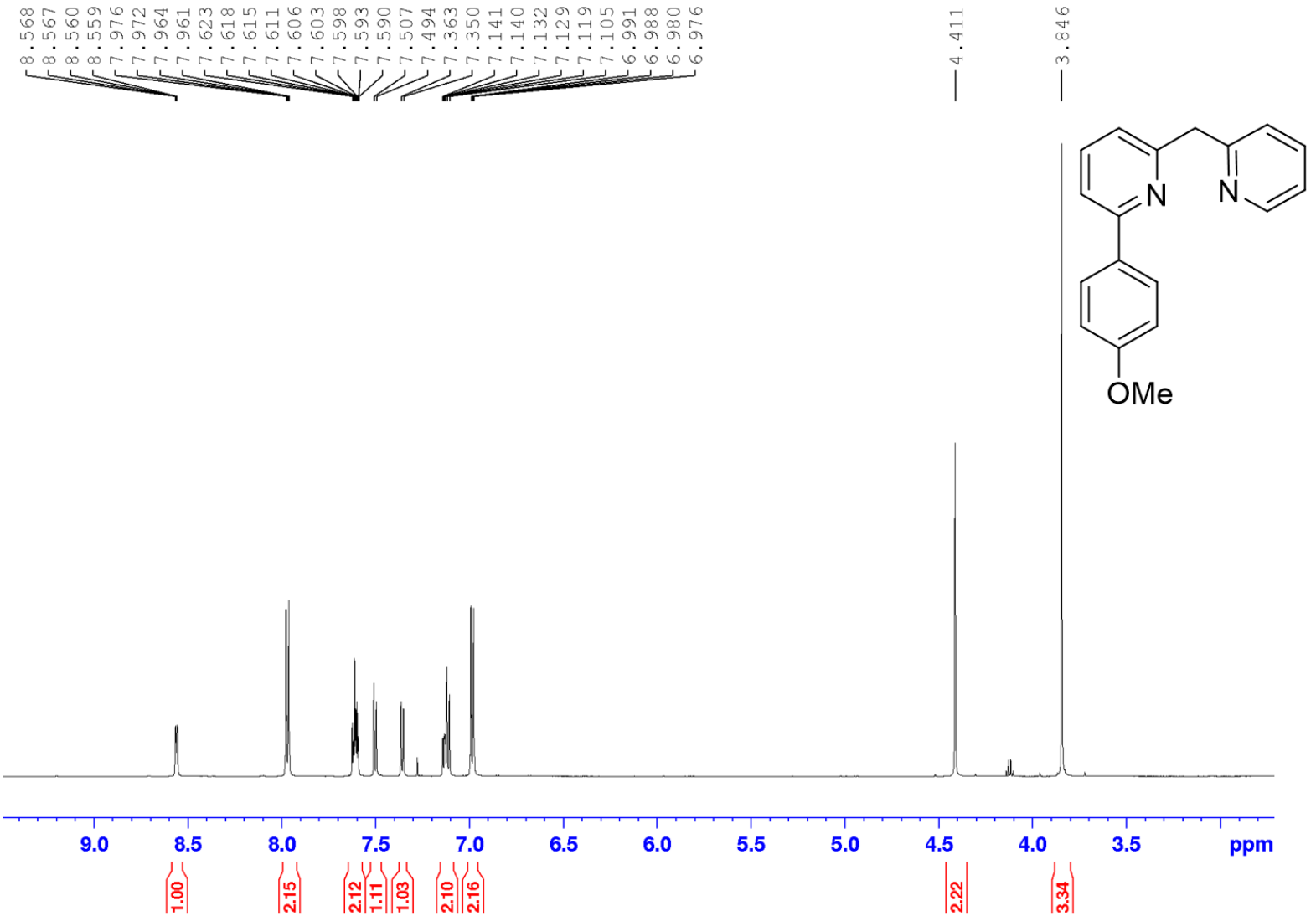

Figure S4.31. ^{1}H-NMR for 2-(4-methoxyphenyl)-6-(pyridin-2-ylmethyl) pyridine, **4.6-OMe** in $CDCl_3$

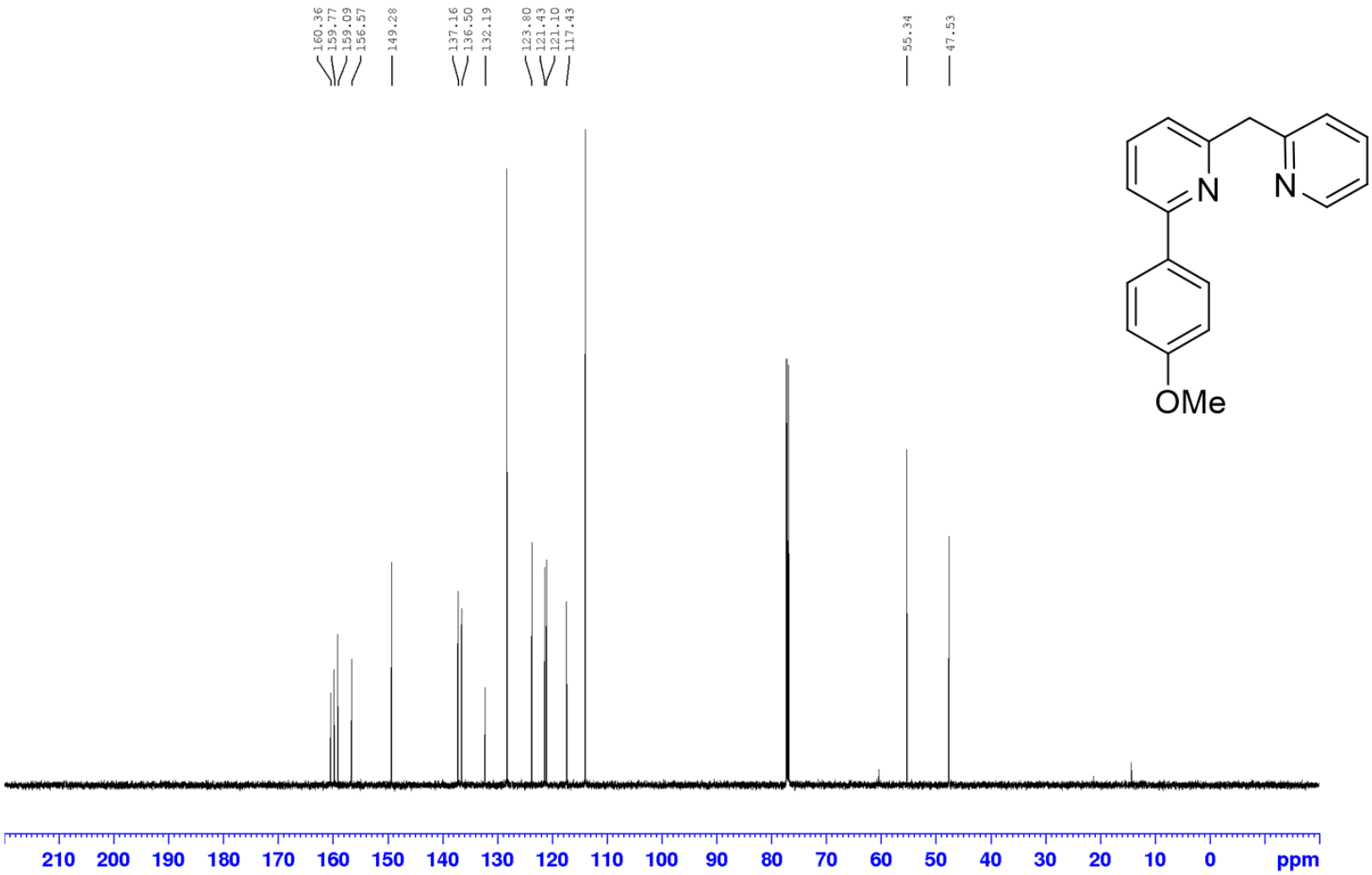

Figure S4.32. ^{13}C-NMR for 2-(4-methoxyphenyl)-6-(pyridin-2-ylmethyl) pyridine, **4.6-OMe** in $CDCl_3$

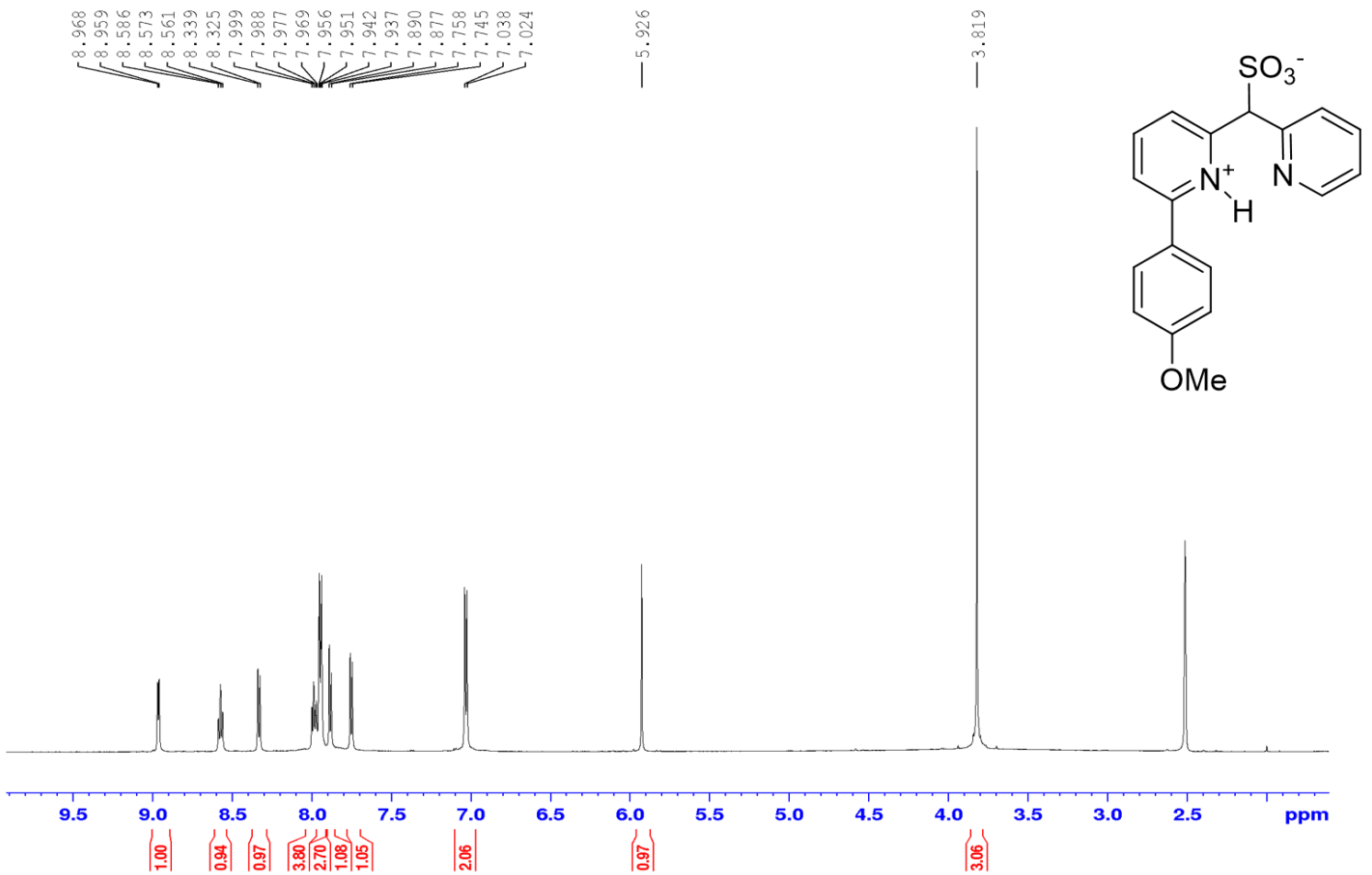

Figure S4.33. ^{1}H-NMR for 2-(4-methoxyphenyl)-6-(pyridin-2-ylmethyl) pyridinium sulfonate, **4.7-OMe** in DMSO-d_6

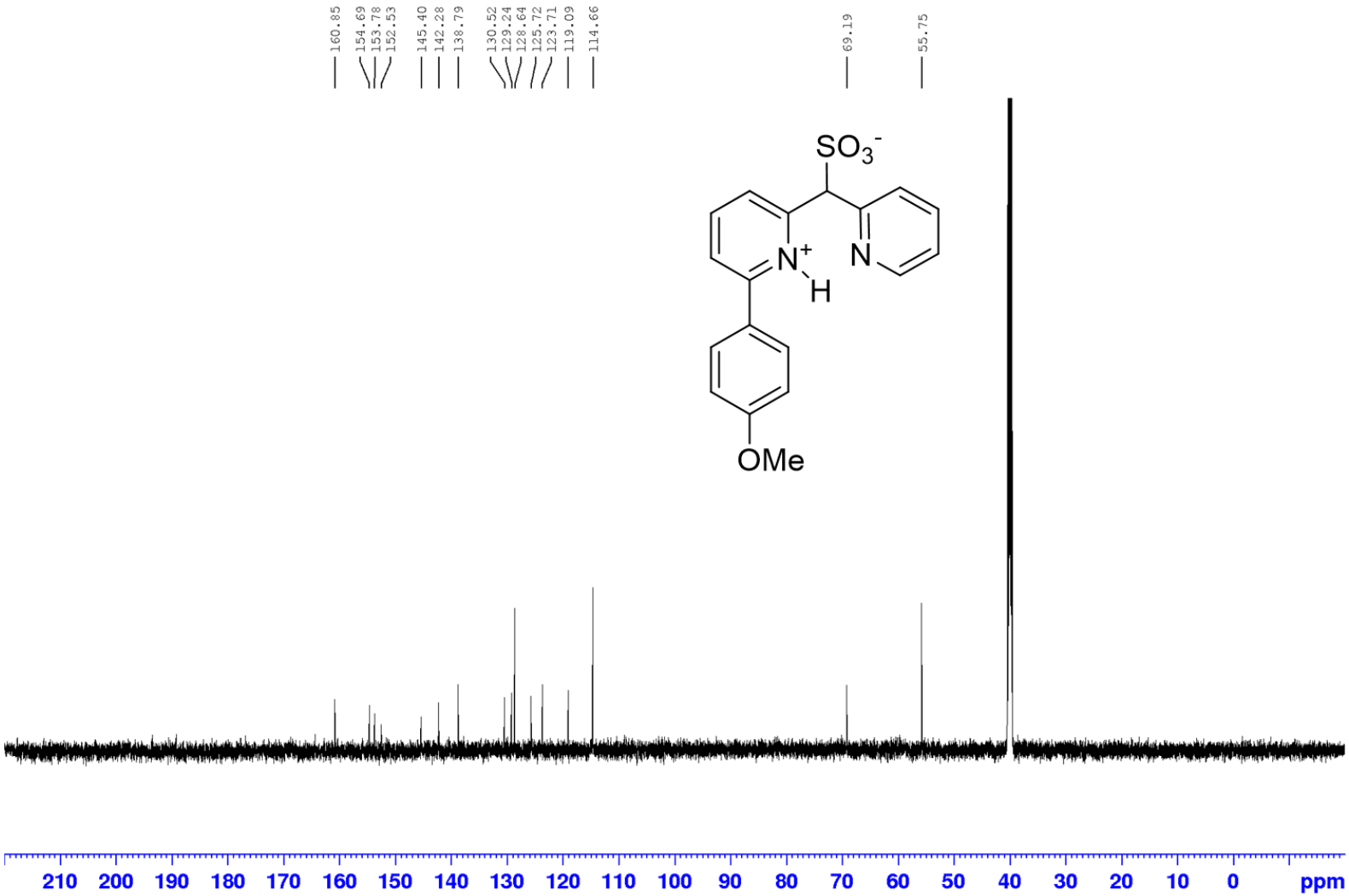

Figure S4.34. ^{13}C-NMR for 2-(4-methoxyphenyl)-6-(pyridin-2-ylmethyl) pyridinium sulfonate, **4.7-OMe** in DMSO-*d*$_6$

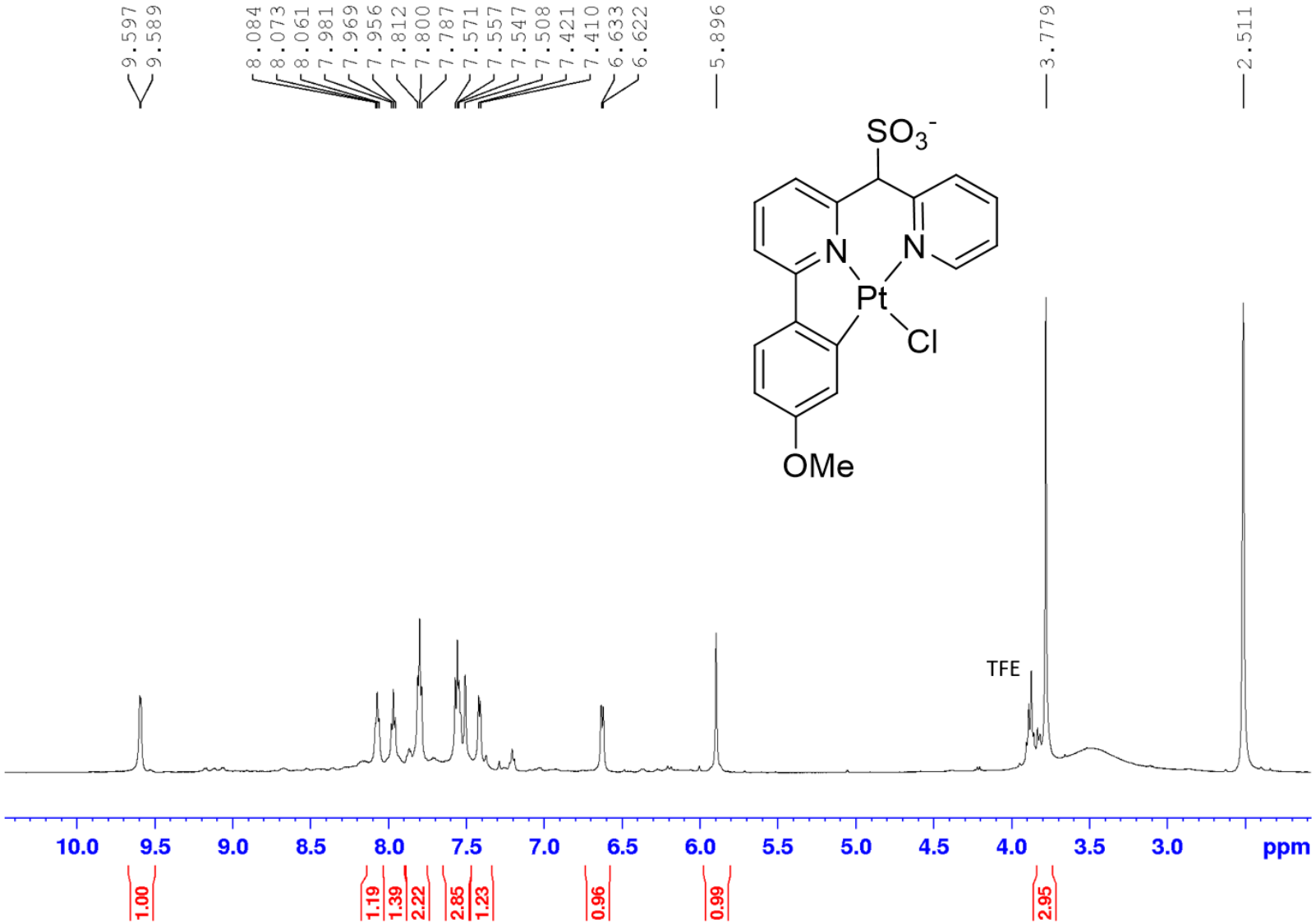

Figure S4.35. ^{1}H-NMR for 2-(4-methoxyphenyl)-6-(pyridin-2-ylmethyl) pyridine Pt-Cl Complex, **4.8-OMe** in DMSO-d_6

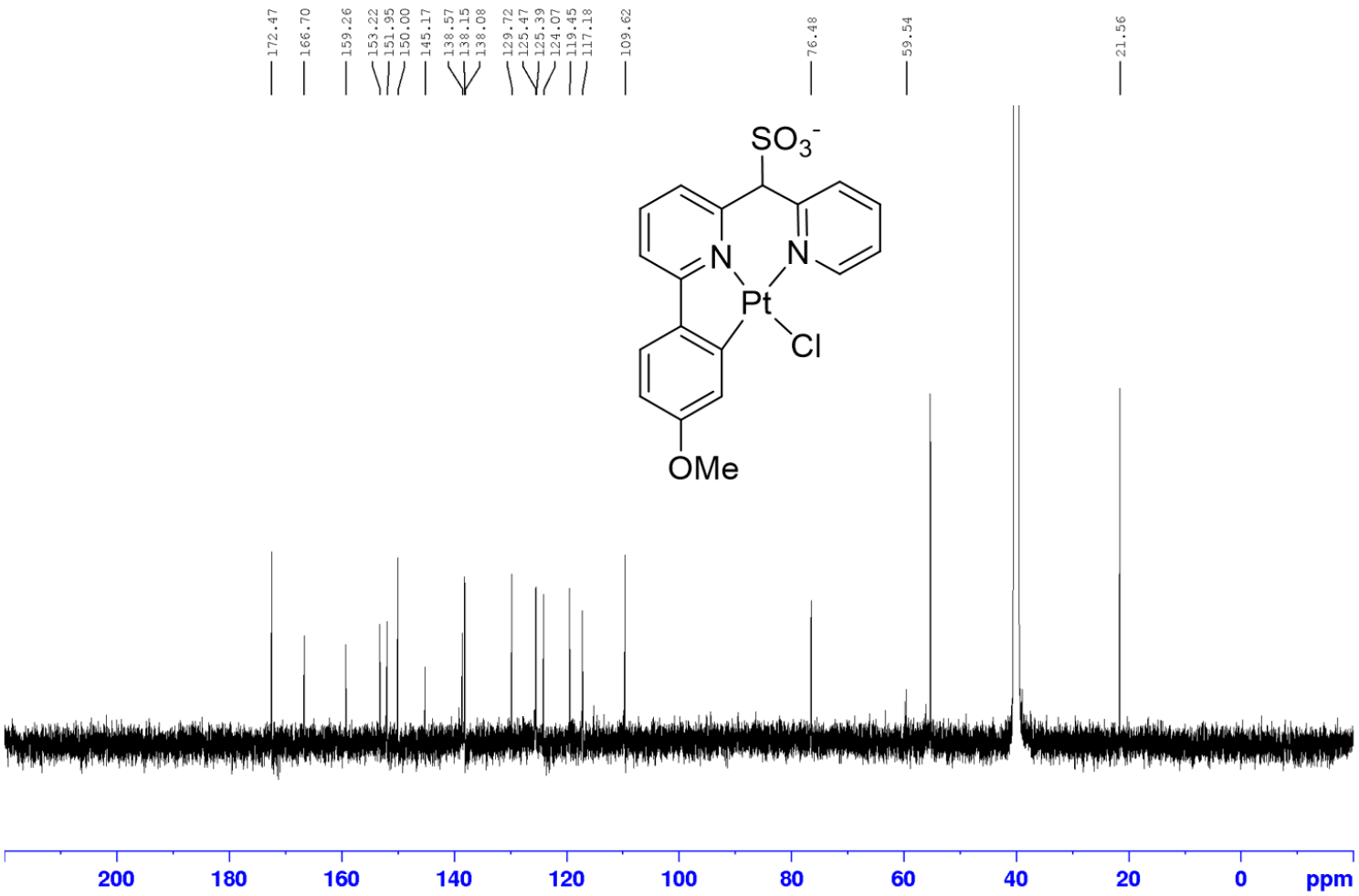

Figure S4.36. ^{13}C-NMR for 2-(4-methoxyphenyl)-6-(pyridin-2-ylmethyl) pyridine Pt-Cl Complex, **4.8-OMe** in DMSO-d_6

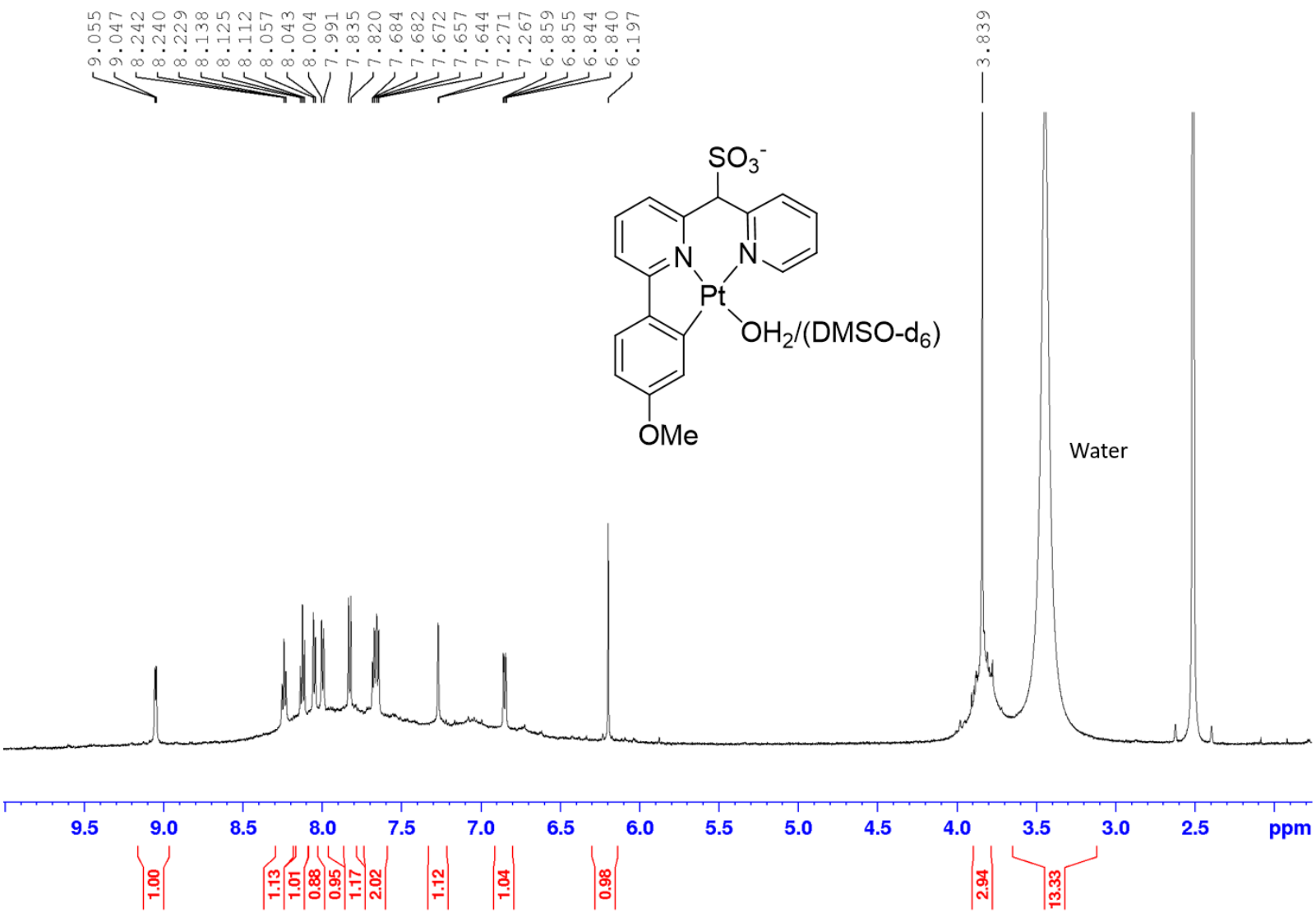

Figure S4.37. ^{1}H-NMR for **4.1-OMe** in DMSO-d_6

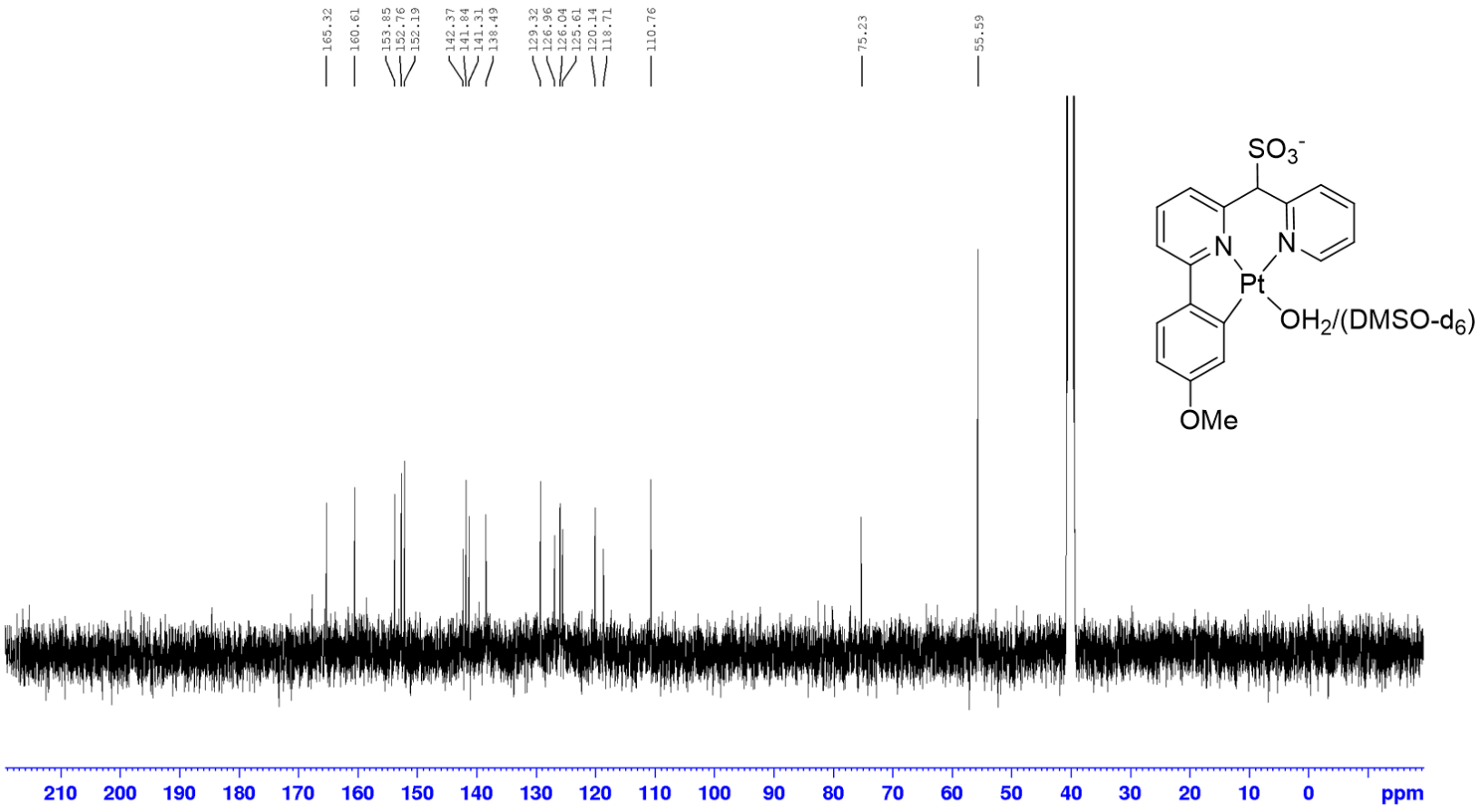

Figure S4.38. ^{13}C-NMR for **4.1-OMe** in DMSO- d_6

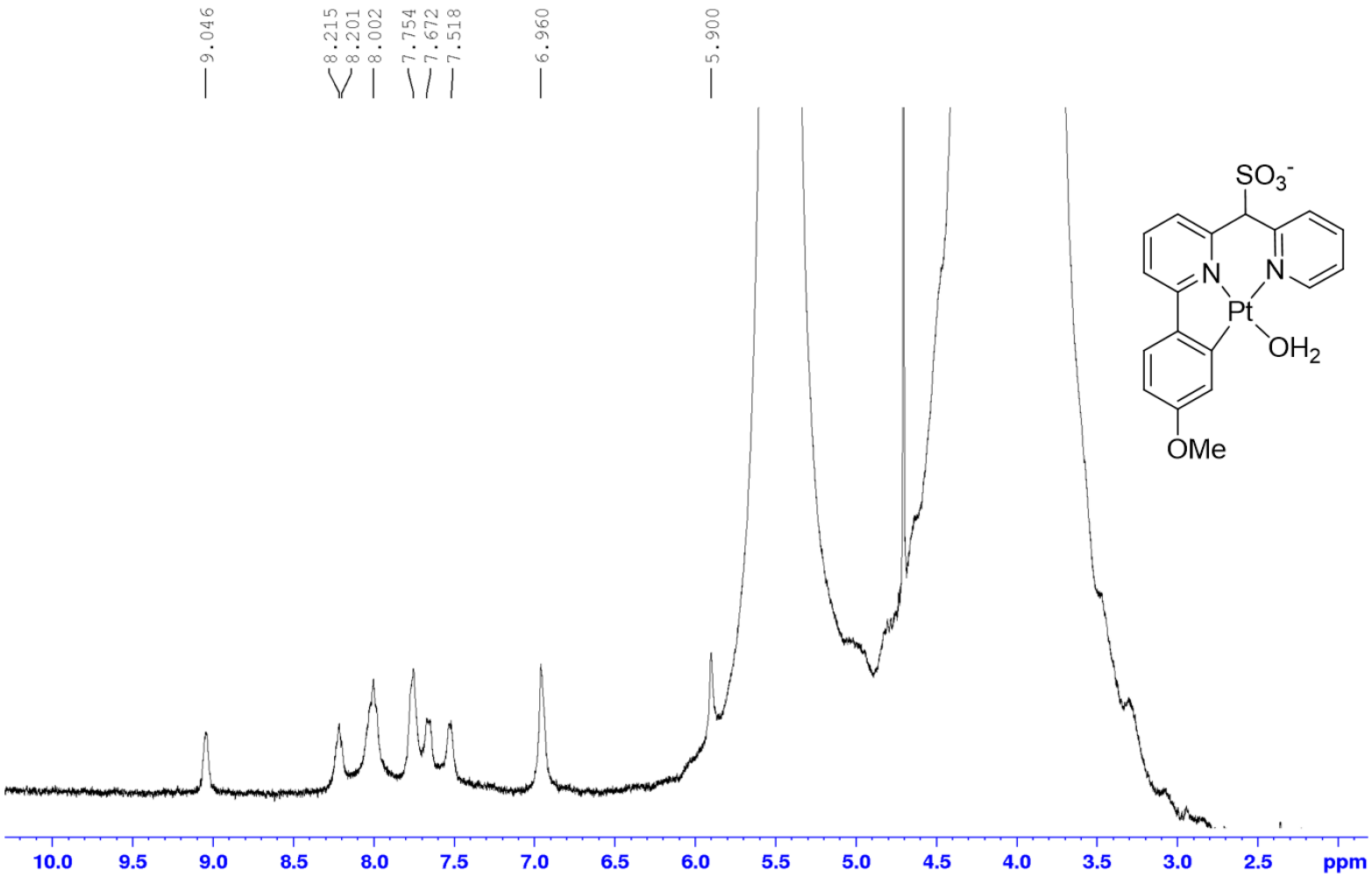

Figure S4.39. ^{13}C-NMR for **4.1-OMe** in TFE-d_1

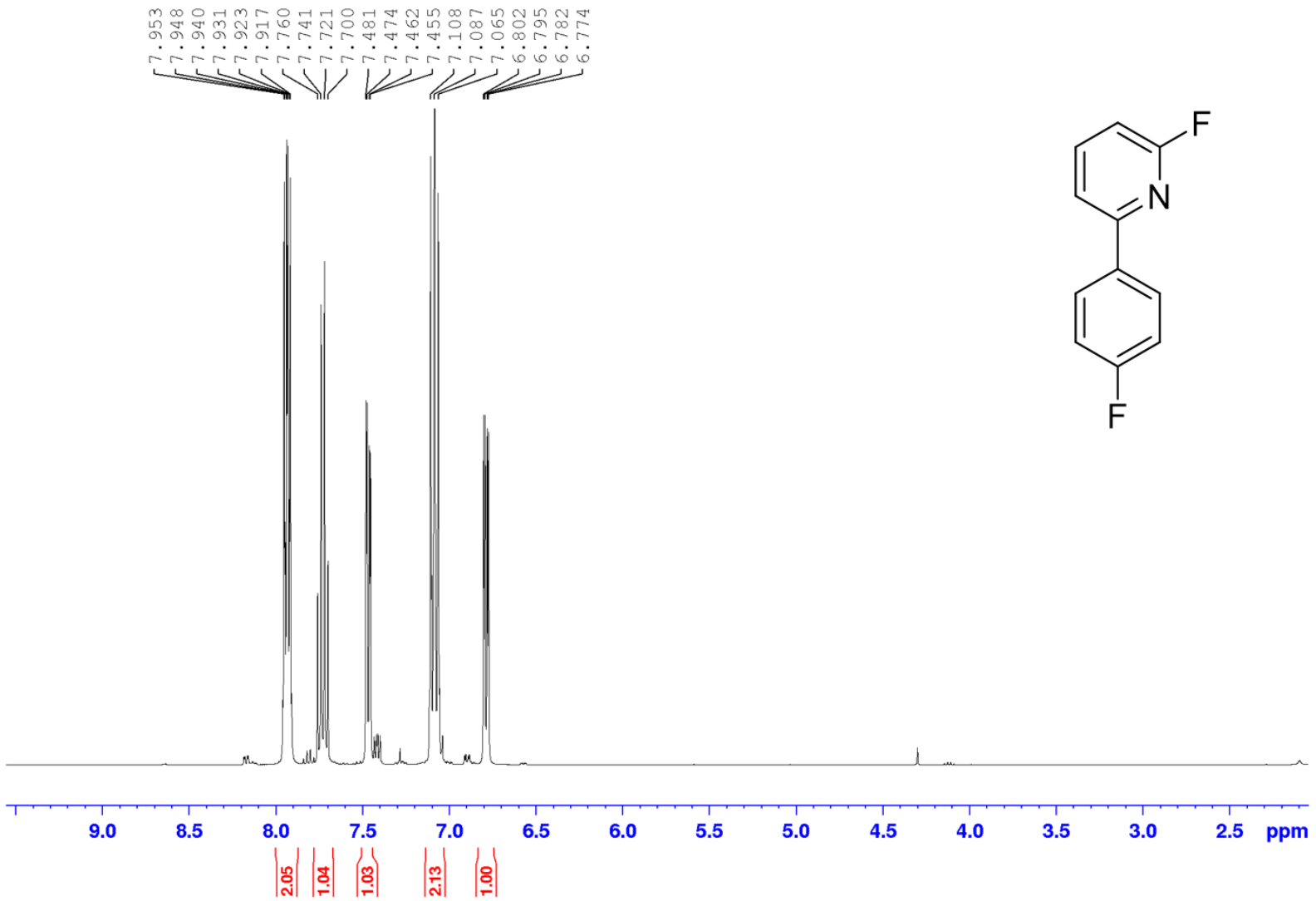

Figure S4.40. ^{1}H-NMR for 2-fluoro-6-(4-fluorophenyl) pyridine, **4.5-F** in $CDCl_3$

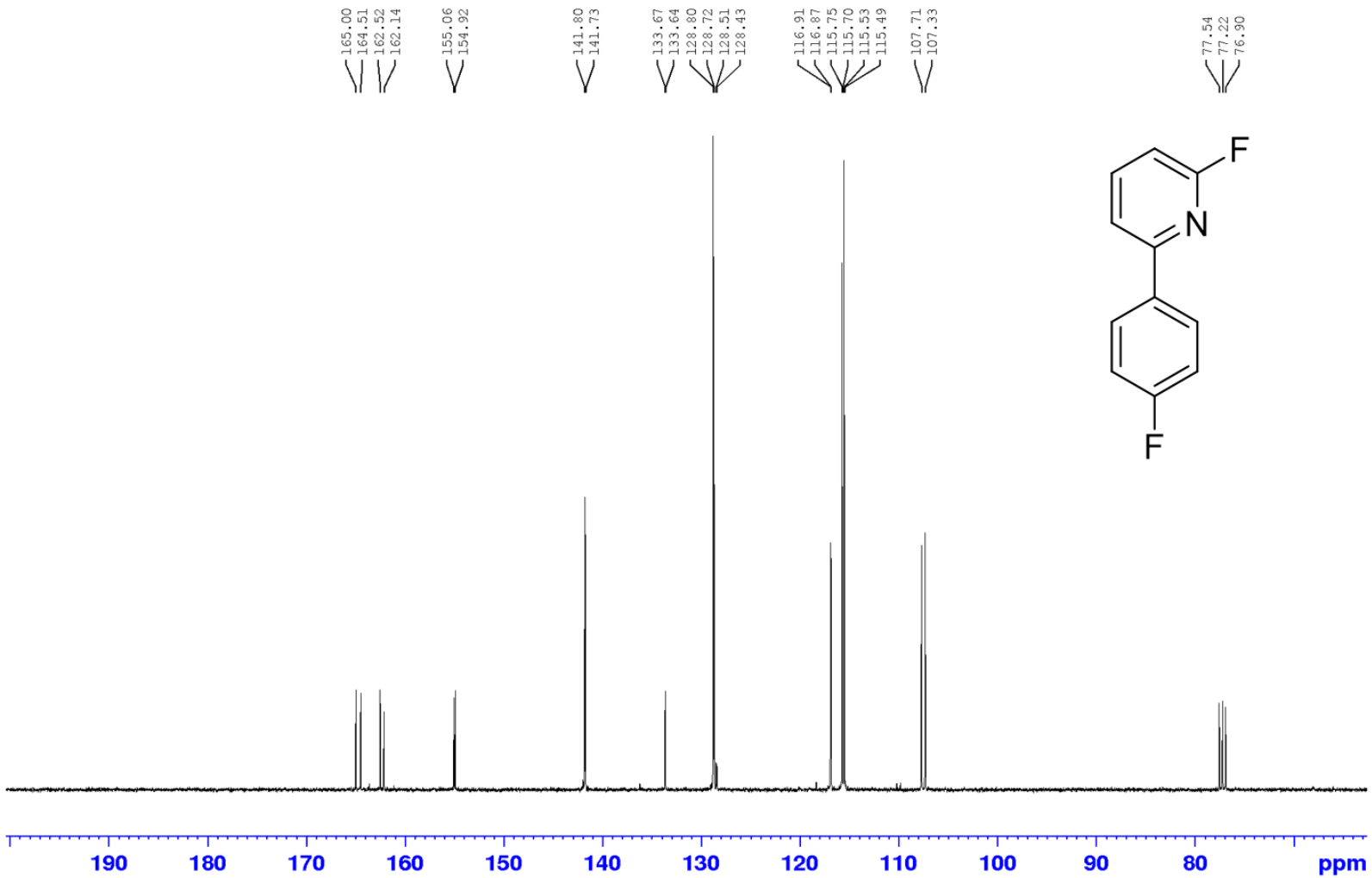

Figure S4.41. ^{13}C-NMR for 2-fluoro-6-(4-fluorophenyl) pyridine, **4.5-F** in $CDCl_3$

Figure S4.42. ^{19}F-NMR for 2-fluoro-6-(4-fluorophenyl) pyridine, **4.5-F** in $CDCl_3$

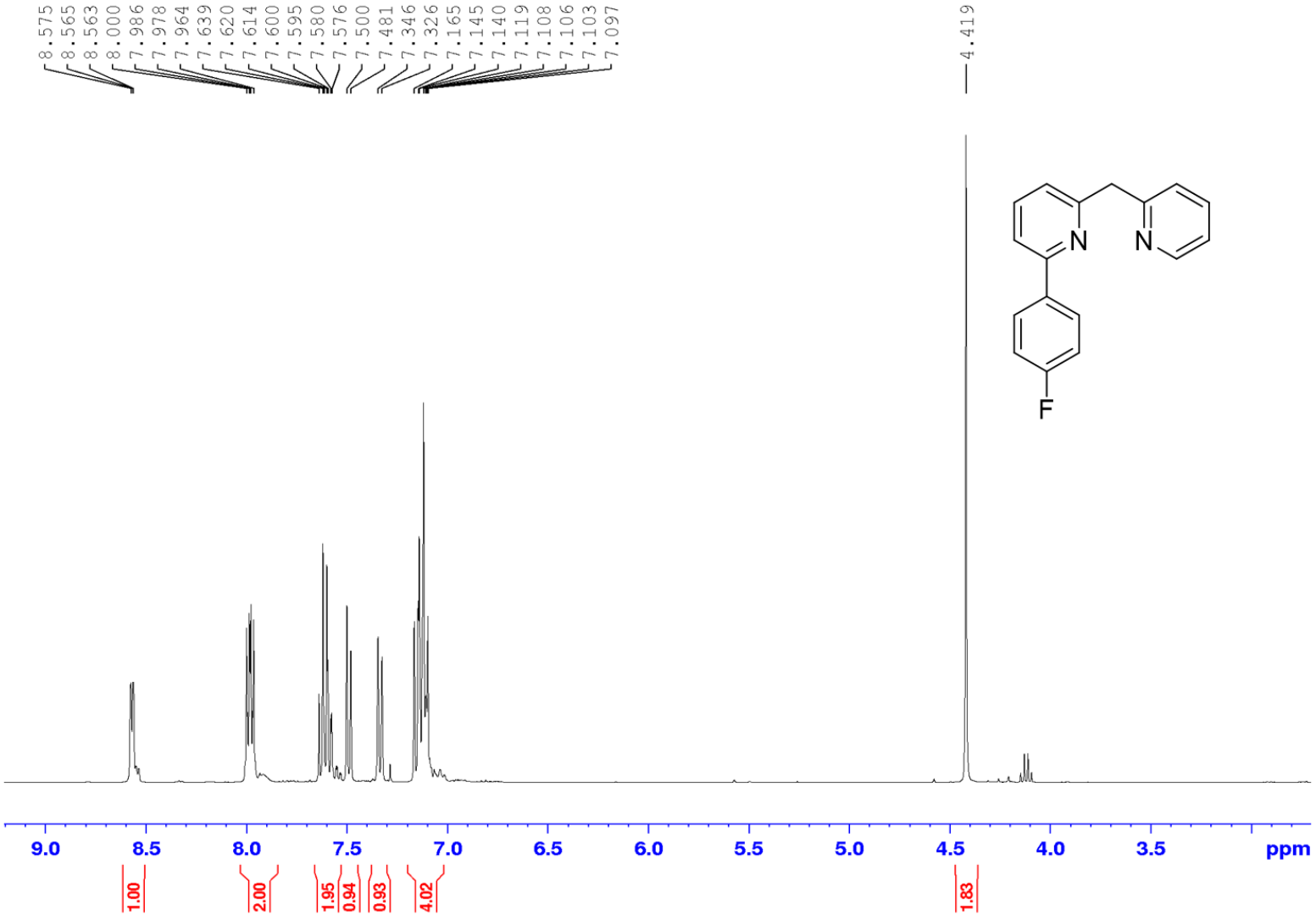

Figure S4.43. ^{1}H-NMR for 2-(4-fluorophenyl)-6-(pyridin-2-ylmethyl) pyridine, **4.6-F** in $CDCl_3$

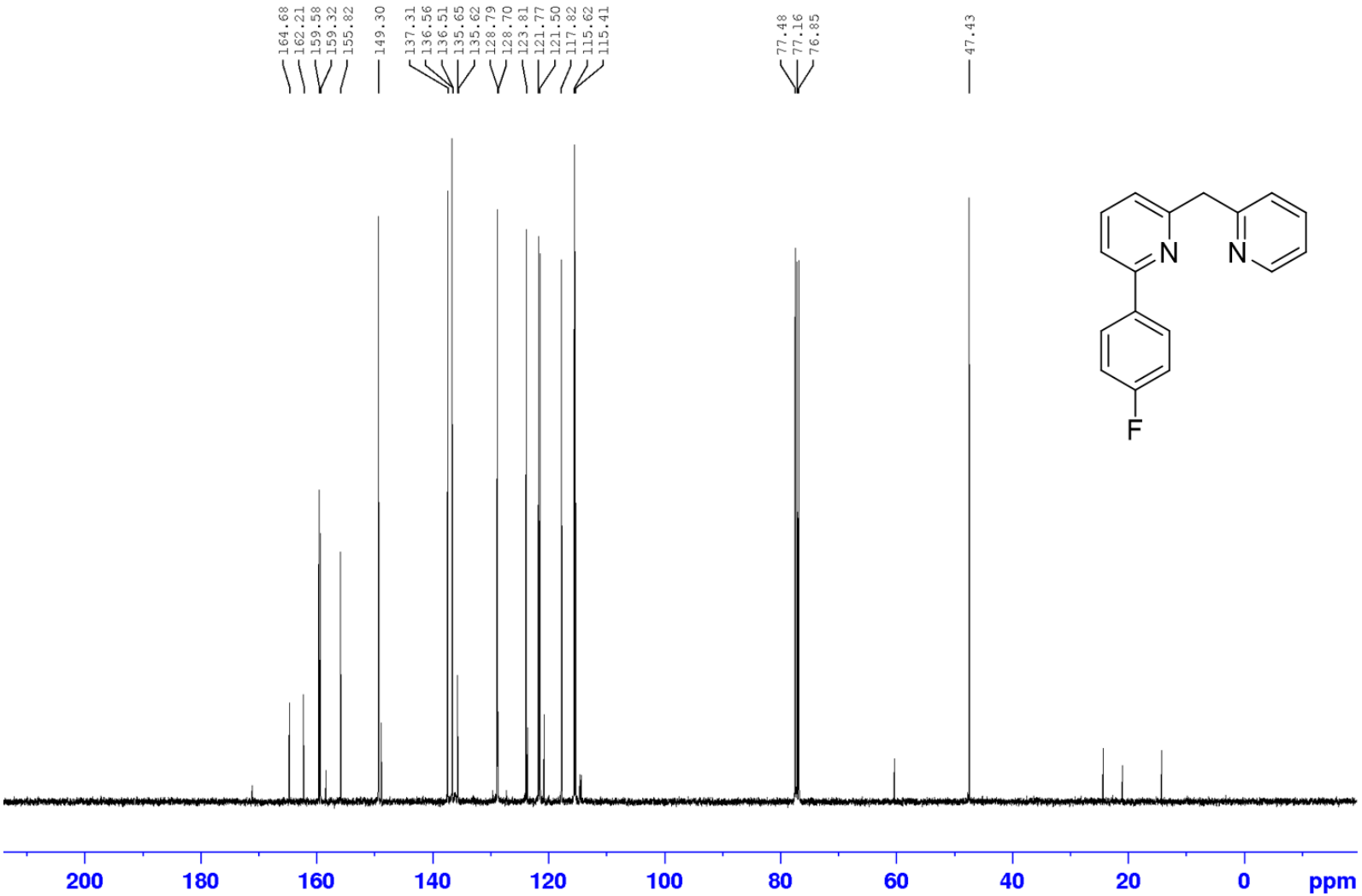

Figure S4.44. ^{13}C-NMR for 2-(4-fluorophenyl)-6-(pyridin-2-ylmethyl) pyridine, **4.6-F** in $CDCl_3$

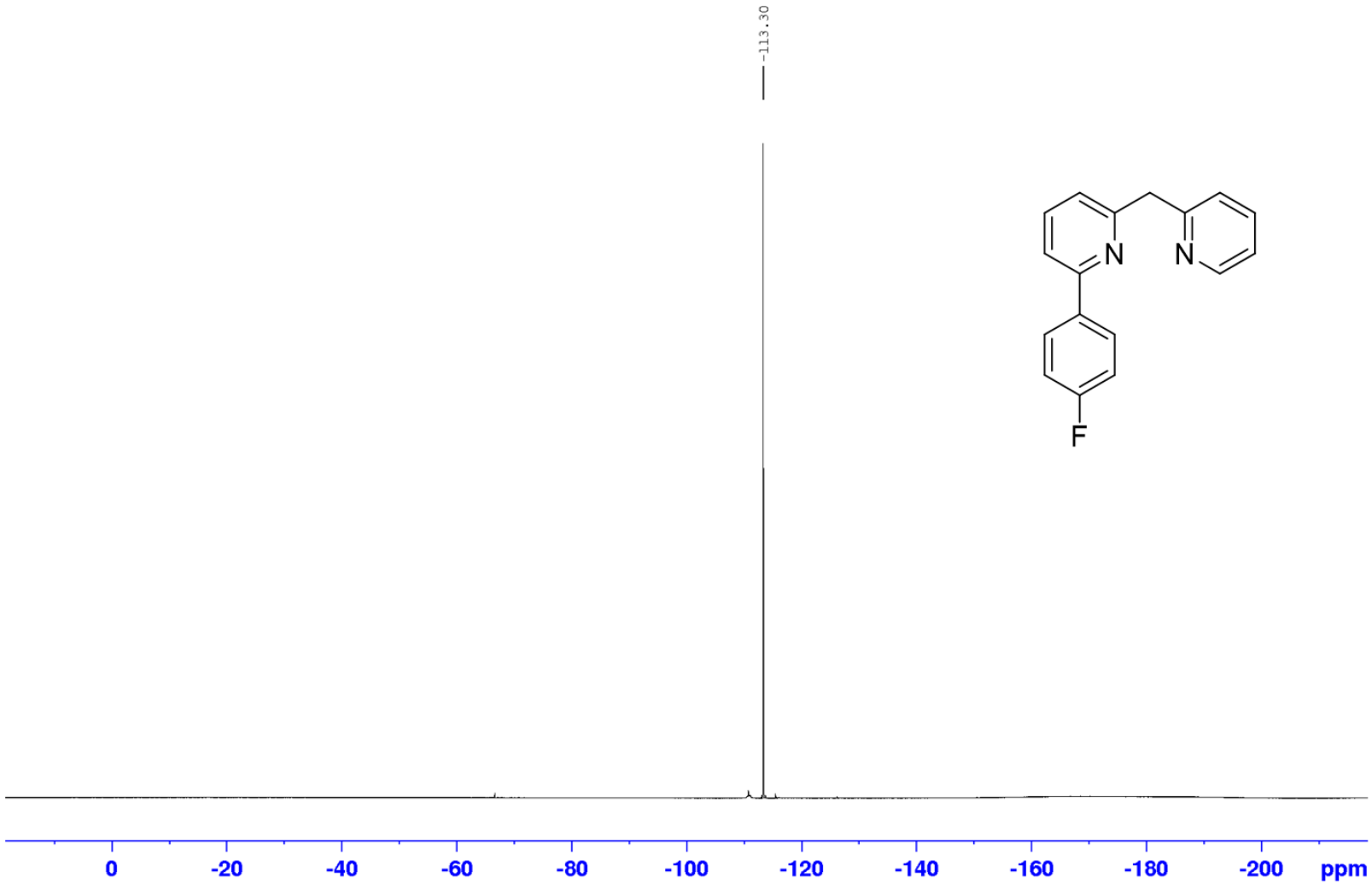

Figure S4.45. ^{19}F-NMR for 2-(4-fluorophenyl)-6-(pyridin-2-ylmethyl) pyridine, **4.6-F** in $CDCl_3$

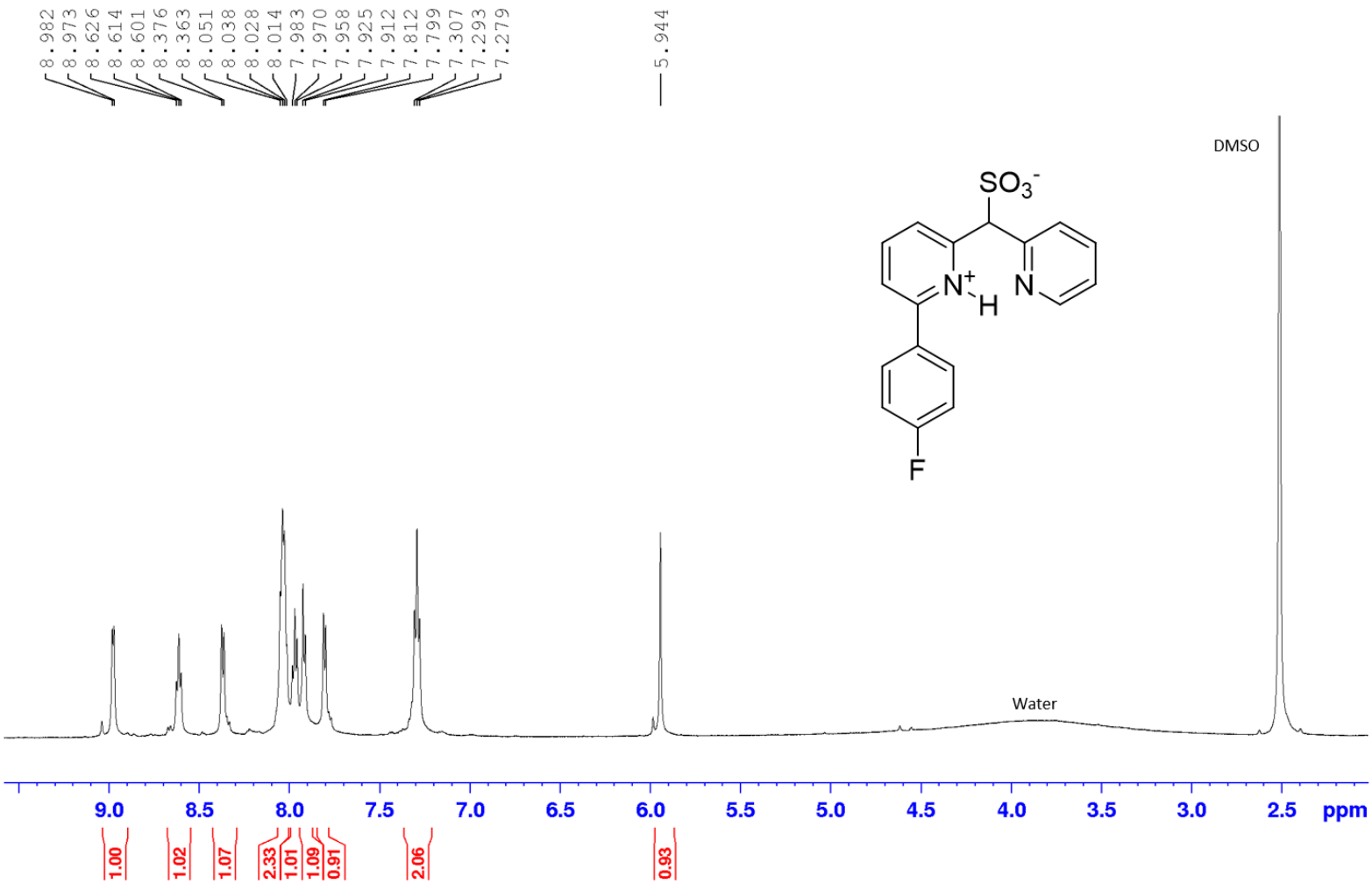

Figure S4.46. ^{1}H-NMR for 2-(4-fluorophenyl)-6-(pyridin-2-ylmethyl) pyridinium sulfonate, **4.7-F** in DMSO- d_6

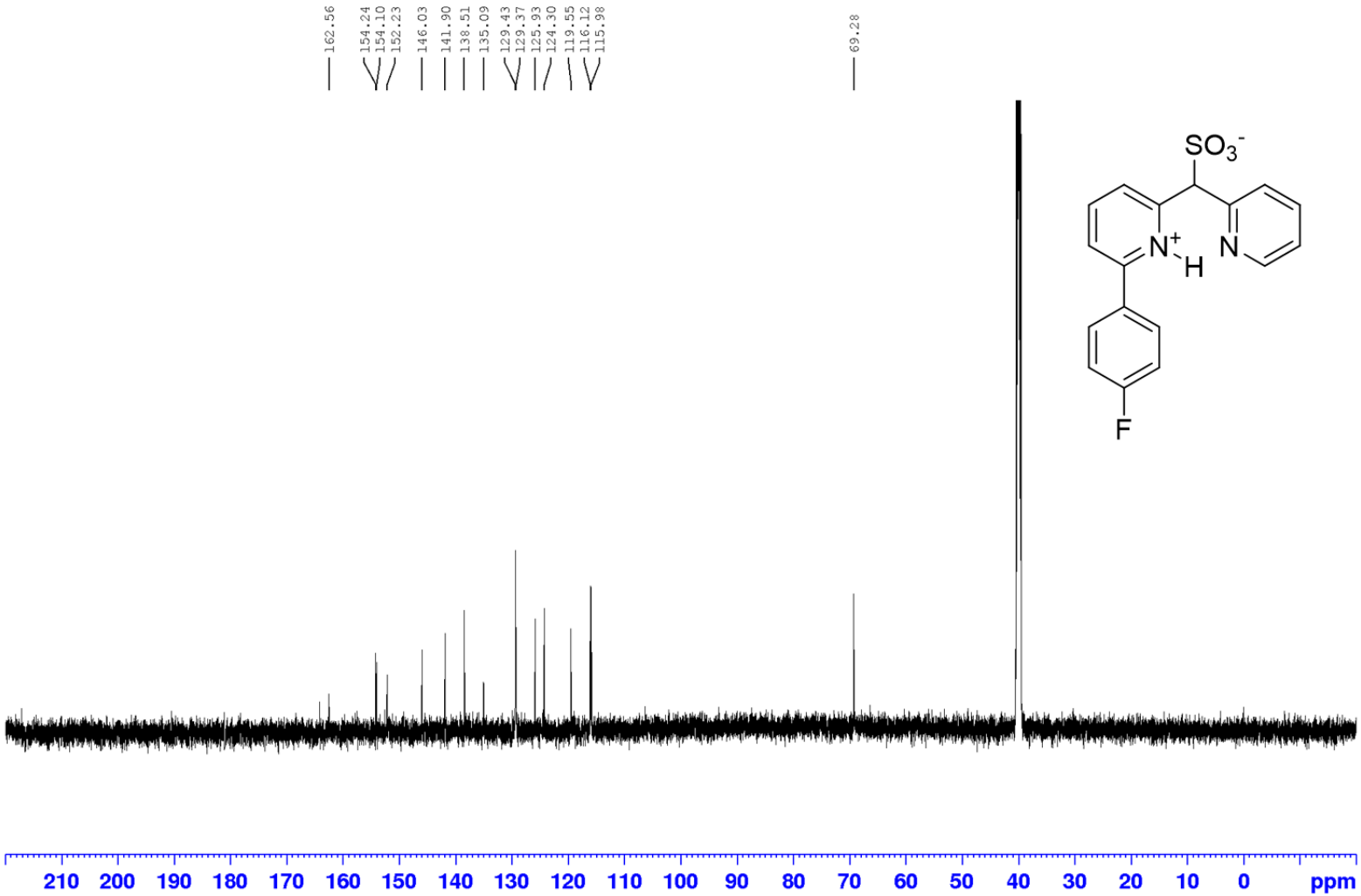

Figure S4.47. ^{13}C-NMR for 2-(4-fluorophenyl)-6-(pyridin-2-ylmethyl) pyridinium sulfonate, **4.7-F** in DMSO- d_6

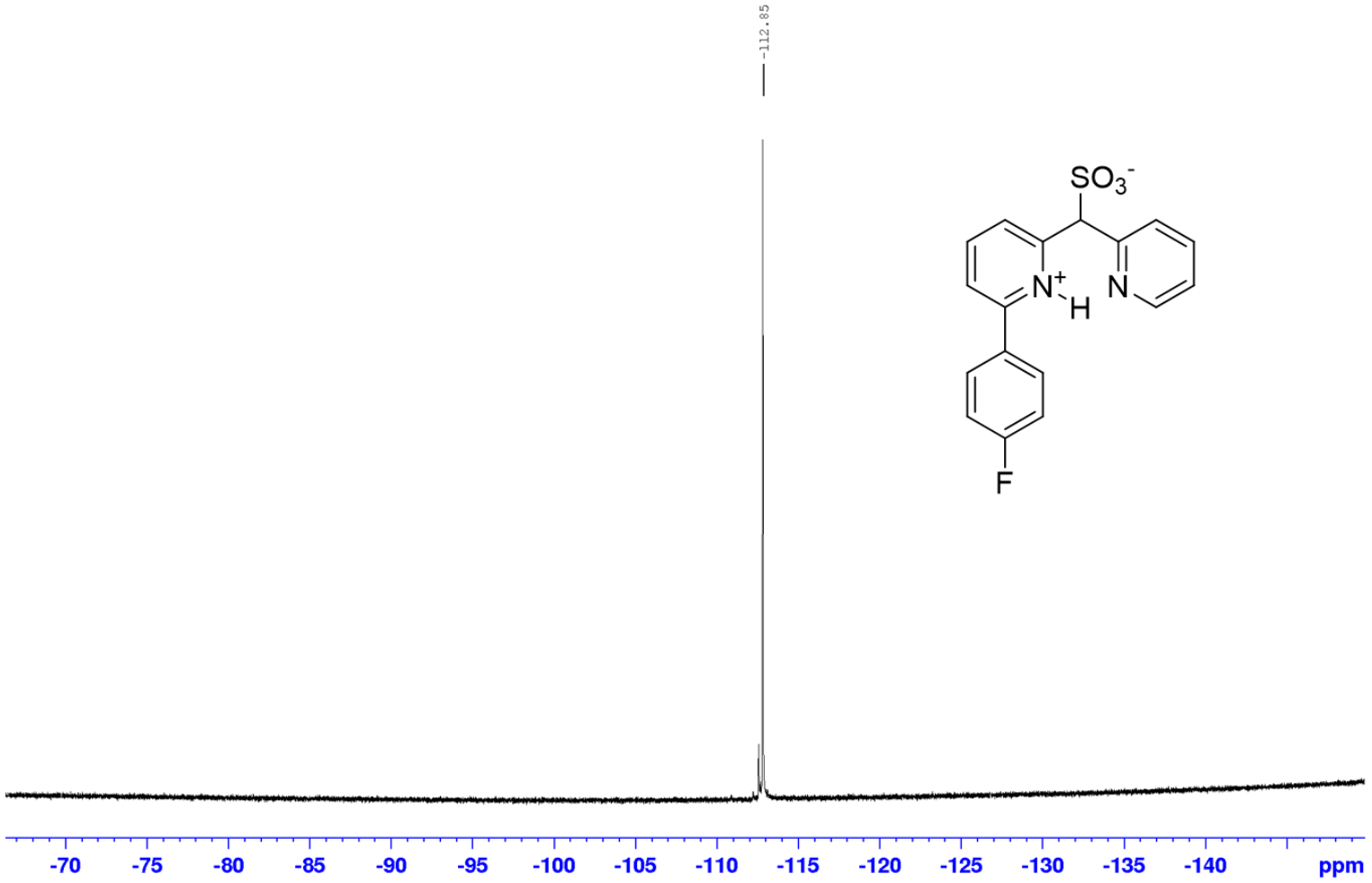

Figure S4.48. ^{19}F-NMR for 2-(4-fluorophenyl)-6-(pyridin-2-ylmethyl) pyridinium sulfonate, **4.7-F** in DMSO- d_6

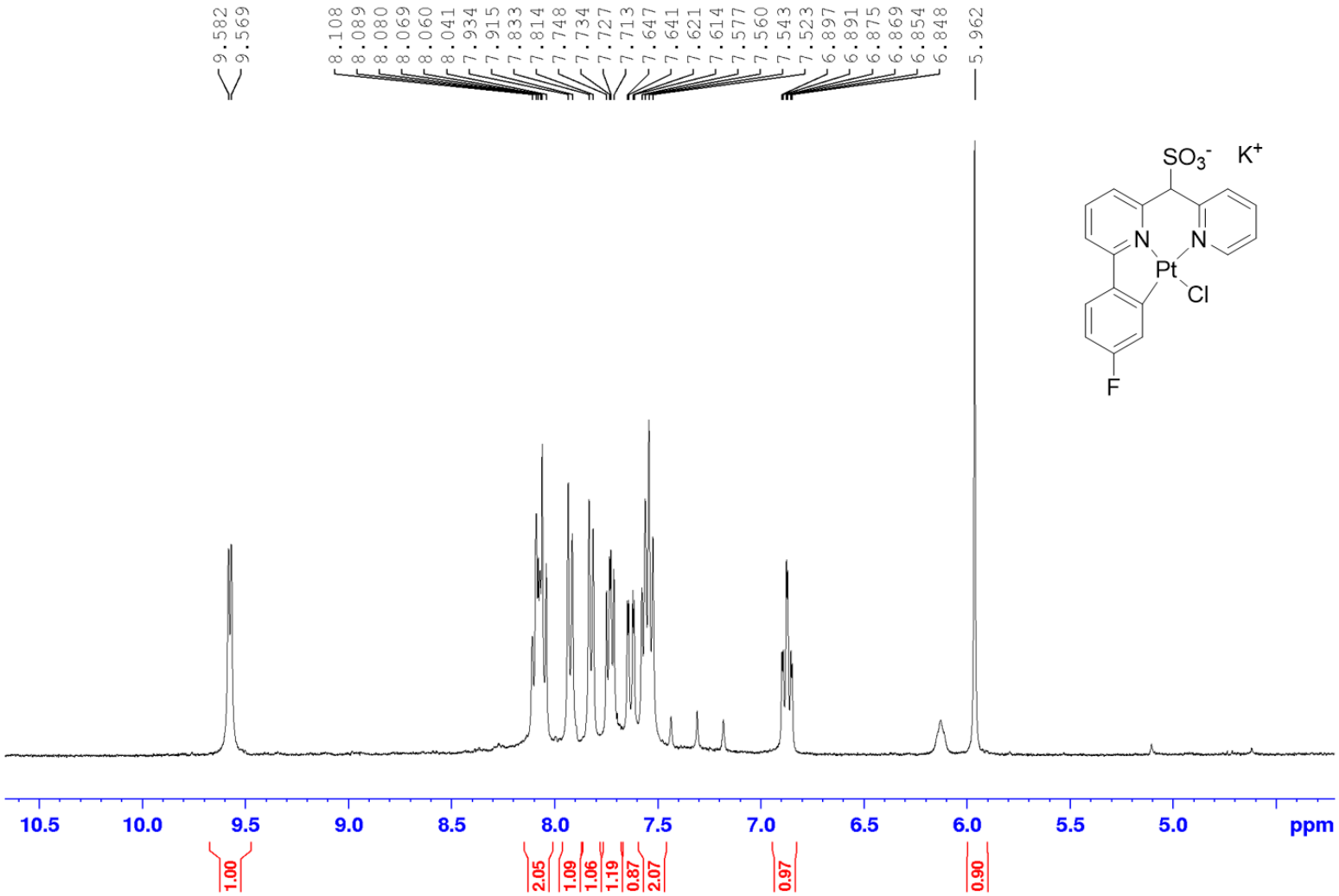

Figure S4.49. ^{1}H-NMR for 2-(4-fluorophenyl)-6-(pyridin-2-ylmethyl) pyridine Pt-Cl Complex, **4.8-F** in DMSO- d_6

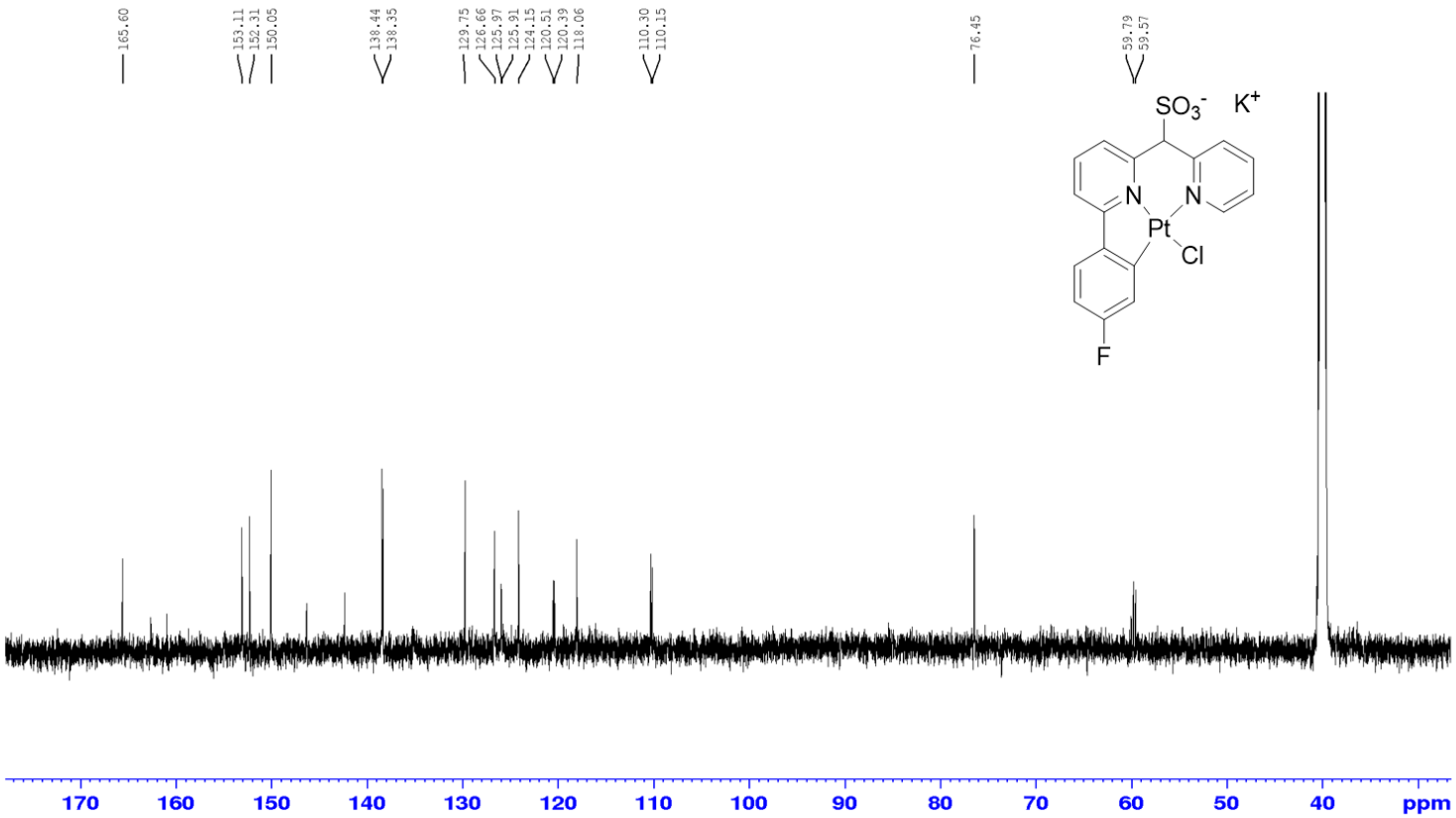

Figure S4.50. ^{13}C-NMR for 2-(4-fluorophenyl)-6-(pyridin-2-ylmethyl) pyridine Pt-Cl Complex, **4.8-F** in DMSO- d_6

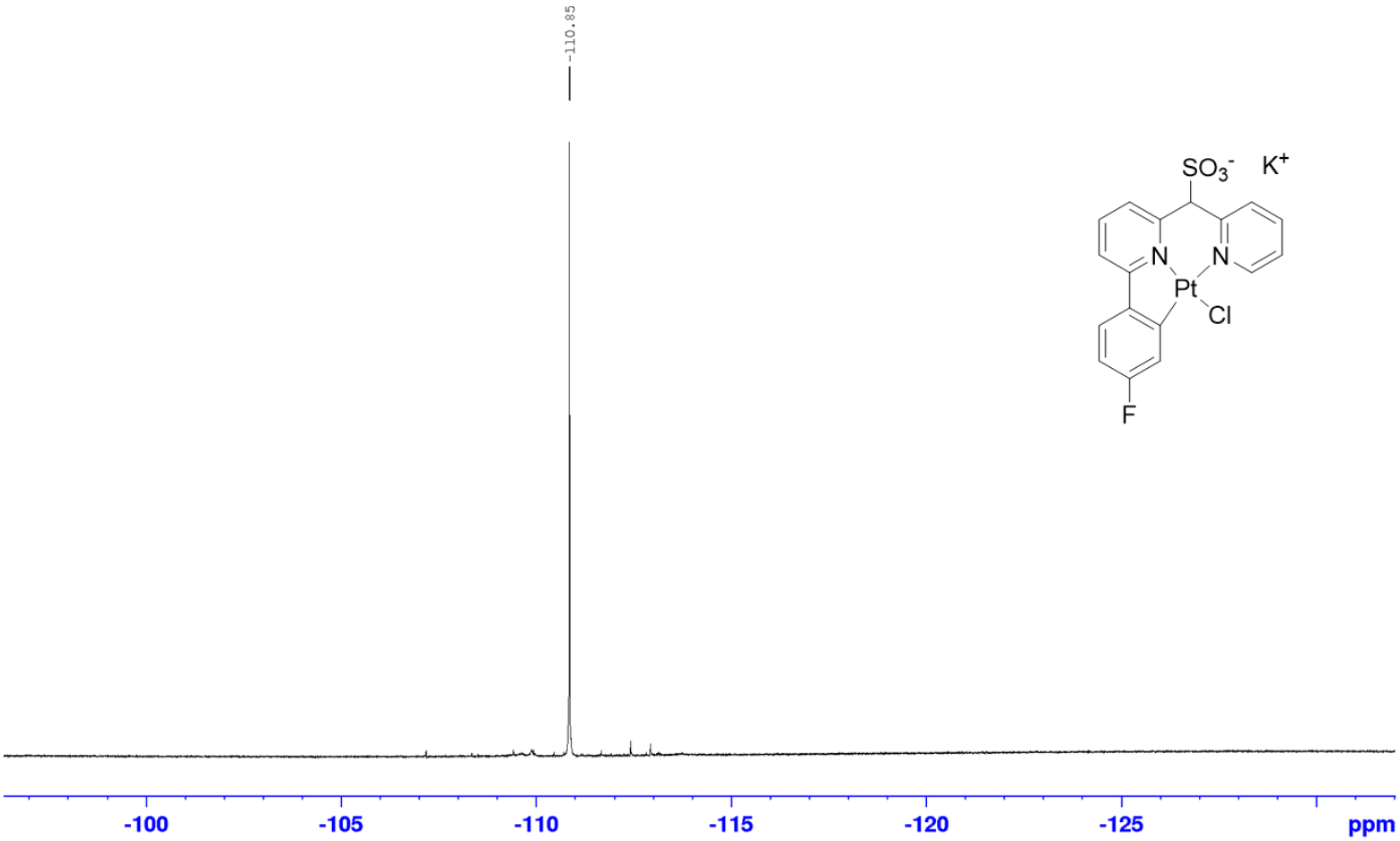

Figure S4.51. ^{19}F-NMR for 2-(4-fluorophenyl)-6-(pyridin-2-ylmethyl) pyridine Pt-Cl Complex, **4.8-F** in DMSO- d_6

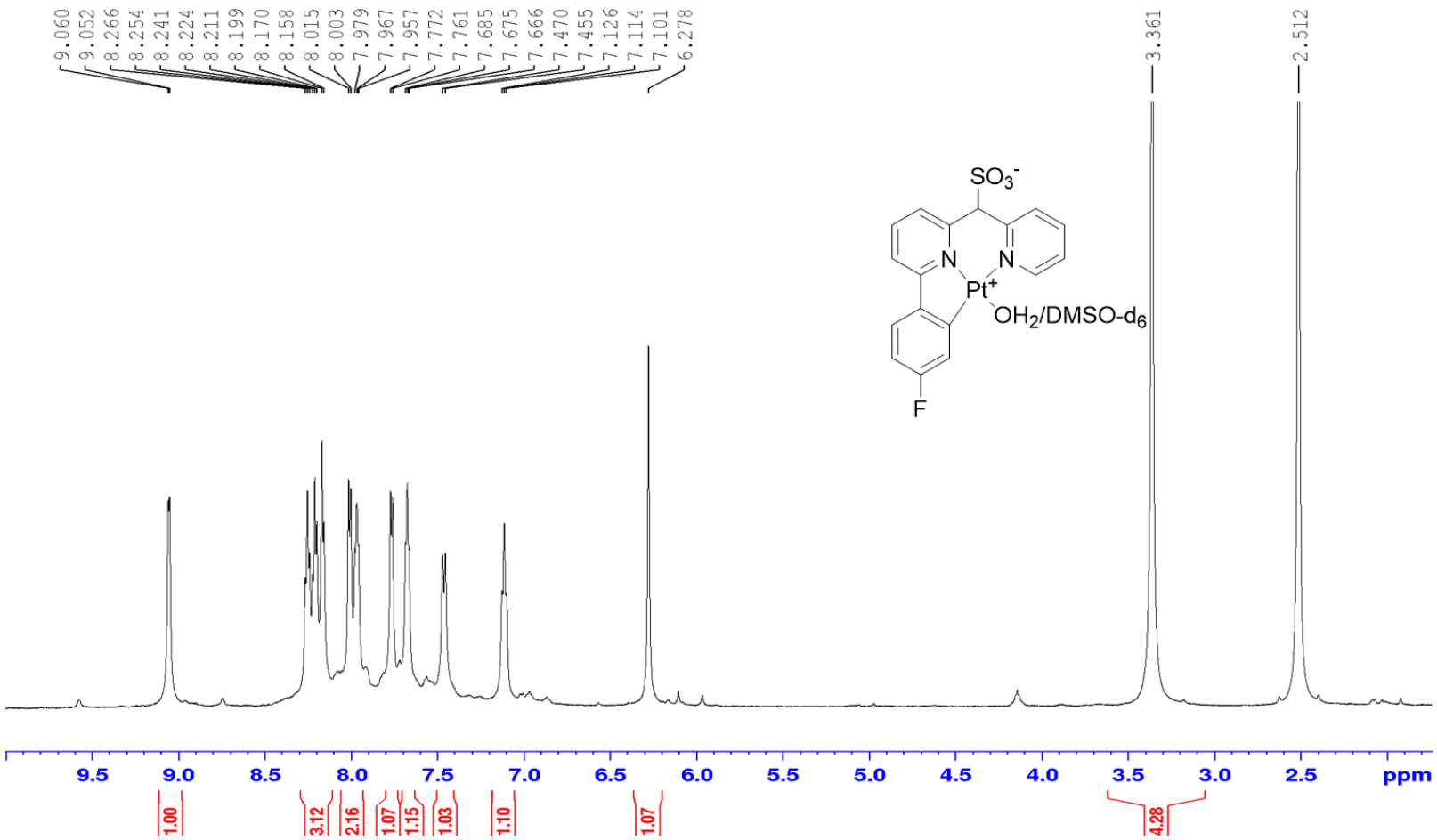

Figure S4.52. ^{1}H-NMR for **4.1-F** in DMSO- d_6

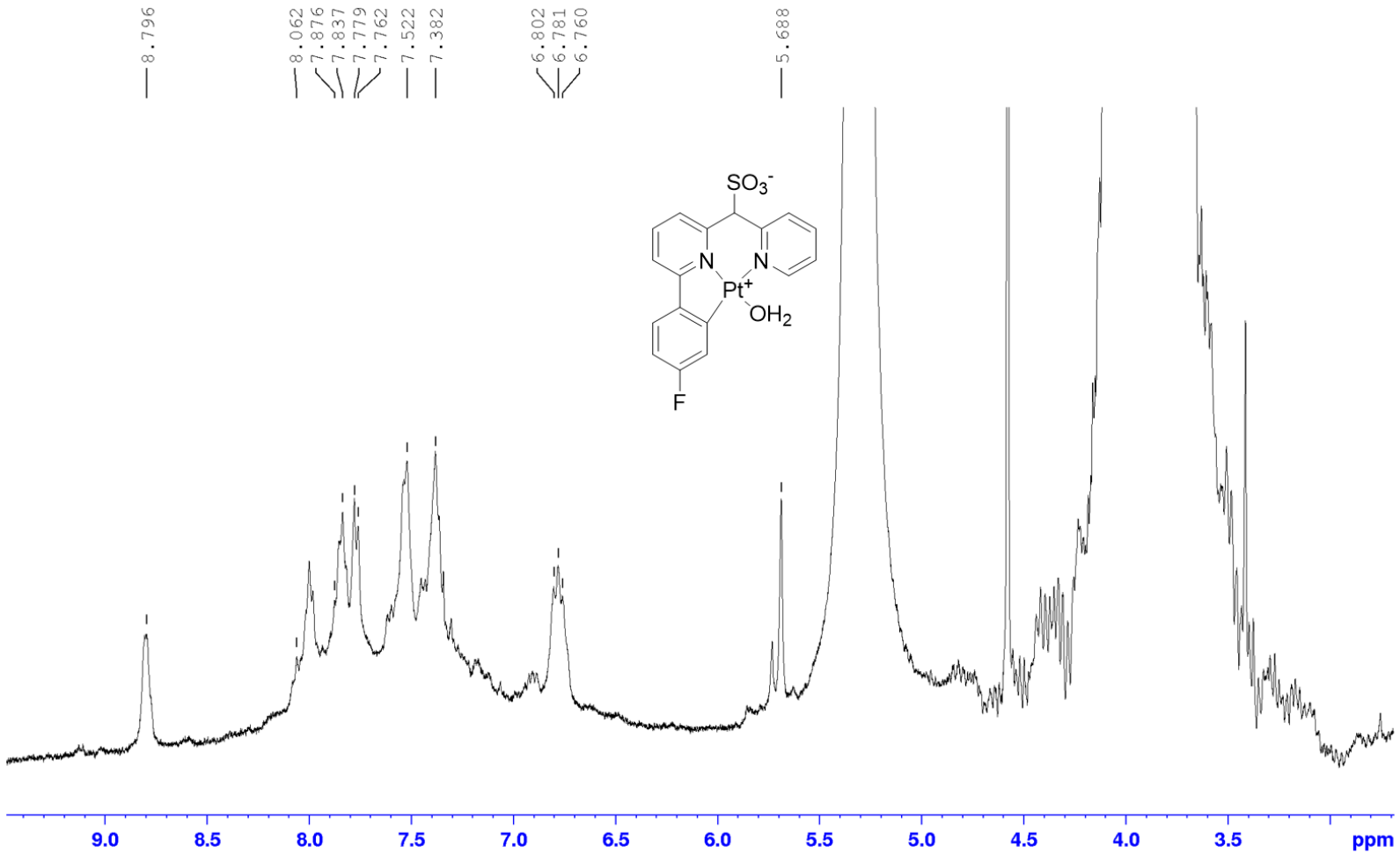

Figure S4.53. ^{1}H-NMR for **4.1-F** in TFE- d_1

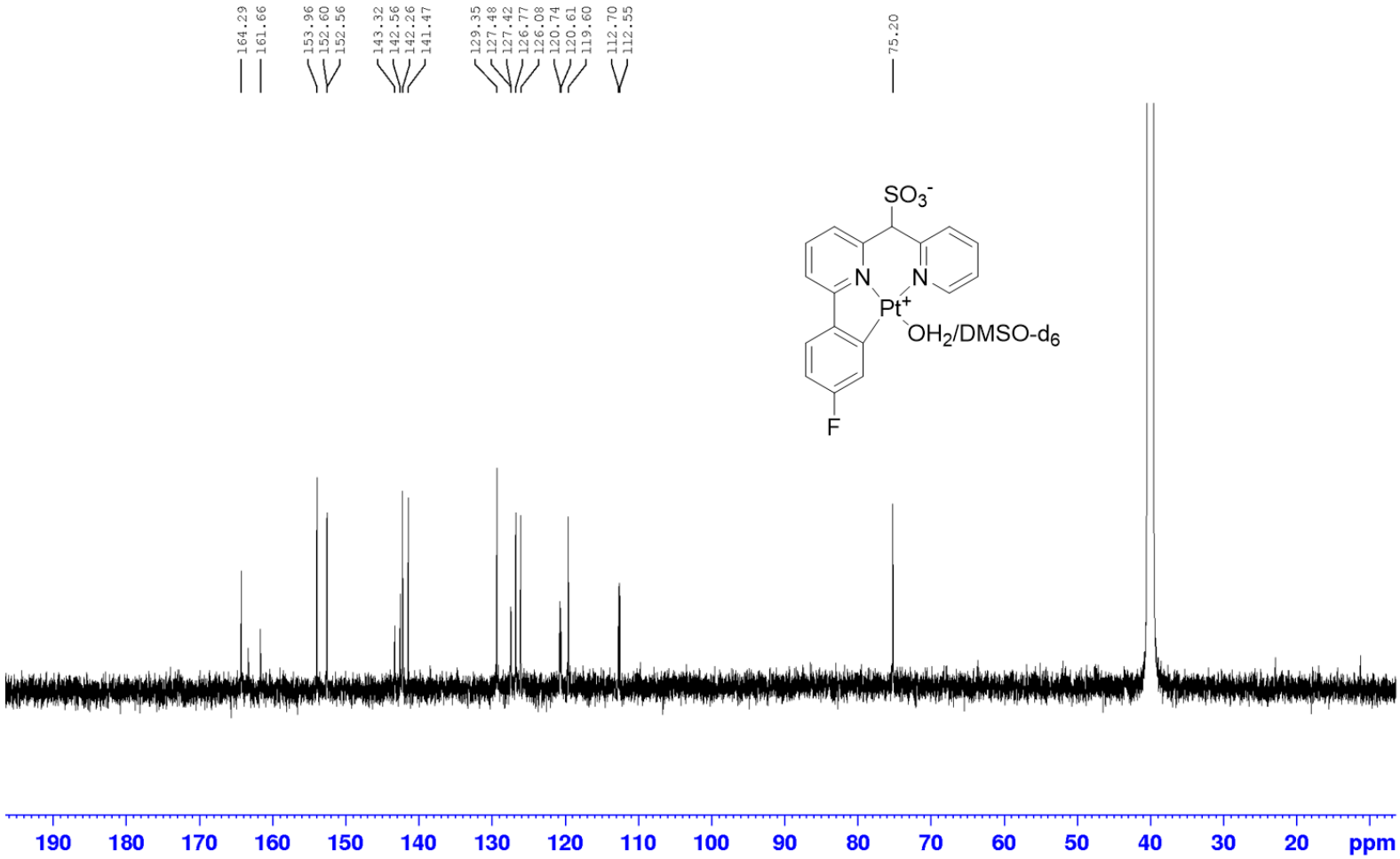

Figure S4.54. ^{13}C-NMR for **4.1-F** in DMSO- d_6

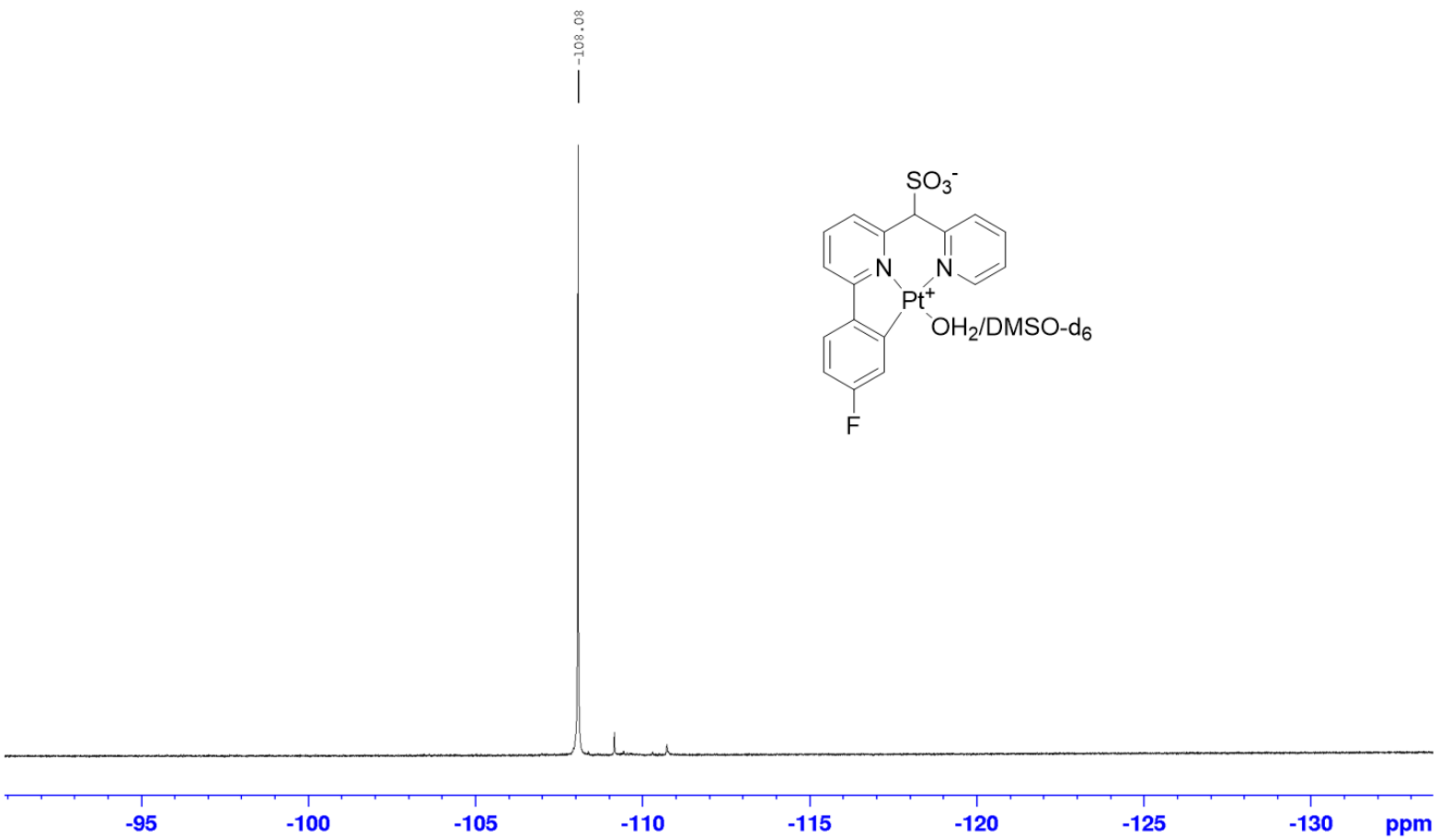

Figure S4.55. ^{19}F-NMR for **4.1-F** in DMSO- d_6

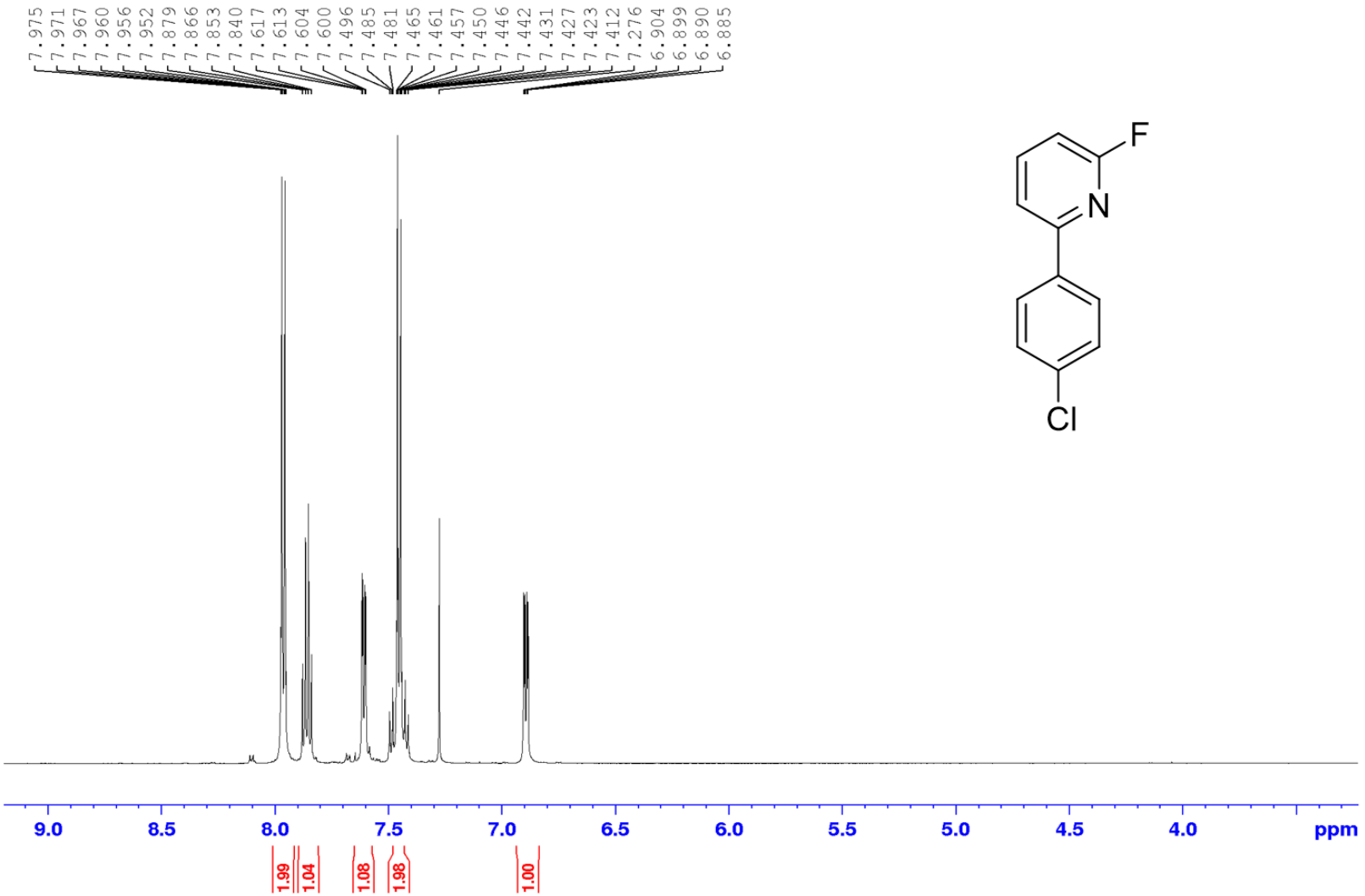

Figure S4.56. ^{19}F-NMR for 2-fluoro-6-(4-chlorophenyl) pyridine, **4.5-Cl** in $CDCl_3$

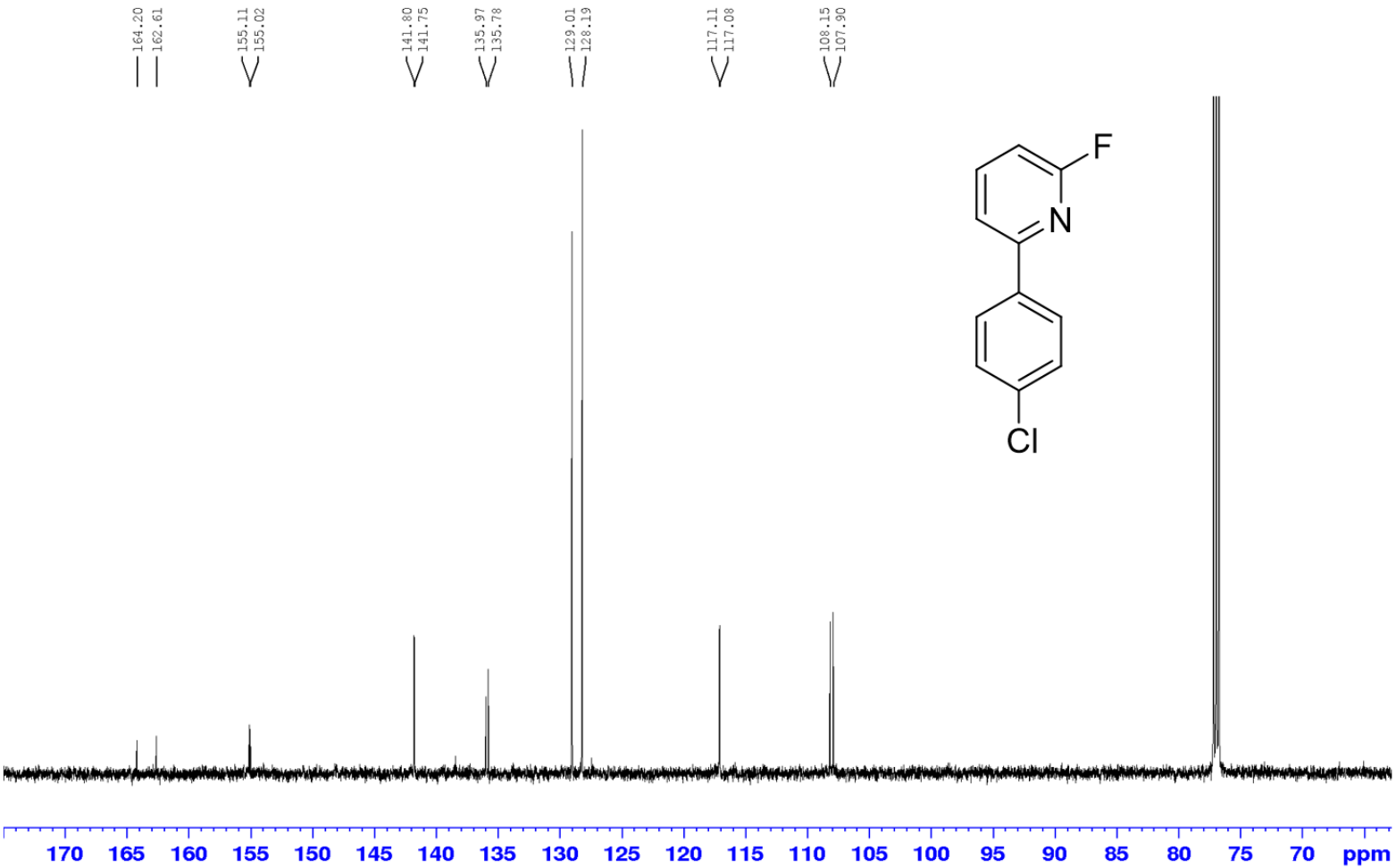

Figure S4.57. ^{13}C-NMR for 2-fluoro-6-(4-chlorophenyl) pyridine, **4.5-Cl** in $CDCl_3$

Figure S4.58. ^{19}F-NMR for 2-fluoro-6-(4-chlorophenyl) pyridine, **4.5-Cl** in $CDCl_3$

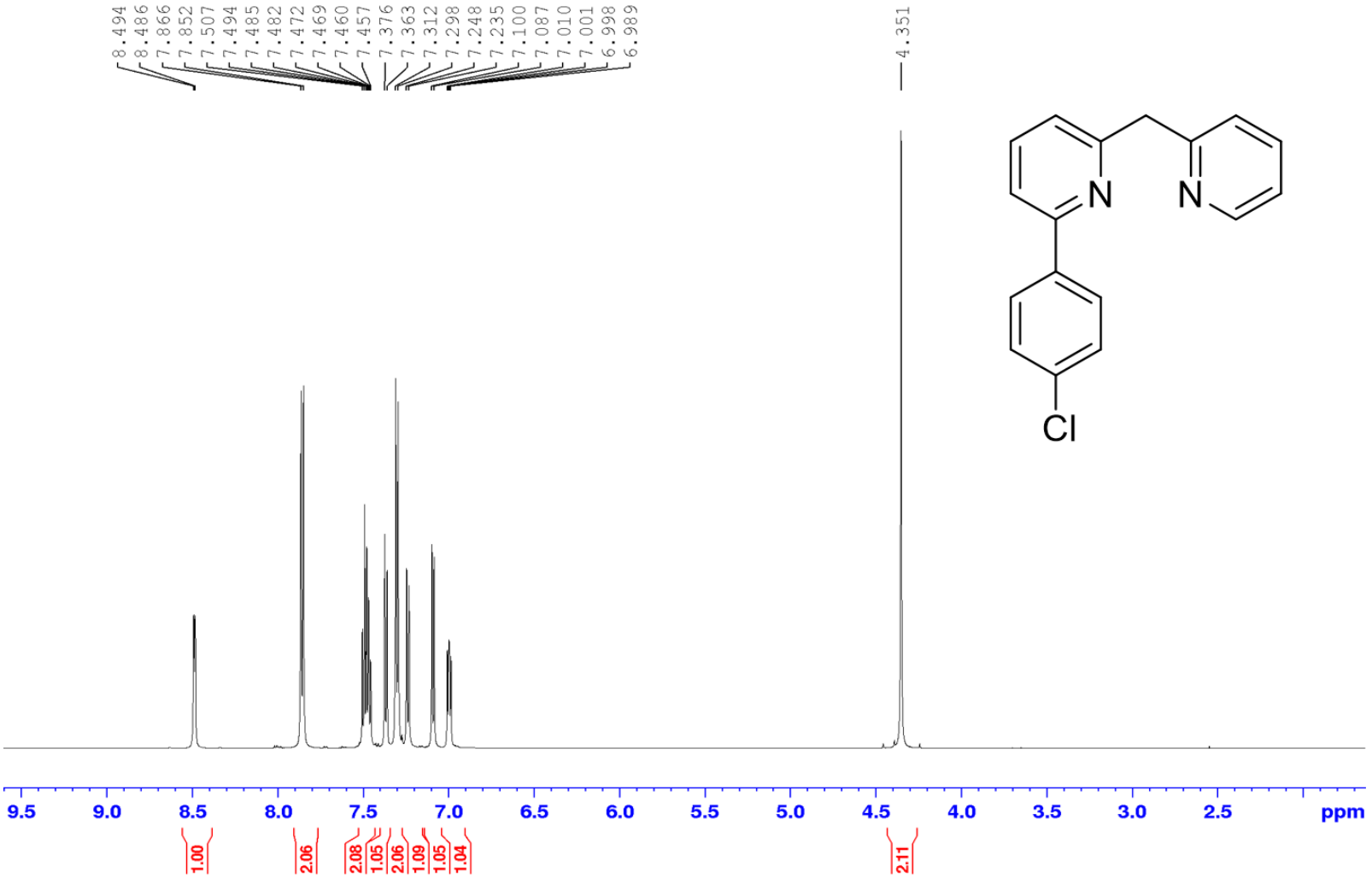

Figure S4.59. ^{1}H-NMR for 2-(4-chlorophenyl)-6-(pyridin-2-ylmethyl) pyridine, **4.6-Cl** in $CDCl_3$

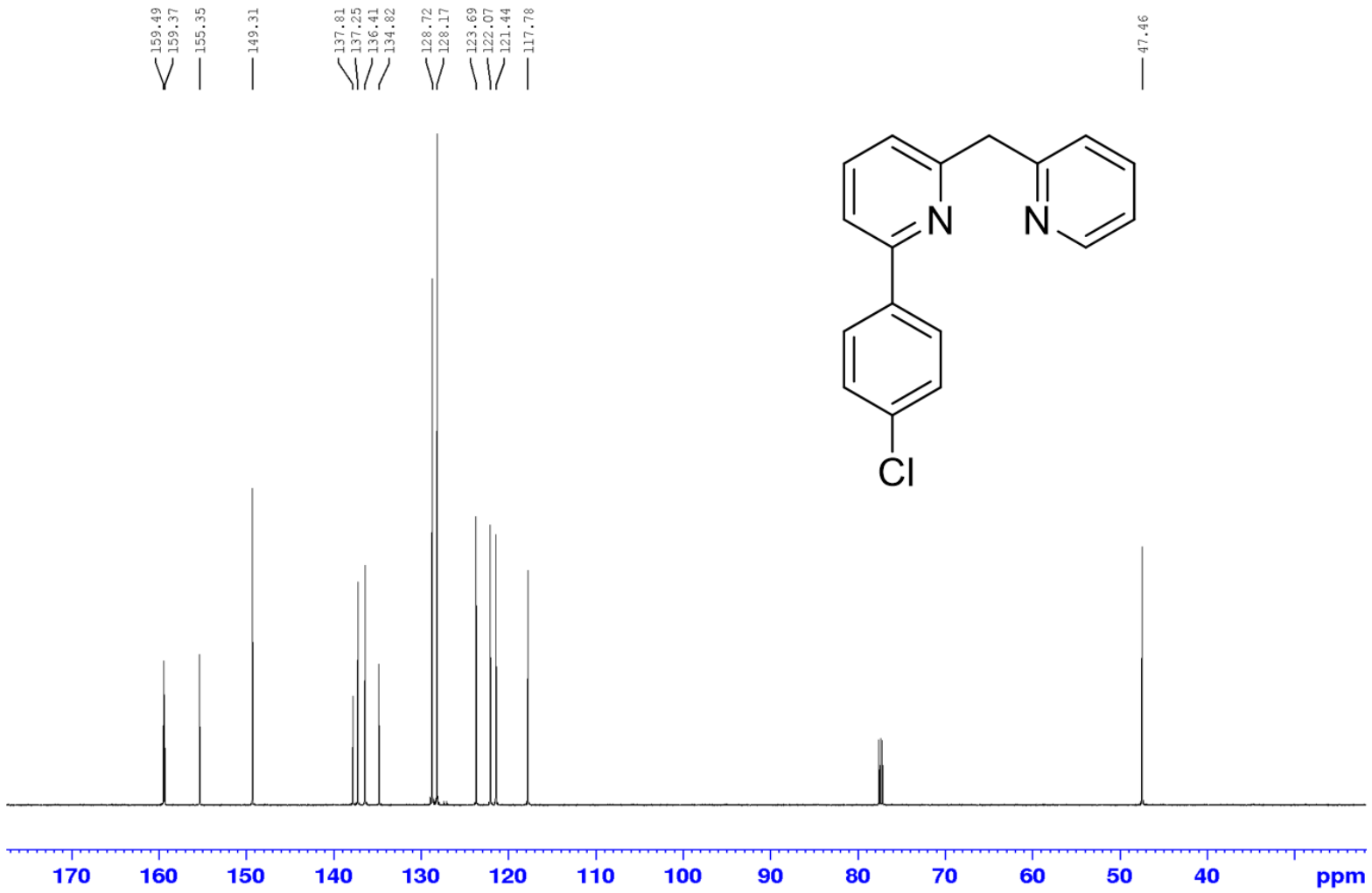

Figure S4.60. ^{13}C-NMR for 2-(4-chlorophenyl)-6-(pyridin-2-ylmethyl) pyridine, **4.6-Cl** in $CDCl_3$

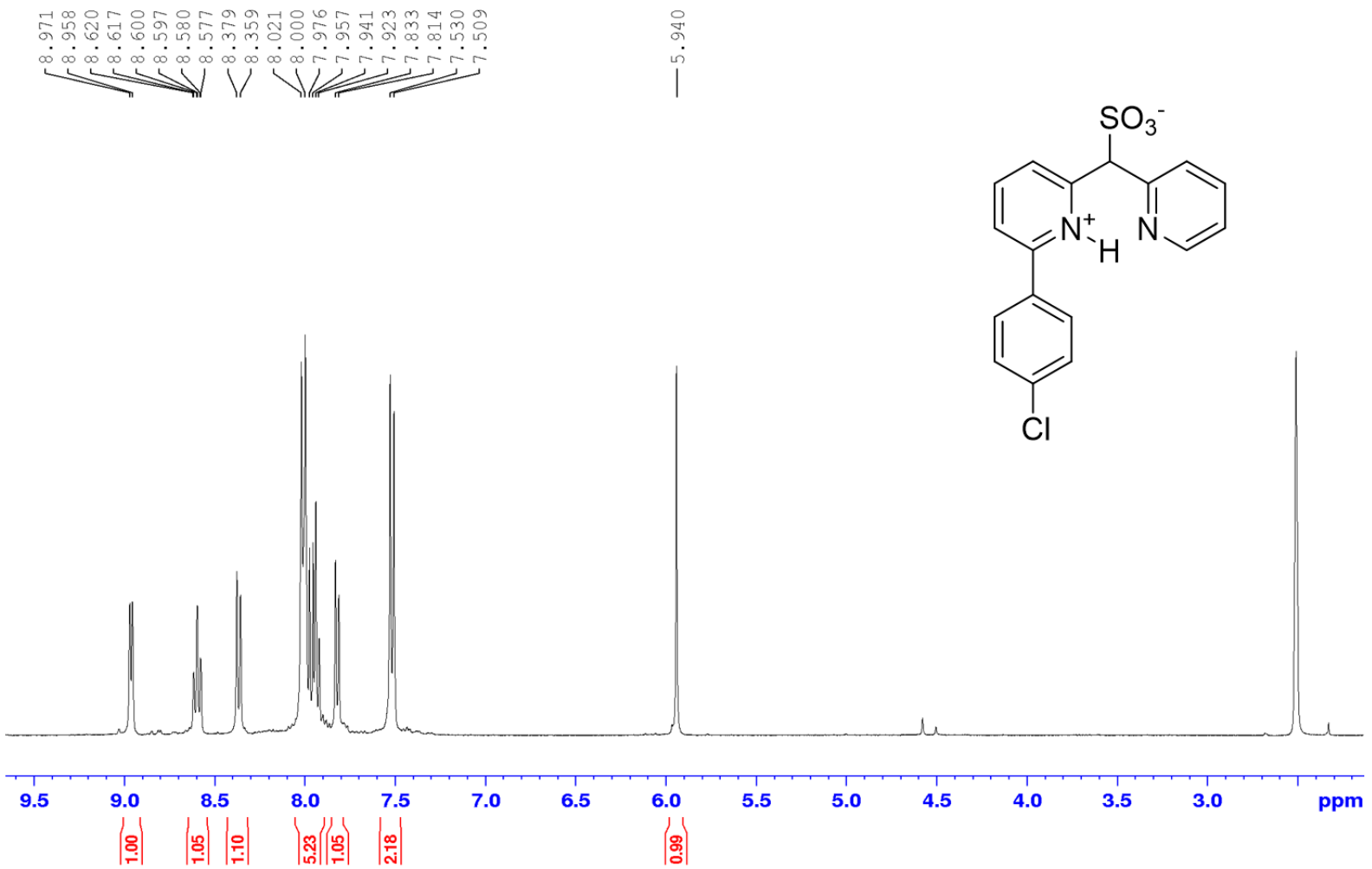

Figure S4.61. ^{1}H-NMR for 2-(4-chlorophenyl)-6-(pyridin-2-ylmethyl) pyridinium sulfonate, **4.7-Cl** in DMSO- d_6

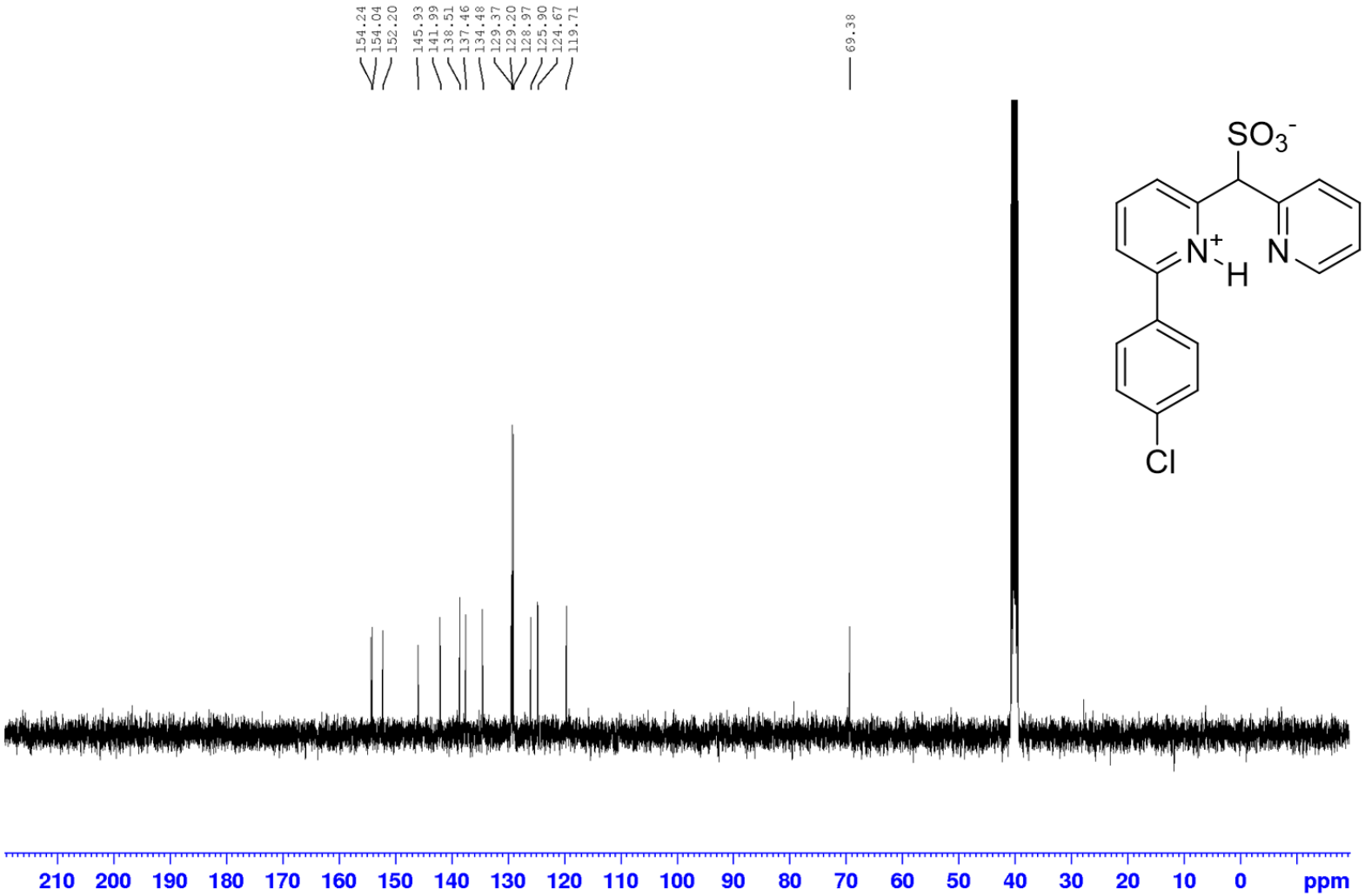

Figure S4.62. ^{13}C-NMR for 2-(4-chlorophenyl)-6-(pyridin-2-ylmethyl) pyridinium sulfonate, **4.7-Cl** in DMSO- d_6

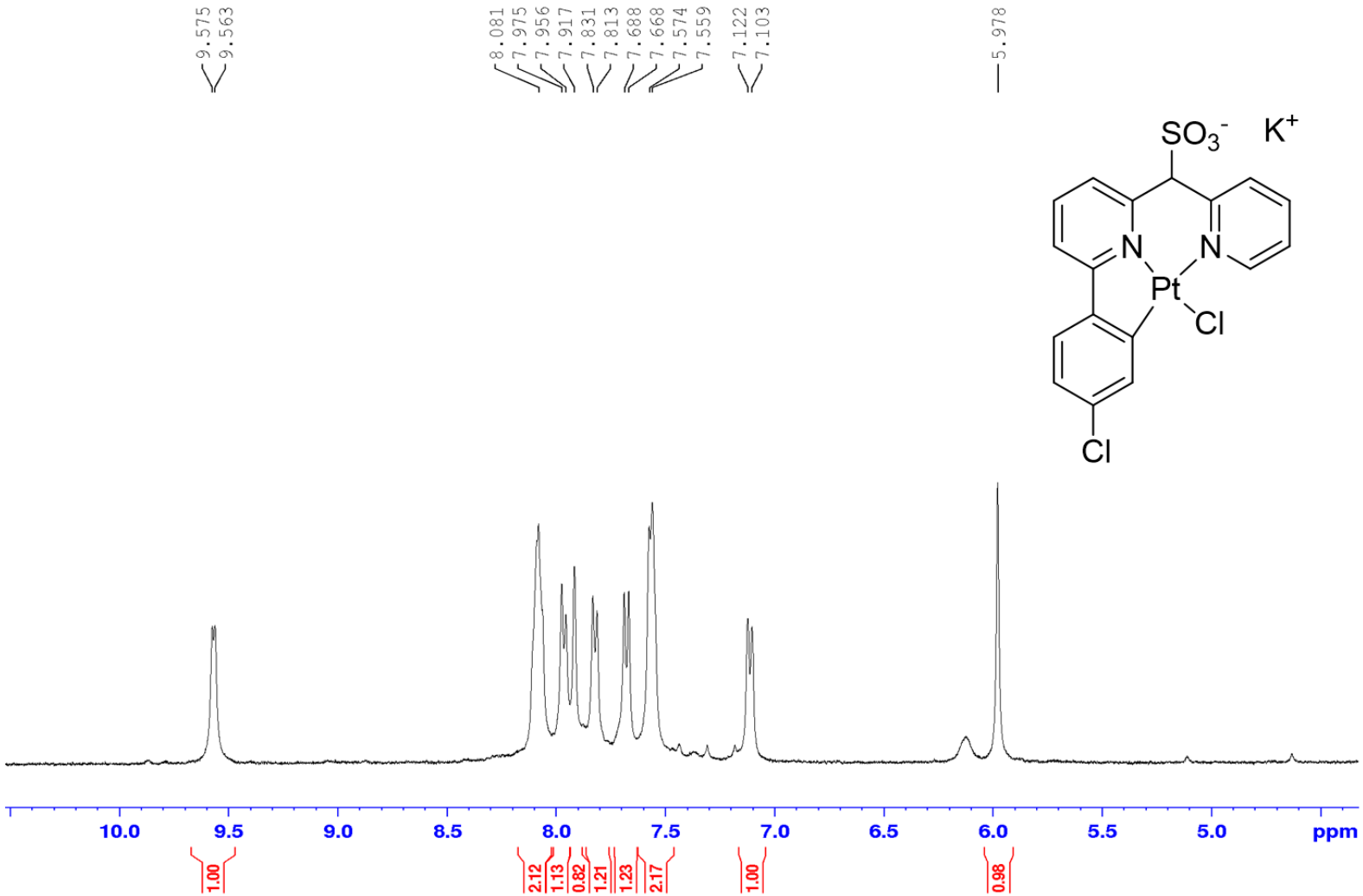

Figure S4.63. ^{1}H-NMR for 2-(4-chlorophenyl)-6-(pyridin-2-ylmethyl) pyridine Pt-Cl Complex, **4.8-Cl** in DMSO- d_6

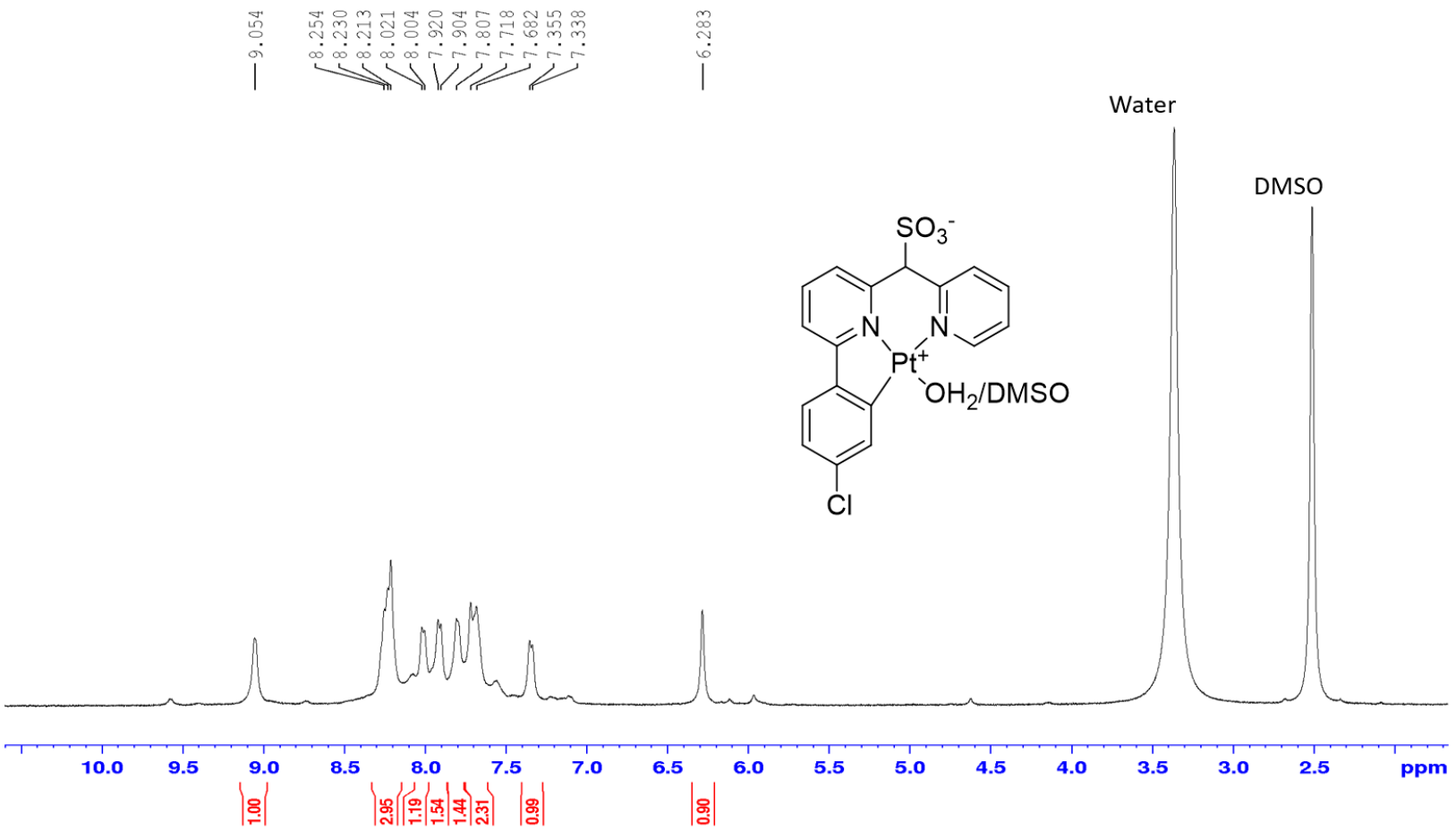

Figure S4.64. ^{1}H-NMR for **4.1-Cl** in DMSO- d_6

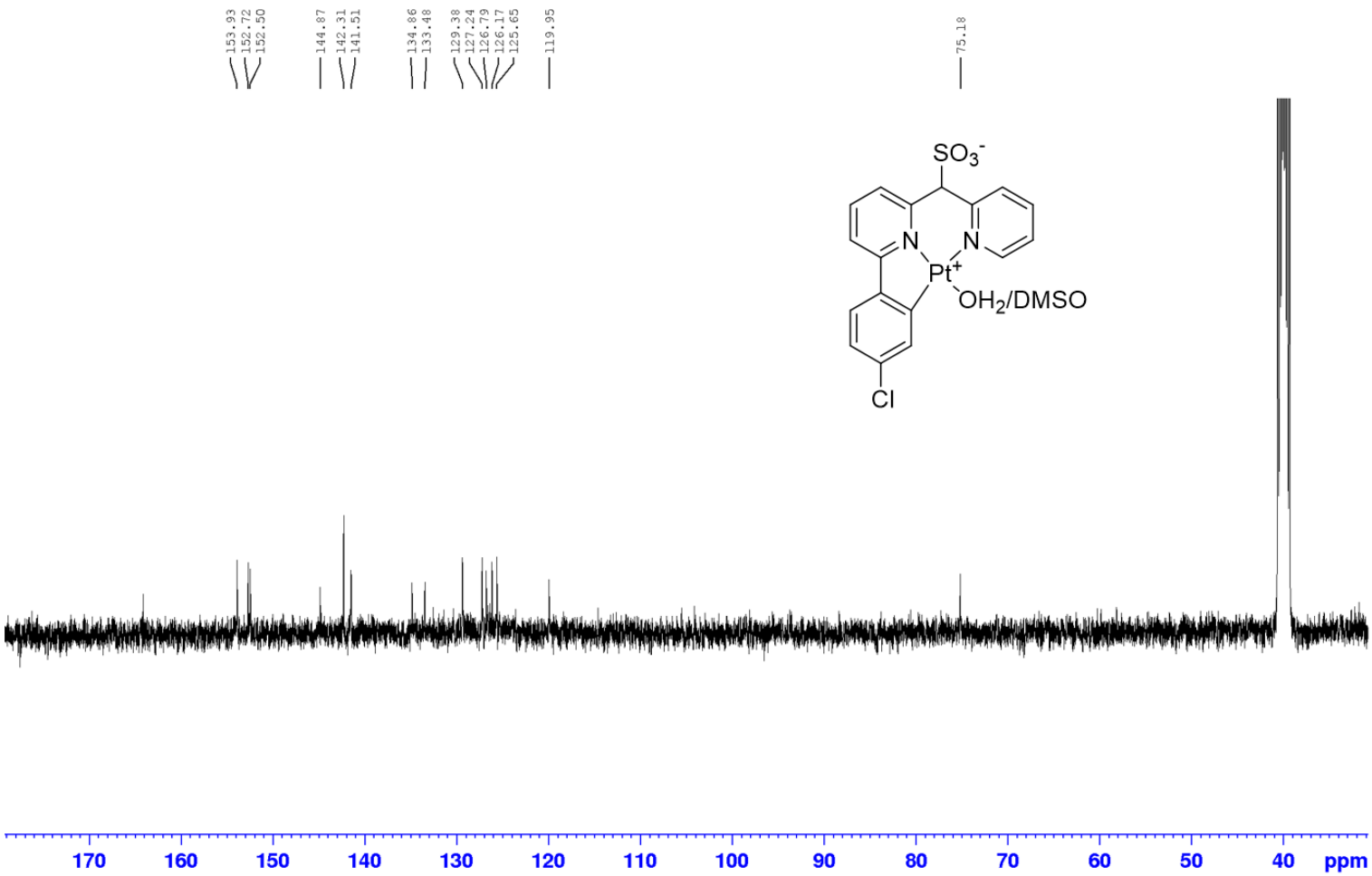

Figure S4.65. ^{1}H-NMR for **4.1-Cl** in DMSO- d_6

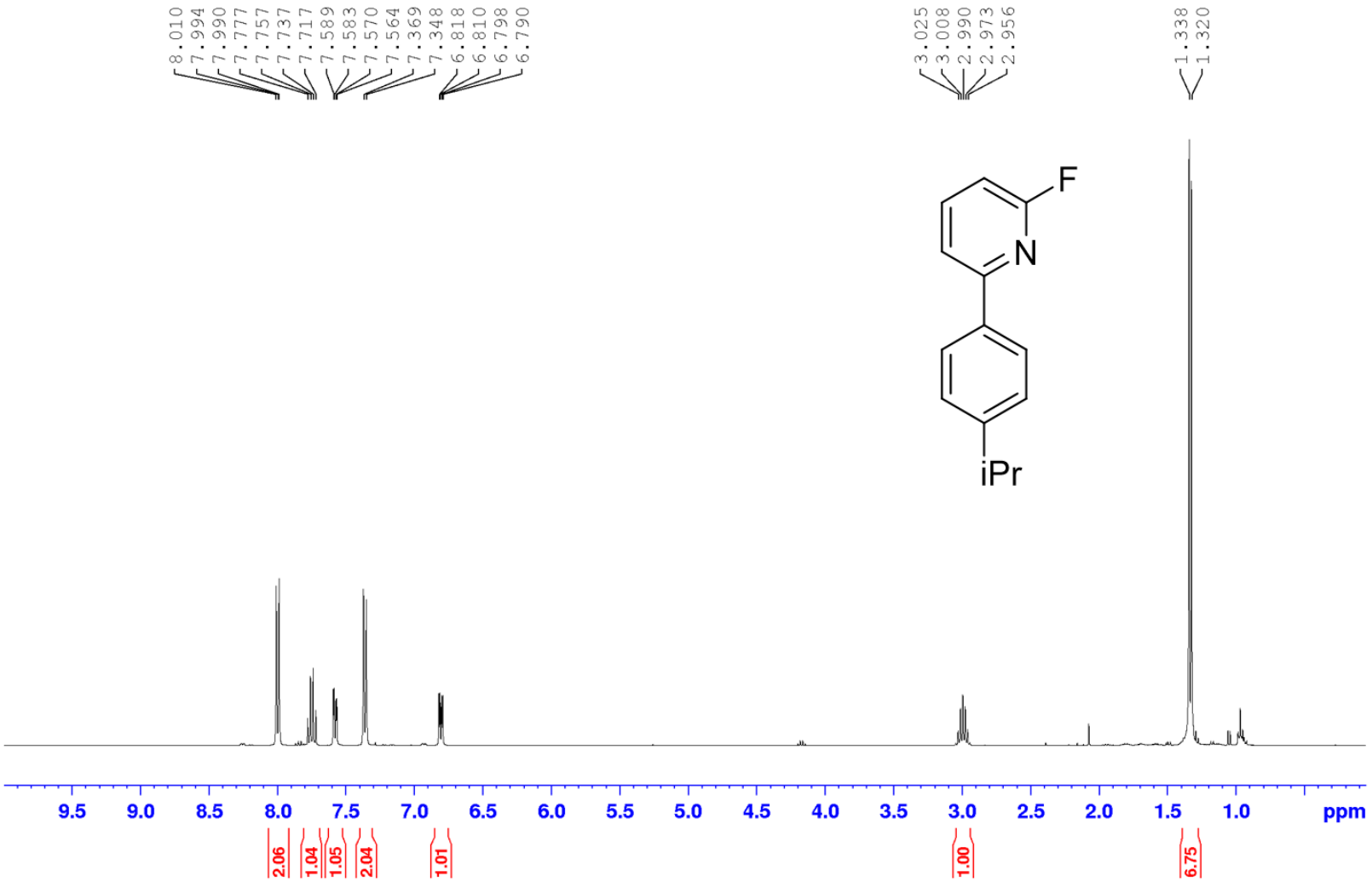

Figure S4.66. ^{1}H-NMR for 2-fluoro-6-(4-isopropylphenyl) pyridine, **4.5-iPr** in $CDCl_3$

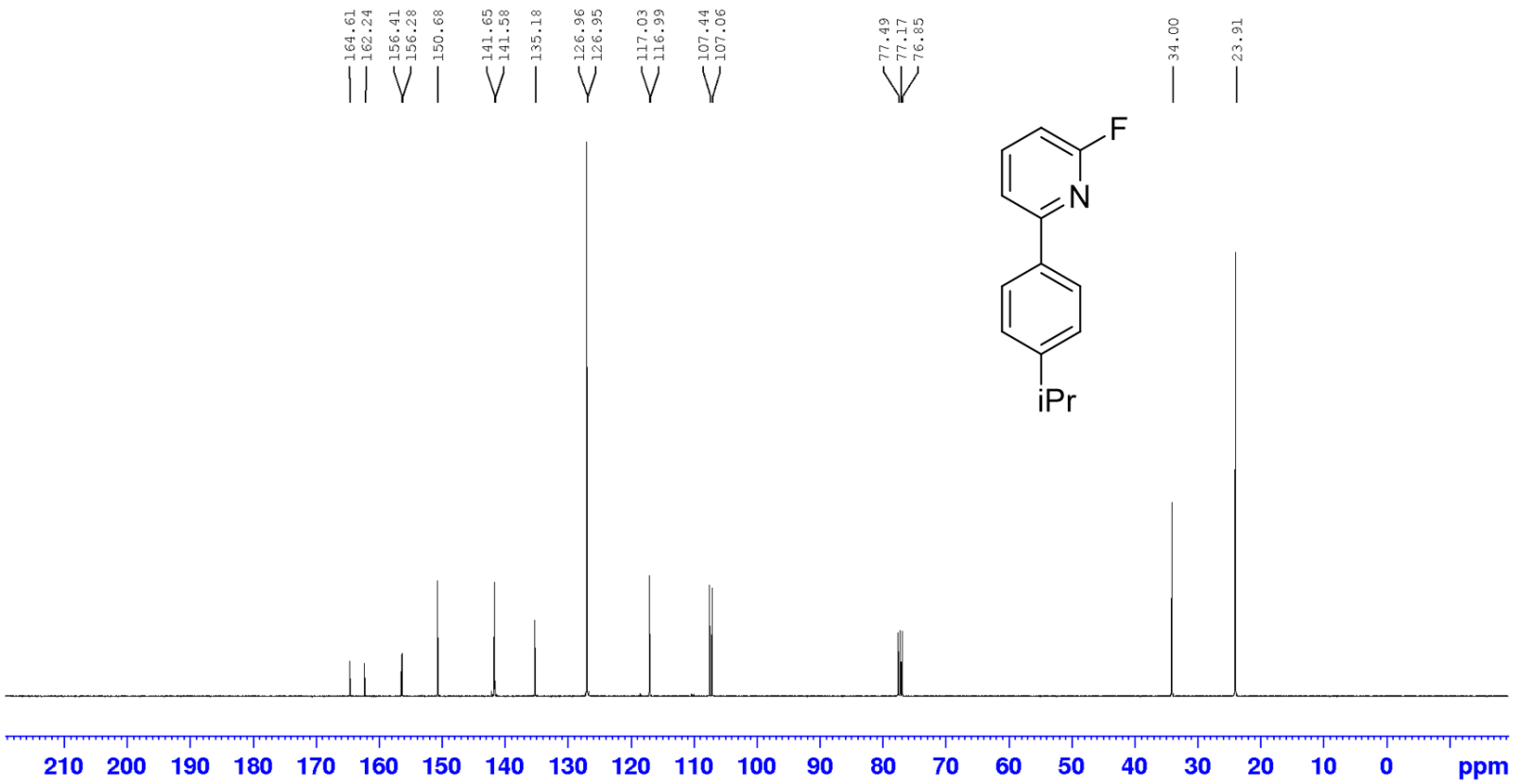

Figure S4.67. ^{13}C-NMR for 2-fluoro-6-(4-isopropylphenyl) pyridine, **4.5-iPr** in $CDCl_3$

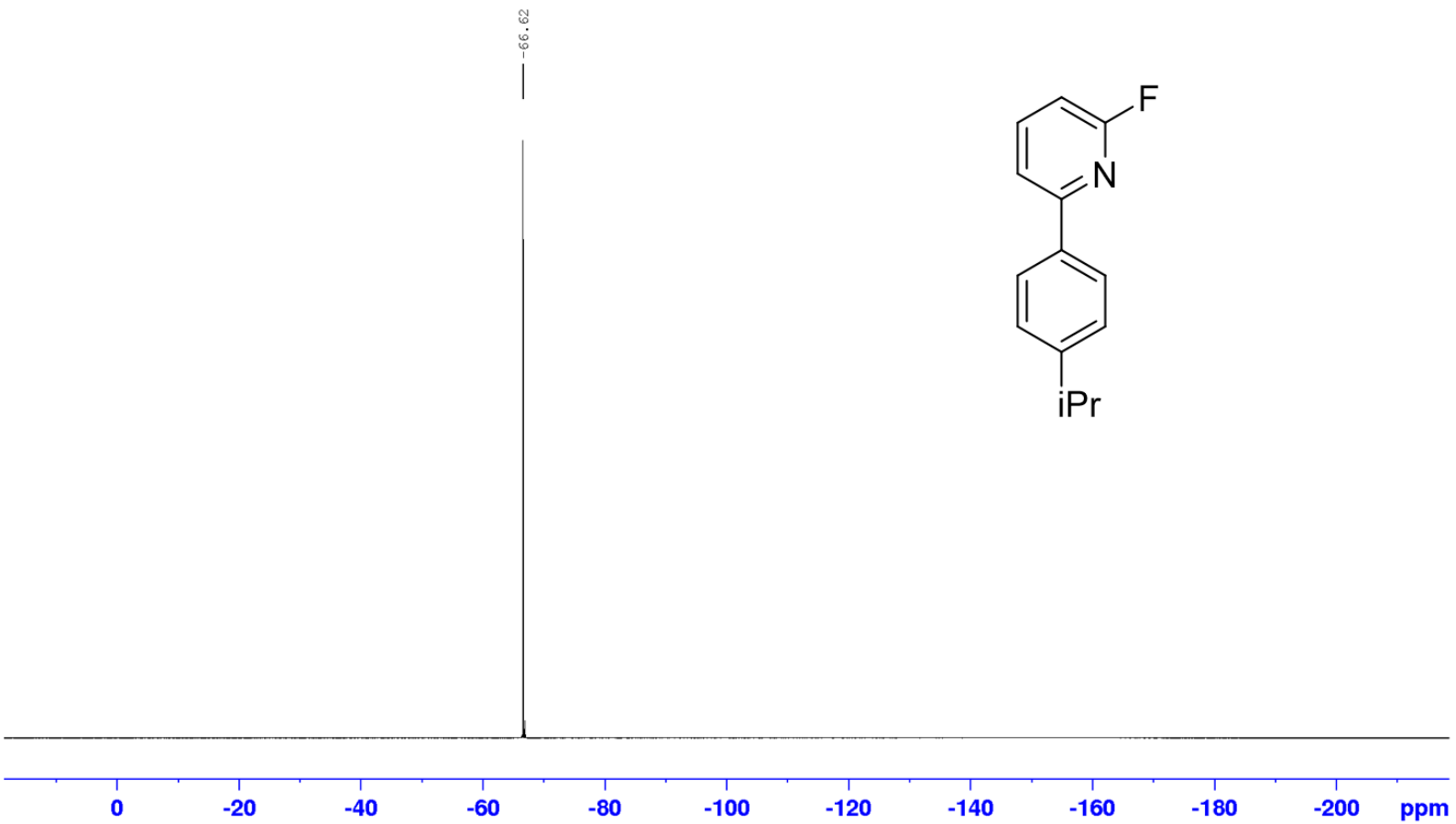

Figure S4.68. ^{19}F-NMR for 2-fluoro-6-(4-isopropylphenyl) pyridine, **4.5-iPr** in $CDCl_3$

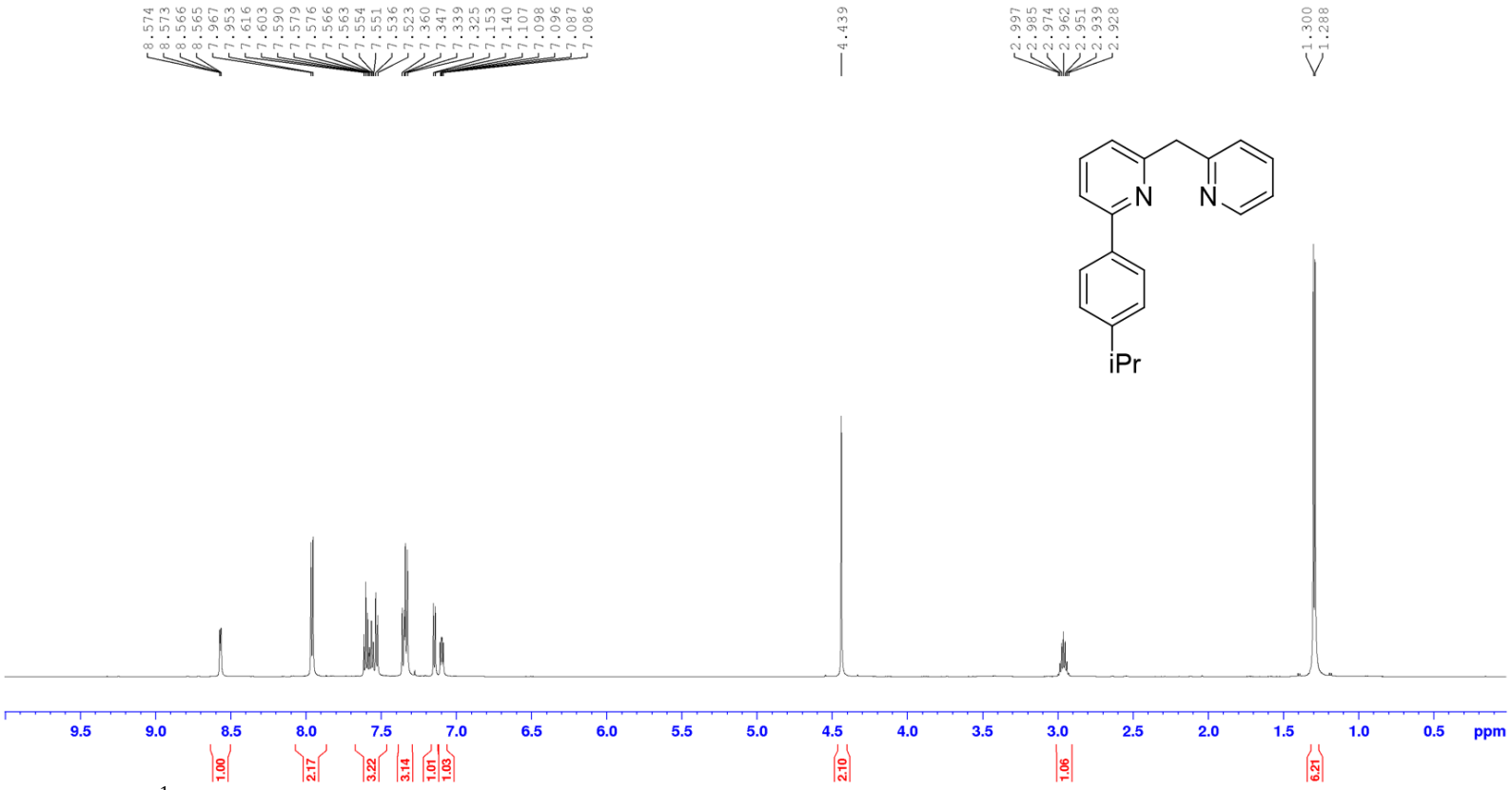

Figure S4.69. ^{1}H-NMR for 2-(4-isopropylphenyl)-6-(pyridin-2-ylmethyl) pyridine, **4.6-iPr** in $CDCl_3$

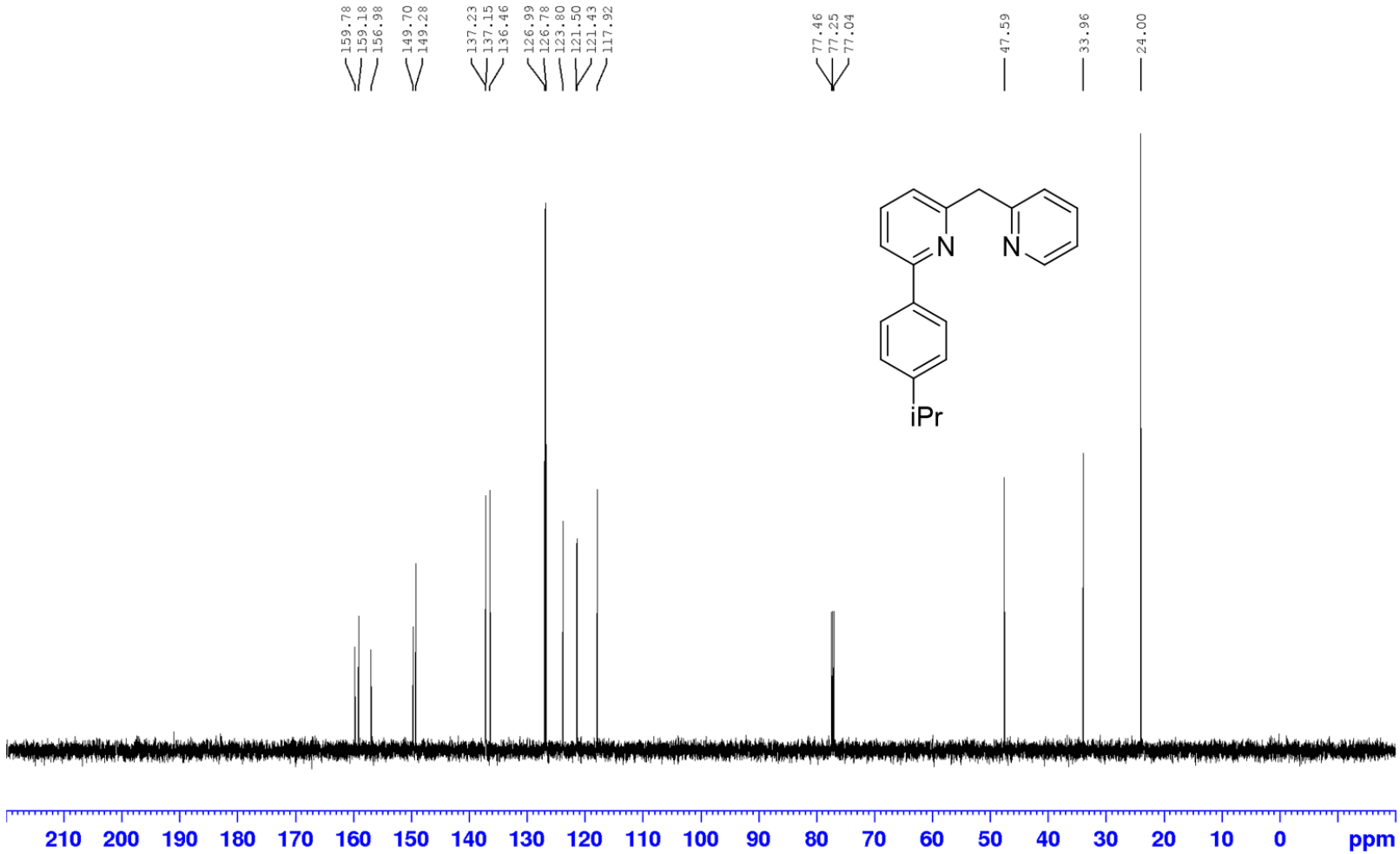

Figure S4.70. ^{13}C-NMR for 2-(4-isopropylphenyl)-6-(pyridin-2-ylmethyl) pyridine, **4.6-iPr** in $CDCl_3$

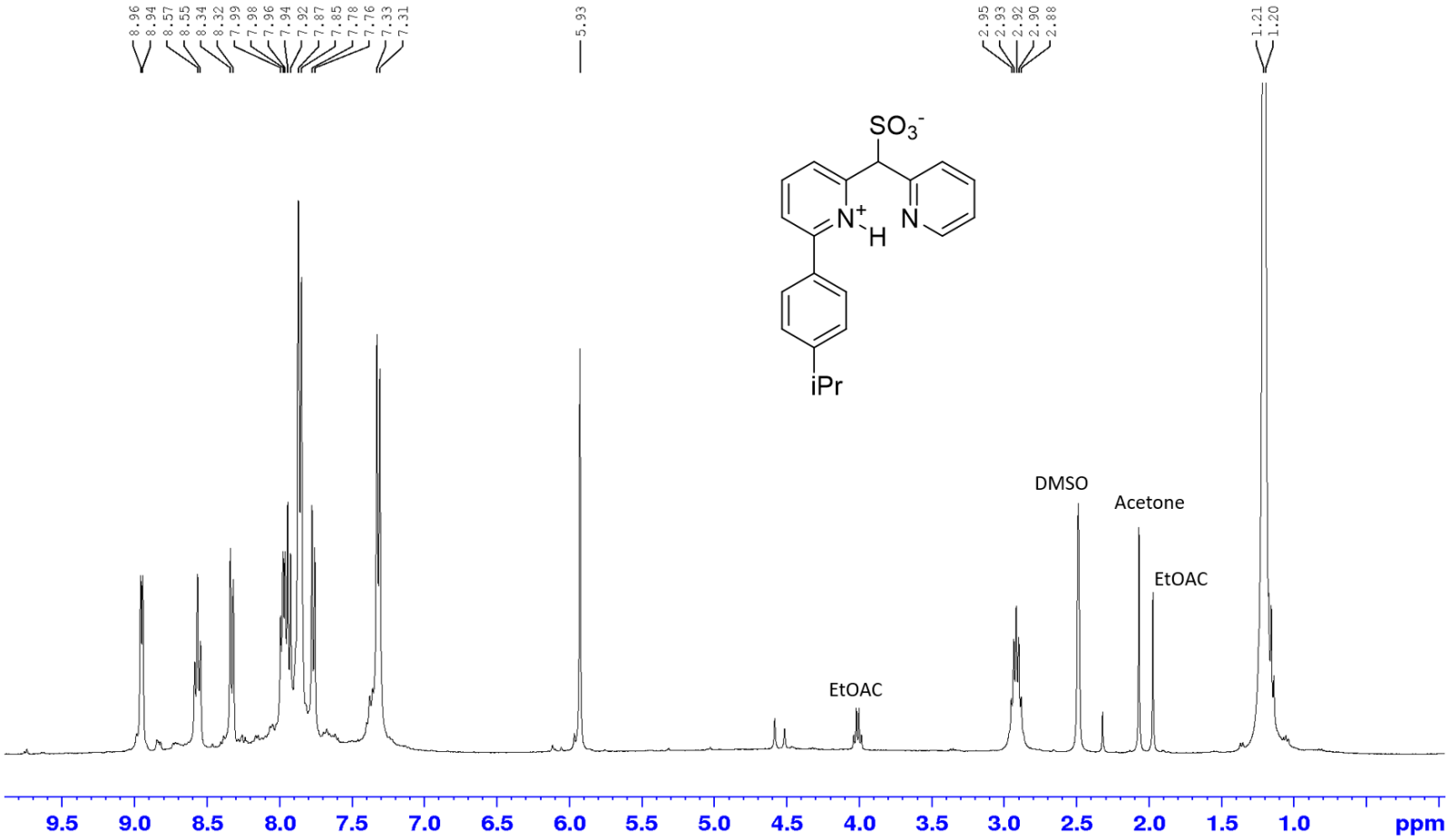

Figure S4.71. ^{1}H-NMR for 2-(4-isopropylphenyl)-6-(pyridin-2-ylmethyl) pyridinium sulfonate, **4.7-iPr** in DMSO- d_6

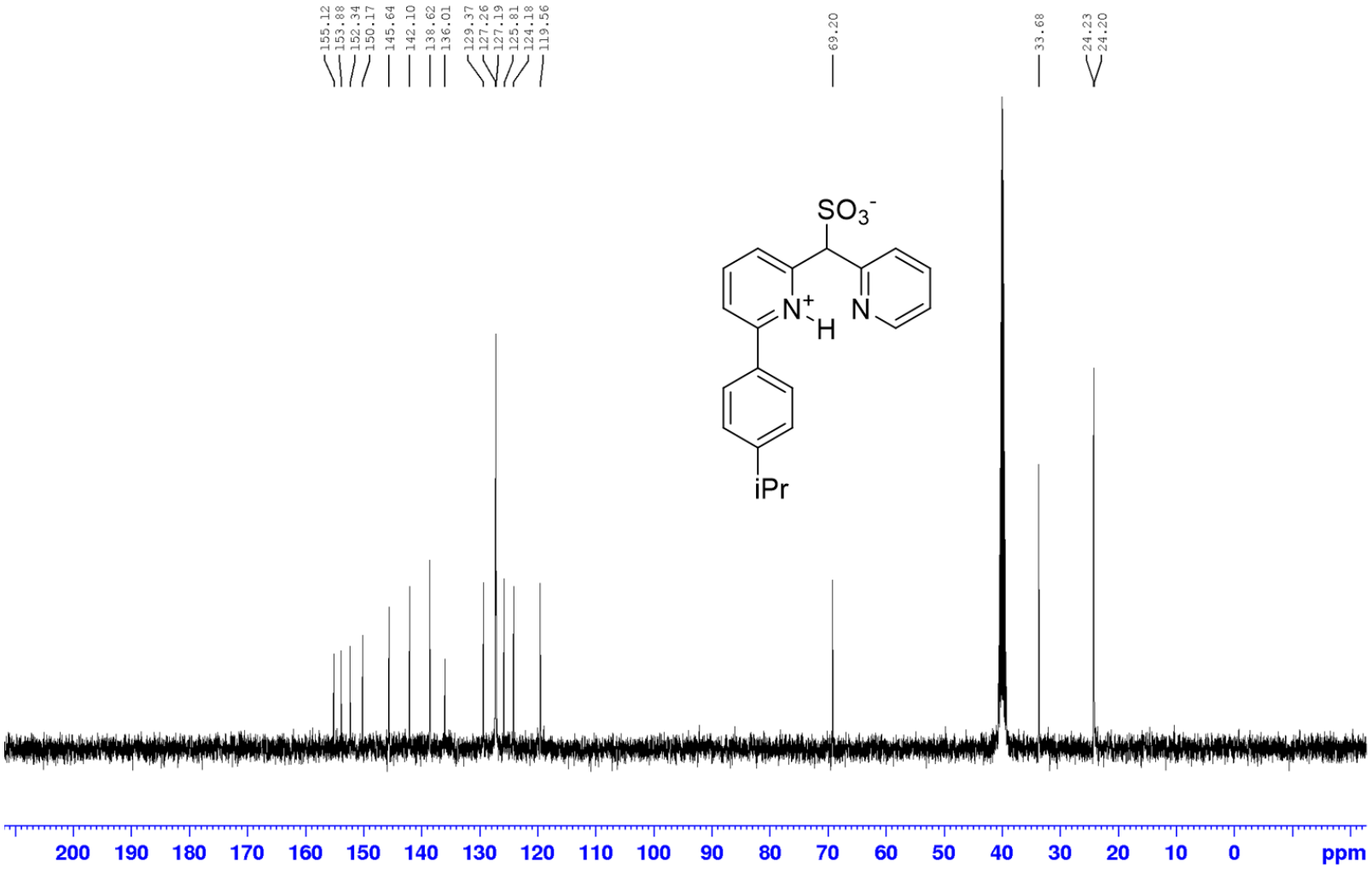

Figure S4.72. ^{13}C-NMR for 2-(4-isopropylphenyl)-6-(pyridin-2-ylmethyl) pyridinium sulfonate, **4.7-iPr** in DMSO- d_6

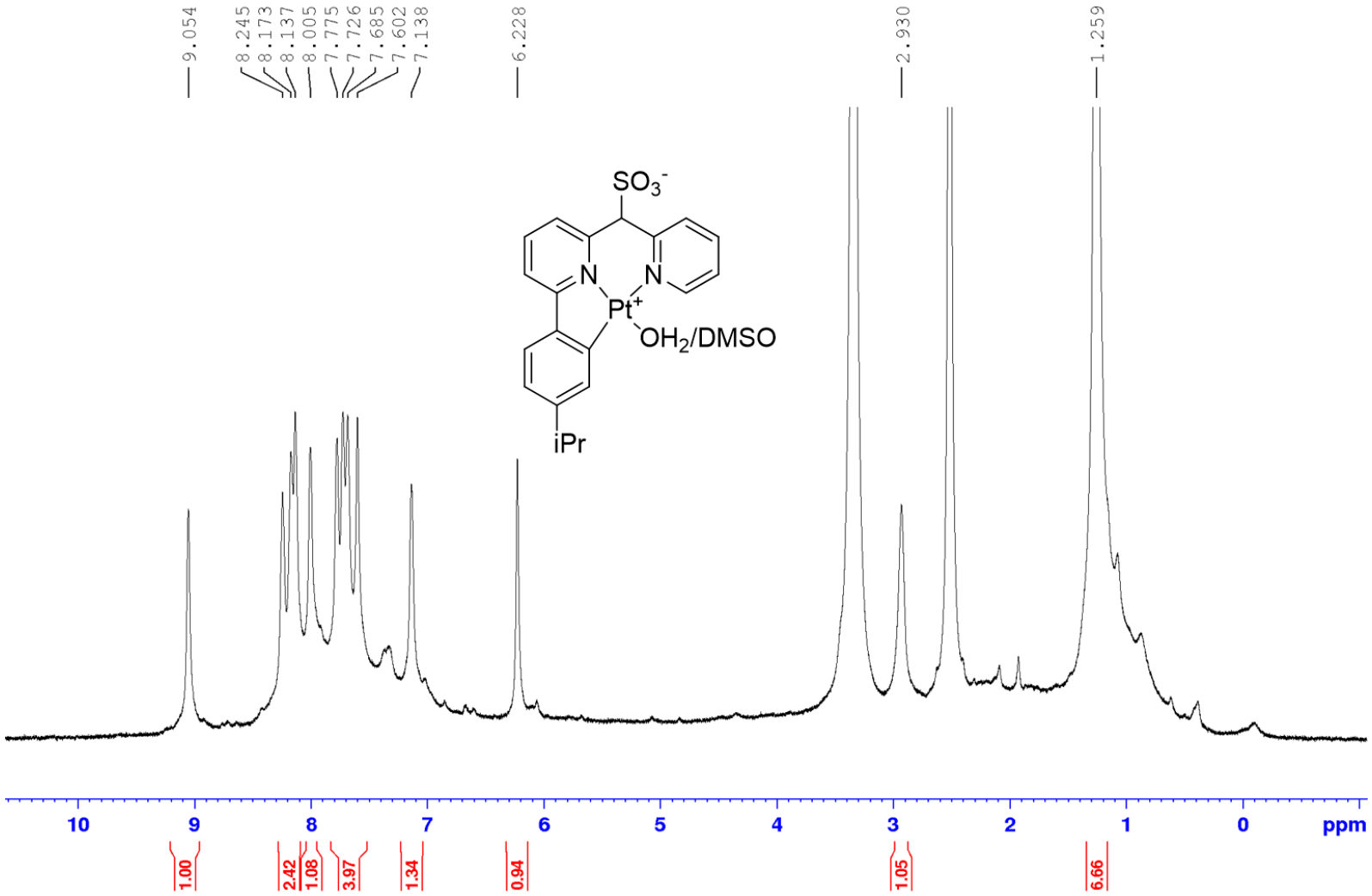

Figure S4.73. ^{1}H-NMR for **4.1-iPr** in DMSO- d_6

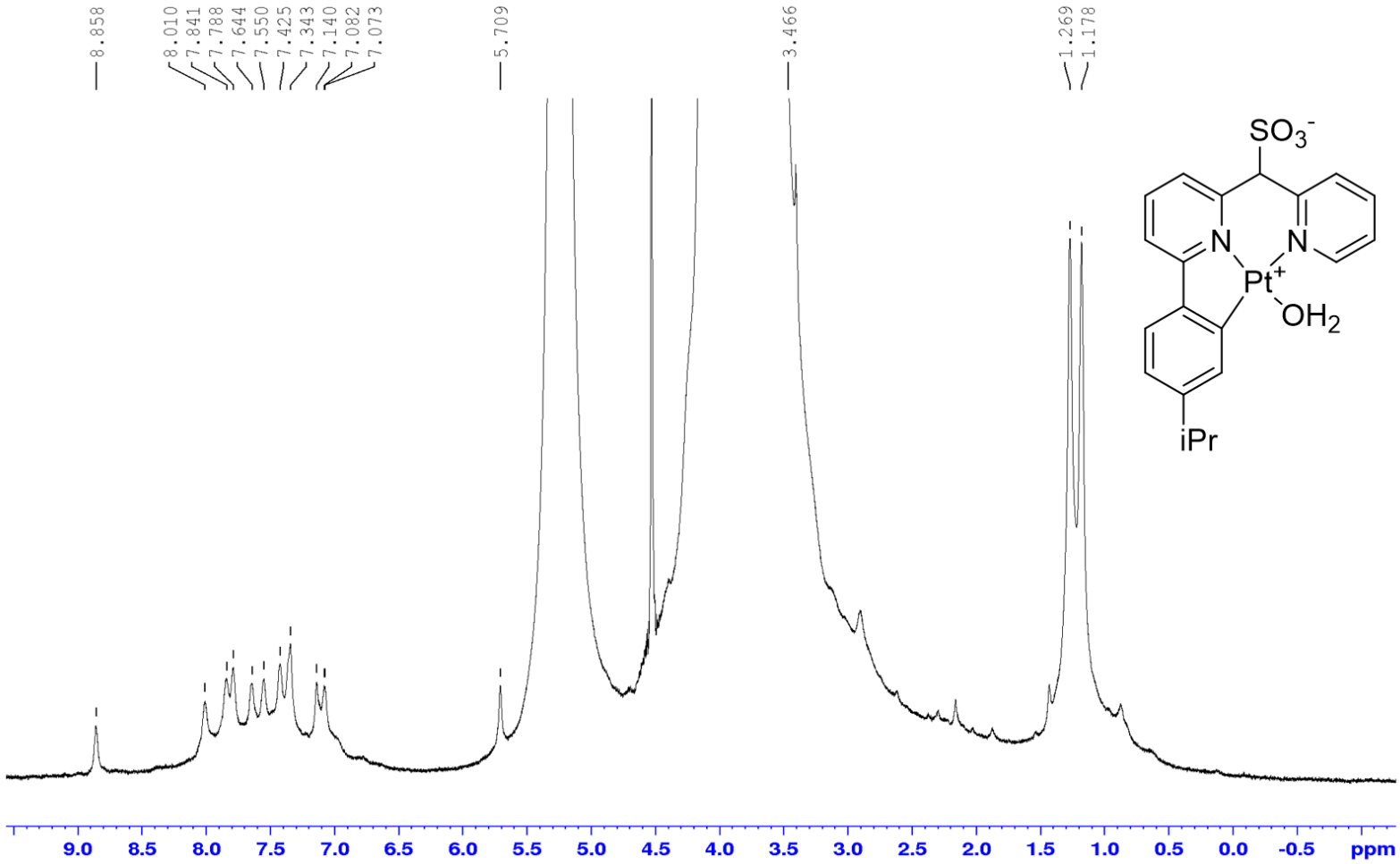

Figure S4.74. ^{1}H-NMR for **4.1-iPr** in TFE- d_1 (isopropyl septet buried under solvent signal)

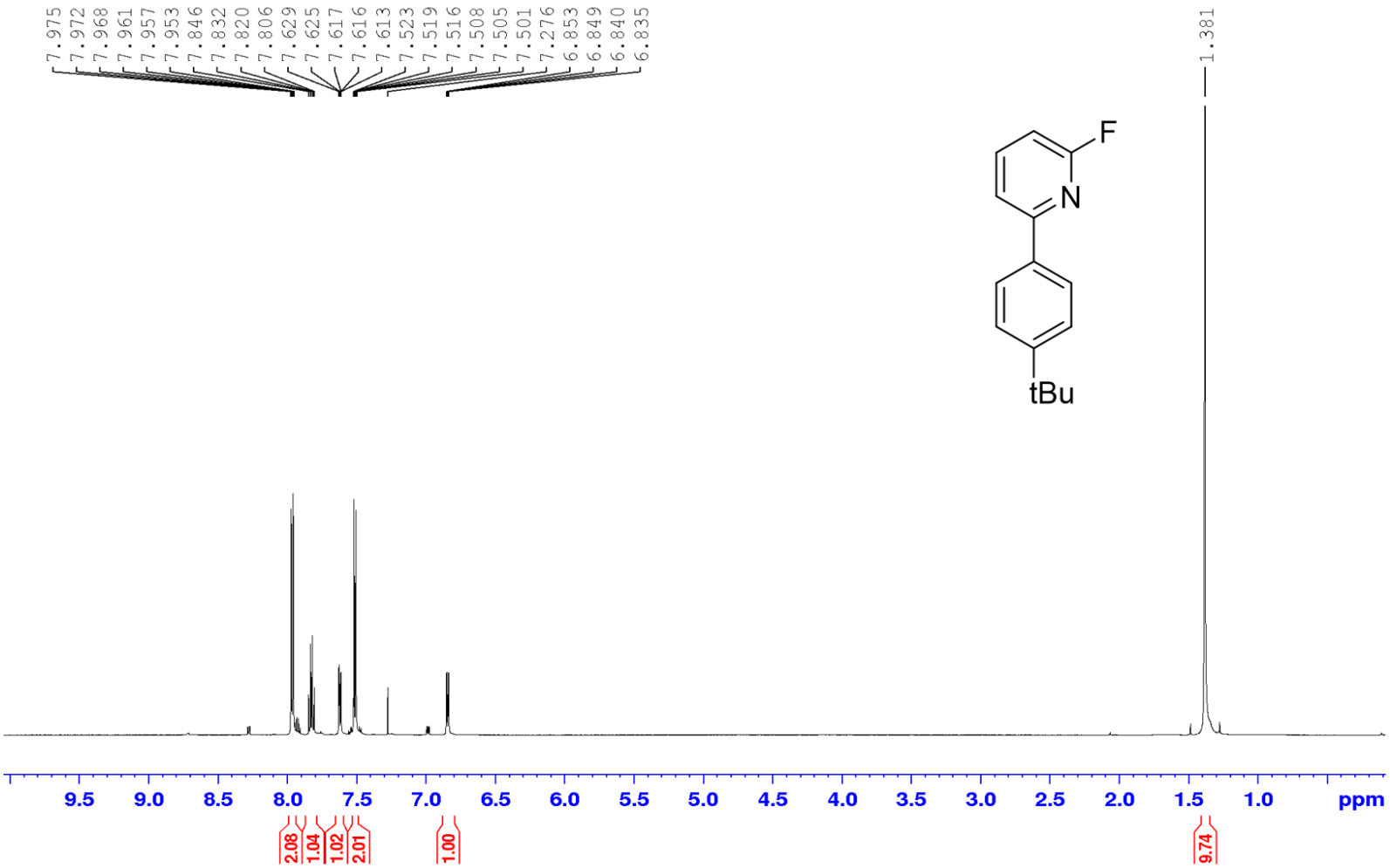

Figure S4.75. ^{1}H-NMR for 2-fluoro-6-(4-*tert*-butylphenyl) pyridine, **4.5-tBu** in $CDCl_3$

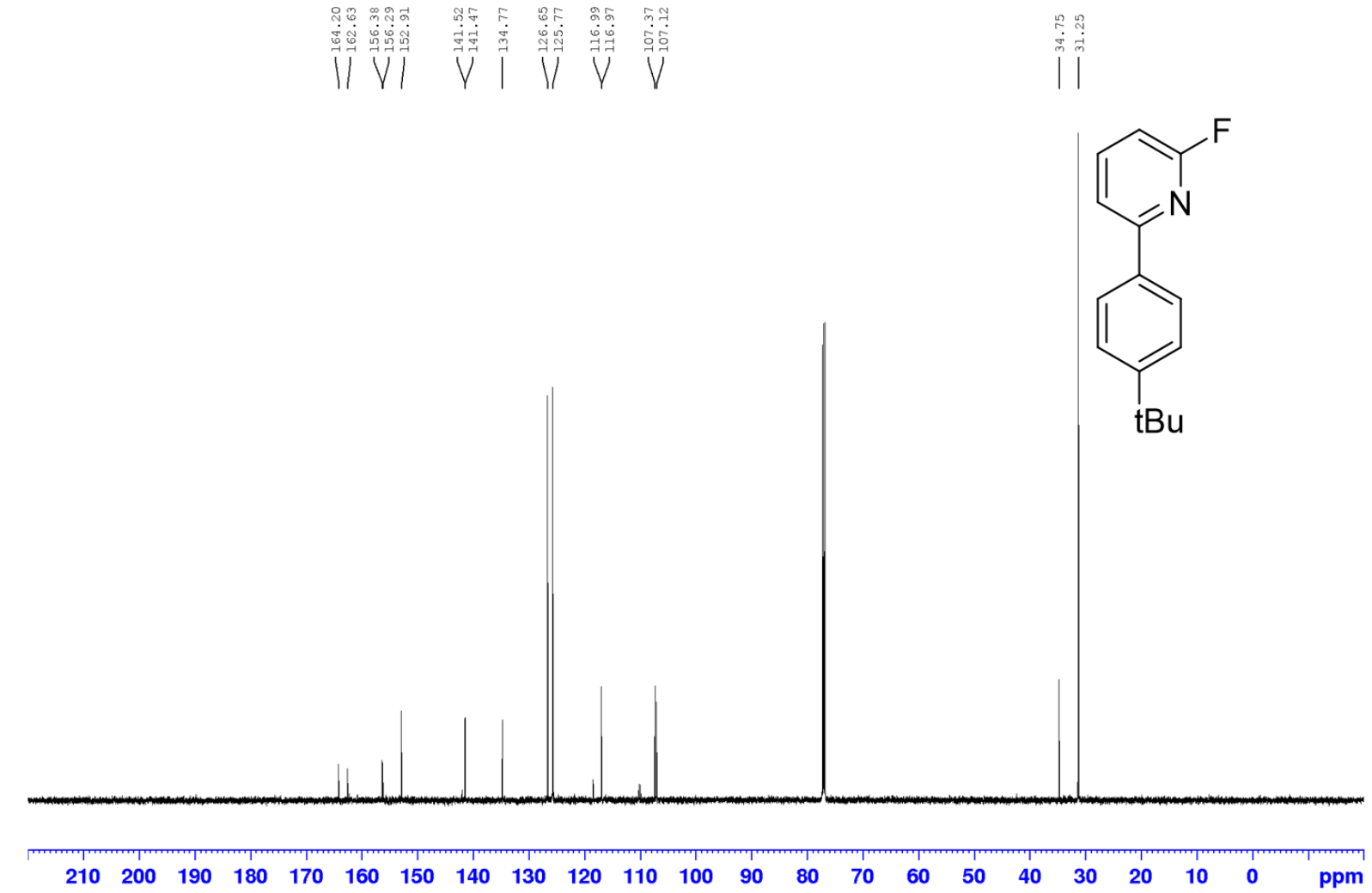

Figure S4.76. ^{13}C-NMR for 2-fluoro-6-(4-*tert*-butylphenyl) pyridine, **4.5-tBu** in $CDCl_3$

Figure S4.77. ^{19}F-NMR for 2-fluoro-6-(4-*tert*-butylphenyl) pyridine, **4.5-tBu** in $CDCl_3$

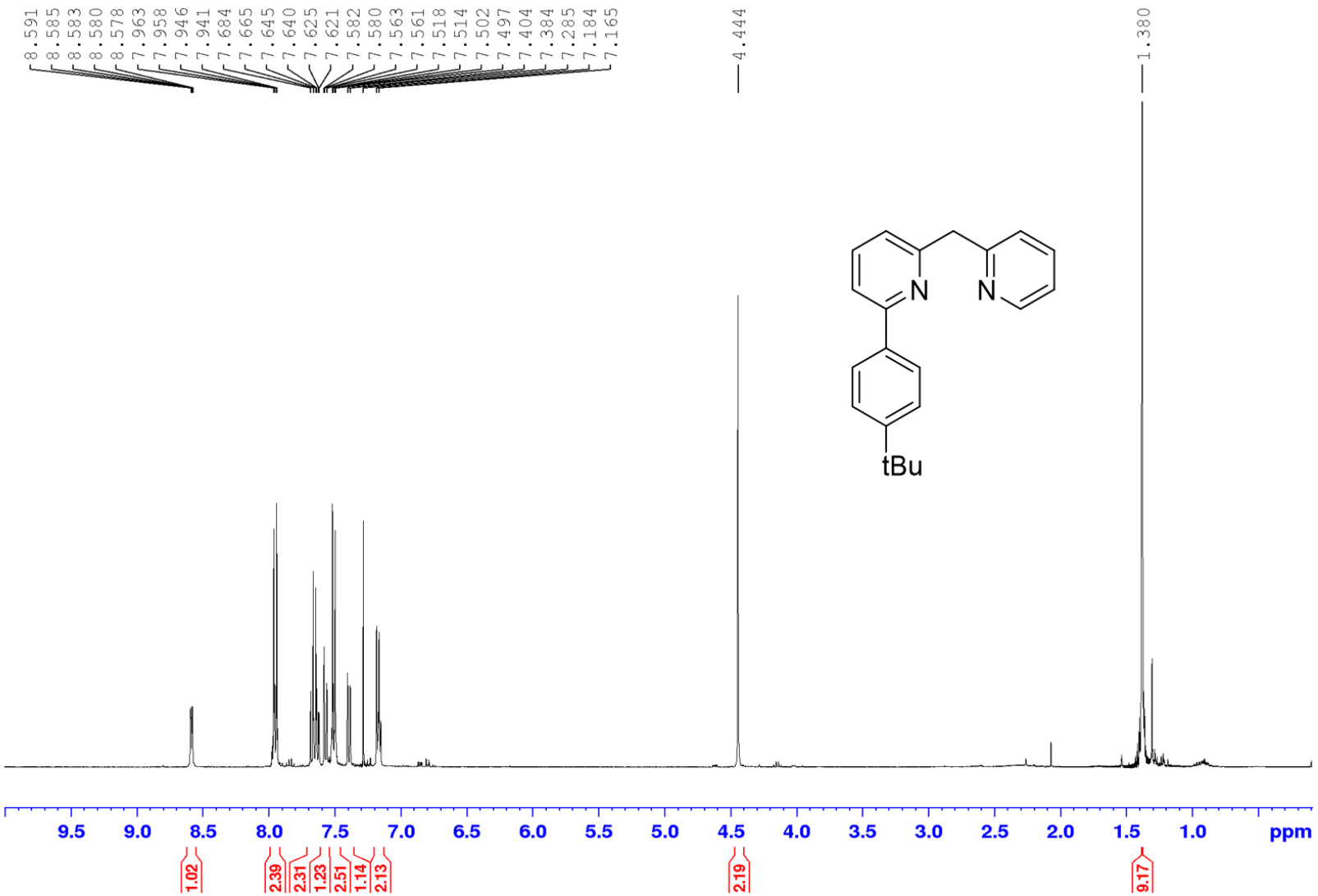

Figure S4.78. ^{1}H-NMR for 2-(4-*tert*-butylphenyl)-6-(pyridin-2-ylmethyl) pyridine, **4.6-tBu** in $CDCl_3$

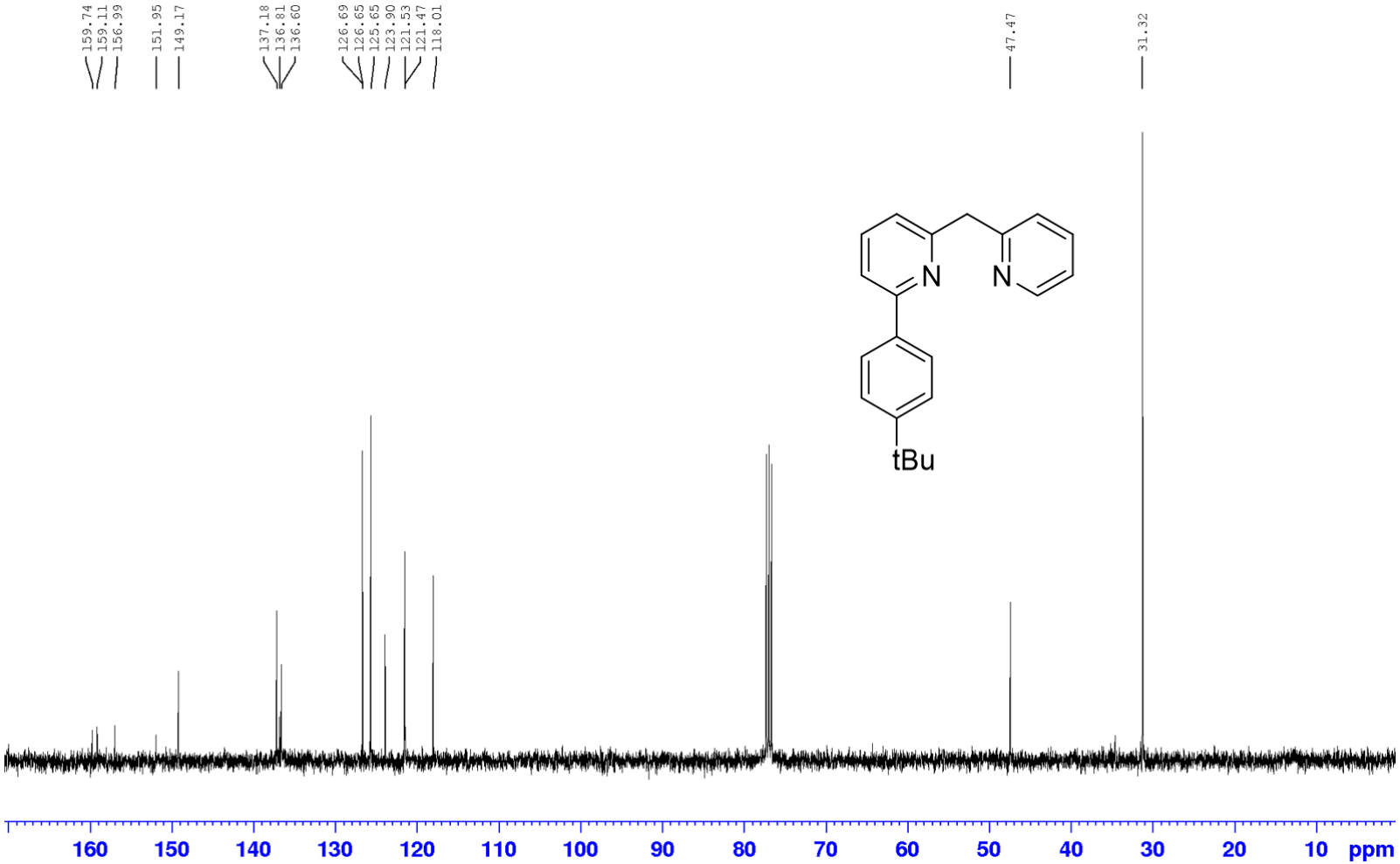

Figure S4.79. ^{13}C-NMR for 2-(4-*tert*-butylphenyl)-6-(pyridin-2-ylmethyl) pyridine, **4.6-tBu** in $CDCl_3$

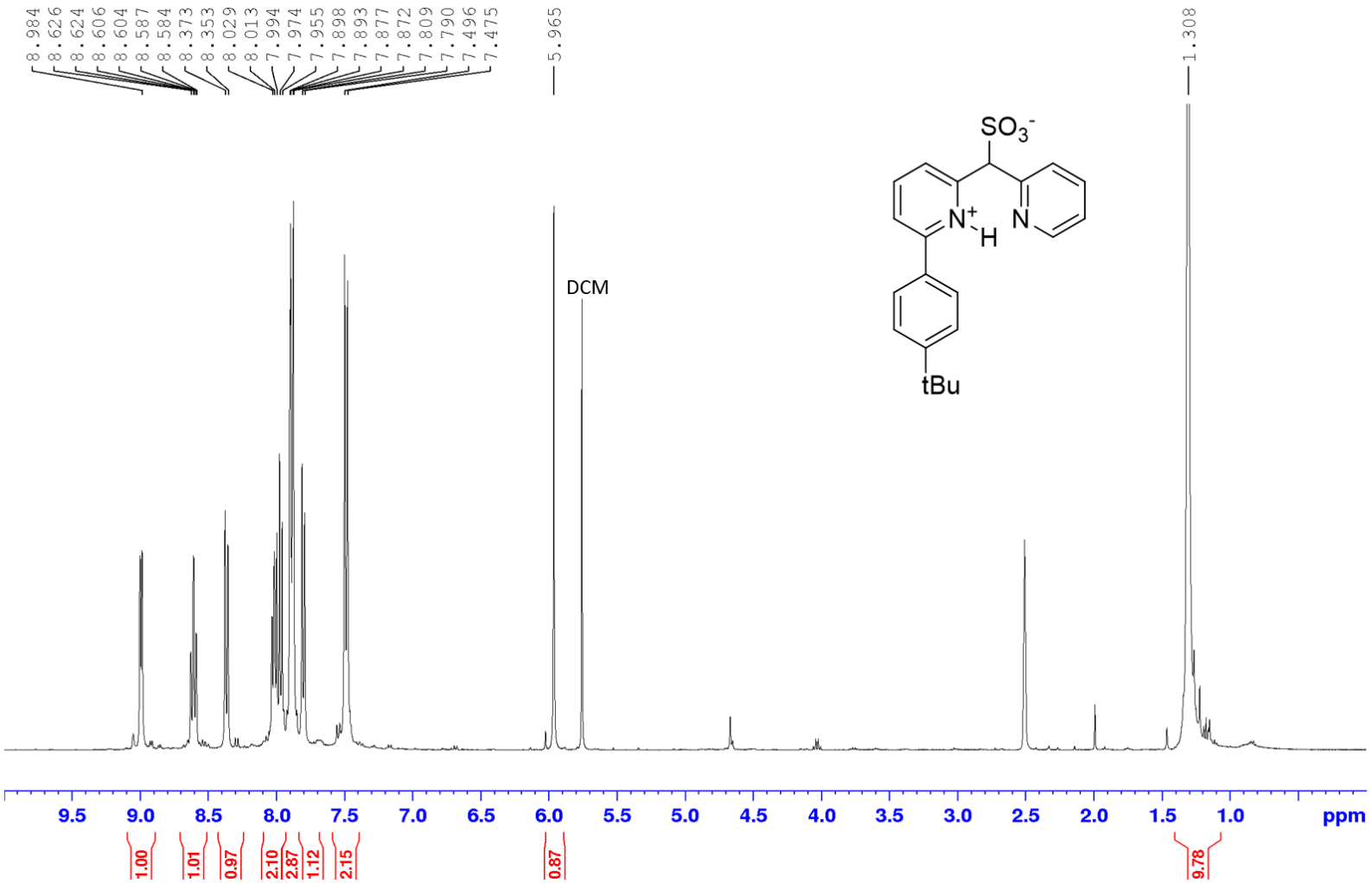

Figure S4.80. ^{1}H-NMR for 2-(4-*tert*-butylphenyl)-6-(pyridin-2-ylmethyl) pyridinium sulfonate, **4.7-tBu** in DMSO- d_6

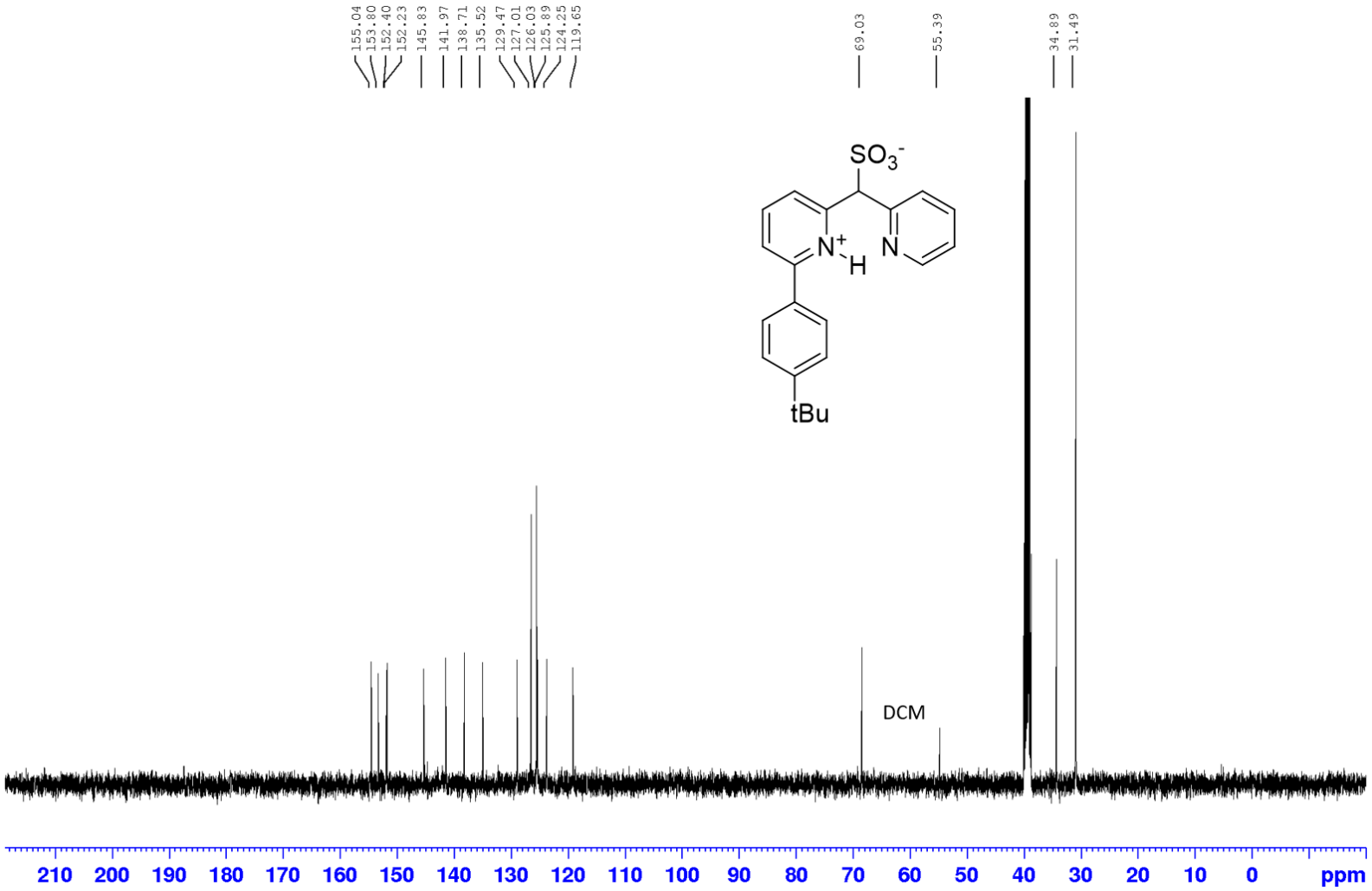

Figure S4.81. ^{13}C-NMR for 2-(4-*tert*-butylphenyl)-6-(pyridin-2-ylmethyl) pyridinium sulfonate, **4.7-tBu** in DMSO- d_6

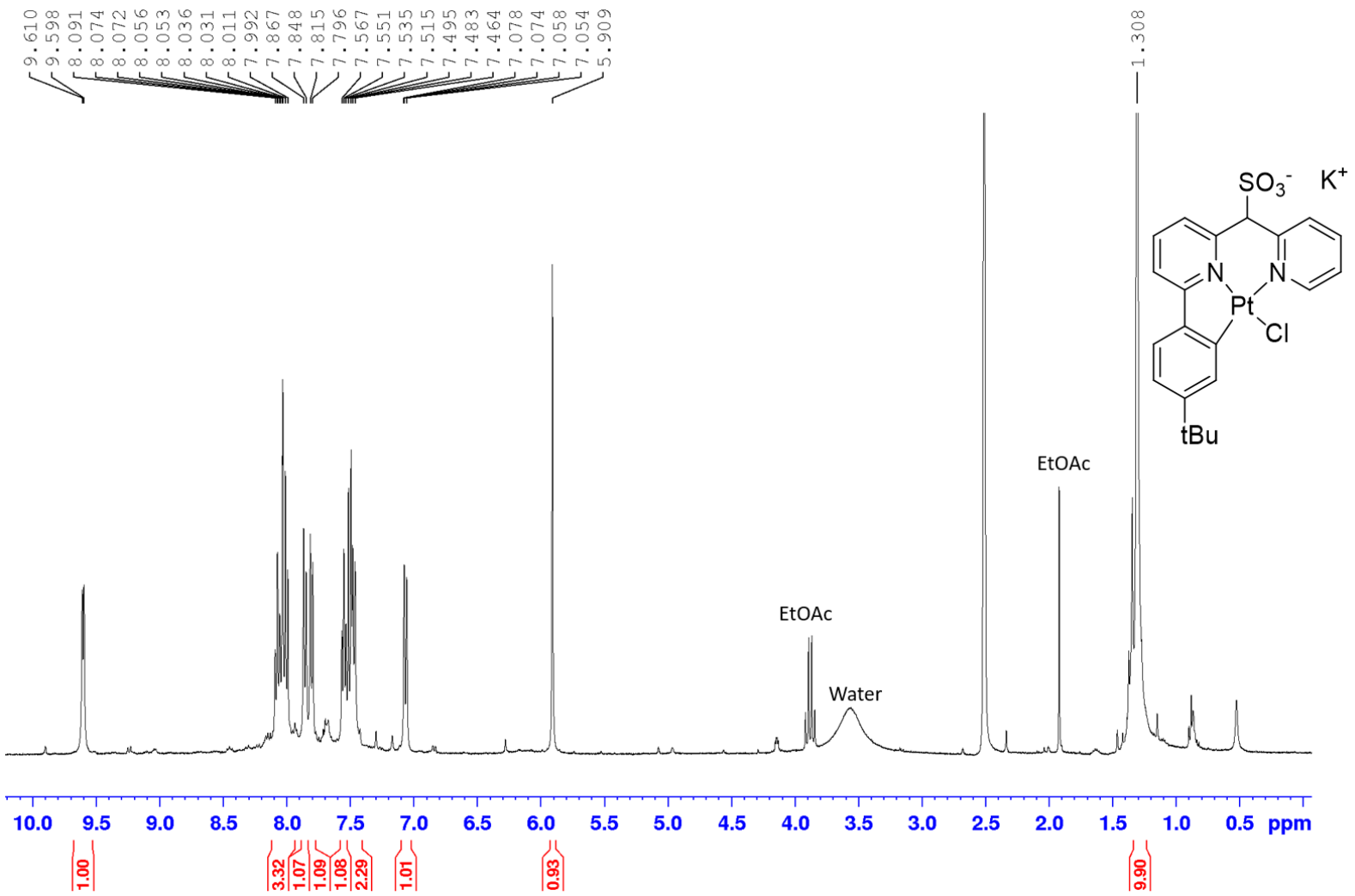

Figure S4.82. ^{1}H-NMR for 2-(4-*tert*-butylphenyl)-6-(pyridin-2-ylmethyl) pyridine Pt-Cl Complex, **4.8-tBu** in DMSO- d_6

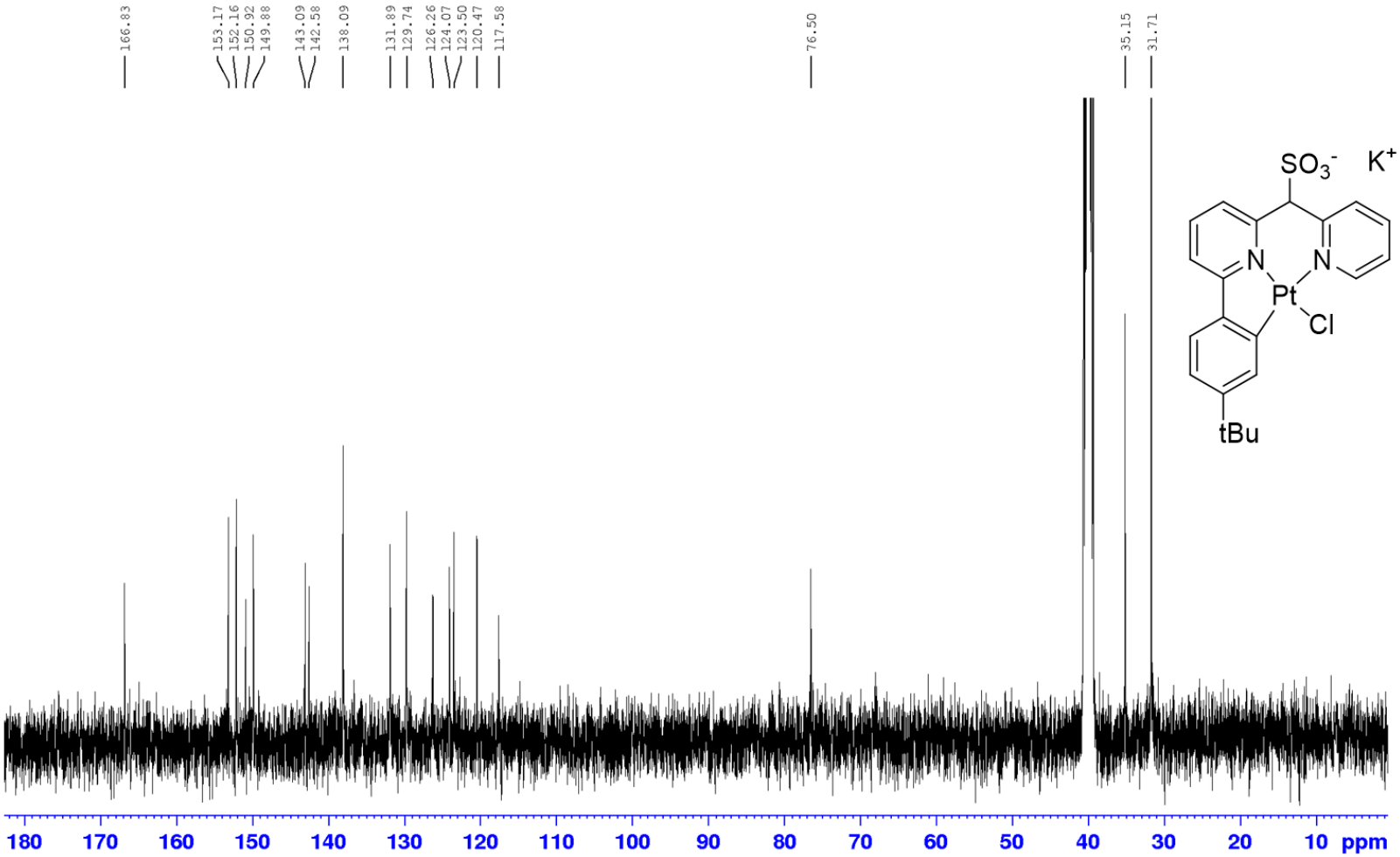

Figure S4.83. ^{13}C-NMR for 2-(4-*tert*-butylphenyl)-6-(pyridin-2-ylmethyl) pyridine Pt-Cl Complex, **4.8-tBu** in DMSO- d_6

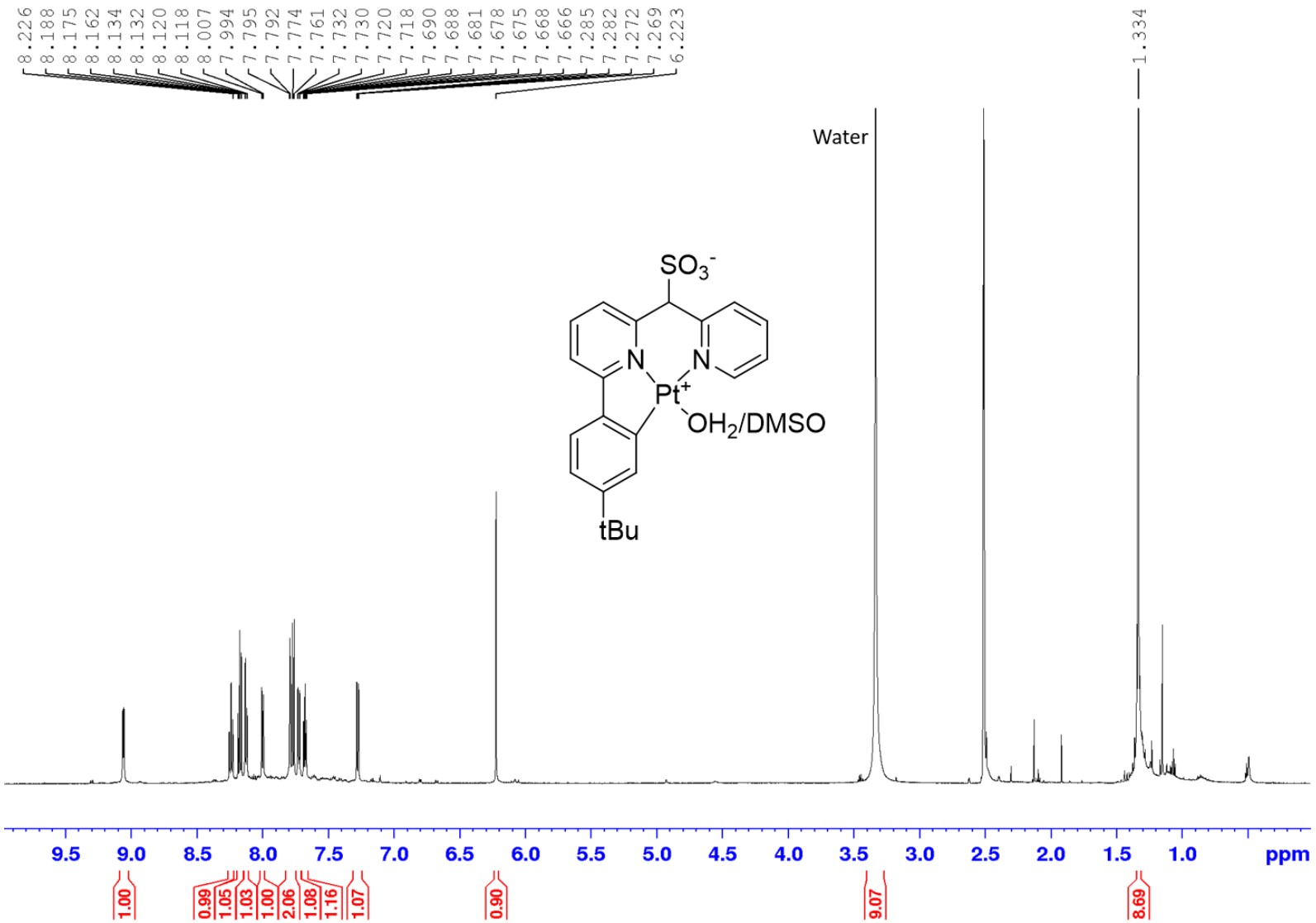

Figure S4.84. ^{1}H-NMR for **4.1-tBu** in DMSO- d_6

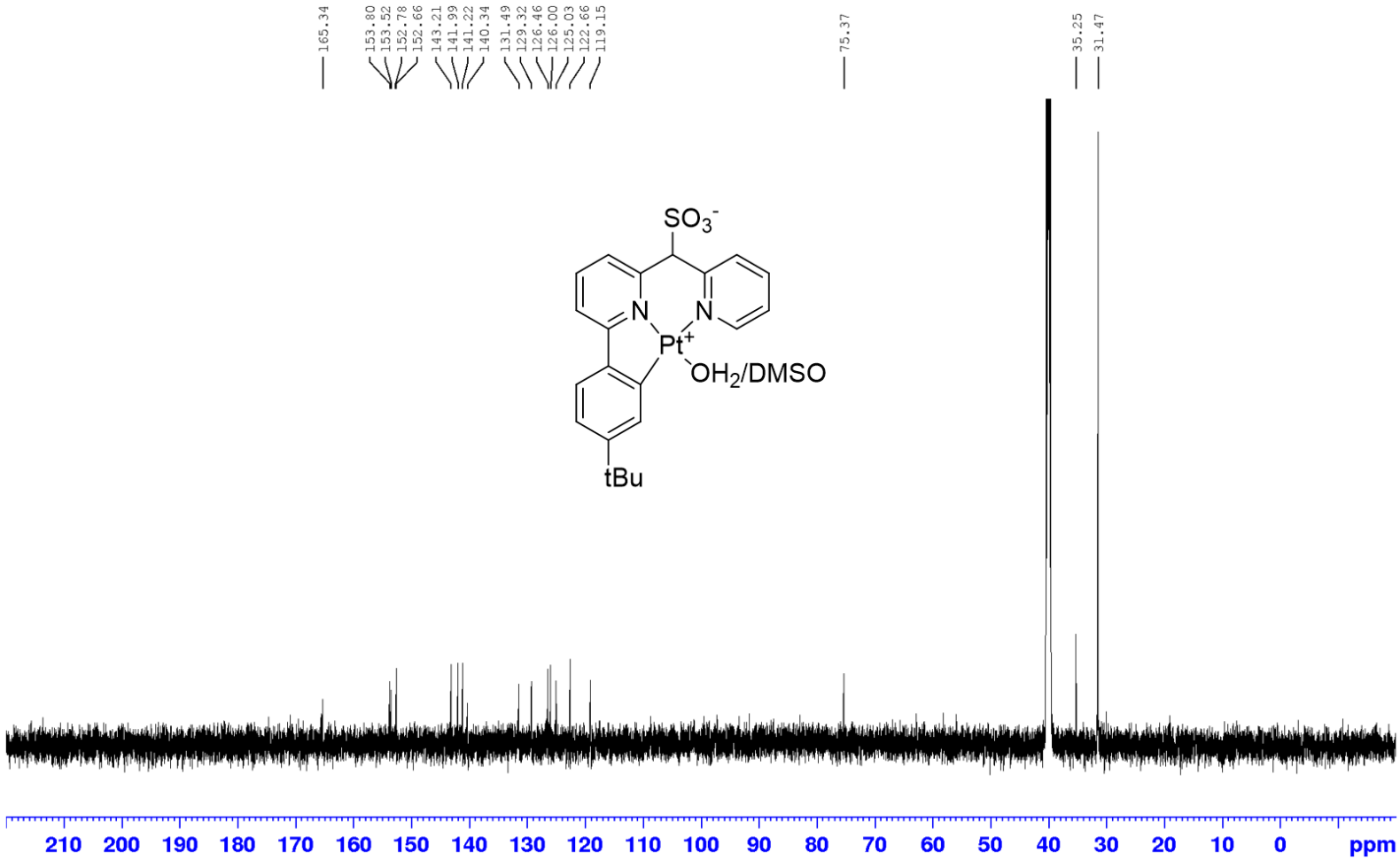

Figure S4.85. ^{13}C-NMR for **4.1-tBu** in DMSO- d_6

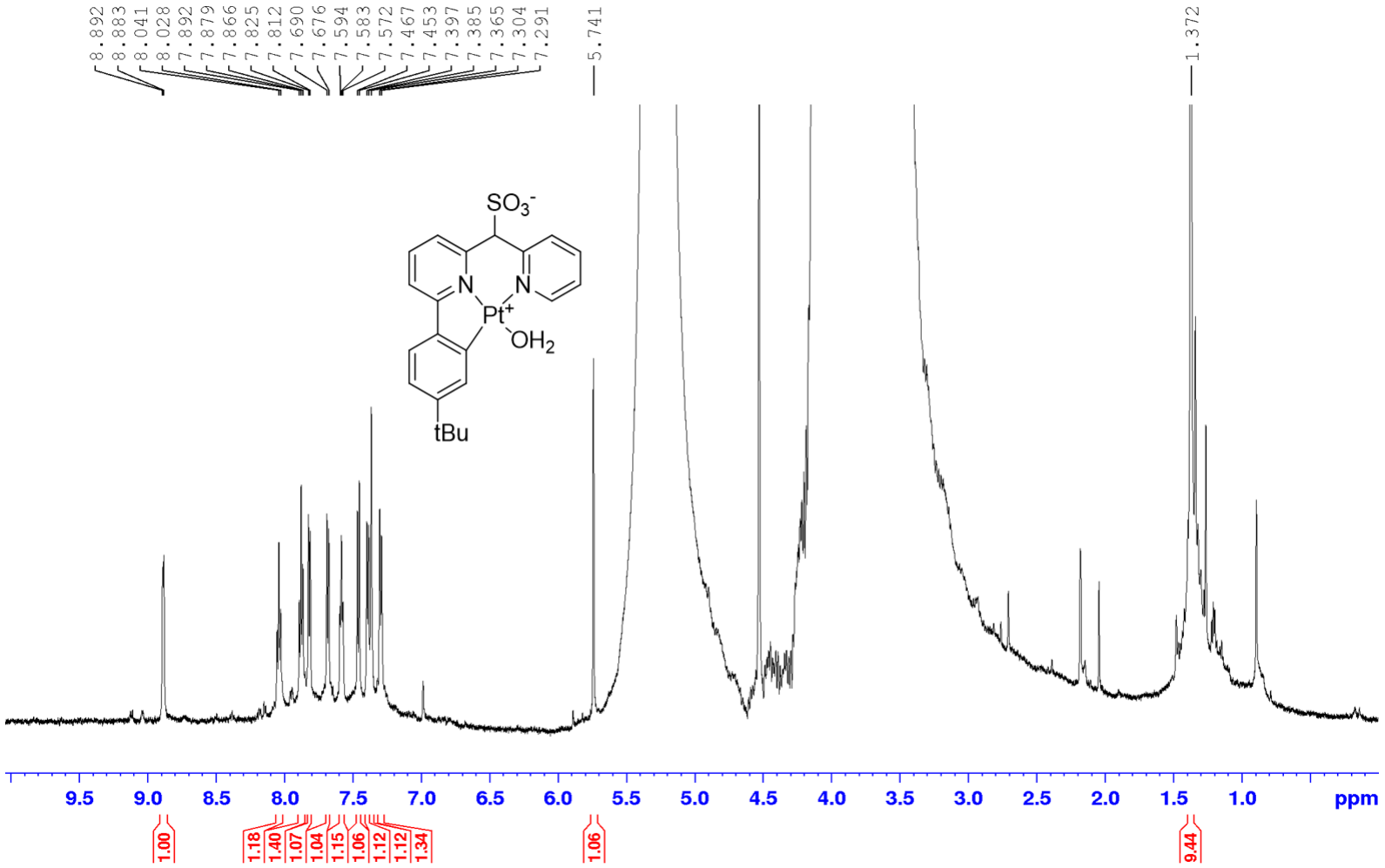

Figure S4.86. ^{1}H-NMR for **4.1-tBu** in TFE- d_1

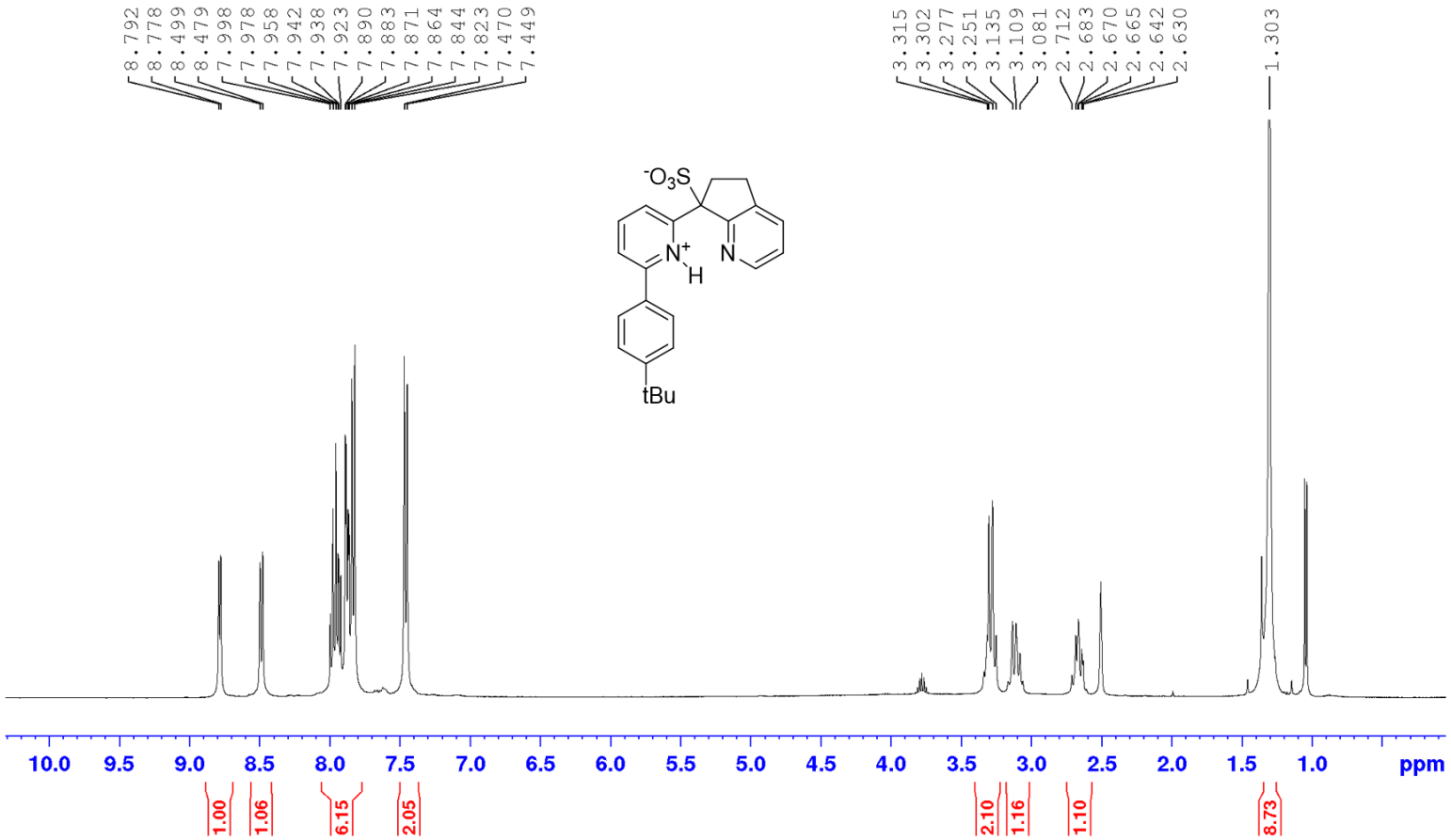

Figure S4.87. ^{1}H-NMR for **4.48-tBu** in DMSO-d_6

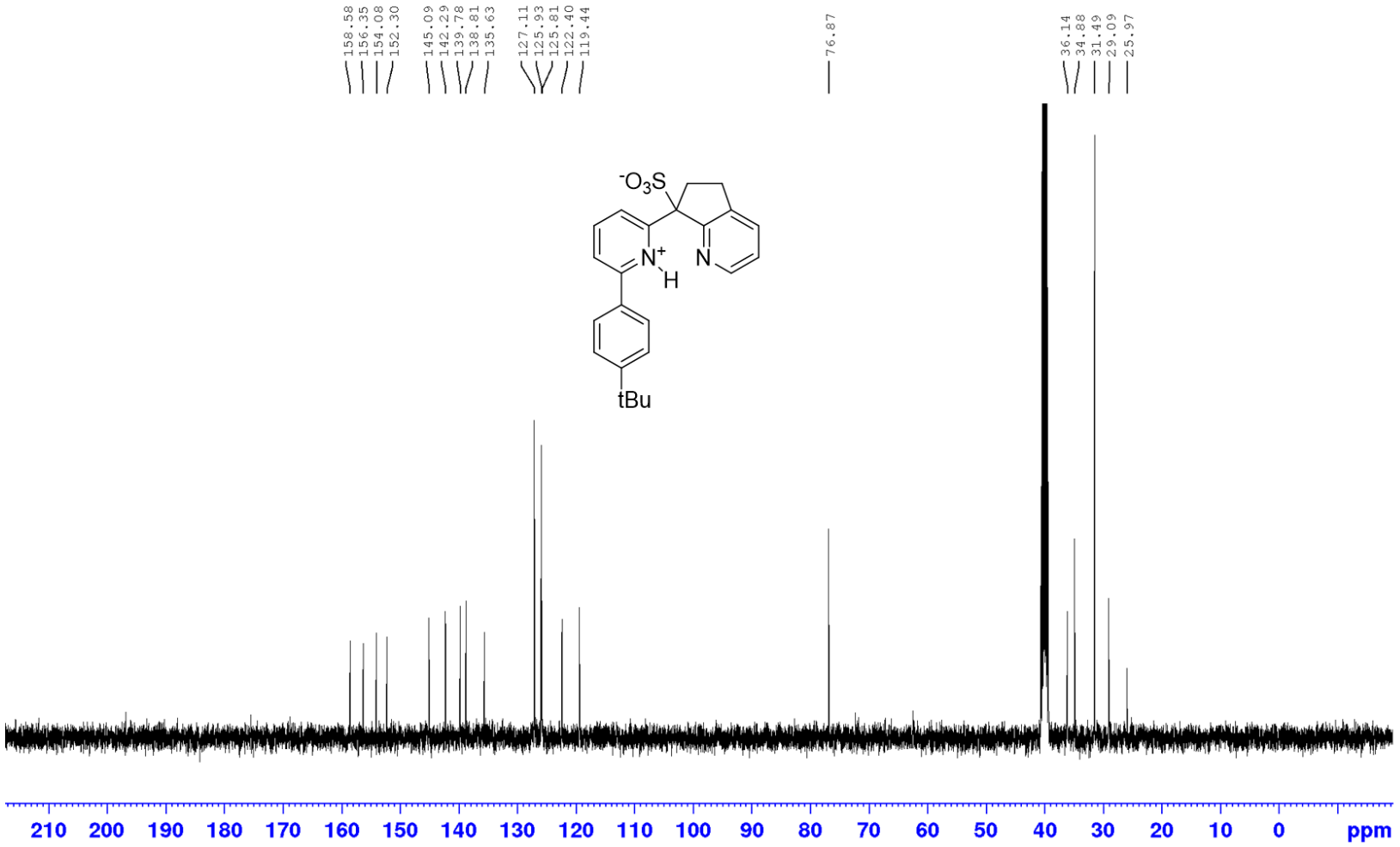

Figure S4.88. ^{13}C-NMR for **4.48-tBu** in DMSO-d_6

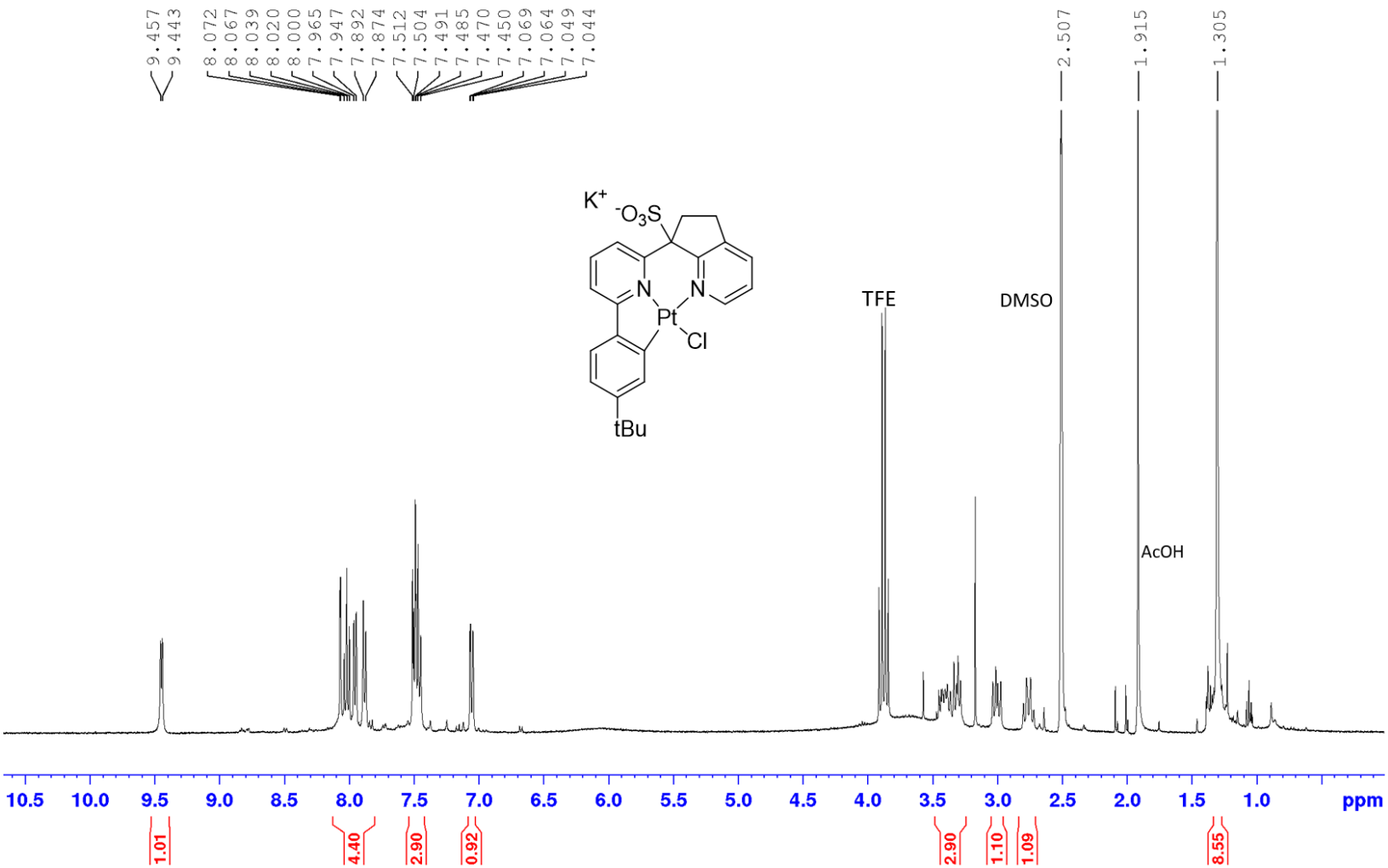

Figure S4.89. ^{1}H-NMR for **4.49-tBu** in DMSO-d_6

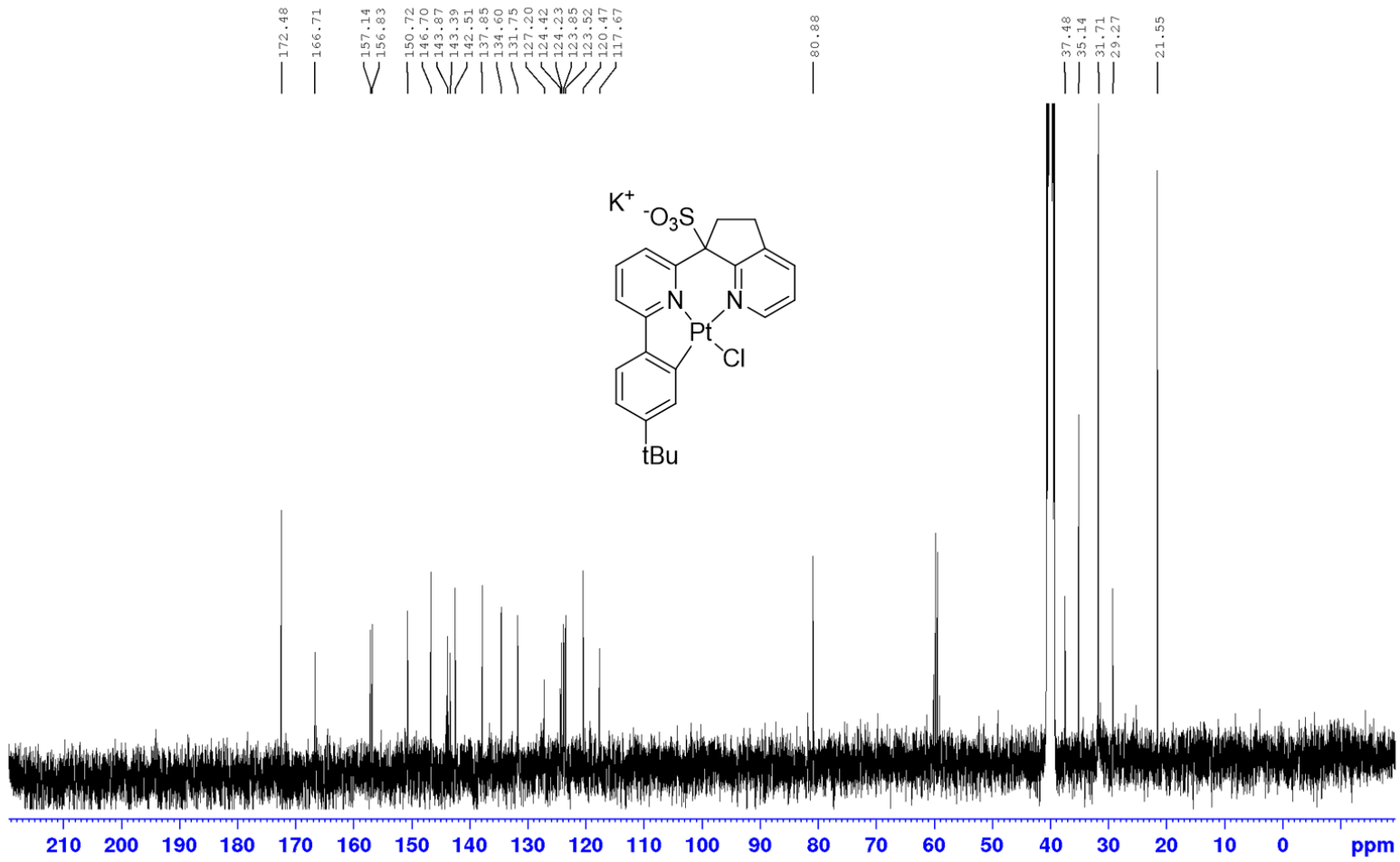

Figure S4.89. ^{13}C-NMR for **4.49-tBu** in DMSO-d_6

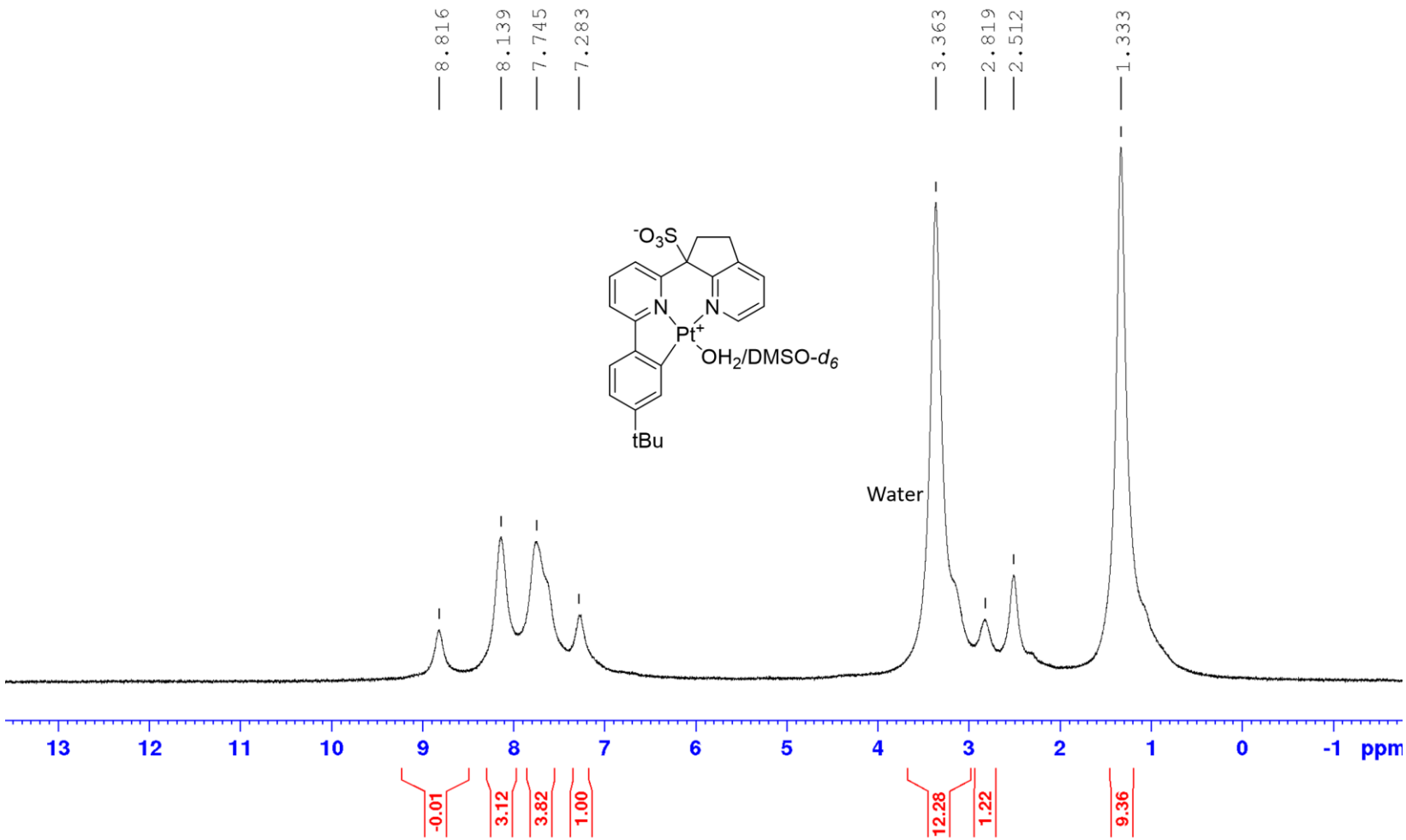

Figure S4.90. ^{1}H-NMR for **4.50-tBu** in DMSO-d_6

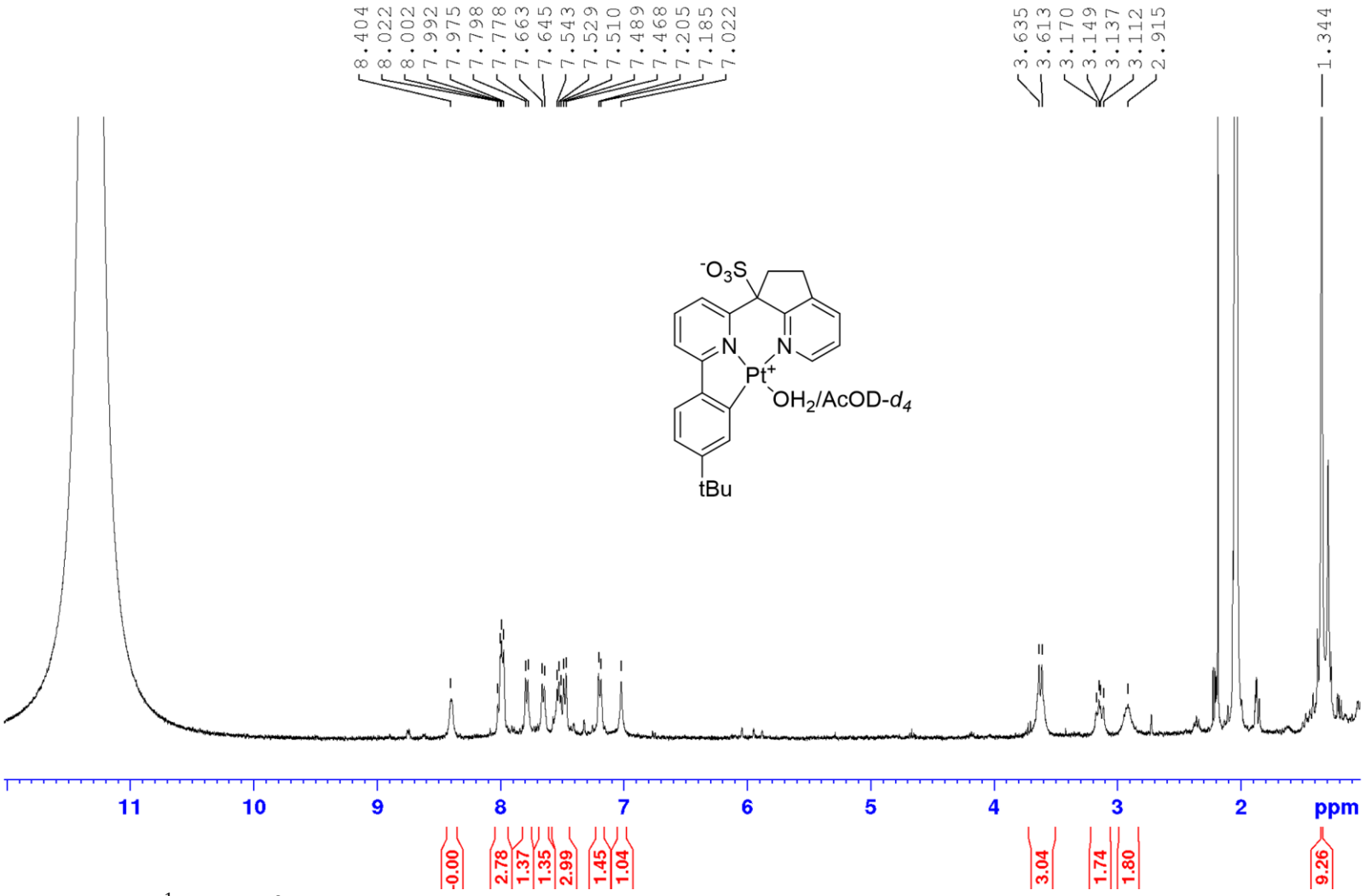

Figure S4.91. ^{1}H-NMR for **4.50-tBu** in AcOD-*d*$_4$

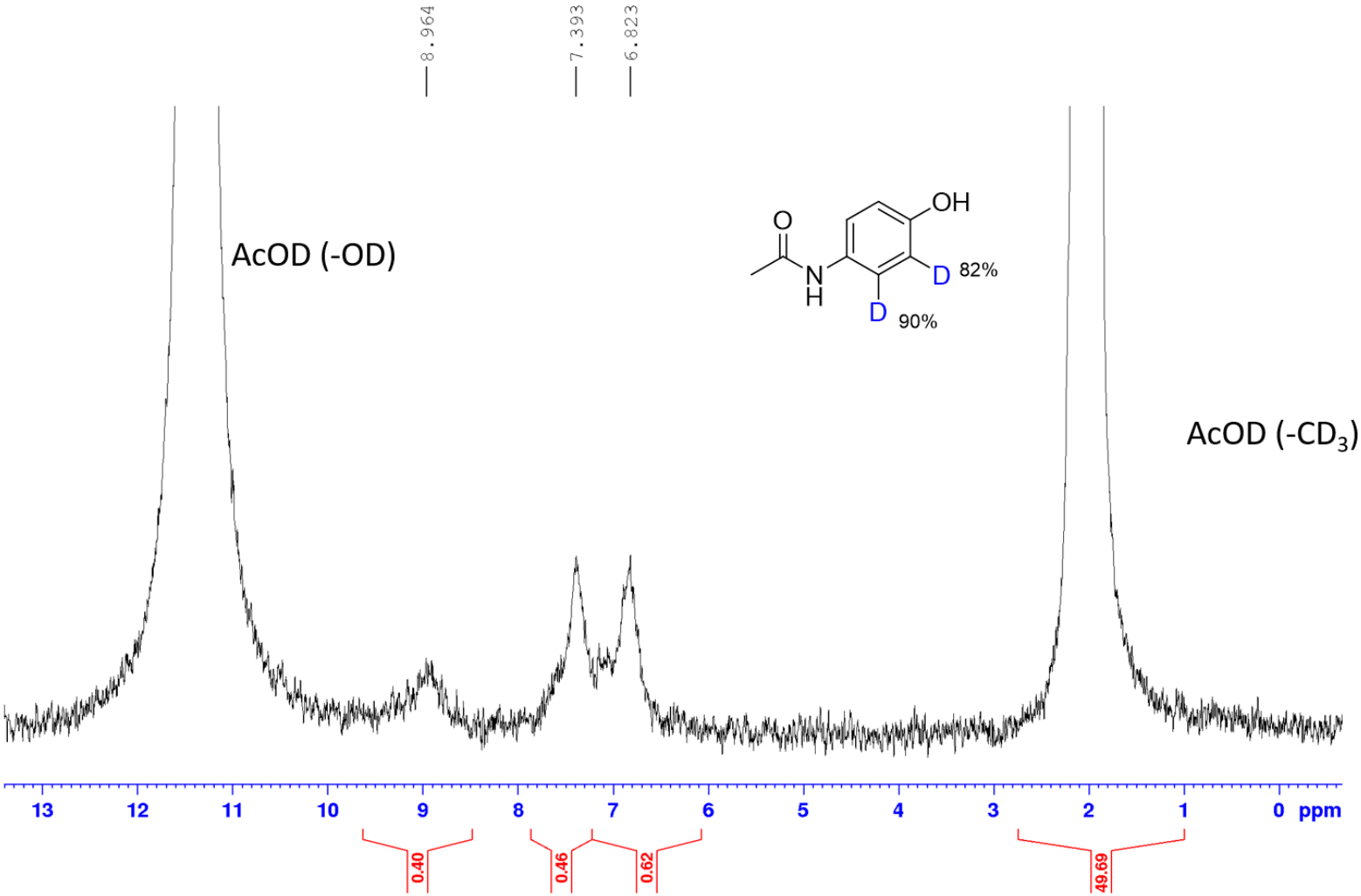

Figure S4.92. ^{2}H-NMR for the H/D Exchange reaction of Acetaminophen in AcOD-*d*$_4$ catalyzed by **4.1-tBu**

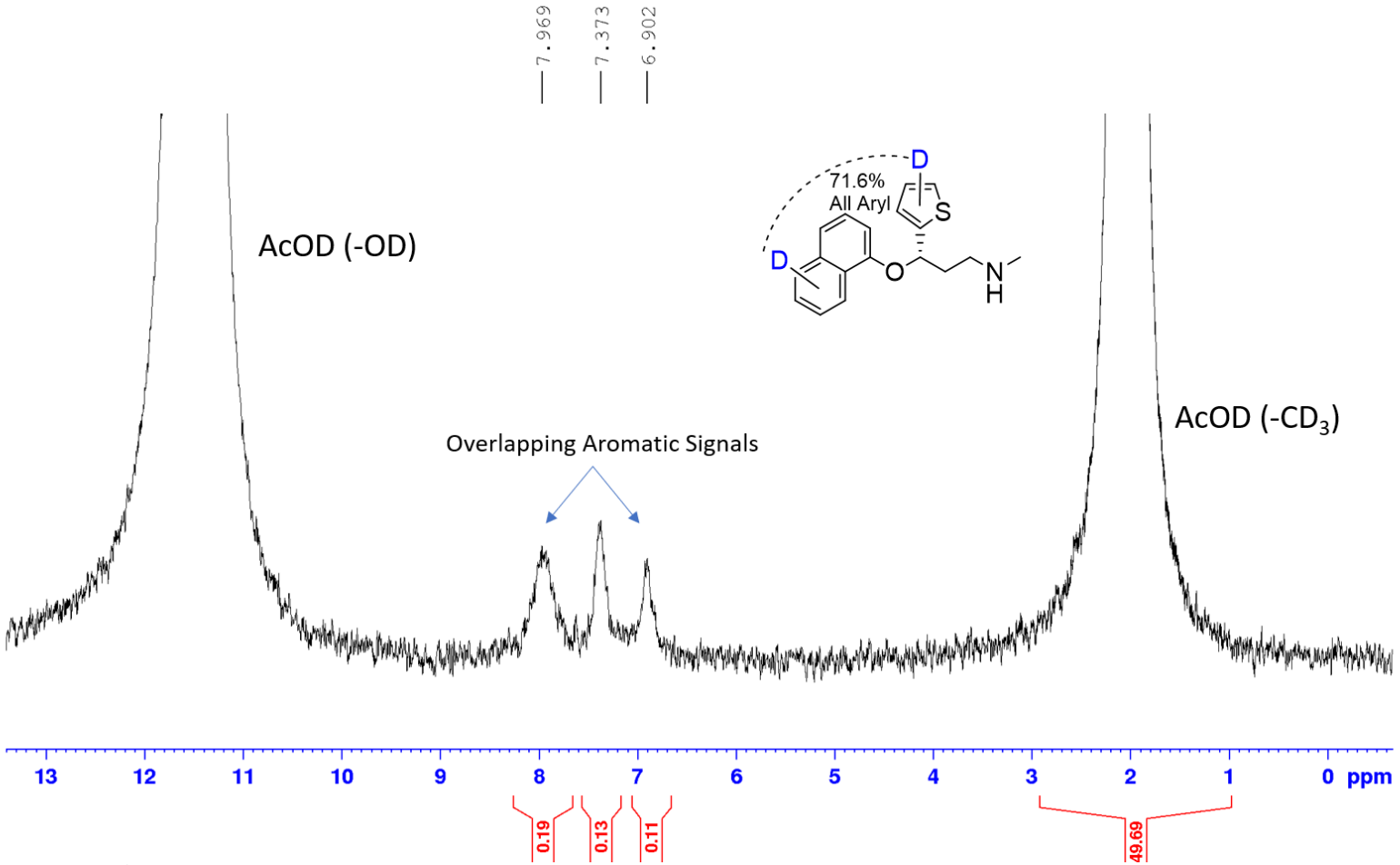

Figure S4.93. ^{2}H-NMR for the H/D Exchange reaction of Duloxetine in AcOD-d_4 catalyzed by **4.1-tBu**

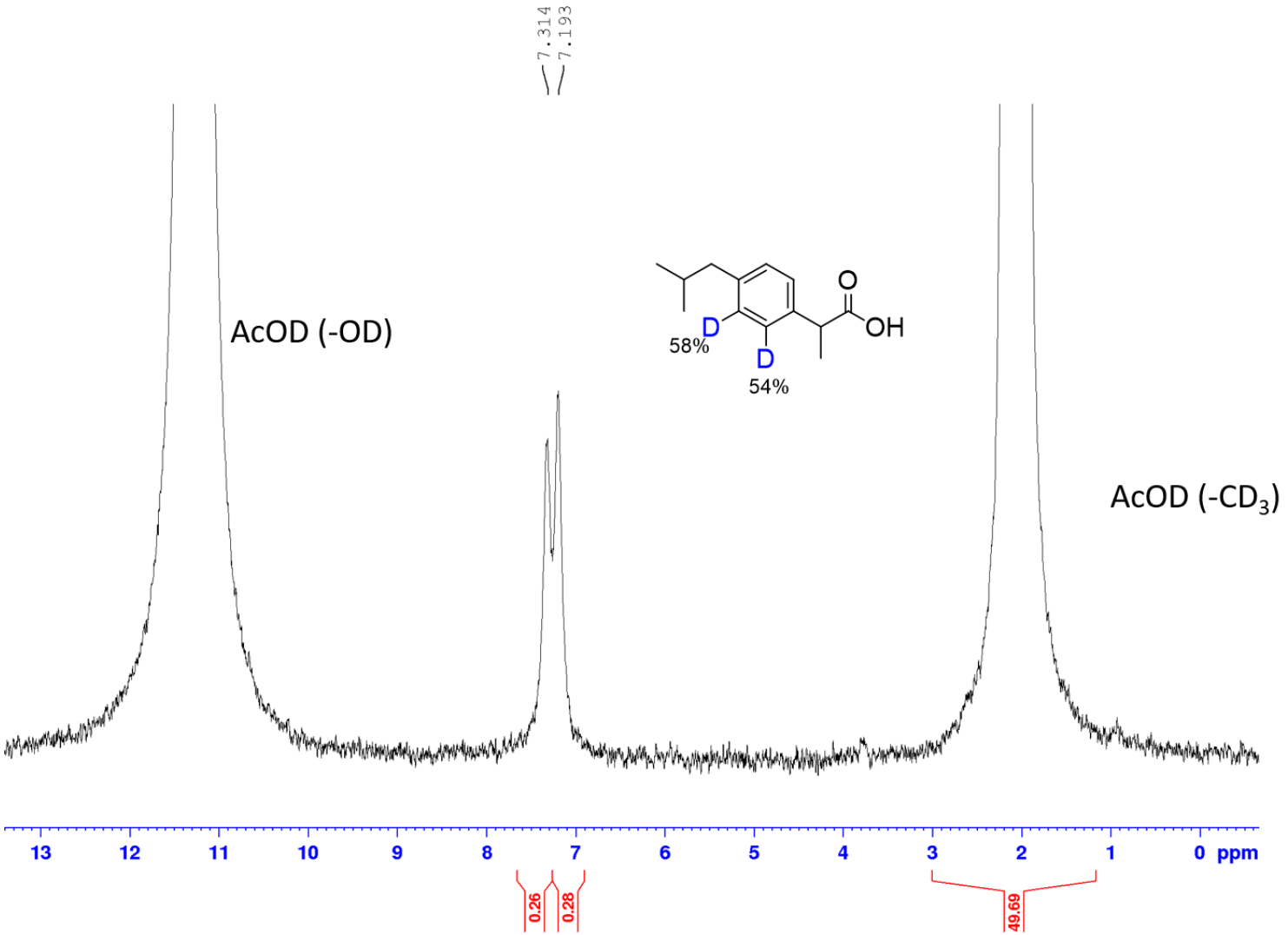

Figure S4.94. ^{2}H-NMR for the H/D Exchange reaction of Ibuprofen in AcOD-*d*$_4$ catalyzed by **4.1-tBu**

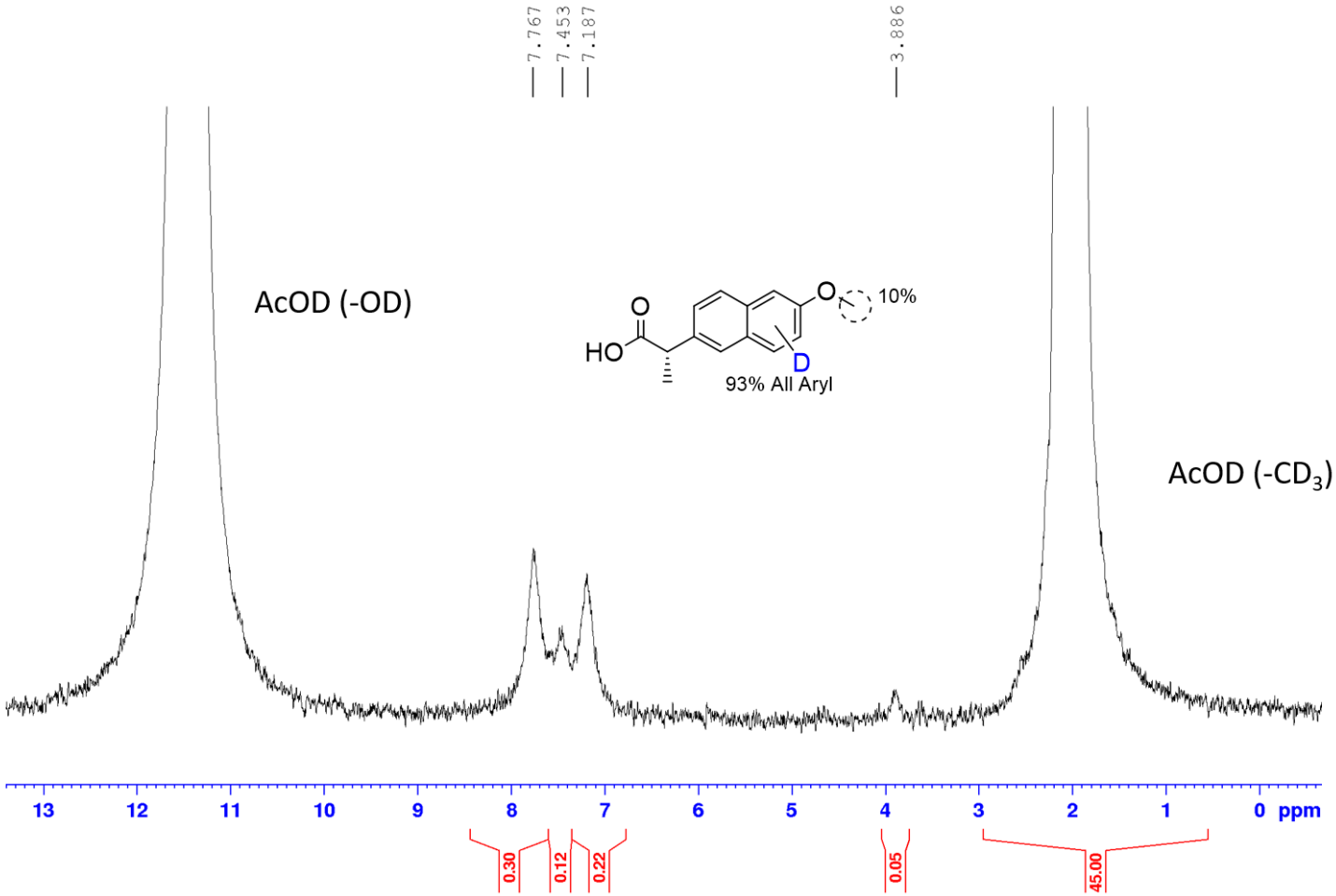

Figure S4.95. ^{2}H-NMR for the H/D Exchange reaction of Ibuprofen in AcOD-*d*$_4$ catalyzed by **4.1-tBu**

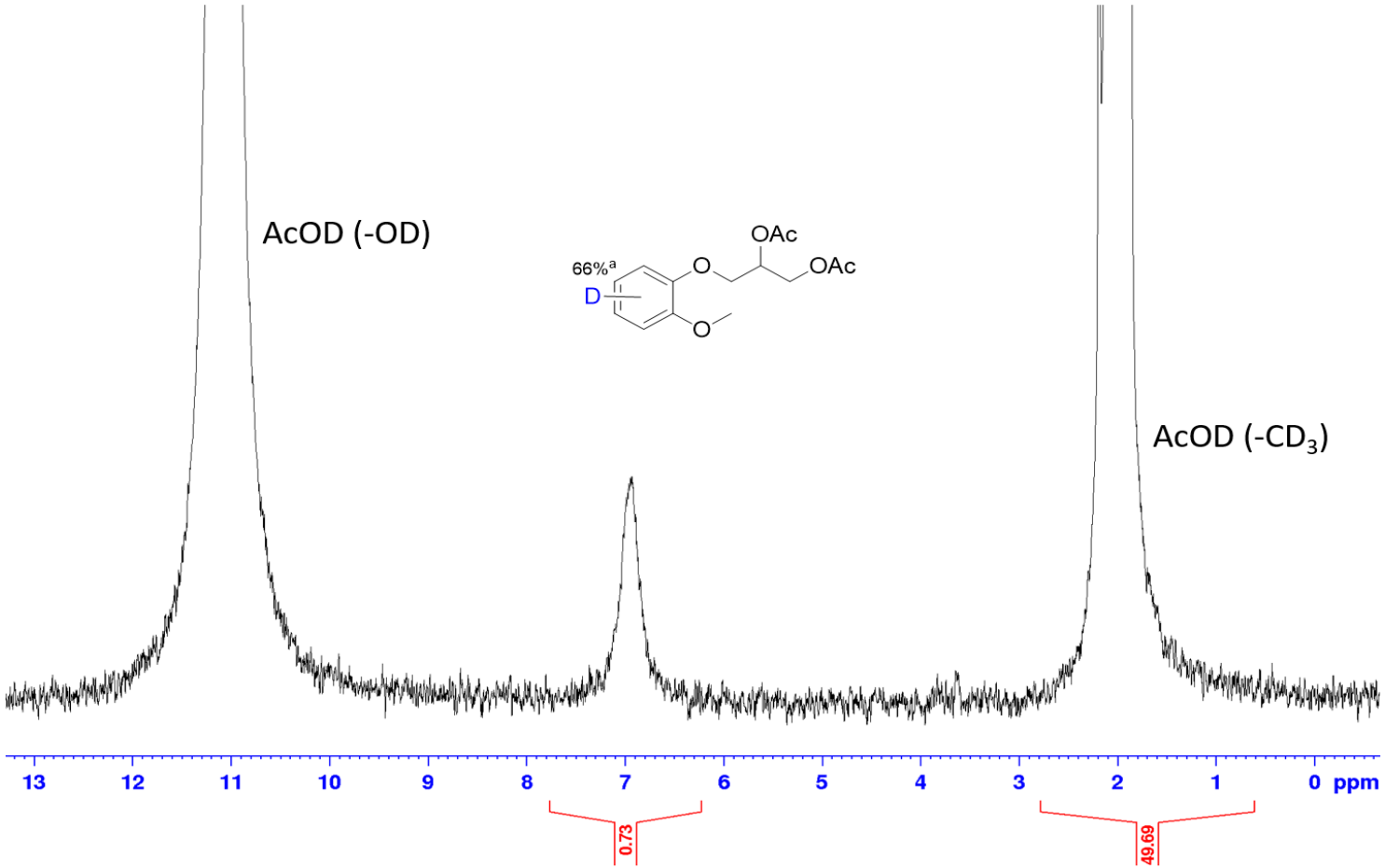

Figure S4.96. ^{2}H-NMR for the H/D Exchange reaction of Guaifenesin derivative in AcOD-*d*$_4$ catalyzed by **4.1-tBu**

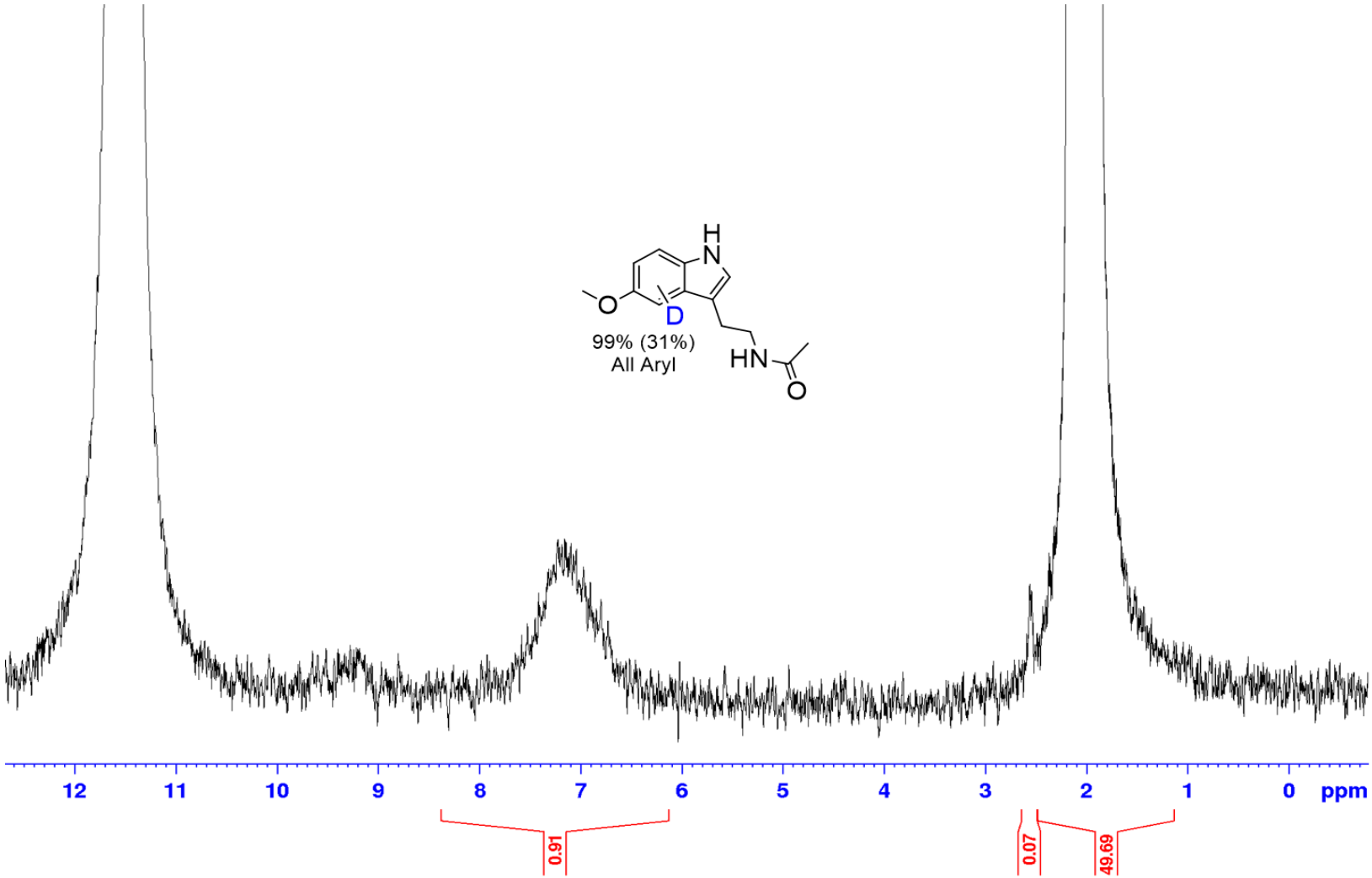

Figure S4.97. ^{2}H-NMR for the H/D Exchange reaction of Melatonin in AcOD-d_4 catalyzed by **4.1-tBu**

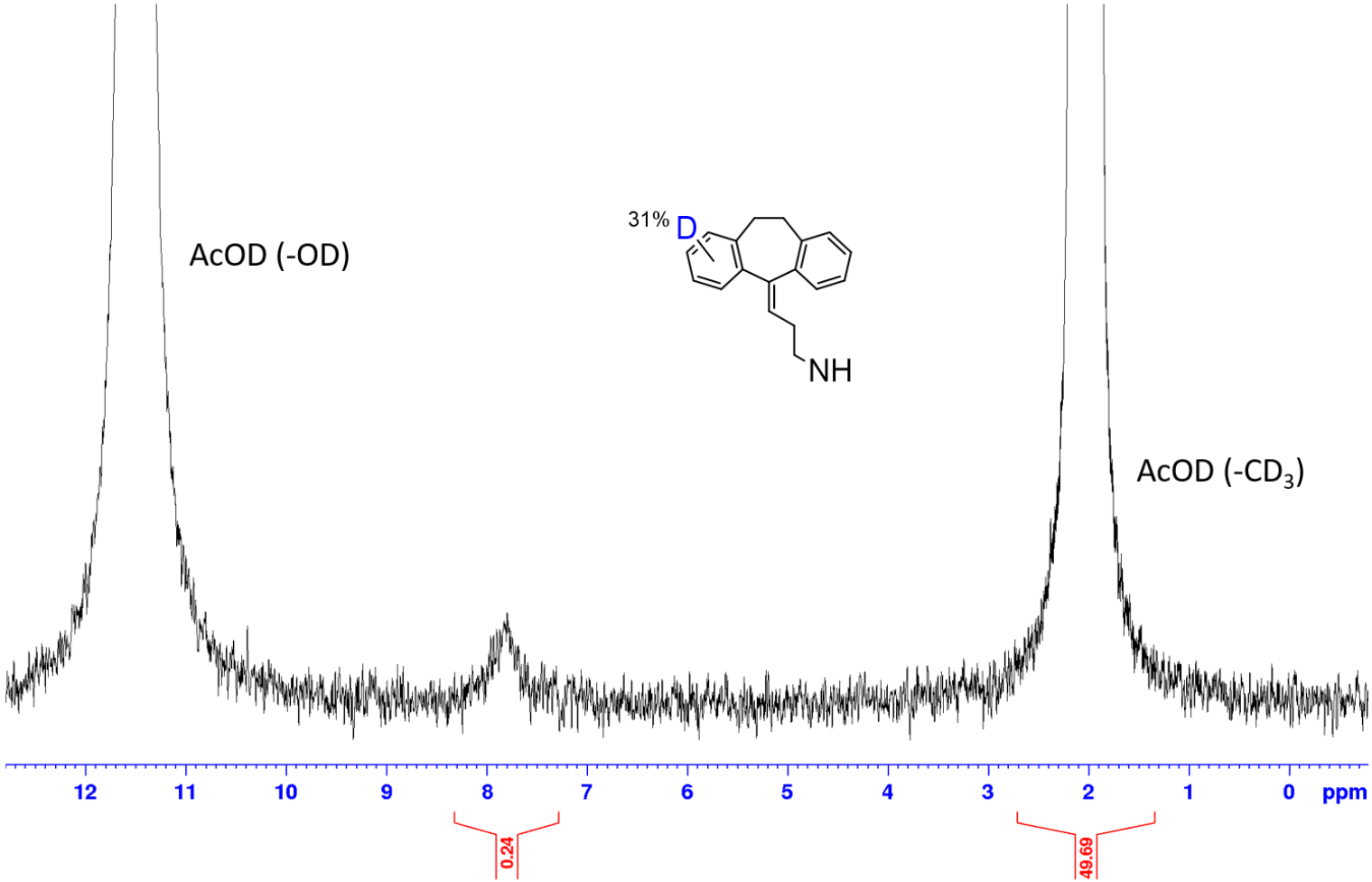

Figure S4.98. ^{2}H-NMR for the H/D Exchange reaction of Amitriptyline in AcOD-d_4 catalyzed by **4.1-tBu**

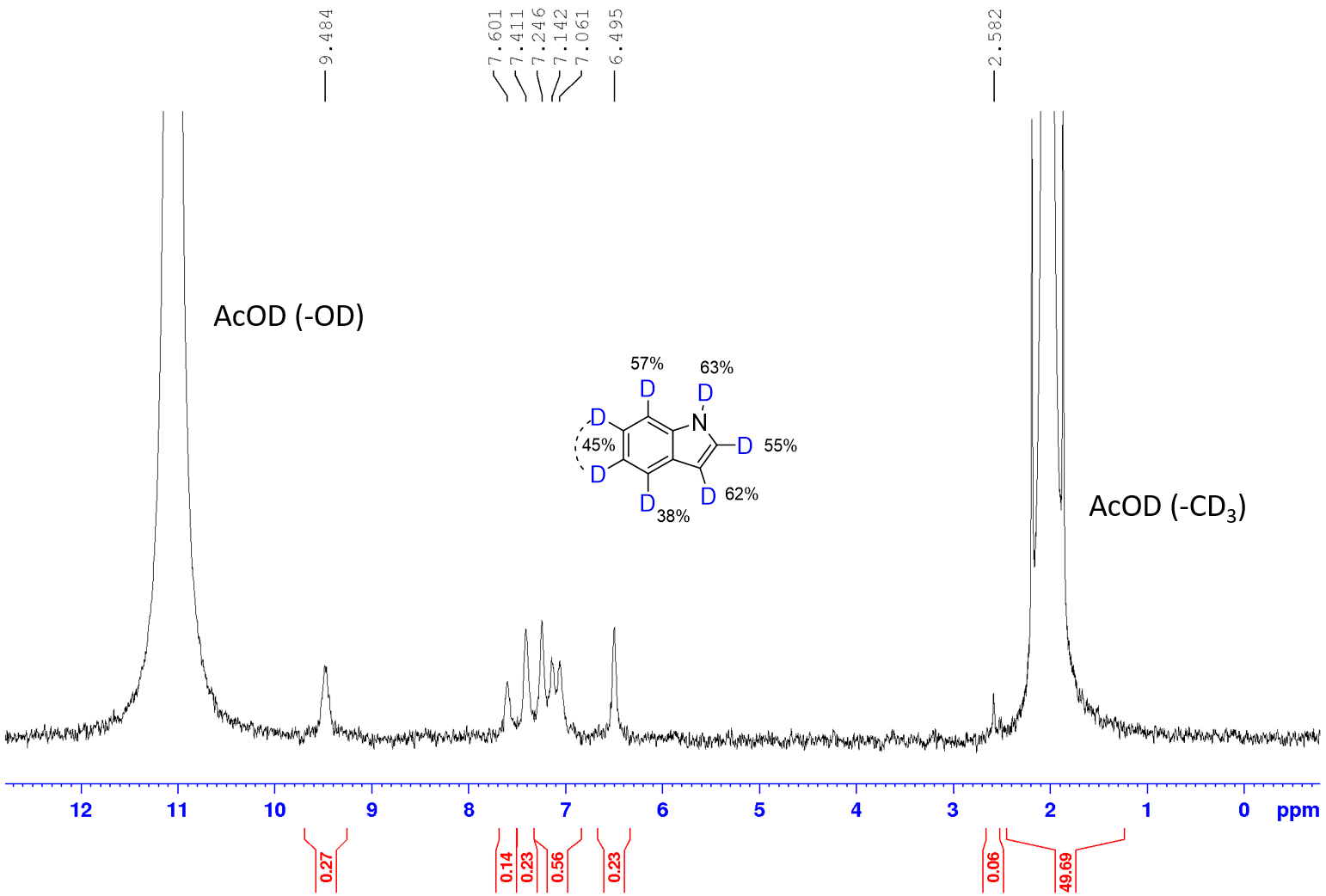

Figure S4.99. ^{2}H-NMR for the H/D Exchange reaction of indole in AcOD-*d*$_4$ catalyzed by **4.1-tBu**

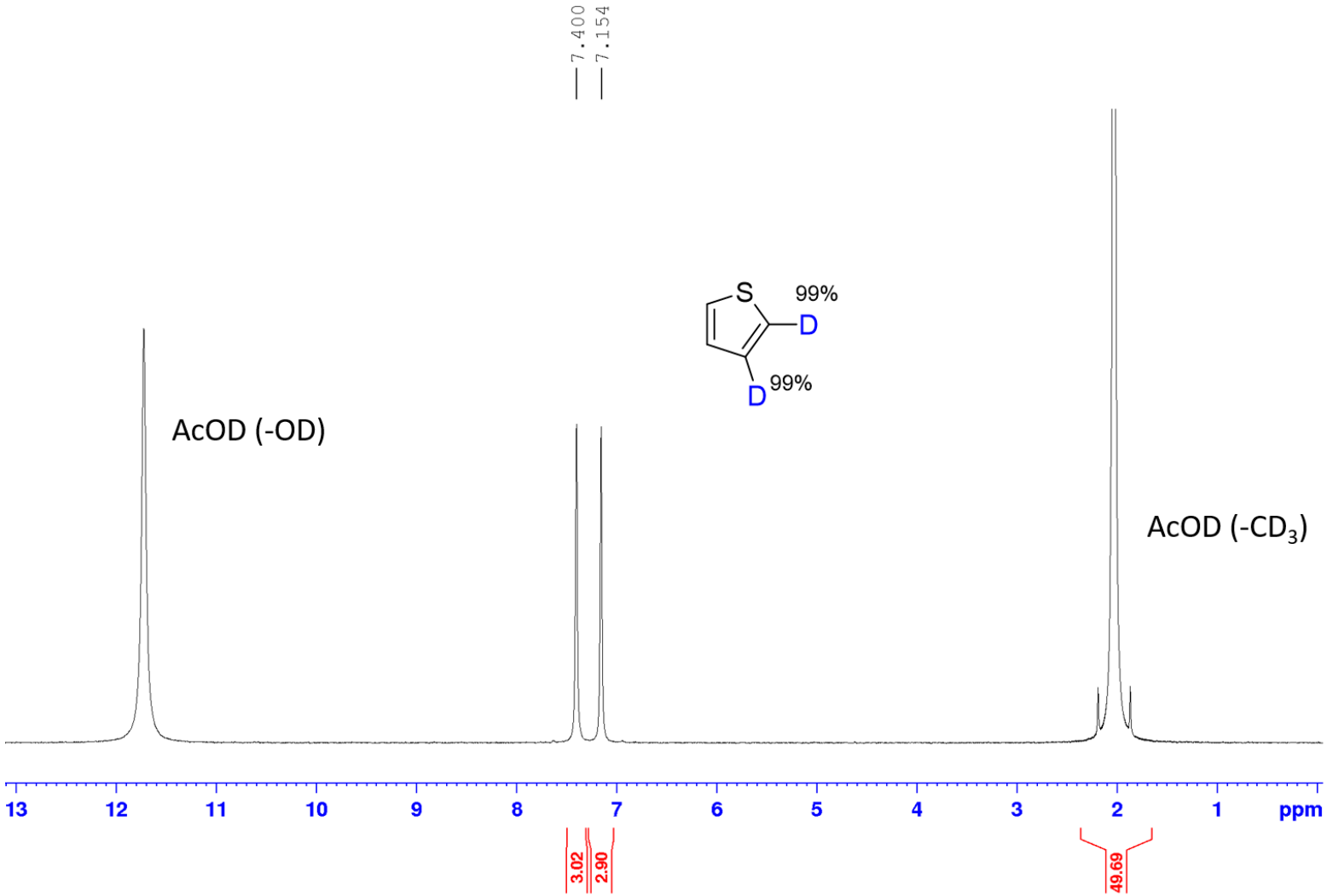

Figure S4.100. ^{2}H-NMR for the H/D Exchange reaction of thiophene in AcOD-d_4 catalyzed by **4.1-tBu**

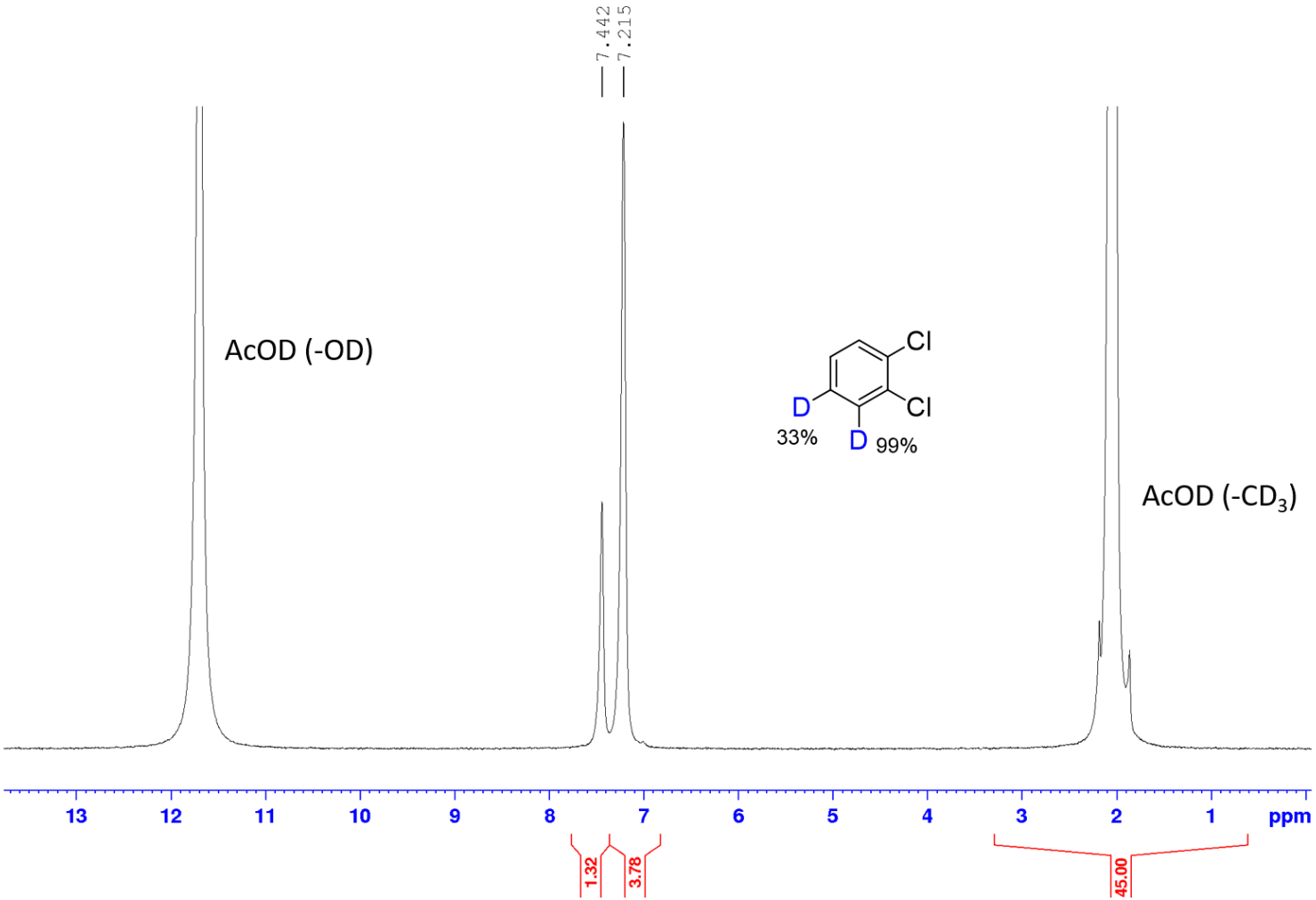

Figure S4.101. ^{2}H-NMR for the H/D Exchange reaction of 1,2 dichlorobenzene in AcOD-*d*$_4$ catalyzed by **4.1-tBu**

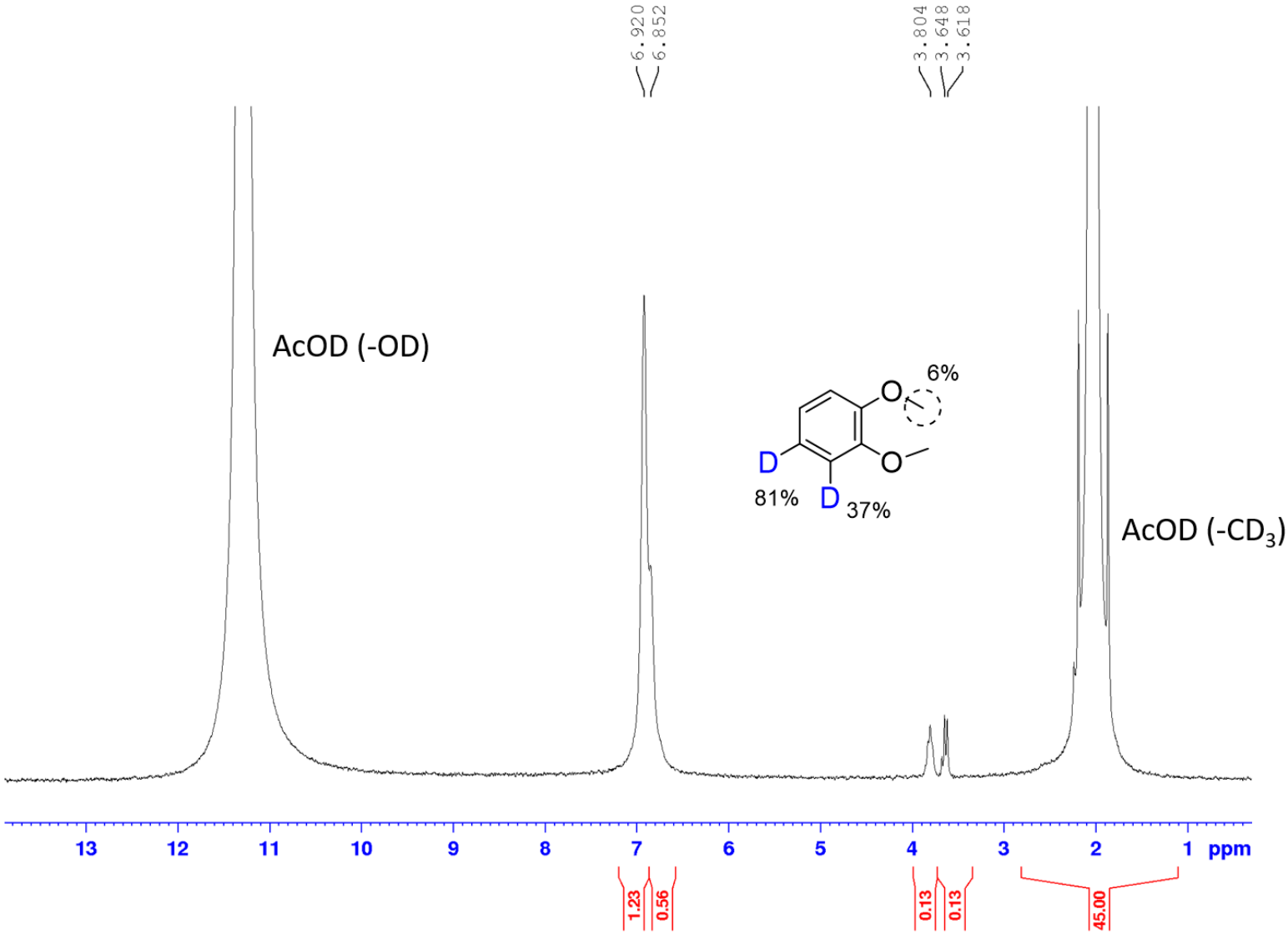

Figure S4.102. ^{2}H-NMR for the H/D Exchange reaction of 1,2 dimethoxybenzene in AcOD-d_4 catalyzed by **4.1-tBu**

Chapter 5: **Conclusions and Future Directions**

5.1. A brief summary

The work presented in this thesis serves as the experimental foundation for the synthesis and applications of sulfonated CNN Pt^{II} complexes for C-H bonds activation. Importantly, we investigated both practical applications of our new Pt^{II} aqua complexes as catalysts of H/D exchange reactions, as well as explored the mechanistic implications of the structural changes of the ligand scaffold and the reaction conditions. This investigation began with the work shown in Chapter 2, where the kinetic regioselectivity of H/D exchange reactivity of complex **1.5** was explored across thirty-four difference aromatic substrates in wet TFE-d_1 in order to develop an understanding of the heteroatom compatibility, characterize rates of regioselective H/D exchange, and to develop a predictive model for the C-H activation reaction of arenes catalyzed by **1.5** (Fig. 5.1).

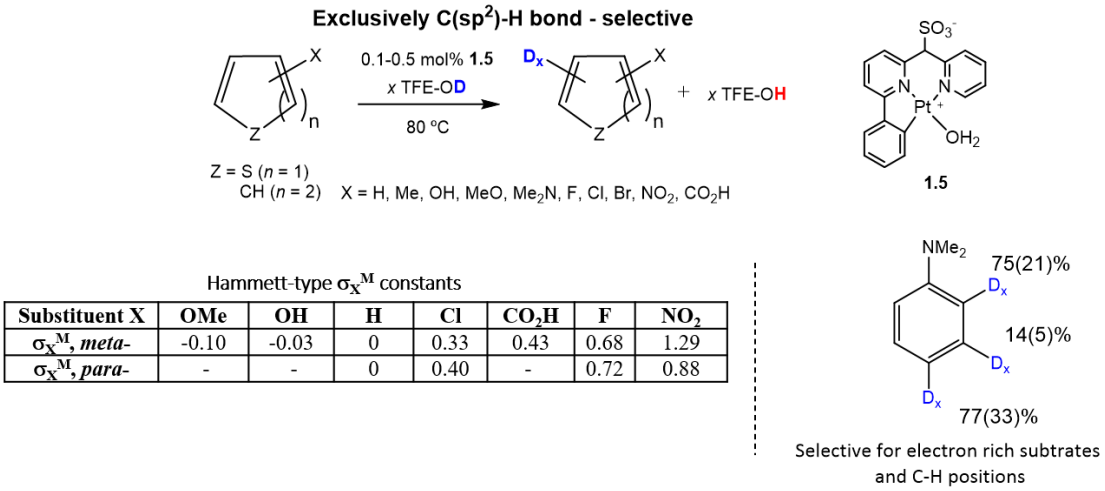

Figure 5.1. Key conclusions from the reactivity of **1.5** towards arene C-H bonds in wet TFE-d_1 at 80 °C.

By varying the identity of the aromatic substrate (H_nSub), a clear reactivity preference for more electron rich aromatic substrates was uncovered. Furthermore, by exploring the kinetic performance of **1.5** towards specific C-H bond positions within each substrate, a clear trend was revealed where the more sterically accessible and electron rich

C-H bonds underwent H/D exchange at a faster rate than their sterically encumbered and/or electron deficient counterparts. Thereby, suggesting a slightly electrophilic behavior of a Pt center in complex **1.5** under these reaction conditions. The rates of regioselective C-H bond activation were then compared to the rate of benzene's C-H bond activation, and a new Hammett-type parameter, σ_X^M, was developed to assist in the predicting of reactivity of a transition metal – assisted C-H activation.

In Chapter 3, the synthesis, characterization, and H/D exchange catalysis by a covalently immobilized sulfonated CNN-pincer ligand Pt^{II}-OH_2 complex was explored. It was expected that through the increased steric rigidity brought on by the fused cyclopenteno bridge, that complexes **3.5-FC** and **3.5** would exhibit a greater reactivity towards C-H bond activation. In some past studies,[51] it was found that these sulfonated CNN ligated Pt^{II}-OH_2 complexes with a more rigid ligand core had both an enhanced reactivity towards C-H bonds and also an increased propensity for bimolecular deactivation through the formation of insoluble dimers. Complex **3.5** was synthesized to exploit this enhanced reactivity brought on by the steric rigidity while eliminating the potential for bimolecular deactivation via a robust tripodal covalent immobilization to MSN.

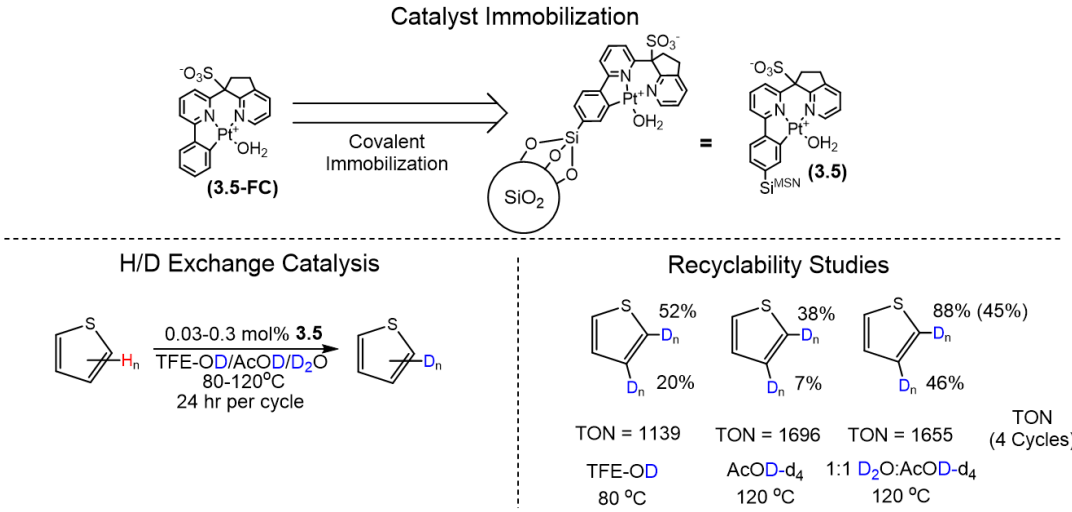

Figure 5.2. Immobilization strategy for **3.5** and some key results from utilizing **3.5** as an H/D exchange catalyst

This immobilization strategy proved to be successful in prolonging catalyst lifetime. Unsurprisingly, this immobilization strategy eliminated the formation of dimer complexes and served as a practical solution to inhibiting catalyst deactivation. Interestingly, complex **3.5** proved to be more reactive than its molecular counterpart **3.5-FC** and the previous catalyst generation **1.5** both in terms of catalyst turnovers and in terms of kinetic performance through the metric $k_{24\text{-}obs}$. With catalyst solubility being eliminated as a factor for H/D exchange catalysis, a wider range of reaction conditions were successfully explored which allowed for the use of more economical, and more practical deuterium sources, such as AcOD, AcOD:D_2O mixtures, and neat D_2O. Finally, complex **3.5** had such a substantial improvement in catalyst longevity over both its predecessor, **1.5**, and its molecular variant **3.5-FC**, that it was efficiently recycled after several 24 hour reaction cycles under various reaction conditions. Cumulative catalytic TON exceeded 1600 for **3.5** and additional recycles were not explored only because of the use of microscale reaction setup and systematic catalyst losses when separating the catalyst from

the reaction mixtures. Hence, complex **3.5** may have a greater potential as a recyclable heterogeneous catalyst than currently presented.

In Chapter 4, the reactivity of a series of 4-R-C_6H_3-dpms Pt^{II}-OH_2 complexes was explored in the H/D exchange of a series of aromatic compounds. The initial goal of this work was to correlate the rate of H/D exchange on a series of electronically diverse aromatic substrates to the substituent effect present on the 4-R-C_6H_3-dpms ligand. The initial kinetic screening included seven derivatives of these complexes, **4.1-X**.

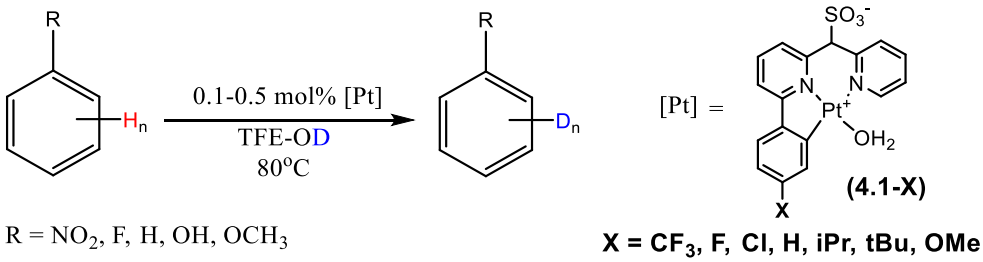

Figure 5.3. Kinetic screening results for **4.1-X** complexes in TFE-d_1 at 80°C.

The substrates chosen for this screening were nitrobenzene, fluorobenzene, benzene, phenol, and anisole. For each catalyst **4.1-X** and each of the substrates a rate constant was calculated for each type of C-H bond using TFE-d_1 as a source of exchangeable deuterium. The logarithm of the rate constants $k_{x,position}$ were plotted against the previously developed σ_X^M, Hammett-type parameters (Fig. 5.3). Generally, there was no clear correlation between the electronic characteristics of **4.1-X** derivatives and and their catalytic performance. The catalysts **4.1-OMe** and **4.1-F**, were the most sensitive to changes in the substrate electronics, with the largest magnitudes of the reaction parameter ρ, -1.82 ± 0.23 and 1.33 ± 0.26, respectively. The most active catalyst **4-CF_3** showed the lowest degree of sensitivity in the Hammett plot, with a reaction parameter ρ of only -0.74 ± 0.18. In fact, this kinetic assay was a poor demonstration of catalyst performance, due to

the complex kinetics associated with catalyst deactivation. The complex **4.1-tBu** proved to be the most practical and potent catalyst for H/D exchange. This increase in catalyst performance was proposed to result from the steric inhibition of its bimolecular deactivation which was not detected either visually (precipitation) or by ^{1}H NMR spectroscopy.

The enhanced catalytic activity of **4.1-tBu** was also evident when it was used with AcOD as a source of exchangeable deuterium at 120 ^{o}C (Fig. 5.4). A number of functional groups present in complex substrates, such as pharmaceuticals, polysubstituted arenes, polycyclic aromatics, and metal-coordinating pyridine moieties are well-tolerated. The observed vs statistically expected deuterium incorporation ratios exceeding 95% were achieved for some substrates. Additionally, the results from the deuteration of 2,6-diphenylpyridine showed somewhat *ortho*-selective deuteration which corroborates the mechanistic observations for the same substrate in reaction catalyzed by **3.5** (Chapter 3). We propose, that a secondary mechanism involving a directing group mediated C-H activation pathway may be accessible for **3.5**, as well as for **4.1-tBu**. Catalytic TON for **4.1-tBu** often exceeded 400, which makes it the most active, and long-lived homogenous Pt^{II} catalyst of this class to date.

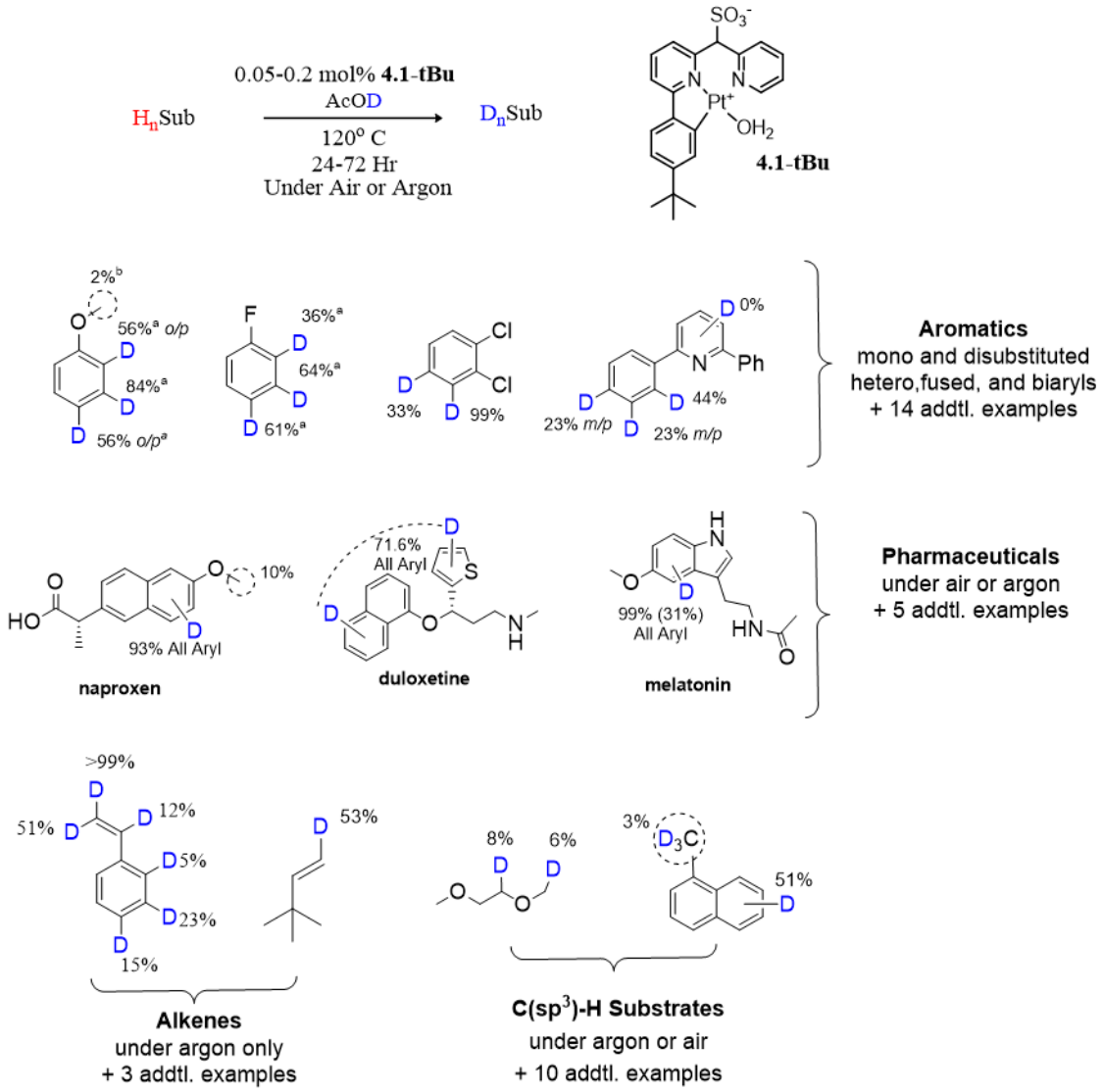

Figure 5.4. Selected results from deuteration studies involving substituted arenes, pharmaceuticals, alkenes, and C(sp^3)-H bearing substrates.

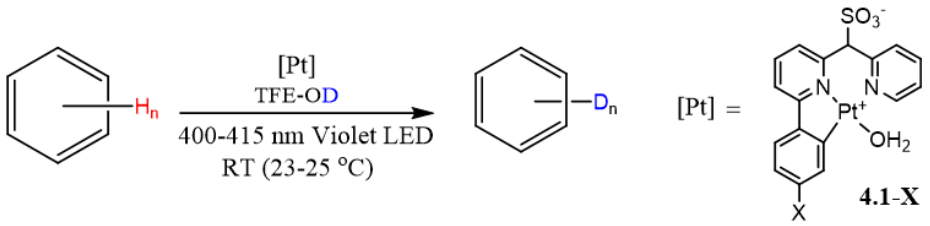

4.1-X	$k_{X,\ all}$	% Deuteration (24 hr)	TON
CF_3	0.06	2.4	2
F	0.11	1.1	12
H	0.32	12	54
iPr	0.09	1.5	7
tBu	0.22	2.8	15
OMe	0.89	15.3	59

Figure 5.5. Photochemically induced H/D exchange between TFE-d_1 and benzene catalyzed by **4.1-X** at room temperature.

It was found the **4.1-OMe** was the clear favorite in terms of kinetic performance with a k_x or 0.89 $M^{-1}hr^{-1}$ and extent of deuteration of 15.3% over 24 hours. The other catalysts screened under the same reaction conditions achieved fewer TON over the same reaction period, thus implying a faster rate of deactivation. While no di(poly)meric precipitates were formed, catalyst deactivation still proved to be problematic for the longevity of this photochemically induced system, regardless of the identity of the identity of the substituent **X** in the catalysts.

A series of competition H/D exchange experiments were then conducted in order to assess whether the reaction substrate selectivity is retained under the photochemical (25 ^oC) vs thermal (80 ^oC) conditions (Figure 5.6).

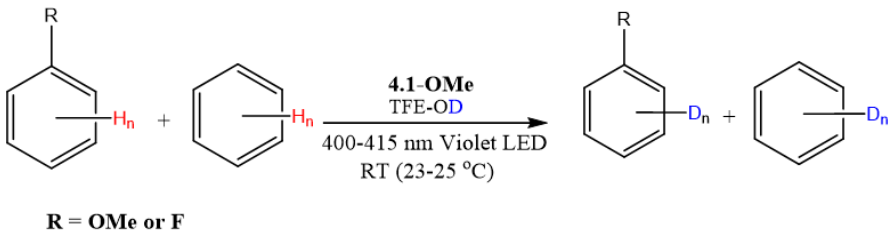

R = OMe or F

Reaction Conditions	Benzene Rel. Rate.	R-Ph, Meta C-H	R-Ph, Para C-H	R-Ph, Ortho C-H
Benzene:PhF @80 °C	1.00	0.62	0.57	0.37
Benzene:PhF Violet *hv*	1.00	0.80	0.86	0.59
Benzene:PhOMe @80 °C	1.00	1.94	1.90	0.97
Benzene:PhOMe Violet hv	1.00	0.72	0.98	0.37

Figure 5.6. Relative rates of H/D exchange of anisole or fluorobenzene vs benzene in TFE-d_1 under thermal (80 °C) and photochemical conditions (25 °C).

There is a significant difference in the substrate selectivity highlighted in the relative rates of the thermal reactions when compared to the photochemical reactions. Under the thermal conditions, the more electron rich anisole reacted at a faster rate than benzene, as highlighted by the relative rates of 1.94 and 1.90 for its *meta* and *para* C-H bonds. In turn, fluorobenzene reacted slower than benzene. These same trends were also observed when **1.5, 3.5**, or **4.1-tBu** were used as catalysts at 80 °C. However, when switching to the photochemical mode of activation, the relative rate of H/D exchange for fluorobenzene increased, and that of anisole decreased. A working hypothesis accounting for these observations is illustrated in Fig. 5.7 using potential energy diagrams for thermal and photochemical reactions.

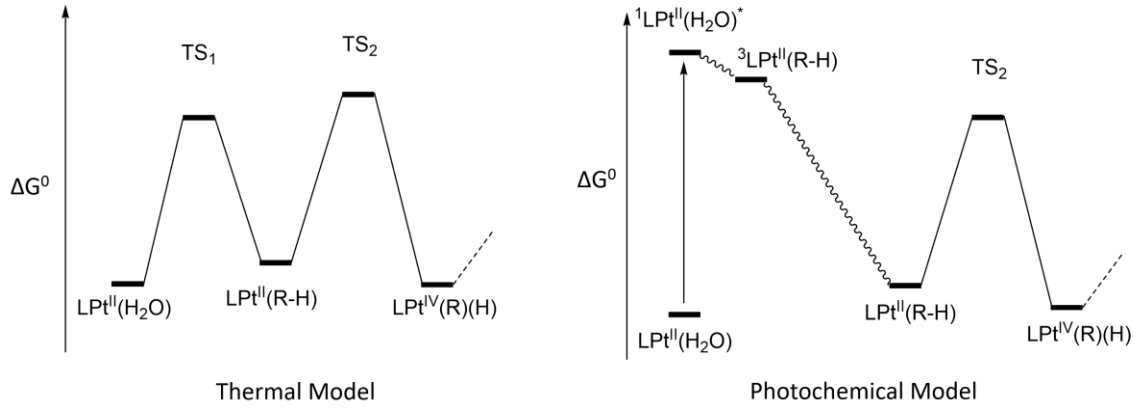

Figure 5.7 Simplified reaction energy diagrams comparing the relative energies of two transition states, TS_1, representing the barrier associated with ligand exchange in **4.1-X** and TS_2 representing the barrier for C-H activation of the resulting Pt^{II}-substrate complex.

Under photochemical conditions, it is expected that the reaction sequence proceeds via the absorption of a photon by **4.1-OMe**. This absorption event causes the promotion of an electron from the HOMO (predominantly a Pt d_{xz} orbital) to a predominantly Pt-O σ^* orbital. This electronic excitation would effectively weaken the Pt-O bond and decrease the activation barrier necessary for aqua ligand substitution with a substrate molecule (TS_1), but have no effect on the barrier for the subsequent C-H bond activation (TS_2) (Fig. 5.7, right). Thus, under photochemical conditions the RDS for the overall H/D exchange reaction will be the C-H activation step (TS_2) with the associated low substrate selectivity. In turn, based on the observed different reaction substrate selectivity under thermal conditions, the TS_1 may now be the reaction RDS (or, at least, contribute substantially to the effective reaction RDS if the energies of both TS_1 and TS_2 are close). A similar comparative study of substrate selectivity under thermal vs photochemical conditions involving other Pt^{II} or other metal complexes may be important when elucidating some

intricate details of their reaction mechanisms, as well as a means to control the selectivity of C-H activation by switching from thermal to photochemical conditions.

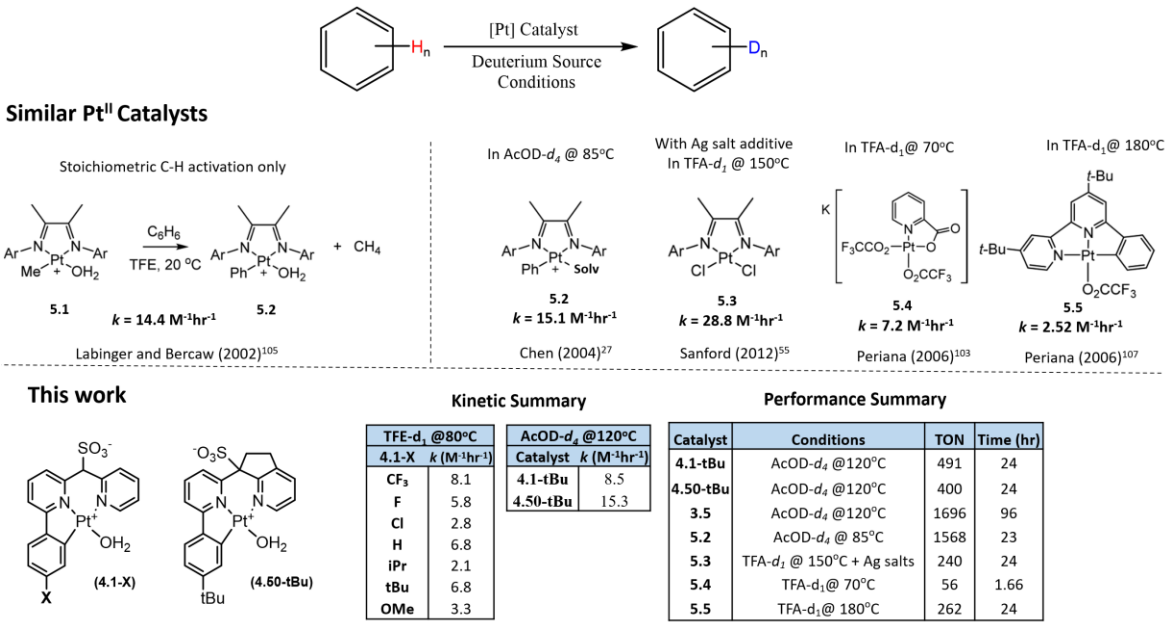

TFE-d_1 @80°C	
4.1-X	k ($M^{-1}hr^{-1}$)
CF_3	8.1
F	5.8
Cl	2.8
H	6.8
iPr	2.1
tBu	6.8
OMe	3.3

AcOD-d_4 @120°C	
Catalyst	k ($M^{-1}hr^{-1}$)
4.1-tBu	8.5
4.50-tBu	15.3

Catalyst	Conditions	TON	Time (hr)
4.1-tBu	AcOD-d_4 @120°C	491	24
4.50-tBu	AcOD-d_4 @120°C	400	24
3.5	AcOD-d_4 @120°C	1696	96
5.2	AcOD-d_4 @ 85°C	1568	23
5.3	TFA-d_1 @ 150°C + Ag salts	240	24
5.4	TFA-d_1@ 70°C	56	1.66
5.5	TFA-d_1@ 180°C	262	24

Figure 5.8. A comparison of the efficiency of various Pt^{II} complexes synthesized in this work and those reported in the literature acting as catalysts of H/D exchange reactions of benzene and selected sources of exchangeable deuterium under thermal conditions.[27, 55, 103, 105, 107]

To summarize how our catalysts perform versus similar Pt^{II}-based H/D exchange catalysts, the initial rate constants, *k*, alongside the respective catalyst and reaction conditions are shown in Fig. 5.8. Complex **5.1** is one of the top-performing species on this list with a very high rate constant of 14.4 $M^{-1}hr^{-1}$ at a very comfortable 20 °C in TFE but the reaction considered here is stoichiometric. Complex **5.3** presents the next fastest homogenous Pt^{II} catalyst with an observed rate constant, *k*, of 28.8 $M^{-1}hr^{-1}$. While this rate constant is ~2x larger than that of our most active complex **4.50-tBu**, the reaction of **5.3** requires a much higher temperature and utilizing a much more aggressive deuterium source, TFA-d_1. Complex **5.2** was able to be demonstrated to be catalytically explicitly for

the H/D exchange reaction between benzene and AcOD at 85 °C. The rate constant for this reaction is among the highest for catalysts of this class at 15.1 $M^{-1}Hr^{-1}$. However, this system requires the production of **5.2** from the dimethyl complex utilizing Et_2OHBF_4 as a proton source in benzene solutions.[27] Additionally, this complex has not been successfully applied as a general aromatic H/D exchange due to its poor heteroatom compatibility.[55] The two other similar complexes **5.4** and **5.5** both also utilize TFA-*d*$_1$ as a deuterium source. For the case of **5.4** the H/D exchange reaction for benzene was run at 70°C with a rate constant of 7.2 $M^{-1}hr^{-1}$, which is comparable to our similar reaction conditions in TFE-*d*$_1$ at 80 °C where complexes **4.1-X** demonstrate very similar rates constants in a more mild solvent mixture. Complex **5.5** was generally less reactive than all of our **4.1-X** series of catalysts. The H/D exchange reaction of **5.5** was run in TFA-*d*$_1$ at 180 °C with a rate constant of only 2.52 $M^{-1}hr^{-1}$. Hence, the novel Pt^{II} complexes developed in this work are some of the most active known Pt^{II}– based catalysts of H/D exchange involving benzene as a benchmark substrate. In addition to being very active catalyst, our novel complexes allow to use more affordable sources of exchangeable deuterium such as AcOD and D_2O.

In terms of catalyst reactivity lifetime and reaction longevity, the catalysts synthesized in this work are also highly competitive or exceed the reported TON of these similar complexes. **4.1-tBu** was the best performing homogenous catalyst in terms of catalytic turnovers and had TON for the H/D exchange reaction of benzene over 24 hours in AcOD-*d*$_4$ at 120°C of 491. In terms of catalytic turnovers for the H/D exchange reaction for benzene, the next highest performing homogenous Pt^{II} catalyst was complex **5.3** in TFA-*d*$_1$ at 150 °C with silver salt additives which had 240 turnovers in 24 hours. In summary, as a result of this work, we have developed several highly active catalysts of

H/D exchange, **4.1-tBu**, **4.50-tBu**, **4.1-CF3**, that are more competitive and/or practical that previously known similar Pt^{II} catalysts. Furthermore, the reaction conditions required for **4.1-tBu** and **4.50-tBu** catalyzed H/D exchange are far milder. Finally, our **4.1-tBu** and **4.50-tBu** outperform similar Pt^{II} complexes in terms of catalytic turnovers, therefore allowing for lower catalyst loadings to be utilized to achieve the same effects as other systems.

5.2. Future Directions: Expansion into Alkyl H/D exchange

Our past attempts utilizing complex **1.5** for the H/D exchange of alkanes or other C(sp^3)-H containing substrates were not successful as they led to the formation of catalytically inert di(poly)mers.[33, 51, 57] Presently, 12 substrates showed some low signs of the H/D exchange involving their C(sp^3)-H bonds in the system **4.1-tBu** / AcOD-d_4 at 120 ^oC. Notably, using violet LEDs - induced H/D exchange experiments in the system **4.1-OMe** / TFE-d_1 at 20 ^oC (Fig. 5.7), we demonstrated that the rates of the catalytic H/D exchange may be limited by the rate of ligand substitution at a Pt^{II} center. Therefore, to be competitive with either the solvent or aqua ligand for coordination to the Pt^{II} center, the donicity of a substrate C-H bond of interest must be sufficiently high to compete.

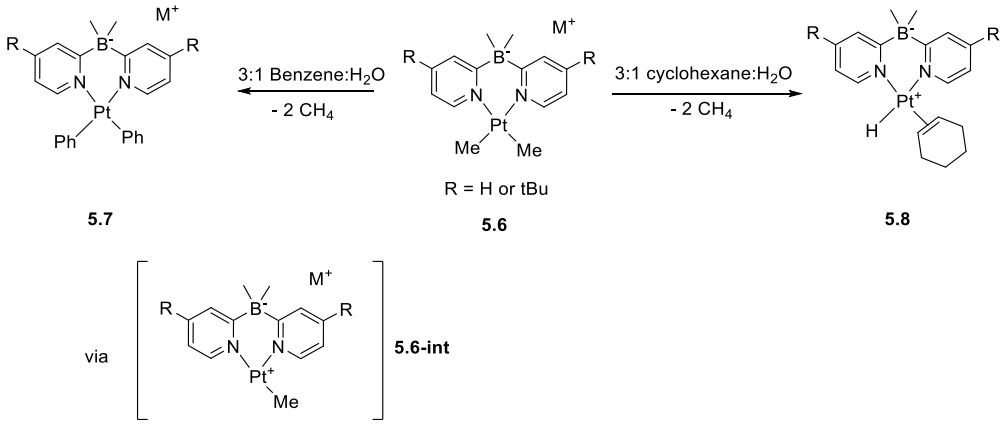

Scheme 5.1. Biphasic reaction conditions for the stoichiometric C-H activation of benzene and dehydrogenation of cyclohexane by **5.6.**

In past works done by our group, facile stoichiometric C-H activation of arenes and alkanes with **5.6** was achieved in biphasic hydrocarbon / water systems at room temperature (Scheme 5.1). In the absence of H_2O, in benzene or cyclohexane carefully dried under Na metal, no reaction was observed over 3 weeks.[113] According to a proposed mechanism, a Pt-Me bond in **5.6** undergoes protonolysis by H_2O to eliminate CH_4 and, formally, produce a 14-electron zwitterionic Pt^{II} intermediate **5.6-int**. With R = tBu, both **5.6** and, presumably, intermediate **5.6-int** are well soluble even in alkanes. In turn, since water solubility in hydrocarbons is very low, water competition for a Pt^{II} center is diminished by several orders of magnitude, which enables the subsequent C-H activation of the hydrocarbon substrates by **5.6-int** to yield complexes **5.7** or **5.8**.

The high solubility of **5.6** in hydrocarbons presents a particularly useful advantage over complexes **4.1-tBu** and **4.5-tBu** for the activation of alkane C-H bonds in water-containing systems. We might gain a similar advantage while designing new Pt^{II} catalysts, if we make them as lipophilic as **5.6**. Then, by using a hydrocarbon as a solvent for an H/D exchange catalyst and a weakly coordinating substrate, an alkane or a similarly poorly reactive substrate, the competitive effects of water co-solvent on the reactivity of the substrate's H/D exchange could be minimized dramatically.[113] Notably, complex **5.6** cannot be used for a catalytic H/D exchange (or Shilov-like C-H functionalization) of substrates that can be dehydrogenated to olefins to form products such as **5.8** (compare to Scheme 5.1, right). In turn, if a XNN-pincer ligand is used instead of dimethyldi(2-pyridyl)borate, an alkane dehydrogenation would not be facile and, potentially, such CNN-pincer – coordinated Pt^{II} complexes might serve as efficient catalysts for alkane H/D

exchange in biphasic alkane / D_2O systems with D_2O as a source of exchangeable deuterium.

Currently, there is no viable way to directly apply this interesting approach for complex **4.1-tBu**. Despite its good solubility in AcOH, the complex is insoluble in liquid hydrocarbons. Instead, in order to take advantage of high reactivity of **5.6** toward alkanes but inhibit the alkane dehydrogenation reaction, a suitable candidate for such a role could be a new Pt^{II} complex **5.9** (Fig. 5.9).

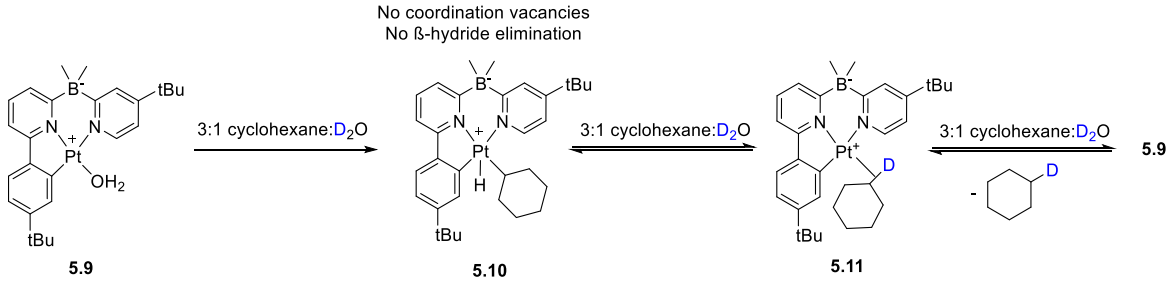

Figure 5.9. Proposed H/D exchange and possible C-H functionalization schemes utilizing complex **5.9**.

The borate scaffold in **5.9** is a modified version of the previous complex, **5.5.** Complex **5.9** shares a similar CNN binding motif as our previously studied **4.1-tBu**. The β-hydride elimination pathway is no longer facile for alkane activation intermediates such as **5.10** due to the phenyl fragment of the CNN-pincer ligand scaffold occupying a coordination site adjacent to the alkyl ligand. This chemistry would enable a competitive formation of a deuterated alkane trough intermediacy of alkane complexes such **5.11**. The presence of a D_2O phase would be sufficient for the H/D exchange of Pt^{IV} alkyl hydrido intermediate **5.10**.

5.3 Conclusions

Overall, two independent solutions have been developed to inhibit the deactivation ('dimerization') of sulfonated CNN Pt^{II}-OH_2 complexes. Along the way, we developed a

thorough heteroatom compatibility profile for complex **1.5** alongside a regioselective kinetics assay probing the rates of reaction for various C-H bond types. Our covalent immobilization strategy to yield complex **3.5** proved to be an effective strategy for prolonging catalyst lifetime alongside preserving the reactivity of the rigid ligand core. The series of **4.1-X** catalysts showed an interestingly small electronic effect on the rate of H/D exchange. Instead, there appeared to be a significant steric effect that enhanced the catalyst lifetime and overall performance. Complex **4.1-tBu** proved to be an extremely highly performing homogenous catalyst for aromatic H/D exchange that outcompetes the similar catalysts reported in the literature. Furthermore, the reaction of **4.1-tBu** and some polyfunctional pharmaceutical substrates yielded high catalytic turnovers even when run under air, and proved to be our most practical H/D exchange catalyst. Finally, we succeeded in our goal to also synthesize complex **4.5-tBu**, which was more active than **1.5** (**4.1-H**), and capable of catalyzing aromatic H/D exchange under air and under mild reaction conditions. We believe that as a result of this work, we have an improved understanding of how to modify our CNN Pt^{II} complexes to enhance their reactivity and how to exploit the structural properties of these complexes to enhance their solubility and catalyst lifetime. Complex **5.9** is proposed to be the "next step" in the advancement of these CNN Pt^{II} complexes in order to achieve sufficient reactivity towards more inert substrates, such as alkanes. Considering the implications of catalytically activating the C-H bonds of alkanes, complex **5.9** presents a unique opportunity for a homogenous Pt^{II} complex for the catalytic C-H activation and H/D exchange of alkanes potentially even at room temperature. This could have a profound impact on the field of homogenous C-H functionalization and mechanistic organometallic chemistry.

References

(1) Kopf, S.; Bourriquen, F.; Li, W.; Neumann, H.; Junge, K.; Beller, M. Recent Developments for the Deuterium and Tritium Labeling of Organic Molecules. *Chem. Rev*. **2022**, 122, 6634– 6718

(2) Urey, H. C.; Brickwedde, F. G.; Murphy, G. M. A Hydrogen Isotope of Mass 2 and Its Concentration. *Phys. Rev.* **1932**,40,1−15.

(3) Schiegl, W. E.; Vogel, J. C. Deuterium Content of Organic Matter. *Earth Planet. Sci. Lett.***1970**, 7, 307−313.

(4) Rosman, K. J. R.; Taylor, P. D. P. Isotopic Compositions of the Elements 1997 (Technical Report). *Pure Appl. Chem.***1998**,70, 217−235.

(5) Perrin, C. L.; Dong, Y. Secondary Deuterium Isotope Effects on the Acidity of Carboxylic Acids and Phenols. *J. Am. Chem. Soc.* **2007**,129, 4490−4497.

(6) Perrin, C. L.; Ohta, B. K.; Kuperman, J.; Liberman, J.; Erdélyi, M. Stereochemistry of β-Deuterium Isotope Effects on Amine Basicity. *J. Am. Chem. Soc.* **2005**,127, 9641−9647.

(7) Atzrodt, J.; Derdau, V.; Fey, T.; Zimmermann, J. The Renaissance of H/D Exchange. *Angew. Chem. Int. Ed.* **2007**, 46, 7744–7765.

(8) Atzrodt, J.; Derdau, V.; Kerr, W.J.; Reid, M. C-H Functionalisation for Hydrogen Isotope Exchange, *Angew.Chem. Int.Ed*. **2018**, 57,3022 –3047.

(9) a) Hashiguchi, B. G.; Bischof, S. M.; Konnick, M. M.; Periana, R. A. Designing Catalysts for Functionalization of Unactivated C–H Bonds Based on the CH Activation Reaction. *Acc. Chem. Res*. **2012,** 45 (6), 885–898 b) Zimmermann, T.; Soorholtz, M.; Bilke, M.; Schüth, F. Selective Methane Oxidation Catalyzed by Platinum Salts in Oleum at Turnover Frequencies of Large-Scale Industrial Processes *J. Am. Chem. Soc*. **2016,** 138, 38, 12395–12400

(10) Garnett, J. L.; Hodges, R. J. Homogeneous metal-catalyzed exchange of aromatic compounds. Isotopic hydrogen labeling procedure. *J. Am. Chem. Soc*. **1967**, 89 (17), 4546–4547.

(11) Gol'dshleger, N. F.; Es'kova, V. V.; Shilov, A. E.; Shteinman, A. A. Reactions of Alkanes in Solutions of Chloride Complexes of Platinum. R *Zh. Fiz. Khim*. **1972**, 46, 1353–1354.

(12) Shilov, A. E.; Shul'pin, G. B. *Chem. Rev*. Activation of C−H Bonds by Metal Complexes. **1997**, 97 (8), 2879–2932.

(13) Geletii, Yu.; Shilov, A. Catalytic Oxidation of Alkanes by Molecular Oxidation. Oxidation of Methane in the Presence of Platinum Salts and Heteropoly Acids. Kinet. Catal. 1983, 24, 413–416.

(14) Hartwig, J. F. Evolution of C–H Bond Functionalization from Methane to Methodology. *J. Am. Chem. Soc*. **2016**, 138 (1), 2–24.

(15) Gunsalus, N. J.; Koppaka, A.; Park, S. H.; Bischof, S. M.; Hashiguchi, B. G.;Periana, R. A. Homogeneous Functionalization of Methane. *Chem. Rev.* **2017**, 117 (13), 8521–8573.

(16) Labinger, J. A. *Chem. Rev.* Platinum-Catalyzed C–H Functionalization. **2017**, 117 (13), 8483–8496.

(17) Chen, X., Hao, X. S., Goodhue, C. E., and Yu, J. Q. Cu(II)-catalyzed functionalizations of aryl C-H bonds using O2 as an oxidant. J. *Am. Chem. Soc.* **2006**, 128, 6790

(18) Luinstra, G. A.; Wang, L.; Stahl, S. S.; Labinger, J. A.; Bercaw, J. E. Oxidation of Zeise's Salt by [PtCl6]2-: A Mechanistic Model for Hydrocarbon Oxidation. *Organometallics* **1994**, 700 (3), 755–756.

(19) Jones, C. J.; Taube, D.; Ziatdinov, V. R.; Periana, R. A.; Nielsen, R. J.; Oxgaard, J.; Goddard, W. A. Selective Oxidation of Methane to Methanol Catalyzed, with C-H Activation, by Homogeneous, Cationic Gold. *Angew. Chem., Int. Ed*. **2004**,43, 4626–4629.

(20) Jones, W. D. Isotope Effects in C−H Bond Activation Reactions by Transition Metals. *Acc. Chem. Res.* **2003**, *36*, 140–146.

(21) Lersch, M. Tilset, M. Mechanistic Aspects of C−H Activation by Pt Complexes. *Chem. Rev*. **2005**, 105, 6, 2471–2526

(22) Gol'dshleger, N.F., Shteinman, Pt(II) complexes in activation of saturated hydrocarbons. A.A. *React. Kinet. Catal. Lett*. (**1977**) 6, 43–50.

(23) Paul, A.; Musgrave, C. B. A Detailed Theoretical Study of the Mechanism and Energetics of Methane to Methanol Conversion by Cisplatin and Catalytica. *Organometallics* **2007**, 26 (4), 793–809.

(24) Ravi, M.; Ranocchiari, M.; van Bokhoven, J. A. The Direct Catalytic Oxidation of Methane to Methanol-A Critical Assessment. *Angew. Chemie - Int. Ed.* **2017**, 56 (52), 16464–16483.

(25) Vargaftik, M. N.; Stolarov, I. P.; Moiseev, I. I. Highly Selective Partial Oxidation of Methane to Methyl Trifluoroacetate. *Chem. Commun*. **1990**, No. 15, 1049.

(26) B. J. Wik, M. Lersch and M. Tilset, J. The Metal Is the Kinetic Site of Protonation of (Diimine)Pt Dimethyl Complexes. *J. Am. Chem. Soc*., **2002**, 124 , 12116 —12117

(27) Gerdes, G. Chen, P. Comparative Gas-Phase and Solution-Phase Investigations of the Mechanism of C−H Activation by [(N−N)Pt(CH3)(L)]+. O*rganometallics* **2004**, 23, 12, 3031–3036

(28) Labinger, J. A.; Bercaw, J. E. Understanding and exploiting C–H bond activation. *Nature* **2002**, 417, 507–514

(29) Pal, S.; Zavalij, P. Y.; Vedernikov, A. N. *Chem. Commun*. Oxidative C(sp3)–H bond cleavage, C–C and C[double bond, length as m-dash]C coupling at a boron center with O2 as the oxidant mediated by platinum(II). **2014**, 50 (40), 5376–5378.

(30) Vedernikov, A. N. Direct Functionalization of M–C (M = Pt^{II}, Pd^{II}) Bonds Using Environmentally Benign Oxidants, O_2 and H_2O_2. *Acc. Chem. Res.* **2012**, 45 (6), 803–813.

(31) Prantner, J.; Kaminsky, W.; Goldberg, K. Methylplatinum (II) and molecular oxygen: oxidation to methylplatinum (IV) in competition with methyl group transfer to form dimethylplatinum (IV). *Organometallics* **2014**, 2–5.

(32) Khusnutdinova, J. R.; Qu, F.; Zhang, Y.; Rath, N. P.; Mirica, L. M. Formation of the Palladium(IV) Complex $[(Me_3tacn)Pd^{IV}Me_3]^+$ through Aerobic Oxidation of (Me3tacn)PdIIMe2 (Me_3tacn = N,N′,N″-Trimethyl-1,4,7-triazacyclononane). *Organometallics* **2012,** 31 (13), 4627–4630.

(33) Watts, D.; Wang, D.; Adelberg, M.; Zavalij, P. Y.; Vedernikov, A. N. C–H and O2 Activation at a Pt(II) Center Enabled by a Novel Sulfonated CNN Pincer Ligand. *Organometallics* **2017,** 36 (1), 207–219.

(34) Munz, D.; Wang, D.; Moyer, M. M.; Webster-Gardiner, M. S.; Kunal, P.;Watts, D.; Trewyn, B. G.; Vedernikov, A. N.; Gunnoe, T. B. Aerobic epoxidation of olefin by platinum catalysts supported on mesoporous silica nanoparticles. *ACS Catal*. **2016**, 2846 (7), 4584–4593.

(35) Vedernikov, A. N.; Fettinger, J. C.; Mohr, F. Synthesis and reactivity of dimethyl platinum (IV) hydrides in water. *J. Am. Chem. Soc.* **2004**, 126, 11160–11161.

(36) Tang, F.; Zhang, Y.; Rath, N. P.; Mirica, L. M. Detection of Pd (III) and Pd (IV) intermediates during the aerobic oxidative C–C bond formation from a Pd (II) dimethyl complex. *Organometallics* **2012**, 31 (18), 6690–6696

(37) Safa, M.; Jennings, M. C.; Puddephatt, R. *J. Chem. Commun*. Easy oxidatively induced silicon–carbon bond activation in organoplatinum chemistry. **2010**, 46 (1), 2811–2813

(38) Prokopchuk, E. M.; Jenkins, H. A.; Puddephatt, R.J. Stable cationic dimethyl (hydrido) platinum (IV) complex. *Organometallics* **1999**, *18, 15, 2861–2866*

(39) Azizpoor Fard, M.; Behnia, A.; Puddephatt, R. J. Activation of dioxygen by dimethylplatinum (II) complexes. *Organometallics* **2017**, 36 (21), 4169–4178.

(40) Vedernikov, A. N.; Binfield, S. a; Zavalij, P. Y.; Khusnutdinova, J. R. Stoichiometric Aerobic Pt^{II}–Me Bond Cleavage in Aqueous Solutions to Produce Methanol and a Pt^{II}(OH) Complex. *J. Am. Chem. Soc.* **2006**, 128 (4), 82–83.

(41) Khusnutdinova, J. R.; Zavalij, P. Y.; Vedernikov, A. N. Facile Aerobic Oxidation of dpms− Platinum (II) Ethylene Complexes (dpms= di (2-pyridyl) methanesulfonate). *Organometallics* **2007**, 26 (II), 2402–2413.

(42) Khusnutdinova, J. R.; Newman, L. L.; Zavalij, P. Y.; Lam, Y. F.; Vedernikov, A. N. Direct C(sp3)−O Reductive Elimination of Olefin Oxides from PtIV-Oxetanes Prepared by Aerobic Oxidation of PtII Olefin Derivatives (Olefin = cis-Cyclooctene, Norbornene). *J. Am. Chem. Soc.* **2008**, 130 (7), 2174–2175.

(43) Khusnutdinova, J. R.; Zavalij, P. Y.; Vedernikov, A. N. Study of aerobic oxidation of phenyl PtII complexes (dpms)PtIIPh(L) (dpms = di(2-pyridyl)methanesulfonate; L = water, methanol, or aniline). *Can. J. Chem*. **2009**,87 (1), 110–120.

(44) Sberegaeva, A. V.; Liu, W. G.; Nielsen, R. J.; Goddard, W. A.; Vedernikov, A. N. Mechanistic Study of the Oxidation of a Methyl Platinum(II) Complex with O_2 in Water:

Pt^{II}Me-to-Pt^{IV}Me and Pt^{II}Me-to-$Pt^{IV}Me_2$ Reactivity. *J. Am. Chem. Soc*. **2014**, 136 (12), 4761–4768.

(45) Khusnutdinova, J. R.; Zavalij, P. Y.; Vedernikov, A. N. C−O Coupling of $LPt^{IV}Me(OH)X$ Complexes in Water (X = ^{18}OH, OH, OMe; L = di(2-pyridyl)methane sulfonate) O*rganometallics* **2007**, 26 (14), 3466–3483.

(46) Hartwig, J. F. Organotransition Metal Chemistry: From Bonding to Catalysis 1st Edition, 1st ed.; University Science Books, **2010.**

(47) Khusnutdinova, J. R.; Zavalij, P. Y.; Vedernikov, A. N. Allylic C–H Deprotonation of Olefins with Pt^{II}(OH) to Form η3-Allyl Pt^{II} Complexes in Water and Aprotic Organic Solvents. *Organometallics* **2011**, 30, 12, 3392–3399.

(48) Khusnutdinova, J. R.; Newman, L. L.; Zavalij, P. Y.; Lam, Y.-F.; Vedernikov, A.N. Direct C(Sp3)−O Reductive Elimination of Olefin Oxides from Pt^{IV}-Oxetanes Prepared by Aerobic Oxidation of PtII Olefin Derivatives (Olefin = Cis Cyclooctene, Norbornene). *J. Am. Chem. Soc*. **2008**, 130, 2174–2175

(49) Kramer, M.; Watts, D.; Vedernikov, A. N. Catalytic Deuteration of C(sp^2)–H Bonds of Substituted (Hetero)arenes in a Pt(II) CNN-Pincer Complex/2,2,2-Trifluoroethanol-d_1 System: Effect of Substituents on the Reaction Rate and Selectivity. *Organometallics* **2020**, 39, 4102– 4114.

(50) Labinger, J. A.; Bercaw, J. E. *J. Organomet. Chem.* Mechanistic studies on the Shilov system: A retrospective. **2015**, *793*, 47– 53,

(51) Watts, D.; Wang, D.; Zavalij, P. Y.; Vedernikov, A. N. Novel Sulfonated CNN Pincer Ligands for Facile C−H Activation at a Pt(II) Center. *Isr. J. Chem.* **2017**, *57*, 1010– 1022

(52) Ziatdinov, V. R.; Oxgaard, J.; Mironov, O. A.; Young, K. J. H.; Goddard, W. A.; Periana, R. A. *J. Am. Chem. Soc.* Carboxylic solvents and O-donor ligand effects on CH activation by Pt (II). **2006**, *128*, 7404– 7405.

(53) Young, K. J. H.; Meier, S. K.; Gonzales, J. M.; Oxgaard, J.; Goddard, W. A.; Periana, R. A. Heterolytic CH Activation with a Cyclometalated Platinum(II) 6-Phenyl-4,4'-di-tert-butyl-2,2-Bipyridine Complex. *Organometallics.* **2006**, *25*, 4734– 4737.

(54) Hickman, A. J.; Villalobos, J. M.; Sanford, M. S. Quantitative assay for the direct comparison of platinum catalysts in benzene H/D exchange. *Organometallics.* **2009**, *28*, 5316– 5322.

(55) Hickman, A. J.; Cismesia, M. A.; Sanford, M. S. Structure Activity Relationship Study of Diimine Pt^{II} Catalysts for H/D Exchange. *Organometallics.* **2012**, *31*, 1761– 1766.

(56) Emmert, M. H.; Gary, J. B.; Villalobos, J. M.; Sanford, M. S. Platinum and palladium complexes containing cationic ligands as catalysts for arene H/D exchange and oxidation. *Angew. Chem., Int. Ed.* **2010**, *49*, 5884– 5886.

(57) Watts, D.; Zavalij, P. Y.; Vedernikov, A. N. Consecutive C–H and O2 Activation at a Pt(II) Center To Produce Pt(IV) Aryls. *Organometallics.* **2018**, *37*, 4177– 4180

(58) Rhinehart, J. L.; Manbeck, K. A.; Buzak, S. K.; Lippa, G. M.; Brennessel, W. W.; Goldberg, K. I.; Jones, W. D. Catalytic arene H/D exchange with novel rhodium and iridium complexes. *Organometallics* **2012**, *31*, 1943– 1952,

(59) Jones, W. D. Alkane Activation Processes by Cyclopentadienyl Complexes of Rhodium, Iridium, and Related Species. In *Activation and Functionalization of Alkanes*; Hill, C., Ed.; Wiley: New York, 1989; pp 111– 149

(60) Jiao, Y.; Morris, J.; Brennessel, W. W.; Jones, W. D. J. Kinetic and Thermodynamic Selectivity of Intermolecular C–H Activation at [Tp′Rh(PMe_3)]. How Does the Ancillary Ligand Affect the Metal–Carbon Bond Strength? *J. Am. Chem. Soc.* **2013**, *135*, 16198– 16212

(61) Eisenstein, O.; Milani, J.; Perutz, R. N. Selectivity of C–H activation and competition between C–H and C–F bond activation at fluorocarbons. *Chem. Rev.* **2017**, *117*, 8710– 8753.

(62) Ma, S.; Villa, G.; Thuy-Boun, P. S.; Homs, A.; Yu, J.-Q. Palladium-Catalyzed ortho-Selective C-H Deuteration of Arenes: Evidence for Superior Reactivity of Weakly Coordinated Palladacycles *Angew. Chem., Int. Ed.* **2014**, *53*, 734– 737,

(64) Ruan, J.; Wang, D.; Kramer, M.J.; Zavalij, P.Y.; Vedernikov, A.N. Oxidation of Methylplatinum(II) Complexes K[(L)Pt^{II}Me] with O_2 and C(sp^3)-X (X = O and C) Reductive Elimination Reactivity of Methylplatinum(IV) Products (L)Pt^{IV}Me(OH): The Effect of Structure of Sulfonated CNN-Pincer Ligands L. *Organometallics*. **2022**, 41, 19, 2764-2783

(65) Janni, M.; Peruncheralathan, S. *Org. Biomol. Chem.* Catalytic selective deuteration of halo (hetero) arenes. **2016**, *14*, 3091– 3097.

(66) Anslyn, E. V.; Dougherty, D. A. *Modern physical organic chemistry*; University Science Books: Sausalito, CA, **2006**; p 609

(67) Huang, Y.; Liu, L.; Liu, W.; Liu, S.; Liu, S. Modeling molecular acidity with electronic properties and Hammett constants for substituted benzoic acids. *J. Phys. Chem. A* **2011**, *115*, 14697– 14707.

(68) Hartwig, J. F. *The Organotransition Metal Chemistry: From Bonding to Catalysis*; University Science Books: Sausalito, CA, **2010**

(69) Perdew, J. P.; Burke, K.; Ernzerhof, M. *Phys. Rev. Lett.* Generalized gradient approximation made simple. **1996**, *77*, 3865– 3868.

(70) *Jaguar, ver. 8.4*; Schrödinger, LLC: New York, NY, **2014.**

(71) Hopmann, K. H. How accurate is DFT for iridium-mediated chemistry? *Organometallics* **2016**, 35, 3795– 3807.

(72) Grimme, S.; Antony, J.; Ehrlich, S.; Krieg, H. Long-range corrected hybrid density functionals with improved dispersion corrections. *J. Chem. Phys.* **2010**, *132*, 154104.

(73) Klopman, G. Chemical reactivity and the concept of charge-and frontier-controlled reactions. *J. Am. Chem. Soc.* **1968**, *90*, 223– 234.

(74) Fleming, I. *Frontier Orbitals and Organic Chemical Reactions*; Wiley, Chichester, UK, 2006; p 27.

(75) Hashiguchi, B. G.; Bischof, S. M.; Konnick, M. M.; Periana, R. A. Designing catalysts for functionalization of unactivated C–H bonds based on the CH activation reaction. *Acc. Chem. Res.* **2012**, 45, 885– 898

(76) Chepaikin, E. G. *Russ*. *Chem. Rev.* **2011**, 80, 363– 396

(77) Ahlquist, M.; Nielsen, R. J.; Periana, R. A.; Goddard, W. A., III. Product protection, the key to developing high performance methane selective oxidation catalysts. *J. Am. Chem. Soc.* **2009**, 131, 17110– 17115

(78) Paek, S. M. Synthesis of tetrabenazine and its derivatives, pursuing efficiency and selectivity. *Molecules* **2020**, 25(5): 1175

(79) Farizyan, M.; Mondal, A.; Mal, S.; Deufel, F.; van Gemmeren, M. Palladium-catalyzed nondirected late-stage C–H deuteration of arenes. *J. Am. Chem. Soc.* **2021**, 143, 40, 16370–16376

(80) Junk, T.; Catallo, W. J. Hydrogen isotope exchange reactions involving C–H (D, T) bonds. *Chem. Soc. Rev.* **1997**, *26*, 401– 406,

(81) Trewyn, B. G.; Slowing, I. I.; Giri, S.; Chen, H. T.; Lin, V. S. Y. Synthesis and functionalization of a mesoporous silica nanoparticle based on the sol–gel process and applications in controlled release. Acc. Chem. Res. **2007**, 40, 846– 853

(82) Valenstein, J. S.; Kandel, K.; Melcher, F.; Slowing, I. I.; Lin, V. S. Y.; Trewyn, B. G. Functional mesoporous silica nanoparticles for the selective sequestration of free fatty acids from microalgal oil. *ACS Appl. Mater. Interfaces* **2012**, 4, 1003– 1009

(83) Manoso, A.S.; Deshong, P. Improved synthesis of aryltriethoxysilanes via palladium (0)-catalyzed silylation of aryl iodides and bromides with triethoxysilane. *J. Org. Chem.* **2001**, 66, 22, 7449–7455

(84) Manoso, A.S.; Chuljin, A.; Soheili, A.; Handy, C.J.; Correia, R.; Seganish, W.M.; Deshong, P. Improved synthesis of aryltrialkoxysilanes via treatment of aryl grignard or lithium reagents with tetraalkyl orthosilicates. *J. Org. Chem.* **2004,** 69, 24, 8305–8314

(85) Seganish, W. M.; DeShong, P. Application of directed orthometalation toward the synthesis of aryl siloxanes. *J. Org. Chem.***2004**, *69*, 6790−6795.

(86) Brunauer, S.; Emmett, P. H.; Teller, E. Adsorption of Gases in Multimolecular Layers. *J. Am. Chem. Soc.* **1938**, 60, 309– 319

(87) Barrett, E. P.; Joyner, L. G.; Halenda, P. P. The Determination of Pore Volume and Area Distributions in Porous Substances. I. Computations from Nitrogen Isotherms. *J. Am. Chem. Soc.* **1951**, 73, 373– 380

(88) Huo, Q. S.; Margolese, D. I.; Stucky, G. D. Surfactant Control of Phases in the Synthesis of Mesoporous Silica-Based Materials. *Chem. Mater.* **1996**, 8, 1147– 1160

(89) Stöber, W., Fink, A., and Bohn, E. J. Controlled growth of monodisperse silica spheres in the micron size range. *Colloid Interface Sci*. **1968**, 26, 62– 69

(90) Sing, K. S. W., Everett, D. H., Haul, R. A. W., Moscou, L., Pierotti, R. A., and Rouquérol; Siemieniewska, T. REPORTING PHYSISORPTION DATA FO GAS/SOLID SYSTEMS with Special Reference to the Determination of Surface Area and Porosity. *Pure Appl. Chem.* **1985**, 57, 603– 619.

(91) Gobin, O.C.; Wan, Y.; Zhoa, D.; Kleitz, F.; Kaliaguine; S. Mesostructured silica SBA-16 with tailored intrawall porosity part 1: Synthesis and characterization. *J. Phys. Chem. C* **2007**, 111, 7, 3053–3058

(92) Zhao, L.; Liu, W.; Zhang, Z.; Zhao, H.; Wang, Q.; Yan, X. Ruthenium-Catalyzed ortho- and meta-H/D Exchange of Arenes. Organic Letters **2019** *21* (24), 10023-10027

(93) Sawama, Y.; Nakano, A.; Matsuda, T.; Kawajiri, T.; Yamada, T.; Sajiki, H. H–D Exchange deuteration of arenes at room temperature. *Org. Process. Res. Dev.* **2019**, *23*, 648– 653,

(94) Lide, David R., ed. **2006**. CRC Handbook of Chemistry and Physics (87th ed.). Boca Raton, FL: CRC Press.

(95) Crespo, M.; Font-Bardia, M.; Solans, X. Compound [PtPh2(SMe2)2] as a Versatile Metalating Agent in the Preparation of New Types of [C,N,N'] Cyclometalated Platinum Compounds. *Organometallics* **2004**, 23, 8, 1708–1713

(96) a) Pony, Y., R., Hesk, D., Rivera, N., Pelczer, I. & Chirik, P. J. Iron-catalysed tritiation of pharmaceuticals. *Nature* **2016,** 529, 195–199 b) Zarate, C.; Yang, Haifeng, Y.; Bezdek, M.J.; Hesk, D.: Chirik, P.J. Ni(I)–X Complexes Bearing a Bulky α-Diimine Ligand: Synthesis, Structure, and Superior Catalytic Performance in the Hydrogen Isotope Exchange in Pharmaceuticals. *J. Am. Chem. Soc.* **2019**, 141, 12, 5034–5044

(97) Li, R., Wu, Y., Wang, C. One-pot H/D exchange and low-coordinated iron electrocatalyzed deuteration of nitriles in D2O to α,β-deuterio aryl ethylamines. *Nature Commun* **2022,** 13, 5951

(98) Loh, Y.; Nagao, K.; Hoover, A.J.; Hesk, D.; Rivera, N.; Colletti, S.L.; Davies, I.W.; MacMillan, D.W.C. Photoredox-catalyzed deuteration and tritiation of pharmaceutical compounds. *Science* **2017,** 358, 1182–1187

(99) Farizyan, M.; Mondal, A.; Mal, S.; Deufel, F.; van Gemmeren, M. Palladium-catalyzed nondirected late-stage C–H deuteration of arenes. *J. Am. Chem. Soc*. **2021**, 143, 40, 16370–16376

(100) Uttry, A.; Mal, S.; van Gemmeren, M. Late-Stage β-C(sp3)–H Deuteration of Carboxylic Acids. *J. Am. Chem. Soc.* **2021**, 143, 10895– 10901.

(101) Kopf, S.; Beller, M. Recent developments for the deuterium and tritium labeling of organic molecules. *Chemical Reviews* **2022,** *122* (6), 6634-6718.

(102) McKeown, B. A.; Foley, N. A.; Lee, J. P.; Gunnoe, T. B. Hydroarylation of unactivated olefins catalyzed by platinum (II) complexes. *Organometallics* **2008**, 27, 4031– 4033

(103) Ziatdinov, V. R.; Oxgaard, J.; Mironov, O. A.; Young, K. J. H.; Goddard, W. A.; Periana, R. A. Carboxylic solvents and O-donor ligand effects on CH activation by Pt (II). *J. Am. Chem. Soc.* **2006**, 128, 7404– 5

(104) Driver, T.; Day, M. W.; Labinger, J. A.; Bercaw, J. E. Mechanism of C− H Bond Activation of Alkyl-Substituted Benzenes by Cationic Platinum (II) Complexes. *Organometallics* **2005**, 24, 3644

(105) Zhong, H. A.; Labinger, J. a; Bercaw, J. E. C− H Bond Activation by Cationic Platinum (II) Complexes: Ligand Electronic and Steric Effects. *J. Am. Chem. Soc.* **2002**, 124, 1378– 99

(106) Hickman, A. J.; Cismesia, M. A.; Sanford, M. S. Structure Activity Relationship Study of Diimine Pt^{II} Catalysts for H/D Exchange. O*rganometallics* **2012**, 31, 1761– 1766

(107) Young, K.; Meier, S.; Gonzales, J.; Periana, R. A. Heterolytic CH Activation with a Cyclometalated Platinum(II) 6-Phenyl-4,4'-di-tert-butyl-2,2-Bipyridine Complex. *Organometallics* **2006**, 25, 4734– 4737

(108) Liu, C.; Han, N.; Song, X.; Qiu, A General and Highly Efficient Method for the Construction of Aryl-Substituted N-Heteroarenes. *J. Eur. J. Org. Chem*. **2010**, 5548–5551

(109) Pal, S.; Zavalij P.Y, Vedernikov A.N. Concurrent B-to-Pt Methyl Migration and B-Center Retention in Aerobic Oxidation of Methylborato Platinum (II) Complexes. *Organometallics.* **2015,** 34: 5183-5190.

(110) Pal, S.; Zavalij P.Y, Vedernikov A.N. Oxidative C (sp^3)–H bond cleavage, C–C and C [double bond, length as m-dash] C coupling at a boron center with O_2 as the oxidant mediated by platinum (II). *Chem.Commun.* **2013,** 50: 5376-5378.

(111) Pal, S.; Vedernikov A.N. Oxidation of dimethyldi (2-pyridyl) borato Pt II Me n complexes, n= 1, 0, with H 2 O 2: tandem B-to-Pt methyl group migration and formation of C–O bond. *Dalton Transactions.* **2012**, 41: 8116-8122.

(112) Khaskin E, Lew DL, Pal S, Vedernikov A. N. Homogeneous catalytic transfer dehydrogenation of alkanes with a group 10 metal center. *Chem.Commun*. **2009,** 6270-6272.

(113) Khaskin, E.; Zavalij, P. Y.; Vedernikov, A. N. Facile Arene C−H Bond Activation and Alkane Dehydrogenation with Anionic $LP^{tII}Me^{2-}$ in Hydrocarbon−Water Systems (L = Dimethyldi(2-pyridyl)borate). *J. Am. Chem. Soc.* **2006**, 128, 13054